The regulation of peripheral nerve homeostasis, regeneration and tumourigenesis

Salome Stierli

Thesis submitted for the degree of Doctor of Philosophy

MRC Laboratory for Molecular Cell Biology

University College London

Declaration

I, Salome Stierli, confirm that the work presented in this thesis is my own. Where Information has been derived from other sources, I confirm that this has been indicated in the thesis.

Signed……. Date…….

Abstract

Peripheral nerves are regenerative, with Schwann cells (SCs), the main glial cells of the peripheral nervous system, orchestrating multiple aspects of the multicellular regenerative process. A regenerating nerve resembles tumours that form in this tissue in patients with Neurofibromatosis Type 1 (NF1) and in a mouse model we have developed, we have identified a key role for the injured microenvironment in stimulating tumour formation derived from adult $Nf1^{-/-}$ myelinating Schwann cells (mSCs).

Here, we have investigated the homeostatic turnover of peripheral nerve and how this changes following injury in order to understand how the injured microenvironment could contribute to tumour formation. We find that mSCs do not turnover in adulthood. Following injury however, all mSCs proliferate and dedifferentiate to progenitor-like SCs, which contribute to the nerve regeneration process without the requirement for a distinct SC stem cell population. Moreover, lineage analysis, demonstrated that mSC derived cells retain the SC lineage but can switch from a mSC to a non-myelinating SC fate during nerve regeneration. In contrast, during tumourigenesis, $Nf1^{-/-}$ mSCs lose this lineage restriction.

To identify the microenvironmental pro- and anti- tumourigenic signals involved in the early stages of tumourigenesis, we have characterised the early stages of tumour formation in our mouse model to identify the point of divergence between tissue regeneration and tumour formation. We subsequently performed a molecular analysis at this time-point that identified several potential pro- tumourigenic signals at the injury site.

This work provides a further illustration of the distinct mechanisms that tissues use to maintain and repair themselves. Moreover, it provides insight into links between tissue repair and tumourigenesis and how studying these processes may provide new approaches for the treatment of this disease.

Impact statement

The PNS differs from the CNS, in that the PNS has much greater regenerative potential. Key to the regenerative process is the major glial cell of the PNS, the SC, which orchestrates the regeneration of this tissue.

In the first part of this thesis, using a combination of long-term labelling studies and lineage analysis, we have addressed the homeostatic state of adult peripheral nerve and how this cell state changes during and after regeneration. Importantly, we find that peripheral nerve uses a distinct mechanism, compared to the CNS and compared to other tissues, in order to maintain itself and repair following injury in that both processes are independent of a stem cell population and instead involve the remarkable plasticity of the mature cell types within the nerve. These mature cell types rarely turnover, if at all, in the homeostatic state, whereas all cell types in the tissue proliferate and contribute to the repair of the damaged nerve. Our findings also highlight the remarkable stability of glia in the PNS, despite retaining the ability to efficiently convert to a progenitor-like SC following injury, thus providing a further illustration of the diversity of stem/progenitor cell phenotypes that exist in mammalian tissues.

This work therefore has broad implications for our understanding of tissue homeostasis and repair and also provides insights into the different requirements of CNS and PNS environments in terms of plasticity and regenerative capability.

A regenerating nerve has similarities to tumours that form in this tissue in patients with NF1. Research in the NF1 field has mainly focused on investigating the tumour driving SCs and on targeting Ras signalling pathways, however, treatment options are very limited emphasising the great need for new therapeutic approaches. More recently, the importance of several other cell types within the tumour microenvironment has been recognised and it has been suggested that targeting the TME could be an alternative therapeutic approach for neoplasms including neurofibroma.

In the second part of this thesis, I have generated a powerful in vivo mouse-model to study the early stages of NF1 tumour formation and to elucidate the role of the microenvironment in neurofibroma formation. I have used this in vivo mouse-model to perform a RNA seq. analysis

at a defined timepoint at which the earliest tumourigenic changes can be observed. The RNA seq data once fully analysed will be deposited in order to make it publicly available. The differential expression analysis of our dataset should identify signalling pathways responsible for creating a pro-tumourigenic environment at the site of injury in contrast to signalling pathways providing an anti- tumourigenic environment in a normal nerve microenvironment. Identification of either signals may identify new molecular targets which may be important for the development of therapeutics for this disease, some of which may be used prophylactically. Moreover, we demonstrated that neurofibromas arise from multiple Nf1-deficient SCs indicating that the loss of Nf1 and the contribution of the injury environment is sufficient for tumour formation.

Acknowledgments

I would like to thank Alison Lloyd for allowing me to work on this project, for her guidance throughout this project and for her feedback and editing on the first drafts of this thesis.

Special thanks also to all the current and previous members of the Lloyd lab for their support throughout this project. In particular, I would like to thank Ilaria Napoli for her guidance and endless scientific discussions during the first half of my PhD, as well as Anne-Laure Cattin and Noelia Garcia Calavia for their contribution to this project. I also am very grateful to Elizabeth Harford-Wright for proof reading my thesis. Furthermore, I would like to thank Liza Malong for being the best colleague and friend I could have wished for.

Special thanks to Christina Venturini who performed the RNA seq analysis and has provided invaluable advice throughout the process, and to the members of my committee Yanlan Mao, Robin Kettler and Rob de Bruin for their advice.

My appreciation goes out to all my friends here in London and back home in Basel who have supported me in multiple ways over the last few years. Moreover, I would like to thank my family, especially my mother, for her constant encouragement and support in the times when I needed it most.

Finally, I would like to express my deepest gratitude to my boyfriend, Artur Faria, who has always been there listening to my endless complaints during the past years. Thanks for sticking with me during difficult moments, I could not have done this without you.

Table of Contents

List of Figures and Tables

List of Abbreviations and Acronyms

ADAM22	A disintegrin and metalloproteinase
BAF	Braham associated factor
BDNF	Brain derived neurotrophic factor
BNB	Blood nerve barrier
BrdU	Bromodeoxyuridine
BV	Blood vessel
CAF	Cancer associated fibroblasts
cAMP	Cyclic adenosine monophosphate
CCNB2	Cyclin B2
CFP	Cyan fluorescent protein
CILP	Cartilage intermediate layer protein
CLEM	Correlative light electron microscopy
CMT	Charcot-Marie-Tooth disease
CNS	Central nervous system
CRC	Colorectal cancer
CSP	Chondroitin sulfate proteoglycan
CSRD	Cysteine/serine rich domain
CTF	C-terminal fragment
CXCL14	C-X-C motif chemokine ligand 14
CX3CL1	C-X3-C motif chemokine ligand 1
Cx32	Connexin 32
Dhh	Desert hedgehoc
DNA	Deoxyribonucleic acid
DRG	Dorsal root ganglia
DTT	Dithiothreitol
ECM	Extracellular matrix
Edil3	EGF like repeats and discoidin domains 3
EdU	5’ethynyl-2’-deoxyuridine
EGF	Epidermal growth factor
EM	Electron microscopy
EMILIN1	Elastin microfibril interfacer 1
EphB2	Ephrin type-B receptor 2
ERK	Extracellular signal-regulated kinases
ESM1	Endothelial cell specific molecule
FC	Fold change
GAP	GTPase activating protein

GDP	Guanosine diphosphate
GEF	Guanine nucleotide exchange factors
GFAP	Glial fibrillary acidic protein
GFP	Green fluorescent protein
GO	Gene ontology
Gpr126	G-protein coupled receptor
GTP	Guanosine triphospate
HDAC	Histone deacetylase
KO	Knock-out
IF	Immunofluorescence
IGF1	Insulin growth factor 1
IL6	Interleukin 6
ITGAE	Integrin Subunit Alpha E
IP	Intraperitoneal injection
JAK	Janus kinase
LHS	Left hand side
MAG	Myelin associated glycoprotein
MAPK	Mitogen activated protein kinase
MBP	Myelin basic protein
MEK	Mitogen-activated protein kinase
MPNST	Malignant peripheral nerve sheath tumour
MPZ	Myelin protein zero
mRNA	messenger RNA
mSCs	myelinating Schwann cells
mTOR	Mammalian target of rapamycin
NCAM	Neural cell adhesion molecule
NCSC	Neural crest stem cells
NEB	New england biolabs
Necl	Nectin-like proteins
NFAT	Cytosolic nuclear factor of activated T cells
NF1	Neurofibromatosis type I
NLS	Nuclear localisation sequence
Nmat	Nicotinamide mononucleotide adenylyltransferase
NMJ	Neuromuscular junction
nmSCs	non-myelinating Schwann cells
NRG1	Neuregulin 1
NT	Neurotrophin
NTF	N-terminal fragment
NTP	Nucleoside triphosphate

Oct-6	Octamer binding transcription factor-6
OL	Oligodendrocyte
OMGP	Oligodendrocyte myelin glycoprotein
OPC	Oligodendrocyte progenitor cell
O/N	Overnight
Par3	Partitioning defective-3
PBS	Phosphate buffered saline
PCA	Principal component analysis
PCR	Polymerase chain reaction
PDGF	Platelet derived growth factor
PFA	Paraformaldehyde
PI3K	Phosphoinositide 3-kinase
PLP	Myelin proteolipid protein
PLC-γ	Phosphoinositid-Phospholipase C
PNS	Peripheral nervous system
P0	Myelin protein zero
Raf	Rapidly accelerated fibrosarcoma
RafTR	Raf-kinase/estrogen receptor fusion protein
RalGDS	Ral guanine dissociation stimulator
Ras	Rat sarcoma
RFP	Red fluorescent protein
RHS	Right hand side
RIN	RNA integrity number
RNA	Ribonucleic acid
RNA seq	RNA sequencing
rRNA	ribosomal RNA
SCs	Schwann cells
SCPs	Schwann cell precursors
SEM	Standard error mean
Sema4F	Semaphorin 4F
SKPs	Skin derived progenitors
SLI	Schmidt-Lantermann incisures
SLITRK6	SLIT and NTRK like family member 6
SMA	Smooth muscle actin
Sox-10	SRY-related HMG-box 10
SPOCK3	SPARC (Osteonectin), Cwcv and Kazal like Domains Proteoglycan 3
SPON1	Spondin-1
STAT	Signal transducer and activator of transcription
TBS	Tris-buffered saline

TBD	Tubulin-binding domain
TEM	Transmission electron microscopy
TGFβ	Transforming growth factor-beta
TME	Tumour microenvironment
Tmx	Tamoxifen
TNFSF18	Tumour necrosis factor 18
TSC	Tuberous sclerosis complex
UCL	University College London
UTP	Uridine triphosphate
VCAN	Versican
WD	Wallerian degeneration
Wld^s	Wallerian degeneration slow
WT	Wild type
YFP	Yellow fluorescent protein

Chapter One: Introduction

1.1. Glial cells in the peripheral nervous system

The nervous system consists of the central and the peripheral nervous system (Figure 1.1A) and its glial cells were long thought to be passive components, acting solely to support neuronal function. Only recently have glial cells moved to centre stage with an acknowledgment of their multiple roles in controlling and regulating nervous system development, plasticity and disease (Fields et al., 2015). Consequently, glial cells have been described as master regulators of the nervous system (Barres, 2008) (Zuchero and Barres, 2015).

In the adult peripheral nervous system (PNS), glial cell types can be divided into three major categories: Schwann cells (SCs), enteric glial cells, satellite cells and olfactory ensheating glial cells. SCs are by far the most abundant glial cell type and are found closely associated with axons throughout the PNS. SCs can be divided into three classes, myelinating Schwann cells (mSCs), non-myelinating Schwann cells (nmSCs) and perisynaptic Schwann cells (also called terminal SCs or teloglia) (Jessen and Mirsky, 2005). The majority of SCs are mSCs and nmSCs, which reside within peripheral nerve trunks, where they ensheath axons (Figure 1.1B).

mSCs ensheath and myelinate larger diameter axons (>1μm) in a 1:1 ratio (Taveggia et al., 2005). This is distinct from oligodendrocytes in the CNS, which are the comparable cell type to mSCs, that generally myelinate several axons (Bercury and Macklin, 2015; Nave and Werner, 2014). mSCs form a compact myelin sheath, which is composed of layers of SC membrane, that provides electrical insulation to the axons and allows rapid, saltatory conduction of action potentials over long distances.

In contrast, nmSCs individually ensheath several small calibre axons forming a structure known as a Remak bundle and these nmSCs appear to metabolically support the small calibre axons in order to maintain axonal integrity (Viader et al., 2011). Compared to mSCs, nmSCs are much less studied due to the lack of specific mouse models, as lineage specific

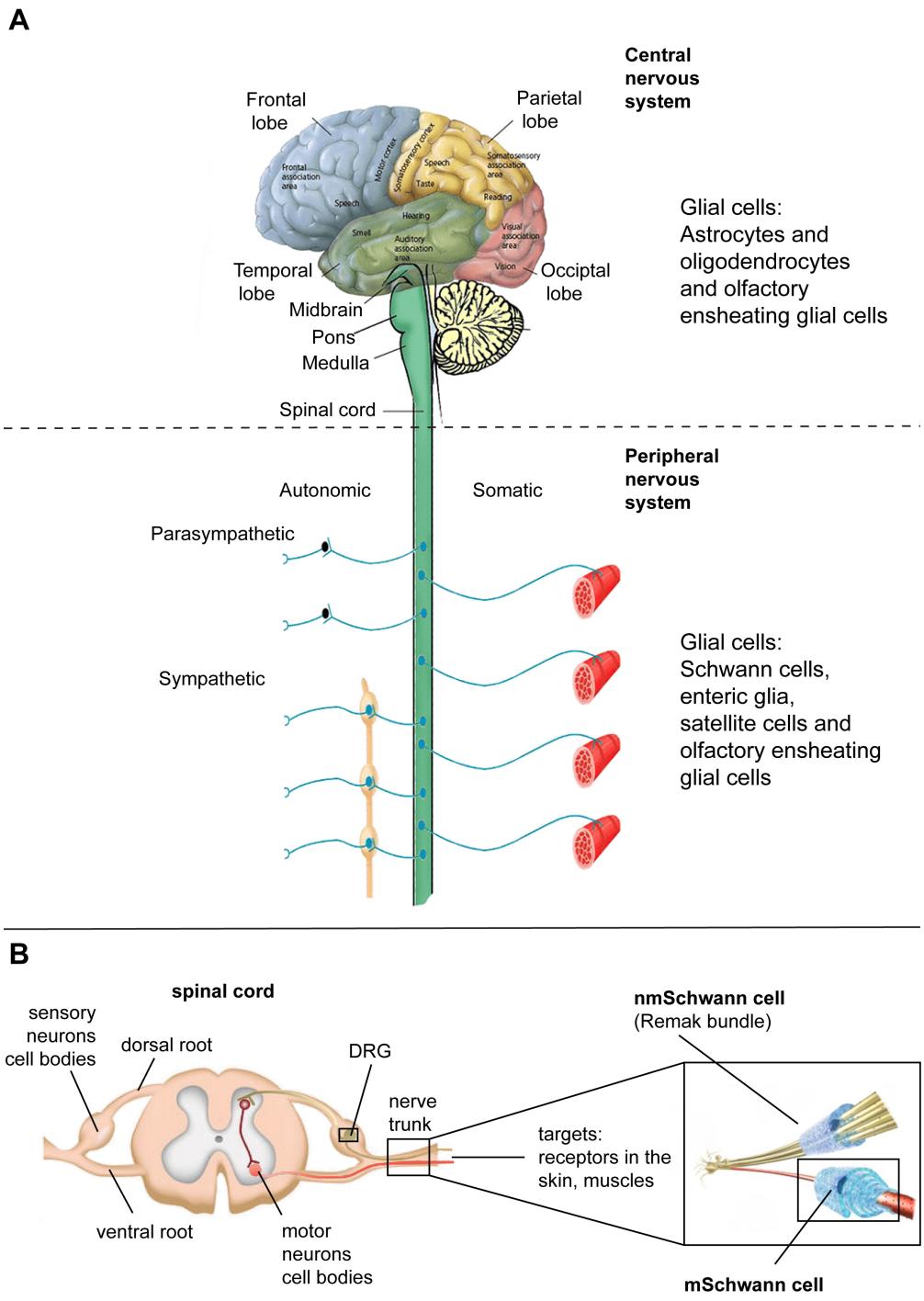

Figure 1.1. The nervous system and its glial cells

A) The nervous system consists of the central nervous system and the peripheral nervous system. Peripheral nerves consist of sensory, motor and autonomic nerves that connect tissues and organs to the central nervous system and transmit signals back and forth from tissues and organs to the CNS. **B)** Schematic representation of the spinal cord from which peripheral nerves emanate. The cell bodies of sensory neurons reside in the dorsal root ganglion (DRG) within the PNS, in contrast motor neuron cell bodies remain in the CNS. Spinal peripheral nerves are mixed nerves consisting of motor neurons that emanate from the ventral roots and sensory neurons that emanate from the dorsal roots. The main peripheral nerve glial cells (nmSCs and mSCs) that reside within peripheral nerve trunks are depicted within this box. Figure is adapted from AP biology, 2015 retrieved from http://carignanapbio.weebly.com/nervous-system1.html

drivers have not been identified (Harty and Monk, 2017; Jessen and Mirsky, 2005; Jessen et al., 2015).

Perisynaptic SCs (tScs) cover the axon terminal at the skeletal neuromuscular junction (NMJ) and have active roles in the formation, function, maintenance and repair of the NMJ (Barik et al., 2016; Feng and Ko, 2008; Kang et al., 2014; Ko and Robitaille, 2015; Smith et al., 2013). Each perisynaptic SC is associated with more than one synaptic site at the NMJ, and these specialised SCs provide a substrate for the regrowing axons to re-enter the former synaptic sites following nerve injury (Kang and Lichtman, 2013; Kang et al., 2014).

Less common than SCs are the enteric glia of the enteric nervous system that reside in the intestinal wall (Grubisic and Gulbransen, 2017), where they maintain the intestinal barrier (Savidge et al., 2007) and support enteric neuron function and survival (Coelho-Aguiar Jde et al., 2015; Ruhl, 2005). Ablation of enteric glia cells in the gut leads to increased permeability of the intestinal epithelia and loss of enteric neurons, demonstrating the critical role of enteric glia in maintaining intestinal homeostasis (Bush et al., 1998; Coelho-Aguiar Jde et al., 2015).

Satellite cells ensheath neuronal cell bodies in the sensory ganglia, (Ohara et al., 2009) (Figure 1.1A) control the neuronal environment within the ganglia and their close interactions with the neurons appears to regulate neuronal activity (Hanani, 2012; Suadicani et al., 2010; Takeda et al., 2009). Recent studies suggested a role for satellite cells in gastrointestinal pain by promoting the excitability of DRG neurons that innervate the colon (Hanani, 2012; Ji et al., 2013).

Olfactory ensheathing glial cells are found associated with non-myelinated axons both within the CNS and PNS (Barraud et al., 2010; Ramon-Cueto and Avila, 1998). These glial cells have been shown to be phagocytic (Nazareth et al., 2015; Panni et al., 2013) and play an instrumental role in the constant regeneration of the olfactory system (Chehrehasa et al., 2012).

1.1.1. Schwann cell development

The different stages of SC development have been intensively studied and have been shown to strongly depend on axonal signals. Three transient cell populations have been identified

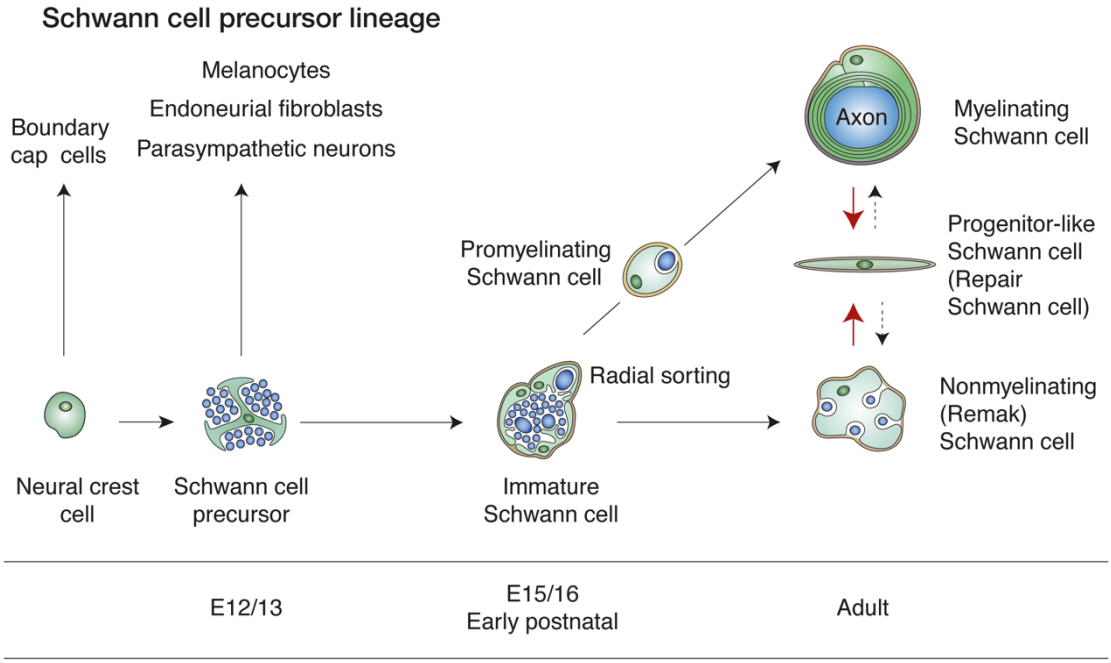

Figure 1.2. The different stages of Schwann cell lineage development
Peripheral glial cells originate from neural crest cells, which progressively differentiate to produce SCPs (Zurkirchen and Sommer, 2017). SCPs are the second transient SC precursor cell population and are tightly associated with axons. SCPs can also give rise to non- glial cells such as melanocytes (Adameyko et al., 2009), enteric neurons (Uesaka et al., 2015), endoneurial fibroblasts (Joseph et al., 2004) and parasympathetic neurons (Dyachuk et al., 2014; Espinosa-Medina et al., 2014). SCPs then differentiate into immature SCs, which undergo radial sorting. The process of radial sorting leads to the 1:1 association of large calibre axons with pro-myelinating SCs and the remaining small calibre axons are bundled together to form Remak bundles by nmSCs. Figure is adapted from (Jessen et al., 2015)

during embryonic SC development: the migrating neural crest cell population, Schwann cell precursor cells (SCPs) and immature SCs (Jessen and Mirsky, 2005; Jessen et al., 2015) (Figure 1.2). Molecular differentiation markers have been identified, which can be used to differentiate the transient cell populations throughout embryonic SC development (Jessen and Mirsky, 2005; Monk et al., 2015) such as the exclusive expression of glial fibrillary acidic protein (GFAP) by the immature SC population that allows characterisation of this transient SC population.

1.1.2. Neural crest cells

The neural crest forms at the border between the neural plate that will give rise to the central nervous system and the non-neuronal ectoderm, which will develop in the epidermis. Neural crest cells are located within the dorsal most regions of the neural tube, where they undergo an epithelial to mesenchymal transition into migratory neural crest cells, which delaminate from the neural tube around E8.5 in the mouse. Migrating neural crest progenitor cells can be classified according to the neural tube region from which they migrate and the region has been shown to determine their subsequent development (Bronner and Simoes-Costa, 2016; Smith M.M., 1993; Zurkirchen and Sommer, 2017).

The majority of neural crest cells are multipotent, with only a few neural crest cells found to be lineage restricted progenitors (Baggiolini et al., 2015). Neural crest cells migrate in two streams: The dorsolateral stream that gives rise to melanocytes and the ventral stream that gives rise mainly to dorsal root ganglia (DRG) neurons and SCs, but also to enteric neurons (Uesaka et al., 2015), satellite glial cells (Jessen and Mirsky, 2005), melanocytes (Adameyko et al., 2009), endoneurial fibroblasts (Joseph et al., 2004) and parasympathetic neurons (Dyachuk et al., 2014; Espinosa-Medina et al., 2014; Le Douarin and Teillet, 1974; Weston, 1963; Zurkirchen and Sommer, 2017).

Moreover, neural crest cells also give rise to boundary cap cells that are a secondary transient multipotent cell type that can differentiate into both neuronal and glial cells. These cells produce almost all SCs within the dorsal and ventral nerve roots and a substantial number of glial cells within the skin (Gresset et al., 2015). Boundary cap cells can be

identified in the mouse embryo around E10 by for example the expression of the transcription factor Krox-20 and transiently reside at the dorsal root entry zone and motor exit points of the embryonic spinal cord (Maro et al., 2004). The markers that identify boundary cap cells during early embryonic development, are also expressed by other cell types after E15.5, hence although boundary cap cells are thought to be a transient cell population, it remains to be shown whether some boundary cap cells persist into adulthood and provide a reservoir of multipotent neural cells in the PNS (Gresset et al., 2015; Hjerling-Leffler et al., 2005; Zujovic et al., 2011).

1.1.3. Transition from neural crest cells to Schwann cell precursor cells

Several factors have been shown to control neural crest differentiation, however these factors mainly act to suppress neuronal or glial cell development, whereas signals that solely drive glial cell lineage differentiation remain to be determined. Neuregulin 1 (NRG1) is known to be a major regulator of SC development, as ablation of NRG1 leads to an almost complete loss of SCs (Adlkofer and Lai, 2000; Esper et al., 2006; Garratt et al., 2000; Meyer and Birchmeier, 1995; Morrison et al., 1999). NRG1 is expressed by axons and binds to SCs via the ErbB3/ErbB2 receptors (Birchmeier and Bennett, 2016; Newbern and Birchmeier, 2010). Migrating neural crest cells also express ErbB3/B2 (Meyer and Birchmeier, 1995) and ablation of NRG1, ErbB2 and ErbB3 severely decreased their number (Britsch et al., 2001; Meyer et al., 1997; Morrison et al., 1999; Riethmacher et al., 1997; Woldeyesus et al., 1999). In addition to the prominent role of NRG1 at later stages of SC development that is discussed in more detail below, it was also shown to be involved in neural crest cell specification as it suppresses neurogenesis and thereby increases gliogenesis (Riethmacher et al., 1997; Shah et al., 1994).

The transcription factor SRY-related HMG-box 10 (Sox-10) a factor required for SC identity (Bremer et al., 2011; Finzsch et al., 2010), seems to be expressed by all migrating neural crest cells (Britsch et al., 2001; Paratore et al., 2001) and is required for the generation of SCPs by inhibiting neurogenesis (Kuhlbrodt et al., 1998). However, neither Sox-10 nor NRG1 is sufficient to drive glial cell differentiation, but appears to require cooperating factors such as

Notch-1 and Pax3. Similarly to NRG1 and Sox10, Notch1 supresses neurogenesis but is only transiently upregulated upon glial cell differentiation in neural crest cells (Morrison et al., 2000; Wakamatsu et al., 2000). Furthermore, neural crest cells express the transcription factor Pax3 that was recently shown to be essential for neural crest cell differentiation by sustaining Sox10 expression and initiating the transcription of SC lineage genes (Jacob et al., 2014).

1.1.4. Schwann cell precursor cells (SCPs)

Neural crest cells give rise to Schwann cell precursors (SCPs) around E12/E13 in mouse (E14/E15 in rat) and the NRG1/ErbB2/B3 signalling pathway is critical for SCP differentiation as homozygous ErbB3 mutant mice lack SCPs and exhibit severe degeneration of peripheral nerves (Figure 1.2) (Riethmacher et al., 1997). Similarly to neural crest cells, SCPs are migratory and proliferative but are distinguishable from neural crest cells by the expression of differentiation markers such as myelin protein zero (P0) and desert hedgehog (Dhh). Moreover, these cells are tightly associated with axons and their survival depends on axonal neuregulin 1 type III signalling (Dong et al., 1995; Dong et al., 1999; Meier et al., 1999). Moreover, neuronal survival is highly dependent on SC signals emphasising the interdependence of glial-axonal signalling.

SCPs further differentiate into immature SCs at around E15/16 in the mouse (E17/18 in rat) (Jessen et al., 1994), but they can also give rise to melanocytes, which migrate out from the developing nerve into the skin and this transition is known to involve the transcription factor FoxD3, which is downregulated upon melanocyte development (Adameyko et al., 2009; Nitzan et al., 2013). Moreover, SCPs also give rise to endoneurial fibroblasts (Joseph et al., 2004), enteric neurons (Uesaka et al., 2015) and parasympathetic neurons (Dyachuk et al., 2014; Espinosa-Medina et al., 2014) (Figure 1.2).

1.1.5. Immature Schwann cells

The transition from SCP cells into immature SCs is not understood completely, however Notch1, which upregulates ErbB3 receptor expression in SCP cells is thought to be essential,

as loss of Notch 1 decreased SCP proliferation and prevented immature SC formation (Woodhoo et al., 2009). Importantly, SCP differentiation to immature SCs is a cell intrinsic process that occurs even when SCPs are cultured without neurons *in vitro* (Jessen and Mirsky, 1991; Jessen et al., 1990). Furthermore, this transition appears to be irreversible and involves extensive changes in gene expression such as elevated expression of the pan SC marker S100 in immature SCs (Jessen et al., 1994).

In contrast to SCPs, which require axonal signals such as NRG1 for their survival and proliferation (Dong et al., 1995), immature SCs maintain their own survival by secreting autocrine signals (Monk et al., 2015). These autocrine secreted signals include insulin growth factor 2 (IGF2), leukemia inhibitory factor, platelet derived growth factor (PDGF) and neurotrophin3 (NT3) (Dowsing et al., 1999; Meier et al., 1999). In adulthood, following an injury and prior to axonal regrowth SC survival likely depends on these autocrine signals and thus may be important in ensuring SC survival while axons regrow.

Immature SCs surround groups of axons forming a so called axon-Schwann cell unit, which is covered by basal lamina and further enclosed by extracellular matrix (ECM) (Webster et al., 1973). From this unit, radial sorting takes place around E19/20 and proceeds until postnatal day P10 in rodent nerves (Figure 1.3) (Feltri et al., 2016). This process sorts the axons according to their size and is strongly dependent on axonal neuregulin1 type III signalling, which determines the ensheathment fate of the axons. Large diameter axons express higher levels of neuregulin1 type III and consequently will become myelinated during development (Taveggia et al., 2005). Axon-SC units usually consist of about 3-8 immature SCs, which surround axons of mixed calibre. Immature SCs insert cytoplasmic processes into the axonal bundles to select and segregate the larger diameter axons to the periphery of the axon-SC unit. Due to the extensive proliferation of the immature SCs and further segregation of the axonal bundles, the large diameter axons are able to establish a 1:1 relationship with a (pro-myelinating) Schwann cell, which forms its own basal lamina around this axon-SC unit resulting in its defasciculation from the immature axon-SC structure. The pro-myelinating SCl will further develop into a mSC and establish its characteristic myelin sheath around the large calibre axon. Within the immature Schwann cell-axon structure, SC proliferation and axonal

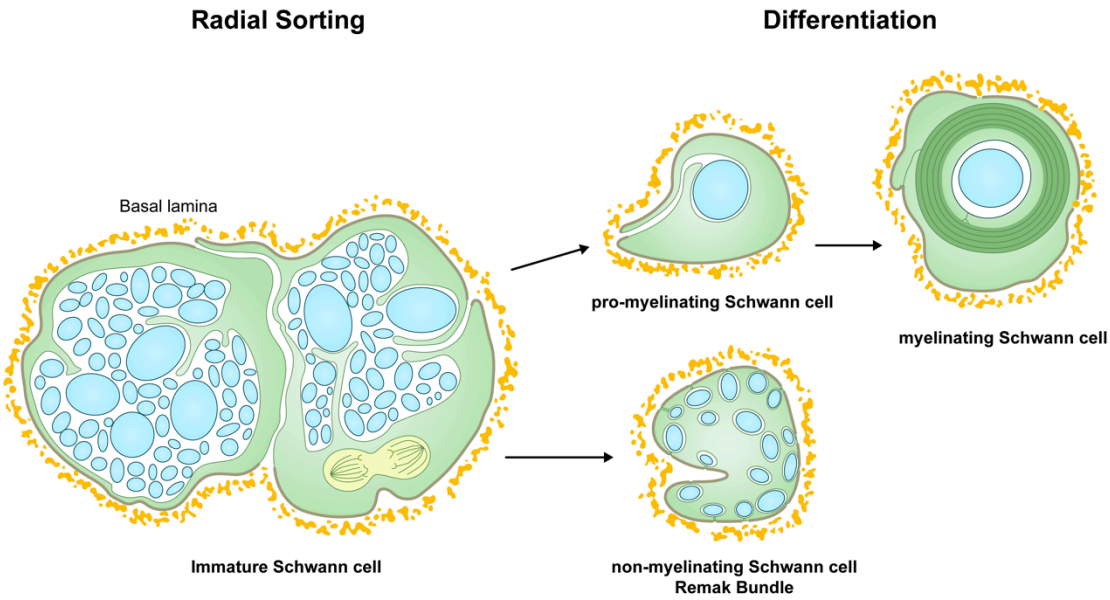

Figure 1.3. Radial sorting

Immature SCs undergo a process called radial sorting. Initially, an axon-SC unit is formed, which consists of several immature SCs and mixed calibre axons that are surrounded by a common basal lamina. The immature SCs insert cytoplasmic processes into axonal bundles, which recognise large calibre axons and segregate them to the periphery of the axon-SC unit. A 1:1 relationship between a pro-myelinating SC and a large calibre axon is established and this large calibre axon will become myelinated after deposition of the (pro-myelinating) SC basal lamina. Due to subsequent SC proliferation and large calibre axon segregation, the remaining axon bundles become smaller and will become Remak bundles. Figure is adapted from (Feltri et al., 2016).

segregation continues until it solely contains small calibre axons, which subsequently become Remak bundles (Feltri et al., 2016; Jessen and Mirsky, 2005; Jessen et al., 2015).

SC differentiation into both nmSCs and mSC is dependent on cell cycle exit, which is controlled by several molecular mechanisms such as Jun activation domain-binding protein (Jab1) that regulates the expression levels of cyclin kinase inhibitor 1b (p27) (Li et al., 2011; Porrello et al., 2014; Stevens and Fields, 2002). Furthermore, SC cell cycle exit is also controlled by cyclic adenosine monophosphate (cAMP) levels (Morgan et al., 1991; Stevens and Fields, 2002).

Immature SCs also control the developing architecture of the nerve by secreting signals that promote the formation of connective tissue sheaths that form around the nerve fibers. Moreover, signals from immature SCs promote arteriogenesis within the developing nerve (Mukouyama et al., 2005; Parmantier et al., 1999). Subsequently, the developing nerve will undergo further organisation steps such as the establishment of the perineurial sheath that surrounds mature nerves, in order to give rise to a mature functional peripheral nerve (Figure 1.4). Adult peripheral nerves consist of groups of axons that are ensheathed by SCs (mSCs or nmSCs) and these axon-SC bundles are embedded in a collagen-rich, vascularised ECM, termed as endoneurium (Zochodne, 2008) (Figure 1.4). Several other cell types reside within the peripheral nerve such as resident macrophages and endoneurial fibroblasts. The endoneurium is enclosed by specialised fibroblasts that form the perineurial sheath and this unit is defined as a nerve fascicle. Larger peripheral nerves contain several fascicles that are surrounded by a common epineurium.

1.1.6. Non-myelinating Schwann cells (nmSCs)

The benefits of myelination decrease with reduced axonal diameter and according to biophysical calculations no velocity advantage is obtained with axons < 1µm in diameter. Three quarters of mature axons are at or below this size and are not myelinated in the human PNS (Ochoa and Mair, 1969). Most of these axons are fully ensheathed by non-myelinating Schwann cells (nmSCs) that ensheath several small calibre axons to form Remak SC structures, except for some sensory nerves called C-fibers, which have free nerve endings

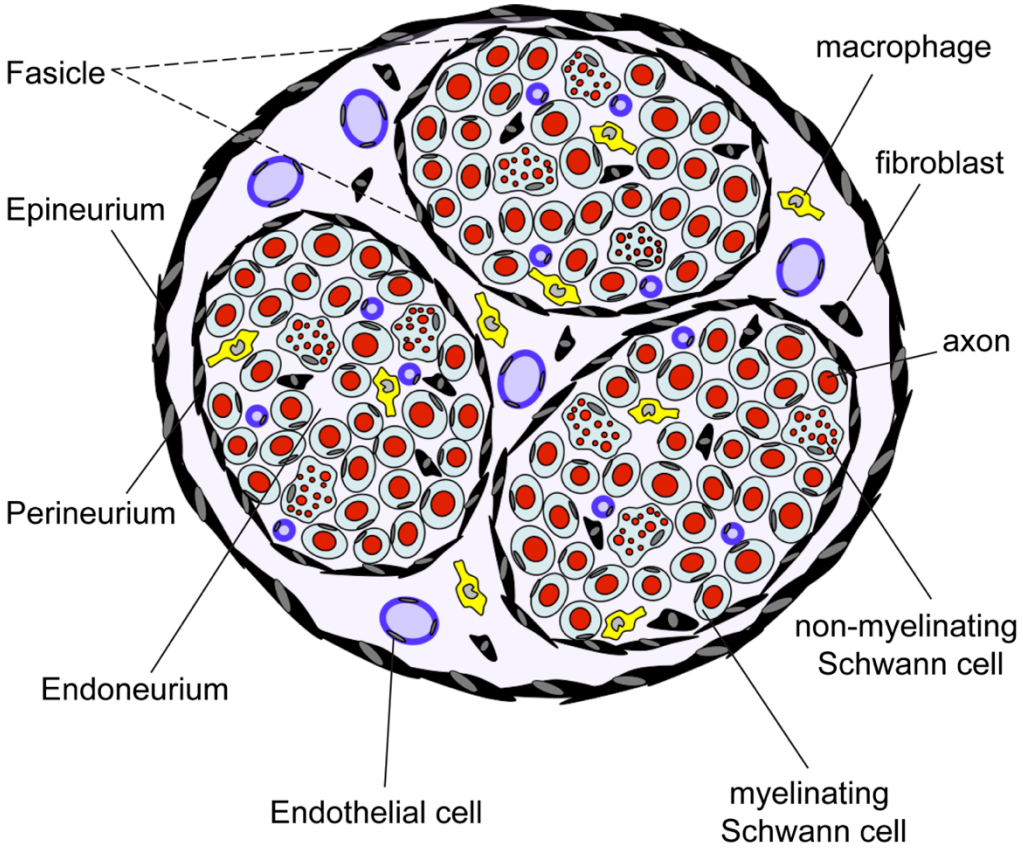

Figure 1.4. Structure of the peripheral nerve

The peripheral nerve is composed of bundles of nerve fibers enclosed by connective tissue sheaths. Small calibre axons are surrounded by the cytoplasm of nmSCs and form a structure termed Remak bundle. Axons with a larger diameter are wrapped by mSCs in a 1:1 ratio that form a myelin sheath around these axons. These axon-SC units are surrounded by the endoneurium composed of connective tissue and enclosed within a perineurial sheath. This entity is called a nerve fascicle. Nerve fascicles are bound together by fibrous tissue known as epineurium. The nerve endoneurium also contains other cell types such as tissue fibroblasts and macrophages and is well vascularised with the presence of numerous blood vessels.

that are not associated with SCs, within the epidermis (Hsieh et al., 1994). Furthermore, at the neuromuscular junction, non-myelinating terminal SCs (tSCs) cover the axonal surface but do not surround the axons in the region, where the synaptic “gutters” or regions with a high concentration of acetylcholine receptors are located (Griffin and Thompson, 2008; Lee et al., 2017).

Both adult SC types, mSCs and nmSCs, express many of the same markers such as cytoplasmic S100 that is known as a pan SC marker. However, nmSCs lack myelin protein expression but do maintain the expression of cell adhesion molecules and cell surface receptors, which are downregulated in mSCs, such as the cell adhesion molecule L1, neural cell adhesion molecule (NCAM) and the neurotrophin receptor p75 (Jessen and Mirsky, 2002).

In contrast to mSCs, the function of nmSCs is poorly understood mostly due to a lack of mouse models as nmSC lineage specific drivers have not been identified. However, recent studies reported that nmSCs metabolically support small calibre axons and SC mitochondrial function was shown to be critical for this process (Beirowski et al., 2014; Viader et al., 2011; Viader et al., 2013). Consistent with this SC-specific mitochondrial dysfunction resulted into progressive axonal degeneration, particularly in small unmyelinated axons, indicating that the metabolic support of axons by nmSCs is critical for long term axon maintenance.

Up until now, the signals that drive nmSCs generation are yet to be identified, however a recent study reported that mice with a targeted ablation of laminin at the immature SC stage lack nmSCs, suggesting that basal lamina deposition is required for the successful generation of nmSCs (Yu et al., 2009). Nevertheless, it remains to be shown if these effects are due to a direct defect in nmSC differentiation or merely due to an abnormal radial sorting process. Furthermore, abnormal numbers of axons per Remak bundle were observed in NRGI Type III deficient nerves indicating that NRGI may, in addition to regulating mSC development, also be required for the proper function of nmSCs (Fricker 2009, Taveggia 2005). In line with this, disruption of ErbB signalling in adult nmSCs results in a progressive sensory neuropathy with the loss of numerous unmyelinated C-fibers axons indicating that nmSCs are critical for the survival of these axons (Chen et al., 2003).

As described above, SC differentiation into nmSC and mSCs requires exit of the cell cycle, however it was postulated that nmSCs provide a reservoir of potentially mitotic glial cells within the adult peripheral nerve, as although associated with small calibre axons, nmSC were reported to undergo mitosis in the adult nerve (Murinson et al., 2005).

1.1.7. Myelinating Schwann cells (mSCs)

Large calibre axons (> 1um) require myelination to increase membrane capacitance in order to allow the propagation of action potentials without decreasing conduction. To allow the rapid propagation of action potentials, myelinated axons use a process called saltatory conduction that transports the action potential along myelinated axons from one unmyelinated axon region (Node of Ranvier) to the other (Salzer, 2015). As the axon is isolated from the extracellular milieu by the myelin sheath and far from the nucleus, mSCs likely nurture the axons. This process is thought to involve the non-compact myelin that transports metabolites from the glial cytoplasm close to the periaxonal space (Nave and Werner, 2014).

The signals that drive axonal myelination and that determine mSC fate are well characterised and involve complex morphological and genetic changes. These changes involve the downregulation of several genes such as the neurotrophin receptor p75, whereas upregulation of genes known to be involved in the regulation of SC myelination and formation of the myelin sheath such as the transcription factor Krox-20, myelin protein zero (PO), myelin associated glycoprotein (MAG) and myelin basic protein (MBP) and periaxin (Jessen and Mirsky, 2002). The changes are regulated by complex signals, which are discussed below, that cause SCs to adopt a mSC fate (Chernousov et al., 2008; Salzer, 2012).

1.1.8 Molecular signals mediate the myelination programme

Myelination involves complex extracellular signals that need to be properly coordinated in order to drive the initial phase of myelination. In turn, these extracellular signals activate intracellular signalling pathways that transmit signals via downstream effectors. Ultimately, this results in the initiation of a sequential feed forward cascade of pro-myelinating

transcription factors that induces the transcription of genes required for myelination. The different levels of myelination regulation are discussed separately in the subchapters below.

1.1.8.1. Transcriptional control of mSC differentiation

The transition of immature pro-myelinating SCs to a mSC cell fate involves the upregulation of pro-myelinating transcription factors, which initiate a complex genetic program regulating this process (Pereira et al., 2012; Salzer, 2015; Svaren and Meijer, 2008). This genetic program involves the regulated balance between negative and positive regulators of myelination and the proper coordination of these two opposing transcriptional programmes mediates the onset and termination of myelination during development (Figure 1.5).

The positive regulators of myelination consist of the transcription factors Krox-20, octamer binding transcription factor-6 (Oct-6), Sox-10 and Brn-2 and the interplay of these positive regulators drive the transition from a pro-myelinating into a mSC. (Svaren and Meijer, 2008) (Figure 1.5). At the onset of myelination, Krox-20 is activated by a feed-forward loop, in which Sox10 induces Oct6 expression and Oct6 and Sox10 synergistically induce the expression of Krox-20 in mSCs (Jagalur et al., 2011; Svaren and Meijer, 2008). Krox-20 is considered a master regulator of PNS myelination, as it is sufficient to induce the transcription of myelin genes such as P0, MAG, PMP22, MBP and connexin32 (Cx32) and of biosynthetic components of myelin lipid synthesis, even when expressed in non-SC cell types such as fibroblasts (Parkinson et al., 2004). Several of the Krox-20 regulated genes such as PO, MBP and Cx32 also have binding sites for Sox10 in their enhancer region, demonstrating a synergistic regulation of these genes by these two transcription factors (Lopez-Anido et al., 2015; Srinivasan et al., 2012; Svaren and Meijer, 2008). The loss of Krox-20 causes SC differentiation at the pro-myelinating stage and consequently results in the complete loss of myelin formation (Topilko et al., 1994), whereas the loss of Sox-10, that is expressed at high levels at all stages of SC development, leads to the complete loss of peripheral glial cells (Britsch et al., 2001; Schreiner et al., 2007). In contrast, the loss of Oct-6 does not prevent peripheral glial cell differentiation but transiently stalls SC development at the pro-myelinating stage and ultimately leads to a delayed onset of myelination, hypomyelinated nerves and the

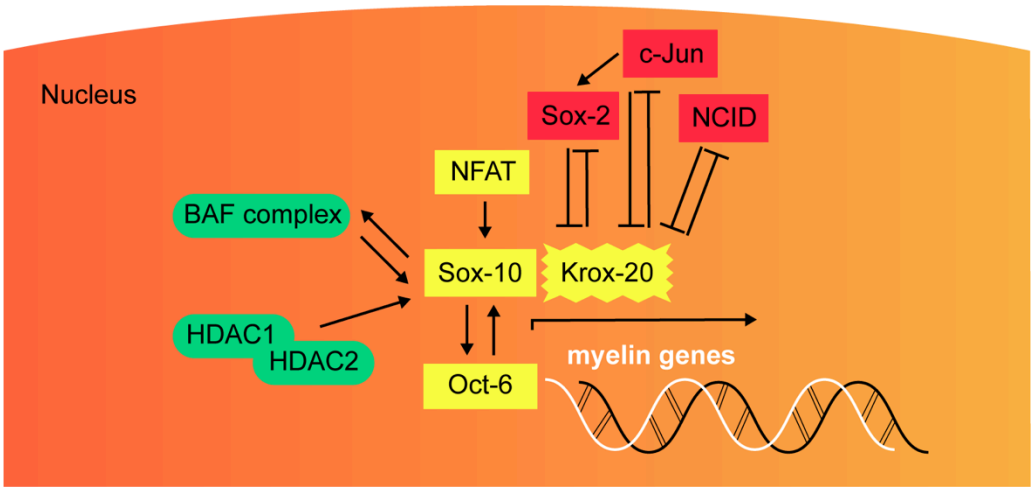

Figure 1.5. Transcriptional programme that initiates Schwann cell myelination
A simplified transcriptional network controlling SC myelination is depicted in this scheme. Positive and negative regulators of SC myelination regulate the initiation of the transcriptional programme. The positive regulators (eg. Krox-20, Oct-6 and Sox-10) are depicted in yellow and the negative regulators (eg. c-Jun, Sox-2 and Notch intracellular domain (NCID) are depicted in red. The epigenetic regulators such as BAF complex and HDAC1 and HDAC2 are displayed in green.

continuous existence of pro-myelinating SCs into adulthood (Bermingham et al., 1996; Jaegle et al., 2003).

In addition to its role during SC development, the continuous expression of Krox-20 in adult mSCs is essential for myelin maintenance, as its loss is associated with SC dedifferentiation and myelin sheath degeneration, which results in a progressive demyelination phenotype (Decker et al., 2006). Similarly to Krox-20, Sox-10 is not only required for SC development but also for the maintenance of mSCs, as its loss in adult SCs also results in demyelination and subsequent axonal degeneration (Bremer et al., 2011). In contrast to the continued expression of Sox-10 and Krox-20 in adult mSCs, Oct-6 is only highly expressed during the transition of pro-myelinating SCs to mSCs, then after ~p14 Oct-6 expression is downregulated indicating that the timely control of Oct-6 expression may be important for myelination (Arroyo et al., 1998; Feltri et al., 2016).

In addition to Krox-20, Sox-10 and Oct-6, the transcription factor NF-κβ was shown to positively regulate myelination *in vitro* (Nickols et al., 2003) but decreased activity of NF-κβ only transiently reduced myelin gene expression and did not prevent myelination *in vivo,* suggesting NF-κβ is dispensable for myelination *in vivo* (Morton et al., 2013).

Known negative regulators of myelination include the transcription factors Notch, c-Jun and Sox2 that are expressed during early SC development, whereas their expression needs to be downregulated by Krox-20 dependent signalling at the onset of myelination (Feltri et al., 2016; Jessen and Mirsky, 2002, 2008; Parkinson et al., 2004; Pereira et al., 2012; Roberts et al., 2017; Salzer, 2015; Woodhoo et al., 2009). Consistent with this, both c-Jun and Sox2 suppress the activity of Krox-20 demonstrating the cross-inhibitory effect of these two transcription factors (Jessen et al., 2015; Parkinson et al., 2008).

The most studied of these negative regulators is c-Jun, which is known to prevent SC myelination and drives the dedifferentiation of pro-myelinating SCs to immature SCs (Parkinson et al., 2008; Parkinson et al., 2004). In addition to c-Jun, Sox-2, which is well known for its role in the maintenance of stem and progenitor cell populations, was identified as a negative regulator of SC myelination in vitro and in vivo (Le et al., 2005; Roberts et al., 2017) (Figure 1.5). In agreement with the role of Sox-2 in maintaining stem cells, it was

shown to prevent SC myelination and maintains SCs in a non-differentiated state (Roberts et al., 2017). Similarly to the role of c-Jun and Sox-2 in SC development, the re-expression of c-Jun promotes SC dedifferentiation and the sustained expression of c-Jun and Sox-2 decreases SC myelination following nerve injury (Fazal et al., 2017; Roberts et al., 2017). Moreover, Notch signalling also negatively regulates SC myelination and was shown to promote demyelination following nerve injury (Woodhoo et al., 2009).

Recently, epigenetic regulators have been demonstrated to be critical for successful myelination (Figure 1.5). The regulation of PNS myelination involves epigenetic modifiers such as the Braham associated factor (BAF) complex, which is a chromatin remodelling complex that regulates access to DNA. The BAF complex interacts with Sox-10 and this interaction was shown to direct the recruitment of BAF complexes to Sox-10 target genes such as Oct-6 and Krox-20 which ultimately results in their enhanced expression (Weider et al., 2013).

In addition to the BAF complex, histone deacetylases (HDACs), which are major epigenetic regulators, have been shown to be critical for SC myelination (Jacob et al., 2011b). HDAC1 and HDAC2 positively regulate Sox10 expression. Moreover, Sox10 recruits both HDAC 1/2 to regulatory regions of Krox-20 and Sox10 loci at which HDAC2 in synergy with Sox10 initiates the myelination transcription program. HDAC1 is dispensable for the transcriptional initiation of myelination, but it controls SC survival by regulating the levels of β-catenin. Although HDAC1 and HDAC2 perform distinct functions, the loss of either is compensated for by the other and consequently, only the loss of both blocks SC differentiation at the immature or the pro-myelinating SC stage (Jacob et al., 2011a). In addition to the role of HDAC1 and HDAC2 in regulating the myelination transcriptional programme, a recent study from our lab has identified HDAC3 as a positive regulator of myelination that is critical for myelin maintenance in adulthood. In contrast to HDAC1/2, HDAC3 is dispensable for myelin formation during development, however it is required for the transition to the homeostatic state, which is associated with the downregulation of myelin gene transcription. Consequently, SCs that have lost HDAC3 failed to exit the biogenic state and maintain high

levels of myelin transcription, which resulted in a progressive neuropathy in adulthood that is associated with severe myelination defects (Rosenberg, Cattin et al, Manuscript submitted). Similar to our study, He et al also investigated the role of HDAC3 in SC myelination and showed that the loss of HDAC3 in SCs both during development and after injury resulted in increased myelination (He et al., 2018). However, they have interpreted their data differently to us, in that they proposed that HDAC3 acts as a negative regulator of myelin transcription. Together, these studies imply a crucial role of epigenetic regulators in SC differentiation and myelination but the exact mechanisms of action are not yet well understood and further studies are required.

1.1.8.2. Extracellular signals that regulate myelination

The intracellular signalling pathways and the transcriptional programme that drive SC myelination are activated by extracellular molecular mediators such as the axonal signal NRG1. In addition to axonal derived mediators, extracellular and basal lamina mediators initiate myelination, either independently or in cooperation with the axonal signal NRG1. All these different classes of extracellular mediators are outlined in this Subchapter: 1. Mediators that establish the initial contact between SCs and axons. 2. Axonal signals. 3. Basal lamina mediators.

1. After the initial contact of SCs with axons, SCs extend processes to associate with axons and the adhesion molecule N-cadherin that is highly expressed at the SC-axon interface was thought to mediate the contact between axons and SCs (Wanner and Wood, 2002) (Figure 1.6). In line with this, the loss of N-cadherin prevents SC process extension and alignment with axons in *in vitro* co-culture systems. However, N-cadherin loss in SCs *in vivo* only causes a minor delay in myelination and does not cause defects in myelin sheath formation (Lewallen et al., 2011). These studies suggest that N-cadherin may be involved in controlling the time of myelin initiation but is dispensable for the formation and maturation of the myelin sheath. Moreover, another adhesion molecule, Nectin-like protein-4 (Necl-4), which is expressed by SCs and binds to the axonal receptor Necl1 was shown to be involved in establishing initial axo-glial interactions (Maurel et al., 2007; Spiegel et al., 2007) (Figure 1.6). The disruption of

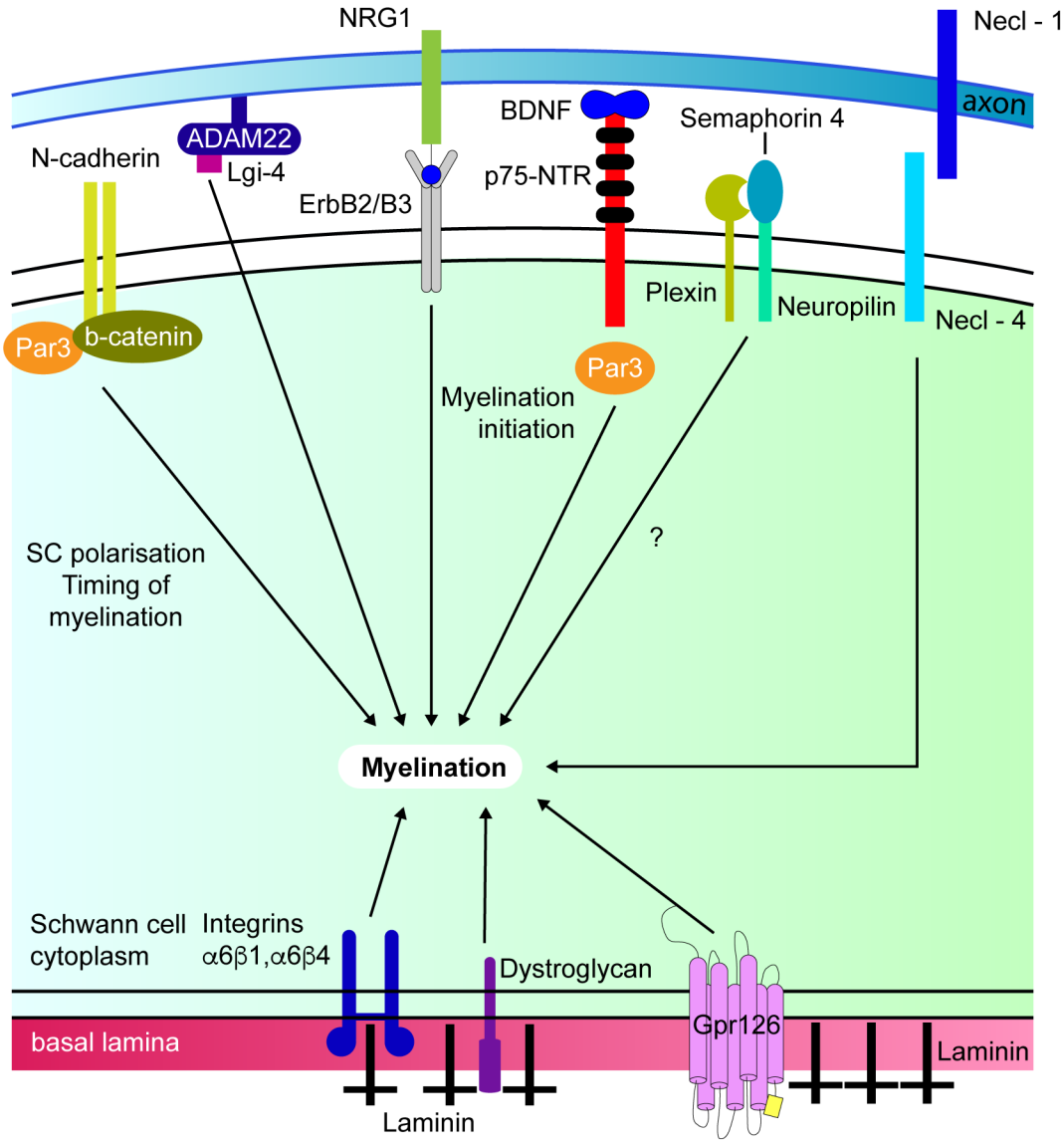

Figure 1.6. Extracellular signals that regulate Schwann cell myelination
The scheme depicts the major extracellular signals that control initiation of myelination. N-cadherin mediates axon-SC interactions and regulates the timing of myelination and probably also contributes to SC polarisation. In addition to N-cadherin, another adhesion molecule Necl-4 that binds to axonal Necl-1 contributes to the initiation of myelination. The polarised localisation of Par3 at the axo-glial site of contact is required for myelination initiation. Importantly, the interaction between axonal NRG1 and ErbB2/B3 expressed by SCs is involved in many aspects of SC development, including myelination. ErbB2/B3 signalling was shown to regulate both myelination initiation and myelin sheath thickness. The basal lamina protein laminin binds to integrins, dystroglycans and Gpr126 to promote SC myelination. For simplification, the SC nucleus is not depicted.

this SC-axon interaction was shown to inhibit myelination initiation demonstrating that adhesion molecules are key players that mediate SC-axon interactions. However, the relevance of Necl4 for axonal myelination *in vivo* is disputable, as the loss of Necl4 did not cause any defect in PNS myelination but this may be due to the compensation of Necl4 function by another unknown adhesion molecule, (Zhu et al., 2013).

After SCs have established an initial contact with axons, subsequent myelination events occur due to the asymmetrical distribution of some proteins such as Partitioning defective-3 (Par-3) protein that is asymmetrically localised at the sites of contact of SCs and axons.

Strikingly, the disruption of this asymmetrical distribution by either knockdown or overexpression of Par3 inhibits myelination (Chan et al., 2006) (Figure 1.6). Although SC myelination is a highly polarised process, the mechanisms that initiate and regulate SC polarity are not well understood. To determine how the asymmetrical distribution of Par3 is regulated, studies investigated whether the homotypic interactions of N-cadherin at the site of axo-glial contact may be involved in this process. However, homotypic interactions of N-cadherin at the SC-axon sites of contact do not appear to play a significant role in the asymmetric localisation of Par3 (Lewallen et al., 2011). It may be that other adhesion molecules such as the nectin like proteins compensate the loss of N-cadherin but this remains to be shown. This demonstrates that although SC-axons interact with each other through adhesion molecules, successful myelination is a complex process, which requires the coordination of many signals.

2. Factors that mediate axon-glial interactions are key players throughout SC development and are instrumental for SC myelination. Amongst them, neuregulin-1 (NRG1), a member of the Neuregulin family of growth factors that share sequence similarities with epidermal growth factor (EGF), is the most well known. From the NRG1 gene at least 16 distinct gene products are produced by alternative splicing and the usage of different promoters with the membrane bound NRG1 Type III being the most abundant form on peripheral nerve axons (Falls et al 2003, Esper et al 2005). NRG1 acts as ligand for ErbB2/B3 heterodimer receptors that are expressed by SCs and it is well established that this signalling complex regulates many aspects of SC development such as the radial sorting of axons, as described above

(Birchmeier and Bennett, 2016; Birchmeier and Nave, 2008; Cohen et al., 1992; Jin et al., 1993). Furthermore, the conditional loss of NRG1 during late SC development leads to hypomyelination of peripheral nerves demonstrating that NRG1 is absolutely required for peripheral nerve myelination (Garratt et al., 2000). Subsequently, the role of NRG1-ErbB signalling in myelination was widely studied and was shown to regulate the initiation of myelination, axonal ensheathment fate and myelin sheath thickness (Figure 1.6). However, it is dispensable for myelin maintenance in the adult (Atanasoski et al., 2006).

In addition to NRG1, other axonal signals have been shown to control SC myelination such as brain derived neurotrophic factor (BDNF) which binds to the neurotrophin receptor p75 that is recruited by Par3 to the site of SC-axon contact (Chan et al., 2001; Cosgaya et al., 2002). Following BDNF binding, p75 and Par3 form a complex, which induces intracellular signalling that is instrumental for myelination. Consequently, BDNF depletion, disruption of the asymmetrical distribution of Par3 and the functional inactivation of p75 was shown to inhibit myelin sheath formation (Chan et al., 2006).

Besides neurotrophins and adhesion molecules, A disintegrin and metalloproteinase (ADAM) 22 has recently been discovered as a key axonal signal that promotes myelination. SCs secrete Lgi4 that binds to axonal Adam22 and this interaction leads through unknown mechanisms to the induction of Krox-20 and consequently is required for SCs to progress beyond the pro-myelinating SC state (Bermingham et al., 2006; Kegel et al., 2013) (Figure 1.6).

Moreover, secreted semaphorins act as axon guidance molecules during development and have also been shown to be involved in myelination. Semaphorins bind to a complex of neuropilin and plexin receptors that are expressed by SCs (Chen et al., 1997; Kolodkin et al., 1997; Takahashi et al., 1999) (Figure 1.6). Initially, semaphorin 3A and F were found to be highly expressed in transiently demyelinated plaques in multiple sclerosis mouse models indicating that they may play a role in remyelination in the CNS (Williams et al., 2007). Additionally, work from the Lloyd laboratory demonstrated that activation of the Ras/Raf/ERK signalling pathway in SCs results in the dissociation of SC-axon interactions and this was shown to be mediated by the Ras/Raf/ERK mediated downregulation of semaphorin 4F.

Restoring semaphorin 4F expression levels restablished axon-SC interactions demonstrating that its expression is required for proper association and alignment of SCs to axons. Consequently, semaphorin4F was identified as a mediator of SC-axon interactions implying potential roles for myelination and neurofibroma formation (Parrinello et al., 2008).

3. SCs secrete ECM components such as laminins and collagen, which are major components of the SC basal lamina and function as autocrine signals essential for axonal ensheathment and myelination. Several studies have shown recently that proper assembly of the basal lamina is required for myelination (Bunge et al., 1986; Chernousov et al., 2008). The main basal lamina mediator of SC myelination was identified as laminins, which are heterotrimeric proteins consisting of a α,β and γ chain that bind to SC integrin and dystroglycan receptors (Bunge et al., 1986). Initially, the role of laminins in SC myelination was observed in a mouse model of muscular dystrophy, which carried mutations in the laminin α2 gene and exhibits a defect in peripheral nerve myelination (Madrid et al., 1975). Furthermore, the SC-specific loss of laminin γ1, the most abundant chain, was shown cause peripheral neuropathy that is associated with impaired myelination (Chen and Strickland, 2003; Yu et al., 2005). Moreover, a more recent study demonstrated that reducing expression levels of laminin γ1 leads to an axonal sorting defect that is connected with hypomyelination (McKee et al., 2012).

Recently, a genetic screen in zebrafish identified the G-protein coupled receptor Gpr126 as an important mediator for SC myelination (Pogoda et al., 2006). Mechanistically, it was shown that the extracellular domain of Gpr126 undergoes autocleavage to produce a N-terminal fragment (NTF) and a C-terminal fragment (CTF) with the latter functioning as a tethered agonist that initiates Gpr126 signalling (Liebscher et al., 2014). Gpr126 was demonstrated to mediate SC-ECM interactions by binding via its NTF domain to the basal lamina ligand laminin 211 (Petersen et al., 2015). The binding to laminin 211 was shown to modulate the availability of the tethered CTF agonist with increased concentrations of laminin 211 activating downstream signalling and initiating myelination. This indicates that elevated levels of laminin 211 induce a conformational change in Gpr126 that leads to activation of its downstream

signalling and importantly this highlights that the proper establishment of the basal lamina is absolutely critical to induce myelination.

Gpr126 was shown to drive SC myelination via induction of cAMP signalling (Mogha et al., 2013; Monk et al., 2009; Monk et al., 2011) demonstrating that Gpr126 signalling regulates intracellular cAMP levels in SCs, which is further discussed in the subchapter below (Figure 1.6) (Mogha et al., 2013). Moreover, a recent study has shown that the loss of Gpr126 prevents remyelination after nerve crush, but whether this defect in remyelination is correlated to altered cAMP levels has not been studied yet (Mogha et al., 2016).

In addition to laminin 211, collagen type IV also binds to Gpr126 indicating that collagen type IV likely acts as a secondary ligand for Gpr126 (Paavola et al., 2014). The identification of the critical role of basal lamina assembly for myelination correlates with previous in vitro studies that showed abscorbic acid, which is a co-factor required for the post-translational modification and assembly of collagen IV, promotes SC myelination (Carey et al., 1986; Eldridge et al., 1987).

1.1.8.3. Intracellular signals that regulate myelination

Following the early events establishing the SC-axon interactions that are required for the initiation of axonal ensheathment, multiple pathways are activated by axonal, extracellular and basal lamina mediators, which ultimately drive myelin sheath formation. The activation of these multiple pathways leads to the initiation of a transcriptional program that promotes the final stages of myelination.

In earlier studies, it was shown *in vitro* that the addition of cAMP was sufficient to induce SC myelination (Glenn and Talbot, 2013; Lemke and Chao, 1988; Morgan et al., 1991; Shuman et al., 1988; Sobue and Pleasure, 1984; Sobue et al., 1986). These studies showed that cAMP promotes myelination by inducing myelin gene protein expression (Figure 1.7). Recent studies discussed in the subchapter above, demonstrated that Gpr126 is the long-sought receptor that regulates cAMP levels *in vivo* (Monk et al., 2009; Monk et al., 2011).

In addition to GPR126 signalling via cAMP, binding of axonal NRG1 type III to ErbB2/B3 receptors on SCs is also essential. The activation of this complex initiates complex

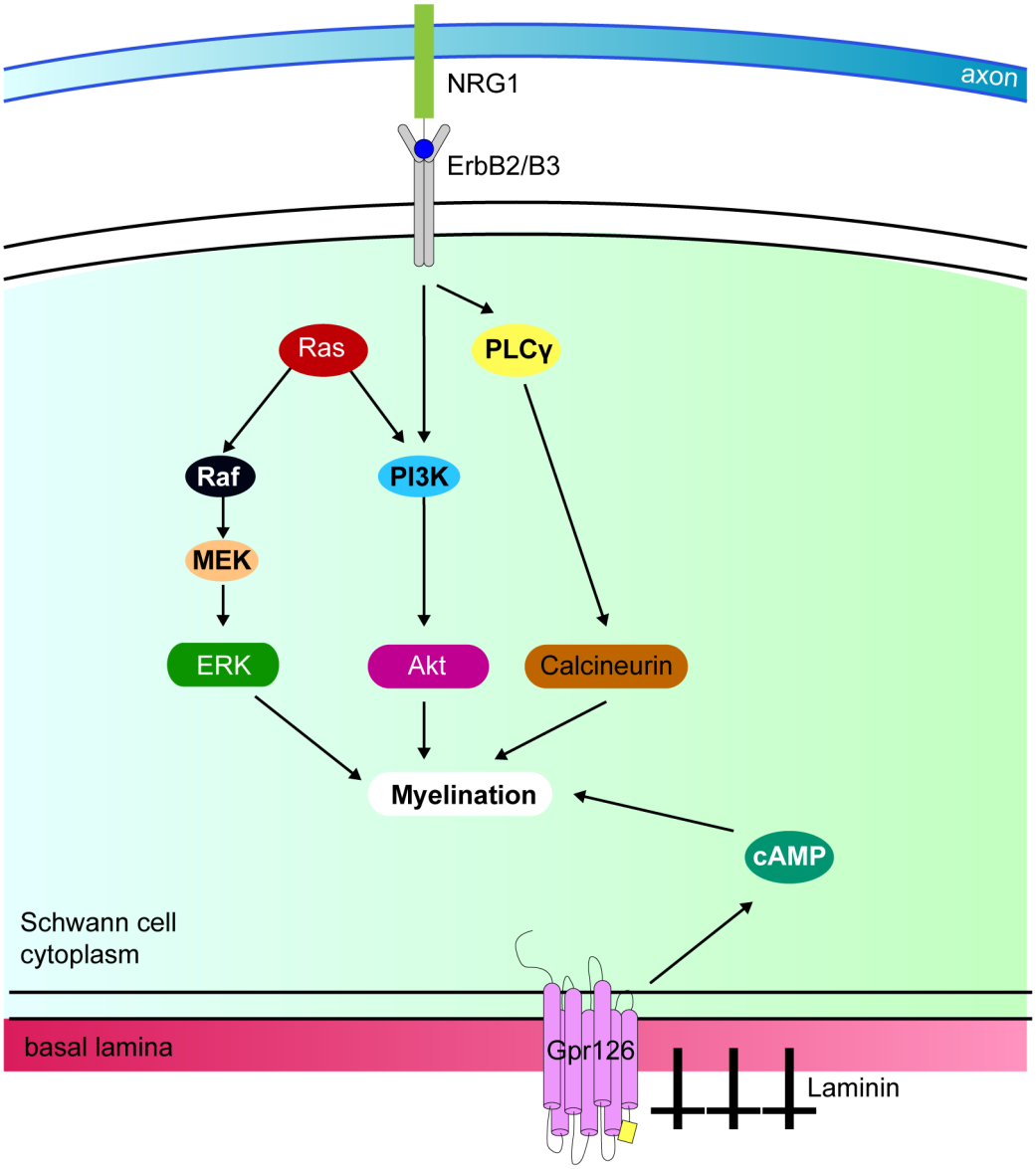

Figure 1.7. Intracellular signalling pathways that regulate Schwann cell myelination
The interplay between several signalling pathways regulates SC myelination. The activation of ERB2/B3 by NRG1 leads to the downstream activation of PI3K/AKT, MAPK and PLC-γ which all contribute to drive myelin sheath formation. The role of the PI3K/AKT signalling pathway has been studied in more detail and it was shown that the extent of PI3K activation correlates to NRG1 expression levels and determines the ensheathment fate of axons. Furthermore, in addition to ErbB2/B3 downstream signalling pathways, elevated levels of cAMP are essential for myelination initiation. The activation of these (and more) signalling pathways ultimately results into activation of the transcriptional programme that regulates SC myelination. For simplification in this scheme, the SC nucleus is not depicted.

downstream signalling pathways that are crucial for successful myelination. Among these signalling pathways are the phosphatidylinositol 3 kinase (PI3K/AKT), ERK and PLC-γ signalling pathways (Nave and Salzer, 2006; Newbern and Birchmeier, 2010; Pereira et al., 2012) (Figure 1.7).

The levels of axonal NRG1, as discussed above, were shown to be absolutely critical to determine the ensheathment fate of axons. Ensheathed axon express low levels of NRG1 type III, whereas myelinated axons high levels and the artificial expression of NRG1 type III was sufficient to induce myelination in axons, which are normally unmyelinated (Taveggia et al., 2005). Low and high levels of NRG1 type III expression was shown to correlate with the extent of PI3K activation demonstrating that PI3K activation is graded to the levels of NRG type III.

In line with this, the conditional deletion of PTEN, a negative regulator of the PI3K kinase pathway, results in aberrant activation of PI3K, which causes enhanced SC wrapping and hypermyelination (Goebbels et al., 2010). These defects in SC development were found to be mainly due to the extensive activation of AKT by PI3K and subsequent downstream signalling to mTOR. Consequently, the effects of loss of PTEN can be alleviated by treatment with the mTOR inhibitor rapamycin (Goebbels et al., 2012).

Moreover, NRG1 signalling activates the PLC-γ signalling pathway that leads to increased intracellular calcium and activation of the phosphatase calcineurin B. Activation of calcineurin B in turn results in dephosphorylation of the cytosolic nuclear factor of activated T-cells (NFAT) proteins, which accumulate within the SC nuclei and induce the transcription of myelin specific genes such as Krox-20 and myelin protein zero (PO) (Kao et al., 2009) (Figure 1.7).

In contrast to PI3K/AKT and PLC-γ, the ERK signalling pathway was shown to have a dual role in myelination. On the one hand, high levels of ERK signalling prevent myelin gene expression and consequently inhibit myelination as shown *in vitro* (Harrisingh et al., 2004; Ogata et al., 2004; Syed et al., 2010) and *in vivo* (Napoli et al., 2012). On the other hand, the ERK signalling pathway also positively promotes SC myelination, as severe hypomyelination was observed in the Dhh-Cre:Erk$^{-/-}$:Erk2$^{fl/fl}$ mouse model, in which ERK1 and ERK2 were ablated during SC development (Newbern et al., 2011). Moreover, moderate elevation of ERK

was shown to increase myelin thickness during SC development (Ishii et al., 2013; Sheean et al., 2014). These studies demonstrated that ERK activation is required for the initiation of myelination (Figure 1.7), but the expression levels of ERK have to be regulated as high levels of ERK prevent mSC differentiation. Recent studies showed that these opposing effects are regulated by the strength and duration of MAPK signalling with moderate levels of MAPK required for SC myelination whilst high levels of MAPK inhibit SC differentiation and induce demyelination in adulthood (Ishii et al., 2016; Napoli et al., 2012). Furthermore, other signalling pathways may interact with ERK signalling and may thereby influence its effect on myelination (Newbern et al., 2011).

1.1.9. Myelin structure and function

The myelin sheath results from the circumferential wrapping of the SC plasma membrane and consists of 40 or more lamellae that wrap around axons with a large diameter (≥1μm) (Peters, 1991). The organisation of the myelin membrane involves two biochemical and structurally different areas. These two areas are the compact myelin regions and the regions of non-compact myelin (Figure 1.8).

The structure of the myelin sheath is highly polarised both longitudinally from node to node and radially from the axon to the SC basal lamina (Pereira et al., 2012; Salzer, 2003) (Figure 1.8). The overall organisation of the SC into nodal, paranodal, juxtaparanodal and internodal compartments demonstrates its longitudinal polarity with the internode being the largest compartment, in which the membrane of the SC and axon are in close contact. Radial polarity is apparent by the distinct membrane surfaces present on opposite sides of the SC; the abaxonal (outer) and adaxonal (inner) membrane surfaces. The compacted membranes of the myelin sheath are localised between these two distinct membrane surfaces (Figure 1.8). The mSC adaxonal membrane is separated from the axonal membrane by the periaxonal space (~15nm), which contains adhesion molecules and receptors that mediate interactions with ligands on the axon (Salzer, 2003, 2015)

The SC basal lamina surrounds mSCs and several of its proteins such as laminin mediate the direct contact with the abaxonal membrane proteins (eg. α6β4 integrin and β-dystroglycan) of

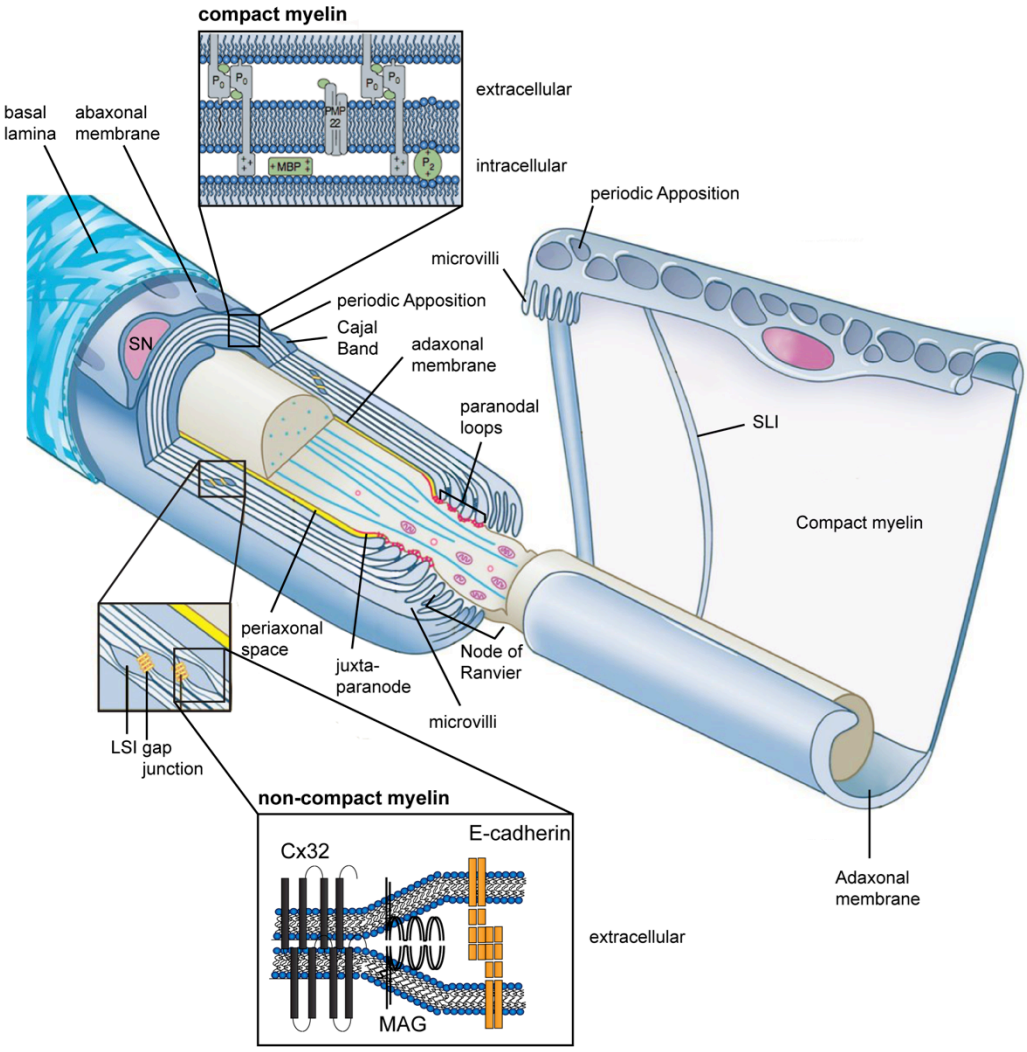

Figure 1.8. Myelin structure and organisation

Schematic representation of a mSC (depicted in blue) that is surrounding an axon (depicted in grey). On the left a longitudinal transverse section is shown and on the right the mSC is displayed "unwrapped". SC basal lamina (shown on the left) is surrounding the mSC and is in direct contact with the abaxonal compartment, which contains the SC nucleus. The periaxonal space (highlighted in yellow) separates the axonal membrane from the abaxonal membrane. The compact myelin (depicted in pale blue) is interrupted by regions of non-compact myelin such as the Schmidt-Lantermann Incisures (SLI), which are cytoplasmic incisures that connect the myelin sheets with the paranodal region that is adjacent to the Node of Ranvier. At the Node of Ranvier the SC microvilli are displayed and the adjacent paranodal junction are depicted in red. Figure adapted from (Salzer, 2015).

the mSC and these interactions, as discussed above, are essential for SC myelination. In addition, to impaired SC myelination, ablation of SC dystroglycan or mutations in laminin-2, were shown to cause abnormal myelin sheath folding, disorganised microvilli, reduced sodium channel density and disrupted cytoplasmic compartmentalisation indicating that these proteins are also instrumental for the proper compartmentalisation and elongation of the myelin sheath (Court et al., 2009). Furthermore, deficiency of α6β4 integrin in SCs results in abnormal myelin sheath folding in aged mice suggesting that this integrin is crucial for myelin stability (Nodari et al., 2008).

The compact myelin is mainly composed of lipids (~70%) (Saher and Simons, 2010) and is enriched in several proteins such as P0, MBP and tetraspanins such as PMP22 (Kidd et al., 2013). P0 makes up more than half of the PNS myelin protein (Lemke, 1988) and possesses a key role in myelin stabilisation and compaction (Kirschner and Ganser, 1980). Myelin compaction is mediated by specialised adhesive proteins and proteins that prevent myelin compaction are downregulated at the onset of the process (Nave and Werner, 2014; Snaidero and Simons, 2014). As shown in Figure 1.9 compaction of the SC cytoplasm is mediated by electrostatic interactions of MBP with the lipid bilayer and with the intracellular domain of P0 (Aggarwal et al., 2011; Min et al., 2009). Myelin sheath compaction is mediated by extracellular homotypic interactions of PO tetramers on one membrane with P0 tetramers on the opposing membrane (Filbin et al., 1990; Harauz et al., 2009; Martini et al., 1995a; Shapiro et al., 1996). In line with the key role of P0 in myelin compaction and stabilisation, mutations in the P0 protein are associated with demyelinating diseases such as Charcot Marie Tooth 1B (CMT1B), congenital hypomyelination and Dejerine-Sottas Syndrome in humans (Hayasaka et al., 1993a; Hayasaka et al., 1993b; Warner et al., 1996). Furthermore, studies in mice showed that the complete loss of PO causes severe SC differentiation defects and abolishes myelin sheath compaction (Giese et al., 1992), whilst P0 protein reduction leads to instability of the compact myelin indicating that both P0 alleles are required for the long-term maintenance of myelination (Martini et al., 1995b; Shy et al., 1997).

Non-compact myelin is found at the inner and outer periphery of the myelin sheath, at the paranodal loops, the Schmidt Lantermann incisures (SLI), the Cajal bands and the nodal

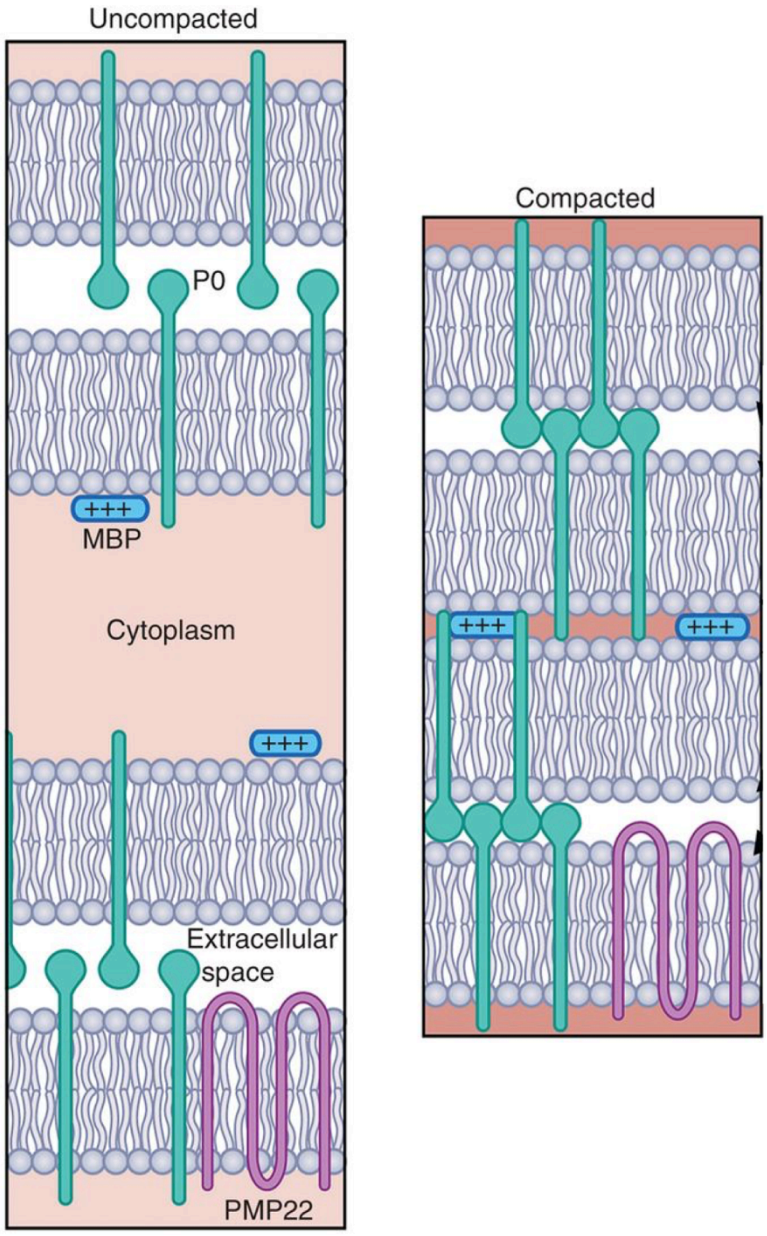

Figure 1.9. Compact myelin sheet organisation
LHS: Illustration depicts the loose wraps of uncompacted myelin that are formed initially. RHS: Following the beginning of myelination, myelin proteins (eg. P0, MBP and PMP22) are upregulated. For simplification in this scheme, P0 tetramers are displayed as P0 dimers. As shown in the scheme, myelin compaction is achieved by the interaction of P0 tetramers (depicted in green) on one membrane with P0 tetramers on the opposing membrane. Furthermore, compaction of the cytoplasm is mediated by electrostatic interactions of MBP (depicted in blue) with the phospholipid bilayer and binding to the cytoplasmic domain of PO. Figure is adapted from (Salzer, 2015).

microvilli. The SLI incisures are cytoplasmic inclusions that are present in each myelin layer and that provide a pathway to transport metabolites from the adaxonal to the abaxonal SC compartment (Arroyo and Scherer, 2000; Salzer, 2003, 2015; Scherer, 1999). The paranodal loops form specialised junctions with the axon and flank the Nodes of Ranvier (Salzer, 2003, 2015). The abaxonal compartment is interrupted by periodic appositions that flank a network of cytoplasmic channels, termed Cajal bands (Sherman et al., 2012), between the abaxonal membrane and the outer turn of the compact myelin (Nave and Werner, 2014; Salzer, 2015). These cajal bands transport proteins and RNA from the SC nucleus to the paranodal regions (Court et al., 2004) and thereby provide the means for the SCs to nurture the axons with metabolites.

Axons are myelinated along their entire length, except of at the Nodes of Ranvier, which are small (~1 micron) gaps between myelinated SCs and are highly enriched in voltage-gated sodium (Na+) channels (Rasband and Peles, 2015; Salzer et al., 2008) (Figure 1.10). The nodes of Ranvier are the only compartment, in which ions are exchanged across the axon membrane, and together with the increased resistance and reduced capacitance of the myelinated regions allows for the rapid saltatory conduction of the action potentials. The proper functionality of the nodes of Ranvier is supported by its surrounding specialised regions: The paranodal region that surrounds the Node of Ranvier at both sides and the juxtaparanodal region that is located between the paranodal region and the internode (Figure 1.10). In the paranodal region, SCs form membrane loops that connect to the axonal membrane (axolemma) by specific axo-glial junctions, the so called-paranodal junctions. These paranodal junctions promote the tight attachment of axons and glial cells and presumably maintain the composition of the nodes by acting as a kind of barrier preventing the lateral diffusion of its proteins (Eshed et al., 2005; Poliak and Peles, 2003; Rios et al., 2000; Rios et al., 2003). Adjacent to the paranodal region and the internode is the juxtaparanode that contains specialised K+ channels that likely contribute to maintain the resting potential of the internode and stabilise action potential conduction (Rasband, 2010; Vabnick and Shrager, 1998; Wang et al., 1993). The nodes of Ranvier contain many SC microvilli that emerge from the outer ends of the cell and were demonstrated to play important

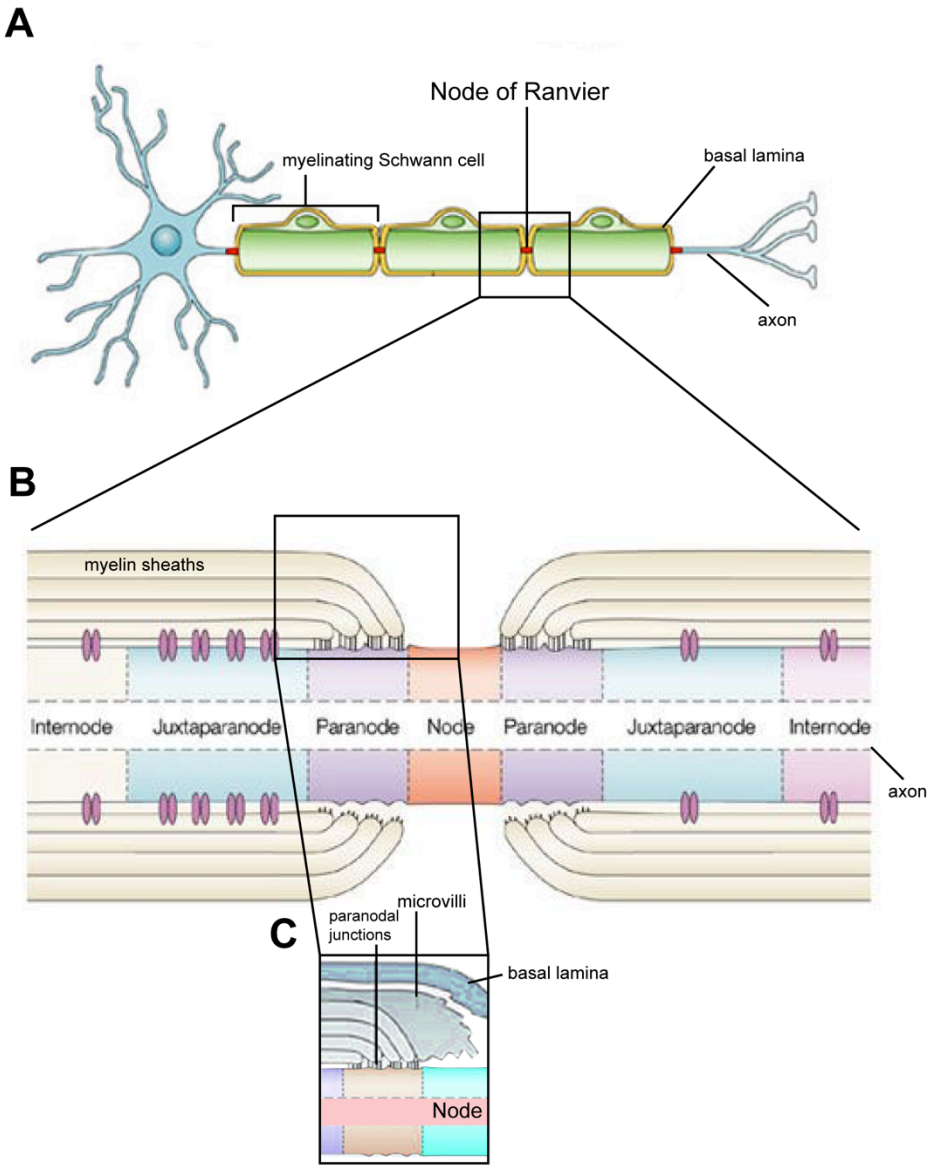

Figure 1.10. The Node of Ranvier

A) Scheme depicts an axon that is surrounded by mSCs that are connected with each other through Nodes of Ranvier. Furthermore, SCs are surrounded by a basal lamina layer. **B)** Scheme depicts longitudinal organisation of two mSCs that are intersected by the Node of Ranvier. mSCs are organised longitudinally into internode, juxtaparanode, paranode and the Node of Ranvier. **C)** The Node of Ranvier is surrounded by the paranodal region in which SCs interact with axons through paranodal junctions. SC microvilli emerge into the Node of Ranvier and are known to contribute to node formation and function. Furthermore, these microvilli intersect the basal lamina of neighbouring SCs to form a continuous tube. Figure is adapted from (Poliak and Peles, 2003).

roles in node formation and function (Salzer, 2015) (Figure 1.10). Among these functions, SC microvilli expand the SC basal lamina across the node and enable the fusion of neighbouring SC basal laminas in order to form a continuous tube.

1.2. Regeneration following nerve injury

In contrast to the CNS, the PNS is able to regenerate efficiently (Figure 1.11) and underlying this regenerative capacity are SCs, which are thought to be central organisers of the regenerative response (Cattin and Lloyd, 2016; Zochodne, 2008) (Figure 1.12).

There are two main types of peripheral nerve injuries (Burnett and Zager, 2004): 1. Axonotmesis, which transects the axons but the SC basal lamina and the enclosing connective tissue sheaths remain intact. Axonotmesis can be modelled by nerve crush in animal models (eg. rodents). 2. Neurotmesis, which transects the axons, SC basal lamina and the connective tissue sheaths, is the more severe form of peripheral nerve injury. Neurotmesis can be modelled by sciatic nerve transection in animal models.

Following both nerve transection and nerve crush, Wallerian degeneration (WD), which is defined as axonal degeneration distal to the injury site, is initiated (Figure 1.11A), nevertheless the extent of a successful repair process varies depending on the type of injury (Conforti et al., 2014). Axonal regeneration is effective and nerve function is restored after 3-4 week following a sciatic nerve crush, whereas functional recovery is quite poor after sciatic nerve transection (Jessen et al., 2015). The recovery after sciatic nerve crush is fostered by the intact SC basal lamina that supports nerve regeneration by providing a directional non-neuronal tube for axonal regrowth (Nguyen et al., 2002). Strikingly, it was shown that the regrowing axons remain within the same tubes and reconnect to the same muscle fibres that they originally reinnervated prior to sciatic nerve crush (Nguyen et al., 2002). In contrast to sciatic nerve crush, following sciatic nerve transection a new tissue, termed the nerve bridge is formed to join the two stumps together (Cattin and Lloyd, 2016) (Figure 1.11B). SCs rapidly dedifferentiate to progenitor-like SCs that possess key roles for successful nerve repair. Downstream of the injury site, axons degenerate and SCs and macrophages clear the axonal and myelin debris to provide a conducive environment for axonal regrowth (Figure 1.11B).

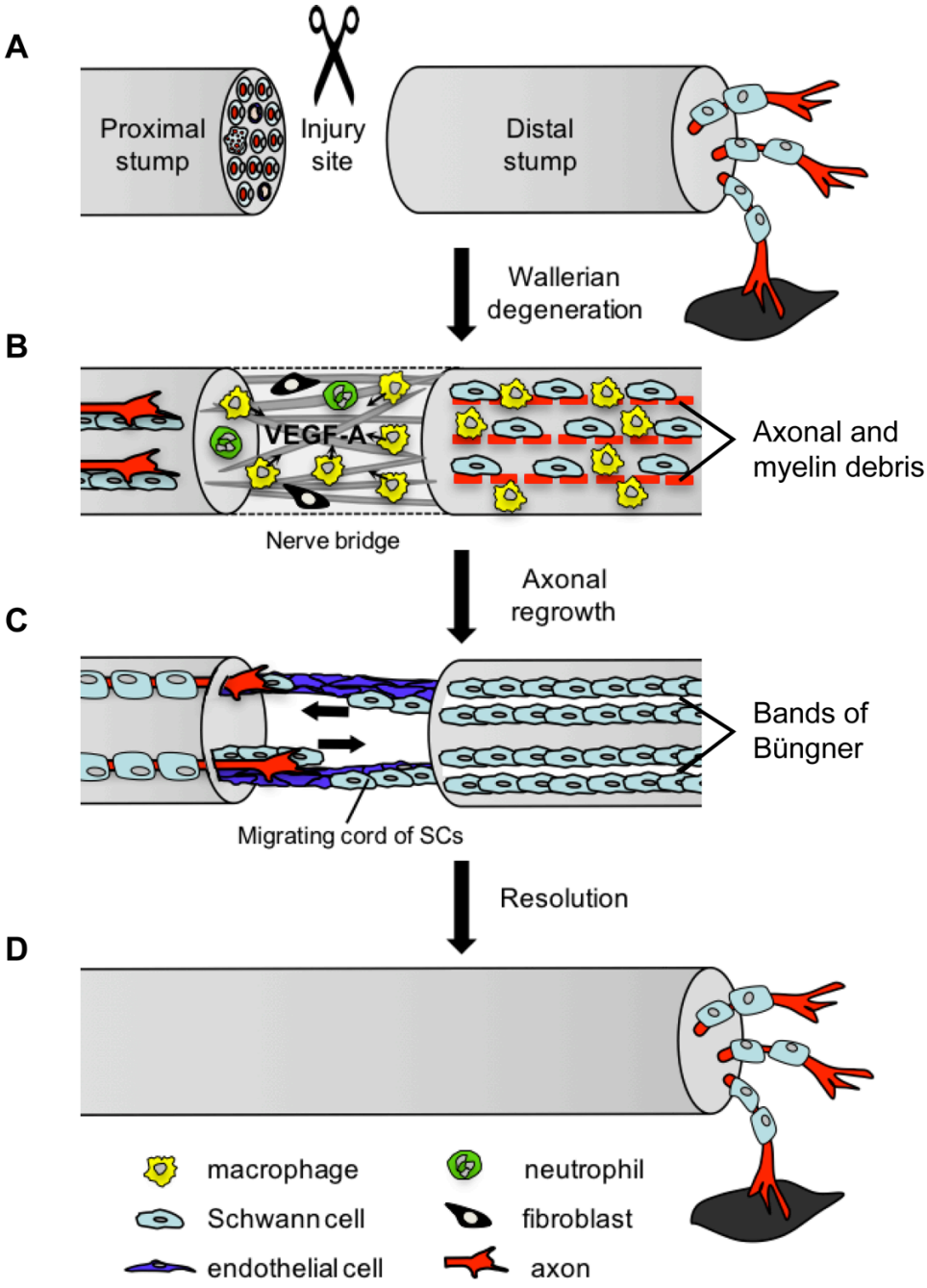

Figure 1.11. Peripheral nerve regeneration

Following nerve injury, the proximal and the distal stump retract **(A)** and a new tissue is formed to join the two stumps, the so-called nerve bridge. **B)** Initially, the nerve bridge is composed mainly of matrix and inflammatory cells and becomes hypoxic due to the lack of vascularisation. Macrophages primarily respond to the hypoxic environment and release VEGF-A that promotes angiogenesis. Downstream of the injury site, the axons degenerate in an active process known as Wallerian Degeneration. SCs dissociate from the degenerating axons and perform many crucial roles for a successful nerve repair process. **C)** In the distal stump, SCs together with macrophages clear the myelin and axonal debris in order to provide a conducive environment for axonal regrowth. SC form Bands of Büngner creating directional tubes, which provide a substrate for axonal regrowth back to the distal targets. After vascularisation of the bridge, SCs migrate along the vasculature and guide the regrowing

axons across the nerve bridge into the distal stump. **D)** In the final stages of nerve regeneration, the inflammatory response resolves and upon axonal regrowth, SCs re-differentiate to their mature form. Figure adapted from (Cattin and Lloyd, 2016)

Initially, the nerve bridge is a hostile environment for axonal regrowth that requires vascularisation, which is initiated by VEGF-A secreting macrophages, for axonal regrowth. Following vascularisation of the nerve bridge, SCs migrate in cords (Parrinello et al., 2010) along blood vessels and take the regrowing axons across the nerve bridge into the distal stump (Cattin et al., 2015). (Figure 1.11C). Within the distal stump, SCs form Bands of Büngner that provide directional tubes to facilitate axonal regrowth back to their original targets (Figure 1.11C). Overall, dedifferentiated SCs orchestrate a complex multicellular response, which is discussed in detail below and upon successful repair of the nerve will resolve to restore normal nerve function (Figure 1.11D) (Hall, 2005; Reichert et al., 1994).

1.2.1. Axonal degeneration

The axolemma and cytoskeleton of the axons rapidly commence to degenerate downstream of the site of injury (Figure 1.11). Axonal degeneration is an active process that is mediated by the activation of calcium dependent axonal proteases such as calpain (Glass et al., 2002). Furthermore, the ubiquitin-proteasome system was shown to be involved in this process, as preventing proteasome activity delayed axon degeneration *in vivo*. (Ehlers, 2004; Hoopfer et al., 2006) and *in vitro* (Gerdts et al., 2011; MacInnis and Campenot, 2005).

Although studies of Wallerian degeneration slow (Wld^S) mice (Mack et al., 2001) provided major insights into the mechanisms of WD, the molecular mechanisms that initiate axonal degeneration following nerve injury have not been identified. Wld^S mice exhibit delayed WD, as axons within the distal stump persist for one or two weeks following nerve injury without any obvious signs of fragmentation (Abbott et al., 2006). These mice overexpress a fusion protein of the first 70 amino acids of Ube4b, which is an evolutionary conserved protein involved in protein polyubiquitination, and the full-length nicotinamide mononucleotide adenylyltransferase 1 (Nmnat1), which is an enzyme that aids NAD synthesis. Axonal levels of Nmnat decrease rapidly after injury *in vitro,* whilst preventing this decrease protects axons

from degeneration indicating that Nmnat may be the key enzyme that mediates axonal degeneration (Araki et al., 2004; Wang et al., 2005). However, studies *in vivo* have shown that overexpression of Nmnat is not sufficient to protect axons from degeneration. Instead, the Ube4b derived sequence and the Nmnat enzyme activity are required, the former probably targeting the fusion protein to specific subcellular sites, at which the Nmnat enzyme then exerts its activity (Conforti et al., 2009; Jia et al., 2007; Yan et al., 2010). Strikingly, SC dedifferentiation was shown to correlate with delayed axonal degeneration in Wld^S mice indicating the requirement of axonal signals for the initiation of the SC dedifferentiation process (Brown et al., 1992).

To date, the exact mechanisms that link axonal degeneration and SC dedifferentiation and demyelination remain poorly understood (Rotshenker, 2011). NRG1 may act as an early axonal signal that mediates myelin breakdown, as ErbB2 phosphorylation is observed at the paranodes within minutes after nerve injury (Guertin et al., 2005). In line with this, treatment with the ErbB1/B2 tyrosine kinase PKI-166 inhibitor delayed demyelination, although axonal degeneration occurred normally following nerve injury. This suggests that that the temporal activation of ErbB2 in SCs is sufficient to induce SC demyelination. However, as the inhibitor also acts on the EGFR, which is also expressed by SCs upon injury, it is not clear if the observed effect is solely through NRG1-ErbB2 signalling or if alternative signalling pathways are involved. In agreement with Guertin et al., other studies demonstrated that high levels of GGF (NRG1 type II) induce demyelination *in vitro* (Zanazzi et al., 2001) and *in vivo* (Huijbregts et al., 2003), which further supports the proposed role of NRG1 as an initiator of the SC response following injury.

1.2.2. Schwann cell response after injury

SCs are highly specialised cells in the adult peripheral nervous system, however following injury, as axonal degeneration commences, SCs lose their contacts with axons and rapidly dedifferentiate into progenitor-like SCs (repair SCs). Recent studies, from us and others, have greatly contributed to the knowledge of the signals and transcriptional programs that control both the SC response after injury and remyelination. Several molecular signalling pathways

and transcription factors which were active throughout SC development ("associated with immature SCs"), are reactivated following nerve injury (Hall et al., 1997; Jessen and Mirsky, 2008; Jessen et al., 2015; Svaren and Meijer, 2008; Taniuchi et al., 1986; Trapp et al., 1988). For example, the expression of molecular markers that are characteristic of the immature SC stage are upregulated, such as L1, NCAM, p75NTR, c-Jun, Sox2 and glial fibrillary acid protein (GFAP). On the other hand, the expression of Krox-20 and other myelin-associated genes (eg. P0, MBP) are downregulated in line with the gradual degradation of the myelin sheath. Once axons regrow, SCs upregulate Krox20 and Oct-6 expression to induce remyelination. However, during SC development Oct6 needs to be downregulated for successful SC differentiation, whereas Krox20 expression remains stable (Ghazvini et al., 2002; Monuki et al., 1990; Scherer et al., 1994; Zorick et al., 1996). Although, several molecular pathways and transcription factors are consistent between immature SCs and progenitor-like SCs (repair SCs), the transcriptional profile of these two SC populations is distinct, as progenitor–like SCs express Olig1, Shh and GDNF at high levels, whereas immature SC express them at a low level (Arthur-Farraj et al., 2012). In addition, progenitor-like SCs differ in length to immature SCs and to SC precursors (Gomez-Sanchez et al., 2017). However, it is not clear from these studies, whether immature SCs and progenitor-like SCs are intrinsically distinct from each other, or these cells are different because they are exposed to a different nerve environment (development vs. injury environment), which may influence their transcriptional profile and cell morphology, whilst maintaining their cell identity.

Several studies from others and us have shown that, remarkably, the activation of some signalling pathways in mSCs is sufficient to induce SC dedifferentiation and to trigger demyelination. A study from the Lloyd lab (Napoli et al., 2012) has demonstrated the central role of the Ras/Raf/ERK signalling pathway in driving SC dedifferentiation (Figure 1.12). Within 20 minutes following nerve injury, ERK was shown to be rapidly activated in mSCs both at the site of injury and along the distal stump. Moreover, this ERK activation is maintained for several days following nerve injury (Harrisingh et al., 2004; Sheu et al., 2000). This rapid activation of ERK following injury induces SC dedifferentiation in vivo and in vitro (Harrisingh et al., 2004; Napoli et al., 2012; Ogata et al., 2004). Using a tamoxifen inducible

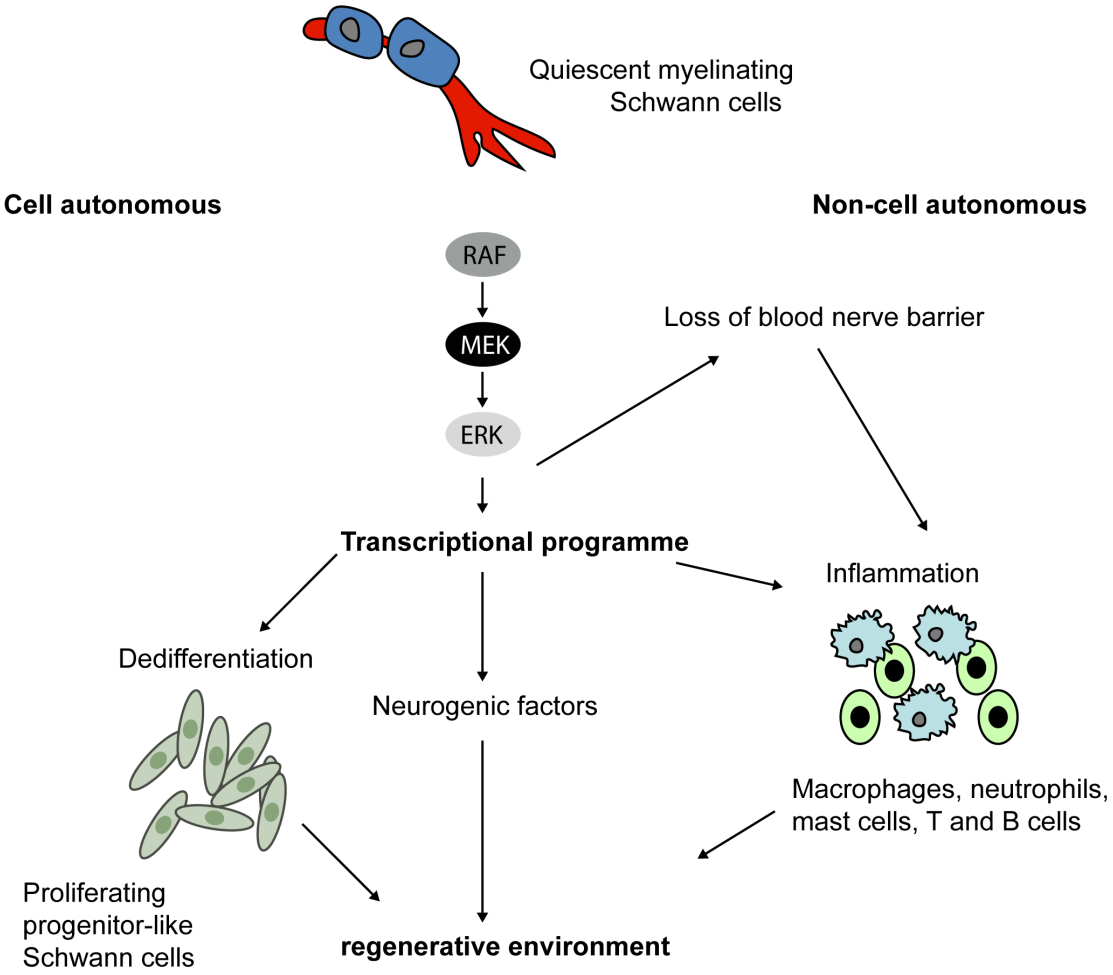

Figure 1.12. Schwann cells act as orchestrators of peripheral nerve regeneration
The activation of the Ras/Raf/ERK signalling pathway regulates key events in SC biology and importantly, plays a major role during the regenerative process. The strong activation of this pathway occurs after injury and has both (LHS) cell autonomous and (RHS) non-cell autonomous effects. The cell autonomous effects drive SC dedifferentiation to progenitor- like SCs. The non-cell autonomous effects initiate the opening of the Blood Nerve Barrier and the induction of the inflammatory response. All these components contribute to the regenerative nerve environment.

Raf-kinase/estrogen receptor fusion protein (RafTR), the Lloyd laboratory demonstrated that activation of the Raf kinase specifically in mSCs is sufficient to induce SC demyelination *in vivo*, although axons remained intact (Napoli et al., 2012). Importantly, this study showed that prior to structural changes of the nerve, myelin genes (eg. P0 and MBP) were downregulated, whereas the SC dedifferentiation marker such as p75 were upregulated. This shows that a transcriptional programme associated with the switch of SC state, similar to that following nerve injury, occurs that is initiated by the activation of Raf in mSCs. Furthermore, it was shown that SCs remain in the dedifferentiated state for as long as Raf activation was maintained. Upon withdrawal of tmx treatment, the activation of the Raf kinase ceased and SCs rapidly redifferentiated and remyelinated axons, which highlights the reversibility of this process. Strikingly, Raf activation in mSCs not only has SC autonomous effects, it also has SC non-autonomous effects, as it was shown to induce the break down of the Blood Nerve Barrier and leads to the recruitment of inflammatory cells to the injured nerve (Figure 1.12). Treatment with the MEK inhibitor PD0325901 was shown to inhibit both SC dedifferentiation and initiation of the inflammatory response following injury (Napoli et al., 2012). These findings demonstrate that the activation of Raf in SCs via the ERK signalling pathway not only drives SC dedifferentiation, it also initiates the SC non autonomous effects such as the recruitment of the inflammatory response to the nerve. Overall, the activation of Raf in mSCs mimics the response of the nerve following injury, even in the absence of axonal degeneration.

The upstream activator of Raf has not been identified, although it was suggested that NRG1 likely activates the Ras/Raf/ERK signalling pathway in SCs following injury. However, *in vitro* NRG1 only transiently activates the Ras/Raf/ ERK signalling pathway in SCs (Echave et al., 2009), implying that there are likely other upstream signals that are responsible for sustaining the activation of the Ras/Raf/ERK signalling pathway. Fibrin, that is deposited within injured nerves, was postulated as an additional upstream activator of ERK, as it was shown to induce phosphorylation of ERK and increased the expression of p75 in SCs (Akassoglou et al., 2002). In line with the crucial downregulation of ERK activation in order to allow SC remyelination, fibrin clearance was shown to correlate with the onset of re-myelination.

In addition to the instrumental role of the Ras/Raf/ERK signalling pathway in driving SC dedifferentiation, other studies showed that c-jun, which negatively regulates myelination throughout SC development, is upregulated in SCs following nerve injury (Arthur-Farraj et al., 2012; Fontana et al., 2012; Parkinson et al., 2008). The loss of c-jun was shown to impair neuronal survival and leads to defects in axonal regeneration and reduced functional recovery. Furthermore, it was shown that the expression of c-Jun is involved in the downregulation of the myelin genes MBP and P0 and actively contributes to the repair program by upregulating the expression of neurotrophic factors (eg. Artemin, GDNF, BDNF) that support axonal regrowth (Arthur-Farraj et al., 2012; Fontana et al., 2012). Moreover, c-Jun, which is a known downstream effector of the Raf/MEK/ERK signalling pathway, was found upregulated following Raf activation in mSCs implying that its activation is regulated by Raf (Napoli et al., 2012).

Following ERK and c-Jun activation, SC dedifferentiate to progenitor-like SCs that contribute to regeneration by performing multiple distinct roles. Work from our laboratory has shown the mechanism that induces a change in SC behaviour from repulsion to attraction is needed for the collective migration across the nerve bridge (Parrinello et al., 2010). Following nerve transection, SCs come into close contact with fibroblasts at the injury site and this interaction induces a dramatic switch in SC behaviour. This switch is mediated by the activation of Ephrin type-B receptor 2 (EphB2) on SCs by ephrinB expressing fibroblasts. The activation of EphB2 in SCs results in modification and stabilisation of Sox-2 that initiates the relocalisation of N-cadherin to cell-cell junctions, which was shown to mediate SC clustering into cords. Whilst Sox2 is a known negative regulator of myelination that maintains SCs in their dedifferentiated state (Roberts et al., 2017), as discussed above, our study further suggests that Sox2 is required following nerve injury to induce gene expression changes that are necessary to obtain long-term modifications of cell behaviour. Moreover, consistent with previous studies (Chen et al., 2005; McDonald et al., 2006), we found that SCs enter the nerve bridge prior to axonal regrowth. Importantly, SCs cord formation is necessary for the guidance of axonal regrowth across the nerve bridge, as loss of EphB2 resulted in aberrant axonal regrowth. In line with our study, previous work demonstrated that abolishing SC mitosis and migration at

the site of injury leads to a severe reduction in axonal regrowth (Chen et al., 2005; Pellegrino and Spencer, 1985). Importantly, these SC cords are unable to migrate within a 3D matrix indicating that an additional mechanism is required to allow SC migration into the nerve bridge (Cattin et al., 2015).

A recent study from the Lloyd lab identified the mechanism by which SCs migrate across the hostile environment of the nerve bridge following nerve transection (Cattin et al., 2015). Initially, the nerve bridge is filled with ECM and inflammatory cells and is not vascularised resulting into tissue hypoxia, which is specifically sensed by macrophages within the nerve bridge. In turn, these macrophages produce VEGF-A that is sufficient and required to initiate vascularisation in this region (Figure 1.11B). Importantly, Cattin et al. demonstrated that the newly formed blood vessels provided a substrate for SC migration across the hostile environment of the nerve bridge. Consistent with this, the loss of VEGF-A in myeloid cells was sufficient to block both blood vessel growth and SC migration into the nerve bridge. Moreover, SC migration was found to be independent of focal adhesion formation, whilst dependent on actomyosin contractility. Importantly, despite that many other cell types populate the nerve bridge after injury, this study showed that only macrophages exhibited a hypoxic response, whilst the other cell types responded differently to the bridge microenvironment. This demonstrated a specific role for macrophages in the regenerative response, which can be compared to their role in tumourigenesis in which macrophages were shown to promote vascularisation in hypoxic regions of tumours (Murdoch et al., 2008; Qian and Pollard, 2010).

Within the distal stump, SCs and macrophages (see also inflammatory response paragraph below) clear the myelin and axonal debris in order to provide a more conducive environment for axonal regrowth (Figure 1.11B) (Cattin and Lloyd, 2016). The clearance of axonal and myelin debris is integral for successful axonal regrowth as myelin contains proteins such as myelin associated glycoprotein (MAG) that inhibit axonal regrowth (Chen et al., 2007; Kang and Lichtman, 2013; Mukhopadhyay et al., 1994; Schafer et al., 1996; Shen et al., 1998). Dedifferentiated SCs activate a cell-intrinsic myelin breakdown process, which accounts for the majority of the myelin breakdown during the first 5-7 days after injury (Hirata and Kawabuchi, 2002; Rotshenker, 2011). In this intrinsic process, SCs use autophagy to degrade

the myelin, which was shown to be dependent on mTOR activation after injury (Gomez-Sanchez et al., 2015). Moreover, this process is dependent on the interaction of galactose-specific lectin MAC-2 that is expressed by SCs, with Galoctosylceramidase (GalC and sGalC) presented on myelin debris following injury (Reichert et al., 1994).

Following SC dedifferentiation, SCs re-enter the cell cycle and proliferate at the site of nerve injury and throughout the entire distal stump following nerve injury (Liu and Shen, 1985).

Different mechanisms seem to control SC proliferation throughout SC development and following nerve injury, whereas the mechanisms controlling SC redifferentiation and remyelination seem largely similar in development and throughout nerve repair (Chen et al., 2007; Hall, 2005; Walikonis and Poduslo, 1998; Zhang et al., 2000). Initially, it was thought that NRG1-ErbB2/B3 signalling initiates SC proliferation following injury, as it is critical for SC proliferation and survival during development. However, studies using SC-specific ErbB2 conditional knockout mouse models showed that the ErbB2 signalling pathway is dispensable for SC proliferation and survival but critical for SC remyelination following nerve injury (Atanasoski et al., 2006; Fricker et al., 2011; Stassart et al., 2013). In addition, using cyclin D1 knockout mice it was shown that SC proliferation is independent of cyclin D1 during development, whereas cyclin D1 was required to initiate SC proliferation following sciatic nerve crush (Kim et al., 2000). Surprisingly, in contrast to studies performed following nerve transection (Chen 2005), Kim et al showed that although SC proliferation was absent, axonal regrowth occurred normally suggesting that SC proliferation is dispensable for successful nerve repair after sciatic nerve crush.

1.2.3. Inflammatory response

As discussed above, the activation of Raf in mSCs triggers the infiltration of inflammatory cells into peripheral nerves, which was shown to correlate with breakdown of the Blood Nerve Barrier, similar to that after injury, implying that Raf activation in mSCs may lead to release of signals that initiate these processes (Napoli et al., 2012). The signals that mediate the breakdown of the Blood Nerve Barrier remain unknown (L.Malong, ongoing study in the lab), however Napoli et al. showed that following Raf activation dedifferentiated SCs initiate

inflammatory cell recruitment by secreting pro-inflammatory cytokines and chemokines such as monocyte chemoattractant protein-1, c-kit ligand, tumour necrosis factor α (TNF-α), Interleukin 1α (IL-1α) and Interleukin-6 (IL6). These cytokines are sustained by the infiltration of inflammatory cells such as neutrophils that further contribute to the expansion of this pro-inflammatory network (Chen et al., 2005; Shamash et al., 2002).

Neutrophils are the first inflammatory cells that enter the regenerating nerve to phagocytose debris and to recruit other leucocytes within the first 24 hours (Hall, 2005; Kennedy and DeLeo, 2009; Nathan, 2006; Perkins and Tracey, 2000). A recent study demonstrated that myelin clearance was decreased upon neutrophil depletion following nerve injury (Lindborg et al., 2017) suggesting that neutrophils probably cooperate with SCs and macrophages to myelin debris clearance. However, apart from the clearance of debris, the contribution of neutrophils to the peripheral nerve injury response is not well understood. In the process of nerve repair, neutrophils likely undergo apoptosis, as they have high cell turnover in other tissues (Kennedy and DeLeo, 2009).

Similarly to neutrophils, resident macrophages respond rapidly to tissue damage (Mueller et al., 2001) and monocyte derived macrophages are recruited to aid the resident population following nerve injury (Cattin and Lloyd, 2016; Mueller et al., 2003). In addition to the role of macrophages in initiating vascularisation of the nerve bridge, as discussed above, macrophages are considered as the major cell type, along with SCs, that remove cellular and axonal debris in the distal stump (Cattin and Lloyd, 2016; Martini et al., 2008). Monocytes are recruited by pro-inflammatory cytokines such as macrophage inflammatory protein and tumour necrosis factor-alpha (TNFα) to the injured nerve, where they differentiate into macrophages (monocyte-derived macrophages). The contribution of these monocyte-derived macrophages was shown to be important for efficient myelin clearance (Klein and Martini, 2016). Furthermore, B-lymphocytes promote macrophage recruitment to the injured nerve by secreting antibodies against myelin proteins, which was also shown to be important for the efficiency of the myelin clearance process (Vargas et al., 2010). Macrophages produce cytokines that can recruit and/or activate SCs such as Il-1 (La Fleur et al., 1996) and CCL3 (L.

van Emmenis, ongoing study in the lab). Additionally, macrophages may also secrete trophic factors that stimulate neuronal regrowth, as shown *in vitro* (Hikawa and Takenaka, 1996).

In addition to macrophages and neutrophils, other inflammatory cells such as mast cells and T-cells are recruited to the injured nerve. T-cells are known to secrete both pro- and anti-inflammatory cytokines and have been shown to be the last immune cells to reach the injured nerve around 14-28 days following nerve injury (Moalem et al., 2004). Mast cells are though to increase the permeability of the Blood Nerve Barrier by secretion of vasoreactive agents (Hall, 2005). However, the contribution of mast cells and T-cells to nerve repair is not very well understood and requires further investigation. Following nerve repair, the inflammatory response resolves and most macrophages either undergo apoptosis or migrate to the lymph nodes and the spleen (Kuhlmann et al., 2001). The mechanisms and kinetics of the resolution of the inflammatory response remains poorly understood. However, in addition to providing insight into the mechanism of SC dedifferentiation, Napoli et al showed that downregulation of Raf actively resolves the inflammatory response suggesting that SC differentiation status may regulate both the initiation and termination of the inflammatory response (Napoli et al., 2012).

1.2.4. Final steps of nerve repair: Axonal regrowth and Schwann cell redifferentiation and remyelination

Successful nerve regeneration depends on axonal reinnervation of the correct distal target sites (Nguyen et al 2002). In this process, SCs provide trophic support and physical guidance to the regrowing axons by forming Bands of Büngner in the distal stump, which provide a sustaining substrate and guidance cues for axonal regrowth to reconnect with their original distal targets (Figure 1.11D) (Chen et al., 2007; Nguyen et al., 2002). Furthermore, dedifferentiated SCs also secrete many neurotrophic factors such as NGF, BDNF, NT3 and Artemin (Fontana et al., 2012; Funakoshi et al., 1993) and express adhesion molecules such as N-cadherin, L1 and NCAM, which have been shown to increase neurite outgrowth *in vitro* (Bixby et al., 1988; Bixby and Zhang, 1990; Tacke and Martini, 1990; Thornton et al., 2005). In addition to the crucial contribution of SCs, laminin, collagen and fibronectin expression is strongly upregulated in injured nerves (Lefcort et al., 1992) and the interaction between these

ECM matrix proteins and axonal proteins may facilitate axonal regrowth by providing structural and trophic support (Agius and Cochard, 1998; Toyota et al., 1990; Vogelezang et al., 2001).

At the site of transection, axonal sprouting leads to the emergence of several sprouts from each parental axon and subsequently to an excess of regrowing axons into the distal stump (Aguayo et al., 1973; Sanders and Young, 1946). Axons, which fail to reconnect to their distal targets are pruned away and disappear (Campbell, 2008; Dyck PJ, 1993). During this process, the nerve trunk also reorganises into so called minifascicles, which are surrounded by a perineurium (Geuna et al., 2009). The formation of these minifascicles occurs at the proximal stump, the site of injury and in the distal stump (Morris et al., 1972) and is thought to be an active process which rapidly restores the endoneurial environment to protect the regenerating nerve (Birch, 2013; Lundborg et al., 1981).

Following axonal regrowth, SC redifferentiation is initiated upon re-establishment of SC-axon contact within the regenerating nerve and involves the transient expression of Oct-6, followed by upregulation of Krox-20 and the subsequent induction of myelin genes (Scherer et al., 1994; Zorick et al., 1996). Whilst SC myelination is driven solely by the axonal NRG1 type III isoform during development, a recent study demonstrated that soluble NRG1 type I, which is secreted by dedifferentiated SCs, is required for efficient remyelination following nerve injury (Stassart et al., 2013). This study suggested that SC NRG type I promotes SC redifferentiation in addition to signals from axonal NRG1 type III. Surprisingly, a recent study showed that following sciatic nerve crush remyelination is possible in adult mice that lack NRG1 in all cells, implying that an additional factor that remains to be identified must compensate for the loss of NRG1 (Fricker et al., 2013; Fricker et al., 2011; Mei and Nave, 2014). These studies underline that SC remyelination is not a simple recapitulation of nerve development, as myelination is dependent on different factors during development and nerve injury. Moreover, neurotrophic factors also appear to be involved in SC remyelination, as p75 null mice exhibited reduced numbers of myelinated axons and thinner myelin sheaths following nerve injury (Song et al., 2006).

Strikingly, a regenerating nerve resembles neurofibromas that develop in association with the tumour predisposition syndrome Neurofibromatosis type I. This implies an important link between injury and tumorigenesis, which is consistent with previous reports in other tissues (Balkwill and Mantovani, 2001; Martins-Green et al., 1994).

1.3. Neurofibromatosis type I (NF1)

Neurofibromatosis type 1 (NF1) is an autosomal inherited disorder and is one of the most common tumour predisposition syndromes, affecting 1 in 3500 individuals worldwide. NF1 patients develop a wide spectrum of clinical presentations such as learning disabilities, pigmentary lesions of the skin (café au lait macules) and iris (Lisch nodules) and skeletal abnormalities (eg. spinal deformations, scoliosis). Additionally, NF1 patients are prone to develop benign and malignant tumours including gliomas, glioblastomas and astrocytomas. However, the development of Schwann cell-derived neurofibromas is the hallmark lesion of NF1. Neurofibromas are heterogenous benign tumours of the peripheral nerve sheath, which can develop in many different parts of the body and can spread to surrounding tissues/organs (eg skin, bones and muscle) (Friedman and Birch, 1997; McClatchey, 2007; Riccardi, 1981, 1992a). Affected individuals are born with one mutated and one wild type *Nf1* allele. The loss of the second *Nf1* allele is required for tumourigenesis, although NF1 heterozygous patients exhibit learning disabilities and pigmentary defects. Consequently, NF1 follows Knudsons two-hit hypothesis of tumour formation, as NF1 heterozyous patients develop neurofibromas upon somatic mutation of the second wild-type *Nf1* allele (Serra et al., 1997; Upadhyaya et al., 1994).

1.3.1. Neurofibromas

Neurofibromas are highly heterogenous, benign tumours that develop along peripheral nerves. Neurofibromas are composed of a mixture of SCs, axons, perineurial-like cells, inflammatory cells (eg. mast cells and macrophages), vascular cells and morphologically appear very disorganised in contrast to a healthy peripheral nerve (Figure 1.13). Furthermore, an abundant collagenous extracellular matrix encloses neurofibromas

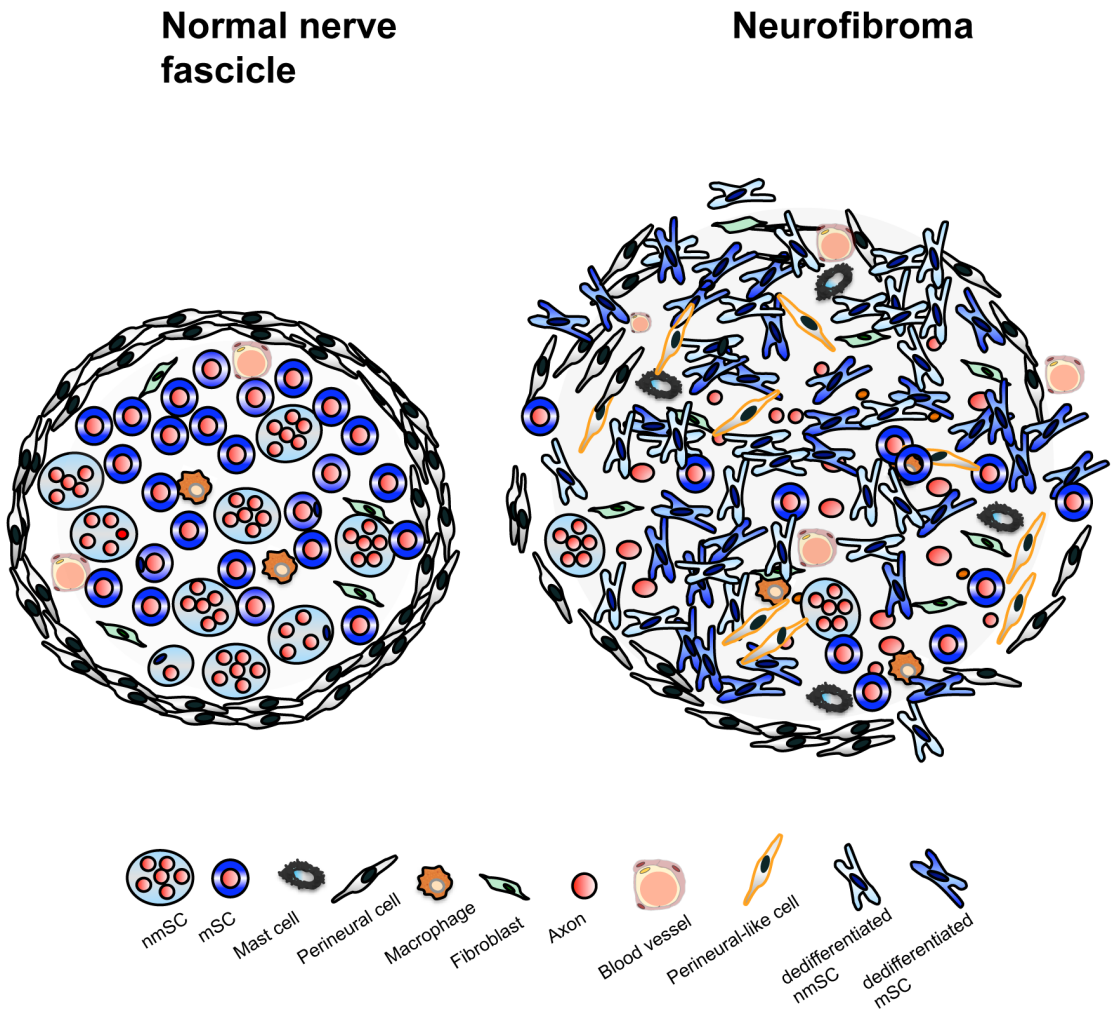

Figure 1.13. Structure of a normal uninjured peripheral nerve and a neurofibromatic nerve

Schematic representation of a normal uninjured peripheral nerve (LHS) and of a neurofibromatic nerve (RHS), in which SC mainly exist in a dedifferentiated state and are devoid of axonal contact. Many other cell types, which are not present in a healthy peripheral nerve, exist in neurofibromas such as mast cells and perineurial-like cells. Furthermore, many macrophages, fibroblasts and vascular cells can be found within neurofibromas.

(Friedman and Birch, 1997; McClatchey, 2007; Riccardi, 1981, 1992a).

Neurofibromas are commonly described as unrepaired wounds, as striking similarities exist between the processes involved in wound healing and the composition of neurofibromas. Similarly to injured nerves, within neurofibromas, SCs exist in a dedifferentiated state and proliferate in the absence of axonal contact whilst surrounded by a complex microenvironment consisting mainly of fibroblasts and inflammatory cells (Ribeiro et al., 2013) (Figure 1.13). The link between tumourigenesis and wound healing has been drawn frequently for many tumour types (Balkwill and Mantovani, 2001; Martins-Green et al., 1994). The wound environment is similar to the tumour environment, suggesting that it may be permissive for tumour growth and in line with this, studies based on patient observations suggested that neurofibroma formation can be triggered by local injury (Ribeiro et al., 2013; Riccardi, 1992b).

Neurofibromas can form in many different parts of the body and they can be classified as dermal, developing in the skin or plexiform, developing along the nerve plexus, neurofibromas. Most NF1 patients develop dermal neurofibromas, which are superficial tumours and are mostly associated with single, small nerves, but they can add up to several thousand and be extremely disfiguring for the affected patient. Dermal neurofibromas usually increase in number throughout puberty and their numbers are known to increase during pregnancy, however they have never been observed to undergo malignant transformation. In contrast, plexiform neurofibromas arise within larger nerves or nerve plexus resulting in extensive enlargement of the nerve. Plexiform neurofibromas are benign tumours, but large benign plexiform neurofibromas can compress vital organs and thereby severely impact the patient's lifespan. Only plexiform neurofibromas can progress to highly aggressive malignant tumours known as malignant peripheral nerve sheath tumours (MPNSTs) that affect approximately 8-13% of NF1 patients and will be discussed in more detail below (Friedman and Birch, 1997; McClatchey, 2007; Riccardi, 1981, 1992a) (Figure 1.14).

1.3.2. *Nf1*

The Nf1 gene was identified and cloned in 1990 and is one of the larger genes in the human

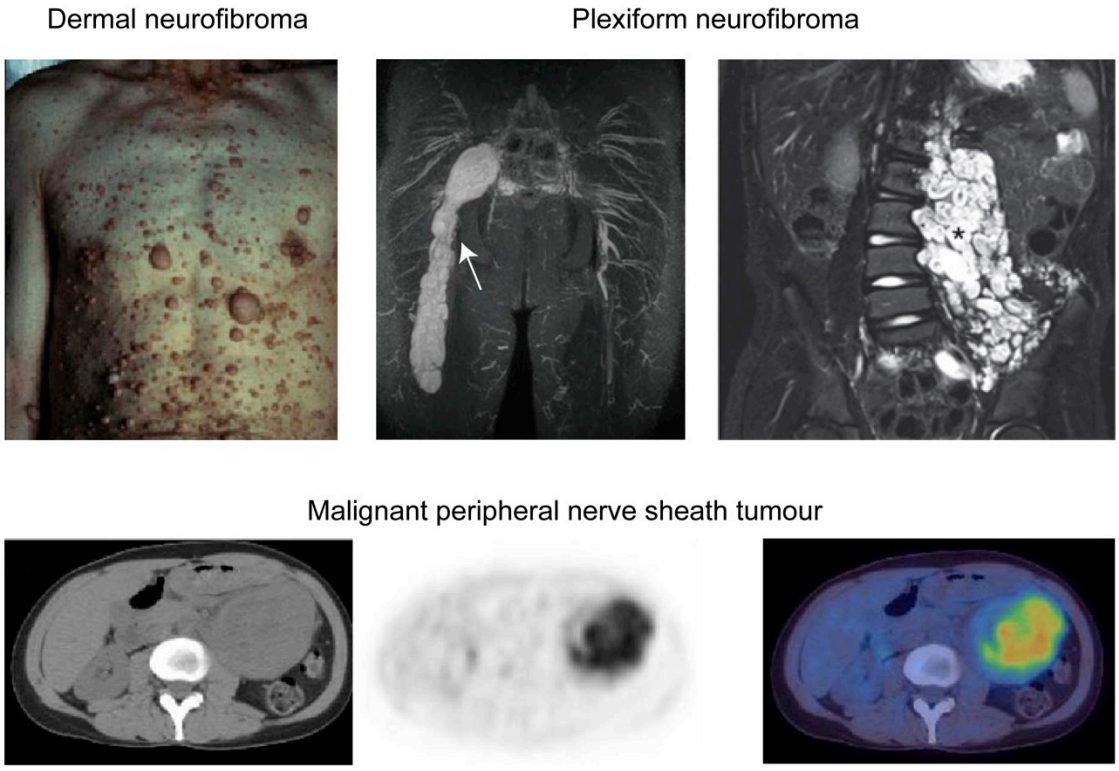

Figure 1.14. Representative images of dermal, plexiform neurofibromas and malignant peripheral nerve sheath tumours

A NF1 patient with dermal neurofibromas growing on the chest and abdomen (LHS). Magenetic resonance images of NF1 patients with plexiform neurofibroma (RHS). The plexiform neurofibroma of the patient on the left, highlighted with an arrow, is growing in the sciatic nerve, whereas the plexiform neurofibroma of the patient on the right is growing in the nerve roots and is compressing the spinal cord. Lower panel: Axial CT, PET and overlayed CT/PET image of high grade malignant peripheral nerve sheath tumour that formed within the left flank. Figure is adapted from (Hirbe and Gutmann, 2014; Savva et al., 2010; Staser et al., 2010; Warbey et al., 2009)

genome. In humans, *Nf1* is localised at chromosome 17q112 (chromosome 11 in mouse) and is comprised of 62 exons, which span over 350kb of genomic DNA with this large size is thought to render Nf1 more susceptible to mutations. Consequently, the mutation rate for Nf1 is one of the highest (~1:10,000) with approximately 50% of the mutations are thought to be *de novo* (Thomas et al., 2010). Most of the reported mutations (90%) are point mutations (nonsense, missense and frameshift mutations), which lead to synthesis of a truncated, non-functional protein. All these mutations are completely penetrant but the clinical presentation of the disease varies wildly, even between family members (Wimmer et al., 2007; Wimmer et al., 2006).

The *Nf1* gene consists of 23 transcripts of which 8 are protein-coding, 4 out of the 62 exons are alternatively spliced (9a, 10a-2, 23a and 28a) (Cawthon et al., 1990b; Marchuk et al., 1991; Wallace et al., 1990). The *Nf1* gene sequence and structure is highly conserved between species and its promoter region contains transcription binding sites that include a cAMP response element, an SPI site, multiple AP2 binding sites and a serum response element (Hajra et al., 1994). To date the transcriptional regulation of *Nf1* is not well understood and it remains to be shown how genetic and/or epigenetic regulators can regulate *Nf1* expression.

Three additional genes are localized within intron 27b on the antisense strand: a membrane glycoprotein called oligodendrocyte myelin glycoprotein (OMGP) and two genes involved in the development of mouse leukemia, EVI2A and EVI2B (Cawthon et al., 1991; Cawthon et al., 1990a). To date, no mutations have been identified in any of these three proteins and none of these three genes have been shown to be involved in NF1 pathogenesis.

In addition to Nf1, many other genes are found mutated in NF1 malignant tumours, including cell cycle regulatory proteins such as TP53, CDKN2A, RB1 and mice carrying cis linked *Nf1* and TP53 mutations undergo malignant progression to MPNST (Stewart et al., 2008; Upadhyaya et al., 2008).

1.3.3. Neurofibromin

Neurofibromin is a large 220-250kDa cytoplasmic protein that is highly expressed in neurons,

SCs, astrocytes, oligodendrocytes and leukocytes (Daston et al., 1992; DeClue et al., 1991; Gutmann et al., 1991). Neurofibromin is a member of the mammalian Ras-GTPase activating proteins (Ras-GAPs) (Brossier and Carroll, 2012) that are negative regulators of Ras, as they downregulate Ras signalling by accelerating the conversion of active Ras-GTP to inactive Ras-GDP (Martin et al., 1990; Xu et al., 1990) and thereby diminish the activity of the Ras signalling pathways (Ballester et al., 1990; Xu et al., 1990). Positive regulators of Ras are called guanine nucleotide exchange factors (GEFs), which stimulate Ras to release GDP and bind to GTP that is the predominant intracellular guanine nucleotide. The balance between GAP and GEFs determine the activation state of Ras and its downstream target pathways (Bos et al., 2007; Vigil et al., 2010) (Figure 1.15).

The binding of Ras by neurofibromin is mediated by the GTPase activating protein (GAP) related domain (GRD domain). This domain is sufficient to stimulate the GTPase activity of Ras and thereby is able to reverse the tumourigenic properties of Nf1 deficient cells (Martin et al., 1990; Xu et al., 1990). The GRD domain of neurofibromin is highly conserved between species and by stimulating the intrinsic GTPase activity of Ras it diminishes Ras-mediated mitogenic signalling, which is consistent with neurofibromin acting as a tumour suppressor.

Many other protein domains of neurofibromin have been identified such as a cysteine/serine rich domain (CSRD), tubulin-binding domain (TBD), a Sec14 homology domain (Sec14), a pleckstrin homology domain (PH), a nuclear localization sequence (NLS) and a FAK interacting domain (Figure 1.16). Two of these domains, the TBD and the CSRD domain, regulate the GAP activity of neurofibromin. The interaction of the TBD domain of neurofibromin with tubulin was shown to inhibit the GAP activity, whereas phosphorylation of the CSRD domain by PKC enhances the GAP activity of neurofibromin (Bollag et al., 1993; Mangoura et al., 2006). Furthermore, neurofibromin contains a functional NLS (Vandenbroucke et al., 2004) and a FAK-binding region at its C-terminal domain that may be involved in controlling cell adherence (Kweh et al., 2009). The function of these domains other than the GRD domain is not well understood.

The molecular mechanisms that regulate neurofibromin expression are not completely understood. Following growth factor (eg PDGF, EGF) treatment of cells *in vitro*, neurofibromin

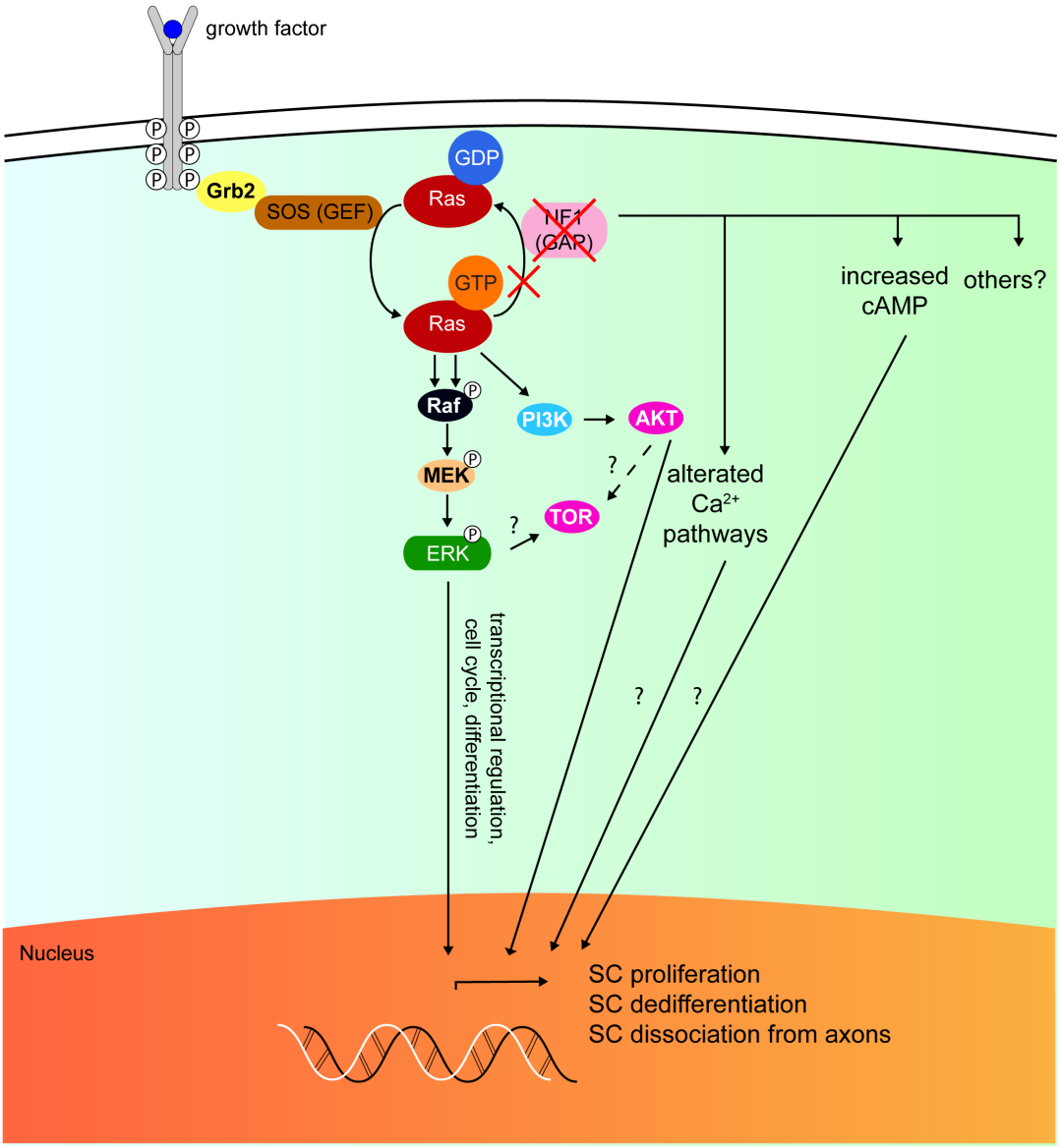

Figure 1.15. Loss of Nf1 impacts many signalling pathways

Scheme displays intracellular pathways that are deregulated upon loss of Nf1 in SCs. The loss of Nf1 is affecting signalling pathways that are dependent on Ras signalling such as MAPK and PI3K but also other pathways are deregulated such as calcium signalling pathways.

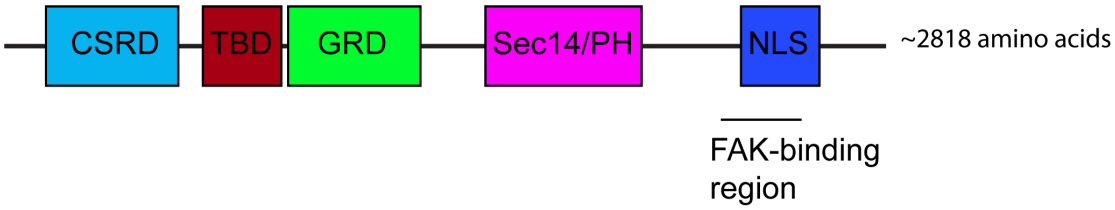

Figure 1.16. Schematic representation of neurofibromin domains
Many domains have been identified within the neurofibromin sequence, some of which are more studied than others. These domains encompass a cysteine/serine rich domain (CSRD), tubulin-binding domain (TBD), a GAP related domain (GRD), a Sec14 homology domain (Sec14), a pleckstrin homology domain (PH), a nuclear localization sequence (NLS) and a FAK interacting domain. The GRD domain defines Nf1 function, as it decreases Ras signalling through stimulation of the intrinsic GTPase activity of Ras.

expression is rapidly degraded due to the activation of receptor tyrosine kinases and G-protein coupled receptors (Cichowski et al., 2003). The rapid degradation of neurofibromin is mediated by the ubiquitin degradation machinery and appears independent of Ras downstream pathways as MEK and PI3K inhibitors did not prevent neurofibromin degradation. Degradation of neurofibromin is instrumental to achieve the maximal activation of Ras and was shown to be dependent on growth factor concentration. Consequently, lowering growth factor concentration correlated with incomplete neurofibromin degradation and lower levels of Ras-GTP. Following neurofibromin degradation, neurofibromin expression levels are rapidly re-elevated and this was shown to correlate with downregulation of Ras activation. In Nf1-deficient cells, Ras-GTP levels were sustained and the levels of Ras-GTP were independent of growth factor concentration. This appears to make Nf1-deficient cells more sensitive to growth factor stimulation as they proliferate in concentrations that were non-mitogenic for Nf1 WT cells. Overall, neurofibromin appears to regulate both the levels of activation of Ras and the duration of its activation.

Loss of Nf1 is linked to malignancy by allowing hyperactivation of the Ras signalling pathway (Basu et al., 1992; Cichowski and Jacks, 2001; DeClue et al., 1992; Kim et al., 1995) (Figure 1.15). Importantly, elevated levels of activated Ras-GTP were found in $Nf1^{-/-}$ SCs isolated from neurofibromas and MPNSTs (Cichowski and Jacks, 2001; Sherman et al., 2000) and maintaining high Ras-GTP levels were demonstrated to be crucial to maintain the transformed phenotype (Basu et al., 1992; DeClue et al., 1992; Kim et al., 1997; Kim et al., 1995).

Furthermore, the loss of Nf1 was shown to impact other signalling pathways other than the ERK signalling pathway. For example, neurofibromin regulates intracellular cAMP levels, so that loss of Nf1 increased cAMP levels in SCs (Kim et al., 2001). Recently, it was shown that cAMP regulation by neurofibromin is not mediated by downstream signalling to MEK or AKT, but by protein kinase C zeta, resulting in $G\alpha$ inactivation and a subsequent increase in cAMP levels (Anastasaki and Gutmann, 2014). Moreover, deregulated calcium signalling was observed upon loss of Nf1 in MPNST cell lines, however the mechanism with which neurofibromin regulates intracellular calcium levels have not been identified yet (Dang and DeVries, 2005) (Figure 1.15).

1.3.4. Ras effector pathways

Many different extracellular stimuli can activate Ras signalling such as growth factors, cytokines, hormones and neurotransmitters (Pylayeva-Gupta et al., 2011; Simanshu et al., 2017). The binding of these extracellular stimuli to receptors on the membrane such as tyrosine kinases receptors (eg. EGFR), G-protein coupled receptors, cytokine receptors and ECM receptors leads to receptor activation and downstream signalling to several adaptor proteins, which then ultimately results in activation of Ras. Activated Ras (Ras-GTP) interacts with and activates multiple downstream effector pathways such as the Raf/MEK/ERK, phosphatidylinositol 3'kinase (PI3K) and Ral guanine dissociation stimulator (RalGDS), that control cell proliferation, migration, cell differentiation and survival (Schubbert et al., 2007) (Figure 1.17). Constitutively active mutations in Ras are frequently associated with human cancers (Downward, 2003; Weiss et al., 1999). Activating point mutations in Ras are found in about 20% of all human tumours and most of these mutations abrogate interactions with Ras-GAPs and thereby cause the accumulation of the GTP-bound active form of Ras (Bos, 1989).

The Ras/Raf/ERK pathway is arguably the best characterised Ras effector pathway (Repasky et al., 2004) and deregulation of the Ras/Raf/ERK pathway is frequently observed in cancer cells and its uncontrolled or maintained activation is associated with uncontrolled cell proliferation. Activation of Ras initiates a kinase cascade that ultimately results in the activation of ERK (Figure 1.17). Raf is a serine/ threonine kinase that is directly activated by Ras (Rapp et al., 1983). GTP- bound Ras binds to Raf kinase, which in turn relocates to the plasma membrane. The relocation of cytosolic Raf kinase is critical for its function, as other proteins contribute to the activation of Raf at the plasma membrane (Leevers et al., 1994; Marais et al., 1995). Activated Raf then phosphorylates and activates the mitogen-activated protein kinase kinases 1 and 2 (MEK1 and MEK2), which are dual specificity kinases that phosphorylate and activate the mitogen activated protein kinases (MAPKs) ERK1 and ERK2. ERK phosphorylates and activates several cytosolic proteins and/ or it can translocate into the nucleus, where it regulates transcription by phosphorylating transcription factors such as c-JUN and the ETS family of transcription factors including ELK1. ELK1 is a component of the

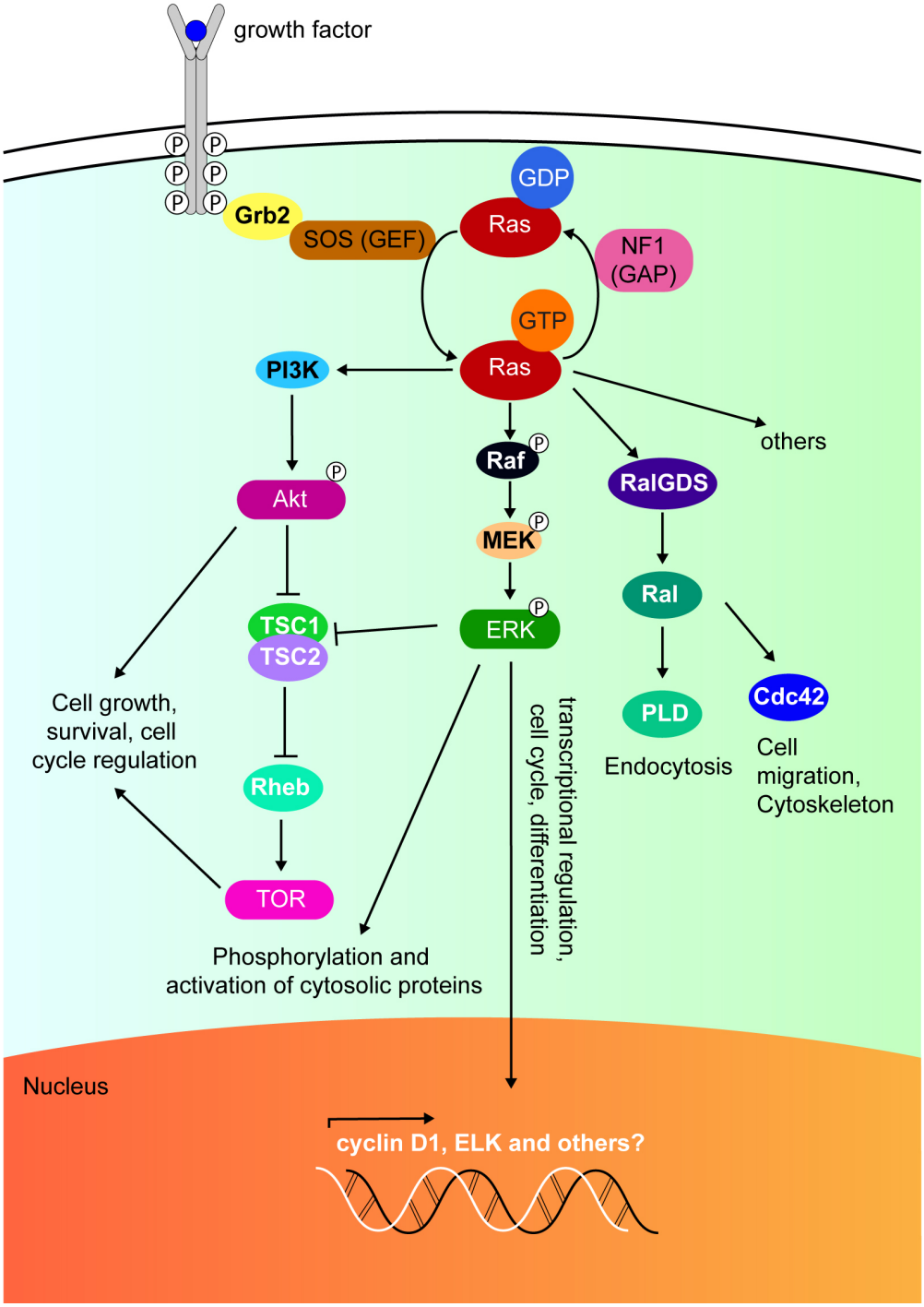

Figure 1.17. Ras activation and downstream effector pathways

Scheme depicts activation of Ras and its downstream effector pathways following growth factor stimulation. Growth factors bind receptor tyrosine kinases (RTKs) and RTK activation results into activation of Ras via adaptor proteins (eg. Grb2). Adaptor proteins interact which Ras-GEFs, the positive regulators of Ras (eg. Sos), which accelerate the conversion of Ras-GTP into the active form of Ras-GTP. Nf1, as a negative regulator of Ras signalling, stimulates the intrinsic GTPase activity of Ras and promotes the conversion of Ras-GTP into Ras-GDP. Activated Ras regulates and interacts with many other effector pathways such as PI3K to transmit signals to cytoplasmic and nuclear targets. The best characterised Ras effector pathway is the Ras/Raf/ERK signalling pathway which ultimately results into activation of ERK.

Serum Response Factor that regulates the expression of FOS, which together with c-JUN forms the AP1 early response transcription factor. Activation of these transcription factors can lead to the expression of proteins involved in cell cycle regulation such as cyclin D1, which in turn enables the cell to progress through the G1 phase of the cell cycle (Pruitt and Der, 2001; Schubbert et al., 2007) (Figure 1.17).

The activation of the Ras/Raf/ERK pathway can cause opposing effects in the same cells depending on the duration and level of the signalling (Marshall, 1995). For example, the activation of this pathway can cause contrary effects in SCs. On one hand Ras/Raf/ERK signalling mediates SC differentiation during development (Newbern et al., 2011), but on the other hand the activation of this pathway in adult SCs drives SC dedifferentiation and proliferation (Harrisingh et al., 2004) with high levels of ERK associated with SC dedifferentiation at very early timepoints and lower levels with SC proliferation at later timepoints following injury.

Beside the activation of the Ras/Raf/ERK signalling pathway, Ras has been shown to activate several other effector pathways such as phosphaditylinositol 3-kinases (PI3K) (Figure 1.17). Ras-GTP directly interacts with the p110α subunit of PI3K, which results in activation of the kinase due to its relocation to the plasma membrane and conformational changes (Castellano and Downward, 2011; Rodriguez-Viciana et al., 1994). PI3K then phosphorylates phosphaditylinositol 4,5- biphosphate to generate phosphaditylinositol-3,4,5 triphosphate (Pylayeva-Gupta et al., 2011; Simanshu et al., 2017). PIP3 binds to many proteins through its pleckstrin homology domain and other domains and thereby regulates the activity of downstream effectors such as 3-phosphoinositide dependent protein kinase (PDK1) and AKT (Bader and Vogt, 2005). AKT can also be activated by PDK1 and is known as mediator of the survival signal downstream of Ras by inactivating several pro-apoptotic proteins such as BAD (Khwaja et al., 1997; Vivanco and Sawyers, 2002). Moreover, AKT activation is known to initiate TOR signalling by inactivating the TOR tuberous sclerosis complex (TSC), which negatively regulates TOR activation (Figure 1.17). Importantly, constitutive activation of TOR is found in *Nf1*$^{-/-}$ SCs and in human neurofibromas (Johannessen et al., 2005) and strikingly treatment with the TOR inhibitor rapamycin led to suppression of tumour growth in a mouse

model of malignant peripheral nerve sheath tumours (MPNSTs) (Johannessen et al., 2008). In addition to AKT, ERK phosphorylates and inactivates TSC (Ma et al., 2005) and it remains to be clarified, if the high levels of mTOR signalling are due to increased signalling through the PI3K or the Ras/Raf/ERK pathway in the absence of *Nf1*. In addition, to the Ras downstream signalling pathways that are discussed here, Ras activates many other effector proteins such as RAS-related RAL proteins (Albright et al., 1993; Ferro and Trabalzini, 2010). Both the loss of Nf1 and activating mutations in Ras lead to aberrant activation of Ras, however the downstream effects are not identical. Whilst activating mutations in Ras render Ras independent of upstream signalling and non-responsive to GAPs, Nf1-deficient cells still depend on upstream activators of Ras signalling and other Ras GAPs, such as p120GAP, might partially compensate the loss of Nf1 and decrease Ras signalling (Brightman and Fell, 2000; Holt et al., 1996). These differences likely explain the increased tumourigenic capacity of Ras activating mutations opposed to the loss of Nf1.

1.4. Mouse models of neurofibromatosis type I

It is well established that neurofibromas arise from SCs (Serra et al., 2000), which have lost the second *Nf1* allele. However, whilst several studies in mice have shown that both SC precursor cells (Parrinello and Lloyd, 2009) and adult SCs (Ribeiro et al., 2013) can initiate neurofibroma formation, it is unclear which cell type within the SC lineage undergoes loss of Nf1 in human tumours. In the next section, I discuss mouse models that were initially developed to study the effect of loss of Nf1 and those that helped to shed a light on the ability of cells within the SC lineage to act as the cell of origin for neurofibromas. Although none of the transgenic mouse models of Neurofibromatosis Type I truly mimic the human disease, each of them contributed to our understanding of possible mechanisms of tumour formation in NF1.

1.4.1. Germline knockout of *Nf1*

To study the role of Nf1 in development and disease, mice were created, which carry a null mutation at the *Nf1* locus. The point mutation was introduced in exon 31 (Brannan et al.,

1994; Jacks et al., 1994) and importantly mutations in this exon are frequently found in NF1 patients (Cawthon 1990). *Nf1*$^{-/-}$ mice die in utero at E13.5 as a result of delayed and abnormal cardiac development, accompanied by severe cardiac dysfunction. However, in contrast to the cardiac abnormalities that arise in homozygous mice, only a few NF1 patients develop congenital heart disease (Brannan et al., 1994; Jacks et al., 1994; Lakkis and Epstein, 1998). This discrepancy is very likely due to that human are heterozygous for *Nf1*. Germline knockout of *Nf1* also resulted in a developmental delayed hypoplasia in other organs such as the liver (Brannan et al., 1994; Jacks et al., 1994).

Nf1$^{+/-}$ mice do not develop neurofibromas (Jacks et al., 1994). However, consistent with the role of Nf1 as a tumour suppressor, *Nf1* heterzygosity does increase the rate of tumourigenesis. It was demonstrated that 75% of *Nf1* heterozygous animals developed a wide spectrum of tumours that includes lymphomas, lung adenocarcinomas, hepatomas and fibrosarcomas over a period of 27 months. Moreover, *Nf1* heterozygous mice also developed tumour types such as neurofibrosarcoma and adrenal tumours that are found in NF1 patients. Consistent with the human disease, most of the these tumours showed loss of the wild type *Nf1* allele (Cichowski and Jacks, 2001).

Despite the predisposition for tumourigenesis, *Nf1* heterozygous mice did not develop the hallmark features of human NF1 and consequently do not provide an adequate model for the human disease (Jacks et al., 1994). However, *Nf1*$^{+/-}$ mice did develop other NF1 related symptoms such as learning disabilities, possibly as a result of increased ERK signalling in inhibitory neurons resulting in greater GABA release and long-term potentiation (Costa et al., 2002; Cui et al., 2008; Silva et al., 1997). Strikingly, genetic or pharmalogical inhibition of ERK rescued the learning defects (Costa et al., 2002).

The isolation of *Nf1*-deficient SCs, prior to embryonic death in utero, allowed the demonstration that they had elevated levels Ras activity (Kim et al., 1997; Kim et al., 1995) and additionally *Nf1*-deficient SCs exhibited functional abnormalities such as enhanced angiogenic and invasive properties (Muir, 1995; Sheela et al., 1990), which are known characteristics of cancer cells. However, *Nf1*-deficient SCs proliferated less in response to the mitogenic signal NRG1 or axonal contact (Kim et al., 1995), which is consistent with high

levels of Ras signalling causing cell cycle arrest in primary cells (Lloyd et al., 1997; Mathon and Lloyd, 2001; Ridley et al., 1988; Serrano et al., 1997). Later studies showed that loss of *Nf1* induced oncogene induced senescence (OIS) in SCs *in vitro* and *in vivo*, which can only be overcome by additional genetic mutations in the p53 or Rb signalling pathways (Courtois-Cox et al., 2006; Mathon and Lloyd, 2001; McGillicuddy et al., 2009; Zhu et al., 2005). Strikingly, cAMP mediated PKA activation induces hyperproliferation in *Nf1*-deficient SCs demonstrating that $Nf1^{-/-}$ SC behavior can be altered by factors from the microenvironment (Kim et al., 2001).

Overall, the benign characteristic of neurofibromas may be due to senescence induction of *Nf1*-deficient SCs (Courtois-Cox et al., 2006) but importantly, senescence induction seems to be a temporal effect, which can be influenced by additional signals from the microenvironment and/or additional genetic mutations (Cichowski et al., 1999).

1.4.2. *Nf1* chimeric mice

The *Nf1* chimeric mouse model is partially composed of $Nf1^{-/-}$ cells and was generated to test whether loss of the second *Nf1* allele is sufficient for the formation of neurofibromas in $Nf1^{+/-}$ mice (Cichowski et al., 1999). Mice with moderate chimerism exhibited frequent myelodysplasia and progressive neuromotor defects and importantly, all of these mice developed neurofibromas. The tumours generally emanated from the dorsal root ganglia and several tumours were found per mouse. However, no dermal neurofibomas, which are very common in NF1 patients, were detected. In contrast, plexiform neurofibromas developed in the *Nf1* chimeric mice. Mice with a low chimerism (~15%) did not develop neurofibromas demonstrating that the number of $Nf1^{-/-}$ cells is rate-limiting and that loss of the second allele is needed to initiate tumour formation.

It is thought that loss of the second Nf1 allele occurs rarely in mice compared to humans and explains the absence of neurofibroma development in the $Nf1^{+/-}$ mouse model. It was hypothesised that the frequency of the loss of the second Nf1 allele might differ between humans and mice because of interspecies differences in target cell number, lifespan and the mutational propensity of the *Nf1* locus, but this remains to be clarified (Cichowski et al., 1999).

Overall, the tumours exhibited many similarities to human neurofibromas, such as the presence of perineurial-like cells within the tumour mass demonstrating that chimeras provide an adequate model for the disease (Cichowski et al., 1999).

1.4.3. Loss of *Nf1* in neural crest stem cells

In recent years, a small subset of cells have been isolated from tumours and identified as stem-cell like cells that possess an unlimited capacity to self-renew and to differentiate into all cell types within the tumour (Pardal et al., 2003; Reya et al., 2001). Their self-renewal capacity made these cells ideal candidates as the cell of origin for tumourigenesis, as the classic multistep model of carcinogenesis postulates that tumour initiation requires a long living cell in which multiple genetic lesions can occur (Kreso and Dick, 2014; Nguyen et al., 2012).

Cells with stem-like properties have been identified as possible tumour initiating cells in brain tumours (Singh et al., 2004) and recently a cancer stem cell population has been isolated from NF1-associated low grade gliomas (astrocytomas) (Chen et al., 2015). However, the contribution of this cancer stem cell-like population to astrocytoma formation is not yet known, although it is hypothesised that they may be contribute to the differential drug responses observed in NF1 patients (Chen et al., 2015; Lee et al., 2010).

Initially, it was believed that the loss of Nf1 in astroglial progenitor cells was sufficient for the development of NF1-associated low grade gliomas (astrocytomas) in the CNS (Bajenaru et al., 2002). However, the conditional loss of Nf1 in astrocyte progenitor cells did not results in CNS tumour formation, implying that other factors are required. Interestingly, it was shown that astrocytoma formation requires both the loss of Nf1 in astroglial progenitor cells and reduced Nf1 expression ($Nf1^{+/-}$) in non-neoplastic cells (eg. Stromal cells) (Bajenaru et al., 2003). Due to the abundance of microglia (resident immune cells of the brain) within NF1-associated astrocytomas it was hypothesised that these cells were likely the Nf1 heterozygous cell population that contributes to tumour formation (Bajenaru et al., 2005; Watters et al., 2005). In line with this, recent studies demonstrated that both the genetic inactivation and the pharmalogical inhibition of microglia reduced NF1-associated

astrocytoma formation in mice (Daginakatte et al., 2008; Daginakatte and Gutmann, 2007; Simmons et al., 2011). Importantly, these studies emphasise the importance of the tumour microenvironment, which will be further discussed below.

In contrast to the CNS, the origin of PNS tumours is not known. In the gut, neural crest stem cells (NCSCs) persist into adulthood (Kruger et al., 2002). However, in all other regions of the PNS, NCSCs have not been found postnatally as they terminally differentiate during embryogenesis (Kruger et al., 2002). NCSCs were considered as a potential cell of origin of neurofibromas, because it was suggested that deletion of *Nf1* in embryonic NCSCs may result in their continuous expansion and postnatal persistence, which may enable them to give rise to neurofibromas in the adult nerve. Studies addressed the impact of *Nf1* loss in NCSCs and showed that, although *Nf1*-deficient NCSCs showed increased proliferation, gliogenesis and self-renewal *in vitro*, the loss of *Nf1* in neural crest cells did not induce neurofibroma formation *in vivo* (Joseph et al., 2008). Joseph et al demonstrated that although the loss of *Nf1* in NCSCs increased NCSCs frequency during mid-gestation, their numbers declined progressively during late gestation and *Nf1*-deficient NCSCs did not persist postnatally in the sciatic nerve, DRGs and sympathetic ganglia into adulthood. These findings suggest that *N1*-deficient NCSCs differentiate in a similar manner to WT NCSCs during late gestation. Furthermore, Joseph et al failed to isolate $Nf1^{-/-}$ NCSCs from neurofibromas and the engraftment of E13 $Nf1^{-/-}$ NCSCs did not lead to neurofibroma formation in $Nf1^{+/-}$ animals (Joseph et al., 2008). Overall, these studies indicate that loss of *Nf1* in neural crest cells does not render them tumourigenic and suggests that more differentiated SCs are likely the cell of origin of neurofibromas.

1.4.4. P0A-Cre:$Nf1^{fl/-}$ mouse model

The P0-promoter drives the inactivation of *Nf1* at E12.5 in SCPs during nerve development (Zheng et al., 2008). This mouse model develops neurofibromas in adult nerve trunks in old age with 70% of the mice developing plexiform neurofibromas, which have clinical presentations similar to the human disease such as the appearance of elongated spindle shaped cells and infiltrating mast cells in a collagenous matrix. Importantly, Zheng et al.

demonstrated that, *Nf1*$^{-/-}$ SCPs developed normally and there was no persistence of stem/progenitor cells in adulthood. The only phenotypic abnormality, prior to tumour formation, was the presence of a subpopulation of Remak bundles with a Schwann cell "pocket defect", which probably derives from a failure in the axonal segregation process. This Remak-phenotype resembles mice with a targeted mutation in NRG1 type III (Taveggia et al., 2005), which may suggest that Nf1 is acting on the NRG1/ErbB2/3 signalling pathway at this stage of development. These abnormal Remak bundle progressively degenerate and dissociate from the axons and ultimately develop into smaller abnormal Remak bundles with less axons per Remak bundle. Finally, several abnormal Remak bundles, which contained dissociated SCs, were observed and SCs devoid of any axonal contact could also be found within these nerves and some of them seemed to ensheath collagen fibers. In summary, Zheng et al. postulated that an abnormal nmSC population was likely responsible for neurofibroma initiation (Zheng et al., 2008).

1.4.5. Dhh-Cre:Nf1$^{fl/fl}$ mouse model

The Desert Hedgehoc (Dhh) driver leads to loss of *Nf1* at E12.5 in both boundary cap cells and SCPs but not in neural crest cells, neurons or in the CNS (Wu et al., 2008). As described earlier, boundary cap cells do not contribute to the formation of the spinal nerve trunks, but these cells differentiate into the SCs of the ventral and dorsal roots. The loss of *Nf1* at E12.5 in SC precursors gave rise to plexiform neurofibromas, neurofibromas in peripheral nerve roots and hyperplasia in nerve trunks. These tumours formed very rapidly and exhibited high morbidity and mortality by 15 months of age. In contrast to the P0A-Cre and Krox-20-Cre Nf1$^{fl/-}$mouse model, dermal neurofibromas were observed and their number increased with the age of the animals.

The location and the rapid development of these tumours suggested that boundary cap cells were the cell of origin, opposed to a SC precursor cell. Although no neoplastic lesions were found in Dhh-Cre:Nf1$^{fl/fl}$ sciatic nerves, examination of the nerve demonstrated hyperplasia with disrupted Schwann cell-axon interactions within Remak bundles. Interestingly, these observations are similar to the first neoplastic events detected in the P0A-Cre mice that

develop tumours in old age, making it likely that if the Dhh-Cre:Nf1$^{fl/fl}$ mice survived longer, they would also develop neurofibromas in peripheral nerves.

Overall, both Dhh-Cre and P0A-Cre mouse models emphasise the importance of the disruptions of Schwann cell-axon interactions as a key event in neurofibroma formation and also suggest that tumour initiation can occur during development. Importantly, both mouse models show that despite of loss of Nf1 in the SC lineage the vast majority of the SCs developed normally.

1.4.6. Krox20-Cre:Nf1$^{fl/-}$ mouse model

The Krox-20 mouse model induces the loss of *Nf1* at E10.5 in boundary cap cells and at E15.5 in immature SCs. However, the loss of Nf1 in the SC lineage is required but is not sufficient to induce tumour formation in this mouse model (Zhu et al., 2002). Strikingly, neurofibromas only developed in a *Nf1*$^{+/-}$ background and neurofibroma formation was shown to be dependent on interactions between Nf1$^{-/-}$ SCs and Nf1$^{+/-}$ cell types in the tumour microenvironment. Later studies then showed that c-kit signalling in Nf1$^{+/-}$ mast cells was necessary for neurofibroma development in this mouse model (Yang et al., 2008a). These studies demonstrated for the first time the contribution of the tumour microenvironment in neurofibroma formation.

Furthermore, these mice only developed multiple neurofibromas in cranial nerves or spinal nerve roots but not within the sciatic nerve at 15 months of age. Although no neurofibromas were observed within the sciatic nerve, microscopic regions of hyperplasia were found. Comparing the Krox20-Cre:Nf1$^{fl/-}$ with the P0A-Cre:Nf1$^{fl/-}$ and Dhh-Cre:Nf1$^{fl/fl}$ mouse models led to the conclusion that the timing of *Nf1* loss is important and suggested that to induce neurofibromas, *Nf1* loss needed to occur at the earlier SCP stage. This may partially explain why neurofibromas develop in the absence of an *Nf1*$^{+/-}$ background in both Dhh-Cre:Nf1$^{fl/fl}$ and P0A-Cre:Nf1$^{fl/-}$ mouse models, as it could be that the *Nf1*$^{+/-}$ background is required to compensate for the fewer numbers of *Nf1*$^{-/-}$ SCPs in the Krox-20 mouse model.

1.4.7. Conclusions drawn from Nf1 mouse models

Together these studies suggest that an important cell of origin for neurofibromas is the transient SC lineage progenitor cell that undergoes loss of Nf1 during development. However, while these cells go on to form tumours, the majority of *Nf1*$^{-/-}$ SC precursor cells differentiated normally and generated normal proportions of both nmSCs and mSCs, implying that in absence of Nf1 the Ras/Raf/ERK signalling pathway may be regulated by additional mechanisms to ensure appropriate levels of ERK activation in order to allow SC differentiation during development. Although SC development appeared normal, Nf1 mutant nerves often exhibited axonal segregation failures within Remak bundles that progressively disintegrated and led to neurofibroma formation at an older age (Wu et al., 2008; Zheng et al., 2008).

Importantly, it seems like that the timing of *Nf1* loss is a key event for neurofibroma formation, as neurofibroma development within a peripheral nerve requires the inactivation of *Nf1* at the late SC precursor- early immature SC stage (E12-E13). Consistent with this, tumours did not form in the Krox-20-Cre:Nf1$^{fl/fl}$ mouse model, in which Krox-20 expression induces the loss of Nf1 at E15.5. Consequently, it was hypothesised that the loss of Nf1 at this later timepoint leads to lower numbers of Nf1-deficient SCs suggesting that tumour formation requires the contribution of Nf1$^{+/-}$ mast cells in this model (Zhu et al., 2002) (Figure 1.18). Additionally, the comparison of the Krox20-Cre:Nf1$^{fl/-}$, P0A-Cre:Nf1$^{fl/-}$ and Dhh-Cre:Nf1$^{fl/fl}$ mouse models led to the hypothesis that *Nf1* loss in boundary cap cells at E10.5 can induce neurofibroma formation in the nerve roots, whereas *Nf1* loss in SC-precursors cells at E12.5 can drive neurofibroma formation in the nerve trunks.

These findings could partially explain the broad clinical manifestations of the disease in Nf1 patients, especially among members of the same family (Parrinello and Lloyd, 2009). For example, affected siblings often have different clinical manifestations with one sibling developing multiple neurofibromas whereas the other only a few (Carey et al., 1979; Friedman, 1999; Rieley et al., 2011). Consequently, it was speculated that the somatic inactivation of the second allele of Nf1 occurred earlier in the sibling with the more severe symptoms and therefore affected a larger number of SCs, whereas in the sibling that

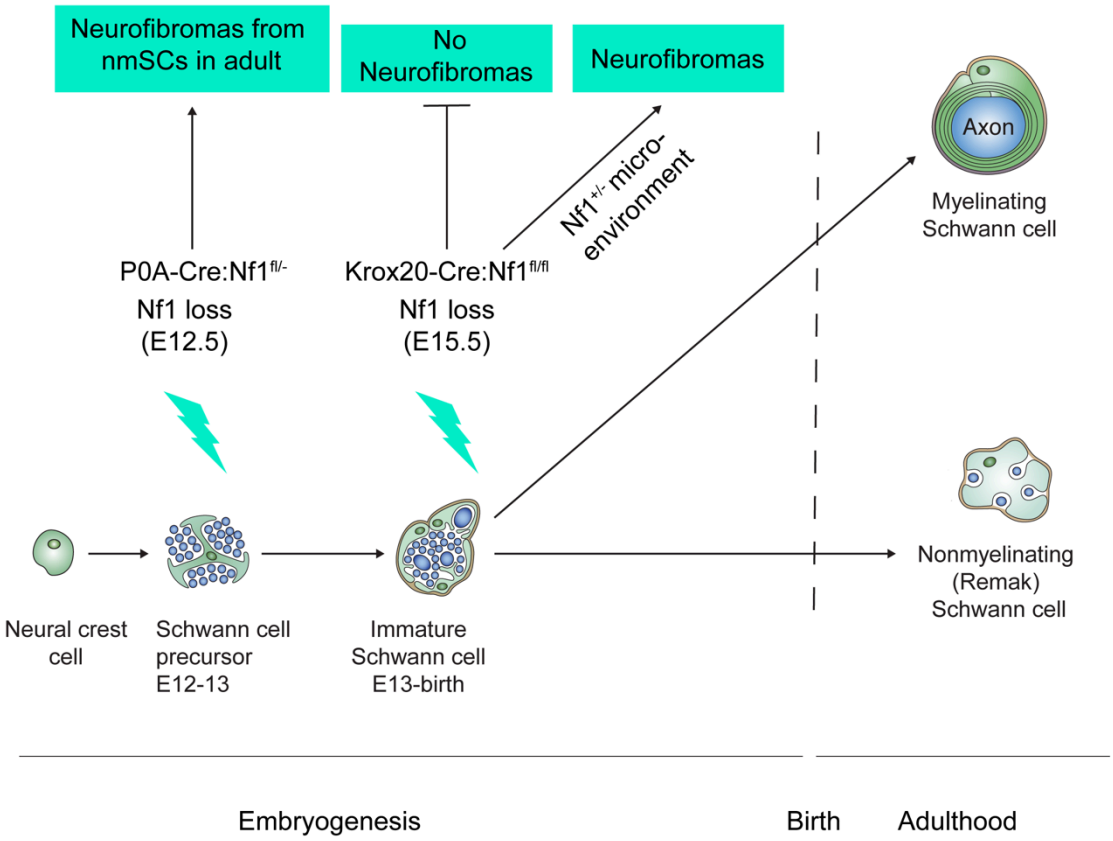

Figure 1.18. Timing of Nf1 loss in Schwann cell precursors is critical for neurofibroma development in peripheral nerve trunks

Scheme displays the timeframe of SC development and the transient SC precursor cells that originate from neural crest cells. Furthermore, this scheme indicates neurofibroma development from transient $Nf1^{-/-}$ SC precursor cells within the sciatic nerve. Neurofibroma formation requires the loss of Nf1 at the late precursor/ early immature SC stage (E12-13 in sciatic nerve), as highlighted in the scheme. Loss of Nf1 in immature SCs at a later stage is not sufficient to induce neurofibroma formation and requires the contribution of the microenvironment. Figure adapted from (Parrinello and Lloyd, 2009).

exhibited less severe symptoms, the loss of the second Nf1 allele occurred later (Parrinello and Lloyd, 2009).

In addition, the broad clinical manifestations may also be caused by modifying genes (Easton et al., 1993; Rieley et al., 2011; Sabbagh et al., 2009). Recently, SUZ12, which is a component of the polycomb repressive complex, has been identified as a modifying gene in NF1 patients. This gene was discovered in NF1 patients that carry large germline deletions of *Nf1* and exhibit a fourfold increased risk of malignancies (De Raedt et al., 2014). Further studies then showed that loss of SUZ12 increased the risk of malignant progression of NF1, demonstrating that it acts as a cooperating tumour suppressor (De Raedt et al., 2014; Lee et al., 2014; Zhang et al., 2014b).

Mechanistically, it was shown that the loss of SUZ12 potentiates Ras driven transcription indicating a potential mechanistic link between loss of SUZ12 and Nf1, which may provide a new therapeutic strategy for NF1. Moreover, further supporting the role of modifying genes in NF1 are studies that reported race and gender specific differences in the clinical manifestation of NF1 (Diggs-Andrews et al., 2014; Ratner and Miller, 2015; Zhang et al., 2014b).

The studies using Dhh-Cre and P0A-Cre:$Nf1^{fl/fl}$ mice also underline the importance of the loss of SC-axonal interactions at the onset of neurofibroma formation. As explained above, axonal signals control SC survival, proliferation and differentiation during SC development and likely maintain SC differentiation and function in the adult nerve (Chan et al., 2006; Corfas et al., 2004; Michailov et al., 2004; Taveggia et al., 2005). Consistent with the importance of SC-axonal interactions during development, previous studies demonstrated that the loss of SC-axon interactions can results in neuropathy and the majority of SCs within neurofibromas are found devoid of axonal contact (Corfas et al., 2004).

A study from the Lloyd lab has provided mechanistic insight in SC-axonal dissociation (Parrinello et al., 2008). This study demonstrated that the loss of Nf1 in primary SCs led to SC dissociation from the axons *in vitro* and mechanistically we showed that axonal dissociation is due to Ras-Raf-ERK dependent downregulation of semaphorin 4F (Sema4F), which is expressed on the SC surface. Interestingly, Sema4F expression is detectable in adult nerves

in *vivo* but is strongly downregulated in neurofibromas. Moreover, in established SC-axon co-cultures, SCs associated with axons, do not proliferate in response to mitogen stimulation, but strikingly the loss of Nf1 renders SCs susceptible to the stimulation with mitogens and induces them to proliferate. Importantly, in the absence of serum, $Nf1^{-/-}$ SCs did not proliferate demonstrating that Sema4F does not have a direct impact on the cell cycle but rather induces proliferation indirectly by triggering SC-axon dissociation. Our findings confirm the anti-proliferative impact of axons on SCs and also demonstrate that these anti-proliferative axonal signals seem to be dominant over pro- environmental mitogenic stimulation. Furthermore, we demonstrated the potential impact of axonal- SC dissociation at the onset of tumourigenesis, as it renders SC more responsive to pro-proliferative stimuli from the environment.

1.4.8. Mouse model of dermal neurofibromas

Many mouse models, which develop plexiform neurofibromas such as Krox20-Cre:$Nf1^{fl/-}$ and P0A-Cre, fail to develop dermal neurofibromas and consequently it was argued that dermal and plexiform neurofibromas originate from a different cell type. Subsequently, it was hypothesised that dermal neurofibromas derive from adult tissue stem cells, as these increase in numbers during adolescence. Skin-derived progenitors (SKPs), which are neural crest-like stem cells present in both human and mouse dermis, have been suggested as a potential cell of origin of dermal neurofibromas, as SKPs possess a certain pluripotency and can differentiate into glial, neuronal and melanocytic cell lineages (Fernandes et al., 2006; Fernandes et al., 2008; McKenzie et al., 2006; Toma et al., 2001; Toma et al., 2005). Moreover, the loss of Nf1 in SKPs can lead to plexiform and dermal neurofibroma development (Le et al., 2009). Isolated SKPs from CMV-CreER:$Nf1^{fl/-}$ mice were treated to recombine *Nf1 in vitro* and then re-transplanted. The *Nf1*-deficient SKPs formed plexiform neurofibromas when implanted close to the nerve plexus. However, no formation of dermal neurofibromas was observed, when Nf1 deficient SKPs were implanted subcutaneously. Dermal neurofibroma formation was only observed in female mice that were pregnant at the time of Nf1-deficient SKPs implantation indicating a critical contribution of the hormonal milieu to tumour formation. To address whether endogenous SKPs formed dermal neurofibromas in

situ, the authors induced loss of *Nf1* in SKPs by topical tamoxifen administration *in vivo*. Dermal neurofibroma formation was observed, however these tumours developed with a latency period of 7-8 months indicating that additional microenvironmental cues are required for tumour formation. Importantly, as topical tamoxifen administration would induce loss of *Nf1* in all cell types in the skin, including SCs, it cannot be concluded, that SKPs are the cell type of origin of dermal neurofibromas (Le et al., 2009).

1.4.9. Mouse models of malignant peripheral nerve sheath (MPNST) tumours

In humans, MPNSTs frequently arise in the context of plexiform neurofibromas but can also arise sporadically with no obvious precursor lesion (Evans et al., 2002; Ferner and Gutmann, 2002; Tucker et al., 2005; Widemann, 2009). NF1 patients are predisposed for MPNST formation (8-13%) and the 5-year survival rate (both sporadic or NF1 derived MPNST) is poor (42% and 21% respectively). In mouse models, malignant tumours only rarely develop from pre-existing plexiform neurofibromas, which is possibly because mice that develop large plexiform neurofibromas have to be sacrified before the natural progression to MPNSTs can occur. In addition, the life-span of a mouse is significantly shorter compared to humans, indicating that the timeframe in which additional genetic mutations that are required for MPNST formation is shortened.

The most frequently mutated genes in MPNSTs are *p53* and the *CDKN2A* locus that encodes for both the Ink4a gene ($p16^{CDKN2A}$) and the Arf gene ($p19^{CDKN2A}$) tumour suppressors (Mantripragada et al., 2008; Rubin and Gutmann, 2005). Consequently, mouse models, which harbor mutations in these tumour suppressors in addition to Nf1 mutations, have been generated (Evans et al., 2002; Ferner and Gutmann, 2002; Riccardi, 1992b; Tucker et al., 2005; Widemann, 2009; Woodruff, 1999). Both the Ink4a/$Arf^{-/-}$/$Nf1^{+/-}$ and the $Nf1^{+/-}$/$p53^{+/-}$ mouse models develop GEM PNSTs, which are the counterpart of human MPNSTs and recapitulate the mutations in the human disease (Cichowski et al., 1999; Joseph et al., 2008; Vogel et al., 1999). Furthermore, it was shown that the mutation of *Ink4a* or *Arf* alone was not sufficient to induce tumour formation, suggesting that both p53 and Rb pathways need to be deregulated in order to trigger MPNST formation in the context of Nf1 heterozygosity (Joseph

et al., 2008; King et al., 2002). MPNSTs often arise in the context of pre-existing plexiform neurofibromas suggesting that additional mutations likely drive the malignant progression to MPNSTs. Multiple studies have investigated the role of p53 in this process and found a cooperative effect of the loss of Nf1 and p53 in MPNST formation that supports a causal role for p53 mutations in the malignant progression from plexiform neurofibromas to MPNSTs (Cichowski et al., 1999; Menon et al., 1990; Vogel et al., 1999).

In addition to loss of p53, overexpression of the EGFR was observed in many human MPNST tumours and in both human and mouse MPNST cell lines implying the potential involvement of the EGFR in MPNST formation (DeClue et al., 2000; Li et al., 2002; Perry et al., 2002). In line with this, a recent study demonstrated that overexpression of the EGFR in Nf1-deficient SCs was sufficient to drive MPNST progression in a mouse model of NF1. Moreover, EGFR overexpression was shown activate the JAK-STAT3 signalling pathway in Nf1-deficient SCs and inhibiting STAT3 resulted in delayed MPNST growth *in vivo*. This study demonstrated a critical role of the EGFR-STAT3 signalling pathway in the malignant progression of NF1 (Wu et al., 2014).

MPNSTs exhibit reduced expression of SC markers such as Sox10 and S100, but elevated expression of markers that are characteristic for migrating NCSCs such as Twist1 and Sox9, indicating that the loss of SC identity may be an important event for the progression of neurofibromas to MPNSTs (Joseph et al., 2008; Levy et al., 2004; Miller et al., 2009; Miller et al., 2006).

Recent studies also demonstrated an involvement of the CXCR4/CXCL12 signalling in MPNST progression (Mo et al., 2013). The receptor CXCR4 is enriched in *Nf1*-deficient MPNSTs, similarly to other tumours (Kijima et al., 2002; Koshiba et al., 2000; Laverdiere et al., 2005; Muller et al., 2001; Oh et al., 2001; Righi et al., 2011; Sehgal et al., 1998; Sengupta et al., 2012; Zhou et al., 2002) and is associated with a poor clinical outcome (Li et al., 2004; Wang et al., 2008). Strikingly, Mo et al. showed that CXCR4 inhibition decreased MPNST cell proliferation *in vitro* and MPNST tumour growth in *vivo* (Mo et al., 2013). Consequently, inhibiting CXCR4 signalling may provide a promising new therapeutic target for NF1-associated MPNSTs.

Therapeutic options for MPNSTs are very limited and surgical resection is the standard treatment but is often ineffective, as some tumours cannot be completely surgically resected and others exhibit high tumour recurrence and/or metastasis. Although a recent clinical study showed that inhibiting MEK decreased tumour volume in plexiform neurofibroma patients (Dombi et al., 2016) and targeting MEK was shown to decrease MPNST growth in mice (Jessen et al., 2013), single agent therapy against MEK was not successful for MPNST treatment. Similar to MEK, no beneficial effect was observed when inhibiting EGFR in MPNST patients (Albritton et al., 2006). Consequently, combination therapies have been tested and co-targeting MEK together with the TOR pathway has shown some initial success in MPNST mouse models (Watson et al., 2014). The identification of additional targets and broadening of the knowledge about the signals that determine neurofibroma progression to MPNSTs will be instrumental to improve the therapeutic approaches for MPNSTs in the future.

1.4.10. The P0-CreER^{T2}:R26RYFP:Nf1$^{fl/fl}$ mouse model

In P0-CreER^{T2} transgenic mice, the Cre recombinase is driven by the well characterised 1.1kb P0 rat promoter fused to the 5' untranslated region of the human connexin32 gene upstream of CreER^{T2} (Messing et al., 1992; Messing et al., 1994). The activity of the P0 promoter is confined to mSCs in adult mice and is not active in nmSCs (Messing et al., 1992). The P0-CreER^{T2} mice express a tamoxifen (tmx) inducible variant of Cre recombinase, in which Cre is fused to a mutated estrogen receptor ligand- binding domain (ER). The CreER^{T2} fusion protein is not able to bind the endogenous estrogen and instead binds to the synthetic ligand 4-hydroxy tamoxifen (4-OHT). Tmx is metabolized in the liver into active metabolites such as 4-OHT. In the absence of the ligand, the CreER^{T2} fusion protein is inactive as it is prevented from entering the nucleus due to binding to HSP90 (Nagy, 2000). Upon tmx administration, 4-OHT binds the CreER^{T2} fusion protein, HSP90 is released and CreER^{T2} enters the nucleus. Thus the CreER^{T2} recombinase under the myelin specific promoter permits recombination of a specific gene, at a defined timepoint in adult mSCs.

The Lloyd laboratory previously showed that activation of Ras is sufficient to cause fully dedifferentiated SCs to revert to a progenitor-like state and dissociate from axons. Therefore,

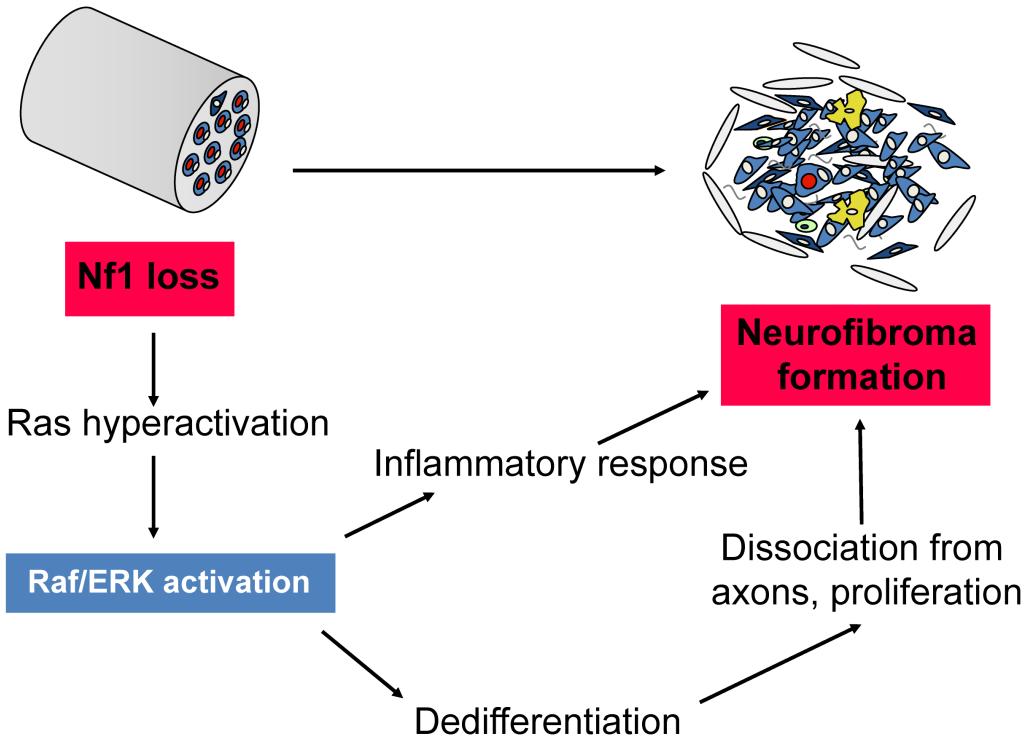

Figure 1.19. Neurofibroma formation upon loss of Nf1 in adult mSCs
Scheme displays the hypothetical neurofibroma formation upon loss of Nf1 in adult mSCs. The hypothesis was that the loss of Nf1 in adult mSCs will results in the hyperactivation of Ras, which in turn will trigger an inflammatory response and SC dedifferentiation and dissociation from axons. These downstream consequences mediated by the hyperactivation of the Ras signalling pathway would then ultimately lead to neurofibroma formation within peripheral nerve.

it was suggested that loss of Nf1 in SCs should be sufficient to drive the formation of neurofibromas (Napoli et al., 2012) (Figure 1.19). However, recent mouse models, which were designed to lose Nf1 in SCs during embryonic development, showed that this appeared not to be the case, as these mice developed structurally normal nerves (Joseph et al., 2008; Le et al., 2011; Wu et al., 2008; Zheng et al., 2008). Nevertheless, spontaneous tumour formation occurred in adulthood, suggesting that loss of Nf1 is not sufficient for tumour formation but requires, in addition, a triggering event in adulthood.

To investigate the acute loss of Nf1 in adult mSCs, the Lloyd laboratory developed a mouse-model that enables the deletion of Nf1 specifically in adult mSCs (Ribeiro et al., 2013). A tamoxifen- inducible Cre-line driven by the P0 promoter was crossed with mice containing an Nf1 floxed allele in both $Nf1^{+/+}$ and $Nf1^{+/-}$ backgrounds. Hence, Nf1 is floxed out upon treatment with tamoxifen, specifically in adult mSCs. These mice additionally express YFP in recombined cells, which allows the tracking of SCs that lack Nf1. Using this mouse model, the Lloyd laboratory was able to show that loss of Nf1 in adult mSCs was not sufficient to induce the activation of ERK in mSCs and consistent with this, no tumour formation was observed. This finding is in line with previous studies, as discussed above, and underline that neurofibroma formation requires an additional triggering event in adulthood. However, we found that after nerve injury, Nf1- deficient mSCs formed neurofibromas specifically at the wound site (Ribeiro et al., 2013). The frequency of tumor formation was independent of the genetic background, eliminating a role for Nf1 haploinsufficiency in this model. Remarkably, Nf1- deficient SCs redifferentiated normally in the distal stump in contrast to the tumorigenic behavior at the wound site. Consistent with this, activation of ERK appeared to be sustained at the wound site, whereas it is decreased seven days after injury in the distal stump.

Therefore, it was suggested that the normal nerve environment suppresses neurofibroma formation, whereas the injury site of the nerve converts to a tumour-promoting environment that fosters the development of neurofibromas. These findings suggested an essential role of the injury microenvironment that cooperates with loss of Nf1 to drive tumour formation.

1.5. The tumour microenvironment

The tumor microenvironment (TME) is complex, consisting of multiple cell types such as endothelial cells, pericytes, smooth muscle cells, fibroblasts, myofibroblasts, and immune cells such as macrophages and neutrophils (Mueller and Fusenig, 2004; Quail and Joyce, 2013). In addition, connective tissue surrounds the tumour and is composed of multiple cells and a specific ECM; the so called tumour matrix. The formation of the TME resembles a wound healing process in which immune cells, endothelial and mesenchymal cells are recruited to the site of injury (Dvorak, 1986; Mueller and Fusenig, 2004) (Figure 1.20).

The concept that the microenvironment of a developing tumour is a crucial regulator of carcinogenesis was originally proposed by Paget in his famous 'seed and soil' hypothesis (Langley and Fidler, 2011; Paget, 1989). However, for many years the scientific focus concentrated on identifying the molecular determinants of the cancer cell themselves, as tumourigenesis was originally defined as a multistep process during which cancer cells acquire multiple genetic alterations. Recently, the TME has been identified as an important contributor to tumor development and the importance of crosstalk between different cell types within a tumour and the surrounding tissue (the so called tumour stroma) has been recognised (Elenbaas and Weinberg, 2001; Tlsty and Coussens, 2006).

Importantly, recent studies revealed that bidirectional interactions between cancer cells and their microenvironment are critical for tumour formation and progression (Friedl and Alexander, 2011; Hanahan and Coussens, 2012; Hanahan and Weinberg, 2011; Joyce and Pollard, 2009; Quail and Joyce, 2013). Consistent with this, it was shown that the tumour microenvironment accommodates tumour growth by providing a permissive and supportive environment for tumour development and progression. On one hand, factors secreted from cancer cells (eg proteases, growth factors) can modulate the tumour microenvironment and induce angiogenesis, recruitment and activation of inflammatory and stromal cells (Bergers and Benjamin, 2003; Coussens and Werb, 2002; Manabe et al., 2003). On the other hand, cells in the tumour microenvironment undergo phenotypic changes such as shown with macrophages and fibroblasts, which convert into tumour-associated macrophages (TAMs) and cancer associated fibroblasts (CAFs)

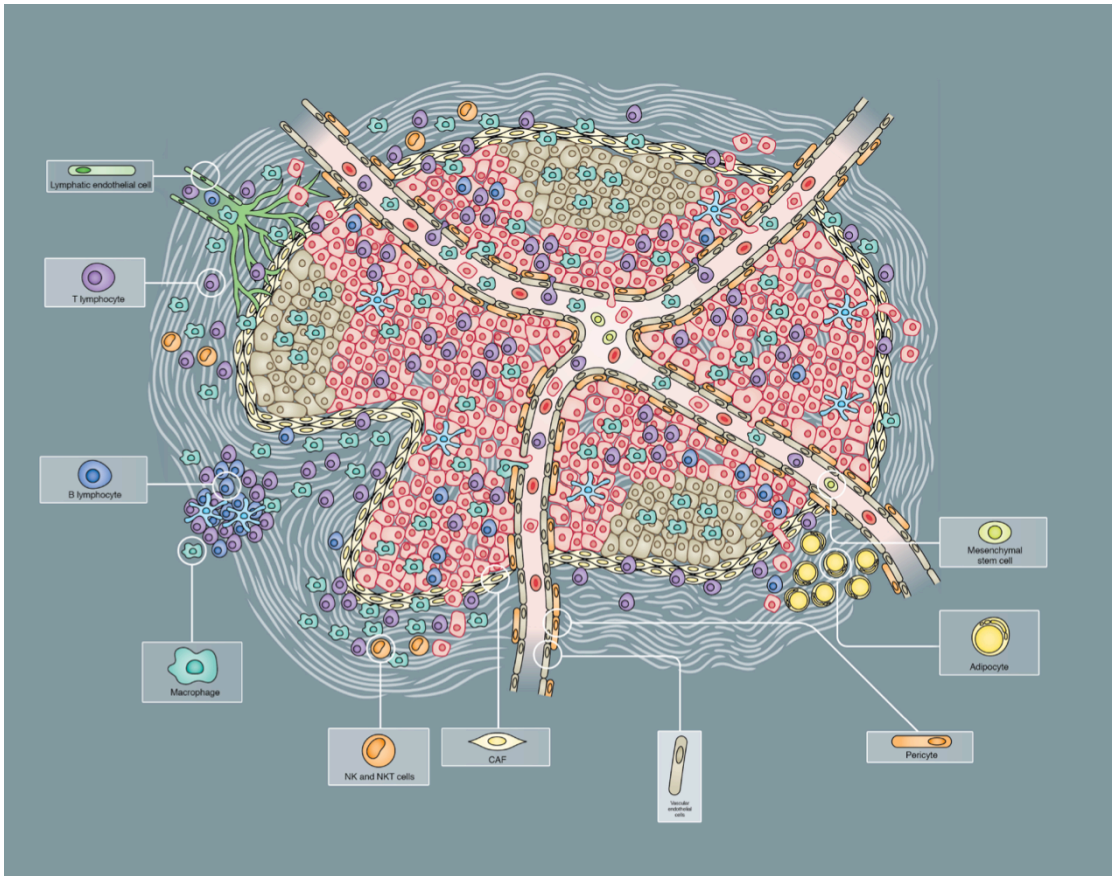

Figure 1.20. The tumour microenvironment
Illustration of the tumour microenvironment, which surrounds the tumour. The different cell types of the TME have been highlighted. Figure is adapted from (Balkwill et al., 2012).

(Condeelis and Pollard, 2006; De Wever and Mareel, 2003; Kalluri, 2016; Kalluri and Zeisberg, 2006). These activated cells then further contribute to the secretion of growth factors (eg. IGF and EGF) and proteases that sustain tumour growth, provide resistance to therapy and induce tumour cell invasion into surrounding tissue (Lin et al., 2008; Straussman et al., 2012; Vermeulen et al., 2010).

One of the earliest pieces of convincing evidence that support an important role for the tumour microenvironment was that many cancers arise in the context of chronic inflammation (~20%) and even cancers, which lack a causal role for chronic inflammation, possess an inflammatory microenvironment (Balkwill and Mantovani, 2001; Elinav et al., 2013; Grivennikov et al., 2010; Grivennikov and Karin, 2011; Mantovani et al., 2008; Martins-Green et al., 1994). This demonstrates an important link between cancer and inflammation that is now widely recognised (Coussens and Werb, 2002; Mantovani et al., 2008). In line with this, inflammatory cells within the tumour microenvironment have been shown to influence almost every aspect of carcinogenesis including the onset of cancer, tumour progression and metastasis (Grivennikov et al., 2010; Hanahan and Weinberg, 2011; Mantovani et al., 2008). For example, it is well documented that tumour associated macrophages contribute to malignant tumour progression by producing a wide range of signals such as cytokines (eg. ILs), growth factors (eg. EGF and TGFβ) and matrix-degrading enzymes (eg, matrix metalloproteases), that promote tumour angiogenesis and invasion (Wyckoff et al., 2007; Yang et al., 2008b).

Moreover, tumour angiogenenesis and the altered ECM are well known to promote tumour growth and may provide resistance to therapy (Bergers et al., 1999; Cox and Erler, 2011; Hanahan and Folkman, 1996; Lu et al., 2012). Furthermore, the tumour matrix can also influence the behavior of neighboring stromal cells and promote angiogenesis and inflammation (Pickup et al., 2014; Weis and Cheresh, 2011).

Targeting the TME could provide an alternative therapeutic approach for neoplasms, including neurofibroma (Joyce, 2005; Valkenburg et al., 2018). The TME provides an attractive target, as it is not as genetically unstable as cancer cells and is therefore less likely to develop drug resistance. Moreover, targeting the TME may complement existing treatment options and

remodeling of the TME may help to enhance drug delivery to the tumour. Consequently, approaches that target the TME have already been undertaken, with some showing initial success. For example, with acute myeloid leukemia and acute lymphoid leukemia cancer cell survival is supported by growth factors and chemokines (eg. CXCL12) of the bone marrow microenvironment. Targeting these factors within the TME has been promising, as inhibiting CXCR4 led to leukemia regression in mouse models (Burger and Peled, 2009; Nervi et al., 2009; Zeng et al., 2009; Zhang et al., 2012; Zhang et al., 2017) and resulted in the increased survival of patients (Habringer et al., 2018). The beneficial effects of targeting the CXCR4-CXCL12 axis are not restricted to leukemia, as targeting of either CXCR4 or CXCL12 showed anti-tumourigenic effects in other cancer models such as breast and epithelial cancer models (Domanska et al., 2013; Lefort et al., 2017; Mao et al., 2017).

Targeting the activated stromal cell population of the TME by limiting the interaction of the tumour with stroma or by converting activated stromal cells to a quiescent state has been shown to improve the survival and delivery of chemotherapeutic drugs in mouse models of pancreatic ductal adenocarcinoma (Ijichi et al., 2011; Sherman et al., 2014). In contrast, targeting matrix metalloproteases, which are known to be essential for cancer progression, with common matrix metalloprotease inhibitors had no beneficial effect on patients (Stetler-Stevenson and Yu, 2001). This suggests that interrupting the pro-tumourigenic effect of the TME is more challenging than expected and underlines the complex contribution of the TME to tumourigenesis (Klemm and Joyce, 2015).

1.5.1. The role of the tumour microenvironment in neurofibromatosis type I

Recent studies, from others, and us have described an important role of the microenvironment in neurofibroma formation. Using the Krox20-Cre:$Nf1^{fl/-}$ mouse model, in which Nf1 is depleted during development, Zhu et al. showed that tumours developed exclusively in a $Nf1^{+/-}$ background implying the contribution of Nf1 heterozygous cells of the tumor microenvironment to neurofibroma development (Zhu et al., 2002). Extensive mast cell infiltration was observed in these tumours and bone marrow transplantations confirmed the important contribution of $Nf1^{+/-}$ mast cells to neurofibroma formation. Later studies then

demonstrated that inhibiting c-kit signalling in *Nf1* haploinsufficient mast cells reduced tumour size confirming the critical role of *Nf1*$^{+/-}$ mast cells (Yang et al., 2008a). Moreover, Nf1$^{+/-}$ mast cells exhibited increased c-Kit receptor expression and the recruitment of Nf1$^{+/-}$ mast cells to the peripheral nerve was fostered by Nf1$^{-/-}$ SCs that secrete c-kit ligand (Ingram et al., 2001; Ingram et al., 2000; Yang et al., 2003), which has a key role in in mast cell development and function and is a known growth factor for the c-kit receptor tyrosine kinase (Huang et al., 1990). In agreement with the contribution of mast cells to neurofibroma formation in the Krox-20 mouse model, extensive mast cell infiltration was observed presumably due to axonal degeneration within Remak bundles in other NF1 mouse models.

Mast cells and other immune cells that infiltrate neurofibromas provide a potential source of growth factors and other factors such as inflammatory mediators (eg. histamines) and pro-angiogenic factors (eg. VEGF) that could promote various aspects of neurofibroma formation and progression (Boesiger et al., 1998; Galli et al., 1993; Sondell et al., 1999). In line with this, another study has shown that Nf1$^{+/-}$ mast cells produce increased levels of transforming growth factor- beta (TGF-β), which induced elevated collagen synthesis and proliferation of Nf1$^{+/-}$ fibroblasts (Yang et al., 2006). The role of TGF-β signalling in neurofibroma formation remains to be addressed, however TGF-β is known to initiate carcinogensis in many organs/tissues and also has been shown to regulate fibroblast proliferation, collagen synthesis and malignant transformation (Bhowmick et al., 2004).

Targeting of the infiltrating mast cells can be achieved using Imatinib mesylate inhibitor, which inhibits c-kit. A human case study demonstrated that imatinib mesylate treatment of a child with a plexiform neurofibroma, which was blocking the upper airways, led to a 70% reduction in tumour volume (Yang et al., 2008a). However, a later clinical study using imatinib mesylate to treat plexiform neurofibromas was only able to reduce tumour growth in 17% of patients, whilst the majority of the patients exhibited side effects ranging from harmless rashes to more severe side effects such as decreased white blood cells and high blood sugar. Although the initial clinical study showed little success, improving the dosage of this drug may provide future clinical benefits (Robertson et al., 2012; Yang et al., 2006).

In our P0-CreER^{T2}:R26RYFP:Nf1$^{fl/fl}$ mouse model, the frequency of tumour formation was

independent of the genetic background, which may be because sufficient wild type mast cells are recruited to the site of injury. Importantly, Nf1-deficient SCs cooperated with unknown signals from the injury environment to produce neurofibromas only at the site of injury, whereas $Nf1^{-/-}$ SCs remyelinated and redifferentiated normally in the distal stump, downstream from the injury site. This suggests that the normal regenerative nerve environment suppresses tumour formation in the distal stump and promotes nerve repair in this region. Importantly, these findings indicate a critical contribution of the injury microenvironment to tumour formation in our injury induced NF1-associated mouse model.

1.6. Thesis aims

As outlined in this introduction, SCs have many key roles in peripheral nerve homeostasis and regeneration and upon loss of the tumour suppressor Nf1 they drive neurofibroma formation in this tissue. Whilst important insights into the biology of SCs and neurofibromas have been gained previously, many outstanding questions remain to be addressed. In this thesis, I will investigate and determine:

1. Peripheral nerve cell composition, structure and plasticity (cell turnover) of the nerve in homeostasis in order to understand how it changes during the regenerative response.
2. mSC behaviour, plasticity and contribution during the regenerative response by performing lineage tracing studies following injury. These lineage tracing studies will determine whether additional (stem) cell populations contribute to replenish the SC population and whether SCs retain multipotency during peripheral nerve regeneration.
3. The early stages of tumour formation in our injury induced NF1 mouse model in order to determine differences in the behaviour of Nf1-deficient SCs.
4. Pro- and anti- tumorigenic signals from the injury microenvironment by performing a molecular analysis at an early timepoint of tumour formation (Figure 1.21).
5. Plasticity of Nf1-deficient mSCs in order to understand whether the loss of Nf1 alters the plasticity of mSCs.

6. Clonality of Nf1-deficient neurofibromas to determine whether neurofibromas are monoclonal or polyclonally derived.

Overall, I am aiming to demonstrate both the mechanism by which the peripheral nerve maintains itself in homeostasis and how this changes during the regenerative response in order to be able to understand the link between tissue repair and tumourigenesis. Moreover, I aim to identify signals in the injury microenvironment that could contribute to neurofibroma formation. Finally, with this work I endeavoured to contribute to the understanding of the NF1 tumour biology by determining novel mechanisms important for the development of neurofibromas and potentially identify new approaches for the treatment of neurofibromas and other neuropathies.

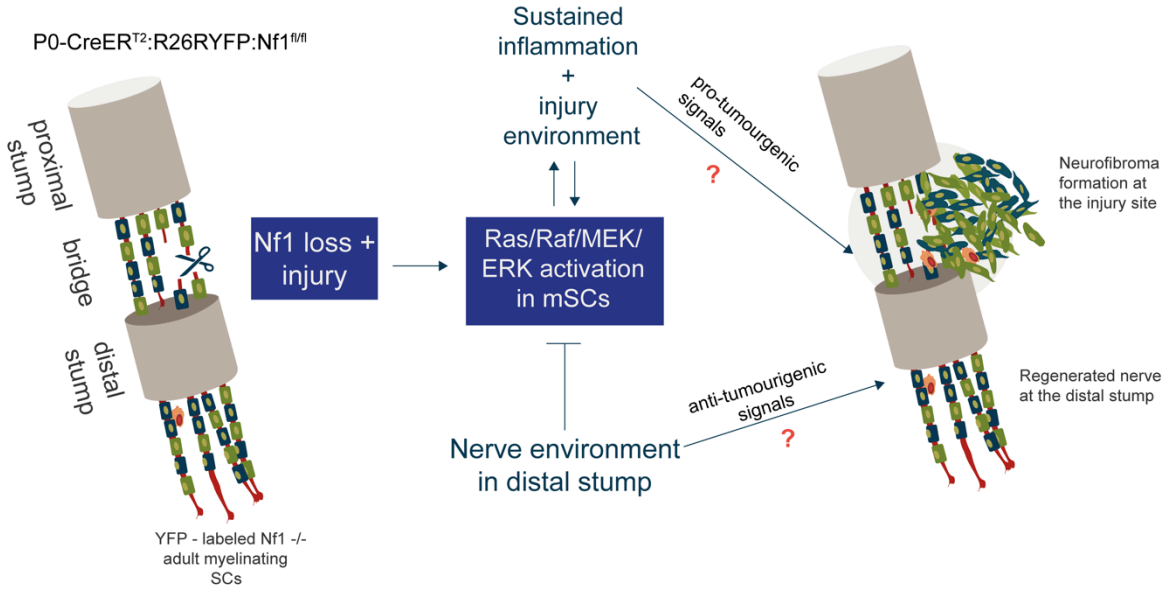

Figure 1.21. Nf1 loss and peripheral nerve injury initiates neurofibroma formation at the site of injury

Loss of Nf1 in adults mSCs in not sufficient to induce neurofibroma formation but requires a tumour promoting environment that can be provided by an injury environment. The nerve environment is normally tumour suppressive and blocks the activation of ERK upon loss of Nf1 in adult mSCs in the absence of nerve injury. The loss of Nf1 in combination with injury of the sciatic nerve results in Ras hyperactivation in mSCs. At the injury site, ERK activation is maintained, whereas at the distal stump the nerve environment ablates p-ERK levels, which ultimately results in normal regeneration in this area. Unknown factors from the injury microenvironment are pro-tumourigenic at the injury site and induce neurofibroma formation from Nf1-deficient SCs, whereas in the distal stump anti-tumourigenic signals prevent tumour formation and promote nerve repair.

Chapter Two: Materials and Methods

2.1. Materials

2.1.1. Chemicals

All chemicals were purchased bought from Sigma unless stated otherwise.

2.1.2. Antibodies

Please see table Table 2-1 for a full list of primary antibodies and concentrations used. For immunofluorescence staining, Alexa Fluor secondary antibodies were obtained from Invitrogen and used at a concentration of 1:400.

Table 2.1. Primary antibodies

Antibodies	Source	Dilution	Method	
pERK	Cell signaling #9101	1:100 (IF) 1:1000 (WB)	rabbit	polyclonal
Neurofilament (NF)	Abcam #ab4680	1:2000 (IF)	chicken	polyclonal
GFP	Abcam # ab13970	1:1000 (IF and WB)	chicken	polyclonal
anti-nerve growth factor (NGF-receptor) p75	Millipore # 07-476	1:500 (IF)	rabbit	polyclonal
S100β	DAKO # Z0311	1:500 (IF)	rabbit	polyclonal
Iba1	WAKO # 019-19741	1:500 (IF)	Rabbit	polyclonal
CD90.2	Millipore MABF461	1:100 (IF)	Rat	polyclonal
glucose transporter 1 (GLUT1)	Abcam # ab652	1:500 (IF)	rabbit	polyclonal
F 4-80	Bio-Rad / AbD Serotec # MCA497G	1:100 (IF)	Rat	Monoclonal
NG2 chondroitin sulfate proteoglycan antibody	Abcam # ab5320	1:500 (IF)	rabbit	polyclonal
NG2 chondroitin	Thermo Fisher	1:100 (IF)	Rat	Monoclonal

sulfate proteoglycan antibody	# MA5-24247			
actin alpha-smooth muscle- Cy3 conjugated (Clone 1A4)	Sigma-Aldrich # C6198	1:1000 (IF)	Mouse	Monoclonal
CD31 platelet endothelial cell adhesion molecule (PECAM)	BD Biosciences # 553370	1:100 (IF)	Rat	Monoclonal
Laminin	Abcam # ab11575	1:1000 (IF)	Rabbit	polyclonal
collagen III	Abcam # ab7778	1:1000 (IF)	Rabbit	polyclonal
Fibronectin	Sigma-Aldrich	1:500 (IF)	Mouse	polyclonal
PDGF Receptor Beta (Y92)	Abcam # ab32570	1:500 (IF)	Rabbit	polyclonal
myelin protein zero (P0)	Abcam ab39375	1:500 (IF)	Chicken	polyclonal

2.1.3. Genotyping primers

Table 2.2. Genotyping primers

Primers	Name	Sequence
Nf1 flox	P1	5'- CTT CAG ACT GAT TGT TGT ACC TGA-3'
	P3	5'- ACC TCT CTA GCC TCA GGA ATG A-3'
	P4	5'- TGA TTC CCA CTT TGT GGT TCT AAG-3'
Nf +/-	NF31a	5'- GTA TTG AAT TGA AGC ACC TTT GTT TGG-3'
	NeoTkp	5'- GC GTG TTC GAA TTC GCC AAT G-3'
	Nf131b	5'- CTG CCC AAG GCT CCC CCA G-3'
YFP	R26kof1	5'- GCG AAG AGT TTG TCC TCA ACC-3'
	R26wtr1	5'- GGA GCG GGA GAA ATG GAT ATG-3'
	R26wtf1	5'- AAA GTC GCT CTG AGT TGT TAT-3'
Cre	Forward	5'-CGG TCG ATG CAA CGA GTG ATG AG-3'

	Reverse	5’- CCA GAG ACG GAA ATC CAT CGC TC - 3’
11341	Confetti forward	5’- GAA TTA ATT CCG GTA TAA CTT CG- 3’
oIMR8545	Confetti wild type forward	5’- AAA GTC GCT CTG AGT TGT TAT- 3’
oIMR8916	Confetti reverse	5’- CCA GAT GAC TAC CTA TCC TC- 3’
oIMR9020	Wild Type Forward	5’-AAG GGA GCT GCA GTG GAG TA-3’
oIMR9021	Wild Type Reverse	5’-CCG AAA ATC TGT GGG AAG TC-3’
oIMR9103	Mutant Forward	5’-CTG TTC CTG TAC GGC ATG G-3’
oIMR9105	Mutant Reverse	5’-GGC ATT AAA GCA GCG TAT CC-3’
oIMR8699	Forward	5’-TTC CTT CGC CTT ACA AGT CC-3’
oIMR8700	Reverse	5’-GAG CCG TAC TGG AAC TGG-3’

2.1.4. qRT-PCR primers

Primers that target mRNA and span at least 1 or more introns were designed using Primer 3 and Blast tool (https://www.ncbi.nlm.nih.gov/tools/primer-blast/). Please see table 2-3 for primer sequences.

Table 2.3. qRT-PCR primers

Gene	**Forward Primer (5’-3’)**	**Reverse Primer (5’-3’)**
Mouse		
B2M	CAGTCTCAGTGGGGTGAAT	ATGGGAAGCCGAACATACTG
Cilp	GTTCCGAGTTCCTGGCTTGT	AATGTATGGGGTCTCTGCCC
Cre-ER^{I2}	AGCCGAAATTGCCAGGATCA	AACCAGCGTTTTCGTTCTGC
Cre-ER^{I2}	CGCGGTCTGGCAGTAAAAAC	CGCCGCATAACCAGTGAAAC
Cxcl14	GTTATCGTCACCACCAAG	CTCTCAACTGGCCTGGAGT
Cx3cl1	GTGCTGACCCGAAGGAGAAA	CACCCGCTTCTCAAACTTGC
CyclinB2	CGACGGTGTCCAGTGATTTG	GTTCTGAGGTTTCTTCGCCAC
Edil3	CTGTGAGTGTCCAGAAGGCT	AGGCTTCGCTTATCTCACAGG
Emilin1	AGCACCCTCCACACCACT	CTGCTGCACCTTCTCTGAC
Esm	TGTCCCTATGGCACCTTC	TCACGCTCTGTGTGGGAG
Igf1	AGACAGGCATTGTGGATGAG	TGAGTCTTGGGCATGTCAGT
Il6	GAGGATACCACTCCCAACAGACC	AAGTGCATCATCGTTGTTCATACA

Itgae	AAGAAAATGTAACCGTGGCCG	CAGTGATCTTCGTCCTGTGG
Nf1	CAACTTGCCACTCCCTACTGA	CAAGCCCCTTTCAATTCTAGG
Pappa	ATCACAGGGCTGTATGACAAAT	GCGTGGATCTCTGTTGCCTT
Slitrk6	GCTTTACAGAGTCAGATCCAATCAT	AAAGAGTGTCGCAAGAGCCT
Spock3	TCAGGGAGAGGAAGATGCTCA	AGAAAATTACCGCCGTCCGA
Spon1	CTGAGTGCCATACCATCCCG	CCACAGGTCACGCTACAGTC
Tgfb1	CCCTATATTTGGAGCCTGGA	CTTGCGACCCACGTAGTAGA
Tgfb2	CTCCCCTCCGAAACTGTCTG	TGTCTGGAGCAAAAGCTG
Tnc	CCATGCTGAGATAGATGTTCCAA	CTTGACAGCAGAAACACCAATCC
Tnfsf18	TCAAGTCCTCAAAGGGCAGAG	GGCAGTTGGCTTGAGTGAAGTA
Vcan	TCCTGATTGGCATTAGTGAAG	CTGGTCTCCGCTGTATCC
YFP	GAAGTTCATCTGCACCACCG	GCTTCATGTGGTCGGGGTAG

2.2. Methods

2.2.1. In vivo experiments

2.2.1.1. Transgenic mouse strains

All animal work was performed in accordance with the United Kingdom Home Office legislation. Mice were housed in a temperature and humidity controlled vivarium on a 12-hour light-dark cycle with free access to food and water.

Female and male (4 week- to 1 year-old) mice of the following genotypes and strains were used: For lineage tracing of mSCs, P0-CreER^{T2} C57Bl/6 mice (Leone et al., 2003; Ribeiro et al., 2013) were crossed with R26R-YFP (Srinivas et al., 2001), R26R-tdTomato (Madisen et al., 2010) or R26R-Confetti reporter mice (Livet et al., 2007; Snippert et al., 2010) to generate P0-CreER^{T2}:YFP, P0-CreER^{T2}:tdTomato and P0-CreER^{T2}:Confetti mice. To visualise all SCs, P0-Cre mice (Feltri et al., 1999) were crossed with R26R-tdTomato mice to generate P0-Cre:tdTomato and Plp-eGFP transgenic mice (Mallon et al., 2002) were used. NG2-dsRed mice were used to confirm the identity of NG2+ cells (Zhu et al., 2008). For studying the early time points of tumourigenesis and SC plasticity in a nerve tumour environment, P0-CreER^{T2}:YFP:Nf1$^{fl/fl}$ mice were used (Ribeiro et al., 2013). As control animals P0-CreER^{T2}:YFP mice were used. For studying neurofibroma clonality P0-CreER^{T2}:YFP:Nf1$^{fl/fl}$ mice were crossed with R26R-Confetti reporter mice (Livet et al., 2007; Snippert et al., 2010) to generate P0-CreER^{T2}:Confetti:Nf1$^{fl/fl}$ mice. As control animals P0-CreER^{T2}:Confetti mice were used. In all studies, both male and female mice were used. In both Nf1 mutant mice,

administration of tamoxifen activates Cre and thereby produces Nf1 KO in myelinating Schwann cells. Animals were genotyped and identified using earhole punches upon weaning.

Table 2.4. Transgenic mice

Mice strains	Reference	Identifier
P0A-Cre (P0-Cre)		RRID: IMSR_RBRC01459
PLP-eGFP	(Mallon et al., 2002)	N/A
NG2-dsRedBAC (NG2-dsRed)	(Zhu et al., 2008)	RRID: IMSR_JAX:008241
B6.Cg-*Gt(ROSA)26Sor*$^{tm9(CAG-tdTomato)Hze}$ (R26R-tdTomato)		RRID: IMSR_JAX:007909
Tg(Mpz-cre/ERT2)2Ueli (P0-CreER^{T2})	(Leone et al., 2003)	RRID:IMSR_MGI: 2663097
R26R-YFP	(Srinivas et al., 2001)	
Gt(ROSA)26Sor$^{tm1(CAG-Brainbow2.1)Cle}$ (R26R-Confetti)	(Snippert et al., 2010)	RRID: IMSR_JAX:013731
P0-CreER^{T2}:R26R-YFP:Nf1$^{fl/fl}$	(Ribeiro et al., 2013)	

2.2.1.2. DNA extraction from animal tissue

Genomic DNA was extracted from ear notches. Animal tissue was lysed with 100 ul Viagen Direct PCR DNA Extraction Reagent ON and Proteinase K (1:100, Roche Laboratories) at 56°C. The next day the extracts were incubated for 45 min at 85°C in order to deactivate the Proteinase K. Remaining tissue was pelleted by centrifugation and the supernatant was used for PCR reactions.

Table 2.5. Genotyping reactions

	Nf1 flx	Nf1 +/-	YFP		Cre	Tomato WT	Tomato Mutant	NG2		Confetti
DNA	1	1	1	**DNA**	1	1	1	1	**DNA**	2
Buffer 5x	6	6	5	**Buffer 5x**	5	5	5	5	**Buffer HF 5x**	5
$MgCl_2$ (50mM)	4.2	4.2	2	**$MgCl_2$ (50mM)**	1.5	1.5	1.5	1.5	**$MgCl_2$ (50mM)**	0.25
Primer (F+ R 10uM)	1	1	1	**Primer F**	0.15	0.15	0.15	0.15	**Primer 1341 (100uM)**	0.15
				Primer R	0.15	0.15	0.15	0.15	**Primer oIMR8545 (100uM)**	0.15
						0.15	0.15	0.15	**Primer oIMR8916 (100uM)**	0.15
dNTPs (25mM)	0.2	0.2	0.2	**dNTPs (25mM)**	0.2	0.2	0.2	0.2	**dNTPS (25mM)**	0.2
Pol (U)	0.2	0.2	0.2	**Pol (U)**	0.2	0.2	0.2	0.2	**Phusion HS Pol**	0.25
H_2O	17.1	17.1	15.3	**H_2O**	16.8	16.8	16.8	16.8	**H_20**	16.85
Total volume	30	30	25	**Total volume**	25	25	25	25		25

2.2.1.3. Genotyping

Mice were genotyped by PCR. Reactions were set up as described in Table 2-5. Go Taq Green Master Mix (Promega) was used for the Nf1 flx, Nf1 +/-, YFP and P0 PCR reactions; Phusion Hot start polymerase (NEB) was used for the Confetti PCR reaction. The PCR programs used for the amplification of the different genes are shown in Table 2-6 and Table 2-7. Primers used for PCR reactions are detailed in Table 2-2.

Table 2.6. Standard Genotyping PCR program

Step	Temperature (°C)	Time
1. Polymerase activation	94°C	3min
2. Denaturation	94°C	30 sec
3. Annealing	55°C	1
4. Extension	72°C	2min
Repeat Step 1-4 for 35 cycles		
5. Final Extension	72°C	10min
6. Hold	4°C	∞

Table 2.7. Confetti mice PCR program

Step	Temperature (°C)	Time
1. Polymerase activation	94°C	2min
2.Denaturation	94°C	20 sec
3. Annealing	65°C	15sec (-0.5°C per cycle)
4. Extension	68°C	10sec
Repeat Step 2-4 for 10 cycles		
5.Denaturation	94°C	15sec
6. Annealing	60°C	15sec
7. Extension	72°C	10sec
Repeat Step 5-7 for 28 cycles		
8. Final Extension	72°C	2min
9. Hold	4°C	∞

2.2.1.4. Tamoxifen administration

For lineage tracing experiments, Cre-mediated recombination was induced in 4-5 week-old mice by intraperitoneal injection (IP) or oral administration of 2mg of Tamoxifen (Sigma) daily for 5 consecutive days. Tamoxifen was dissolved in EtOH at a concentration of 200mg/ml and diluted 10 times in sunflower oil (Sigma, S5007) to reach a final concentration of 20 mg/ml. To

ensure that the tmx was completely dissolved before storage at -80C, the tamoxifen-oil solution was vortexed for at least 3 hours at RT.

2.2.1.5. EdU administration

To cumulatively label newly generated cells, adult c57bl/6 or PLP-eGFP mice received 0.2mg/ml EdU (Invitrogen) in their drinking water 0.2mg/ml for up to 70 days as indicated (Young et al., 2013). The water was changed every 48h. For pulse-labelling experiments, a single EdU injection (2mg of EdU in PBS) was given IP, 3h prior to tissue collection. For investigation of cell proliferation at the early time points of tumour formation in Nf1 KO animals, a double EdU injection (2mg of EdU in PBS) was given IP, 6h and 3h prior to tissue collection. Cell proliferation was determined by measuring EdU incorporation detected using the Click-iT EdU Imaging kit (Invitrogen) according to the manufacturer's instructions.

2.2.1.6. Sciatic nerve transection

14 days after Tamoxifen administration, mice were anaesthetized with isofluorane under aseptic conditions and the right sciatic nerve was exposed at the sciatic notch. The nerve was fully transected or half-transected, as indicated, and the wound closed with clips (Fine Science Tools). Nerves were dissected at the indicated days for analysis by immunostaining, electron microscopy or RNA expression analysis.

2.2.1.7. Preparation of nerves for immunofluorescence

Harvested nerves were fixed for 4 hours at room temperature (RT) in 4% PFA, unless otherwise stated, and cryo-protected in 30% sucrose (w/v) in PBS overnight at 4°C. The nerves were then incubated for 2 hours at RT in 1:1 w/v 30% sucrose in PBS:optimal cutting temperature (OCT) solution (VWR) solution. Then, the nerves were embedded in OCT in a cryosection mould and snap-frozen in liquid nitrogen.

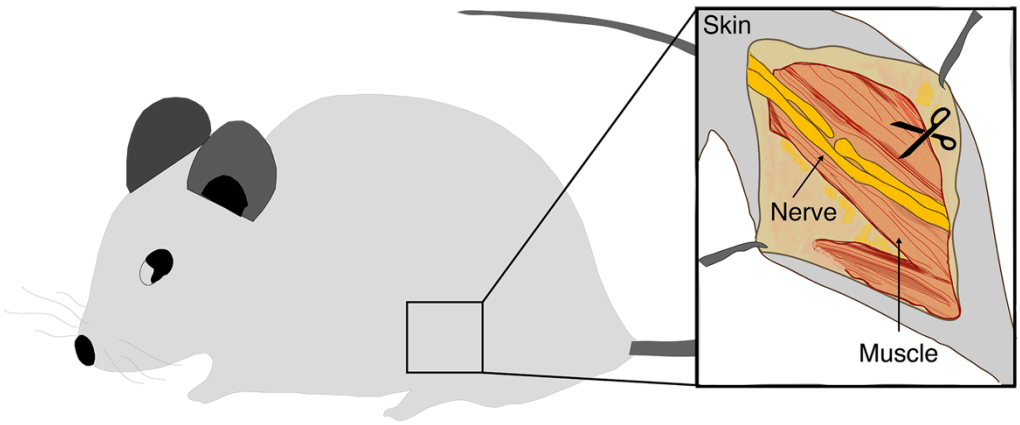

Figure 2.1. Sciatic nerve half transection
Schematic displays sciatic nerve transection that is performed on the right side of mice. Sciatic nerves were exposed just below hipbone under general anaesthesia in aseptic conditions and transected below the sciatic notch. The wound was closed with clips and pain relief was administrated, as required, prior to recovery in heated chambers.

2.2.1.8. Standard Immunofluorescence staining protocol

10-25µm longitudinal or transverse cryosections (Leica) were permeabilised in 0.3% Triton-X100 in PBS for 30 minutes, blocked in 10% goat serum/PBS for ≥1 hour and incubated in primary antibodies (see Table 2-1) diluted in blocking buffer overnight (O/N) at 4°C. The following day, sections were washed 3 times with PBS and the appropriate fluorescent secondary antibodies were used with Hoechst to counterstain the nuclei for 1h at RT. Samples were mounted in Fluoromount G (Southern Biotechnology) before imaging. Sciatic nerves from P0-CreER^{TR}:Confetti mice were fixed in Antigenfix (DiaPath) to preserve the endogenous fluorescence and RedDot (Biotium) or To-Pro-3 (Thermo Fisher) was used as a nuclear counterstain. For better preservation of axonal proteins, PBS containing 1mM $CaCl_2$, 0.5mM $MgCl_2$ was used when needed. For P0 staining, harvested sciatic nerves were instead immediately snap frozen in liquid nitrogen. After cutting 10-25µm transverse cryosections, the sections were post-fixed for 10min using 4% PFA at RT and washed thoroughly with PBS before blocking with 10% goat serum/PBS. The rest of the immunostaining protocol was as the staining protocol for the prefixed nerve.

2.2.1.9. p-ERK Immunofluorescence staining protocol

Nerves that were used to detect pERK by immunofluorescence staining were not fixed in PFA for 4 hours as described in 2.2.1.3, instead after dissection the nerves were embedded in cryosection mould and snap frozen in liquid nitrogen. 10µm longitudinal or transverse cryosections were cut with a Leica cryostat. After cutting, the sections were immediately fixed with 4% paraformaldehyde for 10min. After fixation, the sections were washed with TBSTi (TBS with 0.1% Triton X-100) for 5 minutes, then the intrinsic auto fluorescence quenched for 10min with 0.27% NH_4Cl and 0.37% Glycine in TBSTi. Sections were washed with TBSTi for 5 minutes, then permeabilised with 1% NP-40, 0.1mM tetramisol for 10 minutes. Then, sections were washed three times with TBS and treated with 3% hydrogen peroxide for 20 minutes, in order to block the endogenous peroxidase activity. Sections were washed another three times with TBS, blocked with 3% BSA- TBSTi for 30 minutes and incubated with primary antibodies overnight. The following day, sections were washed three times with TBSTi and the appropriate secondary antibodies (Alexa Fluor, Life technologies) were applied in 3% BSA-TBSTi for 1h. Sections were washed three times with TBSTi, then incubated with tyramide reagent (Tyramide Signal Amplification kit from Molecular Probes T-20935) for 10 minutes in the dark. Next, sections were washed three times with TBSTi before the Click-iT EdU imaging protocol was performed. Sections were washed another three times with TBS before counterstaining nuclei with Hoechst (1:1000) in TBS for 30 minutes**.** Finally, sections were washed another three times in TBS and mounted in Fluormount-G (Southern Biotechnology) before imaging.

2.2.1.10. Click-iT EdU detection protocol

Before sections were mounted with Fluoromount, EdU can be detected using the Click- iT EdU Alexa Fluor Imaging Kit (Thermo Fisher Scientific). Incorporated EdU can be fluorescently labeled with a bright photostable Alexa Fluor dye in a fast and highly specific reaction. For each slide approximately 200ul of EdU reaction mixture was added for 30 minutes in the dark. After staining with EdU it is important to wash the sections at least three times with PBS as the EdU reaction mixture can give quite high background.

Table 2.8. EdU detection

	Vol (ul)
MQ water	324
10x Reaction buffer	32.25
CuSo4	15
Alexa Fluoride	0.9
Buffer additive	3.75
Total volume	375
This volume is sufficient for 2 slides	

2.2.11. RNA extraction from tissue

Nerves were dissected at the indicated time following surgery, and immediately snap frozen in liquid nitrogen and stored at -80°C. Please refer to the molecular biology subchapter for the detailed protocol of RNA extraction from sciatic nerves.

2.2.2. Microscopy

2.2.2.1. Confocal microscopy

Confocal images were acquired using an inverted SPE or SP8 confocal microscope (Leica). A Multiphoton microscope (Zeiss) was used to image confetti samples. Within each experiment, the same acquisition settings were used, the same volume imaged and the same number of z-stacks acquired. Fiji software (https://imagej.net/Fiji/Downloads) was used to make a projection of the z-stacks. Longitudinal reconstructions of nerves were done using the photomerge function in Photoshop CS4.

2.2.2.2. Imaging of confetti samples

The acquisition settings of the confetti samples were optimised in order to excite the four fluorophores without spectral overlap. Initially, the confetti samples were imaged with FluoView FV1200 microscope (Olympus) and the emission spectrum of each fluorescent protein set manually in order to ensure that no spectral overlap occurred. Importantly, CFP requires a laser that excites at ~440-455nm in order to obtain maximum emission.

Furthermore, to achieve faster imaging, the confetti samples were imaged with a multiphoton microscope (Zeiss) in lambda acquisition mode. The lambda acquisition mode acquires all the wavelengths at once and the individual fluorescent proteins are separated from each other by spectral unmixing (linear unmixing) after the acquisition. Depending on the image size, the typical lambda stack consists of thousands to millions of individual spectra, with one spectra for each pixel. Spectral unmixing decomposes the mixed fluorescence signals and determines the relative contribution of each fluorophore to every pixel of the image. Prior to performing the experiment, control samples for each fluorophore in the experiment have to be acquired in order to obtain the individual emission spectra.

2.2.2.3. Transmission electron microscopy (TEM)

Sciatic nerves were dissected and fixed O/N at 4ºC in 2% glutaraldehyde in 0.2M phosphate buffer. Nerves were then post-fixed in 2% osmium tetroxide for 1.5 hours at 4ºC, and incubated in 2% uranyl acetate for 45 minutes at 4ºC. The nerves were washed three times with water and were dehydrated in an ethanol series (5 min in 25%, 5 min in 50%, 5 min in 70%, 10 min in 90% and 4x10 min in 100% ethanol) before being incubated with propylene oxide (3x10 min) to ensure complete removal of the propylene oxide solution. Finally, the nerves were embedded in epoxy resin. Resin was prepared by mixing TAAB 812 (47%), DDSA (18.5%), MNA (32.5%) and DMP30 (2%). Nerves were incubated in 50% resin- 50% propylene oxide for 1 hour and in 100% resin O/N. The resin was renewed the next day and the nerves were embedded in resin at the end of the day. The embedded nerves were incubated at 60 ºC to allow the resin to set. 70nm ultra-thin sections were cut with a diamond knife, collected onto formvar coated slot grids and visualised using a transmission electron microscope (TEM, T12 Tecnai Spirit, FEI) using a Morada camera and iTEM software (Olympus SIS).

2.2.2.4. Correlative light and electron microscopy (CLEM)

Regenerated sciatic nerves from P0-CreER^{T2}:Confetti mice were harvested 3 months following injury and fixed in antigenfix (Diapath) O/N. The following day, nerves were embedded in 2.8%

low melting point agarose in PBS. 200mm sections of the embedded nerve were cut in cold PBS using a vibrating microtome. Sections were screened using a widefield fluorescence microscope to identify sections containing a large number of fluorescently-labelled cells. These sections were imaged with a 40x lens using a SP8 confocal microscope (Leica). YFP, GFP and RFP was acquired (CFP excitation is not possible on this microscope. After image acquisition, samples were fixed in 2% (wt/vol) PFA, 1.5% (wt/vol) glutaraldehyde (both EM grade from TAAB) in 0.1M sodium cacodylate buffer for 30 mins at RT. Samples were then secondarily fixed in 1% (wt/vol) osmium tetroxide, 1.5% (wt/vol) potassium ferricyanide for 1h at 4 °C. After washes in 0.1M sodium cacodylate, samples were incubated in 1% (wt/vol) tannic acid in 0.5M sodium cacodylate at room temperature for 45 min. Further washes in 0.5M sodium cacodylate were followed by a final wash in distilled water, before the samples underwent dehydration by sequential short incubations in 70% (vol/vol) and 90% (vol/vol) ethanol and then two longer incubations in 100% ethanol. Samples were transferred to a 1:1 mix of propylene oxide and Epon resin (TAAB) for 90 min, then 100% Epon for two more incubations, one of several hours and one O/N. Finally, samples were polymerised by baking at 60°C O/N. It is important that the side of the sample that was imaged by confocal microscopy faces the top of the resulting resin block to ensure correlation between LM images and EM section images. Ultrathin sections were collected and imaged as explained below in paragraph transmission electron microscopy.

2.2.3. Molecular biology

2.2.3.1. Standard RNA extraction and cDNA synthesis

Harvested nerves were rapidly snap frozen in liquid nitrogen. As a first step the nerve was disrupted using a pestle and liquid nitrogen. Next, the tissue was immersed in 200µl Trizol Reagent and homogenized using a pellet pestle. Another 300ul of Trizol was added and the sample was incubated for 5min at RT. 0.1ml chloroform was added per sample and the tubes were vortexed for two minutes before centrifugation for 15min at 13000rpm at 4°C. The upper colorless phase was transferred to a fresh RNA free tube and 250ul of isopropanol was added. The samples were incubated for 10min at RT before centrifugation for 10min at

13000rpm. Liquid was decanted and 800ul of 80% ethanol was added. Another centrifugation step of 5min at max. speed was performed, before liquid was decanted again and pellet dried. The pellet was resuspended in RNAse free water. RNA concentration was measured by Nanodrop and 500-1000ng was used to synthesize complementary DNA using the Superscript II kit (Invitrogen). RNA was incubated with 25μM random hexamers (Invitrogen) and 0.5μM dNTPS (Invitrogen) for 5 minutes at 65°C. 40U RNaseOUT, 0.02M DTT and 1x first strand buffer were added to the samples and incubated for 2min at RT. Superscript II was added at 20U/μl and the samples were incubated for 10min at RT, 50 minutes at 42°C and finally the reverse transcriptase was inactivated by incubating for 15 minutes at 70°C.

2.2.3.2. qRT-PCR

The Mesa Blue qPCR Master Mix Plus (Eurogentec) kit was used for the RT-qPCR reaction. Forward and reverse primers were mixed together to a stock solution of 5μM. 5μl of template cDNA (diluted 1:4 in RNase free water), 0.16μM forward and reverse primers, 12.5μl of Mesa Blue Mix and 7.7μl was added in each well. ddH_20 was used as negative control. Primers used for qRT- PCR reactions are detailed in Table 2-3. The Nf1 primers are binding to the exon 31 and 32 which are floxed, hence in the animals with a successful recombination the primers should not be able to bind anymore.

Table 2.9. qRT-PCR program

Step	**Temperature (°C)**	**Time**
1. Meteor Taq activation	95°C	5 minutes
2. Denaturation	95°C	20 seconds
3. Annealing/ extension	58°C	30 seconds
4. Extension	72°C	20 seconds
Repeat Step 2-4 for 40 cycles		
5. Melt curve	60-98 °C	95°C for 10 seconds, 65°C for 5 seconds, 95°C for 5 seconds

2.2.3.3. RNA extraction for RNA seq.

The same protocol was used than for the standard RNA extraction until the separation of nucleic acids from proteins via phase separation. The upper colourless phase was transferred to a fresh RNA free tube and an equal volume of 70% Ethanol was added in order to obtain an ethanol concentration of 35%. The samples were mixed well before transferring to the PureLink columns (Invitrogen). The protocol was performed as described by the manufacturer (see page 51 of the PureLink RNA Micro Kit Protocol). The optional DNA digestion step was performed in order to remove the genomic DNA using RNase free DNase kit (Quiagen) according to manufacturers instructions. RNA was eluted in 30μl of RNAse free water and concentration was measured by Nanodrop.

2.2.3.4. RNA seq

RNA sequencing was performed by the Genomic Facility at the University of Liverpool. The whole procedure including preparation of the samples is explained in detail Chapter 5. Briefly, quality controls were performed, ribosomal RNA was removed and RNA was enriched prior to preparing the RNA library. The quantity and quality of the libraries were determined by Bioanalyzer and subsequently by qPCR using the Illumina Library Quantification Kit from Kapa (KK4854) on a Roche Light Cycler LC480II. The template DNA was denatured and loaded at 300 pM. The sequencing was carried out on two lanes of an Illumina HiSeq4000 at 2x150 bp paired-end sequencing (Borodina et al., 2011; Parkhomchuk et al., 2009). Prior to the bioinformatics analysis, the quality of the raw data was assessed and the data was normalised (Chapter 5 and RNA sequencing reports in Appendix). Two independent bioinformatics analyses were performed: The first by the genomic facility in Liverpool (see Appendix) and the second in collaboration with Dr. Christina Venturini (Group of Judith Breuer, Division of Infection and Immunity, UCL) (see Chapter 5 and Appendix). The analysis of Dr. Venturini was performed using R software (Team, 2014), Bioconductor (Gentleman et al., 2004) packages including DESeq2 (Anders and Huber, 2010; Love et al., 2014) and the SARTools package developed at PF2 (Institute Pasteur). Normalization and differential analysis were performed according to the DESeq2 model and package.

2.2.4. Quantification and Statistical Analysis

2.2.4.1. Cell composition quantification

For the cell type quantifications, z-stack projections were done with an equal number of z-stacks. 4 or more non-overlapping fields of each section were imaged using a 63x objective on a SPE microscope. Three different sections were quantified per mouse (≥4 animals per group). Confocal images were counted manually using Fiji software. To determine the recombination rate by counting GFP+ mSCs, cells were counted both manually and automatically using a pipeline in Icy programmed by L. Malong (http://www.ucl.ac.uk/lmcb/users/alison-lloyd). Within TEM images each cell type was identified and quantified based on their morphology and the presence of a nucleus. mSCs, nmSCs, pericytes and endothelial cells are morphologically very different, however, we were unable to differentiate between the pericyte-like cells and macrophages. Therefore, these cell types were quantified as a single category.

2.2.4.2. Determination of proliferation rates

Turnover of each cell-type was determined by using measurements taken following 30 days of continuous EdU administration. The calculation used was: proportion of each cell-type/(proportion of each proliferating cell-type x the total proliferation rate at 30 days).

2.2.4.3. Area measurements and intensity analysis

For area measurements, 4 or more different fields of each section were imaged, with three sections counted for each mouse (≥4 mice per group). Images were converted to 8-bit grey scale TIFF images using Fiji software. For each image, a threshold was set and made binary. The threshold area was outlined using the “Create Selection” function was used and the immunostained area quantified using the measurement function. For intensity measurements, projections used an equal number of z-stacks. The intensity of 9 different fields per image was measured and averaged using Fiji software (3 images were acquired for each section, 3 sections per animal, 6 animals per group).

2.2.4.4. Axon quantification

The diameter of individual axons measured from 6 images per mouse and 8 mice per group was binned to assess distribution. All measurements were done with Photoshop to draw the axons and Fiji software to measure their diameter.

2.2.4.5. Software

For image quantification Fiji (https://imagej.net/Fiji/Downloads) (Schindelin et al., 2012) and Icy (Institute Pasteur, http:// bioimageanalysis.org) programs were used. For 3D reconstructions Imaris was used (http://www.bitplane.com/imaris).

2.2.4.6. Statistical Analysis

Statistical and graphical data analyses were performed using Prism 7 (GraphPad). For all measurements, three or more biological replicates were used. Information regarding the number of biological replicates or “n” used in each experiment is reported in the relevant figure legends. The data are represented as mean values ± standard error of the mean (SEM). Unpaired two-tailed Student's t test was used for statistical analysis except when ANOVA is indicated. p value significance indicated by asterisks as follows: ns $p \geq 0.05$, $*p < 0.05$, $**p < 0.01$, $***p < 0.001$.

Chapter Three: Mouse models to study the early stages of neurofibroma formation and to determine tumour clonality

3.1. Chapter Introduction

The Lloyd laboratory has developed a mouse-model, P0-CreER^{T2}:YFP:Nf1$^{fl/fl}$, that enables the conditional deletion of Nf1 specifically in adult mSCs and the labelling of these recombined cells with a YFP reporter cassette (Ribeiro et al., 2013). In line with previous studies (Joseph et al., 2008; Le et al., 2011; Wu et al., 2008), we demonstrated that loss of Nf1 in adult mSCs was not sufficient to induce neurofibroma formation (Ribeiro et al., 2013). Importantly however, we found that after nerve injury, Nf1-deficient mSCs formed neurofibromas specifically at the wound site. Remarkably, Nf1-deficient SCs behaved and repaired normally in the distal stump in contrast to their tumorigenic behaviour at the wound site. Therefore, the P0-CreER^{T2}:YFP:Nf1$^{fl/fl}$ mouse model provided a potentially powerful model to study the early events driving neurofibroma formation, as we knew exactly where the tumour would form following a nerve injury (Ribeiro et al., 2013).

However, the use of this mouse model for studying the early events of tumourigenesis was limited by the initial findings that tumours only developed at the site of injury in around 30% of the mice (Ribeiro et al., 2013) preventing a meaningful study of the early events leading to tumourigenesis. Whilst there were potentially several explanations for this lack of penetrance such as a requirement for secondary mutations, variability in Cre-mediated recombination efficiency was considered the most likely explanation, as the efficiency of Cre-recombination is known to vary depending on the target gene and can vary between animals (Richardson et al., 2011).

In the work described in this chapter, we have addressed why tumours only develop in 30% of the P0-CreER^{T2}:YFP:Nf1$^{fl/fl}$ mice and determined how to select the mice, which would eventually develop tumours. Furthermore, we developed a new mouse model, which allows us to track individual SCs and perform lineage and clonality studies specifically on Nf1-deficient SCs, in order to further analyse the role of the microenvironment on neurofibroma formation.

3.2. Optimisation of the Nf1 KO mouse model to study the early stages of tumour formation

In unpublished observations (unpublished data of N. Garcia- Calavia), we noted that the Cre-mediated recombination efficiency appeared to vary between animals in our cohort. To determine whether the Cre-mediated recombination efficiency correlated with tumour growth, we set up a long-term tumour study of the P0-CreER^{T2}:YFP:Nf1$^{fl/fl}$ transgenic mice. These mice express a tmx inducible variant of Cre recombinase specifically in mSCs, hence tmx needs to be administrated to achieve the knock-out of Nf1 and the expression of the YFP reporter cassette. Throughout this thesis, most of the studies described were performed in P0-CreER^{T2}:YFP:Nf1$^{fl/fl}$ mice using P0-CreER^{T2}:YFP:Nf1$^{+/+}$ mice as controls. For simplicity, in this thesis we will refer to the P0-CreER^{T2}:YFP:Nf1$^{fl/fl}$ mouse strain as Nf1 KO and the P0-CreER^{T2}:YFP:Nf1$^{+/+}$ mouse strain as Nf1 WT animals (Figure 3.1).

P0-CreER^{T2}:YFP:Nf1$^{fl/fl}$ mice (24 in total) were injected intra-peritoneally with tmx, sciatic nerve partial transection performed two weeks after injection and the animals were harvested 8 months following nerve injury. Sciatic nerve half transection was performed to facilitate reconnection of the two stumps following injury, in order to reduce the variability between the experiments. Furthermore, the intact half of the nerve provided an internal control. Cre-mediated recombination efficiency was determined by counting the percentage of YFP+ mSCs in the contralateral nerve in each individual animal (Figure 3.2). The quantification of YFP+SCs was performed manually and with an automatic programme (http://www.ucl.ac.uk/lmcb/users/alison-lloyd), which was generated using Icy software (Institute Pasteur, http:// bioimageanalysis.org). Both quantification methods gave similar results. The injured nerves were categorised as either normal regenerated nerves or tumour bearing nerves according to the proportional enlargement of the injury site compared to the distal stump (Figure 3.3). The diameter of a normal regenerated nerve is equal at the injury site and distal stump, whereas the diameter of a tumour bearing nerve was defined as more than twice the size of a regenerated distal stump. Furthermore, the tumours were analysed at the cellular level in order to establish the pathology of the area (Figure 3.4).

Firstly, we observed a large variability in Cre-mediated recombination efficiency (from 0 to

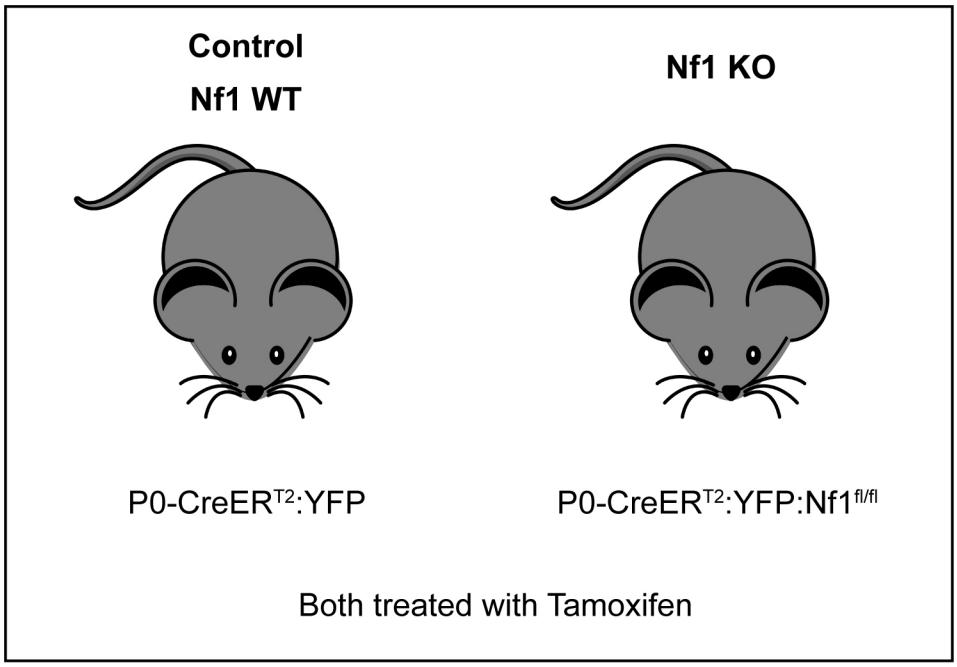

Figure 3.1. Mice used in this study
The P0-CreER^{T2}:YFP mouse line expresses a tmx inducible Cre recombinase under the control of a mSC specific promoter, P0. Upon tmx administration, the Cre recombinase is active and induces recombination of the YFP reporter cassette specifically in the mSC population. YFP expression allows us to determine the Cre mediated recombination efficiency and to track the labelled cells in vivo.
In most of the experiments, P0-CreER^{T2}:YFP:Nf1$^{fl/fl}$ mice (Nf1 KO) and P0-CreER^{T2}:YFP control mice (Nf1 WT) were used, unless otherwise specified. All mice were treated with tmx, unless otherwise stated.

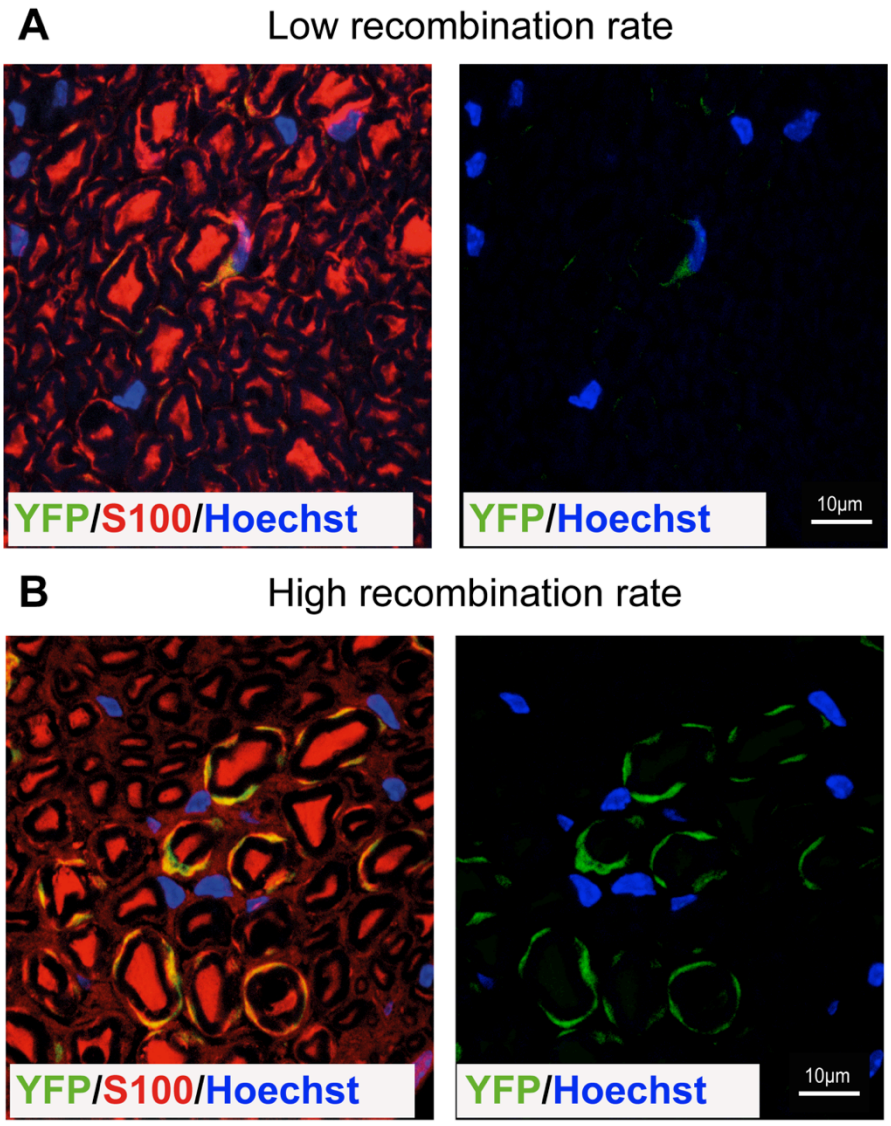

Figure 3.2. Representative images of Cre-mediated recombination efficiency
Cre-mediated recombination efficiency was analysed in the uninjured contralateral nerve, 8 months following injury. Cryosections of Nf1 KO mice were stained for the Schwann cell marker S100 (red) and YFP was detected using an antibody to GFP (green). Nuclei were counterstained with Hoechst. The Cre-mediated recombination efficiency was determined by counting the YFP+mSCS over the total number of mSCs. Representative images are shown of an animal with **A)** low and **B)** high recombination efficiency. Note that axons are also stained by the S100 antibody.

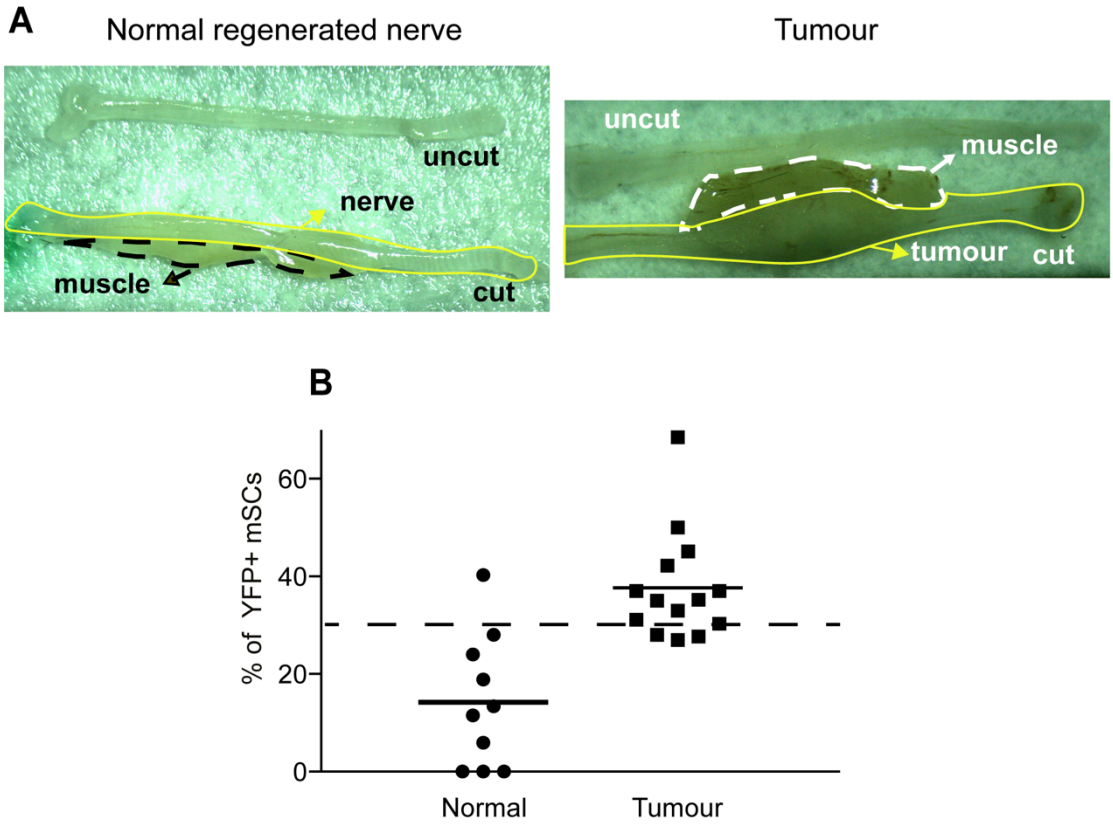

Figure 3.3. Correlation between Cre-mediated recombination and tumour growth at the wound site

Animals were harvested 8 months following nerve injury and sciatic nerves were categorised into tumour bearing or normal regenerated nerves. In the contralateral uninjured nerve, Cre-mediated recombination efficiency was assessed in each individual animal and correlated to tumour growth. **(A)** Left side: Representative image of an animal with a normal regenerated nerve. Right side: Representative image of an animal with a tumour bearing nerve **(B)** Graph shows the average recombination efficiency for all normal regenerated (13.8% average recombination) and tumour bearing nerves (39.7% average recombination) of the Nf1 KO nerves. The dashed line displays the threshold of 30% above which almost all animals (88%) developed tumours at the injury site (n=24).

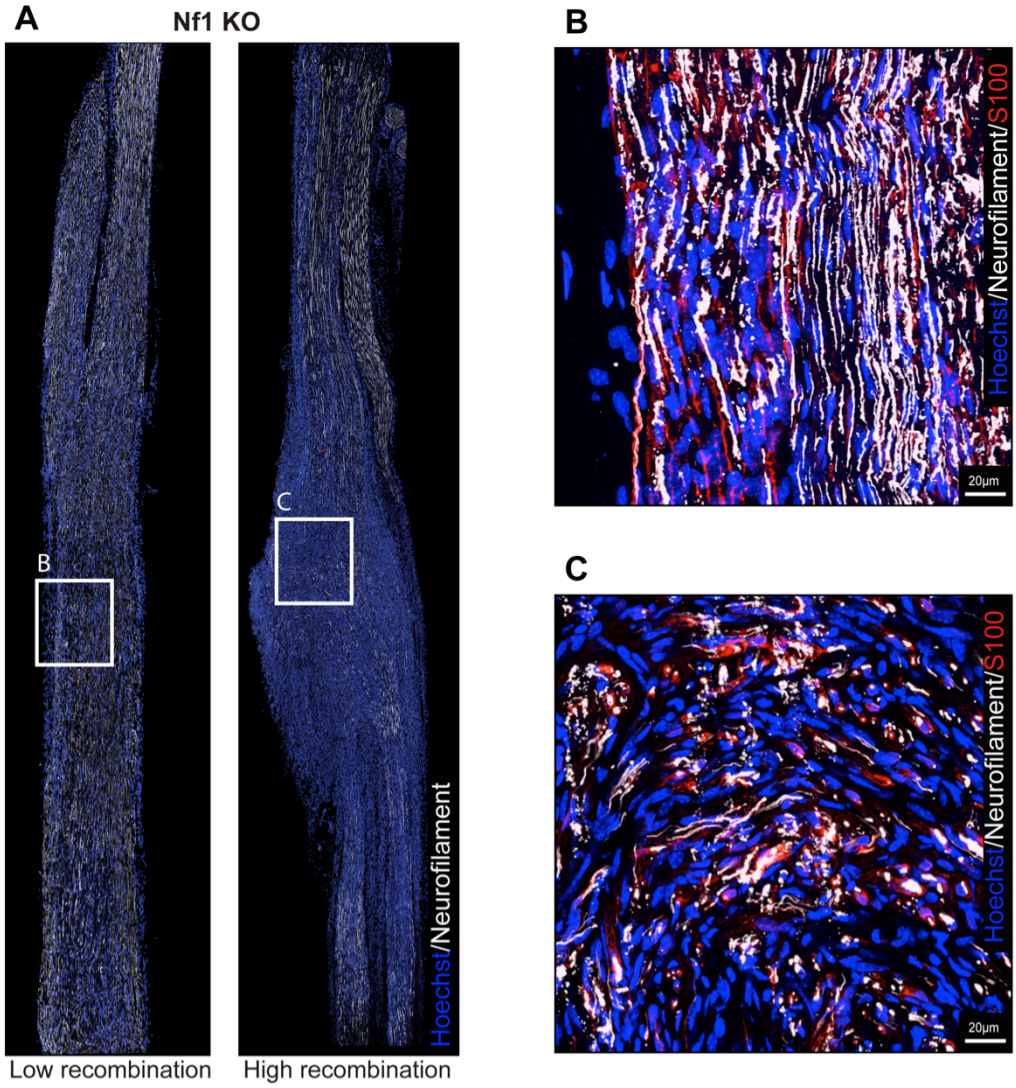

Figure 3.4. Highly disorganised nerve structure of animals with tumour formation at the injury site, 8 months following nerve injury

(A) 8 months following injury, longitudinal cryosections of sciatic nerves from Nf1 KO were immunolabelled for neurofilament (grey), S100 (red) and nuclei were counterstained with Hoechst. High magnification image of **(B)** a normal regenerated Nf1 KO nerve showing no structural abnormality and **(C)** a tumour at the injury site, which showed an increased cell density and a highly abnormal organisation.

80%) with several animals showing zero levels of recombination. Consistent with our previous results (Ribeiro et al., 2013), tumours only arose at the injury site in the Nf1 KO mice. The total tumour formation rate in this experiment was 45%, slightly higher than the 30%, which was previously observed (Ribeiro et al., 2013). In all cases, the injured sciatic nerve of the animals with 0% recombination rate was indistinguishable to a control (Nf1 WT) regenerated nerve at 8 months. As shown in Figure 3.3, all but 1 animal (88%) with more than a 30% recombination rate developed tumours at the injury site, 8 months following injury. One outlier was observed; animal # 6, which had a 40% YFP recombination rate but a normal regenerated nerve.

Importantly, when the tumour bearing nerves were analysed at the cellular level, tumour formation was associated with a highly disorganised structure, whereas the normal-looking nerves had a more organised structure (Figure 3.4). This disorganised structure is consistent with the pathology of Nf1 KO tumours as previously (Ribeiro et al., 2013), whereas a more organised structure indicates that the nerve has regenerated normally.

In conclusion, we have found that animals with a low recombination efficiency did not develop tumours, whereas animals with a recombination efficiency higher than 30% formed tumours at the injury site. These findings demonstrated that recombination rate was sufficient to predict the formation of neurofibromas at the injury site.

The identification of a threshold (YFP recombination > 30%) above which tumour growth is highly likely to occur had key implications for this project, as it allowed the prediction of the fate of a regenerating nerve before a tumour had formed. This provided us with a more powerful and tractable model to investigate the very early stages of tumour development, months before tumours were visible, as we could be confident that animals with a recombination efficiency higher than 30% would go on to form tumours. This should strengthen our analyses to detect the molecular and cellular changes responsible for determining why a tumour only forms at the injury site. For all studies performed after this analysis, only animals with a recombination rate higher than 30% were selected.

3.3. Determination of Cre-mediated recombination variability in P0-CreER^{T2} mice

We next aimed to optimise Cre-mediated recombination efficiency in our mice strain in order to obtain a higher and more consistent recombination efficiency, which would greatly reduce the numbers of animals required for the tumour studies. We have previously noted that the age of the animals at the time of peritoneal tmx injection appeared to affect the Cre-mediated recombination rate, with animals injected at a younger age (P31) showing higher levels of recombination.

This suggested that P0 promoter activity may decrease with the age of the animals or that the nerve perhaps becomes less permeable to tamoxifen, as the Blood Nerve Barrier is established at this developmental stage. Other studies, in line with our observations, demonstrated that the expression of certain transgenes was reduced with the increased age of the animals (Feil et al., 2009; Monvoisin et al., 2006; Robertson et al., 1996). Consequently, we used a standard protocol for tmx administration-the intraperitoneal injection of 2mg of tmx a day over a period of 5 consecutive days in P31 mice, as this protocol has been previously reported to be the most efficient at inducing Cre activity in mSCs (Leone et al., 2003).

We initially determined the Cre-mediated recombination efficiency in a panel of animals, in order to determine the variability of the Cre-mediated recombination efficiency of this age group. For the RNA sequencing analysis, described in Chapter 5, in which large numbers of animals were used, we needed to ensure that the recombination frequency was over 30%, consequently, a large panel of animals was analysed for the percentage of recombination. P0-CreER^{T2} mediated recombination was assessed by the expression of YFP in sciatic nerves of the Nf1 KO and control (Nf1 WT) mice, 15 days following the first tmx injection. Immunostaining with an antibody against GFP (which binds to YFP) and a pan Schwann cell marker, S100 was used to discriminate between the recombined mSCs (YFP+/S100+) and the unrecombined mSCs (YFP- S100+). S100 also labels the nmSCs but these can be morphologically distinguished from mSCs. As shown in Figure 3.5, the average recombination efficiency of this large cohort was only 27% and we observed a large amount of variation in Cre-mediated recombination efficiency, ranging from 0-80%, with many animals (~10%)

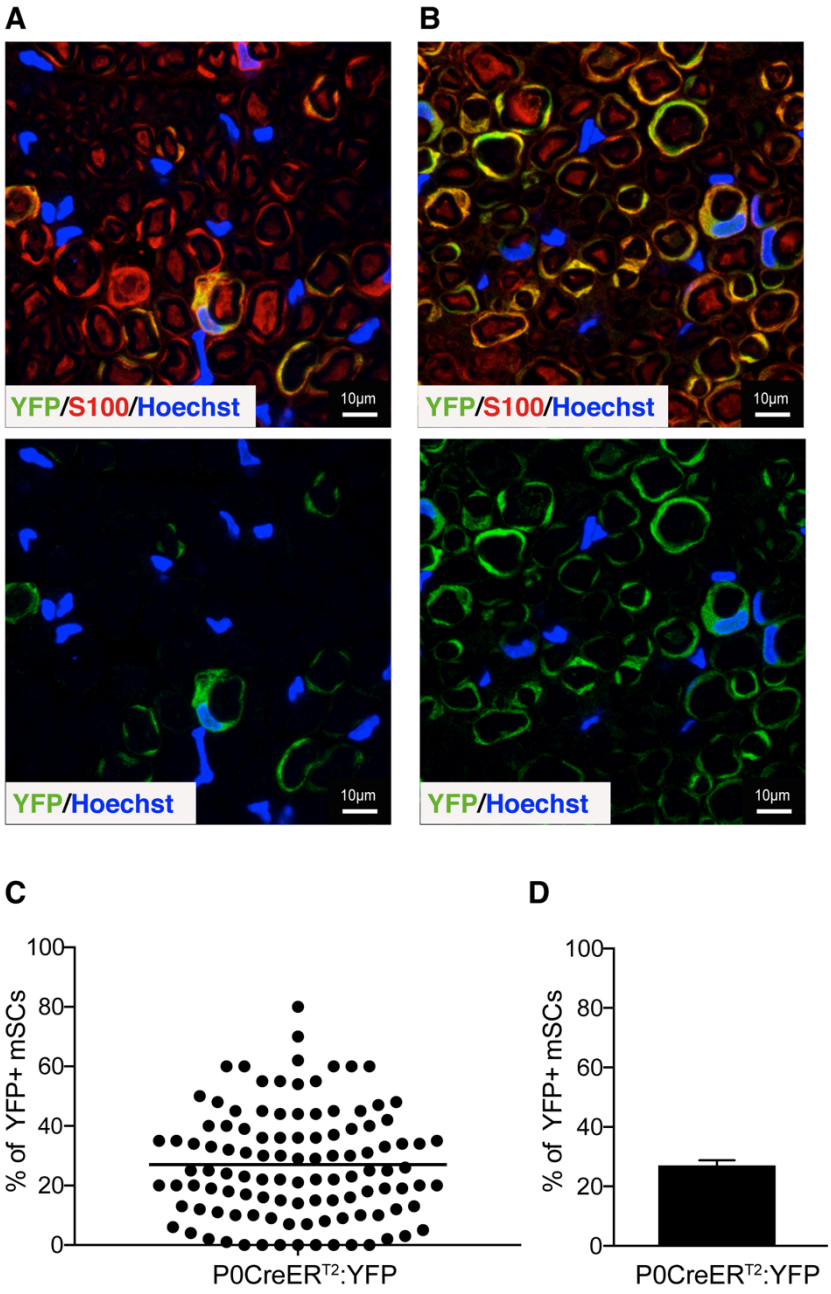

Figure 3.5. High variation of Cre-mediated recombination efficiency in P0- CreER^{T2} mice

Tmx-treated mice were analysed for recombination of the YFP reporter cassette, 2 weeks after peritoneal injection. Cryosections of Nf1 KO and control (Nf1 WT) mice were stained for the Schwann cell marker S100 (red) and YFP labelled with an antibody to GFP (green). Nuclei were counterstained with Hoechst. The efficiency of Cre-mediated recombination was calculated by counting YFP+ mSCs over total mSCs. Representative image of an animal with **(A)** a low and **(B)** a high Cre- mediated recombination efficiency. **(C)** Graph shows the quantification of the percentage of YFP+ mSCs. Each circle in the graph displays the recombination rate of one animal and the average recombination efficiency is displayed as a line. (**D)** Graph shows the average recombination rate of 27% (n=110±SEM).

showing no recombination at all.

After determining the variation in the Cre-mediated recombination efficiency in the P0-CreER^{T2}:YFP mouse strain, we aimed to achieve a higher, less variable recombination rate by testing the effects of: 1. Homozygosity of the P0-CreER^{T2} transgene; 2. Gender of the parental P0-CreER^{T2} carrier and 3. Tamoxifen administration route. Some of these parameters have been shown previously to impact the recombination efficiency or variability in other transgenic mouse models (Heffner et al., 2012; Park et al., 2008; Soriano, 2010).

1. The zygosity of the P0-CreER^{T2} transgene could affect the recombination efficiency, as higher levels of Cre could induce more efficient recombination. In these studies, breeding pairs consisted of parents either heterozygous or homozygous for the P0-CreER^{T2} transgene, which results in a mix of zygosity in the next generation. However, as the P0-Cre genotyping primers cannot discriminate between homozygous or heterozygous animals, we could not test this directly. We therefore used mice which were derived from a breeding pair in which either a P0-CreER^{T2}:YFP female or male was crossed with a Cre negative animal. Crossing with a Cre negative animal ensured that all the Cre positive progenies were heterozygous for the P0-CreER^{T2} transgene (P0-CreER$^{T2+/-}$:YFP:Nf1$^{fl/fl}$).

Following tmx administration, we compared the average recombination rate of the P0-CreER^{T2} heterozygous progenies to the rate determined in the mixed population analysed previously (Figure 3.5). As shown in Figure 3.6, the Cre-mediated recombination efficiency remained highly variable in the P0-CreER^{T2} heterozygous animals, but was on average slightly lower, although this effect was not statistically significant (p-value=0.078). However, the trend towards a lower recombination efficiency in the heterozygous population suggested that while gene dosage may influence the recombination efficiency it was not responsible for the large variability seen in this mouse strain.

To increase the proportion of P0-CreER^{T2} homozygous progenies for future experiments, we decided to select breeding pairs from which all progenies are positive for the P0-CreER^{T2} transgene, which should increase the average Cre-mediated recombination efficiency in the experimental animals.

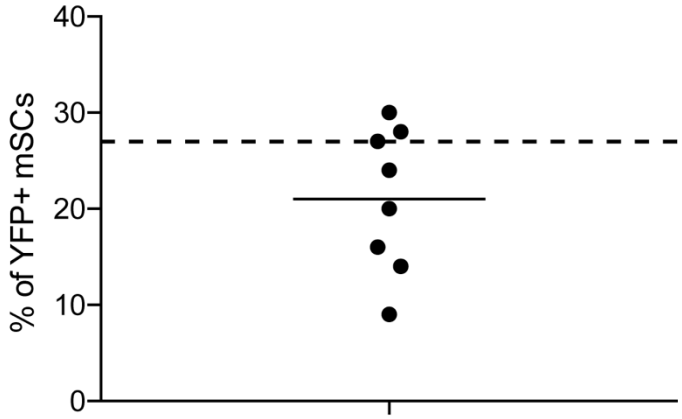

Figure 3.6. Cre-mediated recombination efficiency is lower in Cre heterozygous animas but remains highly variable

All analysed animals carried the P0-CreER^{T2} transgene in heterozygosity (P0-CreER$^{T2\ +/-}$:YFP:Nf1$^{fl/fl}$), were the same sex (males) and were injected at the same age (P31). The tmx-treated Cre heterozygous mice were analysed for YFP expression, 2 weeks after injection. The efficiency of Cre-mediated recombination was calculated by counting the YFP+ mSCs over total mSCs. Cre-mediated recombination efficiency remained highly variable, whereas the average recombination rate was lower, although this was not statistically significant (p-value=0.078) compared to the previously analysed average recombination indicated by the dashed line of the mixed Cre homo- and heterozygous animals. The average recombination efficiency is displayed as a line (n=8).

2. The chromosomal location of the P0-CreER^{T2} transgene is unknown and therefore it could be inserted in a sex chromosome, as been demonstrated for other transgenic mouse strains (Pinkert, 2014). Furthermore, the gender of the transgene carrier may impact Cre recombination at the epigenetic level. Consequently, we tested whether the gender of the parental transgene carrier affects the Cre-mediated recombination efficiency by analysing progenies of breeding pairs in which either the female or male breeder carried the P0-CreER^{T2} transgene. Analysis of the mice showed that the average recombination efficiency and variability in the tmx treated progenies of was not different depending on a female or male P0-CreER^{T2} carrier (Figure 3.7). These findings indicate that Cre expression level and recombination rate variability between the progenies is independent of the gender of the parental transgene carrier in this mouse strain.

3. We tested if the intraperitoneal route of tmx administration might be suboptimal, as it has been shown previously that altering the administration route can result in more efficient recombination. Some studies suggested that oral tmx administration can result in more rapid and uniform Cre mediated recombination and can be less toxic in comparison to intraperitoneal injections, as the latter can cause tamoxifen accumulation in the peritoneum (Park et al., 2008; Soriano, 2010). We tested this by administrating tamoxifen orally (using gavage) instead of intraperitoneally. In agreement with these studies, our results showed that the Cre mediated recombination was much higher (male: 56%, female: 54%, combined: 55%) in mice, in which tmx was administrated orally compared to those with peritoneal administration (27%) (Figure 3.8A-D). Importantly, the vast majority (90%) of the analysed animals had a recombination efficiency > 30%, which is the recombination efficiency previously determined to predispose the Nf1 KO animals to tumour growth at the injury site. The identification of a more optimal administration route for tmx delivery provides a method to obtain more animals prone to tumour development and consequently will help us to reduce the animals required for future experiments. Nevertheless, the variation in recombination frequency between littermates remained (Figure 3.8C).

In summary, we have improved the Cre-mediated recombination efficiency in our mouse model. We have shown that Cre-mediated recombination efficiency is independent of the

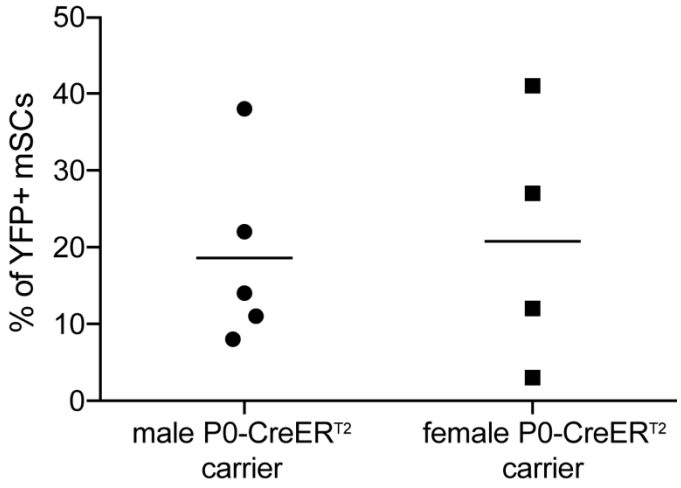

Figure 3.7. Cre-mediated recombination efficiency is independent of the gender of the transgene carrier

Tmx-treated mice were analysed for recombination of the YFP reporter cassette, 2 weeks after injection. All the animals analysed were the same sex (females) and were injected at the same age (P31). Two panels of mice were analysed: Progenies of a male P0-CreER^{T2} carrier and progenies of a female P0-CreER^{T2} carrier. The efficiency of Cre-mediated recombination was calculated by counting the YFP+ mSCs over total number of mSCs. No difference in Cre-mediated recombination efficiency was observed between the two panels indicating that the distribution of Cre mediated recombination rates is independent of the gender of the transgene carrier. The average recombination efficiency is displayed as a line in both panels (n=4-5).

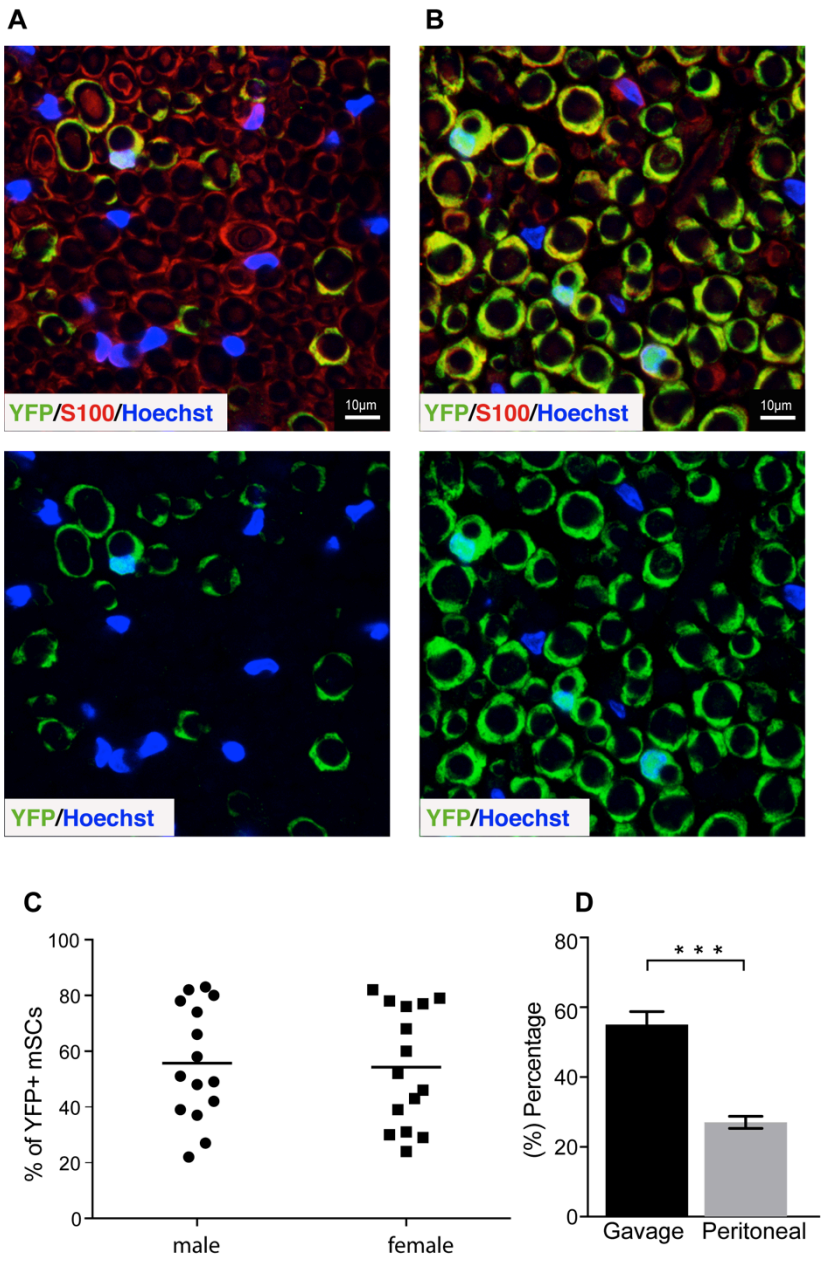

Figure 3.8. Higher average recombination efficiency was obtained by oral tmx administration

Nf1 KO mice were orally administrated with tmx and analysed for YFP expression, 2 weeks after oral administration. Cryosections were stained for the SC marker S100 (red) and YFP was labelled with an antibody to GFP (green). Nuclei were counterstained with Hoechst. The efficiency of Cre-mediated recombination was calculated by counting the YFP+ mSCs over total number of mSCs. Representative images of an animal with **(A)** 30% recombination and **(B)** 80% recombination. **(C)** Graph shows the percentage of YFP+ mSCs. Each circle or square in the graph displays the recombination rate of one animal and the average recombination efficiency of either female (56%) or male (54%) is displayed with a line (n=15). **(D)** Graph shows the average recombination rate of animals administrated with tmx orally (Gavage) or peritoneally. The average recombination rate of animals that were administrated orally with tmx was 55% (n=30), which is significantly higher (p-value of < 0.001) compared to the previous determined average intraperitoneal recombination rate (27%) (Gavage:n=30±SEM, Peritoneal: n=110±SEM).

gender of the P0-CreER^{T2} carrier. Moreover, we have shown that homozygous expression of the P0-CreER^{T2} transgene resulted in a slightly enhanced average recombination rate. Finally, we demonstrated that oral administration of tmx is more efficient at inducing Cre recombination compared to intraperitoneal administrated tmx.

As the optimisation of the Cre-mediated recombination efficiency was performed in parallel with other experiments, many experiments described in this thesis have used the intraperitoneal tmx injection route. However, Cre recombination efficiency was analysed in the contralateral nerve of each animal to ensure that the recombination rate was > 30% irrespective of the administration route. To reduce animal numbers in future projects, oral tmx administration will be the default route of administration.

3.4. Cre expression level correlates with recombination efficiency

Oral tmx administration resulted in increased average recombination efficiency, however the variation in the recombination efficiency amongst animals of the same litter remained. A possible explanation for the variation in recombination rate is that the Cre RNA expression level could be lower in some animals due to transcriptional inhibition by, for example, epigenetic modifications of the promoter sequence (Harno et al., 2013; Schulz et al., 2007). It is known that foreign DNA is prone to methylation and other modifications after integration into the mammalian genome (Doerfler et al., 2001). Furthermore, the Cre gene sequence has a high frequency of CpG dinucleotides, which can lead to epigenetic silencing as demonstrated previously for other CpG dinucleotide sequences (Shimshek et al., 2002). Alternatively, the low level of recombination could be caused by epigenetic modification of the loxP sites, the substrate for the Cre recombinase, in our mouse strain, which could prevent recognition of the site by the Cre recombinase (Rassoulzadegan et al., 2002).

To test this, we performed qRT-PCRs using primers for the P0-CreER^{T2} transgene and the YFP reporter cassette to detect RNA from these two loci. Previous studies have demonstrated robust activation of Cre one week after tmx administration (Reinert et al., 2012). We therefore chose one week after the last tmx administration as the timepoint to analyse Cre and YFP mRNA expression levels. One nerve was analysed for YFP protein

expression levels by immunofluorescence (IF) staining using an antibody to GFP and RNA was extracted in parallel from the contralateral nerve of each animal. According to the YFP protein expression level, the animals were categorised into high or low YFP protein expression (high and low recombination rates) and Cre and YFP mRNA expression levels were determined by qRT-PCR in the contralateral nerve. We used animals, which were constitutively active for P0-Cre and animals negative for the Cre transgene, as positive and negative controls for Cre mRNA expression respectively. As expected, our analysis showed, that the YFP mRNA levels were consistent with the YFP protein expression levels, which were determined by IF and used for categorisation prior to the qRT-PCR (data not shown). However, we found that Cre mRNA expression level varied between littermates in the P0-CreER^{T2} mouse strain and importantly that the level of Cre mRNA expression correlated with recombination efficiency (Figure 3.9). These findings suggest that Cre mRNA expression is transcriptionally silenced, presumably by epigenetic modification, within the low recombined animals implying that the animals may have to be more frequently backcrossed in order to refresh their gene pool.

3.5. Generation of a confetti mouse model for lineage analysis of neurofibromas

In patients with Neurofibromatosis type I (NF1) it is well established that tumours arise from SCs that have lost expression of the Nf1 gene, however it remains unknown whether one or many Nf1 KO SC cell populations drive tumour growth. In the case of a dominant tumour-driving Nf1 KO clone, neurofibromas would be monoclonal, whereas if several Nf1 KO clones contribute to tumour growth the resultant tumour would be polyclonal. Several lineage tracing methods have been developed to address the question of whether one or many cell subpopulations are responsible for tumour development. In mouse models, the most popular technique has been the labelling of cells based on a drug inducible Cre recombinase together with a reporter system (Kretzschmar and Watt, 2012; Van Keymeulen and Blanpain, 2012). Using these systems, the behaviour of a single cell-derived clone can be studied if the tissue is labelled at clonal density.

Multicolour reporter constructs have also been developed for lineage tracing studies, which

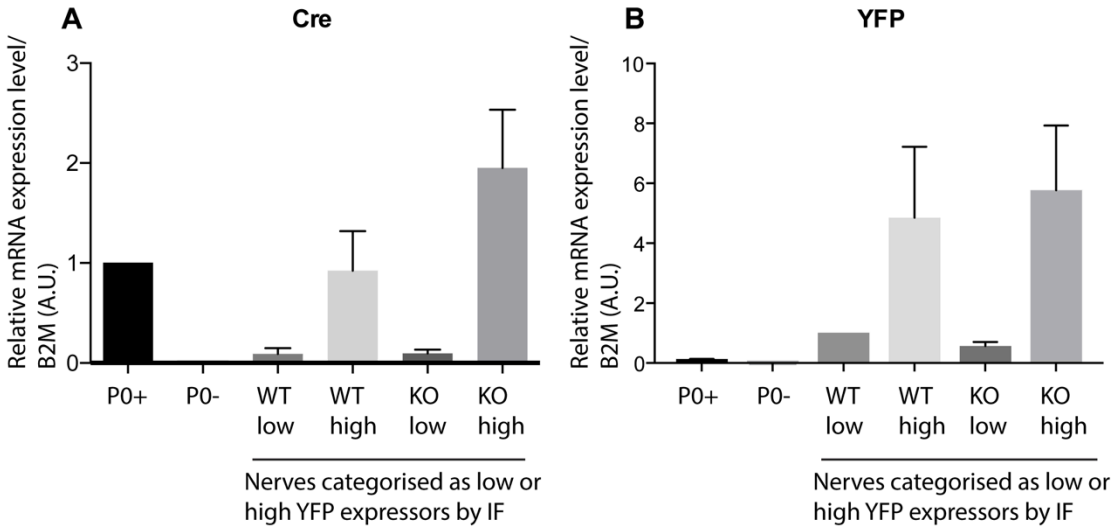

Figure 3.9. qRT-PCR shows that Cre mRNA expression levels correlate with recombination efficiency

Nf1 KO and control mice (Nf1 WT) were analysed 1 week after the last tmx administration. One sciatic nerve was processed for immunofluorescence staining for YFP and the animals categorised as low or high YFP protein expression. RNA was extracted from the contralateral nerve and YFP and Cre mRNA expression levels were analysed. P0-Cre constitutive animals were used as a positive control for Cre expression and P0-Cre negative animals as negative controls. Both the P0-Cre+ (P0+) and P0-Cre- (P0-) mice are negative for the YFP reporter cassette. **A)** Graph shows Cre mRNA expression levels in littermates. Cre mRNA levels correlated with low and high expression of YFP. Fold change was compared to the P0+ sample. **B)** Graph shows YFP mRNA expression levels in the same animals as (A). Fold change was compared to “WT low” sample. Bars show the mean ±SEM for five independent experiments.

allow expression of random different multicolour combinations in order to follow the contribution of individual cell subpopulations to cancer growth, and to facilitate the identification of the cell of origin (Livet et al., 2007; Snippert et al., 2010).

A widely used multicolour reporter system is the R26R-Confetti mouse model (also known as the R26RBrainbow 2.1 mouse model), in which the Brainbow 2.1 construct is inserted into the R26R locus. This mouse model enables the expression of 4 fluorescent proteins in a stochastic manner (Livet et al., 2007). Mice homozygous for the R26R-Confetti conditional allele are viable with a CAG promoter, loxP site, and STOP cassette preventing transcription (Livet et al., 2007; Snippert et al., 2010). The Brainbow 2.1 region contains two loxP-flanked dimers (Figure 3.10B). One dimer contains nuclear-localised green fluorescent protein (hrGFPII) and a reverse-oriented cytoplasmic yellow fluorescent protein (mYFP). The other dimer contains cytoplasmic red fluorescent protein (tdimer2(12)) and a reverse-oriented membrane-tethered cyan fluorescent protein (mCerulean) (Livet et al., 2007).

Using this mouse model, work from the Clevers group (Snippert et al., 2010) has shown that, although an intestinal crypt is initially multiclonal (derived from several stem cells within the crypt), a shift towards monoclonality is observed over time. However, despite their power these multicolour systems have several technical challenges such as the visualisation of the fluorescent reporter proteins after tissue processing and co-staining with antibodies is limited due to the restricted availability of additional fluorophores.

To test if neurofibromas are monoclonal, we required a system that would allow us to distinguish between individual, adjacent recombined SCs. Therefore, we used the R26R-Confetti mouse model, which we crossed to P0-CreER^{T2} mice and to P0-CreER^{T2}:Nf1$^{fl/fl}$ mice to generate P0-CreER^{T2}:Confetti and P0-CreER^{T2}:Confetti:Nf1$^{fl/fl}$ mice (Figure 3.10A). For simplicity, we will refer to these mouse strains as Nf1 KO-Confetti mice and control- (Nf1 WT) Confetti mice throughout this thesis. Another advantage of this mouse model is that it enables us to study the behaviour of individual neighbouring SCs at the early stages following nerve injury (Chapter 4). In order to confirm the crossings, we performed PCRs to detect the insertion of the Brainbow 2.1 construct. PCR showed a band of 300bp (mutant band) in

homozygous animals and a band of 386bp (wt band) and of 300bp in heterozygous animals (Figure 3.10B).

Upon recombination, this mouse model stochastically expresses one of four endogenous fluorophores in different subcellular locations, generating ten possible different colour combinations when two alleles are recombined in homozygous mice (Figure 3.10C). In order to test the functionality of the confetti reporter cassette in the mSC population, we administrated 2mg of tmx a day over a period of 5 consecutive days to Nf1 KO and control confetti mice. 2 weeks following the first tmx administration, the sciatic nerves were harvested and processed for immunostaining, as shown in Figure 3.10C. We optimised nuclear co-staining and confocal imaging conditions to visualise the endogenous fluorescent proteins. As Hoechst cannot be used as a nuclear counterstain, because its excitation spectra would overlap with CFP, we established a protocol to detect TO-PRO-3 (see materials and methods), a nuclear counterstain that is excited at a wavelength of ~640nm. We then established acquisition settings to optimise the lasers to excite the four fluorophores and the nuclear counterstain, without spectral overlap. For example, the excitation wavelengths of GFP and YFP are very close to each other and accordingly, their excitation spectra have to be set to ensure that they do not overlap. In addition, CFP required a laser which excites at ~440-455nm, as we could not obtain sufficient emission using a 405nm laser light. We successfully optimised the imaging conditions for the confetti system and we found that the endogenous confetti reporter cassette expression was detected specifically in mSCs, whereas no expression was observed in nmSCs within the sciatic nerves (Figure 3.11). No fluorescent mSCs were detected in mice, which did not express active Cre recombinase (data not shown) demonstrating that the Confetti reporter cassette expression is not leaky in the absence of Cre recombinase.

Before we set up the lineage tracing and clonality studies described in Chapter 4 and 5 we first tested the efficiency of Cre-mediated recombination to investigate whether we could obtain sufficient recombination to achieve a recombination efficiency of > 30% in order to induce tumourigenesis. Furthermore, it was important to determine the frequency of each colour recombination in order to calculate whether a specific clone expanded in size within

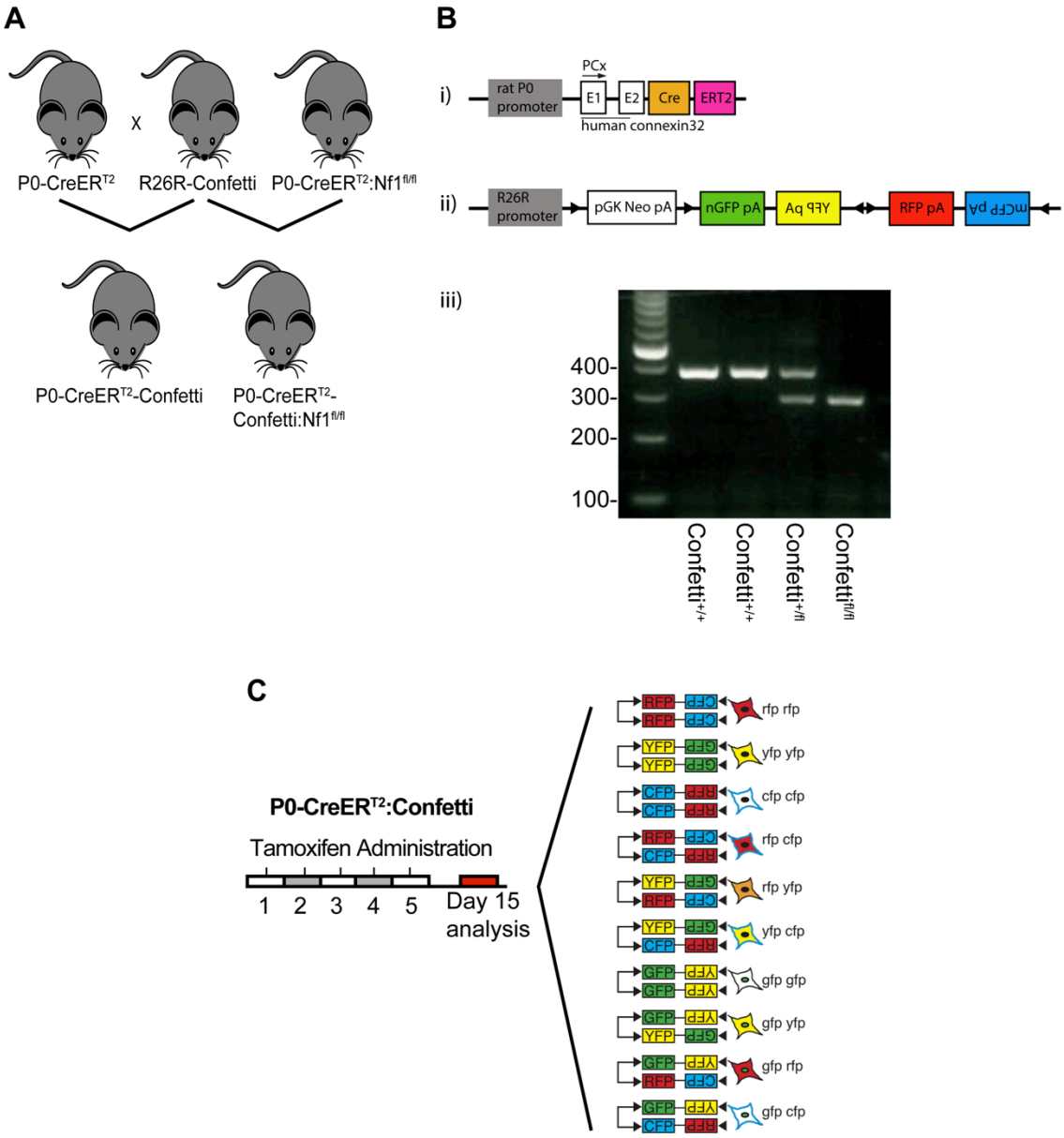

Figure 3.10. Generation of P0-CreER^{T2}:Confetti mouse model

A) P0-CreER^{T2} and P0-CreER^{T2}:Nf1$^{fl/fl}$ mice were crossed to R26R-Confetti mice to generate P0-CreER^{T2}:Confetti and P0-CreER^{T2}:Confetti:Nf1$^{fl/fl}$ mice. **B)** Schematic representation of the (i) P0 promoter and (ii) the R26R-Confetti reporter cassette. iii) PCR detection of the R26R-Confetti construct in genomic DNA from adult sciatic nerve of control, Confetti$^{WT/fl}$ and Confetti$^{fl/fl}$ mice. The WT allele is 386bp and the floxed allele is 300bp. **C)** Schematic representation of the ten different colour recombinations possible in mSCs after tmx treatment.

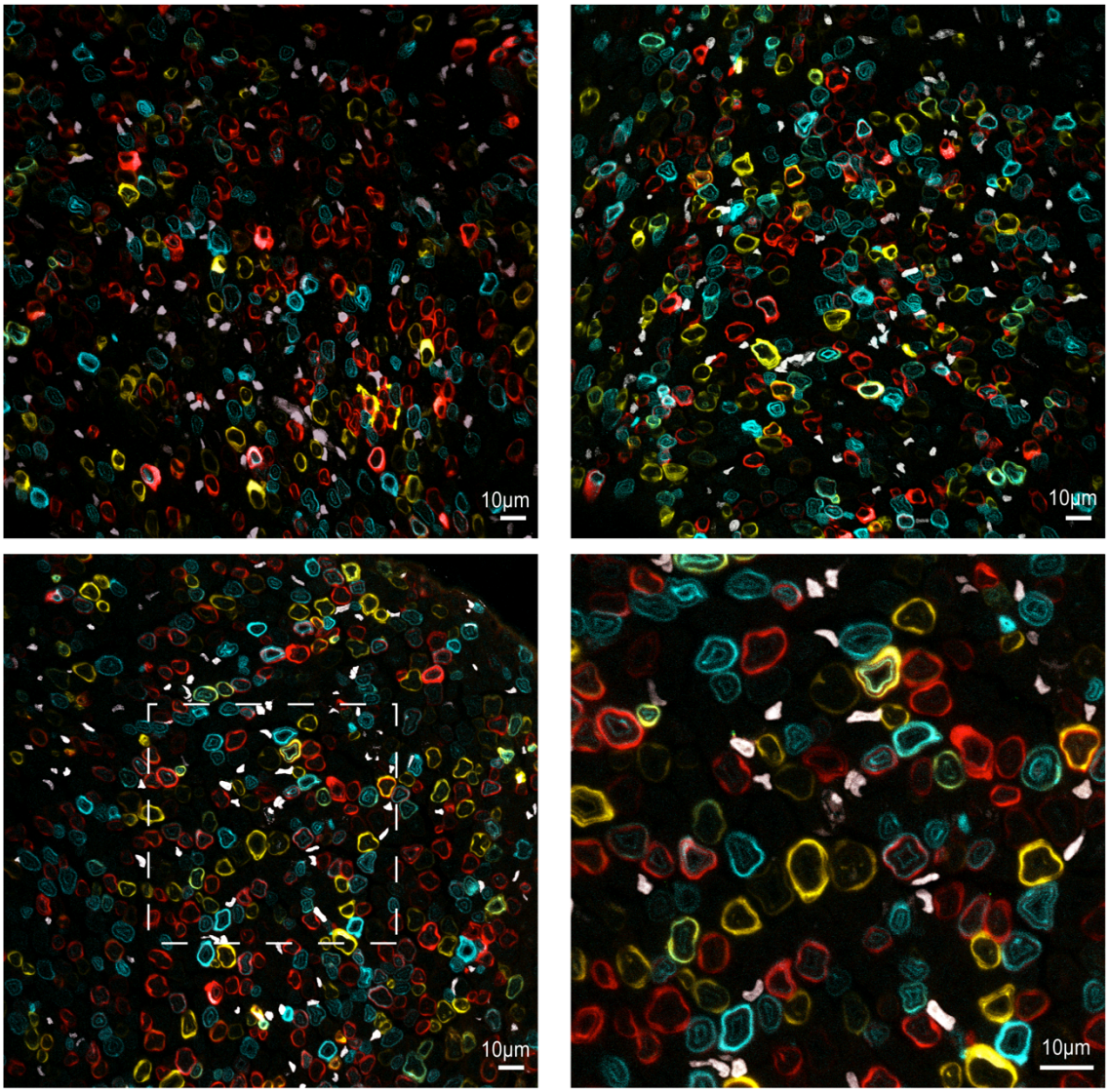

Figure 3.11. mSCs specifically express the fluorescent reporter cassette in the confetti mouse model

Representative confocal images of tamoxifen treated P0-CreER^{T2}:Confetti mice. Mice were analysed 2 weeks after tmx administration. No expression of the Confetti reporter cassette could be detected in P0-CreER^{T2} negative littermates. Nuclei were labelled with RedDot. (white).

the tumour mass.

The overall Cre mediated recombination efficiency was calculated by counting the recombined mSCs over the total number of mSCs. As with the P0-CreER^{T2}:YFP mouse model, we found the Cre-mediated recombination efficiency was highly variable and ranging from 0-80% (Figure 3.12B). The recombination efficiencies of both genotypes were combined in order to compare the average recombination rate of this Confetti mouse model to the previously determined average recombination rate of the P0-CreER^{T2}:YFP mouse model. This showed that the average recombination efficiency of the confetti mouse model was significantly higher (41%) compared to the P0-CreER^{T2}:YFP mouse model (27%) (Figure 3.12D). The increased recombination efficiency of the confetti mouse model was probably due to the "refreshment" of the P0-CreER^{T2} mice gene pool by crossing to a different line. As recombination was induced by peritoneal tmx administration, this suggested that even higher recombination rates should be obtained by using oral tmx administration.

The frequency of each colour recombination was determined by counting the individual colour recombination over the total number of recombined mSCs (Figure 3.12A). Analysis of the nerves showed that red (Nf1 WT 35% and Nf1 KO 28%) was the most frequent single colour recombination followed by similar levels of yellow and blue (blue: Nf1 WT 19% and Nf1 KO 24%, yellow: Nf1 WT 19% and Nf1 KO 24%), whereas green (Nf1 WT 4% and Nf1 KO 4%) and all the double colour recombinations such as blue-red (Nf1 WT 13% and Nf1 KO 11%) and red-yellow (Nf1 WT 5% and Nf1 KO 5%) occurred less frequently. The average colour recombination frequency of each of the 10 colour combinations was not significantly different between Nf1 KO and control confetti mice as shown in Figure 3.12C. However, the colour recombination frequencies differed between animals (Figure 3.12B) and this variation needs to be taken into account when analysing the prevalence of colour recombination within the tumours. Therefore, in order to determine whether a clonal Nf1 KO subpopulation has expanded in size, each colour recombination frequency within the tumours will be compared to the average colour recombination frequencies of all the uninjured contralateral nerves.

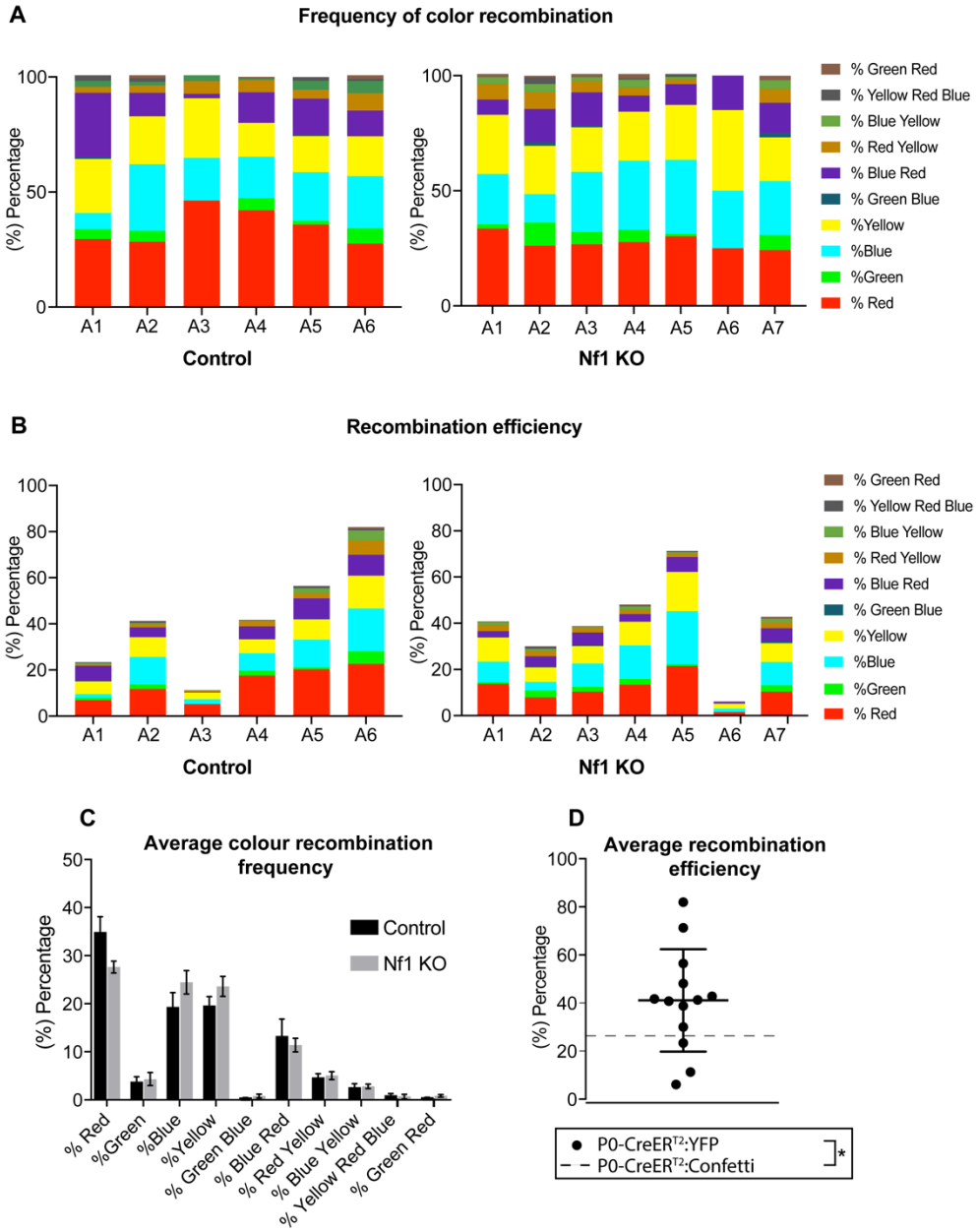

Figure 3.12. Frequency of individual colour recombination and Cre-mediated recombination in Nf1 KO and control (Nf1 WT) confetti mice

Tmx-treated Nf1 KO and control (Nf1 WT) confetti mice were analysed 2 weeks after tmx injection. **A)** Graph shows the colour recombination frequency for the individual colour combinations in each animal. **B)** Graph shows the Cre mediated recombination efficiency in each animal. Note that the recombination efficiency was variable in both genotypes. **C)** Graph shows the average colour recombination frequency for each of the 10 different colour combinations in Nf1 KO and control (Nf1 WT) confetti mice. There is no significant difference between Nf1 KO and control (Nf1 WT) mice (n=6-7±SEM). **D)** Graph shows the average recombination efficiency (41%) obtained with the Confetti mouse model (n=13±SEM). The average recombination rate of the confetti mouse model was observed to be higher (p-value=0.0381) than the previously determined average recombination rate (27%) of the P0-CreER^{T2}:YFP mouse model, which is indicated with a dashed line.

3.6. Chapter discussion and conclusions

Early detection and treatment is significantly improving the long-term survival of cancer patients, however, it remains challenging to detect cancers at their very early stages. Many cancers still elude early detection and are only detectable at later stages (Rempe et al., 2006), as common cancer screening methods fail and tumour-specific genomic, proteomic and epigenetic signatures are not known at these early stages. The generation of mouse models, which imitate these early stages, may contribute to the identification of new tumour - specific signatures and conse

quently to the development of new therapies. The LSL KrasG12D mouse model, for example, is a widely used model for analysing the early stages of lung cancer and has led to the identification of a new cell type, which contributes to the development of the disease (Jackson et al., 2001; Tuveson et al., 2004).

In this chapter, I have described the establishment of a powerful and tractable mouse model, which will enable the study of the early stages of neurofibroma formation. I have shown a direct correlation between Cre mediated recombination efficiency and tumour growth and identified a Cre mediated recombination efficiency threshold of > 30%, above which tumour growth is expected at the injury site of the Nf1 KO animals. The power of this system is that the specific location of tumour formation is known and we have established a methodology to identify the animals prone for tumour development at the later stages. Furthermore, as the tumour only develops at the injury site, our system allows us to follow both how the Nf1 KO SCs together with the injury microenvironment contribute to tumour formation at the site of injury and how Nf1 KO SCs are instructed to re-differentiate within the normal nerve environment at the distal stump. In future experiments, we aim to identify both the signalling pathways responsible for creating a pro-tumourigenic environment at the site of injury and the signalling pathways providing an anti-tumourigenic environment in a normal nerve microenvironment. Identification of either signal may identify new molecular targets, which may be important for the development of therapeutics for this disease, some of which may be of use prophylactically.

We also aimed to optimise the Cre-mediated recombination efficiency in the P0-CreER^{T2} mouse model to reduce the animals needed for our studies. Firstly, we showed that homozygous expression of the P0-CreER^{T2} transgene slightly increases the average recombination rate in our mouse strain. Secondly, we found that the Cre-mediated recombination efficiency is independent of the gender of the P0-CreER^{T2} transgene carrier. Finally, we have chosen the oral tmx administration route as the administration route for future experiments, as we found that oral tmx administration, as opposed to intraperitoneal injection, improved the average recombination efficiency significantly, although variation between animals of the same litter remained. This finding should greatly reduce the number of animals needed for future experiments. We also found that the recombination efficiency variation between littermates was likely due to transcriptional silencing of the Cre construct by for example methylation of the P0-promoter or the Cre recombinase gene. In agreement with our findings, it has been shown previously, that the prokaryotic Cre transgene sequence is a favourable target of methylation (Feng et al., 2001). In future, Cre transgene expression could be improved by for example using iCre (Shimshek et al., 2002), in which the prokaryotic codon of the Cre recombinase has been switched to a mammalian codon that is less prone to methylation. Alternatively, more frequent backcrossing may also contribute to “refresh” the gene pool of the P0-CreER^{T2}:YFP mice line.

Finally, I have described the generation of a new mouse model, the P0-CreER^{T2}:Confetti mouse model, to perform lineage-tracing experiments in order to determine the clonality of neurofibromas and to perform lineage studies of Nf1 KO and control (Nf1 WT) SCs. I have demonstrated functionality of the confetti reporter cassette upon tmx administration and the specificity of its expression in mSCs. I have successfully optimised (nuclear) co-staining and imaging settings and demonstrated the frequency of each single and double colour recombination. Furthermore, I have shown that we can achieve sufficient recombination (>30%) to obtain tumours for our long-term clonality studies.

The power of this inducible genetic labelling system lies in its ability to investigate individual cell-fate or cell population behaviour. Lineage tracing of a cell population, such as the Nf1 KO SCs, will help to investigate potential proliferative lineage hierarchy, cell fate and the

behaviour of neighbouring cells over time. However, these lineage tracing systems harbour several technical and experimental challenges. Technical challenges include the efficiency of cell labelling, as the extent of cell labelling can vary between different areas of the same tissue. In the mammary gland for example, although the recombination efficiency was determined as 30% overall, the degree of cell labelling was observed to be different between distinct areas (Rios et al., 2016). In addition to regional variations in cell labelling efficiency, the emission intensity of the 4 different fluorophors is unequal as for example the RFP intensity is much brighter than CFP, which could lead to an underestimation of certain cell subpopulations. For successful lineage tracing experiments, these technical challenges need to be taken into account whilst designing the experiment. Consequently, prior to starting the clonality analysis we ensured that the CFP emission intensity was equal to the other fluorophors. However, we cannot exclude variations in regional labelling but these should be taken into account by analysing several regions of each animal.

In future studies, we will firstly perform a clonality analysis of the neurofibromas at 8 months following injury in order to determine, whether neurofibromas are monoclonal or polyclonal. This analysis will indicate whether the tumour initiating Nf1 KO SCs requires an additional mutation prior to tumour formation at the injury site. Furthermore, we will perform lineage tracing studies to investigate the contribution of neighbouring mSCs to the regenerative response and to study their plasticity following nerve injury.

Interestingly, a recent study that used the confetti mouse model has demonstrated that the progression from papillomas to skin carcinomas involves a switch from monoclonality to polyclonality implying that the interactions between different subclones and their regional microenvironment is crucial for malignant transformation (Reeves et al., 2018). In order to investigate potential interactions between Nf1 KO mSCs and other neighbouring cell types we will use 3D confocal microscopy. This will allow us to visualise neighbouring Nf1 KO SCs in 3D and allows us to study their behaviour and interaction with other cell types during tumour initiation and progression.

In conclusion, in this chapter we successfully optimised Cre-mediated recombination efficiency in our mouse model and we have generated a mouse model in order to investigate

the clonality of neurofibromas and to perform lineage tracing studies. Importantly, we established a methodology, which allows us to discriminate between animals predisposed for tumour growth at a later stage, and this now provides us with a unique model to study the early stages of tumour initiation in neurofibroma.

Chapter Four: Peripheral nerve homeostasis and regeneration are distinct from the CNS and are independent of a stem cell population

4.1. Chapter Introduction

Once formed in the adult, peripheral nerves are relatively stable structures befitting of their role in transmitting signals back and forth between peripheral tissues and organs and the central nervous system (CNS). However, in contrast to the CNS, peripheral nerves are able to regenerate following an injury (Mahar and Cavalli, 2018). This requires not only the regrowth of the neurons, but the creation of new tissue to repair the wound site, together with the remodelling of the remaining nerve tissue to provide an environment conducive for axonal regrowth (Cattin and Lloyd, 2016; Zochodne, 2008). Following injury, the highly specialised SCs cells rapidly dedifferentiate to a proliferating, progenitor-like SC, which orchestrates the regenerative response, as they initiate an inflammatory response that clears axonal and myelin debris and remodels the nerve environment (Cattin and Lloyd, 2016)

The behaviour of mSCs is in stark contrast to the comparable cell of the CNS, the oligodendrocyte (OL). Once an OL has myelinated a neuron, it is post-mitotic in that it cannot return to a proliferative state. In order to produce new OLs throughout life, the adult CNS maintains a pool of slowly-proliferating oligodendrocyte progenitor cells (OPCs) into adulthood (Birey et al., 2017; Dimou and Simons, 2017; Kang et al., 2010; Young et al., 2013). Previous studies have addressed the cell turnover in the CNS and demonstrated that it is a relatively quiescent tissue (Young et al., 2013). However, to date, it is unclear if and how SCs and other peripheral nerve cells turnover throughout adulthood.

It is not clear why the CNS and PNS have evolved distinct mechanisms to produce new cells and have such different regenerative capabilities. Moreover, the apparent lack of a stem cell/progenitor population in the PNS to produce new cells, either during homeostasis or following injury is unusual for a mammalian tissue. This has led to speculation that an additional stem cell population contributes to the production of new SCs during the regenerative process (Amoh et al., 2005; Chen et al., 2012; McKenzie et al., 2006) and that SCs retain some multipotency that SC precursors exhibit during development in order to

regenerate new nerve tissue (Petersen and Adameyko, 2017).

In this chapter, we have investigated the behaviour of cells within the peripheral nerve in the adult and during the regeneration of a normal nerve. In particular, we determined the normal turnover, cell fate and behaviour of mSCs and showed how this can change following injury. Using lineage analysis we compared the plasticity of mSCs during peripheral nerve regeneration to their plasticity in tumourigenesis in order to understand whether a tumourigenic mutation (loss of Nf1) and a conducive microenvironment impacts SC plasticity. Finally, we performed clonal analysis using the Nf1 KO Confetti mouse model in order to understand whether neurofibromas are monoclonal or polyclonally derived. By studying the clonality of the tumours we should gain a deeper understanding of whether the signals of the injury microenvironment are sufficient to trigger tumourigenesis or if additional genetic mutations may be required.

4.2. Cell composition of peripheral nerve

We initially performed a detailed characterisation of the cell types and their turnover rates within the endoneurium of sciatic nerve. To do this, we used a number of transgenic mice, which express lineage-specific fluorescent labels together with immunofluorescence staining against endogenous specific cell markers. Furthermore, we quantified the different cell types by the analysis of EM images. Consistent with previous findings (Salonen et al., 1988), we found that the majority of cells within the endoneurium are SCs (~ 70%), as determined by staining with the cytoplasmic Schwann cell marker S100 and EM analysis (Figure 4.1A and 4.1B). To confirm this further, we analysed PLP-eGFP mice, in which all SCs express eGFP and found a similar percentage (~70%) of SCs (Figure 4.1A and 4.1B). To distinguish myelinating SCs (mSCs) from nonmyelinating (nmSCs) we performed immunostaining for myelin protein zero (P0, a marker for mSCs) (Figure 4.1C) and p75 (a marker for both nmSCs and dedifferentiated SCs (Jessen et al., 2015) (Figure 4.1D). From this analysis, we observed that the majority of SCs were mSCs with a ratio of mSCs to nmSCs roughly 2:1 (Figure 4.1B and 4.5A). This finding is in agreement with our EM analysis, in which we quantified the cell types by their morphology (Figure 4.1B).

During this analysis, we observed a proportion of p75+ cells that did not appear to be associated with axons and had a distinct morphology (Figure 4.2A). Moreover, these cells were negative for eGFP in nerves from PLP-eGFP mice indicating that they are not SCs (Figure 4.2B). To confirm these studies, we analysed p75+ in a separate mouse model (P0-Cre:tdTomato mice) in which SCs are labelled with tdTomato during development (Madisen et al., 2010). This analysis showed that a proportion of p75+ cells are clearly negative for tdTomato indicating that these cells are not SCs (Figure 4.2C). To test, whether these p75+ cells are SCs or are derived from SCs, we stained for the SC marker S100 and found that these cells were clearly negative as shown in Figure 4.2D.

Interestingly, we found that this p75+ population expressed two commonly used pericyte markers NG2 and PDGFRβ in nerves from PLP-eGFP mice, which was surprising as these cells were often not associated with blood vessels (Figure 4.3A). Furthermore, we determined, whether NG2 is co-expressed with PDGFRβ and we observed complete overlap between the two pericyte markers in these cells (Figure 4.3B). In order to confirm NG2 expression in these cells, we used NG2- dsRed mice (Zhu et al., 2008) that express dsRed in a NG2-driven expression construct and found complete overlap between NG2/PDGFRβ immunostaining and ds-Red expression (Figure 4.3C).

In the progress of this analysis, we identified three populations of NG2+/ PDGFRβ+ cells within the nerve endoneurium. Classical pericytes (Armulik et al., 2011) were identified as the first population, and were defined as cells which co-express NG2,PDGFRβ and α-smooth muscle actin (αSMA), but were negative for p75 (Figure 4.4A). Moreover, morphologically, they were tightly associated with CD31+ blood vessels and EM analysis showed that they were within the basal lamina of the blood vessels (Figure 4.4B). These cells comprised 1.5% of the total cells within the nerve endoneurium (Figure 4.5A).

A much larger population (12.5%) of the total peripheral nerve cell expressed NG2, PDGFRβ, and p75 and were identified as non-associated with axons, as discussed above (Figure 4.2 and Figure 4.5A). We also noticed that a proportion of these cells were found loosely associated with blood vessels, whereas others appeared to be within the endoneurium away from blood vessels (Figure 4.4C and 4.5A).

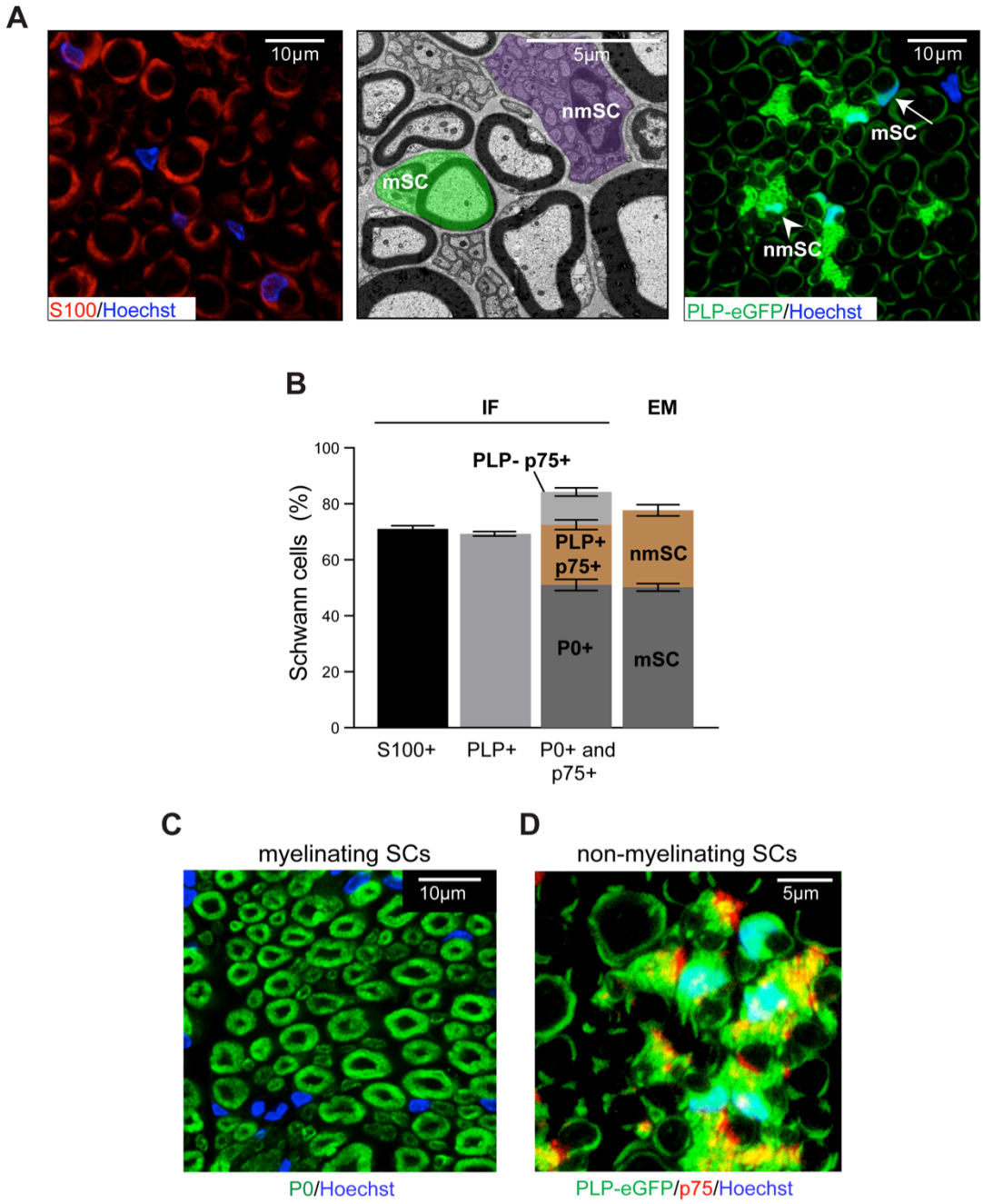

Figure 4.1. Schwann cell population of the peripheral nerve

A) Representative confocal immunofluorescence (IF) and EM images showing the SC population in transverse sections of mouse sciatic nerve. SCs are labelled either by immunofluorescence staining with a S100 antibody (red) or endogenously using PLP-eGFP mice (green). **B)** Graph shows quantification of the proportion of SCs in mouse sciatic nerve. mSCs cells were labelled with P0 and nmSC with p75 in transverse sections of WT animals. (n=4 mice, mean±SEM). Representative confocal images of **C)** mSCs (P0+) and **D)** nmSCs (PLP+/ p75+).

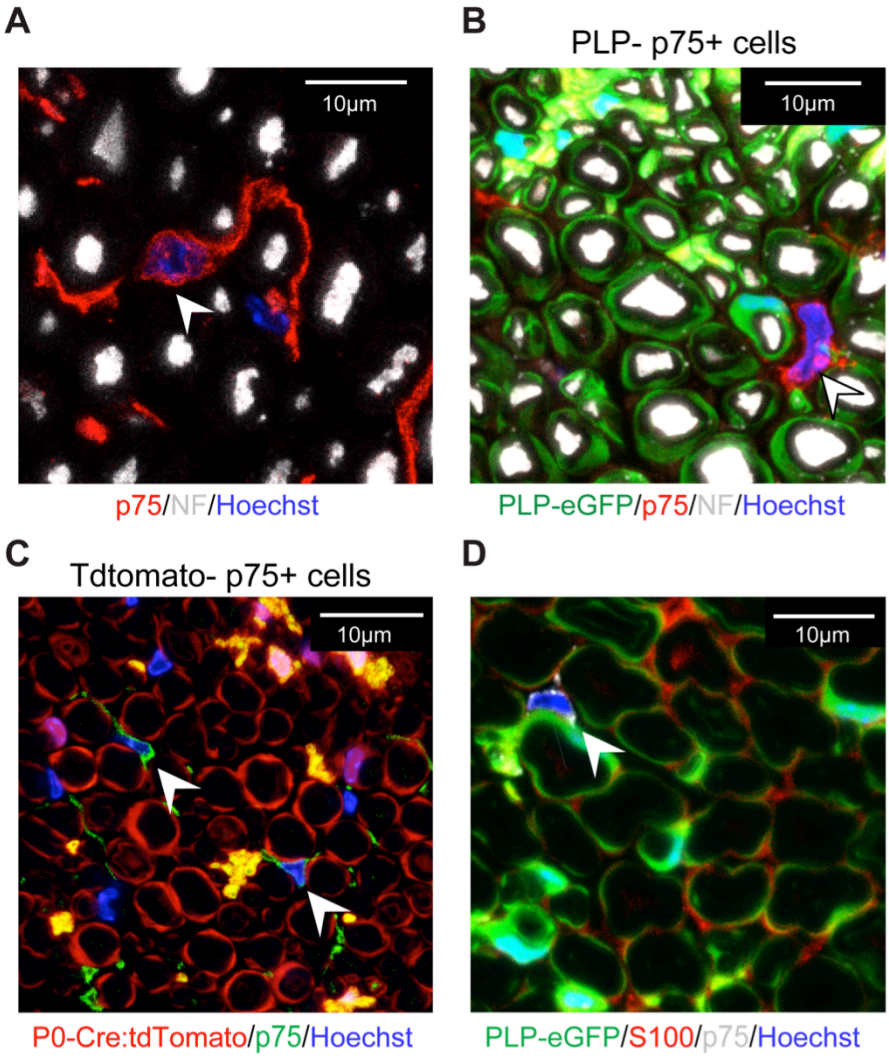

Figure 4.2. p75+ cells that are not associated with axons and are negative for SC markers

Representative confocal images of transverse mouse sciatic nerve sections of nerves labelled as indicated. **A)** Arrowhead indicates a p75+ cell (red) that is not associated with axons (labelled for neurofilament (white)). **B)** Arrowhead indicates a p75+ cell (red) that is not associated with axons (white) and does not express eGFP in nerves isolated from PLP-eGFP mice. **C)** Arrowheads indicate tdTomato-/p75+ cells in nerves isolated from P0-Cre:tdTomato mouse. **D)** Arrowhead indicates a p75+ (grey) S100- (red) and eGFP- cell in nerves isolated from PLP-eGFP mice.

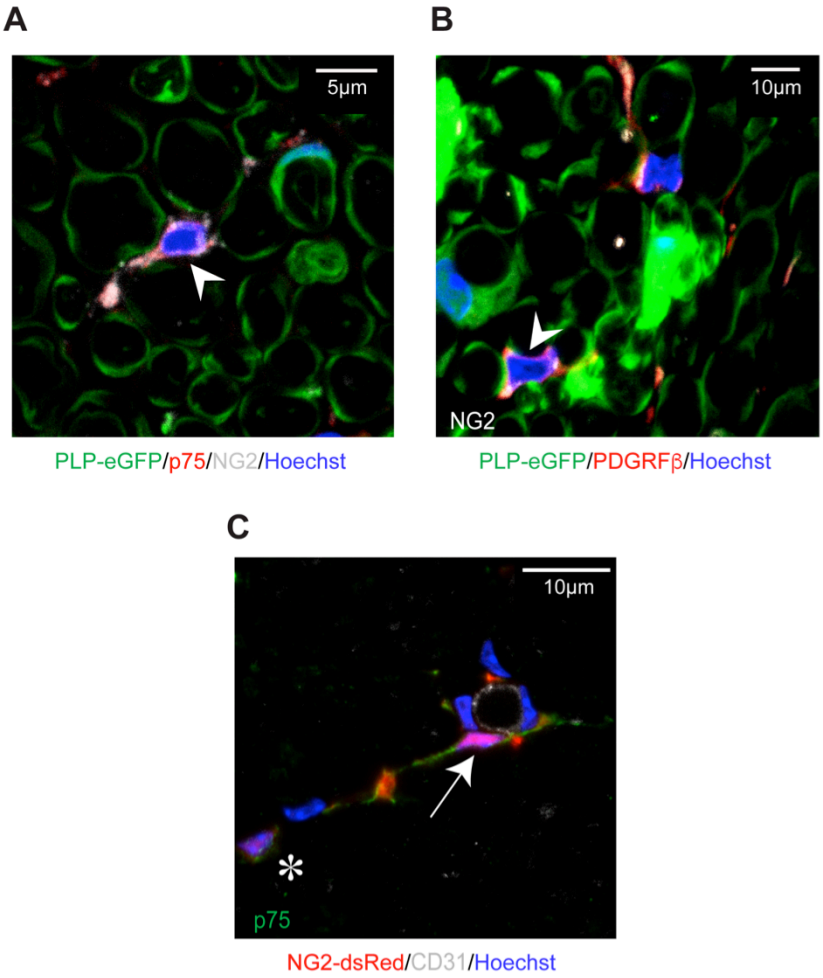

Figure 4.3. p75+ cells co-express the pericyte marker NG2 and PDGFRβ
Representative confocal immunofluorescence (IF) images of transverse mouse sciatic nerve sections, labelled as indicated. **A)** Arrowhead indicates a PLP-eGFP-/p75+/NG2+ cell in nerves isolated from PLP-eGFP mice. **B)** Arrowhead indicates a PLP-eGFP- cell that co-expresses NG2 (white) and PDGFRβ (red) in nerves isolated from PLP-eGFP mice. **C)** Arrow indicates a dsRed+ cell that co-expresses p75 (green) in sciatic nerves isolated from NG2-dsRed mice and is loosely associated with a CD31+ blood vessel. Asterisk indicates a p75+/dsRed+ cell that is not associated with a CD31+ blood vessel.

As we were unable to distinguish these two populations by markers, we classified them as blood vessel associated (4.5%) or blood vessel non-associated (8%) (Figure 4.4C and 4.5A). We next investigated the association of these cells with blood vessels at higher resolution using EM analysis and we found that in contrast to the classical pericytes, they were not found within the basal lamina of the blood vessels (Figure 4.4D). Additionally, in the EM analysis, we also observed high amounts of endoplasmic reticulum within these cells indicating that they may be the same cells previously characterised as neural crest derived fibroblasts (Figure 4.4D) (Joseph et al., 2004).

Finally, we identified the remaining cell types in the peripheral nerve as endothelial cells (6% CD31+) and macrophages (8% F4/80+/Iba1+) (Figure 4.5A and 4.5B). No other inflammatory cells such mast cells, neutrophils or dendritic cells were detected within an uninjured peripheral nerve (data not shown).

In summary, we have identified all cell types within the endoneurium of the peripheral nerve, which enables us to determine their behaviour in adult nerve and following nerve injury.

4.3. Adult peripheral nerve is a quiescent tissue

Following the identification of all the cell types within the peripheral nerves, we aimed to determine the cell turnover within the nerve in order to understand how and if peripheral nerve cells proliferate in the adult PNS. Previous studies have investigated cell turnover in the CNS using cumulative long-term EdU labelling studies and have shown that the CNS is relatively quiescent (Young et al., 2013). These studies showed that all OPCs, which produce oligodendrocytes in the adult CNS, proliferate, though slowly, with turnover times ranging from 1 week to > 1 month in different regions of the brain, spinal cord and optic nerve.

To investigate this mechanism and to determine the overall proliferation rate, we used the same protocol of cumulative EdU labelling as the Richardson lab (Young et al., 2013) to mark proliferating peripheral nerve cells for up 70 days. We used 5-ethynyl-2'-deoxyuridine (EdU), instead of its analogue bromodeoxyuridine (BrdU), as BrdU has been previously shown to be inaccurate in determining the rate of cell division in the CNS (Psachoulia et al., 2009).

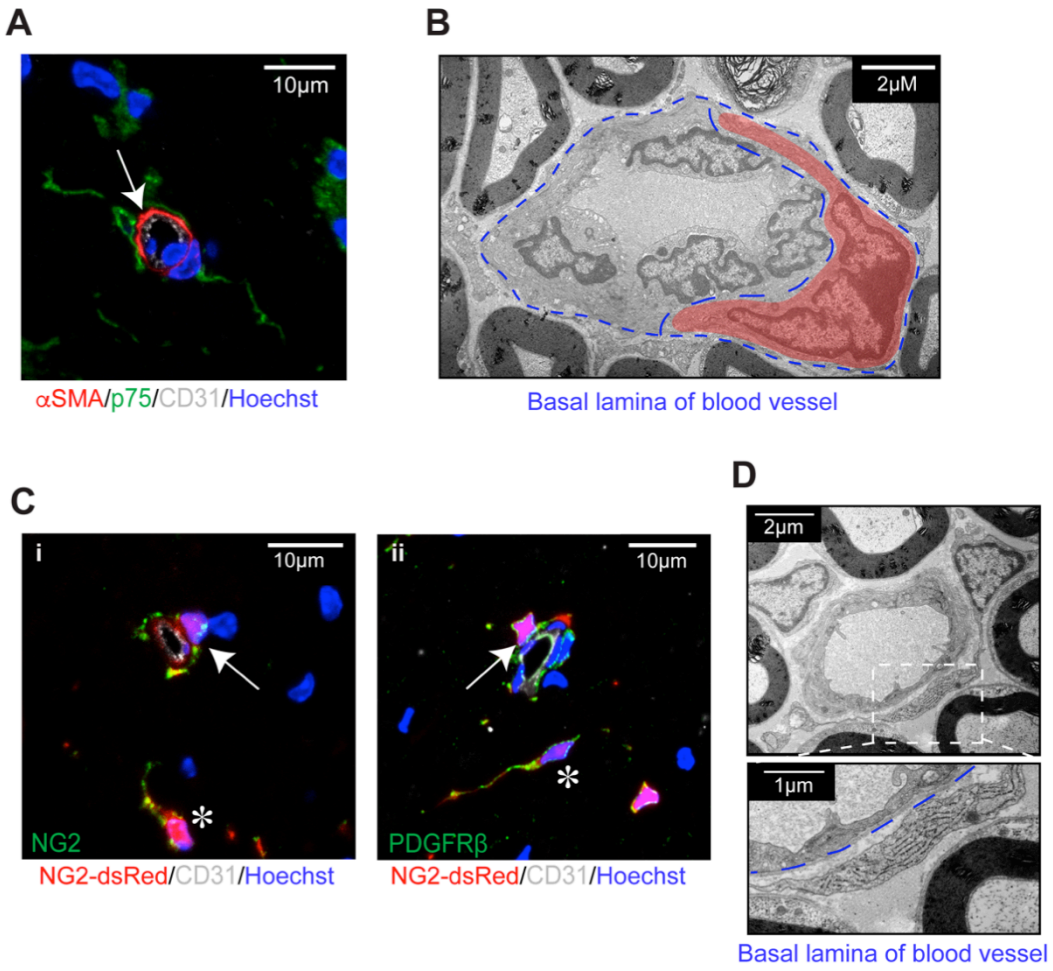

Figure 4.4. NG2 and PDGFRβ staining identifies three populations of cells
A) Representative confocal image of a transverse section of sciatic nerve isolated from WT mice. Arrow indicates a αSMA+/p75- pericyte in close contact with a CD31+ blood vessel (white). **B)** Representative EM image showing a classical pericyte (red), which is in tight contact with a blood vessel and is within the basal lamina. **C)** Sections of sciatic nerve from NG2-dsRed mice were co-stained for (i) NG2 (green) and (ii) PDGFRß (green). Arrows indicate cells that are loosely associated with CD31+ blood vessels, asterisks indicate cells that are non-associated with CD31+ blood vessels. **D)** Representative EM images show an elongated cell, rich in endoplasmic reticulum, closely associated with a blood vessel. The higher magnification image shows that it is not surrounded by the basal lamina.

\

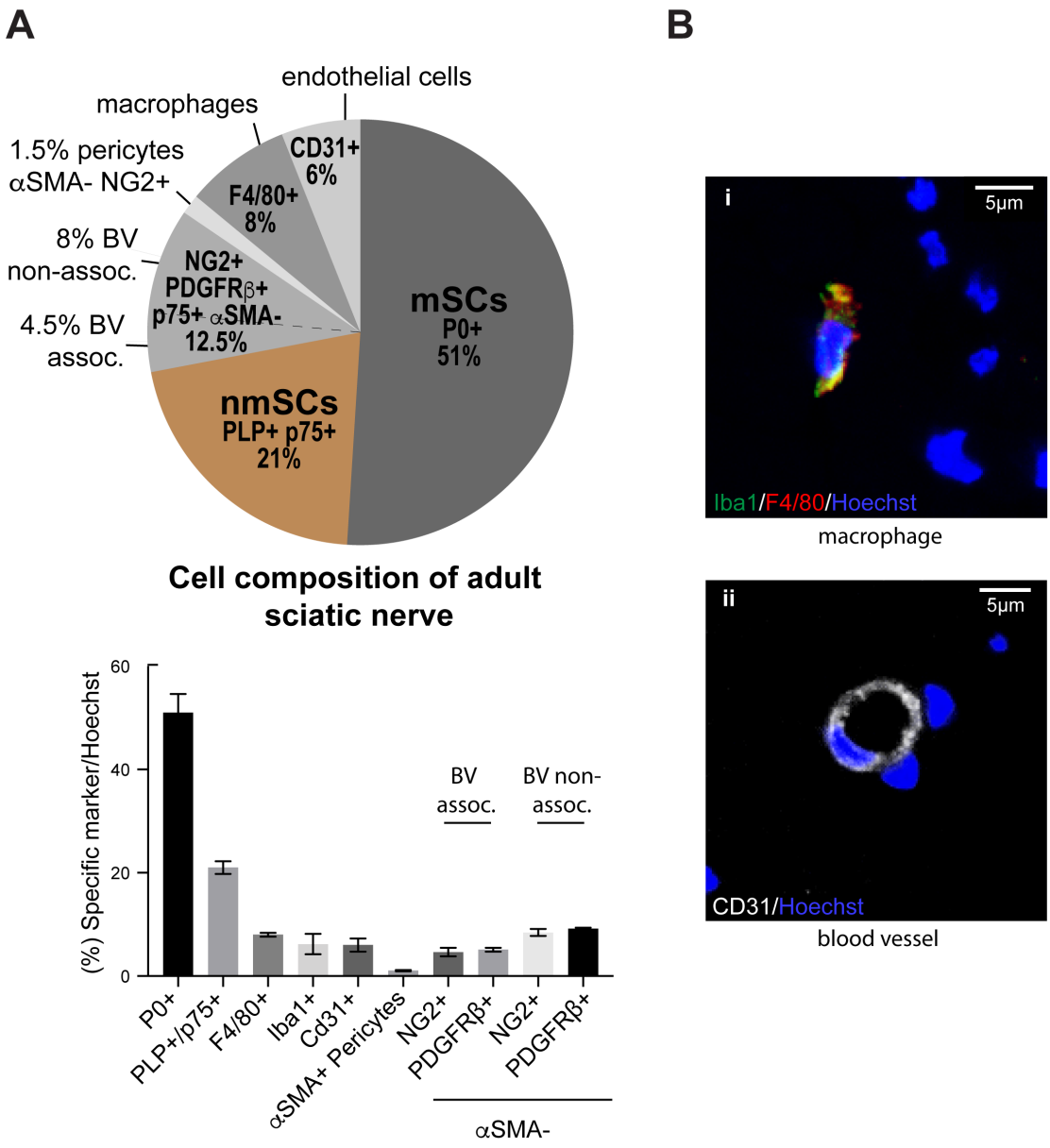

Figure 4.5. Cell composition of peripheral nerve

A) Pie chart and graph showing quantification of the cell types present in sciatic nerve. Both show the percentage of individual cell types within mouse sciatic nerve. Cryosections of sciatic nerves were immunolabelled with cell type specific markers as indicated. Pericytes are defined as NG2+/ PDGFRß+/ αSMA+. The NG2+/ PDGFRß+ / αSMA- cell population is classified as either associated or non-associated with CD31+ blood vessels. Iba1 and F4/80 are both expressed by macrophages. (n=4 mice, mean±SEM). **B)** Representative confocal images of transverse sections of sciatic nerve from WT mice immunolabelled with i) Iba1 (green) and F4/80 (red) to detect macrophages ii) and CD31 (white) to detect endothelial cells.

Furthermore, EdU labelling does not require DNA denaturation for its detection, allowing for better preservation of nerve structure (Cappella et al., 2008; Taupin, 2007). For each time point (8, 30 and 70 days), we calculated the percentage of cells that had accumulated EdU and this increased in a linear manner over time showing that the proliferation rate remains constant during early adulthood (Figure 4.6). However, the overall proliferation rate was very low (~0.8% per week) with less than 10% of the cells having incorporated EdU within the 70 day time period. This implies that if all peripheral nerve cells were proliferating at the same rate, the tissue would turnover within 2.4 years. These findings emphasise the quiescent nature of the peripheral nerve.

To identify the proliferating peripheral nerve cells, we analysed EdU incorporation together with immunostaining against the cell type specific markers defined above (Figure 4.7A and 4.7B). This analysis failed to detect a single EdU+ mSC within the 70 day time period indicating that mSCs do not proliferate within adult peripheral nerve. In contrast, we detected a few EdU+ nmSCs in Remak bundles (Figure 4.7A). To confirm that these nuclei were associated with Remak bundles, as the nmSC marker p75 is also expressed by the NG2+/ PDGFRβ+/ αSMA- cell population, we administrated EdU to PLP-eGFP mice over a time period of 30 days. This analysis detected EdU+/ eGFP+/ p75+ cells and 3D reconstructions clearly showed the association of these cells within eGFP+ Remak structures that contain small calibre axons (Figure 4.8A and 4.8B). However, we found that the nmSC turnover rate was relatively low (~ 72 months) which exceeds the lifespan of a normal mouse (Figure 4.9).

The most highly proliferative cell in peripheral nerve was the resident macrophage, with a turnover rate of ~ 4 months (Figure 4.9, 4.7A and 4.7B), which was similar to the turnover rate of resident macrophages (microglia) in the brain (Askew 2017, Tay 2017). All the other cell types in the nerve also showed detectable but low levels of proliferation. We determined the turnover rate of CD31+ endothelial cells, NG2+/ PDGFRβ+/ p75+/ αSMA- cells and pericytes as 15, 7.5 and 6 months respectively (Figure 4.9, 4.7A and 4.7B). This analysis highlights the slow turnover of cells within peripheral nerve and importantly demonstrated that peripheral nerve glial cells possess very different proliferative dynamics compared to the glial cells of the CNS. Strikingly, mSC do not turnover and nmSC only rarely turnover in the adult peripheral

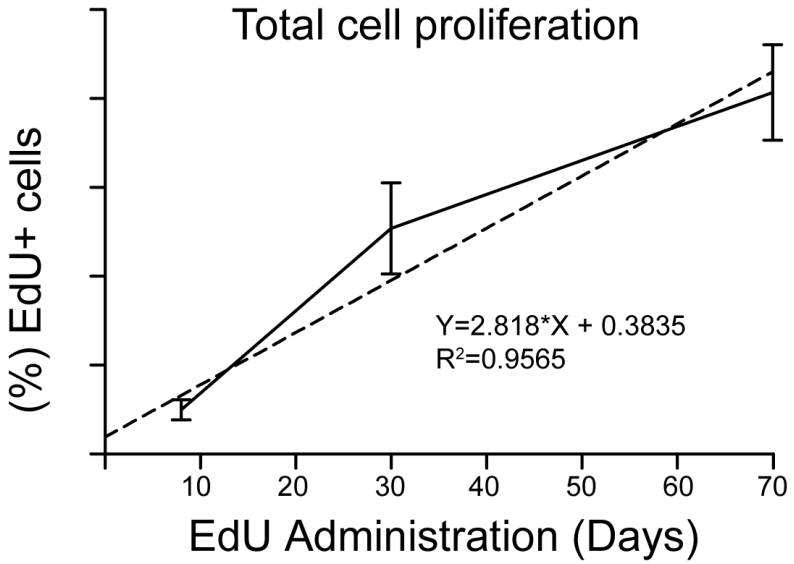

Figure 4.6. Peripheral nerve cell turnover is low and increases linearly
EdU was administered continuously in the drinking water of WT mice for 8, 30 and 70 days. Cryosections of sciatic nerve were processed to detect EdU. The graph shows the mean percentage of EdU+ cells against time of EdU administration. Note that cell proliferation increased linearly over time (n=4-7 mice, mean±SEM).

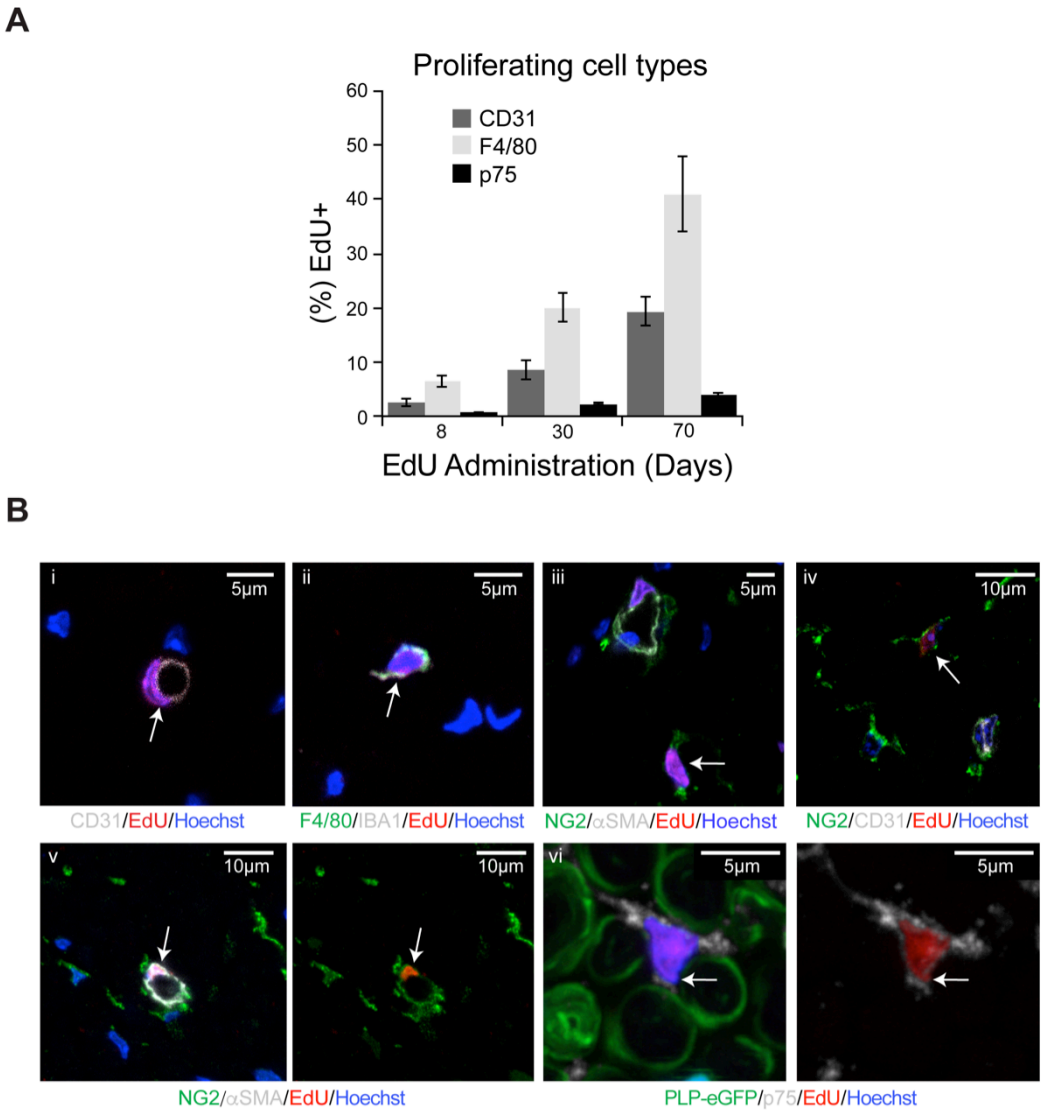

Figure 4.7. Peripheral nerve cells proliferate in a linear manner over time

A) Cryosections of mouse sciatic nerves were labelled with cell specific markers and processed to detect EdU+ cells. The graph shows the mean percentage of EdU+ nmSCs (p75+), endothelial cells (CD31+) and macrophages (F4/80+) within the 70 day labelling period (n=4 mice, mean±SEM). **B)** Representative confocal images of (i-v) transverse sections of sciatic nerve from WT mice and (vi) PLP-eGFP mice treated continuously with EdU for 30 days, processed to detect EdU (red) and immunolabelled for (i) CD31, to detect endothelial cells (white). (ii) F4/80 (green)/ Iba1 (white), to detect macrophages. (iii) NG2 (green) and αSMA (white) to detect pericytes and pericyte-like cells. (iv) NG2 (green), and CD31 (white) to detect NG2+ cells non-associated with CD31+ blood vessels. (v) NG2 (green) and αSMA (white) to detect pericytes. (vi) p75 (white) to detect PLP-/ p75+/ EdU+ cells. Nuclei are stained with Hoechst (blue). Arrows indicate proliferating cells.

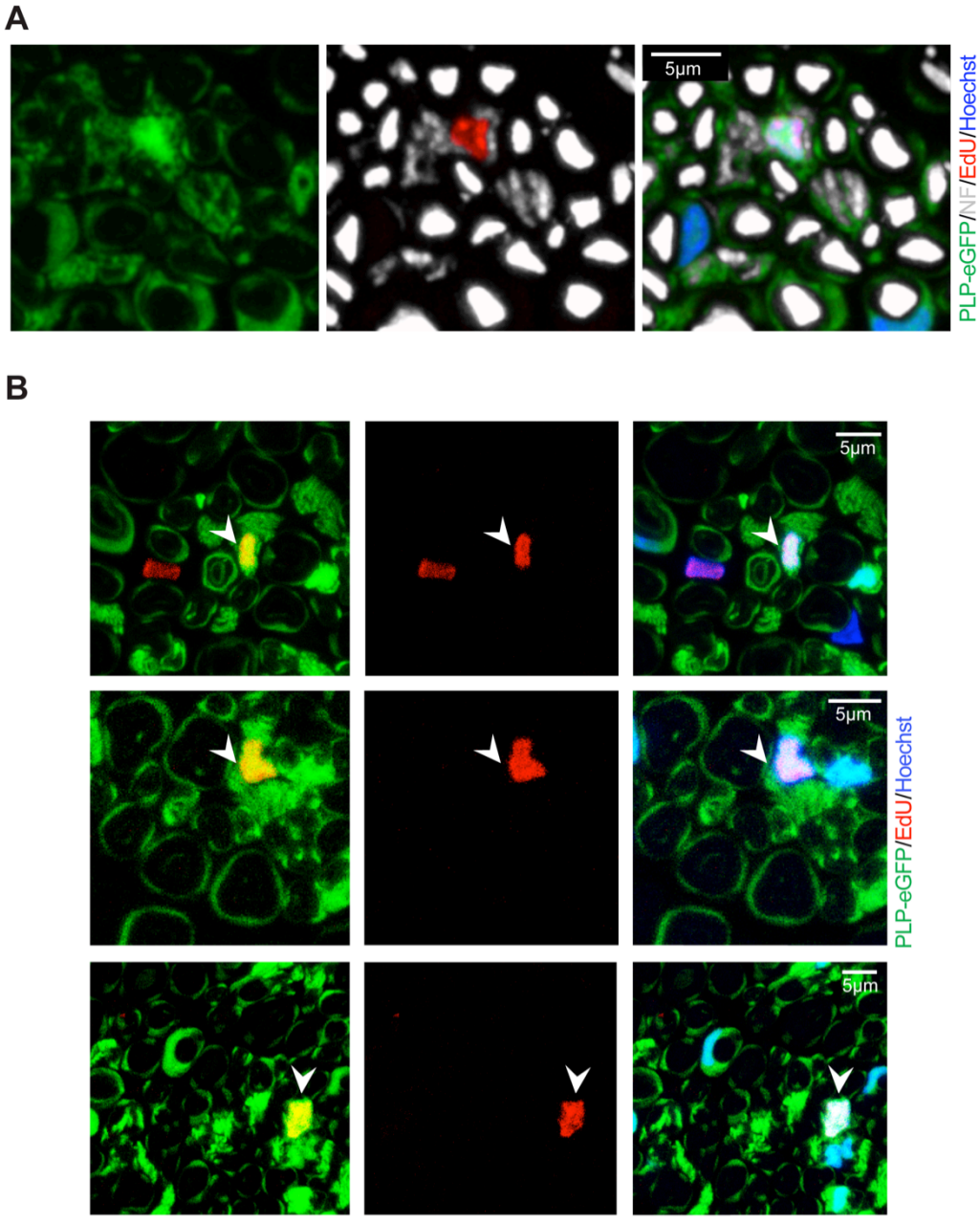

Figure 4.8. nmSC proliferate at low levels in the adult

A) 3D projection of confocal images and **B)** Representative confocal images of 20µm transverse sections of mouse sciatic nerve isolated from PLP-eGFP mice treated continuously with EdU (red) in the drinking water for 30 days. Nuclei are stained with Hoechst (blue). **A)** shows a EdU+ eGFP+ nmSC that is associated with small calibre axons (white). **B)** Arrowheads indicate three separate examples of proliferating nmSCs (PLP+/ EdU+).

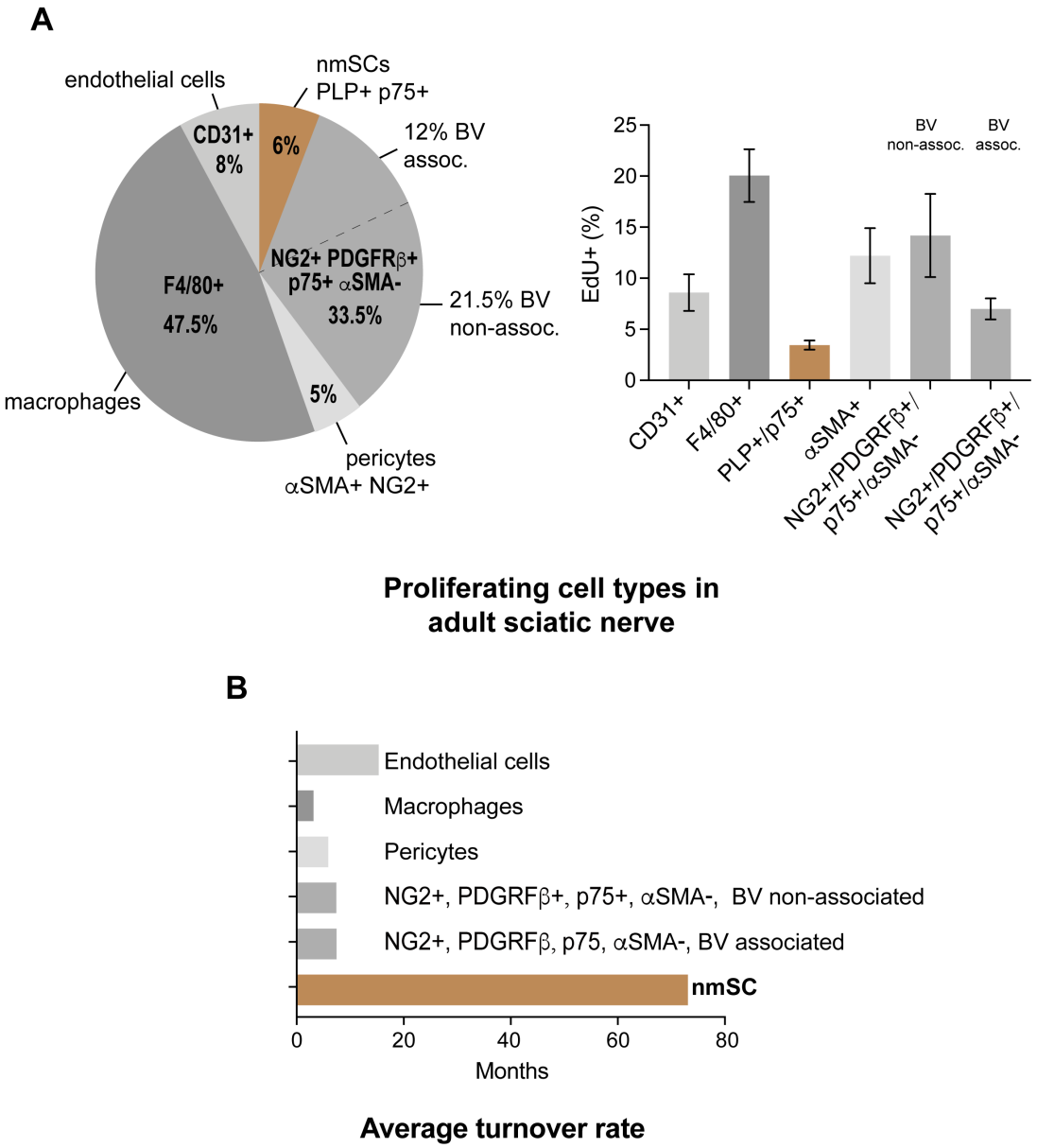

Figure 4.9. Identification of proliferating peripheral nerve cells in homeostasis
A) The mice were treated with EdU in the drinking water for 30 days, the nerves were harvested and cryosections of sciatic nerve were labelled with cell specific markers described above and processed to detect EdU+ cells. Pie chart shows the proportion of proliferating cell types within adult mouse sciatic nerve. The graph shows the mean percentage of proliferating cell types within the 30 Day labelling period (n=4-6 mice, mean±SEM). **B)** Graph shows the calculated turnover time for each cell population.

nerve, whereas new oligodendrocytes are produced throughout life in the CNS.

4.4. All myelinating Schwann cells proliferate following injury

The analysis of adult peripheral nerve demonstrated a mostly quiescent tissue consistent with the stable architecture required for this tissue. However, peripheral nerve is highly regenerative requiring that the tissue retain plasticity. Following an injury, the distal stump of the injured nerve undergoes extensive breakdown and subsequent clearance of the axonal and myelin debris in order to provide an environment conducive to axonal regrowth. Upon axonal regrowth, the nerve then undergoes extensive remodelling to produce a functional nerve (Jessen et al., 2015; Zochodne, 2008).

SCs possess key roles during the peripheral nerve repair process and in order to perform these roles SCs have been shown to dedifferentiate into progenitor-like SCs that re-enter the cell-cycle (Cattin and Lloyd, 2016; Jessen et al., 2015). However, it remains unclear, whether all SCs possess an equal capacity to dedifferentiate into progenitor-like SCs or whether some SCs possess a stem cell-like role and replenish the entire population following nerve injury. Alternatively, other unknown stem cell compartments may be recruited to the regenerating nerve that could replenish SCs (Amoh et al., 2005; Chen et al., 2012; McKenzie et al., 2006).

To determine the proliferative capacity of mSCs and whether all mSCs are capable of re-entering the cell cycle, it is necessary to distinguish them from the non-myelinating population. To do this we made use of a transgenic mouse (PO-CreER^{T2}:YFP), which has been extensively characterised by us and others (Leone et al., 2003; Ribeiro et al., 2013). These mice express a tamoxifen-inducible Cre under the control of the P0 promoter, which directs Cre expression specifically to mSCs in the adult and induces recombination of the YFP reporter cassette. This allows lineage analysis of mSCs because the P0 promoter is highly specific for mSCs in adulthood.

To analyse the initial stages of the regenerative process and to investigate the proliferative potential of the mSCs, we performed cumulative EdU labelling, as shown in Figure 4.10A, following sciatic nerve transection in adult PO-CreER^{T2}:YFP mice. This enabled us to analyse the accumulation of both EdU+ and YFP+ EdU+ cells (those derived from mSCs) over time

following nerve injury. First, we determined the proportion of cells, which proliferated until Day 10 following injury by analysing the distal stump (downstream of the cut). Our analysis showed a dramatic switch in the proliferative status of the nerve with >80% of all cells within the nerve accumulating EdU by Day 8 following injury (Figure 4.10B). Remarkably, despite being completely quiescent in the adult nerve, >80% of the YFP+ cells in the nerve proliferated within 6 days of the injury with close to 100% proliferating by Day 10. This result shows that, despite being such quiescent, specialised cells, all mSCs cells have the capacity to proliferate following an injury (Figure 4.10B-D).

In order to determine the kinetics of mSC proliferation, we performed EdU pulse-labelling as shown in Figure 4.11A, at specific time-points after nerve transection. We found that the peak of mSC proliferation was reached at Day 4 following injury and returned to lower but still detectable levels at Day 8-10 following injury (Figure 4.11B-C). Total cell proliferation followed a similar dynamic and reached its peak at Day 4 following nerve injury (Figure 4.11). We further analysed the cell composition and the proportion of each cell type proliferating at both Day 4 and Day 10 following injury and found that the composition of the nerve changed in that the proportion of SCs decreased, while the macrophage population increased from 8% to 22%, following the recruitment of monocytes from the blood stream. Moreover, the proportion of NG2+/ PDGFRβ+/ αSMA- cells increased from ~12% to 22% reflecting the higher proliferative rate of this cell type (Figure 4.12). Furthermore, neutrophils and other inflammatory cells were recruited into the regenerating nerve, likely accounting for the minor unknown cell population at this timepoint (Figure 4.12A) (Lindborg et al., 2017; Napoli et al., 2012). Both peripheral nerve cell composition and the proportion of proliferating cell types was found to be quite similar at Day 4 and Day 10 following nerve injury (Figure 4.12A and 4.12B). Overall, a dramatic increase in cell numbers occurred at these early time points as shown in Figure 4.13A, in which the cell numbers per field were compared between Day 4 following injury and the uninjured nerve.

Moreover, in parallel, we aimed to determine the cell composition of the injured nerve morphologically by EM analysis at the same time points, however, because the injured nerve drastically changed due to SC dedifferentiation and infiltration of inflammatory cells, we were

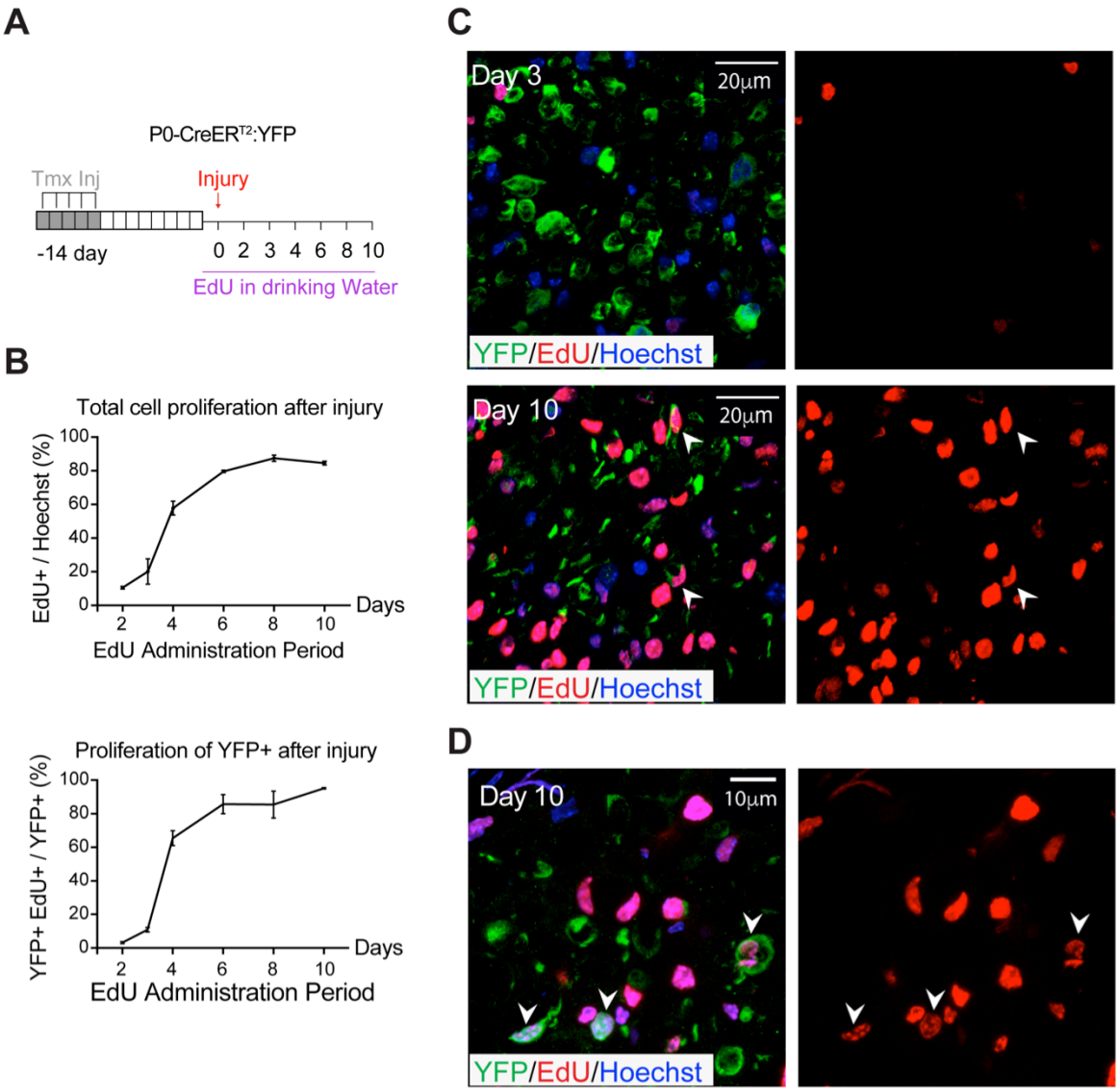

Figure 4.10. All mSCs proliferate following injury

A) Schematic showing the protocol used to assess accumulated proliferation following nerve transection. P0-CreER^{T2}:YFP mice were injected with tmx for 5 consecutive days. 2 weeks following the last injection, the right sciatic nerve was transected and EdU was administered continuously in the drinking water for up to 10 days. Mice were harvested at the indicated time points and EdU+ cells were counted in the distal stump of the injured sciatic nerve. **B)** Graphs show the percentage of proliferating cells (EdU+/Hoechst) and the percentage of proliferating mSCs (YFP+, EdU+/YFP+) plotted against time of EdU administration (n=4 mice, mean±SEM). **C)** Representative confocal images show only few (YFP+) mSCs proliferating at Day 3 following injury, whereas almost all mSCs have proliferated by Day 10. **D)** Higher magnification images show proliferating YFP+ labelled mSCs at Day 10 following injury. Arrowheads indicate proliferating YFP+ mSCs. Analysis was performed in collaboration with a previous master's student, N. Garcia-Calavia.

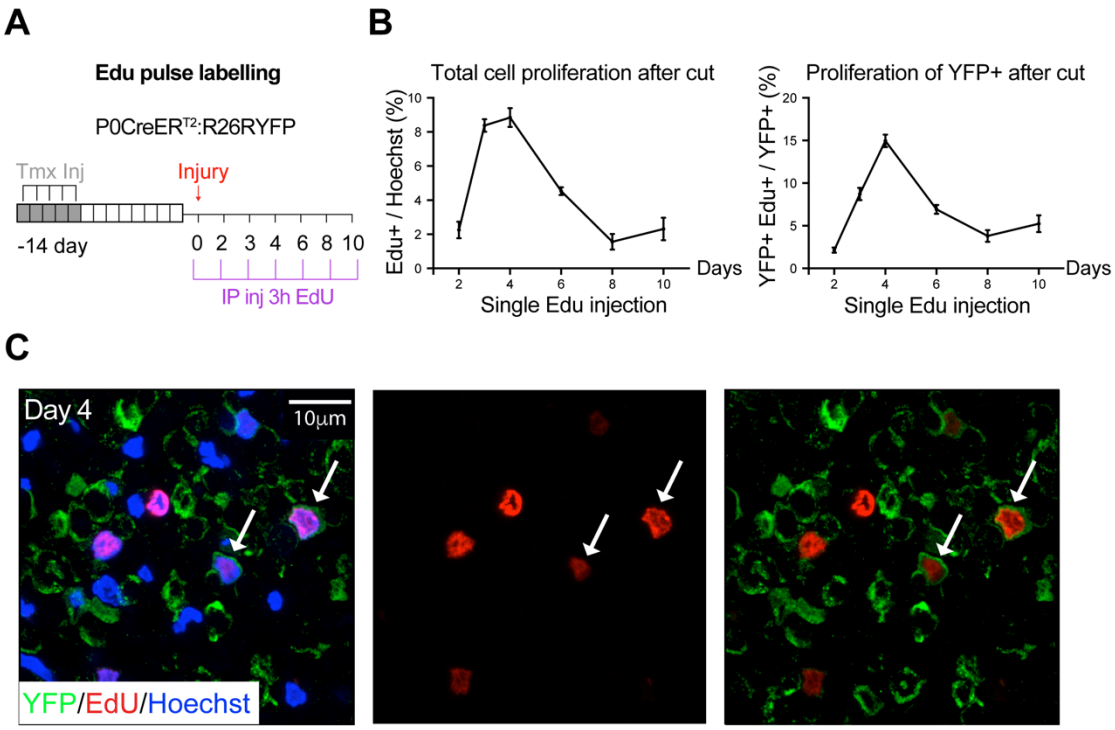

Figure 4.11. The peak of mSC proliferation is at Day 4 following injury

Schematic showing the protocol used to assess mSC proliferation at the indicated early timepoints following nerve injury. Mice were treated as shown in the scheme and as described in Figure 4.10 but EdU was administrated by intraperitoneal injection 3 hours before harvesting at the indicated timepoints. **B)** Graphs show the mean percentage of proliferating cells (EdU+/ Hoechst) and the percentage of proliferating mSCs (YFP+, EdU+/ YFP+) at the indicated timepoints (n=4-6 mice, mean±SEM). **C)** Representative confocal images of transverse sections of the injured distal stump at Day 4 following injury. Arrows indicate proliferating EdU+/ YFP+ SCs.

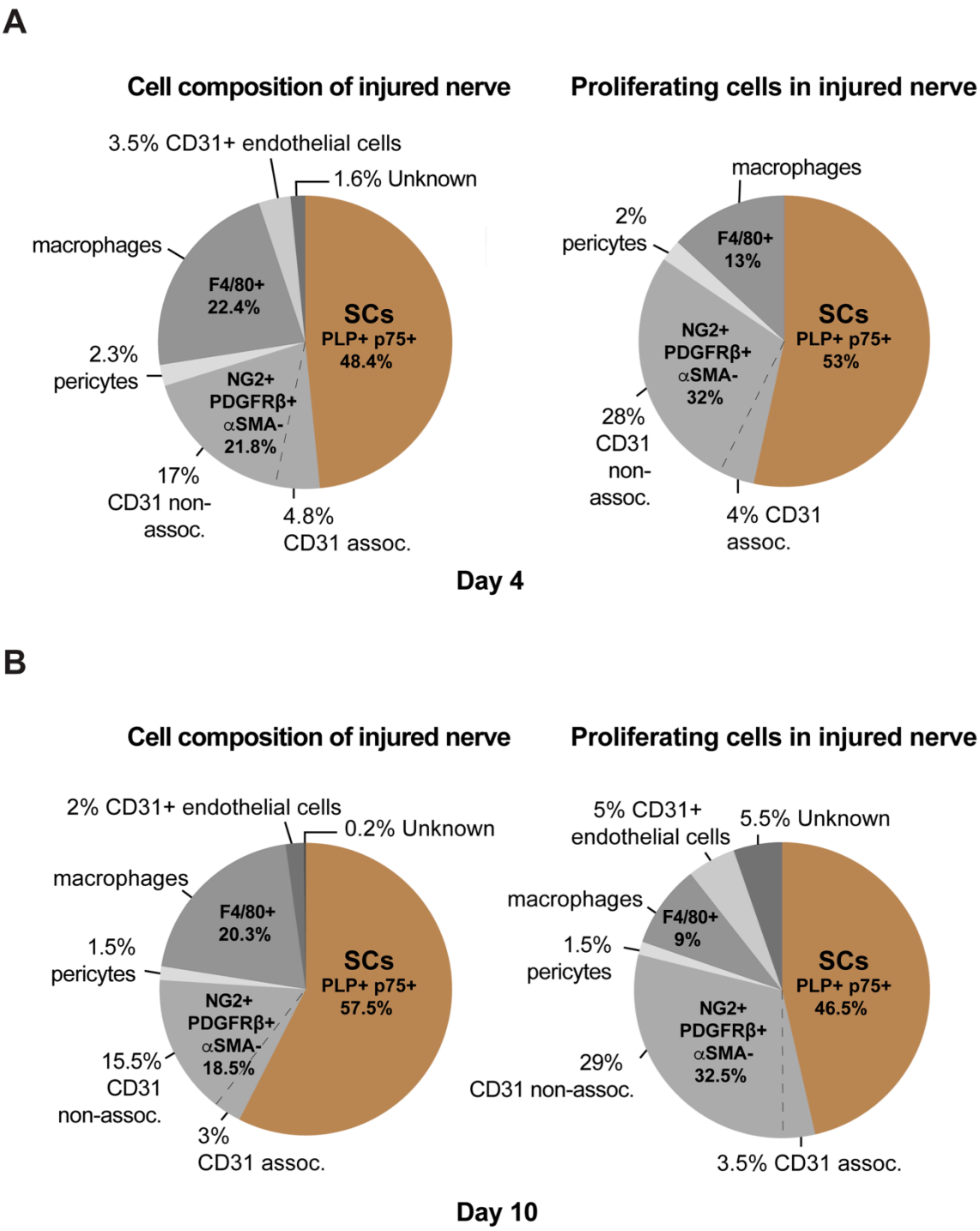

Figure 4.12. The cellular composition of peripheral nerves changes following nerve injury

A+B) P0-CreER^{T2}:YFP mice were injected with EdU 3 hours prior to harvesting at Day 4 **(A)** and 10 **(B)** following injury. Cryosections of injured sciatic nerves were labelled with cell type specific markers and processed to detect EdU+ cells. Pie charts show the cell composition and relative contribution of each cell type to the proliferating population in the distal stump of an injured sciatic nerve at both timepoints, as indicated (n=8 mice, mean±SEM). This analysis was performed in collaboration with a previous Research Assistant, A. Monteza-Cabrejos

not confident in morphological identification of the cell types. The EM analysis showed a few intact axons and myelin sheets, as indicated by arrowheads and arrows respectively, whereas many are in the process of degradation at Day 4 following injury (Figure 4.13B). Both axons and myelin sheaths appeared to be fully degraded by Day 10 following injury (Figure 4.13B) and the nerve filled with extracellular matrix, as shown in the higher magnification image in 4. 13C.

4.5. Myelinating Schwann cells contribute to the regenerative response following nerve injury

Our analysis of the initial stages of the regenerative process has shown that all mSCs are capable of switching from a quiescent state to a proliferating state. We have previously demonstrated that an important function of SCs during peripheral nerve regeneration is to form cellular cords that guide regrowing axons across the nerve bridge into the distal stump (Parrinello et al., 2010). However, to date the source of these migratory SCs, which enter the nerve bridge is not clear. In order to study the behaviour of individual mSCs, we used the P0-CreER^{T2}:Confetti mouse model, which was described in Chapter 3. In this mouse model, recombined mSCs stochastically express a combination of four different fluorophores (nuclear localised GFP, membrane targeted Cyan and cytoplasmic RFP or YFP), which can result in 10 distinctively labelled mSC populations in homozygous mice (Figure 4.14A). This mouse model allowed us to trace the migration of individual mSCs in order to determine their migratory behaviour at early time points following nerve injury.

In order to do this, we performed a sciatic nerve full transection in tmx treated P0-CreER^{T2}:Confetti mice and harvested the injured and uninjured sciatic nerve at Day 5 following nerve injury. We performed immunofluorescence staining with the axonal marker neurofilament to investigate whether the mSC-derived cells are associated with axons in the nerve bridge. Furthermore, we used p75 in order to identify all dedifferentiated SCs.

First, we observed SCs of each colour migrating into the bridge following injury (Figure 4.14B). Higher magnification confocal images showed that different coloured mSC- derived cells migrate next to each other in cellular cords indicating that the migrating mSC- derived

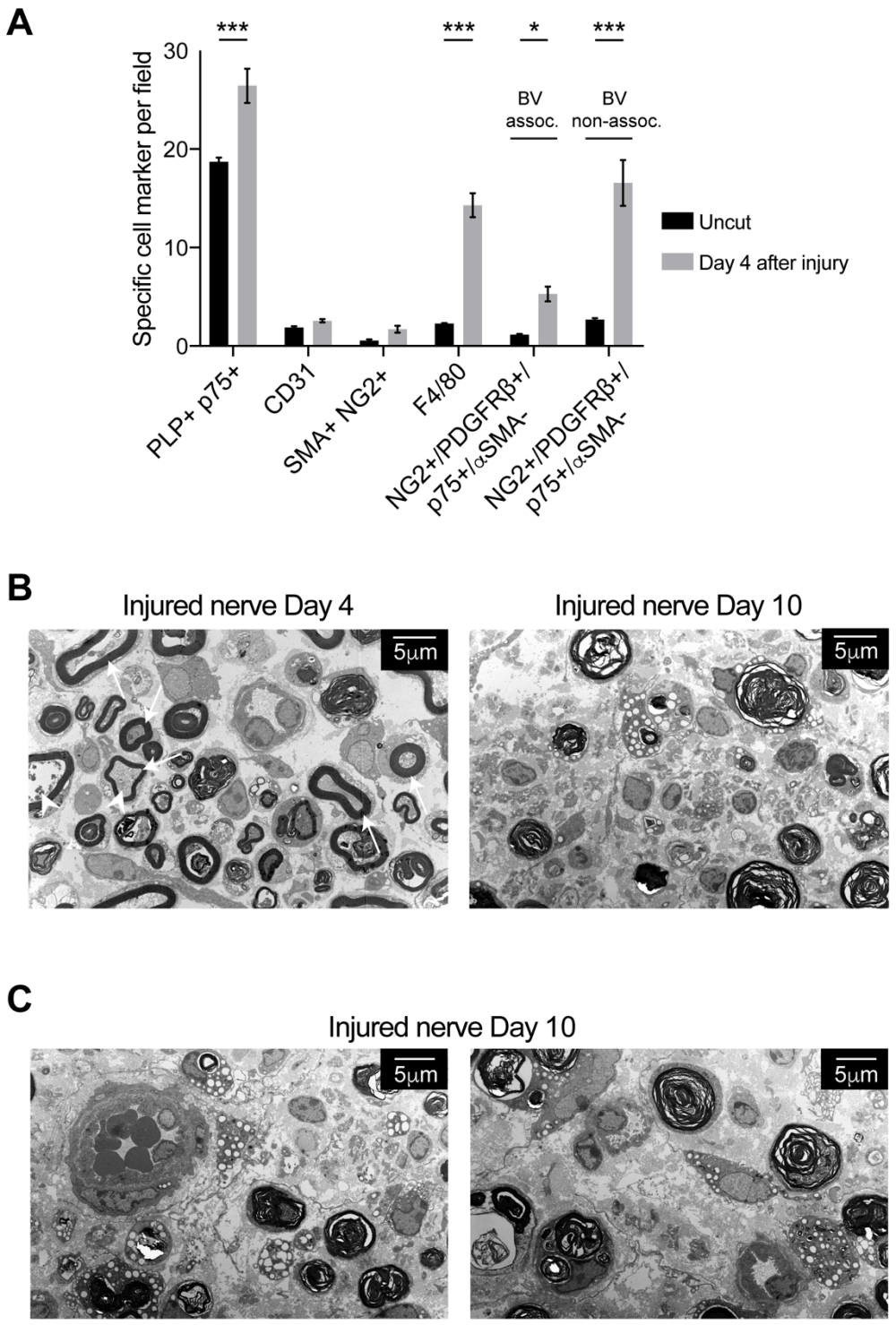

Figure 4.13. Axons and myelin sheets are degraded following nerve injury
A) Cryosections of uninjured and injured nerve at Day 4 following injury were immunolabelled for cell type specific markers, as indicated, and the number of the different cell types were quantified. Graphs shows the quantification of different cell types per field (n=4-10 mice, mean±SEM). **B)** Representative TEM images of the distal stump of the injured nerve at Day 4 and Day 10 following transection. Arrowheads and arrows indicate intact axons and myelin sheaths respectively. **C)** Higher magnification TEM image of the distal stump of the injured nerve at Day 10 following injury.

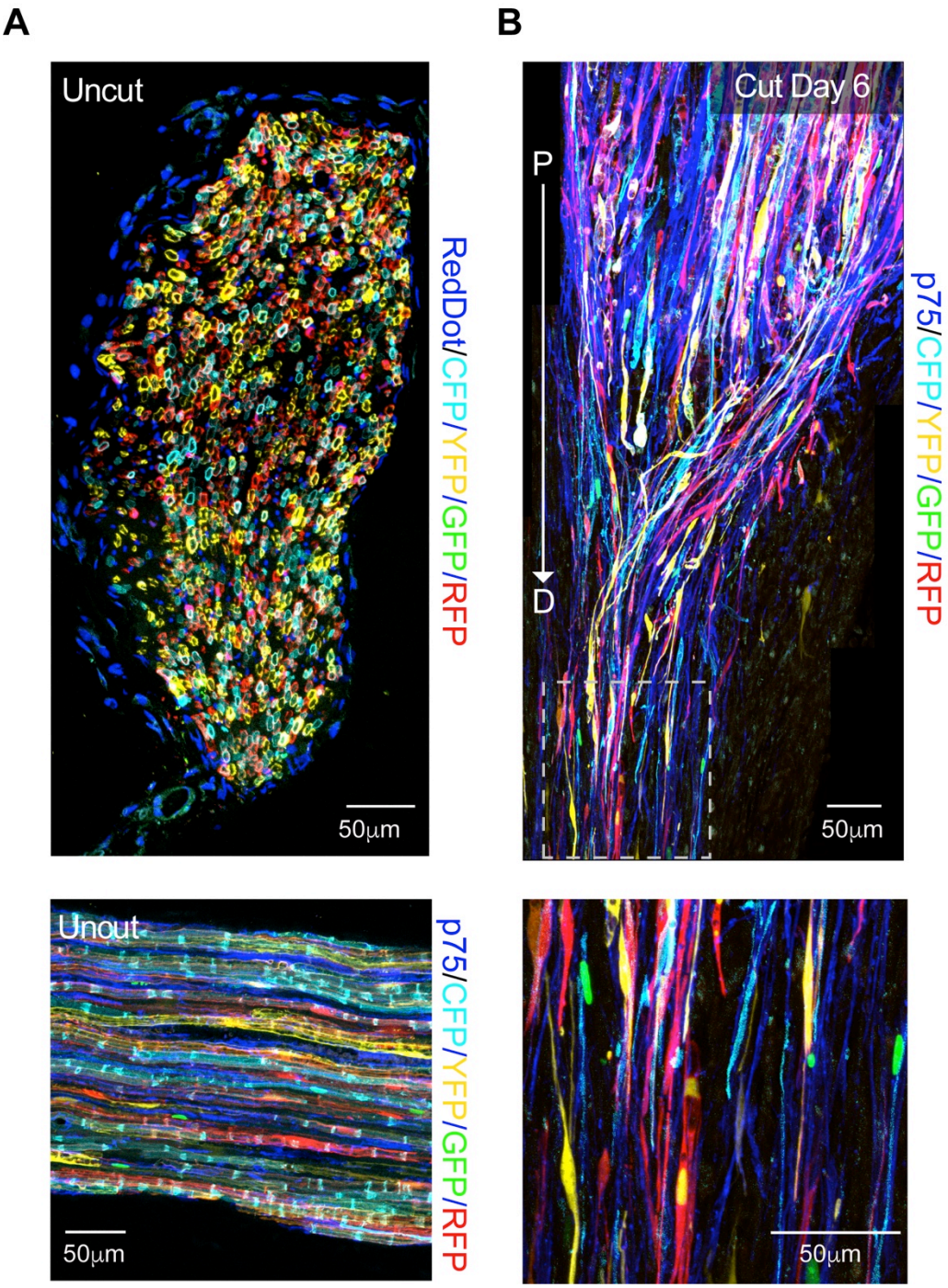

Figure 4.14. mSC-derived cells migrate into the newly formed nerve bridge following nerve injury

A) Representative confocal images of transverse (Upper panel) and longitudinal (Lower panel) cryosections of uninjured contralateral sciatic nerve showing the high recombination rate in P0-CreER^{T2}:Confetti mice. Nuclei were counterstained with RedDot (Upper panel) and nmSCs were labelled with p75 (Lower panel). **B)** Representative images of longitudinal cryosections (Upper panel) and higher magnification (Lower panel) of a transected sciatic nerve showing that mSC-derived cells have migrated into the nerve bridge, at Day 6 following nerve injury. An antibody to p75 was used to label dedifferentiated SCs. This analysis was performed in collaboration with Dr. A. Cattin.

cells are a polyclonal population (Figure 4.15A). Moreover, these SC cords were associated with axons within the sciatic nerve bridge demonstrating that the mSC derived cords transport regrowing axons across the injury site (Figure 4.15B). These results show that previously quiescent mSCs can undergo extensive structural and functional remodelling to become highly migratory cells within a few days of an injury.

We also observed a significant number of p75+ SCs in the migrating cellular cords that were not labelled with a confetti-derived fluorophore (Figure 4.14B). This observation suggested that nmSC-derived cells also contributed to the SC population migrating out of the nerve stumps into the bridge. To determine the proportion of mSCs versus nmSCs, we compared the percentage of recombined SCs in the uncut nerve of individual P0-CreER^{T2}:tdTomato mice (Madisen et al., 2010) compared to those migrating in the bridge region of the injured contralateral nerve (Figure 4.16A). For this analysis, we used the P0-CreER^{T2}:tdTomato mouse model, because staining with additional markers is limited in the confetti mouse model due to the co-emission spectra of the four endogenous fluorescent reporter cassettes. The P0-CreER^{T2}:tdTomato mouse model induces recombination of the tomato reporter cassette specifically in mSCs upon tmx administration.

We performed sciatic nerve injury and harvested the injured and uninjured nerve at Day 6 following nerve injury. First, we determined the recombination rate by quantifying the recombined mSCs over the total mSCs in the uninjured nerve and we observed, as shown in the left panel of Figure 4-16B, high recombination in the P0-CreER^{T2}:tdTomato mice. Then, we determined the percentage of recombined SCs by quantifying the tomato+ mSCs over the total number of SCs in both the uninjured contralateral nerve and at the injury site. This analysis showed that, whereas > 60% SCs were tdTomato+ in the uninjured nerve of all 4 animals (Figure 4-16B), the proportion of recombined mSC-derived cells was lower in the nerve bridge of the injured nerve in 3 out of the 4 mice analysed (Figure 4.16B). This result suggests that both nmSCs and mSC-derived cells migrate into the bridge following injury but that nmSC-derived cells tend to make a greater contribution to this process.

A second role for SCs during the regenerative response is to contribute to the clearance of the axonal and myelin debris that accumulates in the distal stump, as the axons degenerate and

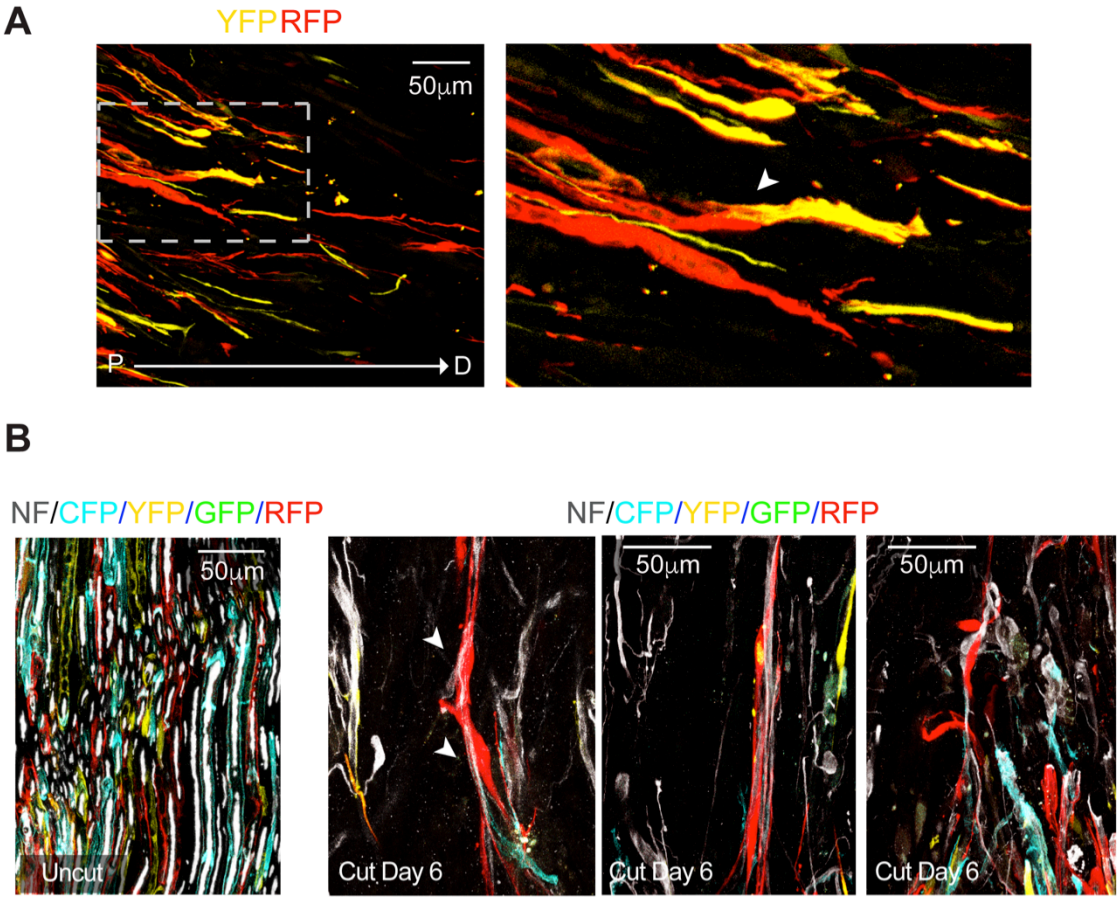

Figure 4.15. Migrating mSC-derived cells are associated with regrowing axons within the nerve bridge following injury

A) Representative longitudinal cryosection (left panel) and higher magnification (right panel) of the newly formed nerve bridge at Day 6 following nerve injury. Right panel: Arrowhead indicates a SC cord that was formed by two migrating SCs that have derived from different mSCs (as seen by their distinct colours, YFP and RFP). **B)** Representative longitudinal cryosections of uninjured (left panel) and injured (right panel) sciatic nerve at Day 6 following nerve injury. Longitudinal sections were labelled with neurofilament (NF) antibody (white) to detect axons in order to show that the migrating mSC-derived cells associate with axons within the nerve bridge. Arrowheads indicate migrating SCs associated with axons. This analysis was performed in collaboration with Dr. A. Cattin.

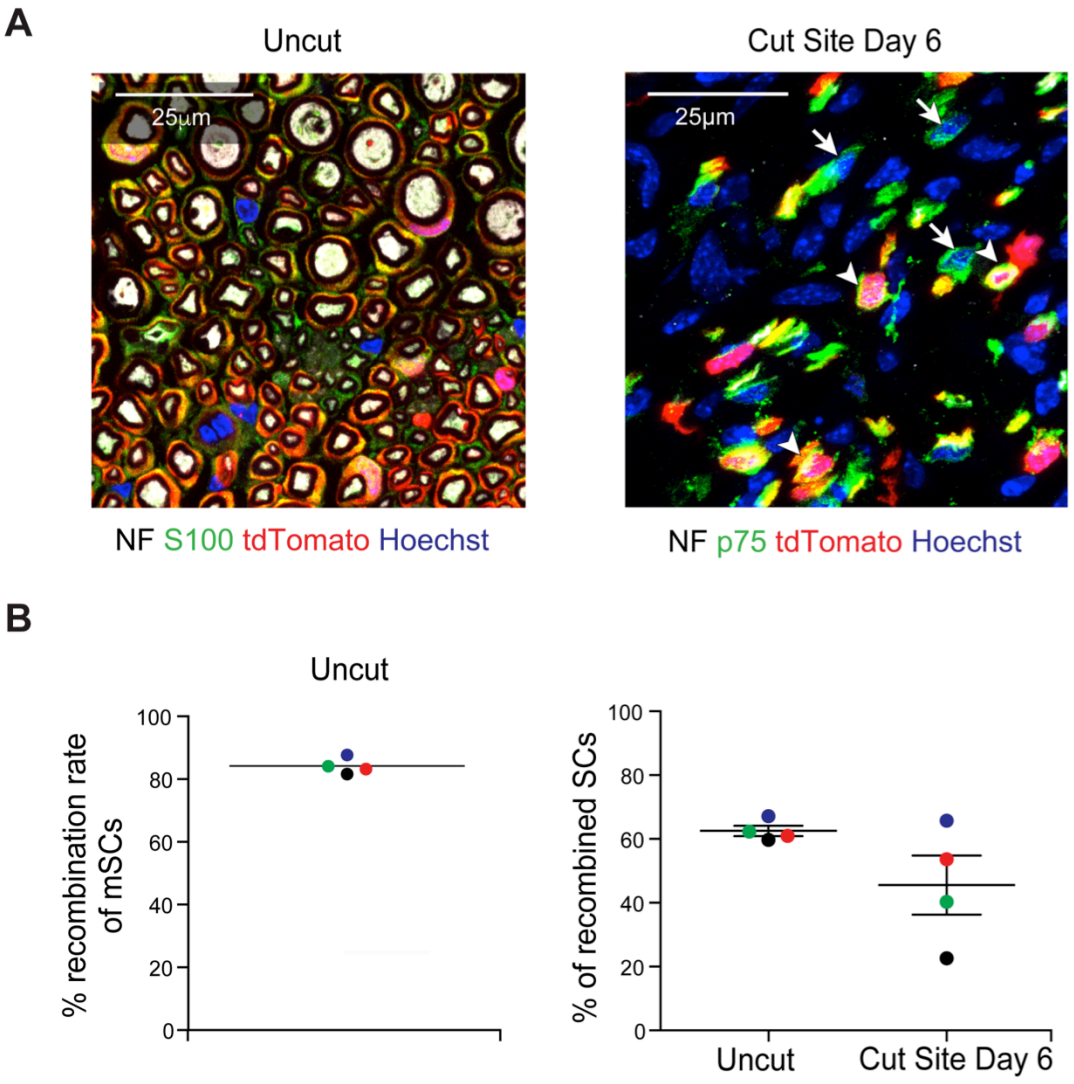

Figure 4.16. mSCs are migratory but nmSCs contribute more to the SC population in the nerve bridge

Representative image of a transverse cryosection of uninjured (left panel) and injured (right panel) sciatic nerve of tamoxifen injected P0-Cre-ER^{T2}:tdTomato at Day 6 following nerve injury. Left panel: Transverse sections were immunostained with antibodies against S100 and neurofilament (NF) to detect SCs and axons, respectively. Right panel: Transverse sections were labelled with antibodies to p75 and neurofilament (NF) to detect dedifferentiated SCs and axons, respectively. Arrowheads indicate Tomato+/p75+ cells and arrows indicate Tomato-/p75+ cells. **B)** Graph shows (left panel) the recombination rate in uninjured nerve and (right panel) the percentage of recombined SCs within the uninjured contralateral nerve and the nerve bridge at Day 6 following nerve injury. The recombination rate was determined by quantifying the recombined mSCs over total mSCs in the uninjured nerve, whilst the percentage of recombined SCs was determined by quantifying the recombined mSCs over all SCs in both the uninjured contralateral nerve and at the injury site. Each coloured dot represents an individual animal. The line shows the mean percentage±SEM. This analysis was performed in collaboration with Dr. A. Cattin.

mSCs dedifferentiate following a transection injury (Zochodne, 2008). To determine whether mSC- derived cells contribute to axonal and myelin debris clearance following injury, we investigated myelin protein zero (P0) expression within the injured distal stump of P0-CreER^{T2}:tdTomato mice. Consistent with previous studies, this analysis showed that mSC-derived cells engulfed myelin debris in the distal stump and therefore, demonstrated that mSC-derived cells contribute to the debris clearance process in injured peripheral nerves (Figure 4.17) (Brosius Lutz et al., 2017).

4.6 The regenerated nerve has structural abnormalities

It is well established that a regenerated nerve is distinct from an uninjured nerve. In particular, that there is an increase in the number of axons due to increased axonal sprouting during the regenerative process and that mSC internodal distances decrease in the regenerated compared to an uninjured nerve (Aguayo et al., 1976a; Bray and Aguayo, 1974; Bray et al., 1972; Schroder, 1972; Zochodne, 2008). However, the changes remain to be fully characterised.

In order to determine the differences in cell composition and nerve structure of the regenerated nerve, we analysed the regenerated nerve at 6 months following nerve injury using EM and the cell type specific markers characterised above. Using EM analysis, we confirmed, as shown in previous studies (Carter and Lisney, 1987; Salonen et al., 1988; Zochodne, 2008) an increase in the density of myelinated axons per field (Figure 4.18A and 4.18B). This finding reflects the axonal sprouting that takes place during axonal regrowth, which may be responsible for this increase in myelinated axons in the regenerated distal stump. Previous studies showed that the normal ratio between axon diameter and myelin sheath thickness (defined as g-ratio) is lost and the regenerated axons were observed as hypomyelinated within a regenerated nerve (Schroder, 1972; Sherman and Brophy, 2005).

In agreement with this, we observed that myelinated axons exhibited a significant decrease in axonal diameter in the regenerated nerve (Figure 4.18C). Moreover, we also found a prominent difference in Remak bundle structure with a large decrease of the number of small calibre axons within each individual Remak bundle (Figure 4.18A and 4-18B).

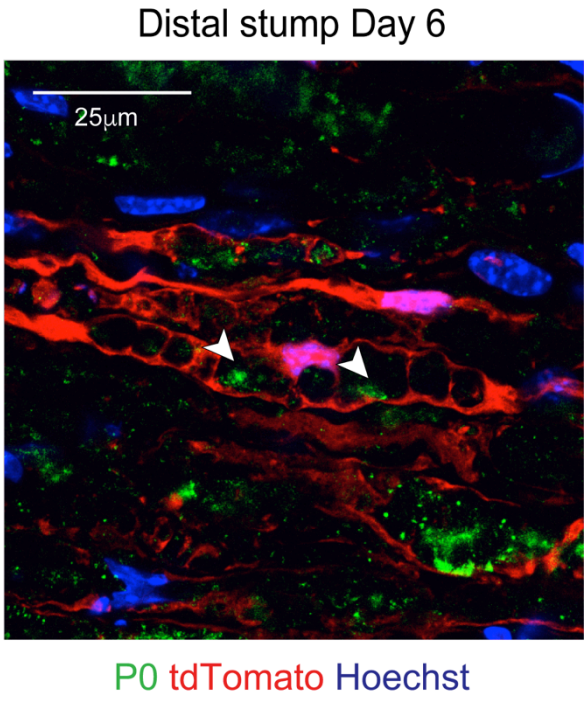

Figure 4.17. mSCs-derived cells contribute to myelin debris clearance following nerve injury

Representative image of a longitudinal section of the distal stump of P0-Cre-ER^{T2}:tdTomato mice. Transverse sections were immunostained with P0 antibody to label degraded myelin. Arrowheads indicate myelin debris that has been engulfed by mSC-derived cells. This analysis was performed in collaboration with Dr. A. Cattin.

Subsequently, we quantified the total number of cells and observed a striking increase in cell density (~three-fold) in the regenerated nerve (Figure 4.19). To determine whether any cell type is over-represented within the regenerated nerve we performed immunofluorescence analysis using the cell type specific markers identified above. In parallel, we also quantified the cell types morphologically by EM analysis. This analysis showed that the increased cell density represented a proportional increase of all cell types within the nerve indicating interactions between the cell types act to maintain the composition of the tissue (Figure 4.20A and 4.20B). Moreover, the previously observed decrease in axons per Remak bundle correlated with the increased cell density, as in the absence of neuronal death its likely more SCs would be needed to form the Remak bundles. Importantly, we were able to identify all of the cells within the regenerated nerve (Figure 4.21A and 4.21B) suggesting that all cell-types retain their identity during the regeneration process.

In other tissues, it is known that extracellular matrix levels increase during a regenerative process (Eming et al., 2017). In keeping with this, we have shown that ECM deposition is high at the initial stages of nerve regeneration (Cattin et al., 2015), however, it is unclear whether the deposited ECM is cleared. To investigate this, we stained for several ECM proteins such as laminin and fibronectin and determined their expression level by quantifying intensity and the percentage of stained area in each confocal image. We observed much higher levels of laminin within the basal lamina of SCs and blood vessels in the regenerated nerve (Figure 4.22A and 4.22B). Moreover, the levels of fibronectin and collagen Type III were considerably higher throughout the regenerated nerve (Figure 4.22A and 4.22B). This analysis showed that the additional ECM was not cleared during peripheral nerve regeneration. These findings are consistent with the perceived fibrotic nature of repaired tissue and suggest that whereas many cellular changes and the inflammatory response associated with a regenerative process successfully resolve, the increased matrix deposition associated with tissue regeneration remains within the tissue. Together these findings demonstrate that the peripheral nerves are regenerative compared to these of the CNS, but the regenerative process cannot fully restore the structure to that prior to nerve injury.

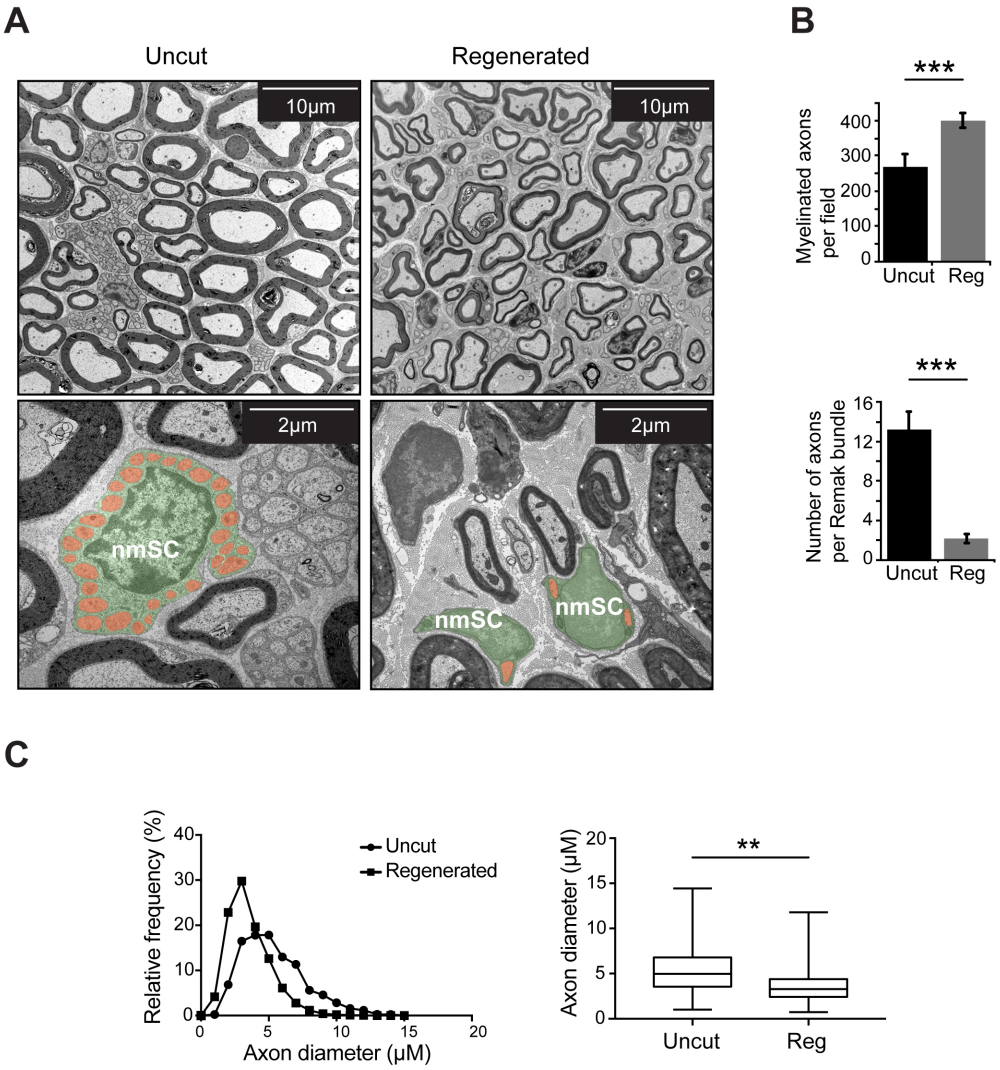

Figure 4.18. Regenerated nerve is structurally distinct from uninjured nerve

A) Representative EM pictures of uncut contralateral (left panel) or regenerated nerve (right panel) at 6 months following injury. Note that the regenerated nerve has a higher density of myelinated axons compared to the uncut nerve. Lower panel: Higher magnification EM images in which nmSCs are highlighted in green and small calibre axons in orange to indicate the decreased numbers of small calibre axons per Remak bundle in the regenerated nerve. **B)** Graphs show the quantification of **A)** to show the density of myelinated axons and number of axons per Remak bundle in uninjured and regenerated nerve (n=3 mice, mean±SEM). **C)** Graphs show the quantification of axon diameters to show that the average axon diameter is significantly decreased in the regenerated compared to the uninjured nerve. Photoshop was used to draw the axon diameters in the EM images and the diameter was measured with Fiji (n=8 mice, mean±SEM). This analysis was performed in collaboration with Dr. I. Napoli.

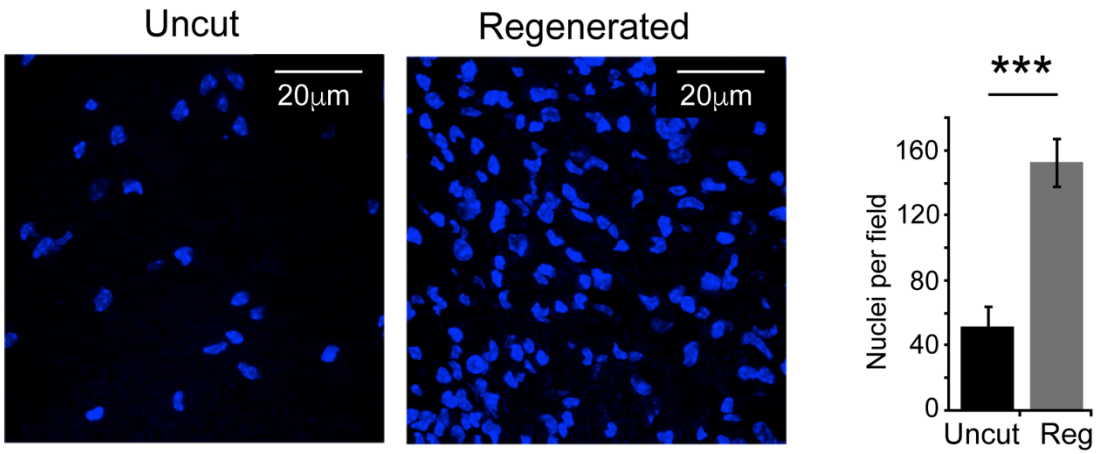

Figure 4.19. Increased cell density in regenerated nerve

A) Representative confocal images of transverse sections of uninjured (left panel) and regenerated (right panel) sciatic nerve, 6 months following injury. Nuclei were labelled with Hoechst (blue) in the uncut or regenerated nerve. Graph shows the quantification of the number of nuclei per field in uninjured and regenerated nerve. Note that the number of nuclei is significantly increased in the regenerated compared to the uninjured nerve. (n=8 mice, mean±SEM).

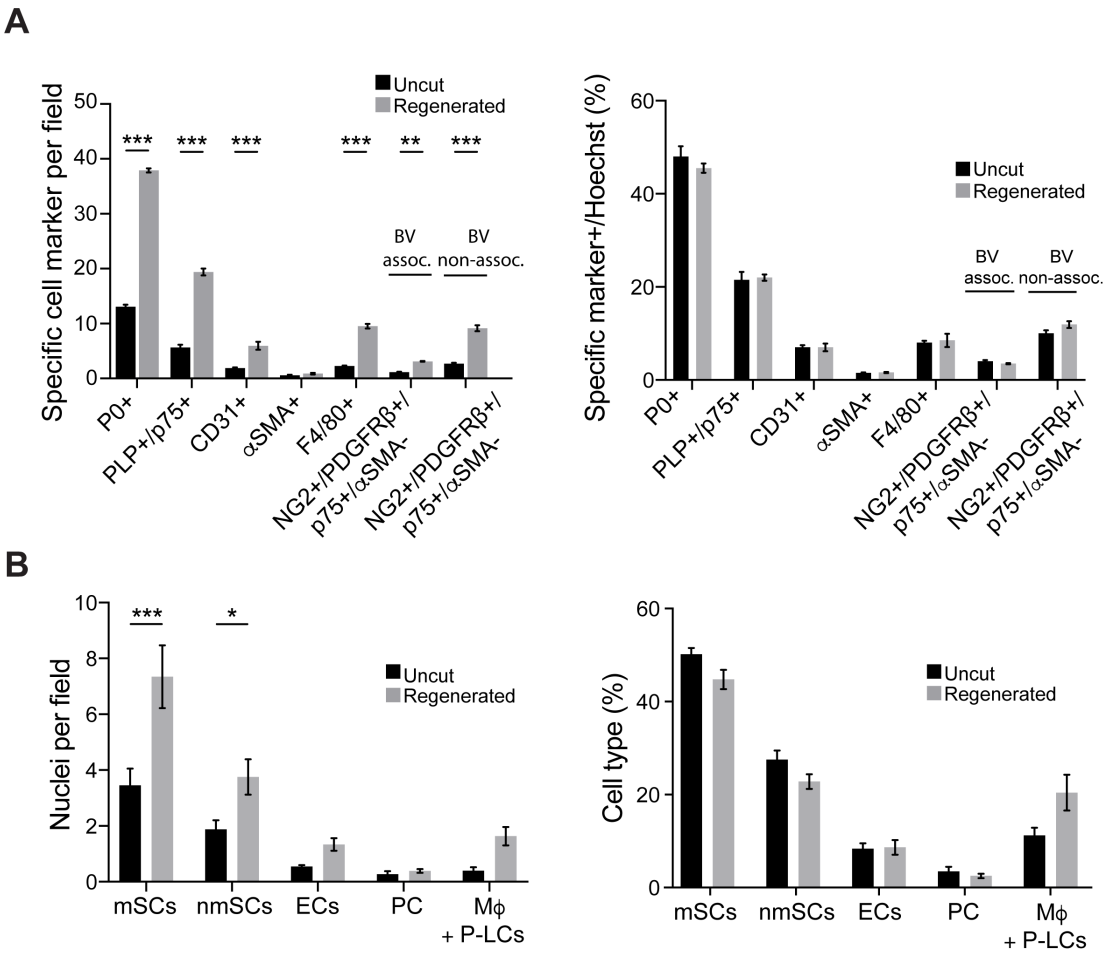

Figure 4.20. Increased cell density represents a proportional increase of all cell types
A) Cryosections of uninjured and regenerated sciatic nerve were immunolabelled for cell type specific markers, as indicated, and the number of different cell types quantified. Graphs show the quantification of different cell types per field (left panel) and the proportion of each cell type (right panel) in the uncut and regenerated nerves, 6 months following injury. The markers used to identify the cell types are indicated in the graph (n=4 mice, mean±SEM). The area of each quantified field was 0.0135mm^2. **B)** Quantification of EM images showing the number of specific cell types per field (left panel) and the proportion of each cell type (right panel) in the uncut and regenerated nerves, 6 months following injury. Cells were identified by morphology. EC= endothelial cells, PC= pericytes. We were not able to distinguish macrophages (Mφ) from NG2+/ PDGFRβ/ αSMA-/ P75+ cells, labelled as P-LCs (pericyte-like cells), and consequently we grouped these two cell types together in one category (n=4 mice, mean±SEM). Statistical analysis: Two-way ANNOVA Sidaks' multiple comparison test. This analysis was performed in collaboration with Dr. I. Napoli.

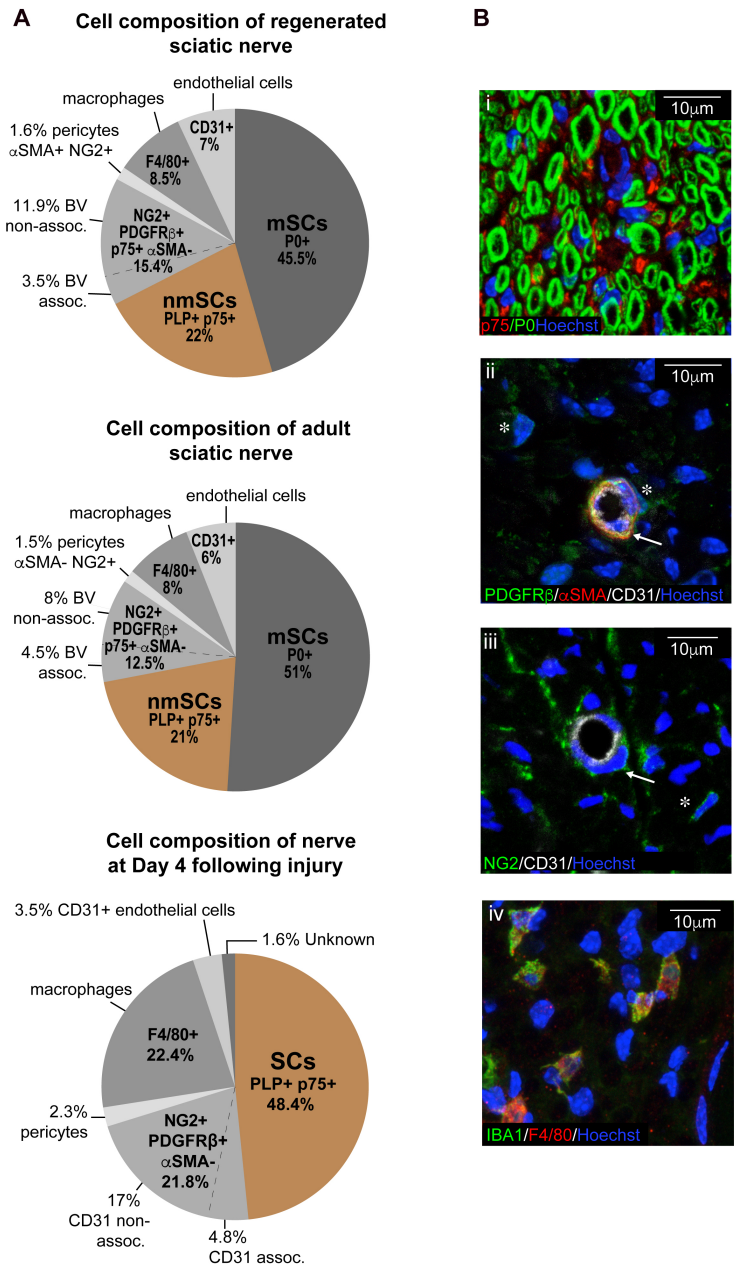

Figure 4.21. Cell composition of fully regenerated nerve

A) Pie chart shows the cell composition of regenerated sciatic nerve, 6 months following nerve injury. The markers used to identify the cell types are indicated in the chart (n=4 mice). Pie charts of uninjured and injured nerve at Day 4 following injury are shown to facilitate the comparison between the different pie charts. **B)** Representative confocal images of transverse sections of fully regenerated sciatic nerve, 6 months following injury showing the different cell types Sections were immunostained with i) p75 (red) and P0 (green) to detect nmSC and mSCs, respectively. ii) PDGFRß (green), αSMA (red) and CD31 (white) to detect pericytes, NG2+/ PDGFRβ+/ αSMA-/ P75+ cells and blood vessels. iii) NG2 (green) and CD31 (white) to detect pericytes, NG2+/ PDGFRβ/ αSMA-/ P75+ cells and blood vessels. iv) Iba1 (green) and F4/80 (red) to detect macrophages. Nuclei were counterstained with Hoechst in blue. ii-iii) Arrows indicate pericytes associated with CD31+ blood vessels and asterisks indicate NG2+/ PDGFRβ+/ αSMA-/ P75+ cells that are either loosely associated or non- associated with blood vessels.

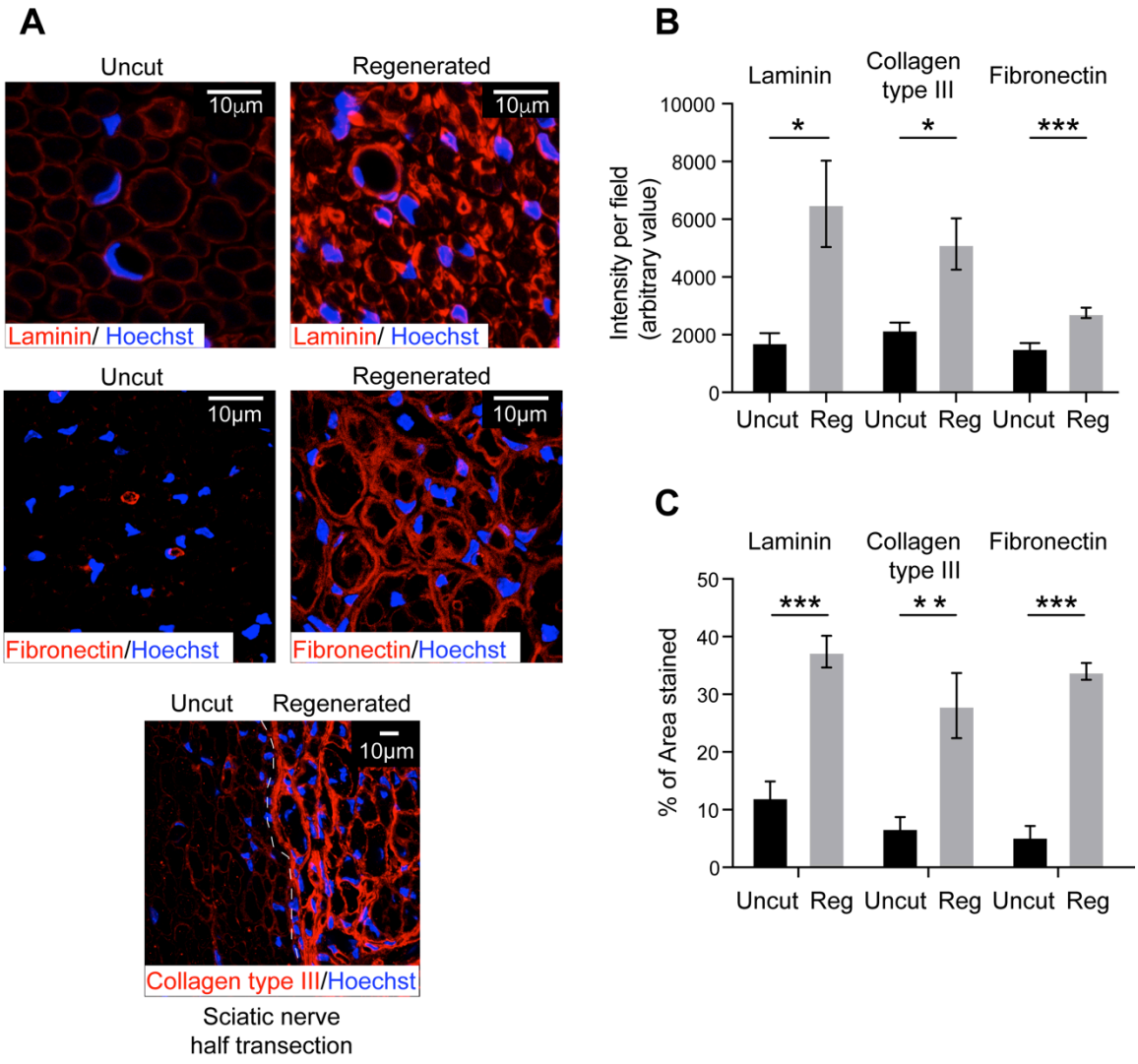

Figure 4.22. Enhanced ECM deposition in regenerated nerve

A) Representative confocal images of transverse sections of uninjured (left panel) and fully regenerated nerve (right panel), 6 months following injury. Cryosections were immunostained for laminin (upper panel, red), fibronectin (middle panel, red) and collagen type III (lower panel, red). Graphs shows **B)** quantification of ECM staining in the regenerated nerve compared to the uninjured nerve. **C)** quantification of ECM area in the regenerated nerve compared to the uninjured nerve (n=6 mice mean±SEM).

4.7. Myelinating Schwann cells retain their SC identity in a regenerated nerve

It has been shown previously that adult SCs retain a certain level of multipotency, however most of these studies have been performed *in vitro* (Real et al., 2005; Widera et al., 2011) or alternatively were performed in relatively non-physiological conditions such as when preventing axonal regrowth *in vivo* (Adameyko et al., 2009). Studies in other tissues have also demonstrated the importance of the physiological environment to maintain cell identity (Anderson, 2001). For example, the reported multipotency of pericytes *in vitro* was contradicted by recent lineage analysis in the brain that showed that pericytes maintain their cell lineage in their physiological environment *in vivo* (Guimaraes-Camboa et al., 2017).

To determine the plasticity of mSCs within the nerve, we performed a lineage analysis to follow the fate of the mSCs following nerve injury. To do this, we used both P0-CreER^{T2}:YFP and P0-CreER^{T2}:Confetti mice. We treated the mice with tamoxifen 2 weeks prior to nerve transection and the injured and uninjured contralateral sciatic nerves were harvested at 6 months following nerve injury. Firstly, we investigated, whether mSCs-derived cells that proliferated early after injury could redifferentiate and remyelinate normally. This study was performed by injecting a single dose of EdU at Day 3 following injury and the nerves of P0-CreER^{T2}:YFP analysed at 6 months following nerve injury. This analysis detected YFP+/ EdU+ mSCs that co-expressed P0 within the regenerated nerve demonstrating that these mSCs have redifferentiated and remyelinated normally in the progress of peripheral nerve regeneration (Figure 4.23A and 4.23B).

We have then used the P0-CreER^{T2}:Confetti mice to trace the cell fate of the mSC-derived cells throughout the regenerative process. To determine whether mSC-derived cells retain their cell identity, we analysed the morphology of the cells and their association with large calibre axons at 6 months following nerve injury. Consequently, we visualised the endogenous fluorescence of the Confetti reporter cassette and in parallel performed immunofluorescence staining to detect the axons within the regenerated nerve. This analysis demonstrated that the majority of the labelled mSCs redifferentiated to mSCs, as shown by their typical mSC morphology and association with large calibre axons (Figure 4.24A).

Although we showed previously that all mSC proliferate following nerve injury, additional stem

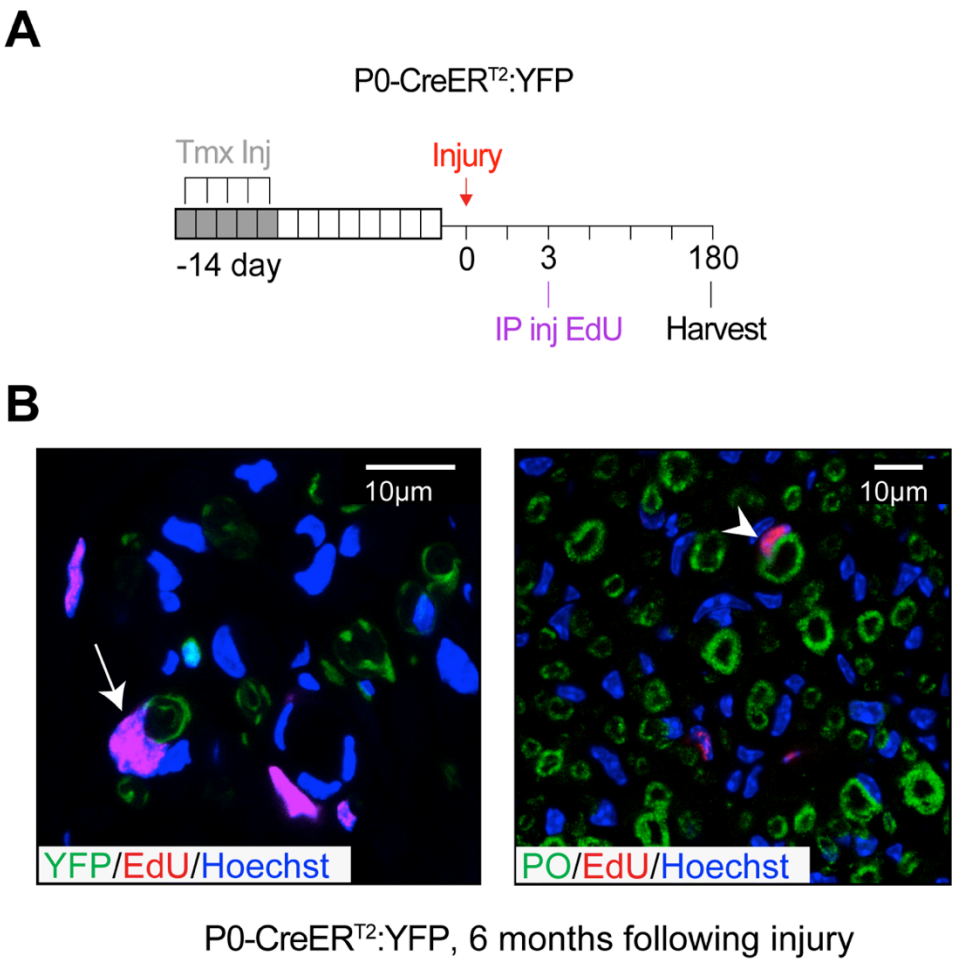

Figure 4.23. Proliferating mSC-derived cells redifferentiate and remyelinate axons
A) Schematic representation of the protocol used to determine whether proliferating cells derived from mSCs redifferentiate and remyelinate axons. P0-CreER^{T2}:YFP mice were injected intraperitoneally with tmx for 5 consecutive days. 14 days following tmx administration, the right sciatic nerve was transected and EdU was injected at Day 3 following injury. Mice were harvested 6 months following injury. **B)** Representative confocal images of transverse sections of the regenerated nerve, 6 months following injury. Left panel: The arrow indicates YFP+ mSC that proliferated at Day 3 following injury and redifferentiated to a mSC within the regenerated nerve. Right panel: The arrowhead indicates a SC that has proliferated at Day 3 following injury and redifferentiated to a mSC, as indicated by P0 staining.

cell populations could still contribute to the production of new SCs during the regenerative process as has been suggested by previous studies (Amoh et al., 2005; Chen et al., 2012; McKenzie et al., 2006). Consequently, we investigated whether cells derived from mSCs contributed proportionally to the new mSC population in regenerated nerve. To do this, we compared the rate of recombination in the contralateral uninjured nerve to the distal regenerated nerve in mice with lower recombination rates. We found that the proportions remained the same (Figure 4.24B) providing strong evidence that an additional stem cell or progenitor population was not contributing to the production of mSCs in the regenerated nerve. In contrast, the percentage of recombined cells was lower in some animals in the region of the cut site (Figure 4.24B). This is consistent with our findings that in some animals, proportionally fewer mSCs migrated into the bridge region compared to those derived from nmSCs (Figure 4.16). This is most likely due to the nmSC population contributing to the mSC population at the injury site. However, to ensure that the original SC populations are not diluted by an influx from stem cells, future experiments will need to compare the proportion of total SCs at the regenerated injury site with the uninjured contralateral nerve by analysing nerves in which all SCs are labelled with a fluorescent reporter cassette.

To determine the plasticity of mSCs following nerve injury, we investigated whether all mSC-derived cells retain their cell fate during nerve regeneration. We initially analysed the new tissue of the bridge region, as the disruption of the perineurium and the SC basal lamina increases the exposure of SCs to factors of the regenerative environment. Strikingly, using immunofluorescence analysis, we observed several examples of labelled mSC-derived cells that were associated with small calibre axons indicating that they had redifferentiated to become nmSCs (Figure 4.25). We also found these cells within the distal stump region, although to a lesser extent than at the injury site. As it is difficult to visualise the small calibre axons by conventional confocal microscopy because spatial resolution is limited, we performed correlation light electron microscopy (CLEM) that combines light with electron microscopy in order to determine whether mSC-derived cells can re- differentiate to nmSCs.

First, we imaged regions of the injury site that contained large number of fluorescently labelled cells. Subsequently the sections were processed for EM analysis and the identical

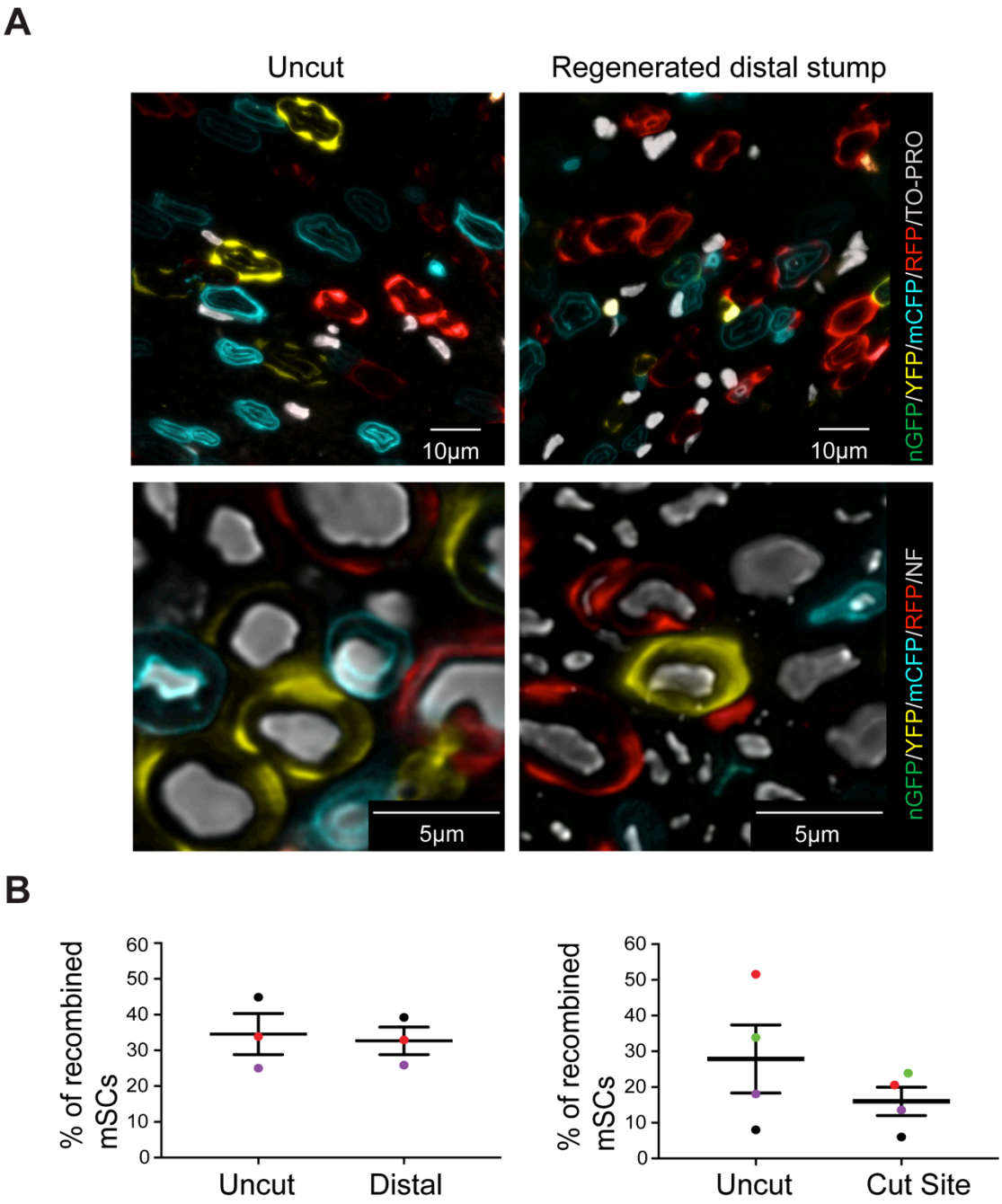

Figure 4.24. Most mSC-derived cells redifferentiate back to a mSC

A) Representative confocal images of uncut and regenerated distal stumps of P0-CreER^{T2}:Confetti mice, 6 months following injury. The majority of the labelled mSCs redifferentiated to become mSCs, as seen by their typical morphology and association with large calibre axons, labelled for neurofilament (white). Nuclei were counterstained with TO-PRO. **B)** Graphs show the percentage of recombined mSCs in the distal stump (left panel) and at the injury site (right panel) of P0-CreER^{T2}:Confetti mice, 6 months following injury compared to the uninjured contralateral nerve. Each coloured dot represents an individual animal and the line shows the mean percentage±SEM.

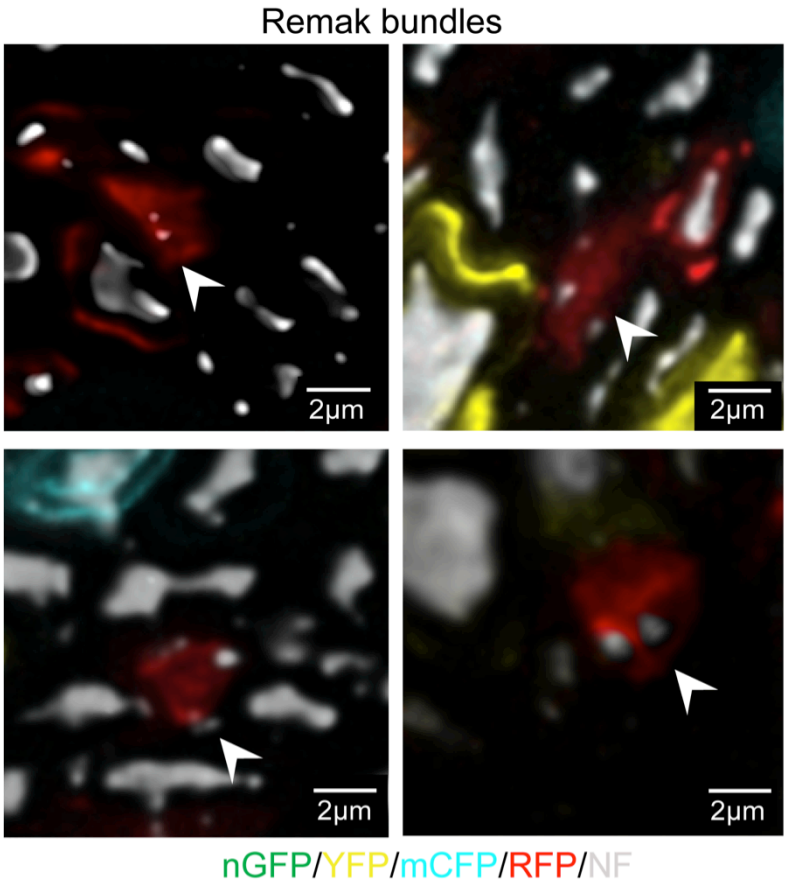

Figure 4.25. Labelled mSC-derived cells are associated with small calibre axons in regenerated nerve

Representative confocal images of transverse sections of regenerated sciatic nerves fromf P0-CreER^{T2}:Confetti mice, 3 months following nerve injury. Transverse sections were immunostained with neurofilament (NF) antibody to detect axons and show labelled mSC-derived cells that have redifferentiated to nmSCs. Arrowheads indicate labelled Remak bundles associated with small calibre axons.

nerve regions imaged by EM and correlated to the immunofluorescence image. Using this technique, we observed multiple examples of labelled Remak bundles within the regenerated injury site (Figure 4.26). We also observed mSC-derived cells that have become nmSCs within the distal stump of the regenerated nerve (data not shown here).

The finding that mSCs can switch to a nmSC fate may imply that nmSCs derived cells can also redifferentiate to mSCs following nerve injury. This could explain the decreased numbers of recombined mSC within the nerve bridge of regenerated sciatic nerves (Figure 4.24B), as nmSCs could contribute to the regenerated mSC population within this newly formed tissue.

Importantly, we did not find any mSC-derived cell that became another cell type within the endoneurium of a normal regenerated nerve. Overall, these findings demonstrate that while mSC derived cells retain their SC identity, they are able to switch to a nmSC fate during regeneration. These findings suggest that as has been shown for other cell types, the reported plasticity of cells is due to the non-physiological environment in which the experiments were performed and that the microenvironment is critical for maintaining cell identity (Guimaraes-Camboa et al., 2017; Snippert and Clevers, 2011).

4.8. mSC plasticity within tumourigenesis

In order to determine whether the loss of Nf1 together with the microenvironment of the injury site influences the cell fate of the Nf1 KO SCs, we performed lineage tracing studies to follow the cell fate of the Nf1 KO SCs. To do this, we used the Nf1 KO mouse model (P0-CreER^{T2}:YFP:Nf1$^{fl/fl}$) that was introduced in Chapter 3. In this mouse model neurofibromas form specifically at the injury site and we have shown that these are derived from Nf1 KO mSCs (Ribeiro et al., 2013). We observed previously that some of the YFP expressing Nf1 KO mSC-derived cells within the neurofibromas co-expressed Glut1 (Ribeiro et al., 2013). Glut1 is a marker for perineurial-like cells within the tumours, whereas in a healthy peripheral nerve it is only expressed by endothelial cells in the nerve endoneurium and by perineurial cells in the perineurium. The expression of Glut1 implies that the Nf1 KO SCs transdifferentiated into perineurial like cells within the tumour mass.

This suggested that Nf1 KO mSC-derived cells were either more plastic than normal SCs, the

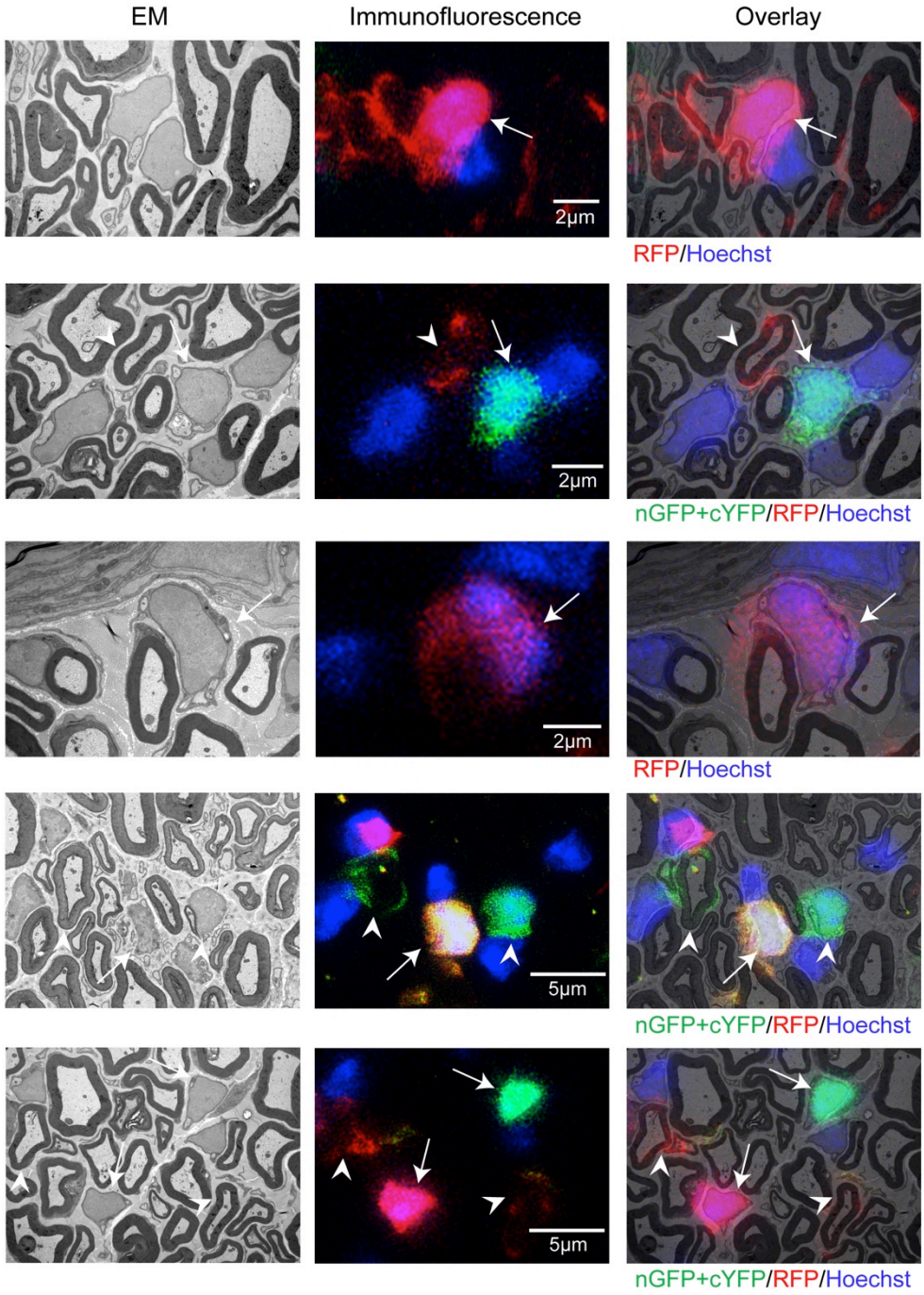

Figure 4.26. mSC-derived cells can redifferentiate to become nmSCs following nerve injury

Correlative light and electron microscopy (CLEM) images of transverse section of regenerated sciatic nerve of P0-CreER^{T2}:Confetti mice, 3 months following nerve injury. Panels show several examples of labelled mSC-derived cells that have redifferentiated to nmSCs during the progress of peripheral nerve regeneration. The arrows indicate mSC-derived cells that have become nmSCs and the arrowheads indicate labelled mSCs.

tumour environment was more conducive to SC plasticity or both. To examine this in more detail, we analysed the fate of Nf1 KO mSCs at both the tumour site and within the distal stump, where the mSCs behave normally. With this analysis, we were aiming to compare the plasticity of mSC during tumourigenesis to mSC plasticity within a normal nerve regeneration process, as shown in chapter 4.7.

To do this, we immunolabelled transverse sections of regenerated control (Nf1 WT) sciatic nerve, regenerated Nf1 KO distal stump and Nf1 KO neurofibromas with Glut1 (Figure 4.27A) to detect perineurial like cells and NG2 to detect pericytes and the NG2+/PDGFRβ+/αSMA- cell population (Figure 4.27B). Analysis of these nerves showed that whilst cells derived from Nf1 KO mSCs redifferentiated into mSCs at the distal stump or became tumour cells at the injury site, a proportion appeared to become other cell types within the tumours, whereas this was never observed within the distal stump. These included a large number of cells that expressed Glut1 and resembled perineurial-like cells within the tumour mass (Fig 4.27Aiv). Moreover, we found several examples of YFP+ cells that had integrated into the perineurium (Fig 4.27Aiii). These cells were never seen in control animals (Figure 4.27Ai) or in the distal stump of Nf1 KO animals (Figure 4.27Aii). Furthermore, we found that some YFP+ cells co-expressed NG2, as indicated by arrowheads in Figure 4.27B, and these cells exhibited a very atypical SC morphology suggesting that they possibly transdifferentiated into a NG2+/ PDGFRβ+/p75+ αSMA- cell population, which has been described in Chapter 4, within the neurofibromas. No abnormal expression of NG2 was observed within the control (Nf1 WT) regenerated nerve (Figure 4.27B) and in the regenerated Nf1 KO distal stump (data not shown) and as shown in Chapter 4.6 no mSC-derived cells were found to become another cell type following normal nerve regeneration.

Interestingly, these results show that Nf1 KO SCs could develop a different cell fate at the injury site, whereas in the distal stump these cells behaved as control (Nf1 WT) SCs, showing that Nf1 KO SCs retain their identity within the context of a regenerating nerve and exhibit limited plasticity, whereas a tumourigenic genetic change and the microenvironment synergise to increase the plasticity of these cells.

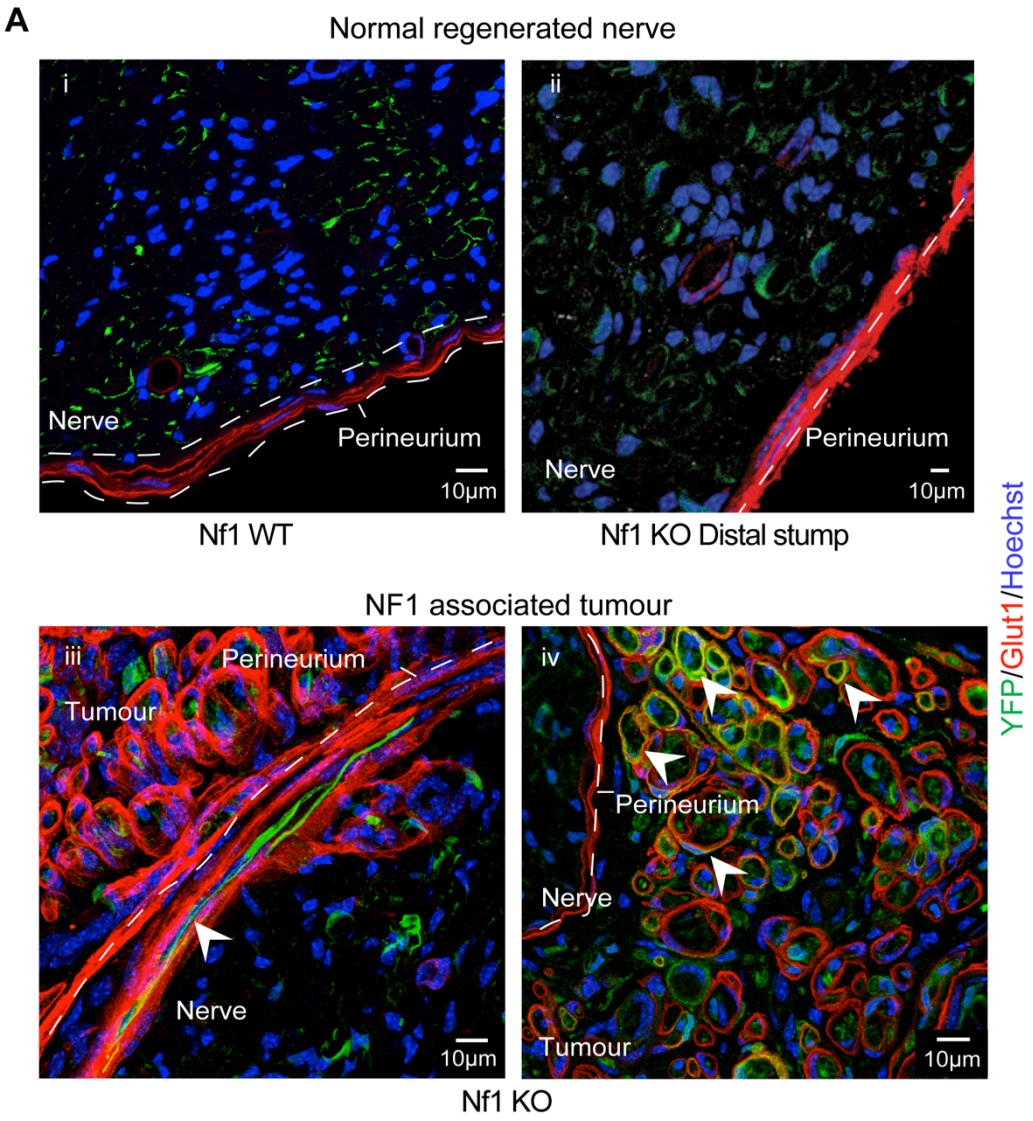
A
Normal regenerated nerve
i
Nerve
Perineurium
10μm
Nf1 WT
ii
Perineurium
Nerve
10μm
Nf1 KO Distal stump
NF1 associated tumour
iii
Perineurium
Tumour
Nerve
10μm
iv
Perineurium
Nerve
Tumour
10μm
Nf1 KO
YFP/Glut1/Hoechst

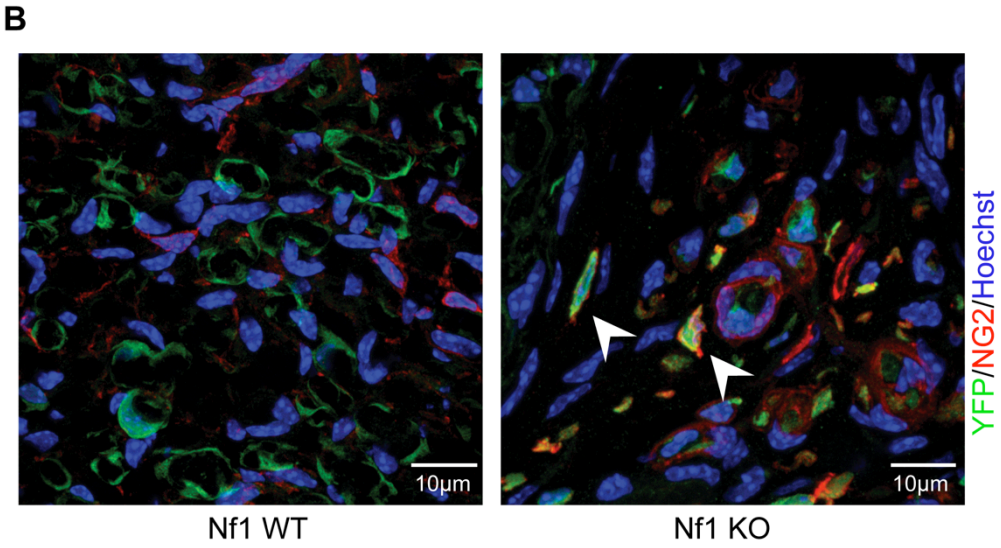

Figure 4.27. Nf1 KO mSC-derived cells become perineurial-like cells within neurofibromas

A) Representative confocal images showing (i) a normal regenerated nerve of a P0-CreER^{T2}:YFP and (ii) regenerated distal stump of P0-Cre:ER^{T2}:YFP:Nf1$^{fl/fl}$ mice in which mSCs retain their lineage as no other YFP+ cells than mSCs were observed and (iii+iv) neurofibromas of P0-Cre:ER^{T2}:YFP:Nf1$^{fl/fl}$ mice that specifically form at the injury site. Arrowheads indicate Nf1 KO YFP+ mSC-derived cells, which have taken a different cell fate within the tumour. (iii) shows a YFP+ cell which has integrated within the perineurium and (iv) shows YFP+ perineurial -like cells that exhibit a typical perineurial-like cell morphology and are labelled with Glut1, which is a perineurial cell marker. **B)** Representative confocal images of transverse sections of regenerated injury site of control animal (Nf1 WT) (left panel) and neurofibromas (right panel) labelled with NG2 (red), GFP(green) and nuclei were counterstained with Hoechst. Arrowheads indicate YFP+ mSC-derived cells that express NG2.

4.9. Analysis of the cellular composition of Nf1-deficient neurofibromas

As we have shown in 4.8 Nf1 KO SCs can transdifferentiate into other cell lineages such as perineurial-like cells within the tumours, however in order to understand whether these cells may play an important role in these tumours, we wanted to determine their prevalence within the tumour mass. Clinical studies have previously shown that perineurial-like cells are very prominent in human neurofibromas and these cells have been characterised morphologically to possess long cytoplasmic processes that contain pinocytotic vesicles (Erlandson, 1985, 1991). In addition to perineurial-like cells, human neurofibromas have been shown to consist of axonal processes, increased numbers of “perineurial-like” cells, endothelial cells, fibroblasts, mast cells and mostly dedifferentiated SCs, all of which are embedded in an abundant collagenous matrix (Carroll and Ratner, 2008; D., 2008; Jouhilahti et al., 2011; Serra et al., 2000; Upadhyaya, 2012). We also investigated the prevalence of activated fibroblasts, as these cells are well known to play a critical role in wound healing, fibrosis and carcinogenesis (Chang et al., 2004) Importantly, these activated fibroblasts secrete several pro-tumourigenic factors that could contribute to drive tumour formation, as shown in other cancers (Bhowmick et al., 2004; Franco et al., 2010; Kalluri, 2016; Kalluri and Zeisberg, 2006).

To determine the prevalence of these two cell types, we performed sciatic nerve half transection on a cohort of tamoxifen treated Nf1 KO and control (Nf1 WT) mice and we harvested the injured nerves at 8 months following injury. Transverse sections of neurofibromas and regenerated injury region of control (Nf1 WT) nerves were immunolabelled with cell type specific markers, as indicated in Figure 4.28. Glucose transporter 1 (Glut-1) was used to label the perineurial-like cells within the neurofibromas, as shown previously (Ribeiro et al., 2013). CD90.2 was used to label fibroblasts as it was shown to be expressed by fibroblasts in other tissues and was previously reported to be expressed by cancer-associated fibroblasts (CAFs) within tumour microenvironments (Franco et al., 2010; True et al., 2010; Zhao and Peehl, 2009; Zhu et al., 2014).

This analysis showed that perineurial-like cells are highly abundant within the neurofibromas at the injury site (Figure 4.28A). Moreover, they have a distinct morphology in that they are

extremely thin with long cytoplasmic protrusions with which they enwrap other cells within the tumour microenvironment (Figure 4.28B). Importantly, these cells appear to form a structural network within the tumour, as shown in the low magnification image in Figure 4.28B, and this network could potentially facilitate intercellular interactions by connecting the different cell types within the tumour. Moreover, the high abundance of the perineurial-like cells and their close contact with other cell types within the tumour microenvironment implies that they likely possess an important role within these tumours and it will be of great interest to investigate their interactions with the Nf1 KO SCs in future experiments.

We also found CD90.2+ fibroblasts throughout the neurofibromas as shown in Figure 4.28C and 4.29, which were not found within a normal regenerated nerve or in the uninjured regions (Figure 4.29A-C), implying that these cells are recruited specifically into neurofibromas. However, we found lower levels of these activated fibroblasts compared to the perineurial-like cells and we also observed that the levels vary regionally, as some regions contained very high levels (Figure 4.29C), of these cells whilst others low levels (Figure 4.28C).

We co-stained for Glut1 in order to determine, whether the perineurial-like cells also expressed CD90.2 within the neurofibromas (Figure 4.29D) and found that Glut-1 and CD90.2 were not co-expressed in the tumour stroma (Figure 4.29D) suggesting that these markers identify two different cell populations. Overall, the observed increase in Glut1+ perineurial- like cells and CD90.2+ activated fibroblasts befits the reported fibrotic characteristic of a neurofibroma.

We also analysed the cell composition of the Nf1 KO distal stump and we observed it was similar to the regenerated control (Nf1 WT) nerve with no detectable expression of CD90.2 (Figure 4.29A-C) and with Glut1 expression restricted to endothelial cells within the regenerated nerve endoneurium and to perineurial cells (Figure 4.29D) within the perineurium. These findings demonstrate that the tumour microenvironment, once it is formed, is different in its cell composition and is highly distinct from normal or regenerated nerve.

Furthermore, to determine whether SCs can myelinate within the tumours, we analysed, whether mSCs are present within the neurofibroma samples. In order to do so, we

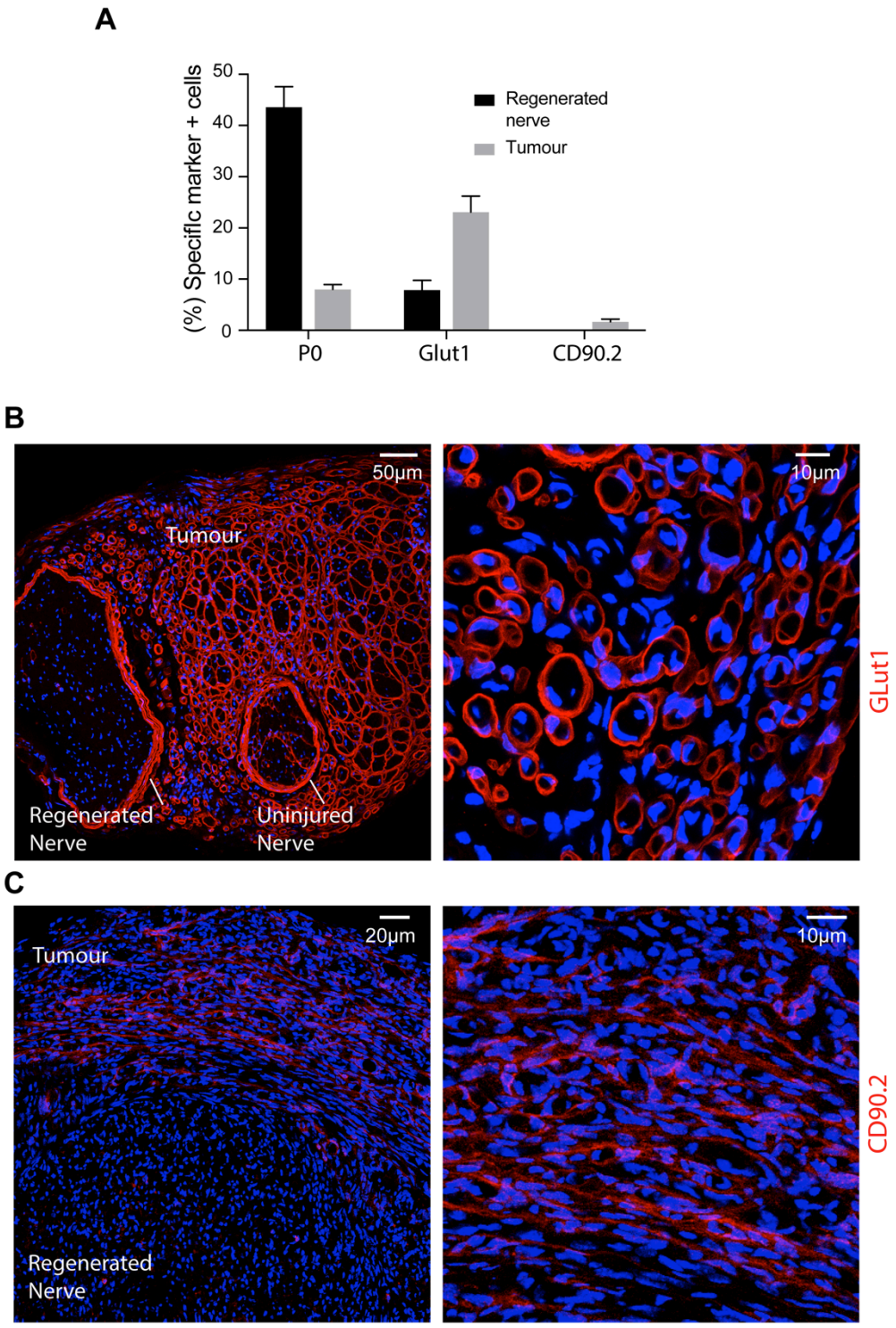
A
(%) Specific marker + cells
50
40
30
20
10
0
Regenerated nerve
Tumour
P0
Glut1
CD90.2
B
50µm
Tumour
Regenerated Nerve
Uninjured Nerve
10µm
GLut1
C
20µm
Tumour
Regenerated Nerve
10µm
CD90.2

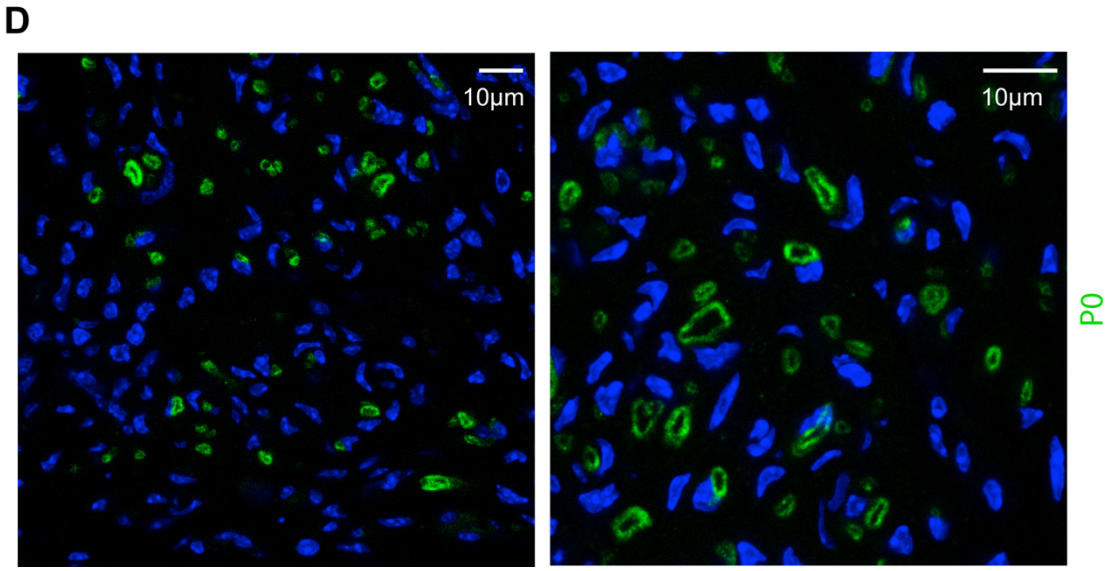

Figure 4.28. Cellular composition of neurofibromas
Sciatic nerves of tmx treated Nf1 KO and control (Nf1 WT) mice were harvested at 8 months following injury and transverse sections were immunolabelled with cell type specific markers, as indicated in the graphs. **A)** Graph shows the proportion of mSCs (P0+), perineurial like cells (Glut1+) and activated fibroblasts (CD90.2+) in the tumours compared to the regenerated injury site of the control animals (n=4, mean±SEM). Representative confocal images of transverse sections of a neurofibroma. Low magnification (left panel) and high magnification (right panel). Transverse sections were labelled with: **B)** Glut1 to detect perineurial-like cells. **C)** CD90.2 to detect fibroblasts. **D)** P0 to detect mSCs.

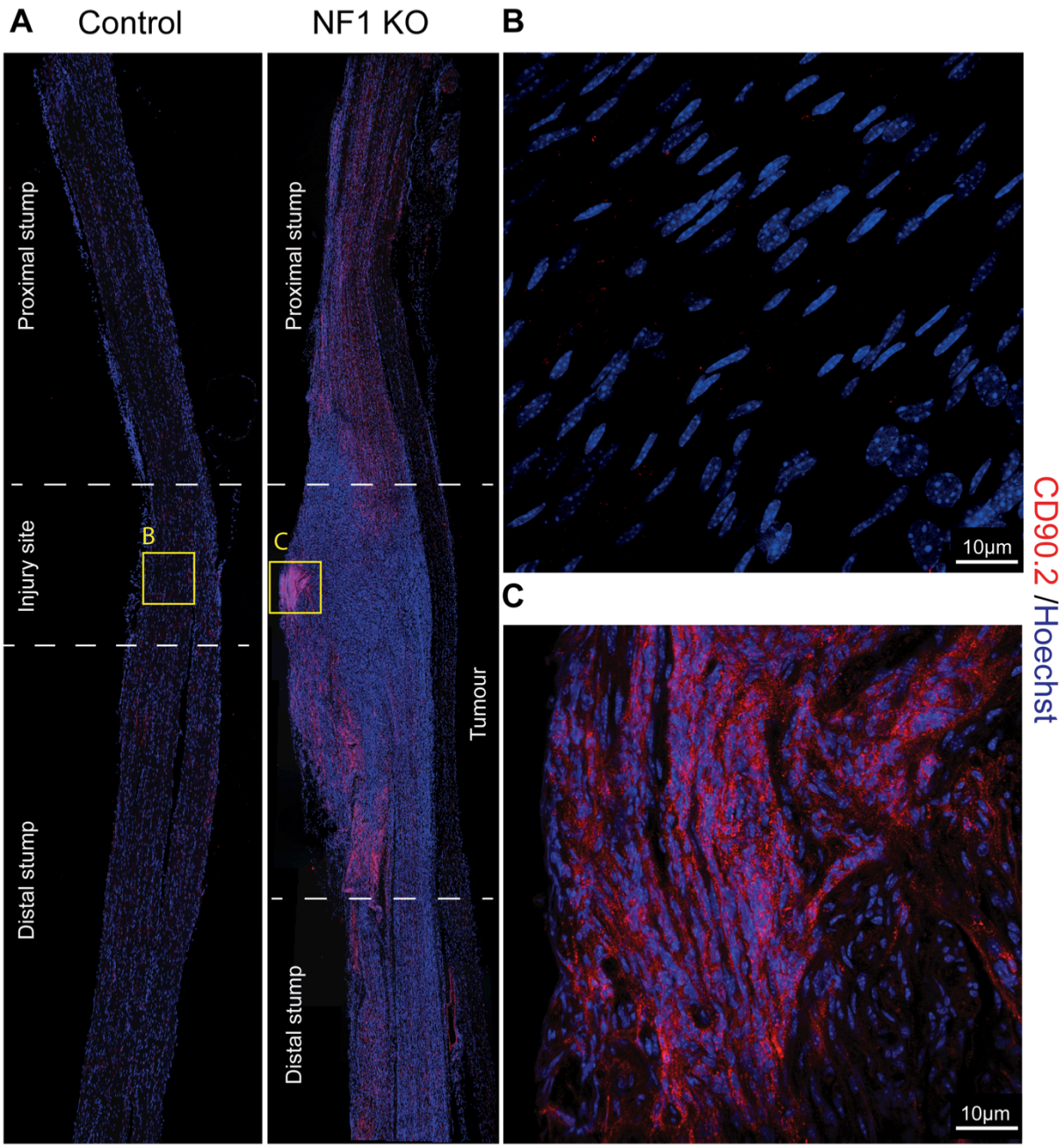
A
Control
NF1 KO
B
Proximal stump
Injury site
Distal stump
B
C
Proximal stump
Tumour
Distal stump
C
10μm
10μm
CD90.2 /Hoechst

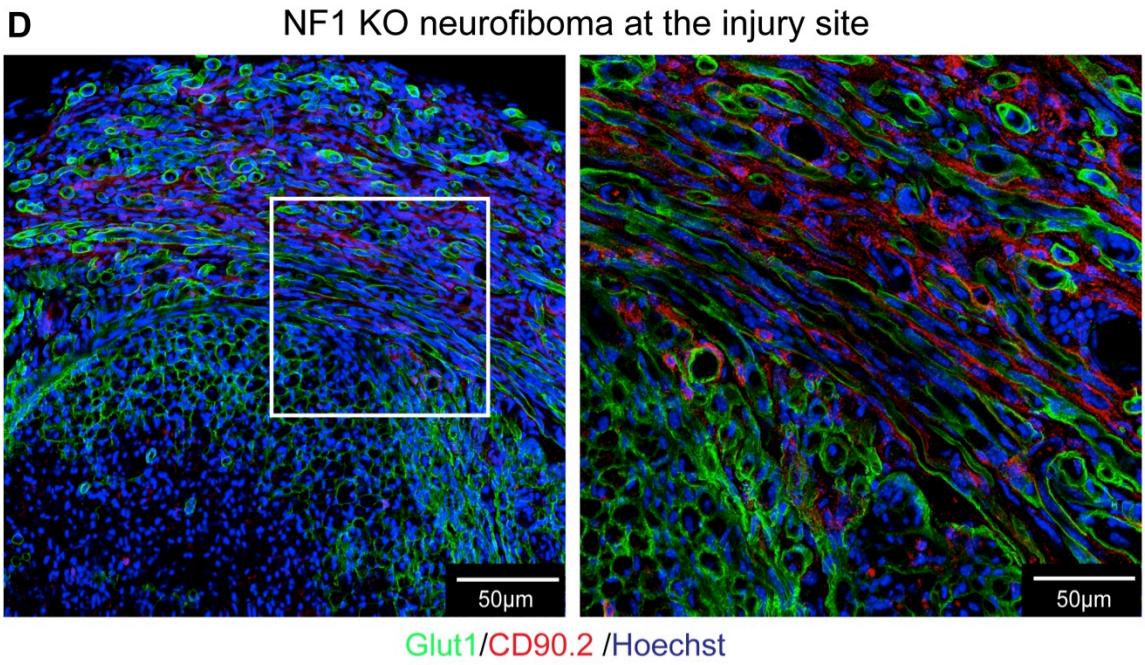

Figure 4.29. Different cell populations express Glut1 and CD90.2 within Nf1 KO tumours

Representative confocal images of longitudinal sections of regenerated control (Nf1 WT) nerve and neurofibromas, 8 months following injury. Cryosections were labelled with CD90.2 (red) and nuclei were counterstained with Hoechst (blue). **A)** Representative confocal images at low magnification showing full length control regenerated and Nf1 KO tumour bearing nerve. Higher magnification confocal images of **B)** regenerated injury site of control (Nf1 WT) animal and of **C)** neurofibroma at the Nf1 KO injury site. **D)** Representative confocal images of transverse sections of Nf1 KO neurofibromas, 8 months following injury. Cryosections were labelled with CD90.2 (red), Glut1 (green) and nuclei were counterstained with Hoechst. Note that Glut1 and CD90.2 were not co-expressed indicating that these markers label two different cell populations within the Nf1 KO tumours.

immunolabelled the neurofibroma samples with the mSC marker PO and as shown in Figure 4.28A and 4.28D, we observed a significant number of mSCs within the tumours. This finding shows that myelination can still occur within the tumour microenvironment, indicating that the signals that maintain SCs in a dedifferentiated state likely act locally, however we don't know yet whether Nf1 KO SC can myelinate within the tumours and this will be addressed in 4.10.

4.10. Tumour Clonality analysis

Neurofibromas are SC derived tumours but to date it is not known, whether they arise from a single transformed SC or are polyclonal. Nf1 KO SCs are highly proliferative and consequently more vulnerable to acquire new mutations, however no studies have addressed the clonality of the Nf1 KO SCs within neurofibromas.

Early studies of tumourigenesis suggested that tumours arise from a single cell, which gradually acquires mutations that ultimately initiate tumour development (Fearon and Vogelstein, 1990; Nowell, 1976). Recent studies updated this model of tumour formation, as next generation sequencing showed that the majority of cancers consist of multiple subclones that carry common but also different mutations (McGranahan and Swanton, 2017). It is important to understand, how this intratumoural heterogeneity contributes to tumour formation and progression and how it impacts cancer treatment, as these various subclones very likely respond differently to therapy.

A recent study using the K5-CreER:Confetti mouse model that labels skin cells demonstrated that benign skin papillomas are usually monoclonal, however malignant transformation was observed to be correlated with the emergence of multiple coloured subclones in the tumour (Reeves et al., 2018). This study suggested that additional mutations have diversified the original clonal population during the course of tumourigenesis and that tumour progression may require interactions between these clonal populations. Similarly, in lung (de Bruin et al., 2014; Zhang et al., 2014a) and colon cancers (Kim et al., 2015; Sottoriva et al., 2015), key driver mutations have been demonstrated to be clonal, but nevertheless the fully grown tumour is highly heterogeneous with spatially distinct subclones.

Similar to the malignant progression of papillomas to skin carcinomas, malignant peripheral

nerve sheath tumours can develop from neurofibromas, however the malignant transformation of neurofibromas to MPNST is poorly understood, although it is thought to involve mutations in tumour suppressor genes and oncogenes, additionally to the loss of Nf1 in SCs (Bradtmoller et al., 2012; Farid et al., 2014; Gregorian et al., 2009; Wu et al., 2014).

Here, we investigated, whether neurofibromas are mono or poly- clonal to understand if additional mutations may be required to initiate neurofibroma formation at the injury site. Moreover, we determined whether Nf1 KO SCs can myelinate within the tumours mass, as mSC can be differentiated from Nf1 KO tumour cells by their morphology and their association with large calibre axons. For this analysis we used the P0-CreER^{T2}:R26RConfetti:Nf1$^{fl/fl}$ (Nf1 KO Confetti mouse model) that I have generated, as described in Chapter 3. This model allows us to distinguish between individual, adjacent recombined SCs. For the clonality analysis, there are two possible outcomes: 1) Monoclonal tumours consisting of uni-coloured Nf1 KO SCs. 2) Polyclonal tumours with equal colour recombination frequencies or unequal colour recombination frequencies. The latter outcome would suggest that one or many colour recombinations have expanded in size probably due to a later mutational event, which provided a survival or proliferative advantage.

Using the confetti mouse model, we performed a half transection of the sciatic nerve on a cohort of tmx injected Nf1 KO and control mice and harvested them at 8 months following injury. Following harvesting of the tumour we processed the tumour tissue for immunostaining and we analysed the distribution, frequency and morphology of the differentially coloured Nf1 KO SCs. This analysis showed that neurofibromas are clearly polyclonal as displayed in Figure 4.30 demonstrating that the loss of Nf1 is sufficient to drive tumourigenesis at the Nf1 KO injury site.

Strikingly, we observed that neighbouring differently coloured Nf1 KO SCs seemed to exhibit distinct cell morphologies within the tumours. Consistent with the previous analysis that showed the presence of mSCs within the neurofibromas, we found that some of these Nf1 KO SCs exhibited the typical morphology of mSCs (outlined with arrows in Figure 4.30). For example, in Figure 4.30, the red Nf1 KO SCs morphologically reassemble dedifferentiated SCs, as indicated with arrowheads, whilst the yellow Nf1 KO SCs reassemble mSCs.

However, as shown in Figure 4.30B, there was no correlation between colour recombination and cell morphology, as some of the red Nf1 KO SC either morphologically resemble dedifferentiated SC or mSCs within the same tumour region. To ensure that these cells are Nf1 KO SCs that have differentiated to mSCs within the tumour, we investigated whether these cells are associated with large calibre axons by labelling the axons with the axonal marker neurofilament. As shown in Figure 4.31, we found several Nf1 KO SCs that are associated with large calibre axons within the tumours demonstrating that these cells have remyelinated. However, we also observed some abnormal SC-axon structures, in that some Nf1 KO SC appear to ensheath several axons and even ensheath other Nf1 KO SCs. These findings further suggest that Nf1 KO SCs likely are a heterogeneous population, as some Nf1 KO SCs become tumour cells that can transdifferentiate to other cell types, whilst others redifferentiate to mSCs. Moreover, these observations indicate that the signals, which maintain Nf1 KO SCs in their dedifferentiated state act very locally within the tumour microenvironment, as Nf1 KO SC can still differentiate to mSCs within the tumour.

Furthermore, we observed spatial segregation of distinctly coloured Nf1 KO cell populations. For example, as shown in Figure 4.30, in some tumour regions there are mainly red Nf1 KO SCs, whereas in others yellow Nf1 KO SCs. Moreover, in some regions, rare colour combinations can be found such as shown in Figure 4.33. In many other cancers, it was shown previously that spatial segregation of tumour cells can involve specific interactions with neighbouring cells and/or the ECM suggesting that spatial segregation may not be random within the neurofibromas (Cleary et al., 2014; Greaves and Maley, 2012).

Because we observed spatial segregation of Nf1 KO SCs in some regions, we tested whether a distinct Nf1 KO SC colour combination was overrepresented within the tumour compared to the uninjured contralateral nerve. To do this, we compared the frequency of colour recombination of the tumour with the average colour recombination frequency of analysed uninjured contralateral nerves. We have excluded the Nf1 KO SCs that resemble morphologically mSCs in this analysis, as these cells do not constitute the Nf1 KO tumour cells. This analysis showed that, although some Nf1 KO SCs colour combinations were highly enriched within certain regions (spatially segregated), none of the distinctly coloured Nf1 KO

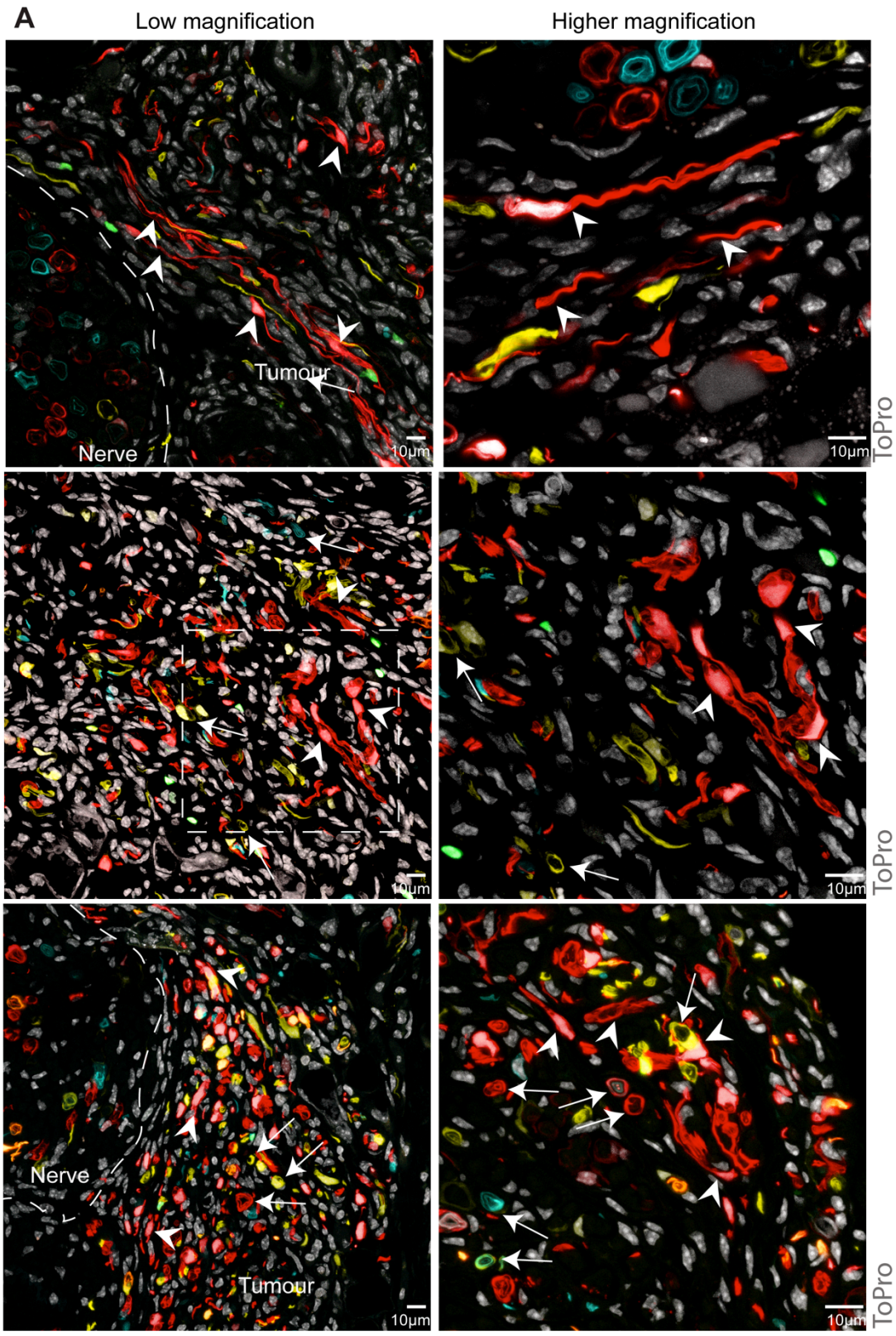
A
Low magnification
Higher magnification
Nerve
Tumour
10µm
ToPro
Nerve
Tumour
10µm
ToPro
10µm
ToPro

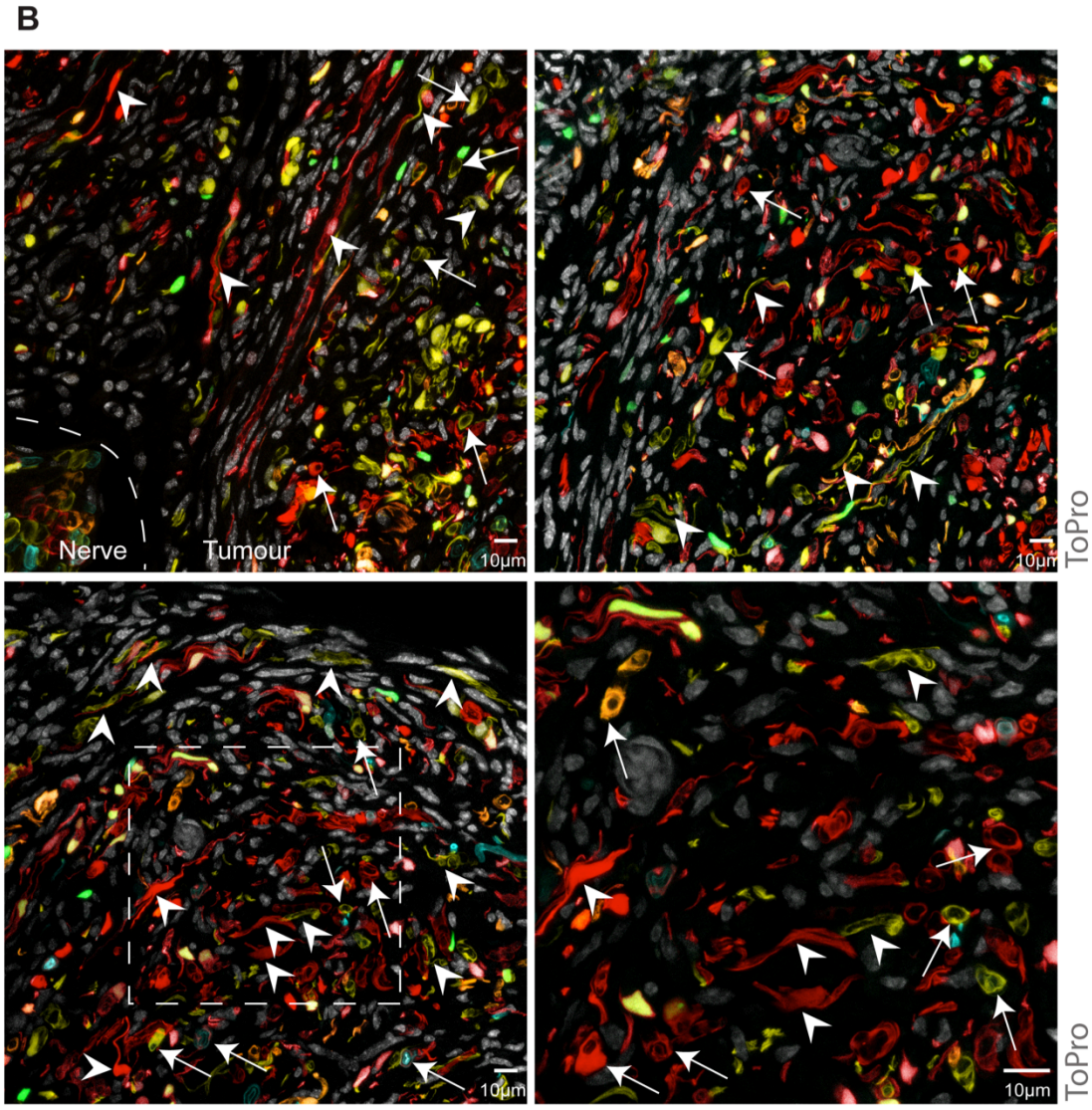

Figure 4.30. Neurofibromas are polyclonal

Representative confocal images of transverse cryosections of Nf1 KO neurofibromas at 8 months following injury. Cryosections were stained with To-Pro-3 (white), which is a far red nuclear counterstain. Note that neurofibromas are polyclonal, however we observed spatial segregation of distinctively coloured Nf1 KO subclones. Furthermore, we also observed recombined mSC-derived cells that exhibit different morphologies such as mSC-derived cells that reassemble morphologically dedifferentiated SCs, as indicated by arrowheads, and others that reassemble mSCs as indicated by arrows. Normal nerve and tumour area is outlined within the image. 6 Animals were analysed in total and representative images of A1 **A)** and A2 **B)** are displayed.

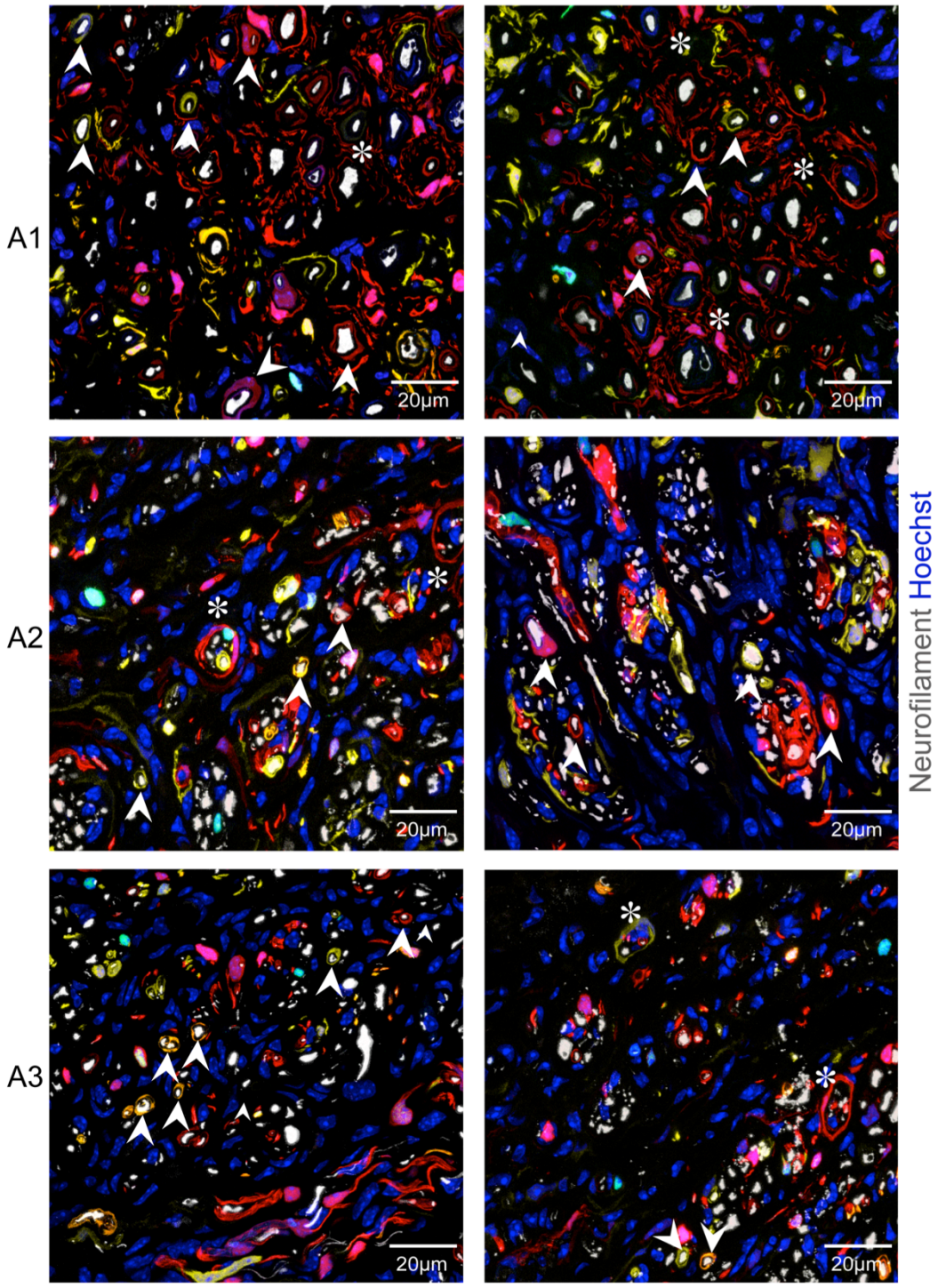

Figure 4.31. Nf1 KO SCs can remyelinate within tumours
Representative confocal images of transverse cryosections of Nf1 KO neurofibromas at 8 months following injury. Cryosections were stained with neurofilament (white) to detect the axons and the nuclei were counterstained with Hoechst (blue). Note that due the Hoechst staining, the CFP positive Nf1 KO SCs cannot be visualised as the CFP emission overlaps with the emission of Hoechst. Arrowheads indicate Nf1 KO SCs that have differentiated to mSCs within the tumours and asterisks indicate abnormal Nf1 KO SC axon structures.

SC subpopulations were found overrepresented within the entire tumour mass (Figure 4.32). These findings suggest that the Nf1 KO SCs do not require any further mutations to trigger tumourigenesis at the injury site, however the observed spatial segregation implies that some Nf1 KO SC subpopulations possess regional preferences for their expansion within the tumour. The latter observation indicates potential interactions of the Nf1 KO SCs with their regional microenvironment, which may correlate with the acquisition of additional mutations that are not driver mutations (not required for tumour initiation) but which may provide regional selective advantage. In future studies, we could use mathematical modelling in order to investigate whether the spatial segregation of the Nf1 KO SCs is random within the tumour mass. In the case that the spatial segregation is significant, it will be important to determine whether it correlates with Nf1 KO SC heterogeneity, as cancer cell heterogeneity is strongly associated with poor prognosis and resistance to therapy.

As shown in Figure 4.30 the tumour mass exhibits high cellularity and seems disorganised in contrast to the neighbouring regenerated nerve. However, we have shown previously that the highly abundant perineurial-like cells form a structural network within the tumour mass (Figure 4.28) and consequently we wanted to investigate whether the Nf1 KO SCs are closely associated with the Glut1+ perineurial-like cells. To test this, we co-stained the confetti neurofibromas with the perineurial–like cell marker Glut1. Interestingly, we observed that the Nf1 KO tumour driving SCs mostly reside within these perineurial-like cell structures suggesting that the Nf1 KO SCs interact with the perineurial-like cells (Figure 4.33). Moreover, these perineurial-like cells appear to spatially organise the Nf1 KO SCs within the tumour and may mediate intercellular interactions between the Nf1 KO SCs and other cell types within the tumour mass. Additionally, we confirmed the transdifferentiation of the Nf1 KO SCs into perineurial-like cells as indicated by the arrowheads in Figure 4.32.

Overall, we showed that the neurofibromas are polyclonally derived, however some distinctly coloured Nf1 KO SC populations appear to be spatially segregated within the tumour mass. Importantly, we found that Nf1 KO SCs can remyelinate within the tumour mass, implying that signals act locally to maintain Nf1 KO SC dedifferentiation, whereas these signals are either absent or suppressed by a pro-differentiating signal that drives myelination in neighbouring

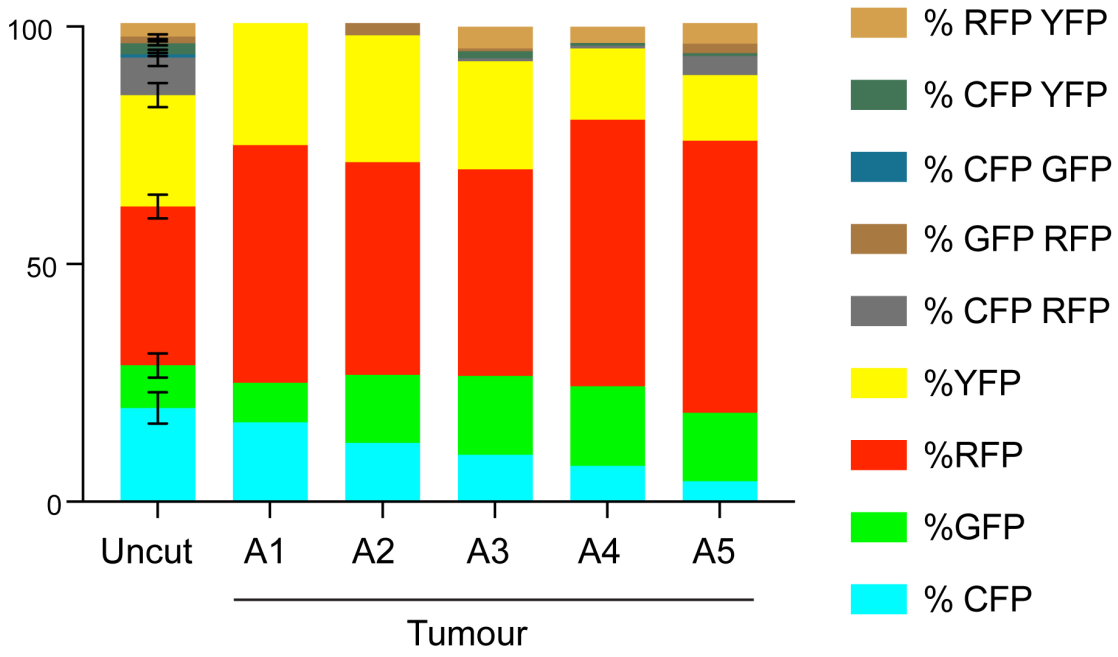

Figure 4.32. Frequency of colour recombination is similar between tumours and uninjured contralateral nerves

Neurofibromas were analysed at 8 months following injury. Transverse sections of tumours and uninjured contralateral nerve were counterstained with nuclear marker To-Pro and the frequency of each individual colour recombination was quantified by counting the number of each coloured Nf1 KO subpopulation over the total number of recombined Nf1 KO mSC derived cells. The colour recombination frequencies were averaged of the uninjured contralateral nerves. We have excluded the Nf1 KO SC that reassemble morphologically mSCs in this analysis, as these cells do not constitute the Nf1 KO tumour cells. This graph shows that none of the individually coloured Nf1 KO subpopulations were found overrepresented within the tumours compared to the average colour recombination frequency of the analysed uninjured contralateral nerves.

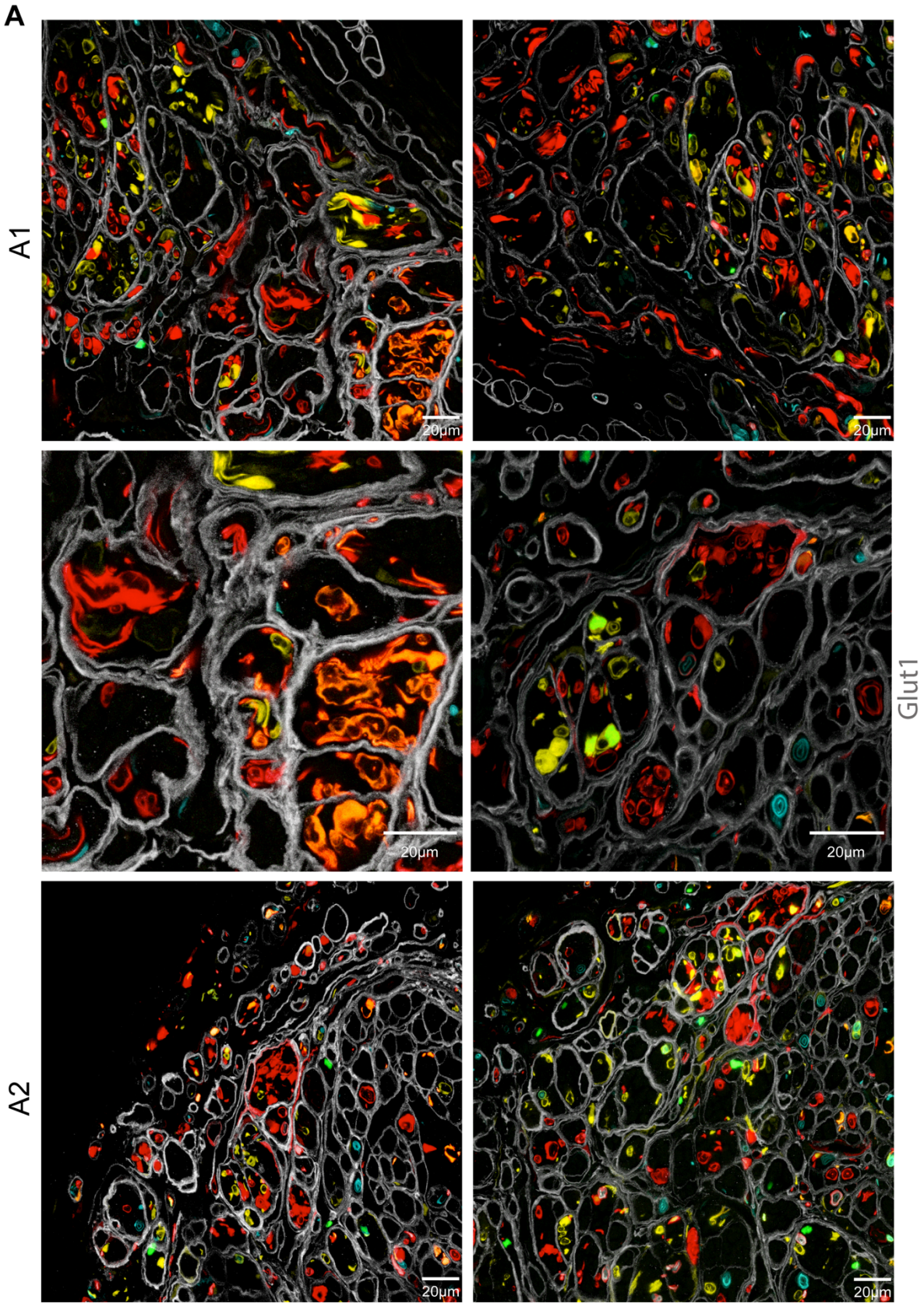
A
A1
A2
Glut1
20µm
20µm
20µm
20µm
20µm
20µm

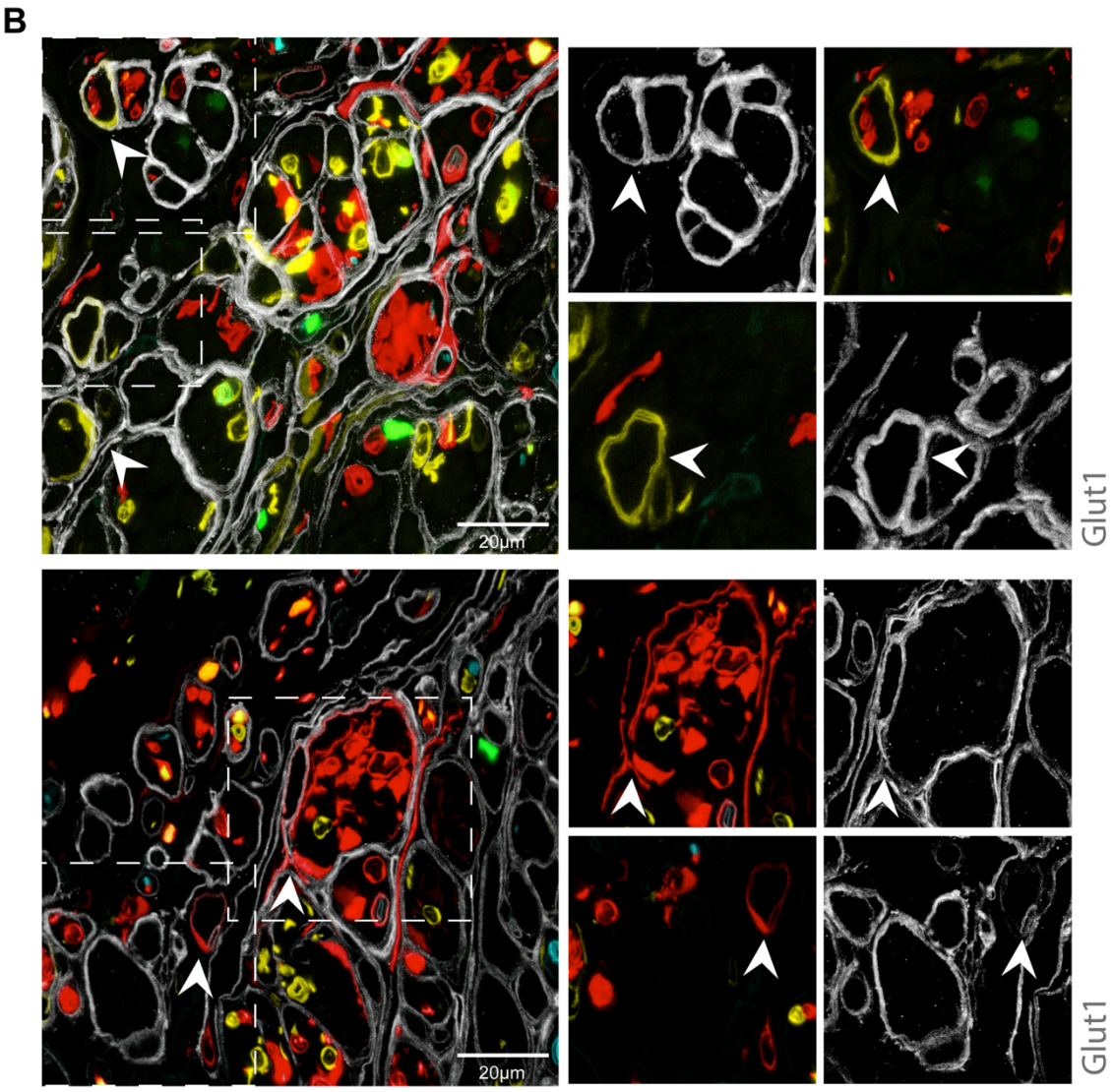

Figure 4.33. Nf1 KO tumour cells are closely associated with perineurial-like cell structures within neurofibromas

A+B) Representative confocal images of transverse cryosections of Nf1 KO neurofibromas at 8 months following injury. Cryosections were stained with Glut-1 (white), which is a perineurial-like cell marker. **B)** Confocal images show Nf1 KO SCs that transdifferentiated into perineurial-like cells, as indicated with arrowheads. 6 animals were analysed in total.

Nf1 KO SCs. It will be of great importance to further characterise the interactions of Nf1 KO SCs with their adjacent microenvironment by performing a temporal 3D analysis, as discussed in Chapter 6. Visualising the interactions of the Nf1 KO SCs in 3D will demonstrate whether the interactions of the dedifferentiated Nf1 KO SCs are different from those of the Nf1 KO mSCs. Furthermore, in addition to the 3D analysis, we could isolate the highly abundant perineurial-like cells from the tumour and analyse their interactions with the Nf1 KO SC *in vitro*.

4.11. Chapter discussion and conclusions

One of the fundamental questions in biology is how tissues maintain cells over a lifetime and how cells are replenished in pathological conditions such as injury. *In vitro* studies have demonstrated previously that plasticity can be induced in almost all somatic cells (Takahashi and Yamanaka, 2006), however, *in vivo*, cell plasticity is mostly linked to tissue damage and injury (Blanpain and Fuchs, 2014; Tata and Rajagopal, 2016; Wells and Watt, 2018). In multicellular organisms, especially in proliferative tissues, multipotent stem cells or pluripotent precursor/progenitor cells have been thought to produce the multiple cell types of a tissue. The peripheral nerve, in contrast to many other tissues (Simons and Clevers, 2011), contains no stem or progenitor cells, implying that the peripheral nerve uses other mechanisms to maintain itself in adulthood.

Consequently, it is becoming increasingly clear that different tissues have distinct mechanisms to maintain themselves in the adult and to repair the tissue following an injury and the classical model of stem and progenitor cells responsible for generating new tissue cells has been recently supplanted by more diverse models (Ge and Fuchs, 2018; Varga and Greten, 2017; Wells and Watt, 2018). These models postulate the existence of stem cells that divide frequently and of reserve stem cell compartments that can be activated upon loss of the primary stem cell compartment (Tian et al., 2011) Furthermore, it has been shown that cell lineage committed cells possess the ability to dedifferentiate into stem cells such as observed in the skin (Donati et al., 2017; Stange et al., 2013), intestine (Beumer and Clevers, 2016), stomach and trachea (Tata et al., 2013) Upon injury, separate stem cell compartments

(such as, amongst others, the reserve stem cell compartment) can become activated (Ito et al., 2005; Tetteh et al., 2016) and committed cells can dedifferentiate and contribute to the stem cell compartment in order to replenish the damaged tissue (Ge and Fuchs, 2018; Ito et al., 2007; van Es et al., 2012; Varga and Greten, 2017; Wells and Watt, 2018). Moreover, the mechanism to produce new cells often varies dramatically between the homeostatic, injured and repairing states. Nevertheless, the replacement of damaged cells by any of these stem and/or progenitor cells has to be tightly controlled in order to prevent tumourigenesis (Simon and Frisen, 2007).

Here, we have systematically characterised the cells that make up the endoneurium of peripheral nerves. We find it is a highly quiescent tissue with most cell types proliferating rarely whereas the main cell type of the nerve, the mSC, does not divide at all in the adult. The stability of this tissue is presumably possible because peripheral nerves once formed and matured tend to retain their structure and their connections. Moreover, peripheral nerves are protected by the Blood Nerve Barrier (BNB), which perhaps contributes to the low turnover rate of cells within this tissue. However, once injured, all cell types within a peripheral nerve are able to re-enter the cell-cycle and do so at very high efficiency, apparently obviating the requirement for a stem cell population to produce new cells for the regenerative process. This switch from a highly quiescent tissue to a highly proliferative tissue - with all cell types contributing to the regenerative response - represents a further model of how tissues maintain and repair themselves.

We have characterised the behaviour of the mSC in most detail, which has been possible because of a highly specific driver for this cell type in adulthood that permits credible lineage analysis. We were unable to detect a single proliferating mSC throughout the nerves of multiple animals, which indicates that once formed, these highly specialised cells do not turnover. Despite being completely quiescent in homeostasis all mSCs dedifferentiate and proliferate following nerve injury, demonstrating that they have retained the necessary plasticity to revert their genetic programme from a very stable to a highly active state. This emphasises the extremely efficient reprogramming process and underlines the non post-mitotic nature of adult mSCs. Moreover, they showed a dramatic change in their behaviour to

become the migratory cells that transport regrowing axons across the injury site.

The ability of all mSCs to proliferate following an injury would seemingly indicate the lack of need for a further stem cell population to produce new SCs during the regeneration of peripheral nerves. This view is further substantiated by lineage analysis of animals with lower levels of recombination, in which we found a similar proportion of recombined mSCs in an individual animal's uncut and contralateral regenerated sciatic nerve, showing the original population is not diluted by an influx of stem cells from another source. It could thus either be argued that there is not a stem cell/progenitor population to produce new mSCs in the adult or that all mSCs have the capacity to act as stem/progenitor cells. The latter argument is augmented by studies showing that dedifferentiated SCs have unlimited proliferative capacity (Mathon and Lloyd, 2001) and retain the ability to redifferentiate back to a more differentiated cell state.

It is particularly striking that very different mechanisms are used to maintain the myelinating cells of the PNS and CNS. The myelinating glial cells of the CNS, the oligodendrocytes (OLs) are produced throughout life. Whilst much of this is thought to be to myelinate new axons and is associated with learning and memory (Kaller et al., 2017; McKenzie et al., 2014), there also appears to be a higher turnover of mature cells, as axons in the optic nerve are fully myelinated yet appear to turnover throughout adulthood (Young et al., 2013).

Why mSCs are more stable than OLs in the optic nerve is not clear, as the environments appear similar in that they are both stable structures and are protected by the BNB and Blood Brain Barrier respectively. The mechanisms to produce new myelinating cells are also completely different. There only appears to be a requirement to produce new mSCs following injury, as normally these cells do not turnover in the adult. However, following injury, new cells are produced by the dedifferentiation and proliferation of the mSCs themselves. In contrast, the CNS is populated throughout by a precursor cell type (OPCs), which proliferate throughout adulthood to maintain themselves and differentiate throughout life to produce new OLs (Birey et al., 2017).

Why such differences exist can only be speculated upon but is likely to reflect a trade-off between the increased plasticity required by the CNS versus the stability required by the PNS.

The presence of a continually proliferating progenitor population whilst allowing a rapid source for new myelination also provides a pool susceptible to tumour development. This has been shown in other tissues previously in which the presence of stem or progenitor cells was correlated to an enhanced tumourigenic potential (de Sousa e Melo et al., 2017; Ge et al., 2017; Petersson et al., 2015; Soteriou and Fuchs, 2018; Wang et al., 2011; Wong and Reiter, 2011).

Consistent with this, malignant tumours are more frequent in the CNS compared to the PNS, which perhaps reflects the presence of a more susceptible proliferating progenitor population. Moreover, some studies have demonstrated a correlation between tissue cell turnovers and cancer incidence (Barker et al., 2009; Kong et al., 2011). For example, epithelial tissues such as the intestine are known to have a high cell turnover and also possess one of the highest frequencies of cancer occurrence (Frank, 2007). In line with this, a previous study suggested that neurofibromas may originate from the nmSC population as they were shown to be more proliferative and genetically more unstable at the early stages of tumourigenesis (Zheng, Chang et al. 2008). Consequently, the observed low turnover of nmSCs may increase their vulnerability to acquire new mutations and may predispose them to an enhanced tumourigenic capacity compared to the completely quiescent mSCs. However, our studies demonstrated that adult mSC can form neurofibromas upon loss of Nf1 and exposure to a conducive microenvironment, which is provided by the Nf1 KO injury microenvironment. Interestingly, in agreement with our studies, studies based on patient observations suggested previously that neurofibroma formation can be triggered by local injury indicating a link between small tissue injuries and neurofibroma formation (Riccardi, 1992a).

We have investigated the cell fate of mSC-derived cells throughout nerve regeneration in order to determine whether progenitor-like SCs possess similar multipotent capacities as SC precursors during development, as has been suggested previously by others (Petersen and Adameyko, 2017). Using lineage analysis, we showed that SCs retain their cell identity during the regenerative process. In agreement with our study, Adameyko et al. demonstrated previously that in order to render SCs multipotent, axonal regrowth needs to be prevented by deflecting the nerve following injury (Adameyko et al., 2009). It was speculated that by

preventing axonal regrowth SCs can escape the lineage restricting influence of axonal signals and can give rise to melanocytes. Interestingly, NRG1, which is a very well described axonal signal regulating SC development and myelination (Newbern and Birchmeier, 2010) may act to inhibit melanocyte differentiation as reported previously in vitro (Buac et al., 2009). A recent study demonstrated that NRG1 type I which is secreted from dedifferentiated SCs promotes SC redifferentiation in addition to signals from axonal NRG1 type III (Stassart et al., 2013). Both signals may contribute to maintain SC lineage differentiation, however, this remains to be clarified and the signals that maintain SC lineage differentiation during peripheral nerve repair remain to be identified.

Overall, our study and the study of Adameyko et al. emphasise the importance of the physiological environment in restricting cell plasticity. Moreover, modulating the physiological environment can release this restriction and may enable cells to produce cells from other cell lineages. Furthermore, *in vitro* culture environments are considered non- physiological environments and recent *in vivo* lineage analysis has contradicted the findings of previous *in vitro* studies (Anderson, 2001; Guimaraes-Camboa et al., 2017). In line with this, our study contradicts the findings of previous *in vitro* studies that have shown that adult SCs retain multipotency and can give rise to other cell types. (Dupin et al., 2003; Widera et al., 2011).

Whilst retaining a SC identity, we did find that dedifferentiated mSCs were able to become nmSCs, showing that these cells retained the ability to respond to the axonal environment and choose between a myelinating or non-myelinating fate. Moreover, this clearly shows that mSC- derived cells are not predisposed to produce myelin and possess the capacity to differentiate into a nmSC that ensheaths multiple small calibre axons. This is in agreement with previous cross-anastomose experiments, which joined myelinated to unmyelinated nerves and vice versa (Aguayo et al., 1976b), that suggested that SCs could switch from one form to the other.

In contrast, SCs are more plastic within the tumourenvironment as they can transdifferentiate into other cell types within a neurofibroma (Ribeiro et al., 2013). We find that this requires both a conducive microenvironment (such as the injury environment) and an oncogenic genetic change such as the loss of Nf1 in SCs in neurofibromatosis type 1 (NF1). In

agreement with this, NF1 patients, who develop peripheral nerve sheath tumours also show skin hyperpigmentation which could possibly derive from Nf1 KO SCs that have become melanocytes (Fetsch et al., 2000). Moreover, Nf1 KO SCs are mostly devoid of axonal contact within neurofibromas and this may allow them to escape the potential SC lineage restricting signals from axons and may increase their multipotent potential. Consequently, it is of great interest to further characterise the interactions of the Nf1 KO SCs with the regrowing axons at the early timepoints, as discussed in Chapter 6 in order to investigate whether the proliferating Nf1 KO SCs are associated with axons. Additionally, Nf1 KO SCs are invasive (Sheela et al., 1990) and this may expose them to different microenvironments that similarly to the non-physiological in vitro environment may enhance their multipotent potential. Furthermore, previous studies have postulated that Nf1 KO SCs resemble more closely multipotent SC progenitor cells (Kim et al., 1997; Kim et al., 1995), as Nf1 KO SCs for example express the EGFR, which is not expressed by adult SCs but by neural crest cells. The closer resemblance of Nf1 KO SCs to SC progenitor cells could also contribute to their increased multipotent capacity, as SC progenitor cells are known to differentiate into other cell lineages such as melanocytes (Adameyko et al., 2009) and endoneurial fibroblasts (Joseph et al., 2004). The mechanisms that regulate SC multipotency are not known, but it may be that ERK signalling (that is deregulated in NF1) is involved in regulating SC plasticity (Rizvi et al., 2002), however this hypothesis remains to be proven.

Finally, our characterisation of the cell composition of adult peripheral nerve has identified a new cell population that makes up a considerable proportion out of all cell types within a peripheral nerve. Here, we have defined this cell population as NG2+/PDGFRβ+/p75+/αSMA- cell population or pericyte-like cells, as we found that these cells express the nmSC marker p75 and are also positive for the pericyte markers NG2 and PDGFRβ. However, these cells are not associated with axons, instead they can be found either non associated or loosely associated with blood vessels. In contrast to pericytes, these cells are not localised within the basal lamina of the blood vessel. We are highly interested in the role of these cells as we observed in our EM analysis that they emanate long cytoplasmic protrusions into the nerve endoneurium that could potentially establish interactions between the different cell types and

that may form a plexus that supports the integrity of the peripheral nerve. Interestingly, in agreement with the potential supporting role of these cells, we observed that they contain a high density of endoplasmic reticulum implying that these cells are highly biogenic and likely produce factors that maintain peripheral nerve integrity or mediate intercellular communication. Due to the high density of endoplasmic reticulum, these cells probably have been identified previously as fibroblasts by other groups (Martin et al., 2001; Morgenstern et al., 2003; Richard et al., 2014). Interestingly, these cells seem morphologically similar to a stromal cell, a so-called telocyte, that has been identified in various tissues recently (Popescu and Faussone-Pellegrini, 2010). These telocytes were shown to express NG2 and PDGFRβ in certain tissues (Mirancea, 2016) and were characterised as having unique extremely long cytoplasmic processes (telopodes) (Popescu and Faussone-Pellegrini, 2010). Importantly, telocytes were shown to form a tissue supporting interstitial plexus in other tissues such as the heart and the intestine (Bani et al., 2010; Gherghiceanu et al., 2010; Rusu et al., 2012; Shoshkes-Carmel et al., 2018). In the latter, a recent study demonstrated that these cells provide a supporting niche for intestinal stem cells by providing Wnt signals that are required for the stem cells to proliferate (Shoshkes-Carmel et al., 2018). This study has demonstrated the importance of this cell type in regulating homeostatic cell renewal in the intestine and implies that these cells likely possess a similar role in other tissues such as in the peripheral nerve.

To identify the role of this cell type in the peripheral nerve, we will isolate these cells from mice that express dsRed by virtue of an NG2-driven expression construct (NG2-dsRed mice) (Zhu et al., 2008) and perform a transcriptomic analysis. The transcriptomic analysis will clarify their cell identity and identify the factors, which they produce. Moreover, in order to gain a better understanding of the three-dimensional nature of these cells we will perform a 3D analysis following tissue clearing of the peripheral nerve. Additionally, we will co-culture these cells with SCs in order to study their interactions *in vitro*.

Peripheral nerves regenerate even following a full transection and functionality can be restored in contrast to the poor regenerative capability of the CNS. However, our studies, and others, show that a regenerated nerve differs markedly from an uninjured nerve (Napoli et al., 2012;

Salonen et al., 1988; Zochodne, 2008). This includes a large increase in the cellularity of regenerated nerve. Interestingly, the relative proportion of all cell types remained the same indicating a homeostatic mechanism exists to ensure the structure of the nerve. However, a major difference appears to be increased matrix levels in regenerated nerve. Matrix deposition is a key aspect of an injury response (Eming et al., 2017), and it is likely that the failure to clear injury-induced matrix contributes to the inability of repaired tissue to return to the uninjured state. Targeting the clearance of accumulated matrix could thus provide a strategy for improving tissue repair.

Chapter Five. Characterisation of the early stages of neurofibroma formation and molecular analysis of the microenvironment

5.1. Chapter introduction

The loss of Nf1 in mSC is not sufficient to induce tumourigenesis, however, we found that after nerve injury, Nf1- deficient mSCs formed neurofibromas specifically at the wound site (Ribeiro et al., 2013). Remarkably, in contrast to the tumorigenic behaviour of Nf1- deficient SCs at the wound site, they behaved and repaired normally in the distal stump. This indicated that whereas the normal nerve environment suppresses neurofibroma formation, the injury site of the nerve is a tumour- promoting environment, fostering the development of neurofibromas.

In Chapter 3, I defined a Cre-mediated recombination threshold, above which the Nf1 KO animals were prone to develop tumours at a later stage. The optimisation of this model provides a more powerful and tractable model to investigate the very early stages of neurofibroma development. We decided to take a transcriptomic approach in order to explore the initial mechanisms underlying tumour formation. Importantly, this should allow the study of both the early stages of tumour formation at the injury site and how Nf1 KO SCs are instructed to redifferentiate within the distal section of the nerve.

The first part of this chapter, describes the cellular changes of mutant and normal nerve following an injury in order to shed light on the early stages of neurofibroma formation and to select a timepoint at which the cellular behaviour of Nf1 KO SCs at the injury site diverges from normal SC behaviour following nerve injury. In the second part of this chapter, I describe a molecular analysis using RNA seq at the selected timepoint with an aim to identify pro-tumourigenic signals of the injury microenvironment and tumour suppressive signals of the normal regenerating nerve environment. Identification of either pro- or anti- tumourigenic signals of the nerve microenvironment could have important clinical implications and may be helpful for the development of new therapeutic approaches for neurofibromas and other neuropathies.

5.2. Definition of regenerating nerve following injury

Following injury, we defined three main regions of the regenerating nerve: the proximal stump, the bridge region and the distal stump. The proximal stump is located upstream of the site of injury, where the nerve structure remains intact except at the very distal region. At the site of injury, a bridge of new tissue forms spontaneously (defined as the sciatic nerve bridge) to rejoin the proximal and distal stump. The sciatic nerve bridge initially consists of inflammatory cells, fibroblasts and vascular cells, before the repair of the nerve (Cattin et al., 2015). The distal stump is defined as the region downstream of the bridge and reaches to the distal target. Proximal and distal stump were each further segmented into two parts: the part closer to the injury site (P1 and D1) and the more distal part starting 0.5cm away from the injury site (P2 and D2) (Figure 5.1). Importantly, in contrast to Chapter 4 but consistent to the previously performed study with the Nf1 KO mice (Ribeiro et al., 2013), sciatic nerve partial transection was performed throughout this Chapter.

5.3. Increased cell proliferation in regenerating Nf1 KO nerve following nerve injury

Following an injury, SCs dedifferentiate to a progenitor-like state at both stumps and along the length of the distal stump and these dedifferentiated SCs enter the cell cycle and proliferate (Jessen et al., 2015). Our earlier studies indicated that there is increased proliferation in the sciatic nerve bridge of Nf1 KO mice upon nerve injury when compared to control (Nf1 WT) mice (Ribeiro et al., 2013) and it is clear that inappropriate proliferation has to occur for a tumour to form.

Initially, we investigated if there was a difference in total cell proliferation within the regenerating nerve of the Nf1 KO mouse model. The total number of proliferative cells was analysed following the injection of EdU prior to harvesting the animals at Day 7 following injury. Analysis of confocal sections showed that proliferation occurred in all regions of the injured nerve but was highest in the nerve bridge and in the proximal stump close to the injury site (P1) decreasing with distance from the injury site in both Nf1 KO and control (Nf1 WT) animals (Figure 5.2). Furthermore, we found that there was higher levels of proliferation both within the nerve bridge and along the length of the distal stump in the Nf1 KO mice compared

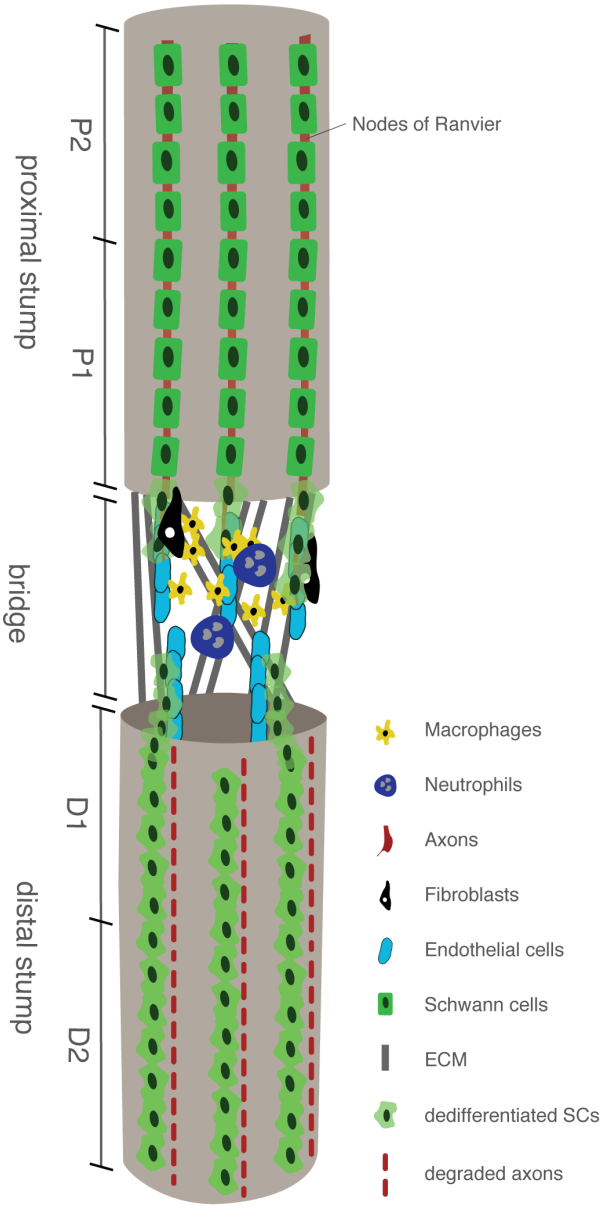

Figure 5.1. Illustration of a sciatic nerve post-injury
The proximal and distal stumps were separated into two regions: the section closer to the injury site (P1 and D1) and the more distal section starting 0.5cm away from the injury site (P2 and D2). Following nerve transection, the proximal and distal stump are reconnected by newly formed tissue, termed the nerve bridge. Initially, the nerve bridge is composed mainly of matrix and inflammatory cells. Downstream of the injury site in the distal stump, the axons degenerate in a process known as Wallerian degeneration. SCs disassociate from the degenerating axons and dedifferentiate to a progenitor-like state that mediates many aspects of the regenerative process. After vascularisation of the nerve bridge, SCs migrate along the vasculature, taking the regrowing axons across the bridge and into the distal stump. Upon axonal regrowth, SCs redifferentiate and the inflammatory response resolves. For simplification in this scheme, only the injured nerve fascicle is displayed.

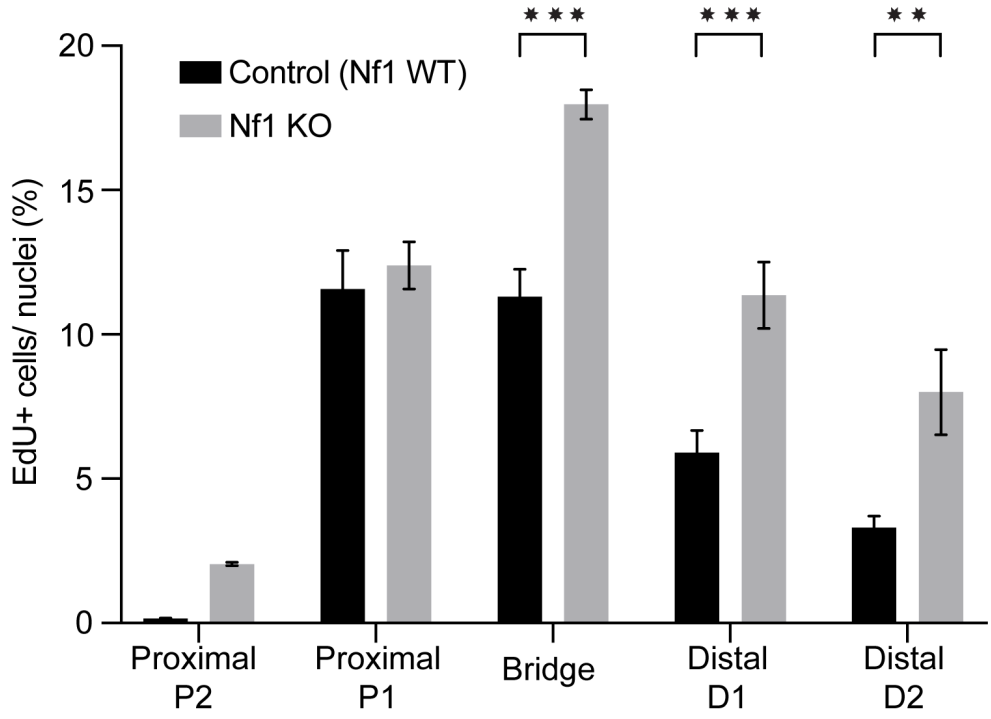

Figure 5.2. Total cell proliferation is increased after injury in Nf1 KO mice.
7 days after injury, Nf1 KO and control (Nf1 WT) mice were injected with EdU, 3 and 6 hours before harvesting. Sciatic nerves were harvested and processed for immunostaining to detect EdU+ cells. Bars show the mean of EdU+ cells/ total nuclei ±SEM for 4 independent experiments. Only animals with a recombination rate higher than 30% were included in this analysis. Statistics: Two-way ANOVA Sidaks' multiple comparison test.

to control animals. This indicates that depletion of Nf1 in a subpopulation of mSCs is sufficient to increase the proliferative response of the nerve after injury. Interestingly, elevated cell proliferation was also observed in the more distal part of the Nf1 KO proximal stump (P2), whereas in control animals, cell proliferation remained at a very low level. This observation was quite surprising, as the nerve structure remains intact in this part of the nerve and, as shown previously, SCs dedifferentiate only in the tip of the proximal stump (Carroll et al., 1997). This finding indicates that despite the intact nerve structure, pro-proliferative signals in the Nf1 KO animals can act on cells within this region.

5.4. Nf1 KO SC proliferation is maintained at the injury site

It is well established that neurofibromas originate from SCs that have lost Nf1, implying that these tumour-driving cells must behave differently compared to control SCs at the onset of the disease. Therefore, we performed a temporal analysis to investigate if YFP-labelled Nf1 KO SCs proliferate differently at the injury site compared to the distal stump.

The aim was to identify a timepoint at which Nf1 KO SC proliferation remained high at the injury site, but returned to control levels in the distal stump. To do this, we quantified the proliferation of the cells derived from Nf1 KO mSCs by counting EdU+ YFP+ cells in the bridge region and distal stump (D2) at day 7, 10 and 14 after injury. The mice were injected with EdU before harvesting at the indicated time points and EdU detection was performed in parallel with immunofluorescence staining for YFP.

This analysis showed that Nf1 KO SCs maintained high levels of proliferation at the injury site (Figure 5.3A and 5.3C), whereas Nf1 KO SC proliferation rate decreased gradually in the distal stump to levels equal to the control at Day 14 following injury (Figure 5.3B and 5.3C). This suggested that the Nf1 KO SCs maintain a proliferative advantage that is stimulated by unknown factors in the injury microenvironment and identified a timepoint of Day 14 when Nf1 KO SC behaviour differs from control SCs at the injury site.

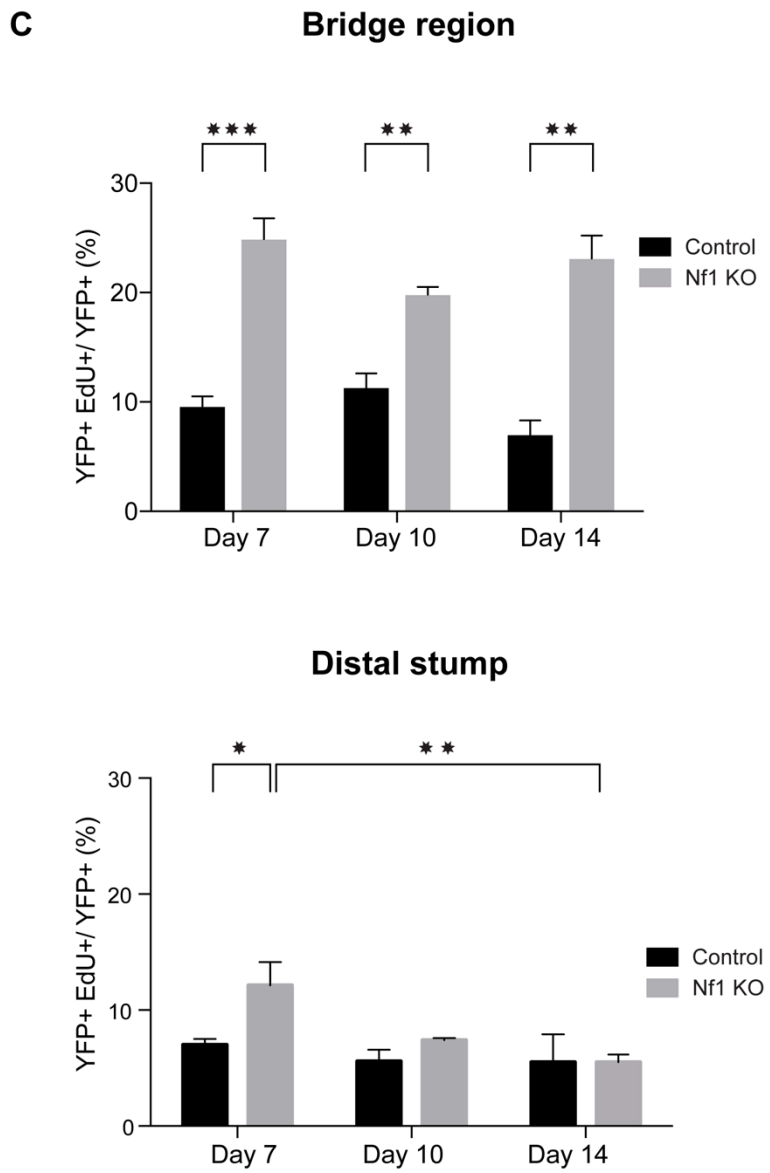

Figure 5.3. Nf1 KO SC proliferation is maintained in the bridge region compared to the distal stump

Following injury, Nf1 KO and control (Nf1 WT) mice were injected with EdU at 3 and 6 hours prior to harvesting at the indicated timepoints. Transverse sections were stained for EdU (red) and YFP (green). Representative images of the **A)** bridge region and **B)** distal stump from Nf1 KO and control mice. Arrows indicate proliferating YFP+ SCs. **C)** Graphs show the percentage of EdU+/YFP+ SCs in Nf1 KO and control mice. EdU+/YFP+ SCs were quantified by counting EdU+/YFP+ cells over total YFP+ cells at the indicated time points. Bars show the mean EdU+,YFP+/YFP+ ±SEM (n=5 mice). Only animals with a recombination rate higher than 30% were included in this analysis. Statistics: Two-way ANOVA Sidaks' multiple comparison test.

5.5. Nf1 KO SCs possess a proliferative advantage in the bridge region

To test whether Nf1 KO SCs possess a proliferative advantage compared to normal SCs in the same microenvironment, we compared the proliferation rate of recombined YFP+ p75+ Nf1 KO SCs to neighbouring unrecombined SCs (YFP-/p75+) within the same nerve and with YFP+ and YFP-/p75+ SCs from control (Nf1 WT) animals. As discussed in Chapter 4, p75 does not only label dedifferentiated and non-myelinating SCs, it also labels the NG2+/PDGFRβ+/αSMA- cell population. Consequently, the YFP-/p75+ cells of both genotypes may also include NG2+/PDGFRβ+/αSMA- cells.

In this analysis, we observed that the YFP+ Nf1 KO SCs proliferated at higher levels and importantly this was maintained at Day 14 following injury (Figure 5.4A and 5.4C), whereas the proliferation rate of the neighbouring YFP- Nf1 WT SCs returned to control levels. This finding indicated that signals derived from the injury microenvironment provide a proliferative advantage to the Nf1 KO SCs over the neighbouring YFP- Nf1 WT within the same nerve (Figure 5.4B and 5.4C). Consistent with the previous analysis (Figure 5.3C), in the distal stump Nf1 KO SC proliferation decreased to control levels by Day 14. A surprising result was that the YFP-/p75+ control cells proliferated at higher levels than the YFP+/p75+ control cells at the injury site at Day 7 following injury. The increased proliferation of these YFP-/p75+ cells may be due to the previously observed high proliferation rates (Chapter 4) of the NG2+/PDGFRβ+/p75+/αSMA- cell population, which would be included in the YFP-/p75+ population. In future experiments, the NG2+/PDGFRβ+/p75+/αSMA- cell population would be differentiated from the YFP- p75+ cells by co-staining with NG2 or PDGFRβ, which is not expressed in dedifferentiated SC.

To test whether the increased cell proliferation within the Nf1 KO bridge is associated with an expansion in tissue size in this region, we compared the area of the Nf1 KO bridge to its distal stump and to both regions of the control (Nf1 WT) animal. Consistent with the high level of cell proliferation, the Nf1 KO injured nerve was significantly enlarged at the injury site, at Day 14 following injury. This analysis shows that even at this early timepoint, the increased cell proliferation in the Nf1 KO injury site is sufficient to result in a detectable enlargement of tissue that will progressively increase over time to ultimately form neurofibromas (Figure

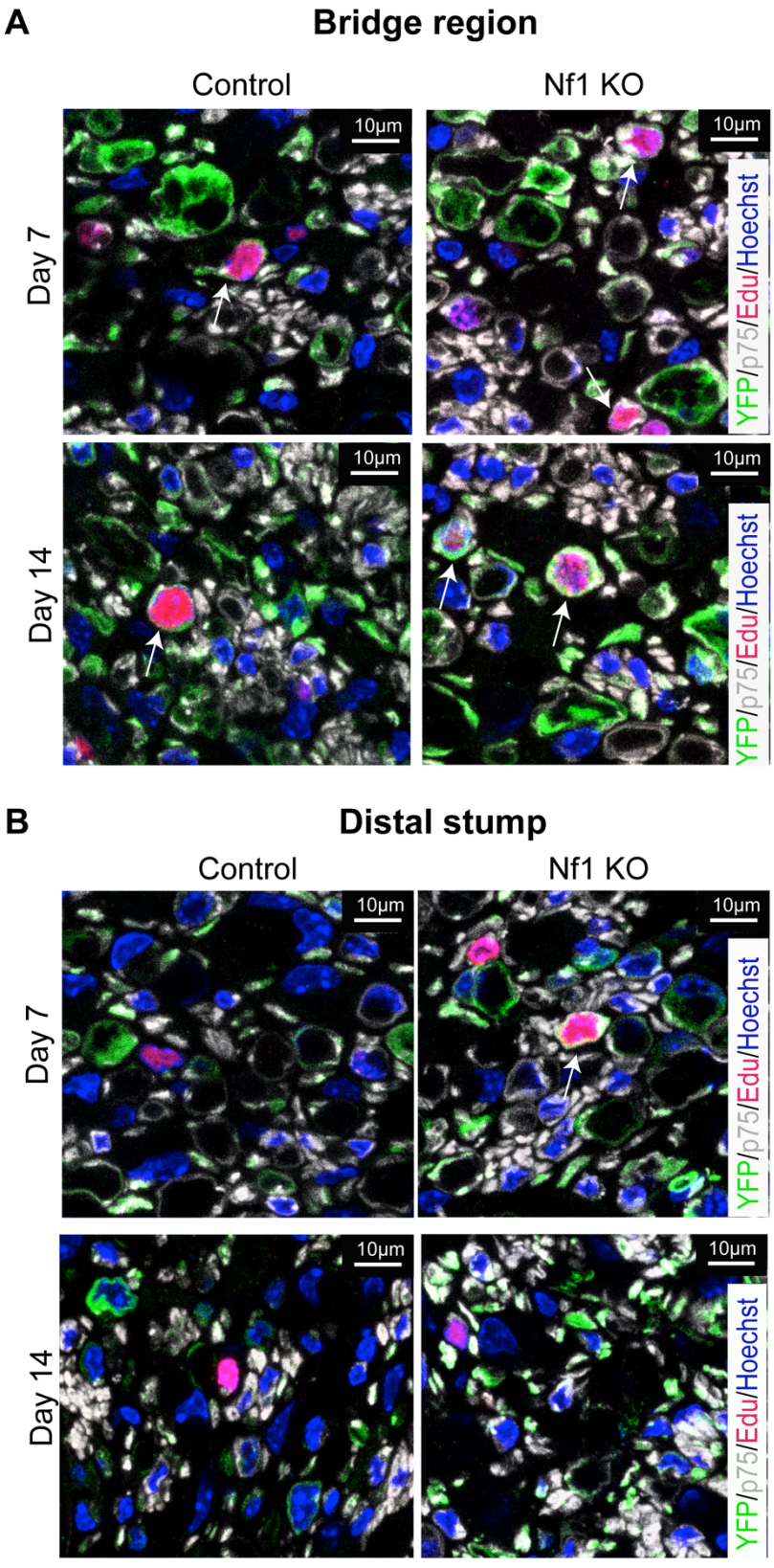
A
Bridge region
Control
Nf1 KO
Day 7
Day 14
10μm
YFP/p75/Edu/Hoechst
B
Distal stump
Control
Nf1 KO
Day 7
Day 14
10μm
YFP/p75/Edu/Hoechst

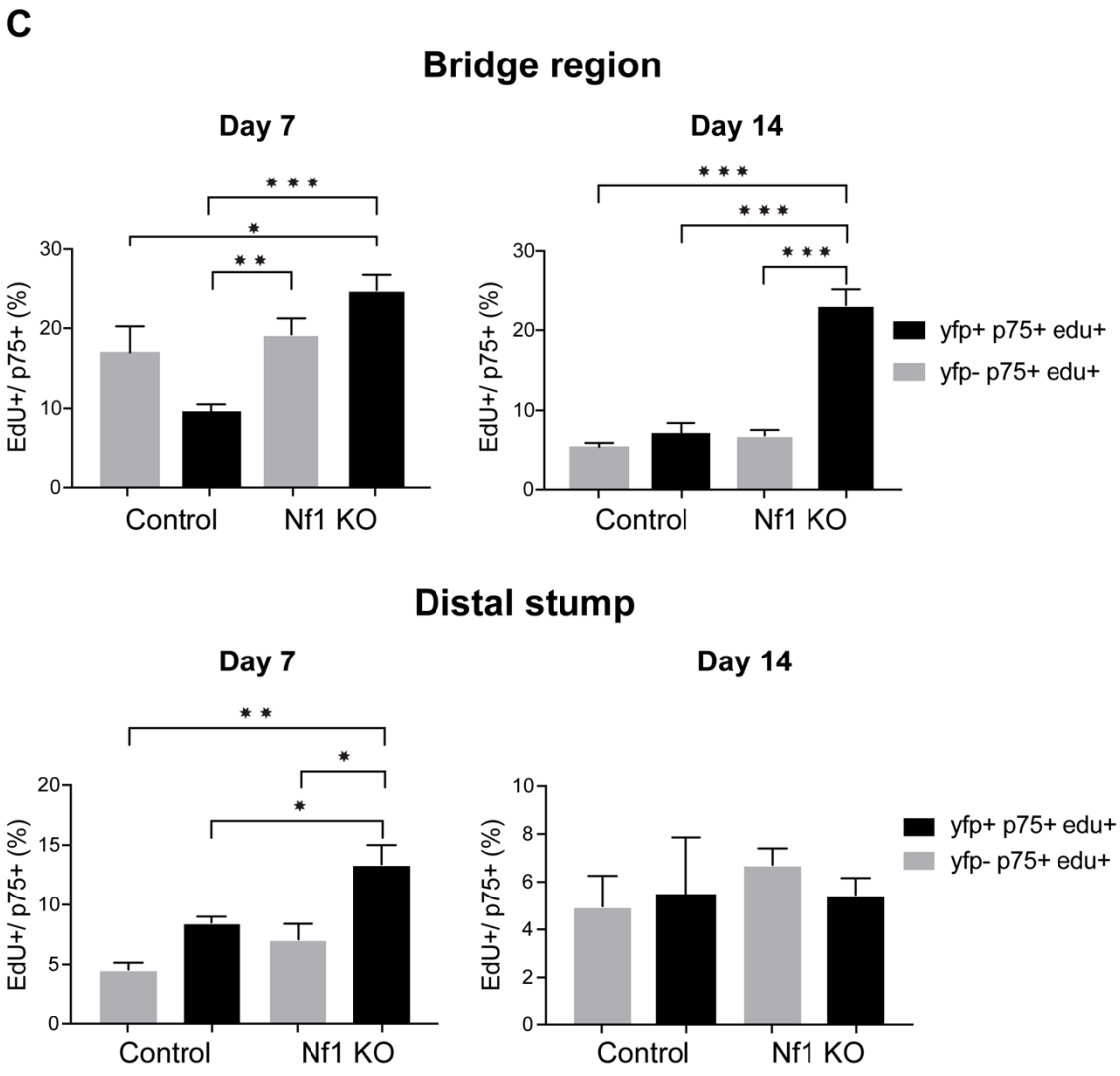

Figure 5.4. Nf1 KO SCs proliferate at a higher rate compared to neighbouring Nf1 WT SCs

Following injury, Nf1 KO and control (Nf1 WT) mice were injected with EdU, 3 and 6 hours prior to harvesting at the indicated timepoints. EdU detection was performed together with immunofluorescence staining. Transverse sections were stained for EdU (red), YFP (green) and p75 (grey). Representative images of the **A)** bridge region and **B)** distal stump (D2) of Nf1 KO and control mice. Arrows indicate proliferating YFP+ p75+ SCs. **C)** Graphs shows the percentage of EdU+/ p75+ (YFP+ or YFP-) cells in Nf1 KO and control mice at the indicated timepoints. Bars show the mean±SEM (n=6 mice). Only animals with a recombination rate > 30% were included in this analysis. Statistics: Two-way ANOVA Sidaks' multiple comparison test.

5.5).

Overall, we identified Day 14 following injury as the timepoint at which Nf1 KO SC behaviour differs from control SCs at the injury site. Specifically, Nf1 KO SC proliferation was maintained at the injury site, whereas it had decreased to control levels in the distal stump. To identify differences in the microenvironment we chose to perform a RNA seq analysis at this timepoint**.**

5.6. Macrophages and NG2+ cells show higher proliferation rates in Nf1 KO mice

Analysis of the cellular composition of neurofibromas has shown increased numbers of macrophages (Choi et al., 2017; Prada et al., 2013), perineurial-like cells (Riccardi, 1992a) and NG2+/PDGFRβ+/p75+/αSMA- cells (our unpublished data) within the tumours. The functional role of macrophages in neurofibroma formation has been addressed recently using a Dhh-Cre:$Nf1^{fl/fl}$ mouse model, in which Nf1 is ablated in the SC lineage during development and which go on to develop plexiform neurofibromas in peripheral nerve roots (Prada et al., 2013). This study showed that macrophages appear to be anti-tumourigenic initially but pro-tumourigenic at later stages of the disease. We therefore investigated if the conditional loss of Nf1 in adult mSCs influences the proliferative behaviour of macrophages and NG2+/PDGFRβ+/p75+/αSMA- cells at the early stages of tumourigenesis to determine whether they may contribute to tumour initiation in our mouse model. To test this, we injected EdU before harvesting and quantified the number and proliferation rate of these two cell types.

Consistent with the previous analysis (Chapter 4), following nerve injury we observed a dramatic increase in the number of both macrophages and NG2+ cells in both genotypes and regions compared to the uninjured Nf1 WT nerve (macrophages ~2 and NG2+ cells ~3 per field) as determined in Chapter 4 (Figure 5.6 and 5.7). The higher macrophage density showed that the inflammatory response remained elevated in both genotypes. However there are more macrophages in the Nf1 KO bridge. This increase in macrophage density could potentially secrete factors, such as cytokines, that could alter the injury microenvironment (Figure 5.6C). Consistent with the increased macrophage and NG2+ cell density in the Nf1

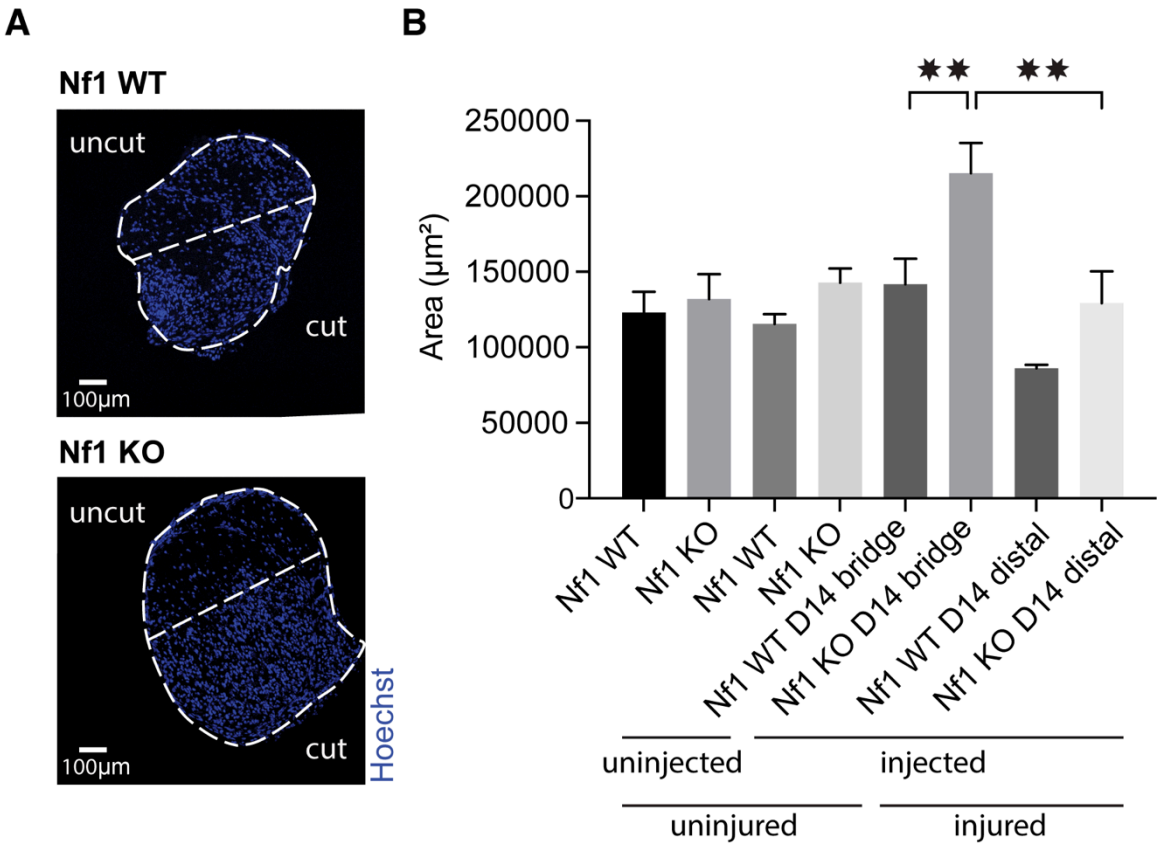

Figure 5.5. The bridge region of Nf1 KO injured nerve is enlarged by Day 14 following injury

Sciatic nerve area was measured in tmx untreated, tmx injected non-injured and injured Nf1 KO and control (Nf1 WT) mice. **A**) Representative images of the measured bridge region of Nf1 KO and Nf1 WT mice at Day 14 following injury. Transverse sections were labelled with Hoechst and the nerve area was outlined and measured using Fiji. **B)** Graph shows quantification of the nerve area. (n= 4 mice, mean±SEM).

KO bridge, this analysis also showed that macrophages and NG2+ cells proliferated slightly more in both the Nf1 KO bridge and distal stump region compared to control (Nf1 WT) animals (Figure 5.6A, 5.6C, 5.7A and 5.7C) and this will contribute to the increased overall proliferation rates, shown in Figure 5.2. Moreover, the high proliferation rates of the NG2+ population will contribute to the higher proliferation rates of YFP-/p75+ cells (Figure 5.4C). However, the proportions of both cell types remained similar to control levels, indicating that the proliferation rate likely increases proportionally in both genotypes (Figure 5.6 and 5.7). In the distal stump, macrophage and NG2+ cell density was similar to control levels, indicating that a normal nerve regenerative process occurs in this region (Figure 5.6B, 5.6C, 5.7B and 5.7C). Consistent with this, the cellular composition of the Nf1 KO distal stump was found to be similar to the control (Nf1 WT) distal stump at 8 months following nerve injury (data not shown) demonstrating that the Nf1 KO distal stump regenerates normally opposed to the Nf1 KO injury site at which a neurofibroma forms.

5.7. High levels of ERK signalling in regenerating Nf1 KO nerve

Sustained ERK signalling is sufficient for SC dedifferentiation and dissociation from axons and is required for SC proliferation following nerve injury (Harrisingh et al., 2004; Napoli et al., 2012; Ribeiro et al., 2013). However, as shown by Ribeiro et al, loss of Nf1 is not sufficient to activate ERK signalling in uninjured adult mSCs nor to drive neurofibroma formation, indicating an additional requirement of signals from the injury microenvironment. In line with this, we have shown previously that p-ERK levels remained elevated in the sciatic nerve bridge in Nf1 KO mice, whereas it decreased to control levels by Day 7 days after injury in the distal stump (Ribeiro et al., 2013). This suggested that activation of ERK signalling is either maintained at the injury site through an unknown factor or that ERK activation is suppressed by a pro- differentiating signal in the distal stump, which is absent at the injury site.

Initially, we decided to perform a more detailed temporal analysis of ERK activation due to the key role of ERK in regulating SC differentiation and proliferation. At first, we harvested the injured nerves at Day 3 following injury and performed immunofluorescence stainings for p-ERK and the axonal marker neurofilament on longitudinal cryosections of the nerve to

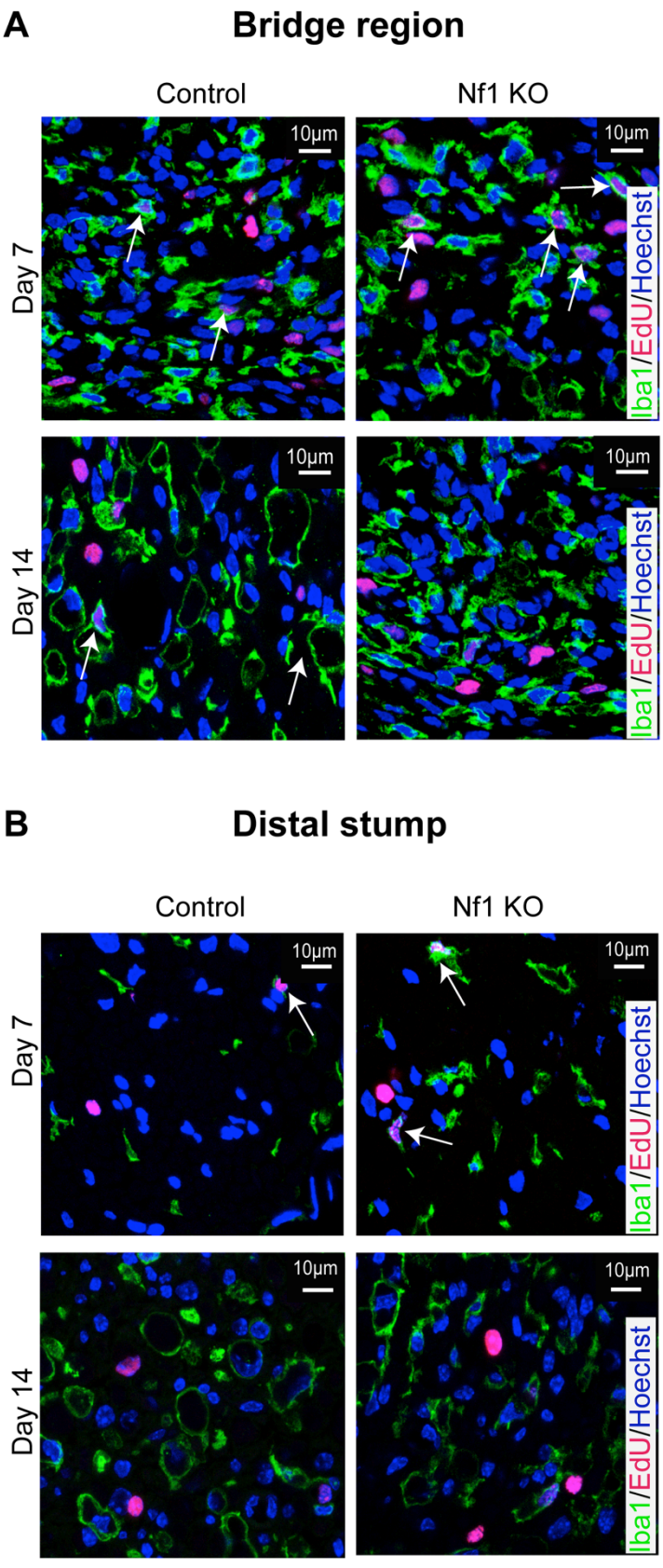
A
Bridge region
Control
Nf1 KO
Day 7
Day 14
10μm
Iba1/EdU/Hoechst
B
Distal stump
Control
Nf1 KO
Day 7
Day 14
10μm
Iba1/EdU/Hoechst

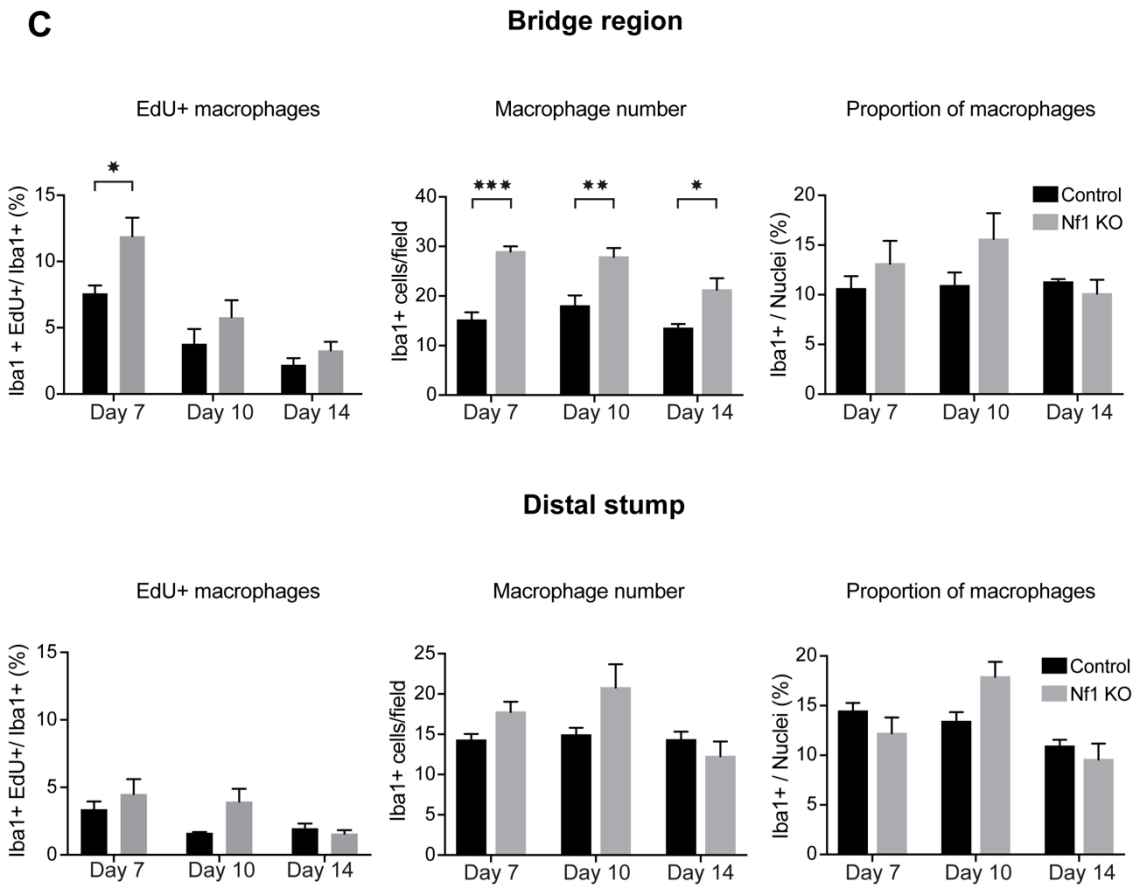

Figure 5.6. Increased numbers of macrophages at the Nf1 KO injury site
Following injury, Nf1 KO and control (Nf1 WT) mice were injected with EdU 3 and 6 hours prior to harvesting at the indicated timepoints. Injured sciatic nerves were harvested and transverse sections of the injury site and distal stump from Nf1 KO and control mice were stained for EdU (red) and Iba1 (green). Representative images of **(A)** The injury site and **(B)** Distal stump. Arrows indicate EdU+ macrophages. **C)** Graphs show EdU+ macrophages, macrophage density and proportion of macrophages in both regions. The area of the field quantified was 0.014mm^2. Bars show the mean±SEM (n=4 mice). Only animals with a recombination rate > 30% were included in this analysis. Statistics: Two-way ANOVA Sidaks' multiple comparison test.

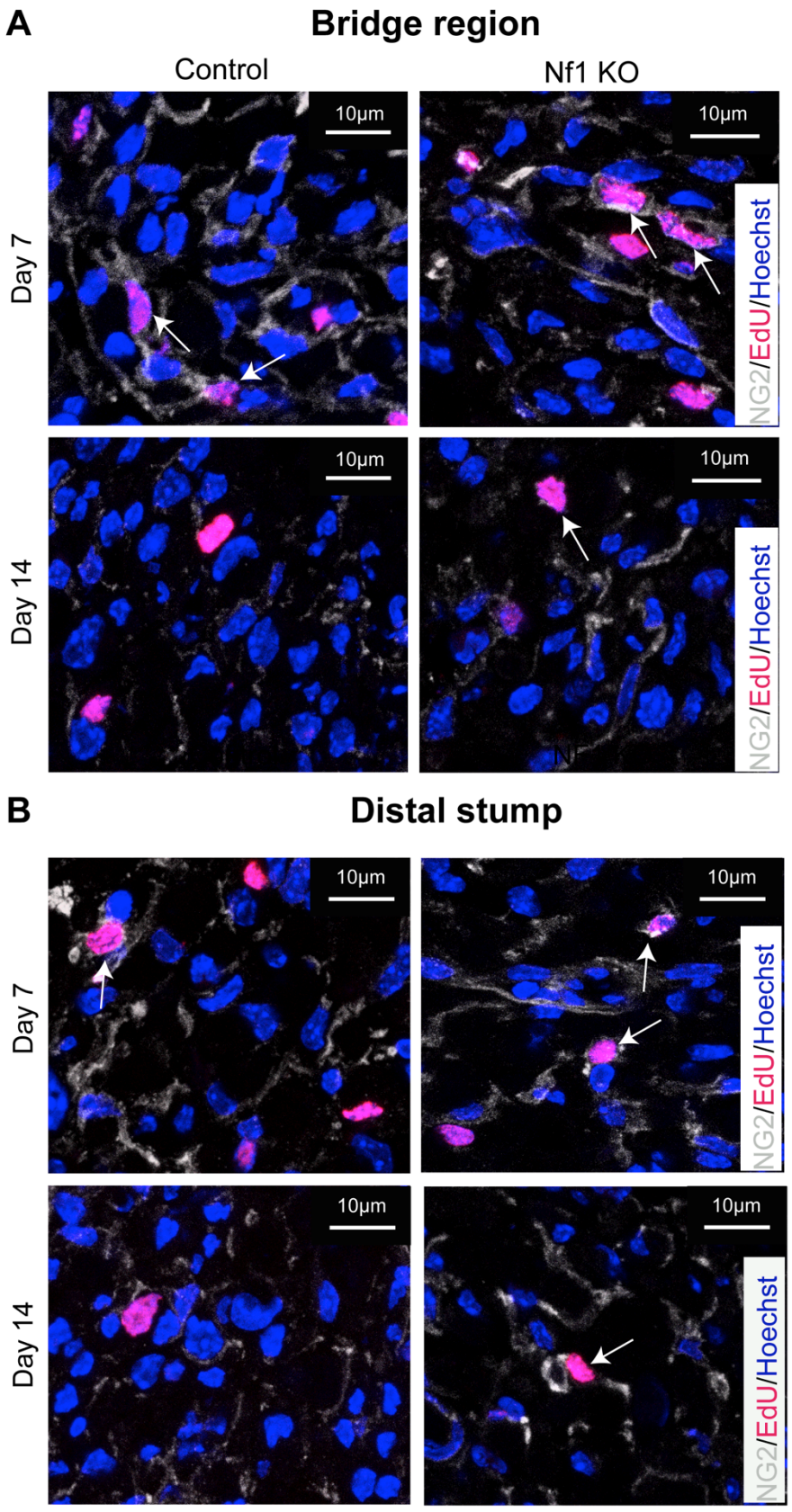
A
Bridge region
Control
Nf1 KO
Day 7
Day 14
10μm
NG2/EdU/Hoechst
B
Distal stump

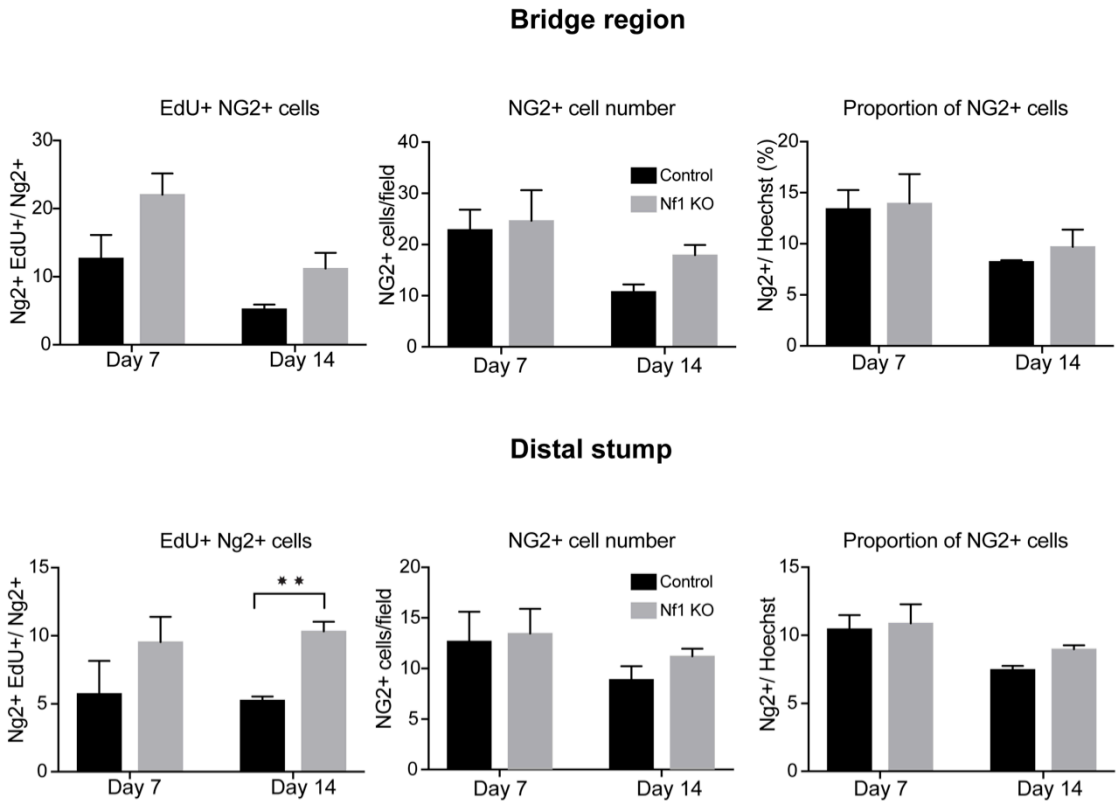

Figure 5.7. NG2+ cells tend to proliferate more in the Nf1 KO mice

Following injury, Nf1 KO and control (Nf1 WT) mice were injected with EdU 3 and 6 hours prior to harvesting the injured sciatic nerve at the indicated timepoints. Transverse sections of the injury site and distal stump from Nf1 KO and control mice were stained for EdU (red) and NG2 (grey). Representative images of **(A)** The injury site and **(B)** Distal stump. Arrows indicate EdU+ NG2+ cells. **C)** Graphs show EdU+ NG2+ cells, NG2+ cell density and proportions of NG2+ cells in both regions. The area of the quantified field was 0.014mm^2. Bars show the mean±SEM. (n=4 mice). Only animals with a recombination rate > 30% were included in this analysis. Statistics: Two-way ANOVA Sidaks' multiple comparison test.

determine ERK activation in the different regions of the nerve. Elevated levels of p-ERK were detected in the proximal stump close to the injury site (P1) and along the entire length of the distal stump (D1 and D2) in both Nf1 KO and control (Nf1 WT) mice, although the levels were higher in the Nf1 KO mice (Figure 5.8A-C). This showed that p-ERK levels were higher in the Nf1 KO nerve, even at the early timepoints, suggesting a potential ablation of signals that downregulate ERK activation. In the newly-formed nerve bridge, p-ERK levels were low, presumably as dedifferentiated SCs have not yet migrated into this area.

As shown in Figure 5.8C, p-ERK levels decreased with distance from the injury site in both genotypes but were surprisingly found to be highest in the proximal stump surrounding the regrowing axonal growth cones in both genotypes. It has previously been reported that axonal ERK signalling is important for axonal regrowth (Chierzi et al., 2005; Perlson et al., 2005; Reynolds et al., 2001), however, high magnification images of the proximal stump (Figure 5.8B) showed that p-ERK staining was more strongly associated with SCs in the area surrounding the axonal growth cones. Axonal regrowth requires local protein synthesis, however axonal cell bodies are located at a great distance from the site of injury (Donnelly et al., 2013; Verma et al., 2005) and consequently previous studies have suggested that SCs may contribute to axonal protein synthesis during axonal regrowth (Court et al., 2008; Lopez-Verrilli and Court, 2012). Consistent with this, our observations indicate that SCs are highly activated around the region of the regrowing axons and possibly act to metabolically support axonal outgrowth from this area.

We also analysed the levels of p-ERK at Day 14 following injury, the timepoint selected for the RNA seq. analysis. As only the bridge region and the distal stump (D2) were compared in the RNA seq analysis, only these two regions were analysed. However, we could not detect p-ERK expression either in the bridge region or in the distal stump (D2) in either Nf1 KO and control (Nf1 WT) mice at Day 14 following injury (Figure 5.9). Consistent with axonal regrowth into the distal stump, we observed that SC remyelination has begun at this timepoint in both genotypes and regions, as shown with P0 staining in Figure 5.9. High level of ERK signalling are associated with SC dedifferentiation, whereas lower levels of ERK activation are required

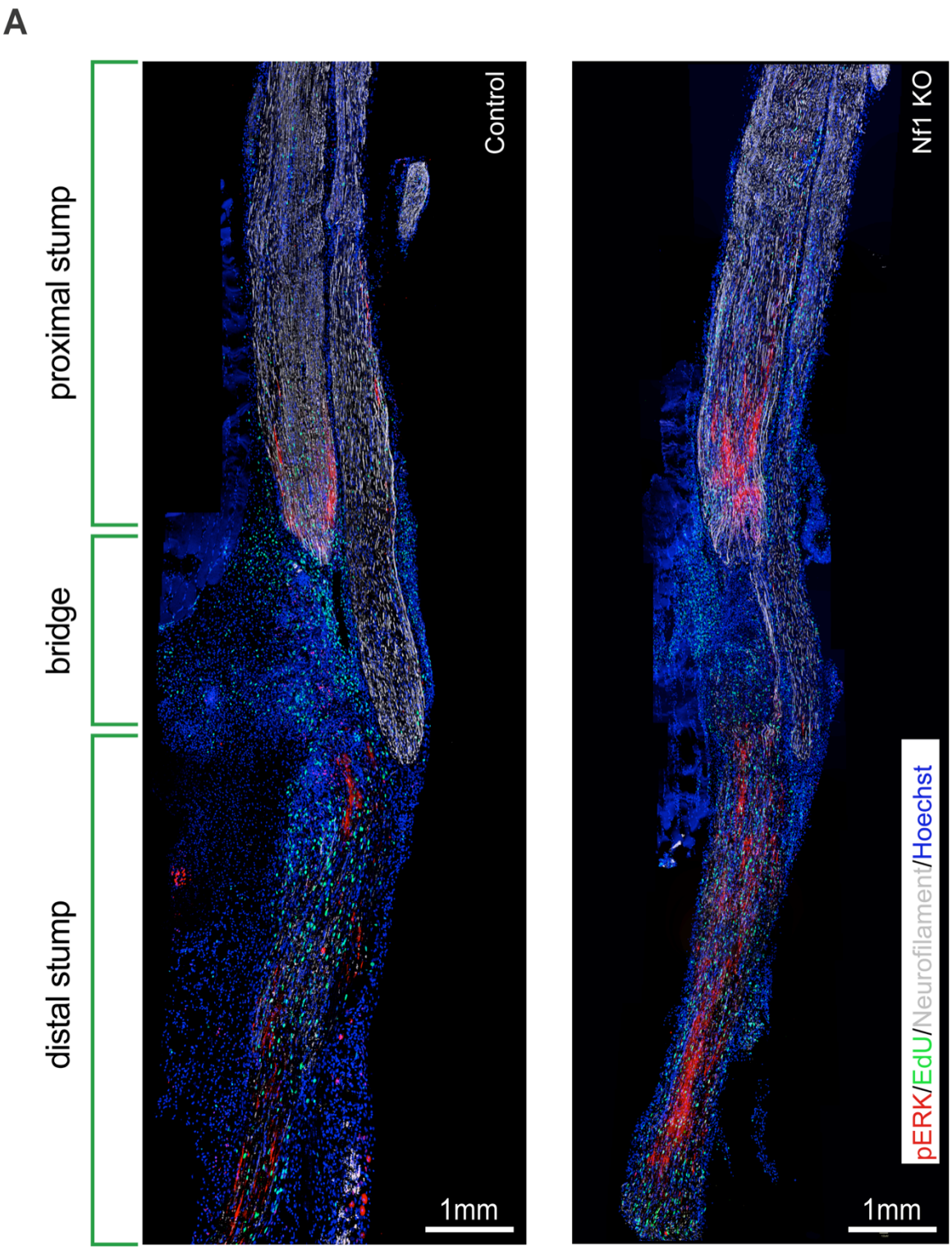
A
proximal stump
bridge
distal stump
Control
1mm
Nf1 KO
1mm
pERK/EdU/Neurofilament/Hoechst

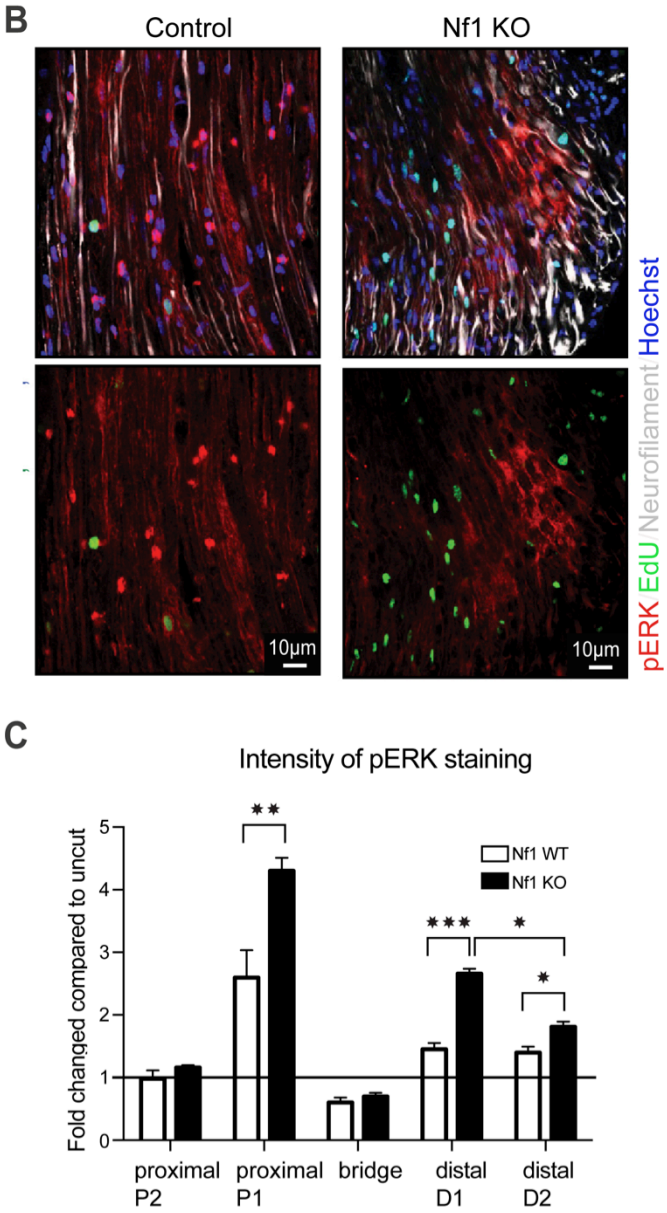

Figure 5.8. High levels of p-ERK are found in the area surrounding the axonal growth cone and along the length of the distal stump

(A) Representative images of longitudinal cryosections of sciatic nerves, Day 3 after injury, immunolabelled for pERK (red), EdU (green) and neurofilament (grey). Nuclei were counterstained with Hoechst. **(B)** Higher magnification images showing ERK activation in SCs and axons in the axonal growth cone area in LHS control (Nf1 WT) and RHS Nf1 KO mice. **(C)** The intensity of p-ERK staining was quantified using Fiji. Graph shows the quantification of the intensity of the p-ERK signal. Only animals with a recombination rate > 30% were included in this analysis. (n=6 animals of each group).

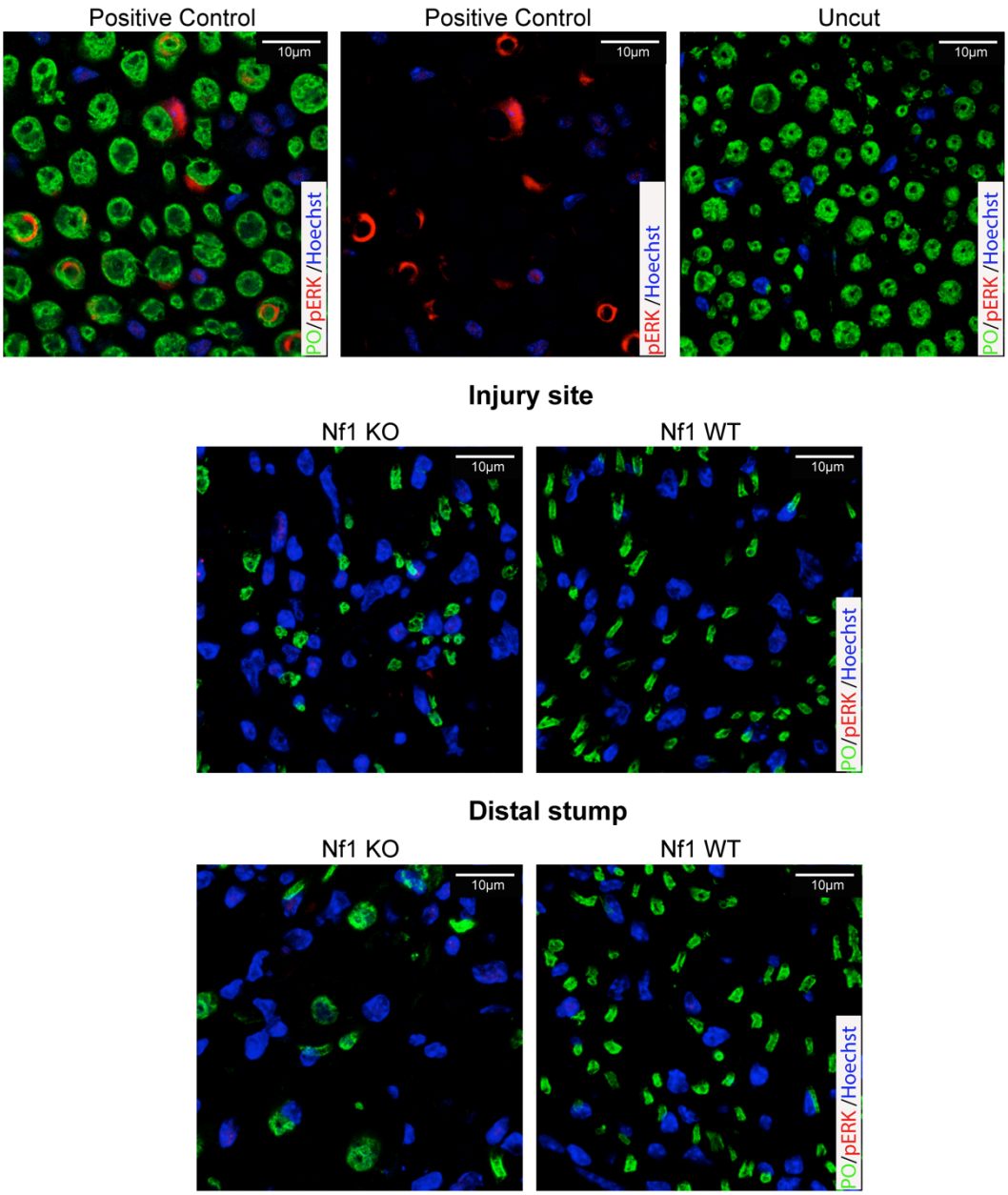

Figure 5.9. p-ERK expression is not detectable in Nf1 KO and control, Nf1 WT mice at Day 14 following injury

5mm nerve fragments were isolated from the sciatic nerve bridge and from the distal stump (D2) of the injured nerve at Day 14 following injury and sections were immunolabelled for p-ERK (red) and myelinating SC marker, P0 (green). Nuclei were counterstained with Hoechst. The positive control is a nerve from a P0-RafTR mouse, Day 4 post-tamoxifen injection (Napoli et al., 2012). An uncut contralateral nerve was used a negative control for ERK activation. Only animals with a recombination rate > 30% were included in this analysis and representative images of the 4 animals analysed for each group are shown.

for SC remyelination and to maintain SC proliferation (Harrisingh et al., 2004; Napoli et al., 2012). Consequently, ERK activation had likely decreased in order to allow SC remyelination and may been too low to be detected. Although, SCs are mostly in their dedifferentiated state in neurofibromas (Ribeiro et al., 2013), this analysis also indicated that high levels of ERK activation are only associated with the SC dedifferentiation process at early timepoints, whilst lower levels together with additional factors likely maintain Nf1 KO SC proliferation and dedifferentiation at later timepoints following injury.

5.8. Quality control of RNA seq. samples

Our findings show that early signals from the injury microenvironment provide a proliferative advantage to Nf1 KO SCs. The proliferation of Nf1 KO SCs was also initially higher in the distal stump compared to Nf1 WT SCs, but whereas levels remain elevated in the bridge region, they returned to control levels by Day 14 following injury in the distal stump. We therefore chose the Day 14 timepoint to analyse differences in the microenvironment of the bridge and the distal stump by performing a RNA seq analysis, as at this timepoint only Nf1 KO SCs maintain high proliferation at the injury site, at which they will go on to form tumours.

We isolated the nerves at Day 14 following injury and we selected nerves for the RNA seq. analysis according to the recombination efficiency (>30%) in the contralateral uninjured nerve. The RNA seq. analysis was performed without purification of the different cell types, as we wanted to analyse the contribution of the entire microenvironment. The injured nerves of both Nf1 KO and control (Nf1 WT) mice were dissected into equally sized fragments (0.5mm) containing either the bridge or the distal stump. We combined 6 nerve fragments from multiple mice for each sample, in order to decrease biological variability and we prepared independent triplicates for each area of interest.

Previously, we tested different RNA extraction methods and determined the protocol that provided the best RNA quality after RNA isolation and purification from mouse sciatic nerve and based on this, RNA was extracted and purified using the Pure Link RNA Micro Scale Kit from Invitrogen. Purified RNA samples were quantified using a Nanodrop to determine RNA concentration and purity, to ensure that the samples had both a 260/280 and 260/230 ratio of

~ 2 (Table 5.1), as expected for high quality RNA. RNA Sequencing was performed by the Genomic Facility at the University of Liverpool, who performed a more sensitive quality assessment of the RNA using a Agilent 2100 bioanalyser (2100 Bioanalyser Software, Agilent Technologies), which produces an electropherogram and a "gel- like image" of the RNA (Figures 5.11-5.12). The integrated software automatically assigns a RNA integrity number (RIN) which is based on a numbering system from 1 to 10 with 1 being the most degraded profile and 10 being the most intact, as shown in Figure 5.10 (Endrullat et al., 2016; Imbeaud et al., 2005; Mueller O., 2004; Schroeder et al., 2006). For each of our samples the software calculated a RIN number (Table 5.1). The ideal RIN number of a sample for RNA seq. analysis should be around 8. All our samples passed this quality control. Table 5.1 below, summarises the quality measurements performed on the RNA samples.

5.9. Ribosomal depletion and library preparation of the RNA seq. samples

After quality control of the samples, the ribosomal RNA (rRNA), typically constituting over 90% of the total RNA of a cell, needs to be removed in order to enrich for the less abundant mRNA prior to preparation of the library. Two methods are commonly used to remove the rRNA: pol(A) selection or depletion of rRNA. We chose to use the ribosomal depletion method, as it is reported to be the more preferable method for mouse samples as poly(A) selection can give a 3'-bias (Weedall, Irving et al. 2015).

750 ng of total RNA was depleted with the Ribo-Zero Gold Kit from Illumina. The Ribo Zero gold kit removes both cytoplasmic and mitochondrial rRNAs and maintains both coding and non-coding RNA. The extent of rRNA depletion was checked on a Bioanalyser RNA pico chip. The NEB Ultra Directional RNA Library Preparation Kit was used to prepare the RNA-Seq libraries from the enriched material using (Figure 5.13). All of the enriched material was used and following 15 cycles of amplification, the RNA was purified using AMPure XP beads. AMPure XP beads are magnetic beads, which bind PCR amplicons longer than 100bp and efficiently remove unincorporated NTPs, primers, salt and other contaminants. The libraries were quantified using Qubit and the size distribution was analysed using the Agilent 2100 Bioanalyser. The final libraries were pooled in equimolar amounts.

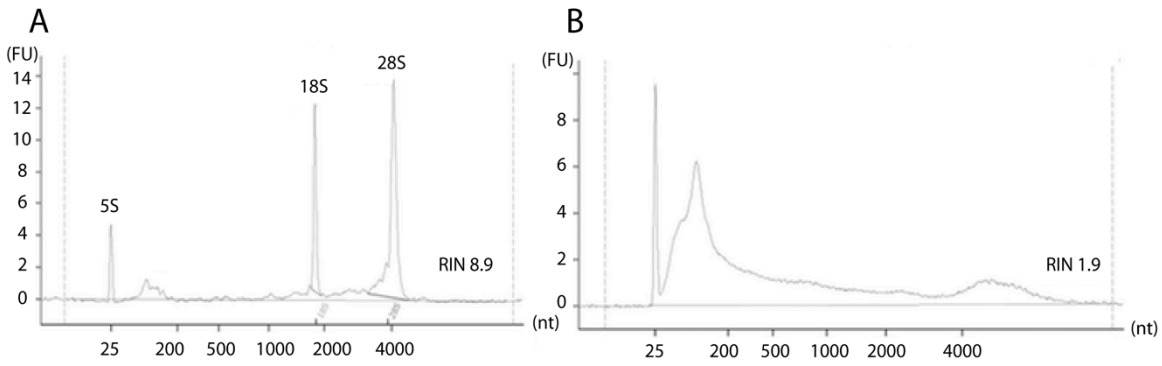

Figure 5.10. Example of electropherogram of an intact (A) and degraded (B) RNA sample

In the electropherogram, a high percentage of fragments with > 200 nucleotides indicates good RNA integrity, whereas a low percentage relates to enhanced RNA degradation and low quality. Important features such as the 5s,18s and 28s rRNA are outlined in the electropherogram. **(A)** Electropherogram of an intact RNA sample with a RIN of 8.9. **(B)** Electrophergoram of a heavily degraded RNA sample with a RIN of 1.9. A shift towards shorter fragment sizes can be observed as RNA degradation is a gradual process. Image adapted from (Peiro-Chova, Pena-Chilet et al. 2013).

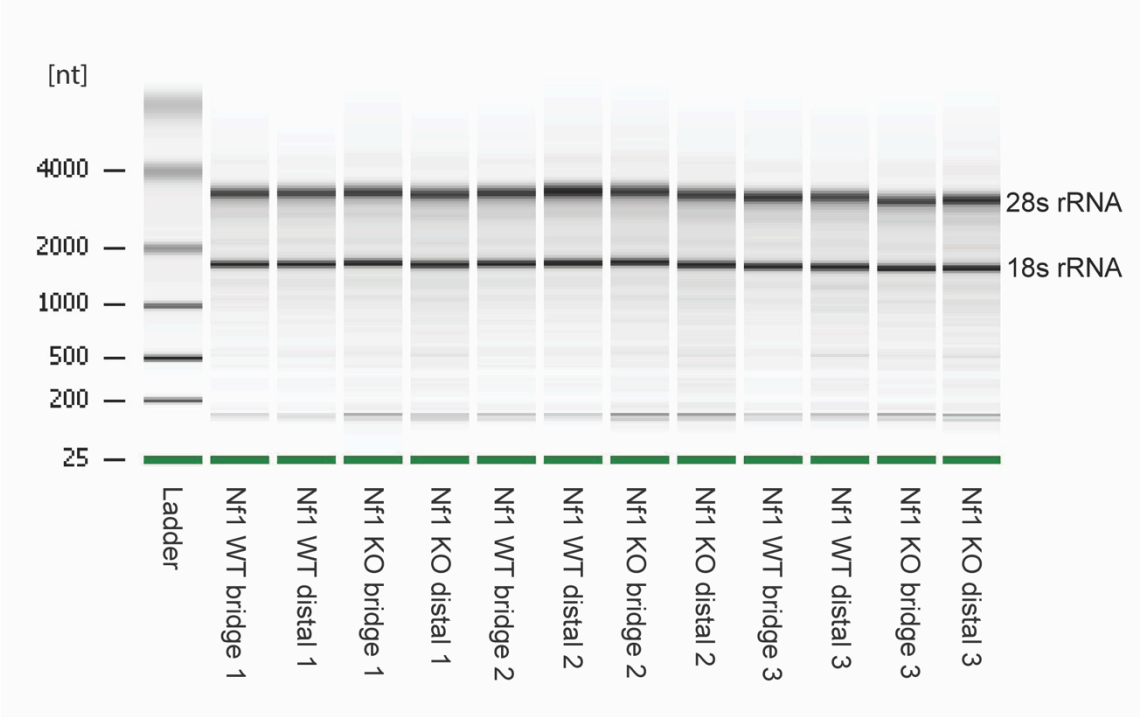

Figure 5.11. Agilent bioanalyser gel-like image of total RNA of samples 1-12
The image shows the total RNA gel like-image of the 12 RNA samples produced by the Agilent bioanalyzer. The 28s and 18s distinctive ribosomal bands are observed for all samples.

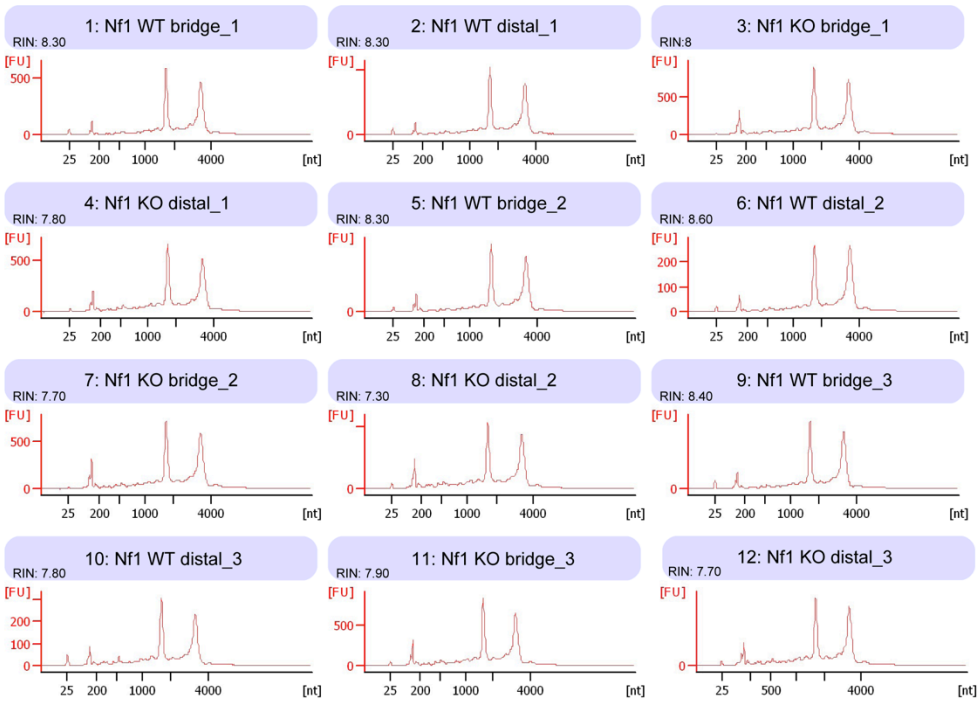

Figure 5.12. Electropherogram of RNA samples 1-12

Sample label and RIN number is displayed in the blue box above the electropherogram. The electropherogram shows a distinct profile for each sample and the amount of measured fluorescence correlates with the RNA concentration of the sample. Note that for example, the measured fluorescence of the sample “Nf1 bridge_1” is clearly higher compared to the sample “Nf1 WT bridge_1”. The 18sRNA subunit can be seen at ~ 2000nt, the 28s large RNA subunit at ~ 3800nt. (FU) =Fluorescence units nt= nucleotides.

Sample Name	Concentration (ng/ul)	260/280	260/230	RIN
1:Nf1 WT bridge_1	94.27	2.03	1.95	8.3
2: Nf1 WT distal_1	89.96	2.01	2.05	8.3
3:Nf1 KO bridge_1	322.46	2.05	2.27	8
4:Nf1 KO distal_1	167.5	2.07	2.17	7.8
5:Nf1 WT bridge_2	105.03	1.98	2.06	8.3
6:Nf1 WT distal_2	73.81	2.01	2.05	8.6
7:Nf1 KO bridge_2	306.8	2.06	2.17	7.7
8:Nf1 KO distal_2	192.35	2.08	1.99	7.3
9:Nf1 WT bridge_3	71.62	2.12	2	8.4
10:Nf1 WT distal_3	62.04	2.14	2	7.9
11:Nf1 KO bridge_3	245.42	2.11	2.06	7.9
12:Nf1 KO distal_3	168.16	2.07	2.06	7.7

Table 5.1. Summary of RNA concentration, 260/280 and 260/230 ratios and RIN number of RNA seq. samples

RNA concentration, 260/280 and 260/230 absorbance ratios were measured with a Nanodrop prior to submission of the samples to the RNA sequencing facility. The RIN number was measured by the Agilent 2100 bioanalyser at the Genomic Facility of Liverpool. RNA seq. samples should have a RIN value of ~8. All our samples, showed a RIN value of 8 ± 0.5 except Nf1 distal_2 which had a RIN value of 7.3. In general, the average RNA concentration was observed to be higher in the Nf1 KO samples than in the control, Nf1 WT samples consistent with the increased number of cells in these nerves.

The quantity and quality of each pool was determined by Bioanalyzer and by qPCR using the Illumina Library Quantification Kit from Kapa (KK4854) on a Roche Light Cycler LC480II. The template DNA was denatured and loaded at 300 pM. The sequencing was performed on two lanes of an Illumina HiSeq4000 at 2x150 bp paired-end sequencing (Borodina et al., 2011; Parkhomchuk et al., 2009).

An important factor to take into account for an RNA seq. analysis is sequencing depth or library size that is defined as the number of sequenced reads for a sample. Deeper sequencing results in the detection of more genes that are expressed at a low level, but it also results in the detection of transcriptional noise and off-target effects (Mortazavi et al., 2008). Increasing sequencing depth increases the cost, hence it is always a trade-off between increasing sequencing depth or the number of biological replicates, as reducing the sequencing depth allows the inclusion of more biological replicates per condition. Differential expression analysis programs such as Deseq2 rely on accurate modelling of the biological variability, as increasing the sequencing depth in an experiment with only a few replicates was shown to increase the number of false-positive differentially expressed genes (mostly low level expressed genes) (Tarazona et al., 2011). In conclusion, increasing the sequencing depth will detect genes, which are expressed at a low level, but their relevance in a biological context can only be assessed when biological variation can be accurately modelled through replication. In general, stable detection of protein coding genes is reached at moderate sequencing depths and ultra- high-throughput sequencing is mainly needed for detection of non-coding, low-expression RNAs. Furthermore, sequencing reads have increased substantially to a maximum of 300bp reads and this has been shown to improve the mapping to the reference genome and also allows the detection of both known splice junctions and novel splice sites. Consequently, we decided to run three biological replicates and the sequencing was carried out for each replicate on two lanes of an Illumina HiSeq4000 at 2x150 bp, which can result in ~50-60 million reads per sample. This is considered a moderate sequencing depth, which we considered most appropriate for our analysis (Chhangawala et al., 2015; Conesa et al., 2016).

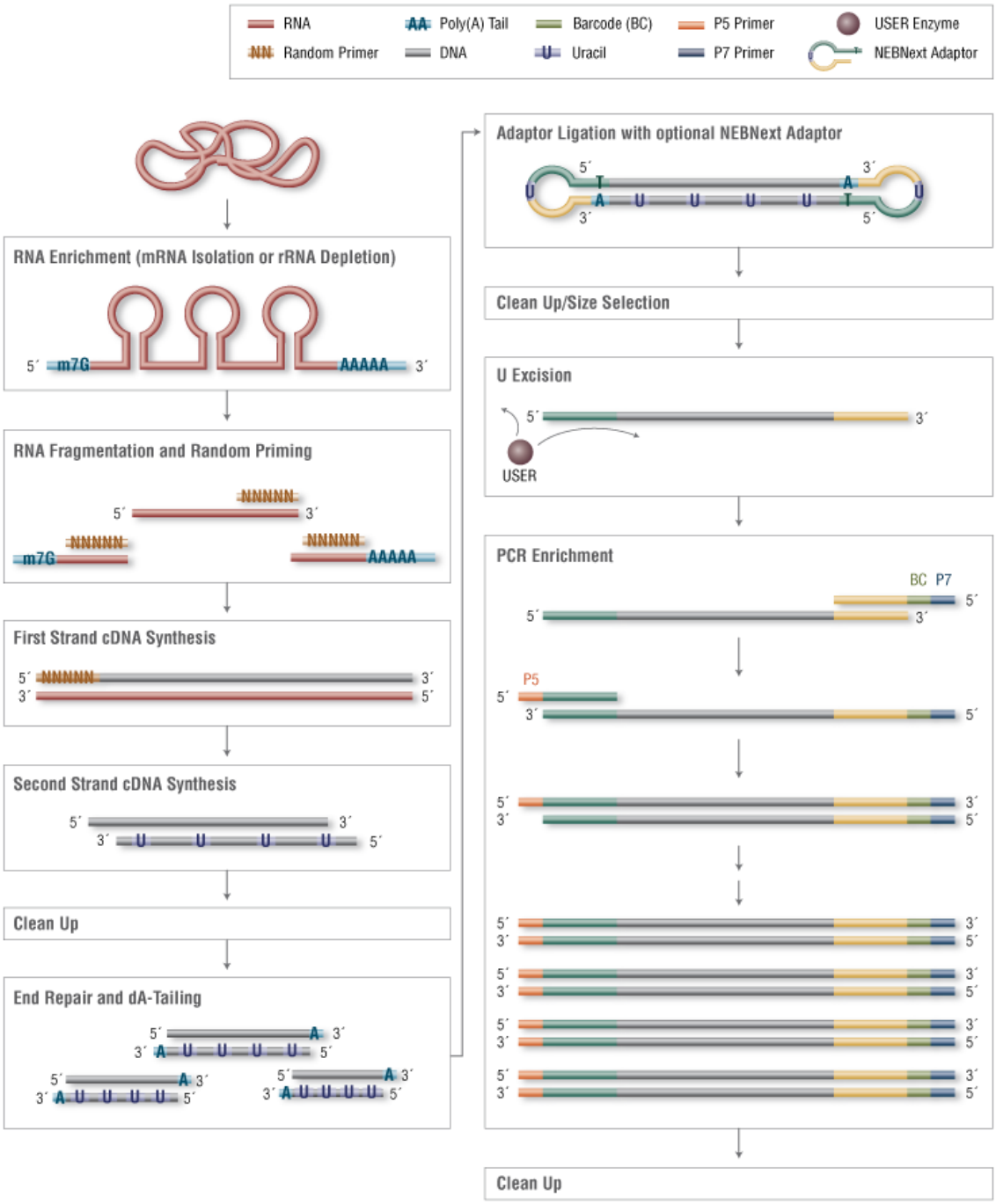

Figure 5.13. RNA- seq. library preparation using NEB Ultra Directional RNA library preparation kit

After rRNA depletion with Ribo Zero gold kit, RNA was fragmented. First strand cDNA was reverse transcribed from fragmented RNA using random hexamers or oligo(dT) primers. In the second strand synthesis, UTP was incorporated in order to conserve strand information. The 5' and/or 3' ends of cDNA were repaired and dA tailed. dA tailing incorporates a non-templated dAMP on the 3' end of the blunt DNA fragments. This process prevents concatamer formation during subsequent ligation steps. Subsequently, the dA tailed fragments were ligated to adaptors, which contain sequences to allow hybridisation to a flow cell with complementary dT overhangs. USER (Uracil-Specific Excision Reagent) enzyme then generated a single nucleotide gap at the location of an uracil which results in custom 3' overhangs, which are required for the PCR enrichment step. The subsequent destruction of the uridine containing strand allowed identification of the orientation of the transcripts.

Libraries were enriched for correctly ligated cDNA fragments by PCR amplification using high fidelity polymerase. Primers, that bind fragments with integrated adapters (yellow) at the 3' end, incorporated a barcode (bc) into each fragment. Library concentration was assessed using Qubit. Figure was retrieved from https://www.neb.com/products/e7530-nebnext- ultra-rna-library-prep-kit-for-illumina#Product%20Information.

5.10. RNA seq. analysis

Prior to the bioinformatics analysis of the RNA seq. data, the quality of the raw data was examined, the variability of the samples was assessed and the data was normalised. Two independent bioinformatics analyses were performed: The first by the genomic facility in Liverpool and the second in collaboration with Dr. Christina Venturini (Group of Judith Breuer, Division of Infection and Immunity, UCL).

The bioinformatics analysis aimed to detect differentially expressed genes between the sample group's, Nf1 WT (control) bridge, Nf1 WT (control) distal, Nf1 KO bridge and Nf1 KO distal. By comparing the different regions, we aimed to identify both the potential pro-tumourigenic signals from the Nf1 KO injury microenvironment and potential tumour suppressive signals from the normal nerve microenvironment.

5.10.1. Processing of raw data

The initial raw data processing steps (basecalling, de-multiplexing and trimming) were performed at the Genomic Facility of the University of Liverpool. Further processing of the raw data was performed both by the Genomic Facility in Liverpool and by Dr. Venturini.

Basecalling and de-multiplexing of the indexed reads was performed using CASAVA version 1.8.2, which is a bioinformatics software package commonly used to process sequencing reads. Demultiplexing divides the sequence reads into separate files for each index tag/sample and generates fastq files, which are required for downstream analysis. Basecalling is the process which determines the sequence of a fragment. Lastly, the raw fastq files were trimmed to remove Illumina adapter sequences using Cutadapt version 1.2.1 (Martin, 2011). Low quality bases were removed from the reads by using Sickle version 1.200 with a minimum window quality score of 20. After trimming was completed, reads shorter than 10 bp were removed.

Both complete bioinformatics analyses are attached in the Appendix of this thesis, however only the analysis of Dr. Venturini is shown in this Chapter. The analysis of Dr. Venturini was performed using R software (Team, 2014), Bioconductor (Gentleman et al., 2004) packages including DESeq2 (Anders and Huber, 2010; Love et al., 2014) and the SARTools package developed at PF2 (Institute Pasteur). Normalization and differential analysis were performed according to the DESeq2 model and package.

For RNA-seq. studies, it is recommended to obtain about 25 million reads per sample, but total read counts could vary between the samples due to slight differences in rRNA contamination and library concentrations between the samples. Figure 5.14 shows the total number of mapped and counted reads for each sample. All the samples have total read counts of ~30 million ± 5, except for sample Nf1 KO_distal_1 with the highest read count (38 million) and Nf1 WT bridge_1 with the lowest read count (~18 million). In addition to total read counts, biological replicates and samples derived from the same tissue are expected to have similar read count distributions. log2(raw counts+1) are used instead of raw counts in order to provide a better readability of the graph. Figure 5.15 shows the distribution of the read counts for each sample and all the analysed samples exhibited a similar distribution of the raw read counts and no abnormal deviations were observed. Furthermore, the graph shows that there were some genes with zero read count (first peak) and some genes, which were very highly expressed.

5.10.2. The PCA plot shows little variation between biological replicates

The main variability within the experiment is expected to come from biological differences between the samples. This can be assessed in two ways: 1. Hierarchical clustering of the whole sample set or 2. Principal component analysis (PCA). We have performed PCA, in which all the genes have been included and each point within the graph represents one biological replicate. The first principal components (PC1 and PC2) of the PCA, as shown in Figure 5.16, separates the samples from the different biological conditions, meaning that the biological variability is the main source of variance in the data. The PCA plot shows that the y-axis separates the bridge from the distal stump samples and the x-axis separates the two

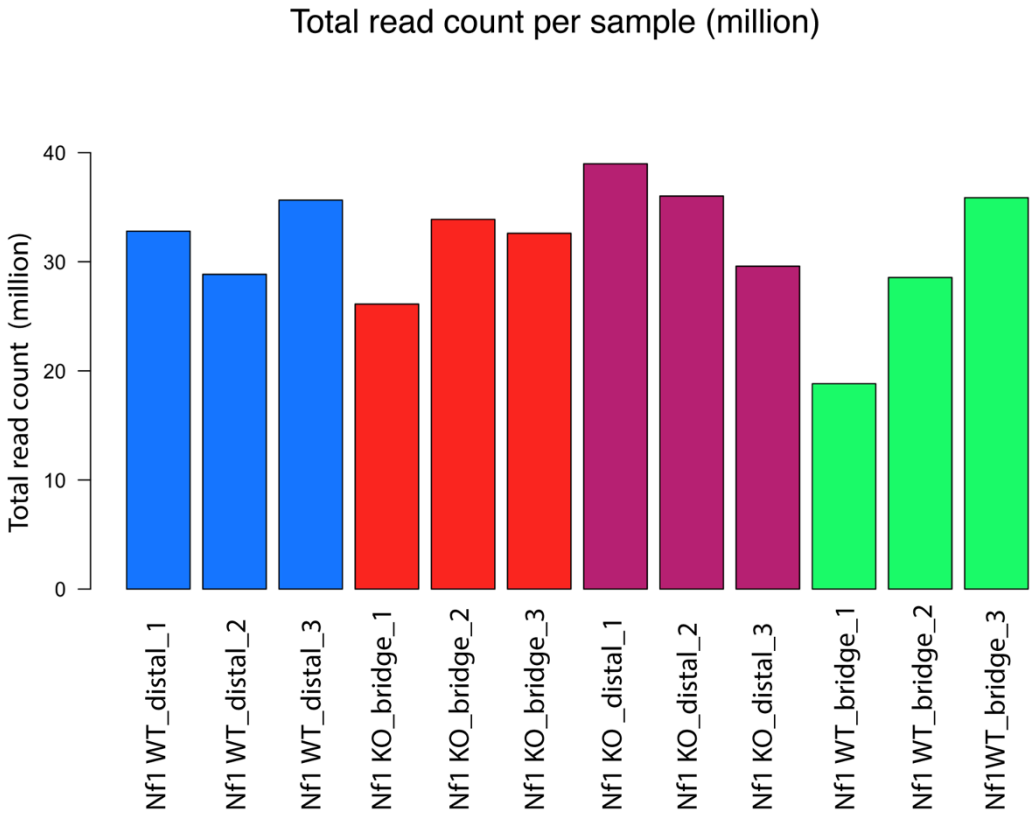

Figure 5.14. Number of mapped reads per sample
The total mapped read counts are displayed in millions. In general, all the samples have a high total read count with in average 30 millions ± 5 total read counts. The highest read counts were obtained with the sample Nf1 KO distal_1 (~ 38 million) and the lowest read counts were obtained with the sample Nf1 WT bridge_1 (~ 18 million). Colours refer to the biological condition of the sample. Figure was generated by Dr. Venturini.

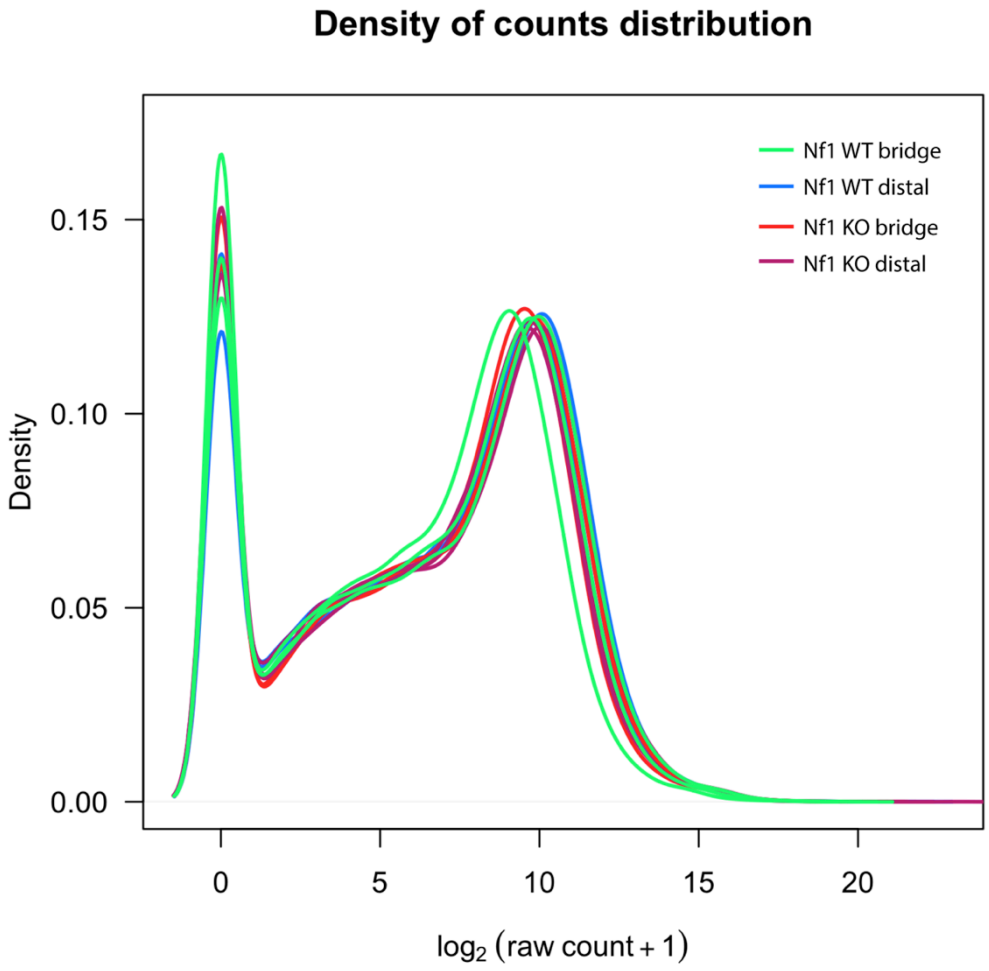

Figure 5.15. Density of counts distribution
This graph displays the distribution of the raw read counts of all analysed samples. All samples show a similar trend and no unusual deviations are observed between the biological replicates. Figure was generated by Dr.Venturini.

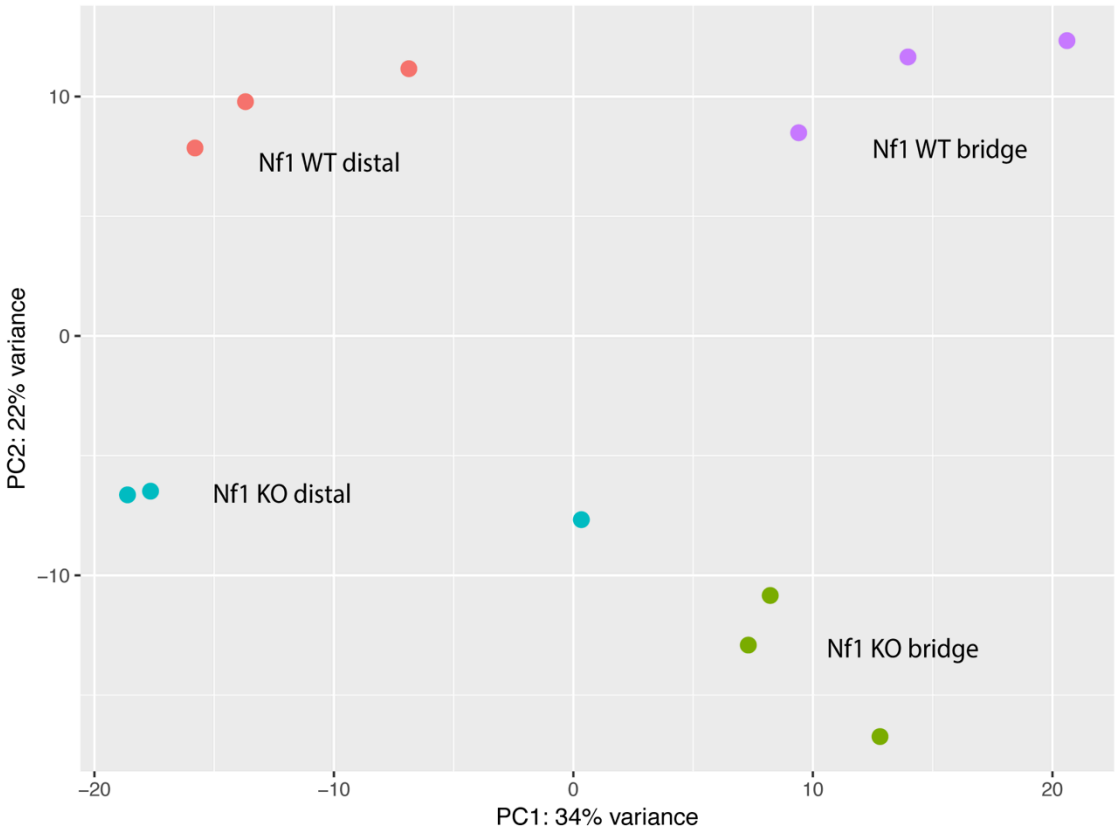

Figure 5.16. The PCA plot shows tight clustering of biological triplicates and separation of biological different samples

The plot shows the first two components of the PCA with percentages of variance associated with each axis (all genes have been included in this analysis). Each point represents one sample and the biological replicates are color-coded. Principal Component 1 (PC1, x-axis) represents 34% and PC2 represents 22% of the total variation in the data. Figure was generated by Dr. Venturini.

genotypes from each other. Overall, the PCA plot of our RNA Seq. data set showed good reproducibility of our samples, as the triplicates of each group are clustered together. However, sample Nf1 KO distal_1 is more different than the other two biological replicates, as it does not cluster so tightly and is more closely associated with the Nf1 KO bridge samples. The reason for the increased variance of the Nf1 KO distal_1 sample is unknown, however we cannot exclude that more of the nerve bridge was included in the Nf1 KO distal_1 sample, which could explain it's increased variance from the other two biological replicates.

5.10.3. Differential expression analysis of the RNA seq. dataset

The differential expression analysis was performed using the Deseq2 package (Love 2014). Outliers were detected by calculating the Cook's distance for every gene (Cook, 1977) with a large Cook's value corresponding to an outlier count. For genes with a large Cooks distance, p-values were not calculated (Love et al., 2014; McCarthy et al., 2012). The calculated p-values must be adjusted for multiple comparisons, as a typical RNA seq. analysis involves comparing a large number of genes (performing a large number of statistical tests) that can lead to false positive results purely by chance. For our analysis, a p-value adjustment using the Benjamini Hochberg procedure was performed (Hochberg, 1995) and the controlled false positive rate was set to 0.05. The Benjamini- Hochberg approach controls the false positive rate, which is the proportion of significant results that are actually false positives.

In Table 5.2, the up-, down- and total number of differentially expressed genes are displayed for all the relevant comparisons. The comparisons Nf1 WT bridge vs Nf1 KO distal and the comparison Nf1 KO bridge vs Nf1 WT distal had the most differentially expressed genes (~4500 genes). This result shows, as already evident in the PCA plot in Figure 5.16, that most differentially regulated genes were found by comparing samples that differ in both regions and genotypes. In contrast, the comparison of the Nf1KO distal stump with the Nf1 WT distal stump had the least number of differentially expressed genes (2190 genes). This is in accordance with the biological similarity of the two samples at Day 14 following injury, as determined earlier in this Chapter.

Test vs Ref	# down	# up	# total
Nf1 KO distal vs NF1 WT distal	1002	1188	2190
Nf1 WT bridge vs NF1 WT distal	1261	1344	2605
Nf1 KO distal vs NF1 KO bridge	1727	1780	3507
Nf1 WT bridge vs NF1 KO bridge	1786	1649	3435
Nf1 WT bridge vs Nf1 KO distal	2374	2196	4570
Nf1 KO bridge vs Nf1 WT distal	2212	2382	4594

Table 5.2. Up-, down- and total number of differentially regulated genes for each comparison

This table displays the number of up-, down and total number of differentially regulated genes in each comparison. As describe above the raw p-values are adjusted for multiple comparisons by performing a false discovery rate p-value adjustment, in which the controlled false positive rate was set to 0.05. This false discovery rate p-value adjustment is done with the Deseq2 (Love et al., 2014) programme and is based on the Benjamini Hochberg approach (Hochberg, 1995).

Both MA and volcano plots are commonly used to visualise high-throughput sequencing analysis (Figure 5.17 and 5.18) and both display the differentially expressed genes of the different comparisons (red dots). We have identified several genes, which are either differentially over or under-expressed in all relevant comparisons. Out of the 6 comparisons made, only the 4 most relevant comparison are shown in Figure 5.17 and 5.18 due to space constraints (the remaining data is in the Appendix of this thesis).

5.10.4. Functional analysis of differentially expressed genes

To test whether genes associated with a specific biological function are over or underrepresented within the differentially upregulated genes of the 4 different comparisons (Nf1 KO ds vs Nf1 WT ds, Nf1 KO b vs Nf1 KO ds, Nf1 KO b vs Nf1 WT b, Nf1 KO b vs Nf1 WT ds), we have performed a non-biased gene ontology (GO) term enrichment analysis using http://pantherdb.org/geneListAnalysis.do (Mi et al., 2013) (Table 5.3). Gene annotation overrepresentation analysis functionally annotates differentially expressed genes and assesses, whether a particular function is over-represented by comparing the frequency of each annotation in the gene list of interest to the background frequency of the reference gene list. The background frequency (defined as “expected value” in Table 5.3) is the expected number of genes annotated to a GO term out of the entire background gene set, whereas sample frequency is the number of genes annotated to the same GO term in the gene list of interest. A biological function is overrepresented when the number of genes out of the gene list of interest that are annotated to a specific GO term exceeds the “expected value”.

In the Nf1 KO bridge compared to all other regions, DNA replication, cell proliferation and cell cycle genes were overrepresented within the differentially upregulated genes (Table 5.3). In contrast, when comparing the differentially upregulated genes in the distal stump of Nf1 KO vs Nf1 WT, none of these groups were found to be enriched (Table 5.3). These findings are in agreement with our previous analysis, which showed increased proliferation in the Nf1 KO bridge at this timepoint. Furthermore, the MAPK (ERK) signalling pathway was overrepresented when comparing the Nf1 KO bridge to both its own and to the Nf1 WT distal stump, but not when comparing the Nf1 KO vs Nf1 WT bridge. As shown in our previous

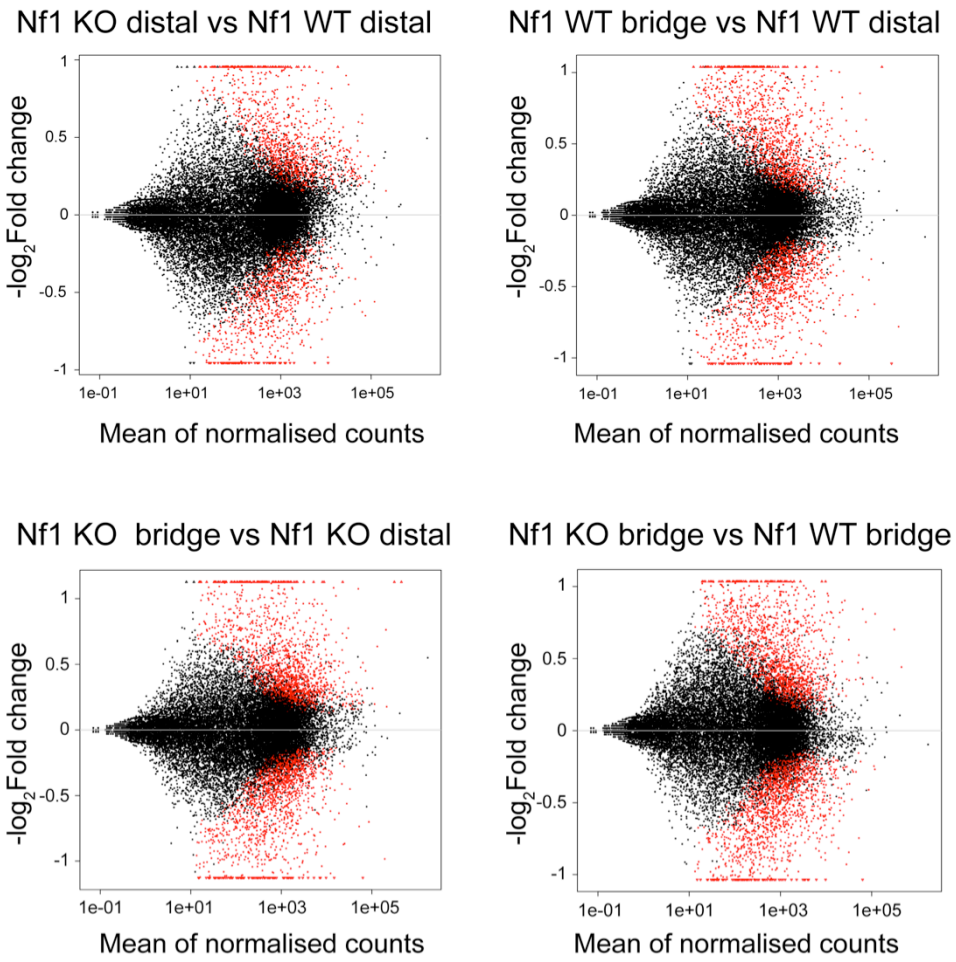

Figure 5.17. MA plots show differentially expressed genes identified between all the conditions

The MA plot provides a useful overview for an experiment with a two-group comparison. In the plot, each data point depicts a gene. The differentially expressed genes (up-and down regulated genes) which possess an adjusted p=value below 0.05 are coloured in red. Genes with a similar expression level in both samples will appear around the horizontal line (y=0) and are coloured in black. A negative change represents down-regulated genes and a positive change represents up- regulated genes. Datapoints, which fall out of the window are plotted as open triangles that are pointing either up or down. x-axis: normalized mean transformed to log10 scale. Y-scale: log2 Fold change. Figure was generated by Dr.Venturini.

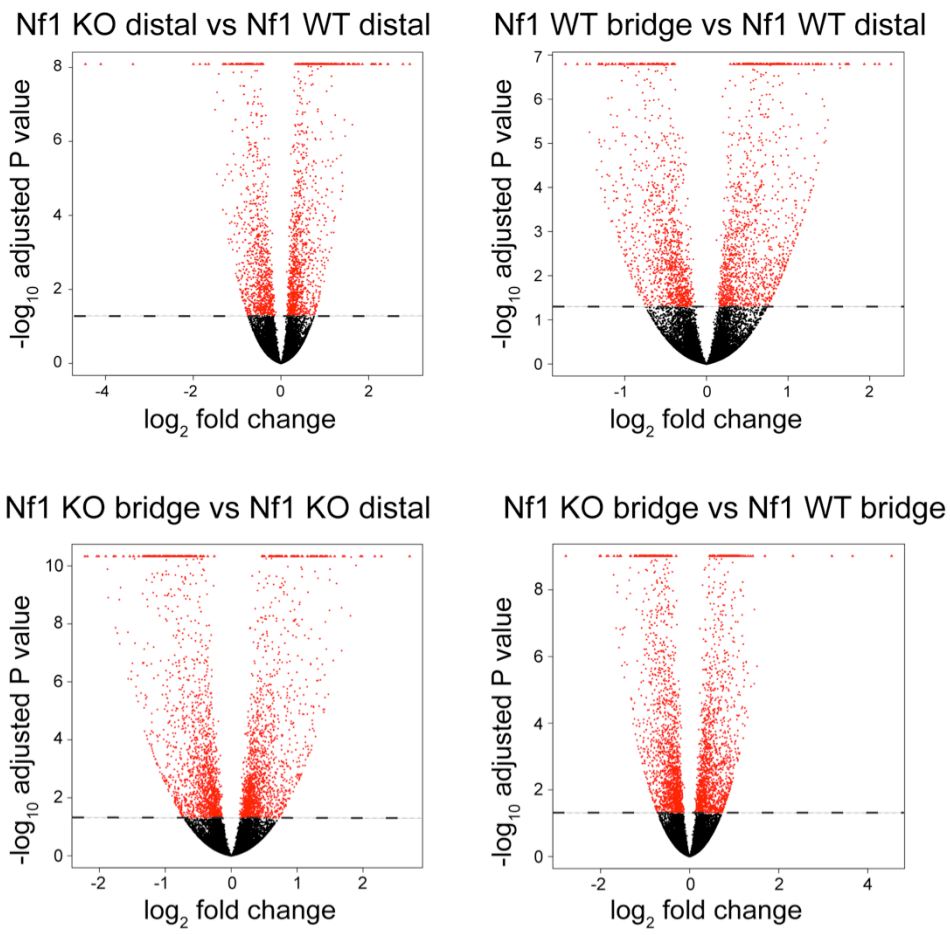

Figure 5.18. Volcano plot shows differentially expressed genes identified between all conditions

In the volcano plot differently expressed genes are highlighted as red dots. Genes with a low p-value (highly significant) appear towards the top of the plot. The log2 of the fold change is plotted so that changes in either direction appear equidistant from the centre. The genes of interest are the genes, which are found towards the top of the plot that are far to either the left- or the right- hand side. These genes have a large fold change as well as being highly statistical significant. A negative change represents the down-regulated genes and a positive change represents the up-regulated genes. x-axis: log2 expression fold change. Y-scale: -log10 of the adjusted p-value. The adjusted p-value of 0.05 is set as threshold and is shown as a dashed line. Figure was generated by Dr. Venturini.

A **Differentially upregulated genes Nf1 KO bridge vs NF1 WT distal comparison**

PANTHER GO-Biological Process	# of genes in Mus musculus reference	# of genes in dataset	expected	Fold Enrichment	raw P-value	FDR
chromatin assembly	30	12	3.08	3.89	3.24E-04	1.98E-03
organelle organization	1133	183	116.5	1.57	3.12E-08	4.48E-07
cellular component organization	1961	280	201.63	1.39	2.03E-07	2.61E-06
cellular component organization or biogenesis	2099	288	215.82	1.33	2.91E-06	2.96E-05
chromosome segregation	86	25	8.84	2.83	2.56E-05	2.09E-04
cellular process	8762	1081	900.92	1.2	4.33E-13	2.11E-11
mitosis	204	55	20.98	2.62	8.31E-09	1.45E-07
cell cycle	650	123	66.83	1.84	3.59E-09	7.97E-08
cell proliferation	66	17	6.79	2.51	1.79E-03	8.55E-03
meiosis	59	15	6.07	2.47	3.78E-03	1.71E-02
protein glycosylation	103	24	10.59	2.27	1.01E-03	5.61E-03
cellular protein modification process	797	113	81.95	1.38	1.66E-03	8.28E-03
primary metabolic process	4839	564	497.55	1.13	1.61E-03	8.38E-03
metabolic process	6009	728	617.85	1.18	1.24E-06	1.38E-05
cell-cell adhesion	157	36	16.14	2.23	5.20E-05	3.85E-04
cell adhesion	359	86	36.91	2.33	5.91E-11	1.80E-09
biological adhesion	359	86	36.91	2.33	5.91E-11	1.60E-09
chromatin organization	258	58	26.53	2.19	7.15E-07	8.72E-06
DNA replication	140	31	14.39	2.15	2.96E-04	1.85E-03
DNA metabolic process	345	69	35.47	1.95	2.09E-06	2.22E-05
nucleobase-containing compound metabolic process	2710	349	278.64	1.25	3.69E-05	2.82E-04
cell growth	98	21	10.08	2.08	3.92E-03	1.68E-02
transmembrane receptor protein tyrosine kinase signaling pathway	148	30	15.22	1.97	1.63E-03	8.27E-03
regulation of cell cycle	175	35	17.99	1.95	7.28E-04	4.23E-03
nervous system development	307	60	31.57	1.9	1.74E-05	1.47E-04
system development	474	82	48.74	1.68	3.20E-05	2.52E-04
developmental process	1514	260	155.67	1.67	5.85E-14	3.57E-12
regulation of catalytic activity	356	64	36.6	1.75	8.78E-05	6.30E-04
regulation of molecular function	436	73	44.83	1.63	2.03E-04	1.38E-03
cell differentiation	547	94	56.24	1.67	9.51E-06	8.59E-05
locomotion	314	53	32.29	1.64	1.44E-03	7.64E-03
cellular component morphogenesis	415	70	42.67	1.64	2.60E-04	1.67E-03
ectoderm development	208	35	21.39	1.64	1.02E-02	4.02E-02
MAPK cascade	346	58	35.58	1.63	9.73E-04	5.52E-03
intracellular signal transduction	1121	168	115.26	1.46	7.06E-06	6.89E-05
mesoderm development	265	44	27.25	1.61	5.52E-03	2.28E-02
cellular component movement	484	80	49.77	1.61	1.71E-04	1.19E-03
cytoskeleton organization	365	59	37.53	1.57	1.77E-03	8.62E-03
regulation of phosphate metabolic process	511	80	52.54	1.52	7.25E-04	4.31E-03
phosphate-containing compound metabolic process	1571	221	161.53	1.37	1.11E-05	9.65E-05

B **Differentially upregulated genes in Nf1 KO bridge vs Nf1 KO distal comparison**

PANTHER GO-Biological Process	# of genes in Mus musculus reference	# of genes in dataset	expected	Fold Enrichment	raw P-value	FDR
angiogenesis	19	7	1.43	4.91	1.61E-03	1.09E-02
system development	474	71	35.58	2	3.72E-07	6.97E-06
developmental process	1514	204	113.64	1.8	2.24E-14	1.83E-12
cell growth	98	26	7.36	3.53	3.59E-07	7.31E-06
cellular process	8762	768	657.68	1.17	1.40E-07	3.41E-06
nervous system development	307	54	23.04	2.34	1.07E-07	2.90E-06
exocytosis	162	27	12.16	2.22	4.34E-04	3.65E-03
vesicle-mediated transport	817	84	61.32	1.37	7.52E-03	3.67E-02
negative regulation of apoptotic process	103	17	7.73	2.2	5.73E-03	2.92E-02
cellular component morphogenesis	415	68	31.15	2.18	3.50E-08	1.07E-06
anatomical structure morphogenesis	139	24	10.43	2.3	5.10E-04	4.01E-03
cellular component organization	1961	193	147.19	1.31	2.72E-04	2.46E-03
cellular component organization or biogenesis	2099	195	157.55	1.24	3.37E-03	2.00E-02
transmembrane receptor protein tyrosine kinase signaling pathway	148	24	11.11	2.16	1.27E-03	9.14E-03
signal transduction	2896	256	217.38	1.18	8.61E-03	3.96E-02
cell communication	3269	295	245.37	1.2	1.33E-03	9.28E-03
cell differentiation	547	85	41.06	2.07	4.95E-09	2.02E-07
cell adhesion	359	55	26.95	2.04	5.54E-06	7.51E-05
biological adhesion	359	55	26.95	2.04	5.54E-06	7.12E-05
locomotion	314	46	23.57	1.95	6.50E-05	6.60E-04
ectoderm development	208	28	15.61	1.79	6.40E-03	3.19E-02
cellular component movement	484	63	36.33	1.73	8.57E-05	8.36E-04
mesoderm development	265	33	19.89	1.66	8.20E-03	3.85E-02
regulation of catalytic activity	356	44	26.72	1.65	2.82E-03	1.72E-02
regulation of molecular function	436	52	32.73	1.59	2.21E-03	1.38E-02
MAPK cascade	346	42	25.97	1.62	4.69E-03	2.66E-02
intracellular signal transduction	1121	129	84.14	1.53	7.92E-06	9.66E-05
regulation of phosphate metabolic process	511	62	38.36	1.62	6.21E-04	4.74E-03
phosphate-containing compound metabolic process	1571	167	117.92	1.42	2.01E-05	2.13E-04
metabolic process	6009	505	451.04	1.12	4.77E-03	2.59E-02
cytoskeleton organization	365	43	27.4	1.57	7.76E-03	3.71E-02
intracellular protein transport	650	74	48.79	1.52	1.06E-03	7.85E-03
protein transport	684	79	51.34	1.54	4.96E-04	4.04E-03
protein localization	494	56	37.08	1.51	5.00E-03	2.65E-02
cellular protein modification process	797	86	59.82	1.44	1.9E-03	1.22E-02
cell cycle	650	70	48.79	1.43	4.71E-03	2.61E-02

C **Differentially upregulated genes in Nf1 KO bridge vs Nf1 WT bridge comparison**

PANTHER GO- Biological Process	# of genes in Mus musculus reference	# of genes in dataset	expected	Fold Enrichment	raw P-value	FDR
chromatin assembly	30	17	2.34	7.26	1.29E-08	1.66E-07
organelle organization	1133	150	88.45	1.7	4.74E-09	7.23E-08
cellular component organization	1961	227	153.1	1.48	1.65E-08	2.02E-07
cellular component organization or biogenesis	2099	236	163.87	1.44	8.54E-08	8.68E-07
chromosome segregation	86	30	6.71	4.47	5.67E-10	1.38E-08
cellular process	8762	845	684.05	1.24	5.68E-14	2.31E-12
cell proliferation	66	18	5.15	3.49	2.61E-05	1.82E-04
DNA replication	140	36	10.93	3.29	1.14E-08	1.55E-07
DNA metabolic process	345	78	26.93	2.9	1.53E-14	7.49E-13
nucleobase-containing compound metabolic process	2710	313	211.57	1.48	1.55E-11	4.74E-10
primary metabolic process	4839	466	377.78	1.23	1.53E-06	1.20E-05
metabolic process	6009	583	469.12	1.24	7.29E-09	1.05E-07
mitosis	204	48	15.93	3.01	5.70E-10	1.26E-08
cell cycle	650	124	50.75	2.44	4.59E-17	3.74E-15
regulation of cell cycle	175	40	13.66	2.93	3.00E-08	3.33E-07
regulation of gene expression, epigenetic	72	16	5.62	2.85	5.29E-04	2.75E-03
DNA recombination	51	11	3.98	2.76	4.58E-03	1.83E-02
protein glycosylation	103	20	8.04	2.49	6.22E-04	3.16E-03
chromatin organization	258	49	20.14	2.43	1.70E-07	1.66E-06
receptor-mediated endocytosis	112	21	8.74	2.4	6.24E-04	3.11E-03
cell-cell adhesion	157	26	12.26	2.12	8.58E-04	4.19E-03
cell adhesion	359	66	28.03	2.35	3.87E-09	6.74E-08
biological adhesion	359	66	28.03	2.35	3.87E-09	6.29E-08
cytokinesis	134	21	10.46	2.01	4.78E-03	1.88E-02
cellular defense response	128	20	9.99	2	6.23E-03	2.37E-02
transmembrane receptor protein tyrosine kinase signaling pathway	148	22	11.55	1.9	7.09E-03	2.66E-02
signal transduction	2896	269	226.09	1.19	4.07E-03	1.71E-02
mRNA splicing, via spliceosome	183	27	14.29	1.89	4.42E-03	1.80E-02
DNA repair	153	22	11.94	1.84	1.17E-02	4.14E-02
nervous system development	307	44	23.97	1.84	3.69E-04	2.14E-03
system development	474	56	37.01	1.51	4.94E-03	1.91E-02
developmental process	1514	190	118.2	1.61	1.46E-09	2.74E-08
apoptotic process	337	47	26.31	1.79	4.51E-04	2.45E-03
cell death	358	52	27.95	1.86	7.23E-05	4.77E-04
death	358	52	27.95	1.86	7.23E-05	4.90E-04
regulation of catalytic activity	356	49	27.79	1.76	4.43E-04	2.46E-03
regulation of molecular function	436	51	34.04	1.5	7.84E-03	2.81E-02
cytoskeleton organization	365	50	28.5	1.75	3.74E-04	2.12E-03
intracellular protein transport	650	89	50.75	1.75	2.30E-06	1.75E-05
protein transport	684	91	53.4	1.7	5.54E-06	3.97E-05
locomotion	314	42	24.51	1.71	1.84E-03	8.46E-03
cellular component movement	484	64	37.79	1.69	1.58E-04	1.01E-03
regulation of phosphate metabolic process	511	66	39.89	1.65	2.31E-04	1.45E-03
phosphate-containing compound metabolic process	1571	187	122.65	1.52	7.53E-08	7.99E-07
cellular component morphogenesis	415	53	32.4	1.64	1.13E-03	5.32E-03
response to external stimulus	377	47	29.43	1.6	3.31E-03	1.42E-02
cell differentiation	547	67	42.7	1.57	8.64E-04	4.13E-03
intracellular signal transduction	1121	135	87.52	1.54	3.16E-06	2.33E-05

D **Differentially upregulated genes in Nf1 KO distal vs Nf1 WT distal comparison**

PANTHER GO-Biological Process	# of genes in Mus musculus reference	# of genes in dataset	expected	Fold Enrichment	raw P-value	FDR
chromatin assembly	30	7	1.56	4.5	1.96E-03	1.29E-02
organelle organization	1133	100	58.78	1.7	9.47E-07	1.78E-05
cellular component organization	1961	158	101.74	1.55	1.23E-07	4.30E-06
cellular component organization or biogenesis	2099	174	108.9	1.6	3.66E-09	2.23E-07
regulation of gene expression, epigenetic	72	14	3.74	3.75	7.61E-05	8.84E-04
translation	212	28	11	2.55	2.73E-05	3.92E-04
protein metabolic process	1700	120	88.2	1.36	1.05E-03	7.77E-03
primary metabolic process	4839	312	251.06	1.24	3.75E-05	5.09E-04
metabolic process	6009	389	311.76	1.25	1.05E-06	1.82E-05
cell-cell adhesion	157	19	8.15	2.33	1.28E-03	9.16E-03
cell adhesion	359	45	18.63	2.42	3.41E-07	9.25E-06
biological adhesion	359	45	18.63	2.42	3.41E-07	8.32E-06
RNA splicing, via transesterificatio reactions	159	19	8.25	2.3	1.43E-03	9.95E-03
RNA metabolic process	1536	106	79.69	1.33	4.47E-03	2.54E-02
nucleobase-containing compound metabolic process	2710	187	140.6	1.33	9.49E-05	9.65E-04
chromatin organization	258	30	13.39	2.24	1.54E-04	1.34E-03
mRNA splicing, via spliceosome	183	21	9.49	2.21	1.56E-03	1.06E-02
mRNA processing	249	24	12.92	1.86	6.75E-03	3.66E-02
nervous system development	307	31	15.93	1.95	8.83E-04	6.73E-03
system development	474	40	24.59	1.63	5.07E-03	2.81E-02
developmental process	1514	123	78.55	1.57	2.61E-06	4.24E-05
cellular component biogenesis	733	74	38.03	1.95	3.16E-07	9.64E-06
DNA metabolic process	345	34	17.9	1.9	7.35E-04	5.98E-03
locomotion	314	30	16.29	1.84	2.40E-03	1.50E-02
regulation of catalytic activity	356	33	18.47	1.79	2.83E-03	1.73E-02
cell differentiation	547	49	28.38	1.73	5.04E-04	4.24E-03
regulation of phosphate metabolic process	511	43	26.51	1.62	3.73E-03	2.22E-02
phosphate-containing compound metabolic process	1571	108	81.51	1.33	4.13E-03	2.40E-02

Table 5.3. Gene ontology term enrichment analysis

These tables display the non-biased gene ontology term enrichment analysis that was performed on the differentially upregulated genes of the 4 different comparisons: **A)** Nf1 KO bridge vs Nf1 WT distal. **B)** Nf1 KO bridge vs Nf1 KO distal **C)** Nf1 KO bridge vs Nf1 WT bridge **D)** Nf1 KO distal vs Nf1 WT distal. The tables are sorted according to the highest fold enrichment value and subcategories are indicated by surrounding boxes and separating dashed lines. Only biological functions that were statistically significant (Fisher exact Test) are shown here and cell cycle related functions are highlighted in red.

analysis, the overall proliferation is higher in the bridge region compared to the distal stump in both genotypes and it is well known that ERK activation is required for SC proliferation, although at lower levels than those required to initiate SC dedifferentiation. As cell proliferation is higher in the bridge regions compared to the distal stump, the difference in ERK activation may be smaller between these two regions than when comparing the bridge region to the distal stump and thereby ERK activation may not been identified as enriched in the Nf1 KO bridge compared to the control bridge region.

Fewer biological functions were found overrepresented when comparing Nf1 KO and Nf1 WT distal stump. This is in line with our previous analyses, which has shown that these two areas are similar at this timepoint.

The heatmap, in which all 21821 genes are included, is displayed in Figure 5.19A and shows that the majority of the genes are similarly expressed across the conditions. The genes that are differentially expressed are displayed in the top panel. Due to the large number of genes, it is difficult to see the expression pattern of the genes that are differentially regulated between the different conditions, as only a subset of these genes reached a fold-change over 2, whilst others exhibited smaller differences. In Figure 5.19B, we selected the 100 genes that changed the most out of the 21821 genes and interestingly some of these genes are more highly expressed in the Nf1 KO bridge and this are candidates as pro-tumourigenic signals. However, many genes appear to be highly expressed in the Nf1 WT bridge region and these may be candidates for anti-tumourigenic signals.

5.10.5. Identification of genes exclusively overexpressed in Nf1 KO bridge region

Thousands of differentially expressed genes were identified between the different conditions, however, for the scope of this thesis, we have focused primarily on the genes, which were more highly expressed in the Nf1 KO bridge compared to the other conditions. The gene lists of the differently downregulated genes can be found in the Appendix of this thesis but because of time constraints have not been further analysed. To obtain the genes, which are exclusively upregulated in the Nf1 KO bridge, we intercalated the different comparisons using Venn diagrams http://bioinformatics.psb.ugent.be/webtools/Venn/. This was performed by

A

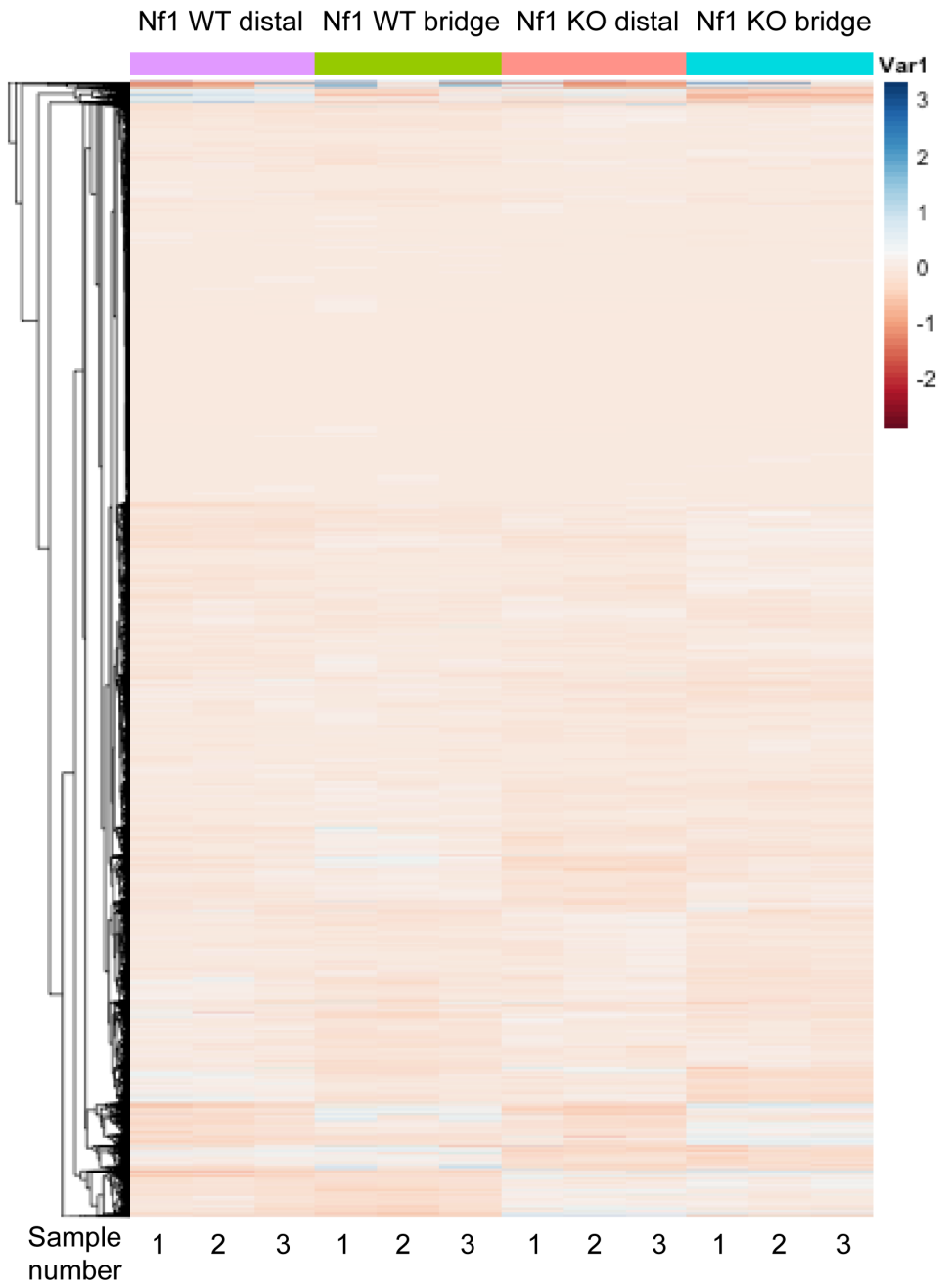
Nf1 WT distal
Nf1 WT bridge
Nf1 KO distal
Nf1 KO bridge
Var1
3
2
1
0
-1
-2
Sample number
1 2 3 1 2 3 1 2 3 1 2 3

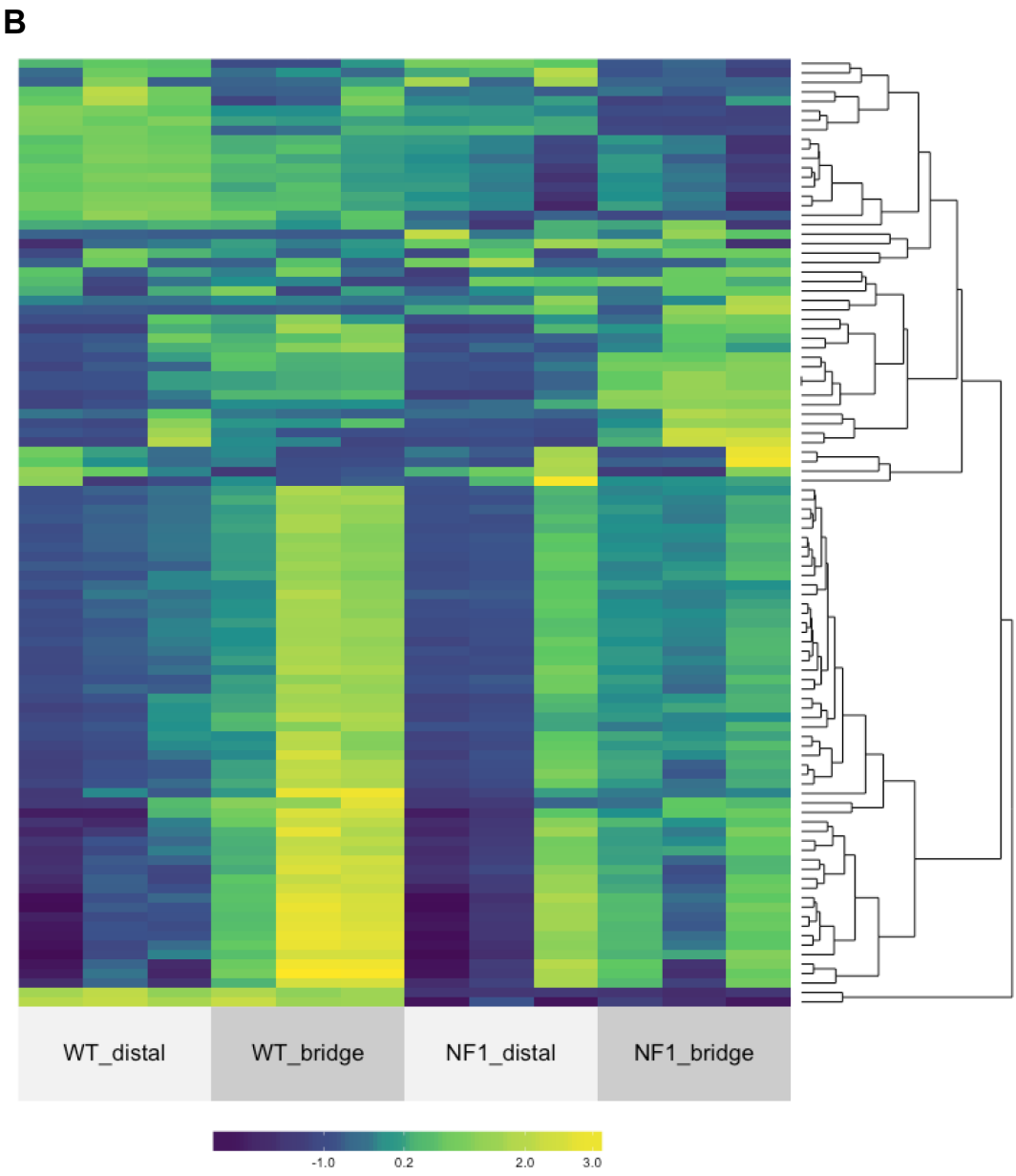

Figure 5.19. Heatmap of all genes

Heatmap of **A)** all 21821 genes and **B)** of the 100 genes that change the most between conditions. The Colour corresponds to per-gene z-score that is computed from the Deseq2 transformed counts (specifically rlog). The *z* -score scale represents mean-subtracted regularised log-transformed read counts. For each gene the distance of each sample from the mean for all samples was calculated and the order of the genes was obtained with hierarchical clustering. Figure was generated by Dr. Christina Venturini using **A)** pheatmap (https://cran.r-project.org/web/packages/pheatmap/index.html) and **B)** superheat (https://github.com/rlbarter/superheat).

intercalating the upregulated genes of the Nf1 KO bridge vs Nf1 WT bridge, Nf1 KO distal vs Nf1 WT distal, Nf1 KO bridge vs WT distal and Nf1 KO bridge vs Nf1 KO distal comparisons (Figure 5.20). The comparison Nf1 KO bridge with Nf1 WT distal stump was included, as although not biologically as relevant, it was important to ensure that the genes were different compared to the Nf1 WT distal stump.

The red Venn diagram intersection contains the 363 genes that are exclusively upregulated in the Nf1 KO bridge compared to the other regions (Figure 5.20), whereas the green intersection contains the 143 genes that are highly expressed in the Nf1 KO bridge but these genes also show different expression levels between Nf1 KO and Nf1 WT distal stump due to their generally low expression in the Nf1 WT animal (Figure 5.20). Furthermore, we were also interested in the genes, which were highly expressed in both the Nf1 KO bridge and Nf1 KO distal stump but not in the Nf1 WT regions (pink and blue intersection). Although these genes are upregulated in both regions in the Nf1 KO animal, they may act very differently in the two regions as the disruption of the basal lamina at the injury site could increase exposure to factors of the microenvironment. These genes are contained in the pink intersection with 276 genes and the blue intersection with 385 genes (Figure 5.20). The difference between these two Venn diagram intersections is that the genes within the pink Venn diagram segment are not differentially regulated between the Nf1 KO and the Nf1 WT distal stump (Figure 5.20).

To investigate, whether particular biological functions are over-represented within the different Venn diagram intersections, we performed a non-biased gene ontology term enrichment analysis using http://pantherdb.org/geneListAnalysis.do. In Table 5.4 the enrichment analysis of the Venn diagram intersections of interest are shown. Importantly, similar to the findings of the GO analysis shown in Table 5.3 above, we observed that cell cycle and mitotic nuclear division were highly overrepresented in the red Venn diagram intersection (which are the genes exclusively upregulated in the Nf1 KO bridge). This finding is in line with our earlier analysis, which showed that cell proliferation is higher within the Nf1 KO bridge at this timepoint (Figure 5.2).

We were especially interested in genes, which encode for secreted proteins such as cytokines, cell surface molecules and ECM proteins, as we considered them likely to

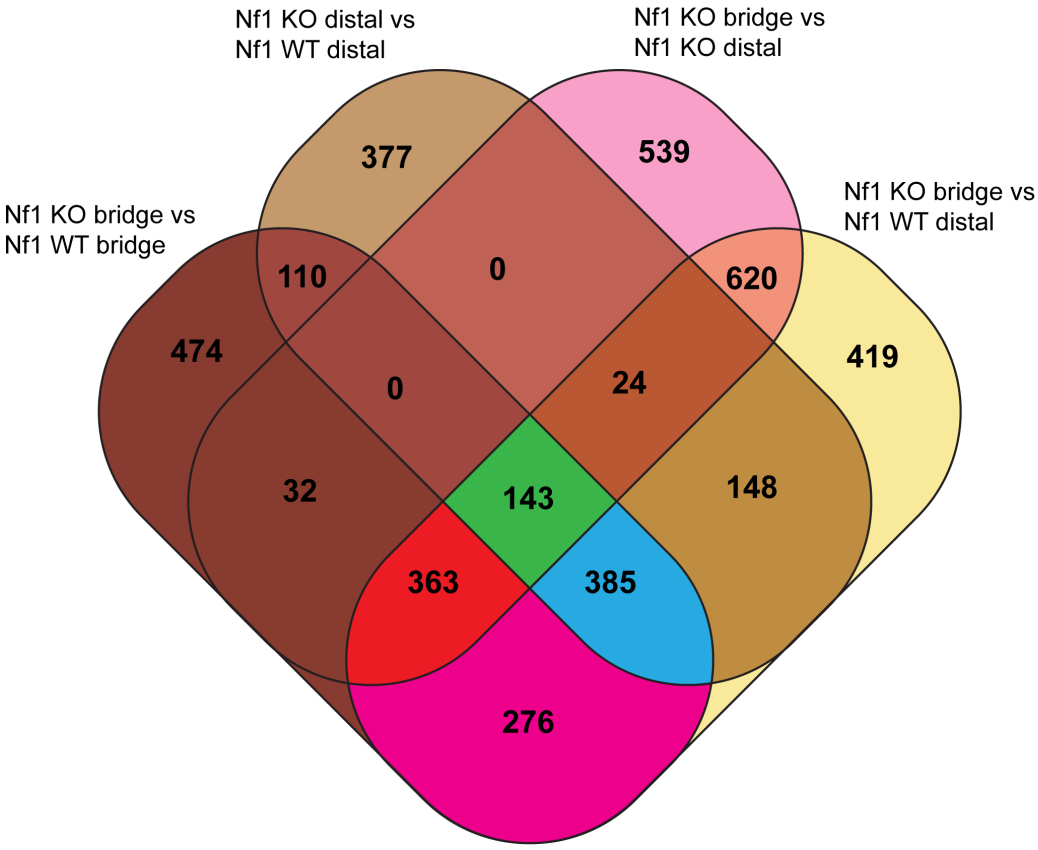

Figure 5.20. Venn diagram intersections

The Venn diagram displays the number of genes upregulated in each intersection. The differentially upregulated genes of the 4 comparisons: Nf1 KO vs Nf1 WT bridge, Nf1 KO distal vs Nf1 WT distal, Nf1 KO bridge vs Nf1 distal and Nf1 KO bridge vs Nf1 WT distal, were intercalated in order to obtain the genes exclusively upregulated in the Nf1 KO bridge (red Intersection). The red Venn diagram section contains the 363 genes, which are exclusively upregulated in the Nf1 KO bridge compared to the other regions, whereas the green intersection contains the 143 genes that are highly expressed in the Nf1 KO bridge, but these genes are also differentially regulated between Nf1 KO and Nf1 WT distal stump. The intersection highlighted in blue (385 genes) and the intersection in pink (276 genes) contains the genes that are highly expressed in both Nf1 KO bridge and distal stump.

constitute the tumour-promoting environment within the Nf1 KO bridge. We have selected genes from the red and the green Venn diagram intersections. Furthermore, we selected genes from the blue (eg. Cytokines CX3CL1 and CXCL14) and pink (eg. cytokine IL6) Venn diagram intersections that contain the genes highly expressed in both regions in the Nf1 KO animals, but expressed at a low level in the Nf1 WT animal.

Table 5.5 and Figure 5.21 display the genes that we have selected from the different Venn diagram intersections. For each gene and sample, the normalised gene reads and the log2 fold changes are displayed for each of the comparisons used in the Venn diagram. The fold change (FC) cut off was set at of 1.5 (log_2 fold change ~ 0.58). Out of these selected candidates, the ECM proteins, CILP and Spondin 1 (SPON1), tumour necrosis factor 18 (TNSF18) and the secreted protein ESM1 were found to be the most highly differentially expressed genes in the Nf1 KO bridge compared to the other conditions. Edil3, is underneath the determined FC cut off of 1.5 in the comparison Nf1 KO bridge to Nf1 KO distal, but was kept it for further validations as it is reported to be expressed in certain cancers and can initiate neo-angiogenesis (Aoka et al., 2002; Beckham et al., 2014; Jiang et al., 2016; Lee et al., 2016; Zou et al., 2009). In this table, we also display cell-cycle related genes to confirm our previous findings. We observed high expression of cell cycle related genes such as cyclin B2 and growth factors such as IGF1 in the Nf1 KO bridge samples. Nevertheless, the cell-cycle related genes have not been included in further validations, as they represent downstream consequences of the pro- tumourigenic signals within the Nf1 KO tumour microenvironment. Furthermore, we also investigated whether TGFβ1 and TGFβ2 are more highly expressed in the Nf1 KO bridge compared to the other areas as it is a known SC mitogen (D'Antonio et al., 2006; Lamouille et al., 2014; Mirsky et al., 2008) and recently TGFβ signalling has been shown to be responsible for reprogramming SCs within the nerve bridge to an invasive mesenchymal cell- type (Clements et al., 2017). As shown in Table 5.5 and Figure 5.21 TGFβ1 was found to be equally expressed in most regions, except for its low expression in the Nf1 WT bridge. Interestingly, in contrast, TGFβ2 was more highly expressed in both Nf1 KO and Nf1 WT bridges compared to both distal stump regions. This is in agreement with a recent study that demonstrated a specific role for TGFβ2 within the nerve

A **Differentially upregulated 363 genes of Venn diagram intersection "red"**

genes that are exclusively upregulated in the Nf1 KO bridge

PANTHER GO- Biological Process	# of genes in Mus musculus reference	# of genes in dataset	expected	Fold Enrichment	raw P-value	FDR
cell growth	98	7	1.57	4.45	1.39E-03	2.62E-02
DNA replication	140	10	2.25	4.45	1.40E-04	5.70E-03
Mitosis	204	10	3.27	3.06	2.22E-03	3.61E-02
Nervous system development	307	15	4.92	3.05	2.02E-04	7.05E-03
System development	474	19	7.6	2.5	3.47E-04	1.06E-02
Cellular component movement	484	17	7.76	2.19	3.04E-04	4.37E-02
Cell cycle	650	22	10.42	2.11	1.33E-03	2.70E-02
developmental processes	1514	50	24.28	2.06	2.38E-06	5.81E-04
Intracellular protein transport	650	21	10.42	2.01	3.87E-03	4.72E-02
protein transport	684	22	10.97	2.01	2.93E-03	4.46E-02
phosphate-containing compound metabolic process	1571	44	25.19	1.75	3.81E-04	1.03E-02
nucleobase-containing compound metabolic process	2710	63	43.46	1.45	3.26E-03	4.19E-02
metabolic process	6009	122	96.36	1.27	3.21E-03	4.35E-02

B

Differentially upregulated 385 genes of Venn diagram intersection "blue"

PANTHER GO-Slim Biological Process	# of genes in Mus musculus reference	# of genes in dataset	expected	Fold Enrichment	raw P-value	FDR
chromatin assembly	30	7	0.5	13.93	2.10E-06	1.28E-04
organelle organization	1133	36	18.98	1.9	3.33E-04	6.76E-03
regulation of gene expression, epigenetic	72	7	1.21	5.8	3.27E-04	7.25E-03
protein glycosylation	103	8	1.73	4.64	5.10E-04	8.29E-03
chromatin organization	258	19	4.32	4.4	1.96E-07	4.78E-05
cellular defense response	128	9	2.14	4.2	4.58E-04	7.98E-03
cell-cell adhesion	157	9	2.63	3.42	1.79E-03	2.42E-02
cell adhesion	359	21	6.02	3.49	1.57E-06	1.92E-04
biological adhesion	359	21	6.02	3.49	1.57E-06	1.28E-04
DNA metabolic process	345	17	5.78	2.94	1.18E-04	3.21E-03
developmental process	1514	47	25.37	1.85	7.23E-05	2.21E-03
signal transduction	2896	71	48.52	1.46	1.11E-03	1.59E-02
cellular process	8762	183	146.81	1.25	1.79E-04	4.36E-03

C **Differentially upregulated 276 genes of Venn diagram intersection "pink"**

PANTHER GO-Biological Process	# of genes in Mus musculus reference	# of genes in dataset	expected	Fold Enrichment	raw P-value	FDR
chromatin assembly	30	7	0.36	19.53	2.25E-07	1.83E-05
organelle organization	1133	37	13.54	2.73	4.73E-08	5.78E-06
cellular component organization	1961	41	23.43	1.75	4.71E-04	7.19E-03
cellular component organization or biogenesis	2099	43	25.08	1.71	6.72E-04	8.20E-03
chromosome segregation	86	9	1.03	8.76	1.89E-06	1.15E-04
meiosis	59	6	0.7	8.51	1.18E-04	2.88E-03
cell cycle	650	23	7.77	2.96	5.63E-06	2.29E-04
DNA recombination	51	5	0.61	8.21	5.16E-04	7.00E-03
DNA metabolic process	345	20	4.12	4.85	1.54E-08	3.75E-06
nucleobase-containing compound metabolic process	2710	58	32.38	1.79	1.21E-05	3.69E-04
primary metabolic process	4839	79	57.82	1.37	2.72E-03	2.89E-02
metabolic process	6009	99	71.8	1.38	2.95E-04	4.80E-03
regulation of cell cycle	175	11	2.09	5.26	1.40E-05	3.79E-04
DNA repair	153	9	1.83	4.92	1.37E-04	3.04E-03
mitosis	204	12	2.44	4.92	1.07E-05	3.74E-04
chromatin organization	258	14	3.08	4.54	4.80E-06	2.34E-04
cytoskeleton organization	365	12	4.36	2.75	1.85E-03	2.15E-02
regulation of nucleobase-containing compound metabolic process	560	15	6.69	2.24	4.63E-03	4.71E-02
nitrogen compound metabolic process	2462	46	29.42	1.56	2.27E-03	2.52E-02

Table 5.4. Gene ontology term enrichment analysis of Venn diagram intersections
These tables display the gene enrichment analysis performed on the gene lists of the 5 different Venn diagram intersections. Only biological functions that were statistically significant (Fisher exact Test) and which had a fold enrichment value > 1.5 are shown. Subcategories are indicated by surrounding boxes and separating dashed lines. Gene enrichment analysis was performed on: **A)** Venn diagram intersection highlighted in red which contains the 363 genes which are exclusively upregulated in the Nf1 KO bridge. Note that cell cycle and cell division are among the most enriched functional annotations in this region. **B+C)** Venn diagram intersection highlighted in blue (385 genes) and pink (276 genes), which contains the genes upregulated in both Nf1 KO bridge and Nf1 KO distal stump. Note that no statistically significant enriched gene classes were found within the green Venn diagram intersection.

Gene name	Mean normalised Nf1 WT distal reads	Mean normalised Nf1 KO bridge reads	Mean normalised Nf1 KO distal reads	Mean normalised Nf1 WT bridge reads	Log_2 fold change Nf1 bridge vs Nf1 distal	Log_2 fold change Nf1 bridge vs Nf1 WT bridge	Log_2 fold change Nf1 distal vs Nf1 WT distal	Log_2 fold change Nf1 bridge vs Nf1 WT distal
CILP	2788	24157	5738	6312	1.499	1.405	-	2.178
EDIL3	472	744	553	345	0.401	1.022	-	0.611
ESM1	34	277	75	73	1.153	1.183	-	1.705
SLITRK6	262	599	224	263	1.271	1.063	-	1.072
SPOCK3	34	76	24	31	1.335	1.036	-	0.965
SPON1	254	1107	362	343	1.184	1.237	-	1.533
TNFSF18	17	68	32	14	0.853	1.626	-	1.447
CX3CL1	157	256	254	111	-	1.034	0.603	0.616
CXCL14	1966	4730	4693	1952	-	1.234	1.215	1.226
CCNB2	454	969	641	456	0.568	1.031	0.476	1.043
IGF1	3641	9769	5053	5477	0.934	0.819	0.464	1.398
ITGAE	69	223	123	79	0.763	1.333	0.707	1.469
VCAN	1385	5872	2588	2566	1.106	1.117	0.839	1.945
EMILIN1	1075	1635	1511	763	-	0.977	-	0.543
IL6	25	97	40	14	-	1.08	-	0.862
TGFβ1	539	599	595	364		0.651		
TGFβ2	147	318	136	260	0.919			0.838

Table 5.5. Overview of selected genes, which are more highly expressed in the Nf1 KO bridge

In this table, the means of the normalised reads are displayed for each gene in each sample. The log_2 fold changes are shown for all the comparisons, which have been used to obtain the Venn diagram. The genes are coloured according to the Venn diagram intersection from which they have been obtained and are sorted according to their colour. CILP, SPON1, TNSF18 and ESM1 are the most differentially expressed genes within the Nf1 bridge compared to the other conditions. All the displayed genes, except for the cell cycle related gene CCNB2 (cyclin B2), are secreted proteins, cytokines or ECM proteins.

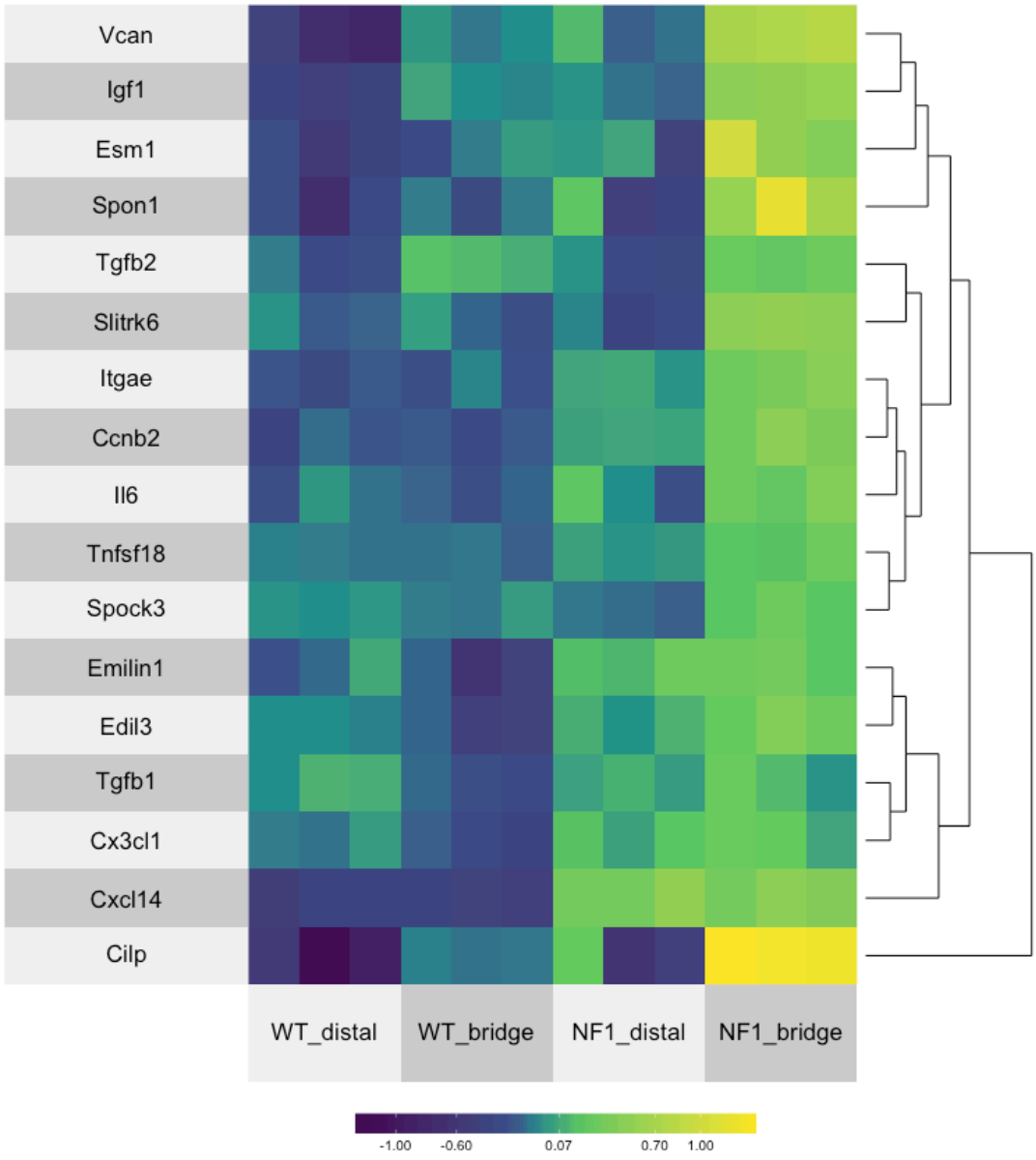

Figure 5.21. Heatmap of selected genes which are upregulated in Nf1 KO bridge
This heatmap displays the expression values of the 14 selected genes that are upregulated in the Nf1 KO bridge. Moreover, TGFβ1 and TGFβ2 and cell cycle protein CCNB2 (Cyclin B2) are also displayed in this heatmap. The Colour corresponds to per-gene z-score that is computed from the Deseq2 transformed counts (specifically rlog). The *z* -score scale represents mean-subtracted regularised log-transformed read counts. For each gene the distance of each sample from the mean for all samples was calculated and the order of the genes was obtained with hierarchical clustering. Figure was generated by Dr. Christina Venturini using superheat (https://github.com/rlbarter/superheat).

bridge region (Clements et al., 2017).

The complete tables of all differentially regulated genes are shown in the Appendix of this thesis. We are also interested in the genes, which are underexpressed in the Nf1 KO bridge as those genes could promote normal nerve repair in the distal stump (anti-tumourigenic properties). A detailed analysis of the underexpressed genes will be undertaken in the future but are outside the scope of this thesis.

In summary, we have selected two main classes of molecules from the differentially expressed genes of the different Venn diagram intersections: 1. Extracellular matrix proteins such as CILP, F-Spondin 1 (SPON1) and Versican (VCAN) and 2. Cytokines such as Il6, CXCL14 and CX3CL1 (Table 5.5 and Figure 5.21). Furthermore, we also selected secreted proteins such as growth factor (IGF1), soluble proteoglycan (ESM1) and integral membrane protein SLITRK6 for further validation.

5.10.6. Validation of the RNA seq. dataset

In order to validate the differential expression of the candidates identified by the RNA seq. analysis, we performed qRT-PCR analysis on freshly isolated nerve fragments from both genotypes. In contrast to the RNA seq analysis, we isolated RNA from single animals for the qRT- PCR analysis. We investigated the expression of 14 genes and confirmed a statistical significant upregulation of 9/14 candidates in the Nf1 KO bridge, although the others also showed a trend of being more highly expressed in the Nf1 KO bridge (Figure 5.22 and 5.23). Out of the 4 cytokines analysed, we confirmed CXCL14, IL6 and TNSFF18 and out of the 7 ECM proteins, we confirmed CILP, EDIL3, SPON1 and VCAN as significantly upregulated in the Nf1 KO bridge (Figure 5.22 and 5.23). Additionally, we confirmed high RNA expression of the growth factor IGF1 and integral membrane protein SLITRK6 in the Nf1 KO bridge samples (Figure 5.23). In future experiments, the function of the identified candidates will be assessed.

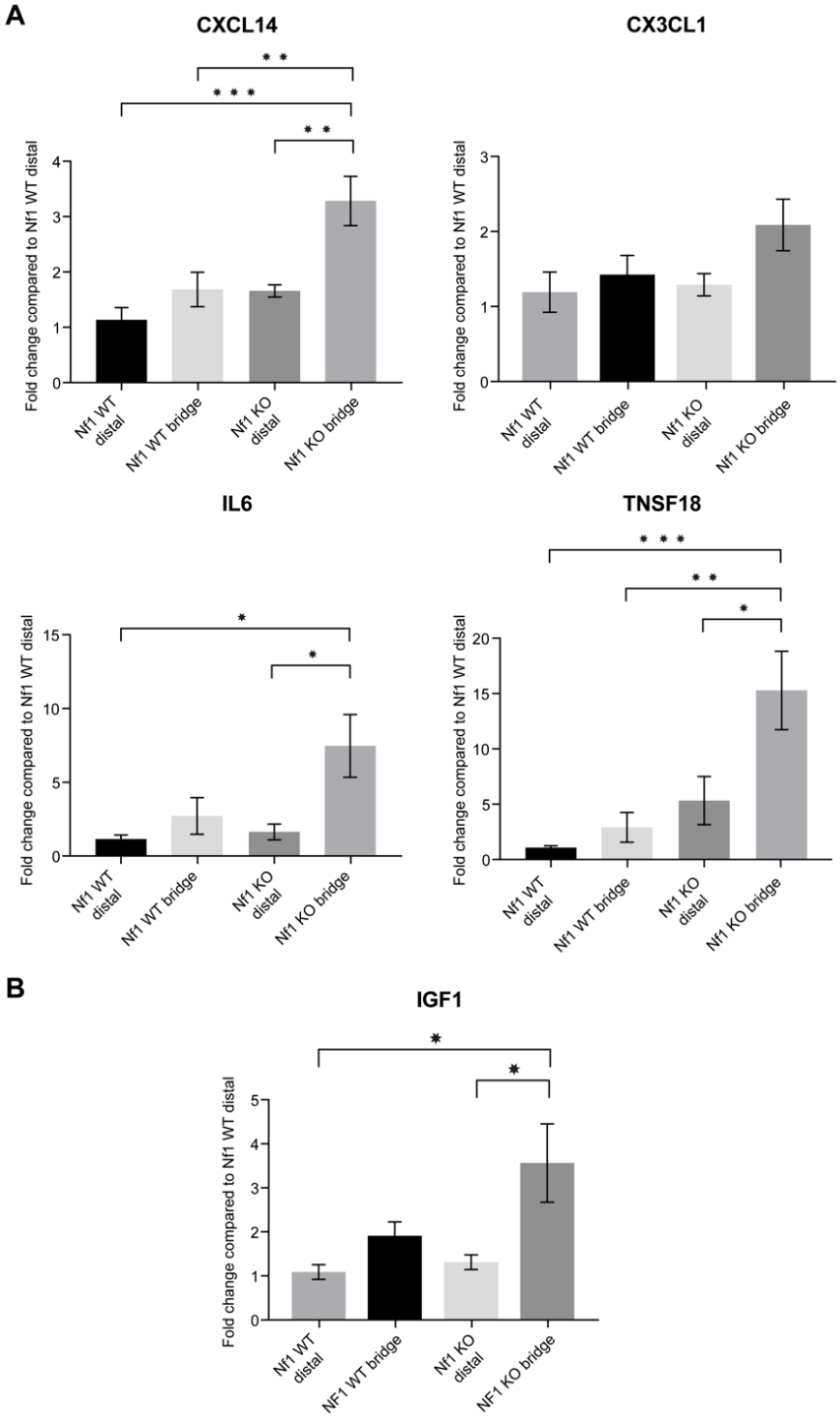

Figure 5.22. qRT-PCR analysis confirms upregulation of cytokines exclusively in the bridge of the Nf1 KO mice

Validation of RNA expression of **A)** 4 cytokines (CX3CL1, CXCL14, IL-6 and TNFSF18) and **B)** 1 growth factor, IGF1 by qRT-PCR. Graphs shows that out of the 4, 3 cytokines (CXCL14, IL-6 and TNFSF18) were confirmed as significantly higher expressed in the Nf1 KO bridge compared to the other conditions. Growth factor IGF1 was also observed as upregulated in the Nf1 KO bridge, whereas CX3CL1 did not reach statistical significance probably due to high variation between the animals. Bars show the mean ±SEM for 8 independent experiments. Fold change was compared to Nf1 WT distal sample. Statistics: Two way ANOVA followed by Sidaks multiple comparison test.

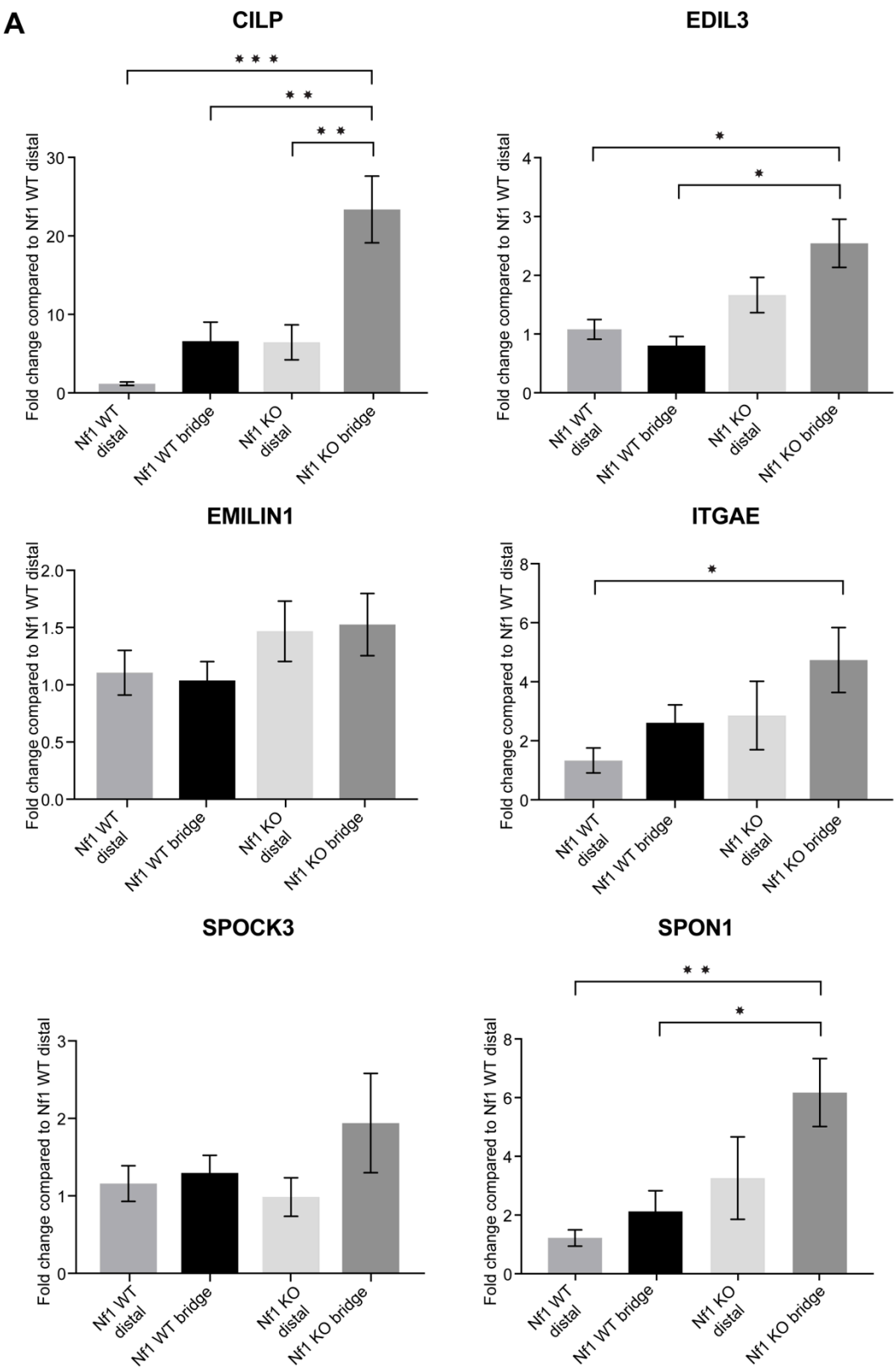
A
CILP
EDIL3
EMILIN1
ITGAE
SPOCK3
SPON1
Fold change compared to Nf1 WT distal
Nf1 WT distal
Nf1 WT bridge
Nf1 KO distal
Nf1 KO bridge

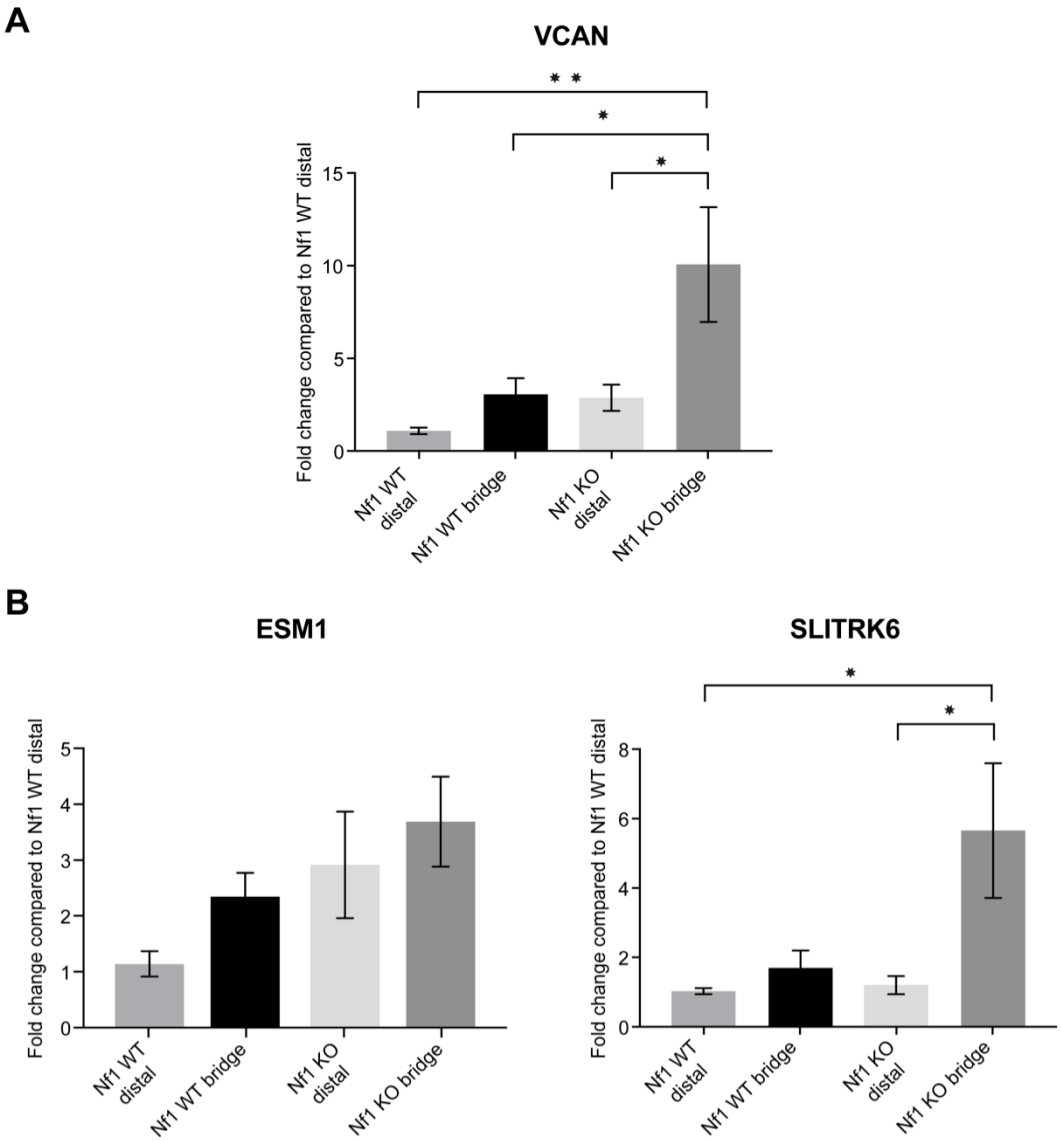

Figure 5.23. qRT-PCR analysis confirms upregulation of (A) ECM proteins and (B) Integral membrane protein SLITRK6 in the bridge of the Nf1 KO mice

Validation of RNA expression of **(A)** 7 ECM proteins (CILP, EDIL3, EMILIN1, ITGAE, SPON1, SPOCK3 and VCAN) and **(B)** integral membrane protein SLITRK6 and secreted protein ESM1 by qRT-PCR. Graphs shows that 4 out of 7 ECM proteins (CILP, EDIL3, SPON1 and VCAN) and integral membrane protein SLITRK6 were confirmed as significantly higher expressed in the Nf1 KO bridge compared to the other conditions. Bars show the mean±SEM for 8 independent experiments. Fold change was compared to Nf1 WT distal sample. Statistics: Two way ANOVA Sidaks multiple comparison test.

5.11. Chapter discussion and conclusions

5.11.1. Investigation of cellular behaviour at the early stages of Nf1 KO tumour formation

In this chapter, we have investigated both the early cellular changes of tumour driving Nf1 KO cells and of stromal cells, such as inflammatory cells, in order to characterise the cellular environment and to select a timepoint to perform a molecular analysis when the cellular behaviour is different at the injury site compared to the distal stump. The ultimate aim was to both characterise the early cellular behaviour associated with tumour formation and to determine the signals from the microenvironment responsible for promoting the development of the tumour.

The generation of transgenic mouse models has led to the identification of many pro-tumourigenic signals such as Wnt signalling that has been shown to have an important role in driving colorectal cancer initiation (Bienz and Clevers, 2000; Groden et al., 1991; Korinek et al., 1997). Whilst Wnt was identified as an early signal, colorectal cancer progression requires the progressive acquisition of other mutations (eg. Activating mutations in proto-oncogene Ras) at later stages (Fearon, 2011). The Nf1 KO mouse model provides an excellent model to study the early stages of tumour formation as we can select the animals prone to tumour formation. Furthermore, as tumours only develop at the injury site it allows us to compare the pro-tumourigenic behaviour of the Nf1 KO SCs in this area to their normal regenerative behaviour in the distal stump. Importantly, the tumour clonality analysis that was shown in Chapter 4 showed that the Nf1 KO SC do not appear to require additional mutations to drive tumourigenesis at the injury site. This result further underlines the important contribution of signals from the Nf1 KO injury microenvironment to tumour initiation and implies the importance of their identification for new therapeutic approaches.

As an initial parameter, we investigated cell proliferation and found that total cell proliferation was enhanced in the Nf1 KO mice in the regenerating part of the nerve, at Day 3 following injury. This indicates that the loss of Nf1 in a subpopulation of mSCs changes the overall proliferative response after injury. Importantly, we observed that the Nf1 KO SCs maintained a higher level of proliferation at the injury site at Day 14 following injury, whereas similar cells

proliferated as control SCs in the distal stump. This finding shows that a hyperproliferative lesion develops at the injury site very early following the injury response, which is associated with an apparent failure of the Nf1 KO SCs to behave normally as the injury response resolves. As the Nf1 KO SCs are genetically identical in both areas, this finding indicates that pro-tumourigenic signals at the site of injury or anti- tumourigenic signals in the distal stump are influencing their proliferative behaviour. Interestingly, *in vitro,* Nf1 KO SCs devoid of axonal contact showed increased proliferation when exposed to cell culture serum suggesting that the serum may mimic the wound microenvironment (Parrinello et al., 2008).

Overall, we have identified the timepoint at which Nf1 KO behaviour differs from control SCs and it will be of great interest to determine the interactions of the Nf1 KO SCs with their adjacent microenvironment in future studies. Particularly, as discussed in Chapter 6, we are highly interested in axonal interactions, as the proliferating Nf1 KO SCs may escape the anti-proliferative signals of the axons and may instead closely interact with other cell types within the nerve bridge.

Consistent with the increase in tissue size at the Nf1 KO injury site, we also found that macrophages and NG2+ cell density is increased in this region. Specifically, elevated numbers of macrophages were found and these cells may secrete factors that could contribute to a pro-tumourigenic microenvironment in this region. In future experiments, we will determine whether Nf1 KO SCs interact with these two cell types and whether these interactions may promote Nf1 KO SC proliferation. In order to do so, we can isolate these cells types from the Nf1 KO bridge and co-culture them with Nf1 KO SCs. The isolation of macrophages will be done via immunopanning, as we have previously established this technique to isolate macrophages from the injured nerve in the lab (L. van Emmenis) and the NG2+ cells can be isolated from mice that express dsRed under the NG2 promoter (NG2-dsRed mice, see Chapter 4).

We also investigated the temporal activation of ERK at the early timepoints following injury and consistent with our previous studies, which showed that high levels of p-ERK were associated with SC dedifferentiation (Harrisingh et al., 2004; Napoli et al., 2012), we found high levels of p-ERK at the early stages following injury. These high levels of ERK activation

likely decrease to lower levels that are sufficient to sustain SC proliferation and allow remyelination of the injured nerve. These low levels may not be detectable via immunofluorescence staining at Day 14 following nerve injury, however, a previous study showed that pERK is still detectable by Western Blot in the distal (D1 and D2) and in the proximal stump (P1) at Day 16 post injury (Sheu et al., 2000), demonstrating that ERK is activated at lower levels at the later timepoints following injury.

5.11.2. RNA seq analysis

In the second part of this chapter, I described the RNA seq. analysis that was performed in an attempt to identify either pro-tumourigenic signals or tumour-suppressive signals of the injury microenvironment and distal stump respectively at the early stages of neurofibroma formation. This analysis has identified several genes as being differentially regulated in the different conditions. We selected genes that are upregulated exclusively in the Nf1 KO bridge or upregulated in both the bridge and distal stump of the Nf1 KO animal for further investigation. Moreover, we have selected mainly ECM proteins, cytokines and other secreted proteins, as these genes most likely constitute the tumour-promoting environment. In the two paragraphs below, I discuss the genes identified within these two categories and their potential impact on neurofibroma formation.

5.11.2.1. Cytokine and chemokine expression is increased in the Nf1 KO injury site

The earliest evidence that the tumour microenvironment plays a critical role in tumourigenesis was the observation that chronic inflammation is associated with tumour formation in many cancers (~20%) and even the cancers, which lack a causal role for chronic inflammation, possess an inflammatory microenvironment that exhibits high cytokine expression (Elinav et al., 2013; Grivennikov et al., 2010; Grivennikov and Karin, 2011; Mantovani et al., 2008). Later studies then demonstrated that inflammatory responses play key roles in tumourigenesis including in tumour initiation, promotion, progression and metastasis (Grivennikov et al., 2010; Hanahan and Weinberg, 2011). Cytokines, that are the main

mediators of the inflammatory response, have been shown to link the wound healing inflammatory response with carcinogenesis and may provide potential therapeutic and preventive targets. Moreover, cytokines are known to possess a dual role in tumourigenesis and these pro- and anti-tumourigenic signals co-exist in developing tumours. However, if the tumour is not rejected, the pro-tumourigenic signals will dominate and contribute to promote growth, invasion and survival of the established tumour by activating many pro-tumorigenic signalling pathways such as AKT, ERK, NF-kB and JAK/STAT (Coussens and Werb, 2002; Hanahan and Weinberg, 2011; Pickup et al., 2014). Consequently, tumour formation and progression is sustained by complex bidirectional interactions between cancer cells and inflammatory cells, in which cytokines can activate critical signalling pathways in cancer cells that in turn can produce chemokines which attract more inflammatory cells into the tumour (Elinav et al., 2013). Furthermore, the production of cytokines by inflammatory and immune cells provides a constant supply of growth factors and survival signals for the cancer cells (Grivennikov et al., 2010; Mantovani et al., 2008).

We have identified three cytokines, IL6, CXCL14 and tumour necrosis factor 18 (TNSF18) as significantly upregulated in the Nf1 KO bridge at Day 14 following injury. The cell type expressing these cytokines has not been identified, but it has been shown previously that the IL6-receptor is expressed by SCs (Ito et al., 2010; Lara-Ramirez et al., 2008). IL6 is one of the best characterised pro-tumourigenic cytokines and is commonly found in tumour microenvironments (Grivennikov and Karin, 2011). After binding to its receptor, the activated IL6 receptor complex signals downstream to JAK/STAT, PI3K-AKT and ERK signalling pathways (Ito et al., 2010; Reichert et al., 1996; Yao et al., 2014). IL6 expression was previously detected during sciatic nerve regeneration *in vivo* and *in vitro* (Bolin et al., 1995; Fregnan et al., 2012) and consistent with this the IL6-receptor was found expressed in dedifferentiated SCs (Parrinello et al., 2008), indicating that dedifferentiated Nf1 KO SCs may be sensitive to IL6 exposure. Interestingly, it was shown that plasma soluble levels of IL6 are upregulated in NF1 cancer patients (Park et al., 2013; Torres et al., 2016) but the relevance of this remains unknown. IL6 is well known as one of the major components of the senescence associated secretory phenotype (SASP) and is associated with oncogenic stress induced

senescence in various cell types (Coppe et al., 2008; Kuilman et al., 2008), whereas in other tissues, IL6 mediated activation of STAT3 can stimulate pre-malignant cell proliferation and inhibits apoptosis at the early stages of tumourigenesis (Bollrath et al., 2009; Waldner et al., 2012). Consistent with this, a recent study demonstrated that STAT3 acts as oncogene by driving neurofbroma initiation in the Dhh-Cre:$Nf1^{fl/fl}$ mouse model (Wu et al., 2016). Further studies support the potential pro-tumourigenic role of STAT3 in the context of *Nf1* loss in NF1 (Banerjee et al., 2010) and in malignant peripheral nerve sheath tumour formation (MPNSTs) (Banerjee et al., 2010; Wu et al., 2014). In MPNSTs, EGFR activation induced the activation of STAT3, whereas the upstream activator remains to be identified. However, it may be that IL6 is fulfilling this role, but this hypothesis requires further testing.

CXCL14 (also called BRAK) belongs to the CXC chemokine family (Shellenberger et al., 2004). CXCL14 was originally defined as a tumour suppressor, as it was shown to recruit anti-tumourigenic leukocytes such as dendritic and neutral killer (NK) cells (Shurin et al., 2005; Starnes et al., 2006). In addition to its known role as a tumour suppressor, CXCL14 has recently been reported to be overexpressed in pancreatic cancer and colorectal carcinoma and was associated with a more aggressive, invasive phenotype and with disease recurrence (Wente et al., 2008; Zeng et al., 2013). This suggests that CXCL14 can act either as a pro- or anti-tumourigenic factor.

TNFSF18, also known as GITRL (Kim et al., 2003) is a transmembrane protein of the tumour necrosis factor superfamily that is mainly expressed by antigen presenting cells including DCs and macrophages and is involved in the regulation of diverse immune system functions (Nocentini and Riccardi, 2009). The role of TNFSF18 in tumourigenesis is not well studied, but it has been shown to be expressed at a high level by cancer cells and can diminish NK cell anti-tumour immunity (Baltz et al., 2008; Baltz et al., 2007).

5.11.2.2. Upregulation of embryonic ECM proteins in the Nf1 KO injury site

In recent years, it has become evident that the tumour microenvironment plays an important role in regulating cancer cell behaviour. To date, the main focus has been set on the cellular components of the microenvironment, however, the impact of the ECM has recently been

recognised (Erler et al., 2009; Erler et al., 2006; Levental et al., 2009). Furthermore, tumours resemble wounds that have not healed and consequently the tumour stroma is similar to the microenvironment that is associated with an unrepaired wound (Bissell and Radisky, 2001; Egeblad et al., 2010). In both, ECM deposition is elevated and results in increased tissue density and stiffness. Elevated ECM deposition or increased tissue stiffness can activate several signalling pathways such as AKT and ERK signalling pathways in adjacent cancer cells (Levental et al., 2009; Provenzano et al., 2009). Furthermore, ECM organisation is altered compared to a normal tissue stroma and the expression of ECM remodelling enzymes is deregulated in various cancers (Egeblad et al., 2010; Frantz et al., 2010; Lu et al., 2011). The ECM, similar to its role in tumourigenesis, is fundamental for many major developmental processes such as branching morphogenesis and bone development (Lu et al., 2011; Rebustini et al., 2009; Stickens et al., 2004). One of the characteristic features of cancer cells is the reactivation of developmental signalling pathways such as Wnt, Hedgehog and Notch pathways in adult cells. These developmental signalling pathways are often deregulated in cancer and increase tumour growth, metastasis, invasion and can initiate the recruitment of stromal cells (Aiello and Stanger, 2016; Bolos et al., 2007; Dempke et al., 2017; Giles et al., 2003; Nwabo Kamdje et al., 2017; Polakis, 2007; Radtke and Raj, 2003).

The expression of three of the four identified ECM proteins EDIL3, F- Spondin 1 (SPON1) and Versican (VCAN) is restricted within adult tissue and they have been reported to mainly play regulatory roles during embryonic development. Consequently, the upregulation of EDIL3, SPON1 and VCAN may indicate the pro-tumourigenic reactivation of developmental signalling pathways in the Nf1 KO bridge.

SPON1 is a secreted extracellular matrix protein which is known to be highly expressed in the floor plate during development and has been shown to promote neural adhesion and neurite extension (Klar et al., 1992). Additionally, it was shown to be expressed in certain cancer stromas such as in breast cancer stroma (Casey et al., 2009), but as it is relatively poorly studied, the mechanisms of action of SPON1 are not yet known.

VCAN is a chondroitin sulfate proteoglycan (CSP), which has been shown to be involved in cell adhesion, and its expression is associated with a proliferative cell phenotype during

development and in a variety of tumours, including breast, brain, prostate and melanoma, in which VCAN expression was shown to correlate with greater tumour invasion and poor disease-specific survival (Shen et al., 2015; Wight, 2002). In the CNS, CSPGs have been found associated with the ECM of reactive astrocytes, whereas in the PNS they are expressed in the ECM of dedifferentiated SCs (Castro and Kuffler, 2006). In contrast to the CNS, where CSPG expression prevents axonal regrowth, in the PNS it only delays axonal regeneration following injury (Zuo et al., 2002). The elimination of CSPGs *in vivo* can be achieved by using an CSPG synthesis inhibitor (eg. beta-D- xyloside) or by enzymatic digestion (Bradbury et al., 2002; Moon et al., 2001; Zuo et al., 1998a) and it was demonstrated previously that injection of the enzyme chondroitinase ABC effectively degraded CSPGs following nerve transection and resulted in enhanced axonal regeneration in the PNS (Zuo et al., 1998b; Zuo et al., 2002).

EDIL3 is a secreted ECM protein that acts as an integrin ligand and was shown to be involved in angiogenesis and cell invasion by activating ERK and TGFβ signalling (Hidai et al., 1998; Rezaee et al., 2002; Xia et al., 2015). Importantly, EDIL3 acts as an embryonic angiogenic factor during development and similarly to VCAN and SPON1 was found to be re-expressed in cancers (Beckham et al., 2014; Lee et al., 2016). The re-expression of EDIL3 in cancers may facilitate neoangiogenesis and cancer invasion as shown previously (Beckham et al., 2014; Lee et al., 2016) and downregulation of EDIL3 can attenuate tumour growth by decreasing cancer cell proliferation and increasing cancer cell apoptosis (Aoka et al., 2002; Jiang et al., 2016; Zou et al., 2009).

In addition to the three ECM proteins associated with the reactivation of developmental signalling programs, CILP, was identified as the most highly upregulated ECM protein in the Nf1 KO bridge. However, CILP is relatively poorly studied and has mostly been described to be abundant in cartilaginous tissue. Functionally, it may regulate TGFβ signalling by antagonising TGFβ1 signalling (Mori et al., 2006; Seki et al., 2005), which may partially explain why we have not identified TGFβ signalling as significantly differentially regulated in the Nf1 KO bridge (Mori et al., 2006; Seki et al., 2005). However, this hypothesis will require further validation.

Lastly, we confirmed the increased expression of insulin growth factor (IGF1) and SLITRK6 that is a poorly characterised integral membrane protein, within the Nf1 KO bridge.

Insulin-like growth factor 1 (IGF1) is a well-known neurotrophic factor in the CNS and PNS that activates several signalling pathways such as PI3K/AKT and MAPK that are instrumental for tumour development and progression (Pollak, 2008, 2012). Interestingly, we showed previously that IGF1 stimulates SC biogenesis and in synergy with NRG1 increases SC proliferation and drives mitochondrial biogenesis *in vitro* (Echave et al., 2009). Consequently, it is of interest that high levels of IGF1 are associated with tumour formation at the Nf1 KO injury site.

SLITRK6 is an integral membrane protein with extracellular sequence homologies to Slit and intracellular sequence homologies to Trk neurotrophin receptors, which both are well known to regulate axon guidance during development. (Aruga and Mikoshiba, 2003; Aruga et al., 2003; Tekin et al., 2013). SLITRK6 is predominantly expressed in the CNS, where it regulates neurite outgrowth and survival during neural development (Aruga and Mikoshiba, 2003; Aruga et al., 2003; Tekin et al., 2013). Furthermore, it was also found to be expressed in the adult brain, but its functional role is not yet understood. Although SLITRK6 is not secreted, it could be involved in neurofibroma formation, as it is not expressed in the healthy PNS and has recently been reported to be expressed at high levels in certain cancers, including brain cancers such as glioblastoma (Aruga et al., 2003; Morrison et al., 2016).

5.11.2.3. Identification of functional role of candidates in future experiments

In future experiments, the functional role and cellular origin of the selected candidate (s), which are discussed above, will be investigated. Initially, the functional role of the candidates will be investigated *in vitro* by determining their impact on SC proliferation, SC-axon association and differentiation. We have established an *in vitro* co-culture system of primary rat postnatal dorsal root ganglion (DRGs) and SCs (Parrinello et al., 2008), which resembles their normal interactions in the PNS. This *in vitro* model will be used 1) to stimulate Nf1 KO and control SCs with IL6, CXCL14 and TNSF18 and other highly expressed secreted proteins such as secreted ECM proteins EDIL3 and SPON1 and 2) to inhibit the identified candidate

(s) by either knockdown of the protein or chemical inhibition. Furthermore, the potential pro-tumourigenic role of the identified ECM proteins VCAN and CILP will be tested by pre-coating culture dishes prior to seeding Nf1 KO and control (Nf1 WT) SCs and the impact on SC proliferation and differentiation will be analysed.

Following any interesting observations, we will identify the cell types expressing the candidates *in vivo* by performing immunofluorescence (IF) stainings or in situ hybridisation together with well-established markers for specific cell types. Alternatively, candidate RNA/protein expression levels can be analysed by isolating the different cell types by FACS or immuno-panning techniques. Furthermore, we will inhibit the candidates by either using transgenic knock-out mouse models or pharmalogical inhibition of the protein and will investigate whether it affects SC proliferation at the early stages and results in reduced neurofibroma formation in the Nf1 KO mouse model.

Following a striking effect upon candidate inhibition on neurofibroma formation, we would determine the clinical relevancy of the candidate by analysing its expression level in human neurofibromas compared to human peripheral nerve. In order to do so, our lab has previously established a successful collaboration with a leading UCL pathologist, Prof. Adrienne Flanagan, a worldwide expert on sarcomas, who can provide us with frozen tissue from human peripheral nerve, neurofibromas and malignant peripheral nerve sheath tumours.

5.11.2.4. Comparison of RNA seq analysis with previously performed microarray analysis

We have compared the candidates from the differential expression analysis of our RNA seq. dataset with a microarray analysis on SCs (Parrinello et al., 2008), which carries an inducible Raf fusion protein (NSΔRafER) (Lloyd et al., 1997). These cells are activated by the addition of tamoxifen (tmx) resulting in rapid and sustained ERK activation. We re-examined this microarray analysis in order to investigate if any of the candidates from our RNA seq. screen were also upregulated in the NSΔRafER cells, which would indicate that these candidates may be expressed by dedifferentiated SCs in the nerve bridge. In line with their high expression in the Nf1 KO bridge, we found that SPON1 (16.9x) and CXCL14 (6x) were both

highly upregulated in the NSΔRafER microarray analysis.

The identification of common candidates between the RNA seq analysis and the microarray analysis implies that CXCL14 and SPON1 are expressed by dedifferentiated Nf1 KO SCs and regulated by the Ras/Raf/ERK signalling pathway. Furthermore, it suggests that SC re-differentiation is delayed within the Nf1 KO nerve bridge as maintained Ras/Raf/ERK signalling prevents SC re-differentiation. This is somewhat in contradiction to our immunofluorescence analysis which did not identify any detectable p-ERK expression in the nerve bridge at Day 14 following injury. However, as discussed earlier, the levels to maintain SC proliferation appear much lower than those that initially drive the dedifferentiation process suggesting that the p-ERK expression levels could be too low to detect by immunofluorescence staining. Future experiments will determine whether CXCL14 and SPON1 are only expressed by dedifferentiated SC in the nerve bridge and determine how the Ras/Raf/ERK signalling pathway regulates their expression. The other candidates that were identified as highly expressed in the Nf1 KO bridge in the RNA seq. screen were not found elevated in the microarray analysis, hence they are likely to be expressed by other cells within the injury environment.

We also compared our candidates with a microarray analysis, which investigated differential gene expression in macrophages and SCs in the Dhh-Cre $Nf1^{fl/fl}$ mouse model, where Nf1 is lost during embryogenesis (Choi et al., 2017). However, Choi et al. did not identify any differentially expressed genes in isolated SCs and macrophages from 1-month-old Dhh-Cre:$Nf1^{fl/fl}$ nerves compared to these isolated from 1- month-old wild type nerves indicating that consistent with no obvious abnormalities no changes in gene expression were detected in this model at the analysed early timepoint. Choi et al. also compared human and mouse neurofibroma gene expression profiles with gene expression profiles of injured rat sciatic nerves and demonstrated that the gene expression profile of neurofibromas reassembled a wounded nerve. These findings are in agreement with the hypothesis that neurofibromas reassemble an unrepaired wound.

In conclusion, in this chapter we identified when Nf1 KO SCs start to behave differently at the injury site on their way to form tumours and we have identified several factors that were

exclusively upregulated in this region. Future studies will further characterise the early cellular changes and determine whether these factors are involved in neurofibroma formation and thereby could result in novel therapeutic approaches for the treatment of NF1.

Chapter Six: Discussion and Conclusion

6.1. Tissue cell turnover

For many years it was thought that multipotent stem cells were mainly responsible for producing new cells for tissue homeostasis and following injury. Moreover, lineage differentiation was considered a uni-directional process in which post-mitotic differentiated cells are irreversibly formed from stem cells (Biteau et al., 2011; Watt and Driskell, 2010). However, recently, it has been shown that different tissues have distinct mechanisms to maintain themselves in the adult and to repair following an injury (Ge and Fuchs, 2018; Varga and Greten, 2017; Wells and Watt, 2018). These distinct mechanisms encompass the activation of resident stem cell populations (Kondo et al., 2003; Osawa et al., 1996; Weissman, 2000), recruitment of reserve stem cell populations (Ito et al., 2005; Tetteh et al., 2016) and the dedifferentiation or transdifferentiation of differentiated cells within the tissue (Ito et al., 2007; van Es et al., 2012). The acknowledgement that differentiated cells can dedifferentiate and re-enter the cell cycle revolutionised the historical concept of lineage specification and determination and has led to the identification of tissues that use specialised cell types in order to produce new cells during tissue homeostasis and following injury.

It is not understood why tissues use different mechanisms to maintain themselves, however it was speculated that these distinct mechanisms reflect the different levels of cell turnover within tissues. For example, highly proliferative tissue such as the skin or the intestine contain continuous cycling resident stem cells to maintain tissue function (Li and Clevers, 2010; Simons and Clevers, 2011; van der Flier and Clevers, 2009). In contrast, tissues with a lower cellular turnover, such as the lung, mainly use progenitor cells to produce new cells in adulthood. Moreover, the mechanism to produce new cells can be different upon injury and can involve the recruitment of reservoir stem cells and lineage dedifferentiation of highly specialised cells. All these tissue maintenance mechanisms need to be strictly controlled to ensure tissue homeostasis and wound healing, as uncontrolled cell turnover is associated with malignant transformation and tumourigenesis (Simon and Frisen, 2007).

Here, we have performed a systematic characterisation of peripheral nerve and have identified all the cell types, which make up the endoneurium of the peripheral nerve. We did not identify a stem cell population that produces new peripheral nerve cells, instead we demonstrated that peripheral nerve possesses a distinct mechanism for maintaining homeostasis in that cells rarely turnover in the homeostatic state. We also found that the peripheral nerve is a more quiescent tissue than the CNS with most cell types proliferating rarely, whereas the main cell type of the nerve, the mSC, does not divide at all in the adult. It is particularly striking that very different mechanisms are used to maintain the myelinating cells of the PNS and CNS, in that in the CNS, the myelinating glial cells, the oligodendrocytes, are replaced throughout life by oligodendrocyte progenitor cells. In this thesis, we investigated the behaviour of mSCs in nerve repair and tumourigenesis by performing several lineage tracing studies, as discussed below.

6.2. Lineage tracing studies

Lineage tracing studies encompass the labelling of a single cell or cell population, moreover, the label will be transmitted to the cell's progeny allowing the investigation of cell fate and cell lineages over time. The most widely used technology for genetic lineage tracing studies is the Cre-loxP recombination system, which has been introduced in the Introduction of this thesis (Sauer and Henderson, 1988). This genetic labelling system has been widely used to investigate stem cell compartments and subsequent lineage differentiation in various tissues such as the intestine (Snippert et al., 2010) and epidermis (Alcolea and Jones, 2014). In the intestine, for example lineage analysis identified that Lrg5, a Wnt target gene, defines the stem cell population, which is localised in the base of the intestinal crypt and that maintains the intestine (Snippert et al., 2010). Moreover, in contrast to the intestine, a single progenitor population was shown to maintain tissue homeostasis in the interfollicular epidermis (Clayton et al., 2007), whereas upon injury a reservoir stem cell population gets activated which produces new cells (Mascre et al., 2012).

Throughout this thesis, a highly specific driver for adult mSCs allowed us to perform credible lineage analysis in order to characterise the behaviour of mSCs and to understand their

contribution to the regenerative response. Moreover, we determined the cell fate of mSCs during the regenerative response. We then compared the behaviour of normal mSCs following injury to those in a mouse model of NF1 tumourigenesis, in which tumours derive from mSCs by performing similar lineage tracing studies (Ribeiro et al., 2013).

6.2.1. Lineage tracing of mSCs following nerve injury

As discussed above, mSC are completely quiescent in homeostasis, however it is known that mSCs retain plasticity and can rapidly dedifferentiate into progenitor-like SCs following nerve injury (Cattin and Lloyd, 2016; Mahar and Cavalli, 2018). Nevertheless, it was not clear whether all mSCs possess the capacity to dedifferentiate or whether a resident or recruited stem-like compartment is responsible for producing new SCs following injury.

Here, we performed lineage tracing studies using transgenic mice that allow Cre expression to be specifically induced in mSCs: P0-CreER^{T2}:YFP and P0-CreER^{T2}:Confetti mice. Our analysis demonstrated that all adult mSCs retained the capacity to dedifferentiate and proliferate following nerve injury implying that there is no need for an additional resident or recruited stem cell population. Furthermore, we showed that mSC derived cells contribute to the regenerative response by migrating in cellular cords into the newly formed nerve bridge following injury.

It is not clear, why some tissues, especially those that possess a resident stem cell population, use dedifferentiation to produce new cells following an injury. To date, two different dedifferentiation processes have been described that are distinguished based on their extent of dedifferentiation. In the first case, dedifferentiation encompasses a smaller step back in the differentiation status of a cell such as in the intestine, in which a progenitor cell can revert to a stem cell like state following injury (Tetteh et al., 2016; van Es et al., 2012). Two different kind of progenitor cells such as the Delta-like protein 1 secretory precursor cells and the more committed enterocyte progenitor cells were shown to be able to dedifferentiate to stem cells following damage to the intestinal crypt. It is not understood why progenitor cells dedifferentiate to stem cells in tissues that possess a resident stem cell population, however speculations argue that the resident stem cells may have been damaged or that the

progenitor cells aid the stem cell population to produce new tissue cells after injury (Merrell and Stanger, 2016).

In the second case, dedifferentiation occurs from highly specialised differentiated cells into progenitor-like cells such as the dedifferentiation of adult SCs into progenitor-like SCs following nerve injury or secretory cells of the lung into stem cells after lung injury (Tata et al., 2013). In this case, dedifferentiation requires that these specialised cell types retain the plasticity to dedifferentiate and involves the reversal of these differentiated cells to a cell state that is similar to a developmental cell state. This reversal process is associated with complex phenotypic and gene expression profile changes and in most cases involves re- entering the cell cycle (Jopling et al., 2011).

In some tissues, it was postulated that dedifferentiation increases the multipotent potential of cells for example in the liver, where it was shown that hepatocytes can transdifferentiate into ductal biliary epithelial cells following injury (Michalopoulos et al., 2005; Tarlow et al., 2014; Yanger et al., 2013). Consequently, it was speculated that dedifferentiated SCs retain some multipotency, similar to SC precursors during development, in order to regenerate new nerve tissue (Petersen and Adameyko, 2017).

However, in this thesis we demonstrated that dedifferentiated mSC derived cells retain their lineage identity during a normal nerve regeneration process. This finding is in contrast to several previously performed *in vitro* studies that postulated that adult SCs maintain multipotency (Dupin et al., 2003; Widera et al., 2011). This suggests that as has been shown for other cell types, the reported plasticity of cells is due to the non-physiological environment in which the experiments were performed and that the microenvironment is critical for maintaining cell identity (Anderson, 2001; Guimaraes-Camboa et al., 2017; Snippert and Clevers, 2011). In line with this, stem cells in the intestinal crypt are maintained by their stem cell niche, which mainly consists of Paneth cells that provide Wnt, EGF and Notch signals that prevent lineage differentiation of the stem cell pool (Sato et al., 2011). The other cells of the crypt are not exposed to the factors of the stem cell niche, however, interestingly progenitor cells of the intestine can dedifferentiate to stem cells when exposed to Wnt factors *in vitro* (van Es et al., 2012). Consequently, it was speculated that upon injury the stem cell niche is

disrupted and progenitor cells of the intestine may be exposed to the stem cell niche factors (eg. Wnt), which can initiate their differentiation into stem cells.

This study further suggests that cell identity depends on the physiological environment and that altering it, by for example inducing an injury, can impact cell identity. In line with this, the injury environment was shown to be similar to the tumour environment indicating that it could likely alters cell plasticity and may be permissive for tumour growth (Arwert et al., 2012; Balkwill and Mantovani, 2001; Dvorak, 1986; Martins-Green et al., 1994). However, as we have shown in this thesis, mSC-derived cells retain SC identity during normal nerve repair demonstrating that the nerve environment maintains cell identity. Although nerve injury is not sufficient and additional factors are required for neurofibroma formation, a link between neurofibroma formation and wound healing has been drawn previously, in that clinical studies reported a correlation between neurofibroma formation and small tissue injuries (Riccardi, 1992a). Consistent with this, we demonstrated here that the genetic loss of Nf1 in adult mSCs requires cooperating factors of the injury environment in order to drive neurofibroma formation and the identification of these would greatly benefit the development of new therapeutic approaches.

6.3. Transgenic mouse models and cancer

The use of transgenic mouse models to study tumourigenesis has greatly advanced in recent years and has helped shed light on interactions of cancer cells with the tumour microenvironment, whose influence was previously underappreciated as it cannot be studied using classical cancer cell culture systems (Folkman and Kalluri, 2004). Amongst these transgenic mouse models, the field is nowadays mainly dominated by conditional transgenic mouse models, such as the P0-CreER^{T2}:YFP:Nf1$^{fl/fl}$, that allow the ablation of a specific gene at a given time (Abate-Shen et al., 2008; Hanahan et al., 2007; Smith and Muller, 2013; Van Dyke and Jacks, 2002).

Transgenic mouse models enable the investigation of pre-malignant lesions and the transformation of these into malignant lesions, which is not accessible to study in human patients. At the early stage of carcinogenesis, these models provide the opportunity to study

molecular pathways responsible for tumour initiation and progression of the disease and to test whether cancer progression can be prevented by targeting specific pathways (Green and Hudson, 2005; Le Magnen et al., 2016).

Overall, transgenic mouse models have their caveats such as their limited heterogeneity and a different immune system compared to humans, however they provide the most experimental accessible mammalian model to study various aspects of human tumour pathogenesis, which we would not be able to investigate otherwise (Rangarajan and Weinberg, 2003; Van Dyke and Jacks, 2002).

The P0-CreER^{T2}:YFP:Nf1$^{fl/fl}$ mouse model provides a powerful model for lineage tracing of the Nf1 KO SCs both at the early stages and within an established tumour in order to identify factors that promote the onset of tumourigenesis and to study to the plasticity of Nf1 KO SCs within the neurofibromas.

6.3.1. Nf1 KO SC plasticity

Lineage tracing of normal SCs demonstrated that SCs retain their identity within the context of a regenerating nerve and exhibit limited plasticity, whereas the loss of Nf1 in adult SCs and the injury microenvironment can synergise to increase the plasticity of these cells. Although, the clonality analysis that we performed demonstrated that the loss of Nf1 is sufficient to initiate neurofibroma formation, Nf1 KO SCs do not behave as a homogenous population as some appear to transdifferentiate into other cell lineages such as perineurial-like cells. Cell plasticity provides adaptive strategies for cancer cells that can facilitate invasion, therapeutic resistance and enables them to adapt to different regions within the tumour microenvironment.

It may also be the case that some Nf1 KO SCs have acquired further mutations that allows them to expand regionally, which could explain the spatial heterogeneity that we have observed in some tumour regions. Genetic diversity is not the only diversity mechanism present within an established tumour as it has been shown that tumour cells with a common genetic lineage are functionally heterogenous, exhibiting differences in growth dynamics and response to therapy (Gay et al., 2016; Marusyk et al., 2012; McGranahan and Swanton,

2017). In these clonal populations, other diversity generating mechanisms such as epigenetic regulation or variability in the tumour microenvironment appear to be responsible for the observed phenotypic differences (Kreso et al., 2013). The relative fitness of a new mutation or of a specific cell phenotype is not only defined by its tumour cell intrinsic advantages such as growth but also by its microenvironmental context. For example, in areas of hypoxia, any mutation that confers anabolic metabolism provides fitness advantages to the tumour cell and consequently results in the expansion of this population (Anderson et al., 2006).

Tumours with high level of intra-tumour heterogeneity have been associated with a worse prognosis as the probability of having a treatment resistant clone is higher in a highly heterogenous population (Bochtler et al., 2013; Mroz et al., 2013; Zhang et al., 2014a). The complexity of intra-tumour heterogeneity may explain certain therapy failures and disease resistances (Misale et al., 2012; Nazarian et al., 2010; Ostman, 2012; Prahallad et al., 2012; Sun et al., 2012). For example, recent publications demonstrated that KRAS mutant clones, which existed at a indictable frequency prior to treatment initiation, expand exponentially upon anti-EGFR treatment (Diaz et al., 2012) and confer resistance to the treatment.

Intra-tumour heterogeneity poses a big challenge to cancer therapies and recent strategies to tackle this issue have arisen. One approach involves suppressing tumour heterogeneity by targeting drivers of genetic instability in order to increase cell homozygosity within the tumour mass, which may render the tumour more sensitive to therapy (Gerlinger and Swanton, 2010).

6.3.2. Interactions of Nf1 KO SC with regional microenvironment

As described previously, neurofibromas only develop at the site of injury in the P0-CreER^{T2}:YFP:Nf1$^{fl/fl}$ mouse model indicating the crucial contribution of the injury microenvironment to neurofibroma formation (Ribeiro et al., 2013). The tumour microenvironment (TME) is known to be highly complex and consists of multiple cell types that have been shown to cross-interact with cancer cells in order to promote various aspects of tumourigenesis such as sustaining tumour growth (Lu et al., 2012; Quail and Joyce, 2013).

In studying the early stages of tumour formation, we observed that Nf1 KO mSC-derived cells maintain proliferation at the injury site at Day 14 following injury, whereas these cells behave

similar to controls cells in the distal stump indicating that the signals that maintain Nf1 KO SC proliferation act regionally. We have identified this timepoint as the point at which the behaviour of Nf1 KO SCs diverges from neighbouring Nf1 WT SCs and we investigated molecular signals that could drive the pro-tumourigenic behaviour of the Nf1 KO SCs at the injury site. Consistent with the regional differences in Nf1 KO SC behaviour at the early timepoints, we observed that some of the Nf1 KO mSC-derived cells were capable of re-myelinating axons within the tumour microenvironment. These observations led to the hypothesis that unidentified signals act locally to maintain the tumour driving Nf1 KO SC in their dedifferentiated state, by for example sustaining their proliferation, whilst neighbouring Nf1 KO SCs may not be exposed to these signals or alternatively are exposed to other signals that initiate their redifferentiation.

As it is known that axonal contact exerts anti-proliferative signals to SCs (Parrinello et al., 2008) and it has been shown previously that the loss of axonal contact is a critical early event in neurofibroma formation (Joseph et al., 2008; Wu et al., 2008; Zheng et al., 2008), it is tempting to speculate that the tumour driving Nf1 KO SCs may escape the anti-proliferative signals of the axons at the injury site.

To determine this, we will investigate interactions of Nf1-deficient mSCs with their local microenvironment *in vivo* in future experiments. These interactions will be investigated by using imaging techniques such as intravital microscopy (IVM) and 3D confocal microscopy that will enable us to perform a systematic 3D analysis in order to determine whether proliferating/dedifferentiated Nf1 KO SCs are associated with axons at the injury site. Moreover, this will enable us to establish the geometry of early tumour formation and the nature of the microenvironment.

Whole mount immunofluorescence techniques (Clarity and PACT) will be used to characterise interactions in 3D of the *Nf1*-deficient SCs (Chung and Deisseroth, 2013; Tomer et al., 2014; Yang et al., 2014). In parallel, we will perform an ultrastructure analysis using correlative light and electron microscopy (CLEM), which allow us to visualise the tumour driving labelled *Nf1*-deficient SCs by light microscopy before being transferred to EM in order to perform a 3D reconstruction of the area of interest.

In contrast to conventional confocal microscopy that provides a static snapshot of a biological process, IVM can be used to study spatiotemporal interactions of fluorescently labelled cells at a single cell level within a specific time window in live animals (Ellenbroek and van Rheenen, 2014; Pittet and Weissleder, 2011). This technique would allow us to specifically investigate axonal interactions of individual cells, however in order to do so, we would have to establish a new transgenic mouse model in which the axons, in addition to Nf1, are labelled with a fluorescent reporter cassette.

Both techniques will contribute to the visualisation of the interactions of the Nf1 KO SCs with their regional microenvironment. In parallel, we will validate the candidates of the RNA seq analysis, as discussed in Chapter 5, in order to determine whether these signals possess SC-specific effects that could mediate these interactions and promote the pro-tumourigenic behaviour of the Nf1 KO SCs.

Both cytokines and ECM proteins that have been identified in the RNA seq. analysis as the most upregulated molecule classes at the Nf1 KO injury site are known to play roles throughout tumourigenesis by for example acting as growth or survival factors, as discussed in Chapter 5 (Coussens and Werb, 2002; Grivennikov et al., 2010; Hanahan and Weinberg, 2011). Moreover, ECM proteins and cytokines also possess major roles during wound healing and many of these factors such as IL6 and TGFβ that are commonly present in both wound healing and cancers have been identified previously (Lin and Karin, 2007; Pedersen et al., 2003; Witsch et al., 2010). However, the level, duration and kinetics of these factors differs between wound healing and cancer, as wound healing is a self-limiting process, whilst tumours are commonly described as unhealed wounds (Arwert et al., 2012). Moreover, this highlights the importance of a controlled wound healing process in order to prevent tumour formation. It is tempting to speculate that elevated levels of the identified candidates may provide a conducive environment for tumour formation at the injury site but this remains to be demonstrated in future.

Overall, these studies will contribute to broaden the understanding of the physical and molecular interactions of the Nf1 KO SCs with their microenvironment at the onset of tumour formation and therefore may identify new treatment approaches for NF1.

References

Abate-Shen, C., Brown, P.H., Colburn, N.H., Gerner, E.W., Green, J.E., Lipkin, M., Nelson, W.G., and Threadgill, D. (2008). The untapped potential of genetically engineered mouse models in chemoprevention research: opportunities and challenges. Cancer Prev Res (Phila) *1*, 161-166.

Abbott, N.J., Ronnback, L., and Hansson, E. (2006). Astrocyte-endothelial interactions at the blood-brain barrier. Nat Rev Neurosci *7*, 41-53.

Adameyko, I., Lallemend, F., Aquino, J.B., Pereira, J.A., Topilko, P., Muller, T., Fritz, N., Beljajeva, A., Mochii, M., Liste, I.*, et al.* (2009). Schwann cell precursors from nerve innervation are a cellular origin of melanocytes in skin. Cell *139*, 366-379.

Adlkofer, K., and Lai, C. (2000). Role of neuregulins in glial cell development. Glia *29*, 104-111.

Aggarwal, S., Yurlova, L., Snaidero, N., Reetz, C., Frey, S., Zimmermann, J., Pahler, G., Janshoff, A., Friedrichs, J., Muller, D.J.*, et al.* (2011). A size barrier limits protein diffusion at the cell surface to generate lipid-rich myelin-membrane sheets. Developmental cell *21*, 445-456.

Agius, E., and Cochard, P. (1998). Comparison of neurite outgrowth induced by intact and injured sciatic nerves: a confocal and functional analysis. J Neurosci *18*, 328-338.

Aguayo, A.J., Bray, G.M., Terry, L.C., and Sweezey, E. (1976a). Three dimensional analysis of unmyelinated fibers in normal and pathologic autonomic nerves. Journal of neuropathology and experimental neurology *35*, 136-151.

Aguayo, A.J., Epps, J., Charron, L., and Bray, G.M. (1976b). Multipotentiality of Schwann cells in cross-anastomosed and grafted myelinated and unmyelinated nerves: quantitative microscopy and radioautography. Brain Res *104*, 1-20.

Aguayo, A.J., Peyronnard, J.M., and Bray, G.M. (1973). A quantitative ultrastructural study of regeneration from isolated proximal stumps of transected unmyelinated nerves. Journal of neuropathology and experimental neurology *32*, 256-270.

Aiello, N.M., and Stanger, B.Z. (2016). Echoes of the embryo: using the developmental biology toolkit to study cancer. Dis Model Mech *9*, 105-114.

Akassoglou, K., Yu, W.M., Akpinar, P., and Strickland, S. (2002). Fibrin inhibits peripheral nerve remyelination by regulating Schwann cell differentiation. Neuron *33*, 861-875.

Albright, C.F., Giddings, B.W., Liu, J., Vito, M., and Weinberg, R.A. (1993). Characterization of a guanine nucleotide dissociation stimulator for a ras-related GTPase. The EMBO journal *12*, 339-347.

Albritton, K.H., Rankin, C., Coffin, C.M., Ratner, N., Budd, G.T., Schuetze, S.M., Randall, R.L., Declue, J.E., and Borden, E.C. (2006). Phase II study of erlotinib in metastatic or unresectable malignant peripheral nerve sheath tumors (MPNST). Journal of Clinical Oncology *24*, 9518-9518.

Alcolea, M.P., and Jones, P.H. (2014). Lineage analysis of epidermal stem cells. Cold Spring Harbor perspectives in medicine *4*, a015206.

Amoh, Y., Li, L., Campillo, R., Kawahara, K., Katsuoka, K., Penman, S., and Hoffman, R.M. (2005). Implanted hair follicle stem cells form Schwann cells that support repair of severed peripheral nerves. Proceedings of the National Academy of Sciences of the United States of America *102*, 17734-17738.

Anastasaki, C., and Gutmann, D.H. (2014). Neuronal NF1/RAS regulation of cyclic AMP requires atypical PKC activation. Human molecular genetics *23*, 6712-6721.

Anders, S., and Huber, W. (2010). Differential expression analysis for sequence count data. Genome Biol *11*, R106.

Anderson, A.R., Weaver, A.M., Cummings, P.T., and Quaranta, V. (2006). Tumor morphology and phenotypic evolution driven by selective pressure from the microenvironment. Cell *127*, 905-915.

Anderson, D.J. (2001). Stem cells and pattern formation in the nervous system: the possible versus the actual. Neuron *30*, 19-35.

Aoka, Y., Johnson, F.L., Penta, K., Hirata Ki, K., Hidai, C., Schatzman, R., Varner, J.A., and Quertermous, T. (2002). The embryonic angiogenic factor Del1 accelerates tumor growth by enhancing vascular formation. Microvasc Res *64*, 148-161.

Araki, T., Sasaki, Y., and Milbrandt, J. (2004). Increased nuclear NAD biosynthesis and SIRT1 activation prevent axonal degeneration. Science *305*, 1010-1013.

Armulik, A., Genove, G., and Betsholtz, C. (2011). Pericytes: developmental, physiological, and pathological perspectives, problems, and promises. Developmental cell *21*, 193-215.

Arroyo, E.J., Bermingham, J.R., Jr., Rosenfeld, M.G., and Scherer, S.S. (1998). Promyelinating Schwann cells express Tst-1/SCIP/Oct-6. The Journal of neuroscience : the official journal of the Society for Neuroscience *18*, 7891-7902.

Arroyo, E.J., and Scherer, S.S. (2000). On the molecular architecture of myelinated fibers. Histochemistry and cell biology *113*, 1-18.

Arthur-Farraj, P.J., Latouche, M., Wilton, D.K., Quintes, S., Chabrol, E., Banerjee, A., Woodhoo, A., Jenkins, B., Rahman, M., Turmaine, M.*, et al.* (2012). c-Jun reprograms Schwann cells of injured nerves to generate a repair cell essential for regeneration. Neuron *75*, 633-647.

Aruga, J., and Mikoshiba, K. (2003). Identification and characterization of Slitrk, a novel neuronal transmembrane protein family controlling neurite outgrowth. Molecular and cellular neurosciences *24*, 117-129.

Aruga, J., Yokota, N., and Mikoshiba, K. (2003). Human SLITRK family genes: genomic organization and expression profiling in normal brain and brain tumor tissue. Gene *315*, 87-94.

Arwert, E.N., Hoste, E., and Watt, F.M. (2012). Epithelial stem cells, wound healing and cancer. Nature reviews Cancer *12*, 170-180.

Atanasoski, S., Scherer, S.S., Sirkowski, E., Leone, D., Garratt, A.N., Birchmeier, C., and Suter, U. (2006). ErbB2 signaling in Schwann cells is mostly dispensable for maintenance of myelinated peripheral nerves and proliferation of adult Schwann cells after injury. J Neurosci *26*, 2124-2131.

Bader, A.G., and Vogt, P.K. (2005). Inhibition of protein synthesis by Y box-binding protein 1 blocks oncogenic cell transformation. Mol Cell Biol *25*, 2095-2106.

Baggiolini, A., Varum, S., Mateos, J.M., Bettosini, D., John, N., Bonalli, M., Ziegler, U., Dimou, L., Clevers, H., Furrer, R.*, et al.* (2015). Premigratory and migratory neural crest cells are multipotent in vivo. Cell Stem Cell *16*, 314-322.

Bajenaru, M.L., Garbow, J.R., Perry, A., Hernandez, M.R., and Gutmann, D.H. (2005). Natural history of neurofibromatosis 1-associated optic nerve glioma in mice. Annals of neurology *57*, 119-127.

Bajenaru, M.L., Hernandez, M.R., Perry, A., Zhu, Y., Parada, L.F., Garbow, J.R., and Gutmann, D.H. (2003). Optic nerve glioma in mice requires astrocyte Nf1 gene inactivation and Nf1 brain heterozygosity. Cancer research *63*, 8573-8577.

Bajenaru, M.L., Zhu, Y., Hedrick, N.M., Donahoe, J., Parada, L.F., and Gutmann, D.H. (2002). Astrocyte-specific inactivation of the neurofibromatosis 1 gene (NF1) is insufficient for astrocytoma formation. Molecular and cellular biology *22*, 5100-5113.

Balkwill, F., and Mantovani, A. (2001). Inflammation and cancer: back to Virchow? Lancet *357*, 539-545.

Balkwill, F.R., Capasso, M., and Hagemann, T. (2012). The tumor microenvironment at a glance. Journal of cell science *125*, 5591-5596.

Ballester, R., Marchuk, D., Boguski, M., Saulino, A., Letcher, R., Wigler, M., and Collins, F. (1990). The NF1 locus encodes a protein functionally related to mammalian GAP and yeast IRA proteins. Cell *63*, 851-859.

Baltz, K.M., Krusch, M., Baessler, T., Schmiedel, B.J., Bringmann, A., Brossart, P., and Salih, H.R. (2008). Neutralization of tumor-derived soluble glucocorticoid-induced TNFR-related protein ligand increases NK cell anti-tumor reactivity. Blood *112*, 3735-3743.

Baltz, K.M., Krusch, M., Bringmann, A., Brossart, P., Mayer, F., Kloss, M., Baessler, T., Kumbier, I., Peterfi, A., Kupka, S*., et al.* (2007). Cancer immunoediting by GITR (glucocorticoid-induced TNF-related protein) ligand in humans: NK cell/tumor cell interactions. FASEB J *21*, 2442-2454.

Banerjee, S., Byrd, J.N., Gianino, S.M., Harpstrite, S.E., Rodriguez, F.J., Tuskan, R.G., Reilly, K.M., Piwnica-Worms, D.R., and Gutmann, D.H. (2010). The neurofibromatosis type 1 tumor suppressor controls cell growth by regulating signal transducer and activator of transcription-3 activity in vitro and in vivo. Cancer Res *70*, 1356-1366.

Bani, D., Formigli, L., Gherghiceanu, M., and Faussone-Pellegrini, M.S. (2010). Telocytes as supporting cells for myocardial tissue organization in developing and adult heart. Journal of cellular and molecular medicine *14*, 2531-2538.

Barik, A., Li, L., Sathyamurthy, A., Xiong, W.C., and Mei, L. (2016). Schwann Cells in Neuromuscular Junction Formation and Maintenance. The Journal of neuroscience : the official journal of the Society for Neuroscience *36*, 9770-9781.

Barker, N., Ridgway, R.A., van Es, J.H., van de Wetering, M., Begthel, H., van den Born, M., Danenberg, E., Clarke, A.R., Sansom, O.J., and Clevers, H. (2009). Crypt stem cells as the cells-of-origin of intestinal cancer. Nature *457*, 608-611.

Barraud, P., Seferiadis, A.A., Tyson, L.D., Zwart, M.F., Szabo-Rogers, H.L., Ruhrberg, C., Liu, K.J., and Baker, C.V. (2010). Neural crest origin of olfactory ensheathing glia. Proceedings of the National Academy of Sciences of the United States of America *107*, 21040-21045.

Barres, B.A. (2008). The mystery and magic of glia: a perspective on their roles in health and disease. Neuron *60*, 430-440.

Basu, T.N., Gutmann, D.H., Fletcher, J.A., Glover, T.W., Collins, F.S., and Downward, J. (1992). Aberrant regulation of ras proteins in malignant tumour cells from type 1 neurofibromatosis patients. Nature *356*, 713-715.

Beckham, C.J., Olsen, J., Yin, P.N., Wu, C.H., Ting, H.J., Hagen, F.K., Scosyrev, E., Messing, E.M., and Lee, Y.F. (2014). Bladder cancer exosomes contain EDIL-3/Del1 and facilitate cancer progression. The Journal of urology *192*, 583-592.

Beirowski, B., Babetto, E., Golden, J.P., Chen, Y.J., Yang, K., Gross, R.W., Patti, G.J., and Milbrandt, J. (2014). Metabolic regulator LKB1 is crucial for Schwann cell-mediated axon maintenance. Nat Neurosci *17*, 1351-1361.

Bercury, K.K., and Macklin, W.B. (2015). Dynamics and mechanisms of CNS myelination. Developmental cell *32*, 447-458.

Bergers, G., and Benjamin, L.E. (2003). Tumorigenesis and the angiogenic switch. Nature reviews Cancer *3*, 401-410.

Bergers, G., Javaherian, K., Lo, K.M., Folkman, J., and Hanahan, D. (1999). Effects of angiogenesis inhibitors on multistage carcinogenesis in mice. Science *284*, 808-812.

Bermingham, J.R., Jr., Scherer, S.S., O'Connell, S., Arroyo, E., Kalla, K.A., Powell, F.L., and Rosenfeld, M.G. (1996). Tst-1/Oct-6/SCIP regulates a unique step in peripheral myelination and is required for normal respiration. Genes Dev *10*, 1751-1762.

Bermingham, J.R., Jr., Shearin, H., Pennington, J., O'Moore, J., Jaegle, M., Driegen, S., van Zon, A., Darbas, A., Ozkaynak, E., Ryu, E.J.*, et al.* (2006). The claw paw mutation reveals a role for Lgi4 in peripheral nerve development. Nat Neurosci *9*, 76-84.

Beumer, J., and Clevers, H. (2016). Regulation and plasticity of intestinal stem cells during homeostasis and regeneration. Development *143*, 3639-3649.

Bhowmick, N.A., Neilson, E.G., and Moses, H.L. (2004). Stromal fibroblasts in cancer initiation and progression. Nature *432*, 332-337.

Bienz, M., and Clevers, H. (2000). Linking colorectal cancer to Wnt signaling. Cell *103*, 311-320.

Birch, R. (2013). Peripheral Nerve Injuries: A Clinical Guide. Springer

Birchmeier, C., and Bennett, D.L. (2016). Neuregulin/ErbB Signaling in Developmental Myelin Formation and Nerve Repair. Curr Top Dev Biol *116*, 45-64.

Birchmeier, C., and Nave, K.A. (2008). Neuregulin-1, a key axonal signal that drives Schwann cell growth and differentiation. Glia *56*, 1491-1497.

Birey, F., Kokkosis, A.G., and Aguirre, A. (2017). Oligodendroglia-lineage cells in brain plasticity, homeostasis and psychiatric disorders. Current opinion in neurobiology *47*, 93-103.

Bissell, M.J., and Radisky, D. (2001). Putting tumours in context. Nat Rev Cancer *1*, 46-54.

Biteau, B., Hochmuth, C.E., and Jasper, H. (2011). Maintaining tissue homeostasis: dynamic control of somatic stem cell activity. Cell stem cell *9*, 402-411.

Bixby, J.L., Lilien, J., and Reichardt, L.F. (1988). Identification of the major proteins that promote neuronal process outgrowth on Schwann cells in vitro. J Cell Biol *107*, 353-361.

Bixby, J.L., and Zhang, R. (1990). Purified N-cadherin is a potent substrate for the rapid induction of neurite outgrowth. J Cell Biol *110*, 1253-1260.

Blanpain, C., and Fuchs, E. (2014). Stem cell plasticity. Plasticity of epithelial stem cells in tissue regeneration. Science *344*, 1242281.

Bochtler, T., Stolzel, F., Heilig, C.E., Kunz, C., Mohr, B., Jauch, A., Janssen, J.W., Kramer, M., Benner, A., Bornhauser, M.*, et al.* (2013). Clonal heterogeneity as detected by metaphase karyotyping is an indicator of poor prognosis in acute myeloid leukemia. J Clin Oncol *31*, 3898-3905.

Boesiger, J., Tsai, M., Maurer, M., Yamaguchi, M., Brown, L.F., Claffey, K.P., Dvorak, H.F., and Galli, S.J. (1998). Mast cells can secrete vascular permeability factor/ vascular endothelial cell growth factor and exhibit enhanced release after immunoglobulin E-dependent upregulation of fc epsilon receptor I expression. The Journal of experimental medicine *188*, 1135-1145.

Bolin, L.M., Verity, A.N., Silver, J.E., Shooter, E.M., and Abrams, J.S. (1995). Interleukin-6 production by Schwann cells and induction in sciatic nerve injury. J Neurochem *64*, 850-858.

Bollag, G., McCormick, F., and Clark, R. (1993). Characterization of full-length neurofibromin: tubulin inhibits Ras GAP activity. EMBO J *12*, 1923-1927.

Bollrath, J., Phesse, T.J., von Burstin, V.A., Putoczki, T., Bennecke, M., Bateman, T., Nebelsiek, T., Lundgren-May, T., Canli, O., Schwitalla, S.*, et al.* (2009). gp130-mediated Stat3 activation in enterocytes regulates cell survival and cell-cycle progression during colitis-associated tumorigenesis. Cancer Cell *15*, 91-102.

Bolos, V., Grego-Bessa, J., and de la Pompa, J.L. (2007). Notch signaling in development and cancer. Endocr Rev *28*, 339-363.

Borodina, T., Adjaye, J., and Sultan, M. (2011). A strand-specific library preparation protocol for RNA sequencing. Methods Enzymol *500*, 79-98.

Bos, J.L. (1989). ras oncogenes in human cancer: a review. Cancer Res *49*, 4682-4689.

Bos, J.L., Rehmann, H., and Wittinghofer, A. (2007). GEFs and GAPs: critical elements in the control of small G proteins. Cell *129*, 865-877.

Bradbury, E.J., Moon, L.D., Popat, R.J., King, V.R., Bennett, G.S., Patel, P.N., Fawcett, J.W., and McMahon, S.B. (2002). Chondroitinase ABC promotes functional recovery after spinal cord injury. Nature *416*, 636-640.

Bradtmoller, M., Hartmann, C., Zietsch, J., Jaschke, S., Mautner, V.F., Kurtz, A., Park, S.J., Baier, M., Harder, A., Reuss, D.*, et al.* (2012). Impaired Pten expression in human malignant peripheral nerve sheath tumours. PloS one *7*, e47595.

Brannan, C.I., Perkins, A.S., Vogel, K.S., Ratner, N., Nordlund, M.L., Reid, S.W., Buchberg, A.M., Jenkins, N.A., Parada, L.F., and Copeland, N.G. (1994). Targeted disruption of the neurofibromatosis type-1 gene leads to developmental abnormalities in heart and various neural crest-derived tissues. Genes Dev *8*, 1019-1029.

Bray, G.M., and Aguayo, A.J. (1974). Regeneration of peripheral unmyelinated nerves. Fate of the axonal sprouts which develop after injury. Journal of anatomy *117*, 517-529.

Bray, G.M., Peyronnard, J.M., and Aguayo, A.J. (1972). Reactions of unmyelinated nerve fibers to injury. An ultrastructural study. Brain research *42*, 297-309.

Bremer, M., Frob, F., Kichko, T., Reeh, P., Tamm, E.R., Suter, U., and Wegner, M. (2011). Sox10 is required for Schwann-cell homeostasis and myelin maintenance in the adult peripheral nerve. Glia *59*, 1022-1032.

Brightman, F.A., and Fell, D.A. (2000). Differential feedback regulation of the MAPK cascade underlies the quantitative differences in EGF and NGF signalling in PC12 cells. FEBS letters *482*, 169-174.

Britsch, S., Goerich, D.E., Riethmacher, D., Peirano, R.I., Rossner, M., Nave, K.A., Birchmeier, C., and Wegner, M. (2001). The transcription factor Sox10 is a key regulator of peripheral glial development. Genes Dev *15*, 66-78.

Bronner, M.E., and Simoes-Costa, M. (2016). The Neural Crest Migrating into the Twenty-First Century. Current topics in developmental biology *116*, 115-134.

Brosius Lutz, A., Chung, W.S., Sloan, S.A., Carson, G.A., Zhou, L., Lovelett, E., Posada, S., Zuchero, J.B., and Barres, B.A. (2017). Schwann cells use TAM receptor-mediated phagocytosis in addition to autophagy to clear myelin in a mouse model of nerve injury. Proceedings of the National Academy of Sciences of the United States of America *114*, E8072-E8080.

Brossier, N.M., and Carroll, S.L. (2012). Genetically engineered mouse models shed new light on the pathogenesis of neurofibromatosis type I-related neoplasms of the peripheral nervous system. Brain Res Bull *88*, 58-71.

Brown, M.C., Lunn, E.R., and Perry, V.H. (1992). Consequences of slow Wallerian degeneration for regenerating motor and sensory axons. Journal of neurobiology *23*, 521-536.

Buac, K., Xu, M., Cronin, J., Weeraratna, A.T., Hewitt, S.M., and Pavan, W.J. (2009). NRG1 / ERBB3 signaling in melanocyte development and melanoma: inhibition of differentiation and promotion of proliferation. Pigment cell & melanoma research *22*, 773-784.

Bunge, R.P., Bunge, M.B., and Eldridge, C.F. (1986). Linkage between axonal ensheathment and basal lamina production by Schwann cells. Annual review of neuroscience *9*, 305-328.

Burger, J.A., and Peled, A. (2009). CXCR4 antagonists: targeting the microenvironment in leukemia and other cancers. Leukemia *23*, 43-52.

Burnett, M.G., and Zager, E.L. (2004). Pathophysiology of peripheral nerve injury: a brief review. Neurosurg Focus *16*, E1.

Bush, T.G., Savidge, T.C., Freeman, T.C., Cox, H.J., Campbell, E.A., Mucke, L., Johnson, M.H., and Sofroniew, M.V. (1998). Fulminant jejuno-ileitis following ablation of enteric glia in adult transgenic mice. Cell *93*, 189-201.

Campbell, W.W. (2008). Evaluation and management of peripheral nerve injury. Clinical neurophysiology : official journal of the International Federation of Clinical Neurophysiology *119*, 1951-1965.

Cappella, P., Gasparri, F., Pulici, M., and Moll, J. (2008). A novel method based on click chemistry, which overcomes limitations of cell cycle analysis by classical determination of BrdU incorporation, allowing multiplex antibody staining. Cytometry A *73*, 626-636.

Carey, D.J., Todd, M.S., and Rafferty, C.M. (1986). Schwann cell myelination: induction by exogenous basement membrane-like extracellular matrix. The Journal of cell biology *102*, 2254-2263.

Carey, J.C., Laub, J.M., and Hall, B.D. (1979). Penetrance and variability in neurofibromatosis: a genetic study of 60 families. Birth defects original article series *15*, 271-281.

Carroll, S.L., Miller, M.L., Frohnert, P.W., Kim, S.S., and Corbett, J.A. (1997). Expression of neuregulins and their putative receptors, ErbB2 and ErbB3, is induced during Wallerian degeneration. J Neurosci *17*, 1642-1659.

Carroll, S.L., and Ratner, N. (2008). How does the Schwann cell lineage form tumors in NF1? Glia *56*, 1590-1605.

Carter, D.A., and Lisney, S.J. (1987). The numbers of unmyelinated and myelinated axons in normal and regenerated rat saphenous nerves. Journal of the neurological sciences *80*, 163-171.

Casey, T., Bond, J., Tighe, S., Hunter, T., Lintault, L., Patel, O., Eneman, J., Crocker, A., White, J., Tessitore, J.*, et al.* (2009). Molecular signatures suggest a major role for stromal cells in development of invasive breast cancer. Breast Cancer Res Treat *114*, 47-62.

Castellano, E., and Downward, J. (2011). RAS Interaction with PI3K: More Than Just Another Effector Pathway. Genes & cancer *2*, 261-274.

Castro, C., and Kuffler, D.P. (2006). Membrane-bound CSPG mediates growth cone outgrowth and substrate specificity by Schwann cell contact with the DRG neuron cell body and not via growth cone contact. Exp Neurol *200*, 19-25.

Cattin, A.L., Burden, J.J., Van Emmenis, L., Mackenzie, F.E., Hoving, J.J., Garcia Calavia, N., Guo, Y., McLaughlin, M., Rosenberg, L.H., Quereda, V.*, et al.* (2015). Macrophage-Induced Blood Vessels Guide Schwann Cell-Mediated Regeneration of Peripheral Nerves. Cell *162*, 1127-1139.

Cattin, A.L., and Lloyd, A.C. (2016). The multicellular complexity of peripheral nerve regeneration. Curr Opin Neurobiol *39*, 38-46.

Cawthon, R.M., Andersen, L.B., Buchberg, A.M., Xu, G.F., O'Connell, P., Viskochil, D., Weiss, R.B., Wallace, M.R., Marchuk, D.A., Culver, M.*, et al.* (1991). cDNA sequence and genomic structure of EV12B, a gene lying within an intron of the neurofibromatosis type 1 gene. Genomics *9*, 446-460.

Cawthon, R.M., O'Connell, P., Buchberg, A.M., Viskochil, D., Weiss, R.B., Culver, M., Stevens, J., Jenkins, N.A., Copeland, N.G., and White, R. (1990a). Identification and characterization of transcripts from the neurofibromatosis 1 region: the sequence and genomic structure of EVI2 and mapping of other transcripts. Genomics *7*, 555-565.

Cawthon, R.M., Weiss, R., Xu, G.F., Viskochil, D., Culver, M., Stevens, J., Robertson, M., Dunn, D., Gesteland, R., O'Connell, P.*, et al.* (1990b). A major segment of the neurofibromatosis type 1 gene: cDNA sequence, genomic structure, and point mutations. Cell *62*, 193-201.

Chan, J.R., Cosgaya, J.M., Wu, Y.J., and Shooter, E.M. (2001). Neurotrophins are key mediators of the myelination program in the peripheral nervous system. Proc Natl Acad Sci U S A *98*, 14661-14668.

Chan, J.R., Jolicoeur, C., Yamauchi, J., Elliott, J., Fawcett, J.P., Ng, B.K., and Cayouette, M. (2006). The polarity protein Par-3 directly interacts with p75NTR to regulate myelination. Science *314*, 832-836.

Chang, H.Y., Sneddon, J.B., Alizadeh, A.A., Sood, R., West, R.B., Montgomery, K., Chi, J.T., van de Rijn, M., Botstein, D., and Brown, P.O. (2004). Gene expression signature of fibroblast serum response predicts human cancer progression: similarities between tumors and wounds. PLoS biology *2*, E7.

Chehrehasa, F., Ekberg, J.A., Lineburg, K., Amaya, D., Mackay-Sim, A., and St John, J.A. (2012). Two phases of replacement replenish the olfactory ensheathing cell population after injury in postnatal mice. Glia *60*, 322-332.

Chen, H., Chedotal, A., He, Z., Goodman, C.S., and Tessier-Lavigne, M. (1997). Neuropilin-2, a novel member of the neuropilin family, is a high affinity receptor for the semaphorins Sema E and Sema IV but not Sema III. Neuron *19*, 547-559.

Chen, S., Rio, C., Ji, R.R., Dikkes, P., Coggeshall, R.E., Woolf, C.J., and Corfas, G. (2003). Disruption of ErbB receptor signaling in adult non-myelinating Schwann cells causes progressive sensory loss. Nat Neurosci *6*, 1186-1193.

Chen, Y.H., McGowan, L.D., Cimino, P.J., Dahiya, S., Leonard, J.R., Lee, D.Y., and Gutmann, D.H. (2015). Mouse low-grade gliomas contain cancer stem cells with unique molecular and functional properties. Cell reports *10*, 1899-1912.

Chen, Y.Y., McDonald, D., Cheng, C., Magnowski, B., Durand, J., and Zochodne, D.W. (2005). Axon and Schwann cell partnership during nerve regrowth. Journal of neuropathology and experimental neurology *64*, 613-622.

Chen, Z., Pradhan, S., Liu, C., and Le, L.Q. (2012). Skin-derived precursors as a source of progenitors for cutaneous nerve regeneration. Stem cells *30*, 2261-2270.

Chen, Z.L., and Strickland, S. (2003). Laminin gamma1 is critical for Schwann cell differentiation, axon myelination, and regeneration in the peripheral nerve. J Cell Biol *163*, 889-899.

Chen, Z.L., Yu, W.M., and Strickland, S. (2007). Peripheral regeneration. Annu Rev Neurosci *30*, 209-233.

Chernousov, M.A., Yu, W.M., Chen, Z.L., Carey, D.J., and Strickland, S. (2008). Regulation of Schwann cell function by the extracellular matrix. Glia *56*, 1498-1507.

Chhangawala, S., Rudy, G., Mason, C.E., and Rosenfeld, J.A. (2015). The impact of read length on quantification of differentially expressed genes and splice junction detection. Genome Biol *16*, 131.

Chierzi, S., Ratto, G.M., Verma, P., and Fawcett, J.W. (2005). The ability of axons to regenerate their growth cones depends on axonal type and age, and is regulated by calcium, cAMP and ERK. Eur J Neurosci *21*, 2051-2062.

Choi, K., Komurov, K., Fletcher, J.S., Jousma, E., Cancelas, J.A., Wu, J., and Ratner, N. (2017). An inflammatory gene signature distinguishes neurofibroma Schwann cells

and macrophages from cells in the normal peripheral nervous system. Sci Rep *7*, 43315.

Chung, K., and Deisseroth, K. (2013). CLARITY for mapping the nervous system. Nature methods *10*, 508-513.

Cichowski, K., and Jacks, T. (2001). NF1 tumor suppressor gene function: narrowing the GAP. Cell *104*, 593-604.

Cichowski, K., Santiago, S., Jardim, M., Johnson, B.W., and Jacks, T. (2003). Dynamic regulation of the Ras pathway via proteolysis of the NF1 tumor suppressor. Genes Dev *17*, 449-454.

Cichowski, K., Shih, T.S., Schmitt, E., Santiago, S., Reilly, K., McLaughlin, M.E., Bronson, R.T., and Jacks, T. (1999). Mouse models of tumor development in neurofibromatosis type 1. Science *286*, 2172-2176.

Clayton, E., Doupe, D.P., Klein, A.M., Winton, D.J., Simons, B.D., and Jones, P.H. (2007). A single type of progenitor cell maintains normal epidermis. Nature *446*, 185-189.

Cleary, A.S., Leonard, T.L., Gestl, S.A., and Gunther, E.J. (2014). Tumour cell heterogeneity maintained by cooperating subclones in Wnt-driven mammary cancers. Nature *508*, 113-117.

Clements, M.P., Byrne, E., Camarillo Guerrero, L.F., Cattin, A.L., Zakka, L., Ashraf, A., Burden, J.J., Khadayate, S., Lloyd, A.C., Marguerat, S*., et al.* (2017). The Wound Microenvironment Reprograms Schwann Cells to Invasive Mesenchymal-like Cells to Drive Peripheral Nerve Regeneration. Neuron *96*, 98-114 e117.

Coelho-Aguiar Jde, M., Bon-Frauches, A.C., Gomes, A.L., Verissimo, C.P., Aguiar, D.P., Matias, D., Thomasi, B.B., Gomes, A.S., Brito, G.A., and Moura-Neto, V. (2015). The enteric glia: identity and functions. Glia *63*, 921-935.

Cohen, J.A., Yachnis, A.T., Arai, M., Davis, J.G., and Scherer, S.S. (1992). Expression of the neu proto-oncogene by Schwann cells during peripheral nerve development and Wallerian degeneration. J Neurosci Res *31*, 622-634.

Condeelis, J., and Pollard, J.W. (2006). Macrophages: obligate partners for tumor cell migration, invasion, and metastasis. Cell *124*, 263-266.

Conesa, A., Madrigal, P., Tarazona, S., Gomez-Cabrero, D., Cervera, A., McPherson, A., Szczesniak, M.W., Gaffney, D.J., Elo, L.L., Zhang, X.*, et al.* (2016). A survey of best practices for RNA-seq data analysis. Genome Biol *17*, 13.

Conforti, L., Gilley, J., and Coleman, M.P. (2014). Wallerian degeneration: an emerging axon death pathway linking injury and disease. Nature reviews Neuroscience *15*, 394-409.

Conforti, L., Wilbrey, A., Morreale, G., Janeckova, L., Beirowski, B., Adalbert, R., Mazzola, F., Di Stefano, M., Hartley, R., Babetto, E.*, et al.* (2009). Wld S protein requires Nmnat activity and a short N-terminal sequence to protect axons in mice. J Cell Biol *184*, 491-500.

Cook (1977). Detection of Influential Observation in Linear Regression. Technometrics.

Coppe, J.P., Patil, C.K., Rodier, F., Sun, Y., Munoz, D.P., Goldstein, J., Nelson, P.S., Desprez, P.Y., and Campisi, J. (2008). Senescence-associated secretory phenotypes reveal cell-nonautonomous functions of oncogenic RAS and the p53 tumor suppressor. PLoS biology *6*, 2853-2868.

Corfas, G., Velardez, M.O., Ko, C.P., Ratner, N., and Peles, E. (2004). Mechanisms and roles of axon-Schwann cell interactions. The Journal of neuroscience : the official journal of the Society for Neuroscience *24*, 9250-9260.

Cosgaya, J.M., Chan, J.R., and Shooter, E.M. (2002). The neurotrophin receptor p75NTR as a positive modulator of myelination. Science *298*, 1245-1248.

Costa, R.M., Federov, N.B., Kogan, J.H., Murphy, G.G., Stern, J., Ohno, M., Kucherlapati, R., Jacks, T., and Silva, A.J. (2002). Mechanism for the learning deficits in a mouse model of neurofibromatosis type 1. Nature *415*, 526-530.

Court, F.A., Hendriks, W.T., MacGillavry, H.D., Alvarez, J., and van Minnen, J. (2008). Schwann cell to axon transfer of ribosomes: toward a novel understanding of the role of glia in the nervous system. The Journal of neuroscience : the official journal of the Society for Neuroscience *28*, 11024-11029.

Court, F.A., Hewitt, J.E., Davies, K., Patton, B.L., Uncini, A., Wrabetz, L., and Feltri, M.L. (2009). A laminin-2, dystroglycan, utrophin axis is required for compartmentalization and elongation of myelin segments. J Neurosci *29*, 3908-3919.

Court, F.A., Sherman, D.L., Pratt, T., Garry, E.M., Ribchester, R.R., Cottrell, D.F., Fleetwood-Walker, S.M., and Brophy, P.J. (2004). Restricted growth of Schwann cells lacking Cajal bands slows conduction in myelinated nerves. Nature *431*, 191-195.

Courtois-Cox, S., Genther Williams, S.M., Reczek, E.E., Johnson, B.W., McGillicuddy, L.T., Johannessen, C.M., Hollstein, P.E., MacCollin, M., and Cichowski, K. (2006). A negative feedback signaling network underlies oncogene-induced senescence. Cancer cell *10*, 459-472.

Coussens, L.M., and Werb, Z. (2002). Inflammation and cancer. Nature *420*, 860-867.

Cox, T.R., and Erler, J.T. (2011). Remodeling and homeostasis of the extracellular matrix: implications for fibrotic diseases and cancer. Disease models & mechanisms *4*, 165-178.

Cui, Y., Costa, R.M., Murphy, G.G., Elgersma, Y., Zhu, Y., Gutmann, D.H., Parada, L.F., Mody, I., and Silva, A.J. (2008). Neurofibromin regulation of ERK signaling modulates GABA release and learning. Cell *135*, 549-560.

D., K. 2008. Monogr Hum Genet Basel, Karger *Vol 16*.

D., K. (2008). Neurofibromatoses. Monogr Hum Genet Basel, Karger *16*, 129–142.

D'Antonio, M., Droggiti, A., Feltri, M.L., Roes, J., Wrabetz, L., Mirsky, R., and Jessen, K.R. (2006). TGFbeta type II receptor signaling controls Schwann cell death and proliferation in developing nerves. J Neurosci *26*, 8417-8427.

Daginakatte, G.C., Gianino, S.M., Zhao, N.W., Parsadanian, A.S., and Gutmann, D.H. (2008). Increased c-Jun-NH2-kinase signaling in neurofibromatosis-1 heterozygous microglia drives microglia activation and promotes optic glioma proliferation. Cancer research *68*, 10358-10366.

Daginakatte, G.C., and Gutmann, D.H. (2007). Neurofibromatosis-1 (Nf1) heterozygous brain microglia elaborate paracrine factors that promote Nf1-deficient astrocyte and glioma growth. Human molecular genetics *16*, 1098-1112.

Dang, I., and DeVries, G.H. (2005). Schwann cell lines derived from malignant peripheral nerve sheath tumors respond abnormally to platelet-derived growth factor-BB. J Neurosci Res *79*, 318-328.

Daston, M.M., Scrable, H., Nordlund, M., Sturbaum, A.K., Nissen, L.M., and Ratner, N. (1992). The protein product of the neurofibromatosis type 1 gene is expressed at

highest abundance in neurons, Schwann cells, and oligodendrocytes. Neuron *8*, 415-428.

de Bruin, E.C., McGranahan, N., Mitter, R., Salm, M., Wedge, D.C., Yates, L., Jamal-Hanjani, M., Shafi, S., Murugaesu, N., Rowan, A.J.*, et al.* (2014). Spatial and temporal diversity in genomic instability processes defines lung cancer evolution. Science *346*, 251-256.

De Raedt, T., Beert, E., Pasmant, E., Luscan, A., Brems, H., Ortonne, N., Helin, K., Hornick, J.L., Mautner, V., Kehrer-Sawatzki, H.*, et al.* (2014). PRC2 loss amplifies Ras-driven transcription and confers sensitivity to BRD4-based therapies. Nature *514*, 247-251.

de Sousa e Melo, F., Kurtova, A.V., Harnoss, J.M., Kljavin, N., Hoeck, J.D., Hung, J., Anderson, J.E., Storm, E.E., Modrusan, Z., Koeppen, H.*, et al.* (2017). A distinct role for Lgr5(+) stem cells in primary and metastatic colon cancer. Nature *543*, 676-680.

De Wever, O., and Mareel, M. (2003). Role of tissue stroma in cancer cell invasion. J Pathol *200*, 429-447.

Decker, L., Desmarquet-Trin-Dinh, C., Taillebourg, E., Ghislain, J., Vallat, J.M., and Charnay, P. (2006). Peripheral myelin maintenance is a dynamic process requiring constant Krox20 expression. J Neurosci *26*, 9771-9779.

DeClue, J.E., Cohen, B.D., and Lowy, D.R. (1991). Identification and characterization of the neurofibromatosis type 1 protein product. Proc Natl Acad Sci U S A *88*, 9914-9918.

DeClue, J.E., Heffelfinger, S., Benvenuto, G., Ling, B., Li, S., Rui, W., Vass, W.C., Viskochil, D., and Ratner, N. (2000). Epidermal growth factor receptor expression in neurofibromatosis type 1-related tumors and NF1 animal models. The Journal of clinical investigation *105*, 1233-1241.

DeClue, J.E., Papageorge, A.G., Fletcher, J.A., Diehl, S.R., Ratner, N., Vass, W.C., and Lowy, D.R. (1992). Abnormal regulation of mammalian p21ras contributes to malignant tumor growth in von Recklinghausen (type 1) neurofibromatosis. Cell *69*, 265-273.

Dempke, W.C.M., Fenchel, K., Uciechowski, P., and Chevassut, T. (2017). Targeting Developmental Pathways: The Achilles Heel of Cancer? Oncology *93*, 213-223.

Diaz, L.A., Jr., Williams, R.T., Wu, J., Kinde, I., Hecht, J.R., Berlin, J., Allen, B., Bozic, I., Reiter, J.G., Nowak, M.A*., et al.* (2012). The molecular evolution of acquired resistance to targeted EGFR blockade in colorectal cancers. Nature *486*, 537-540.

Diggs-Andrews, K.A., Brown, J.A., Gianino, S.M., Rubin, J.B., Wozniak, D.F., and Gutmann, D.H. (2014). Sex Is a major determinant of neuronal dysfunction in neurofibromatosis type 1. Annals of neurology *75*, 309-316.

Dimou, L., and Simons, M. (2017). Diversity of oligodendrocytes and their progenitors. Current opinion in neurobiology *47*, 73-79.

Doerfler, W., Remus, R., Muller, K., Heller, H., Hohlweg, U., and Schubbert, R. (2001). The fate of foreign DNA in mammalian cells and organisms. Dev Biol (Basel) *106*, 89-97; discussion 143-160.

Domanska, U.M., Kruizinga, R.C., Nagengast, W.B., Timmer-Bosscha, H., Huls, G., de Vries, E.G., and Walenkamp, A.M. (2013). A review on CXCR4/CXCL12 axis in oncology: no place to hide. European journal of cancer *49*, 219-230.

Dombi, E., Baldwin, A., Marcus, L.J., Fisher, M.J., Weiss, B., Kim, A., Whitcomb, P., Martin, S., Aschbacher-Smith, L.E., Rizvi, T.A*., et al.* (2016). Activity of Selumetinib in Neurofibromatosis Type 1-Related Plexiform Neurofibromas. The New England journal of medicine *375*, 2550-2560.

Donati, G., Rognoni, E., Hiratsuka, T., Liakath-Ali, K., Hoste, E., Kar, G., Kayikci, M., Russell, R., Kretzschmar, K., Mulder, K.W*., et al.* (2017). Wounding induces dedifferentiation of epidermal Gata6(+) cells and acquisition of stem cell properties. Nature cell biology *19*, 603-613.

Dong, Z., Brennan, A., Liu, N., Yarden, Y., Lefkowitz, G., Mirsky, R., and Jessen, K.R. (1995). Neu differentiation factor is a neuron-glia signal and regulates survival, proliferation, and maturation of rat Schwann cell precursors. Neuron *15*, 585-596.

Dong, Z., Sinanan, A., Parkinson, D., Parmantier, E., Mirsky, R., and Jessen, K.R. (1999). Schwann cell development in embryonic mouse nerves. Journal of neuroscience research *56*, 334-348.

Donnelly, C.J., Park, M., Spillane, M., Yoo, S., Pacheco, A., Gomes, C., Vuppalanchi, D., McDonald, M., Kim, H.H., Merianda, T.T*., et al.* (2013). Axonally synthesized beta-actin and GAP-43 proteins support distinct modes of axonal growth. The Journal of neuroscience : the official journal of the Society for Neuroscience *33*, 3311-3322.

Downward, J. (2003). Targeting RAS signalling pathways in cancer therapy. Nat Rev Cancer *3*, 11-22.

Dowsing, B.J., Morrison, W.A., Nicola, N.A., Starkey, G.P., Bucci, T., and Kilpatrick, T.J. (1999). Leukemia inhibitory factor is an autocrine survival factor for Schwann cells. J Neurochem *73*, 96-104.

Dupin, E., Real, C., Glavieux-Pardanaud, C., Vaigot, P., and Le Douarin, N.M. (2003). Reversal of developmental restrictions in neural crest lineages: transition from Schwann cells to glial-melanocytic precursors in vitro. Proc Natl Acad Sci U S A *100*, 5229-5233.

Dvorak, H.F. (1986). Tumors: wounds that do not heal. Similarities between tumor stroma generation and wound healing. N Engl J Med *315*, 1650-1659.

Dyachuk, V., Furlan, A., Shahidi, M.K., Giovenco, M., Kaukua, N., Konstantinidou, C., Pachnis, V., Memic, F., Marklund, U., Muller, T*., et al.* (2014). Neurodevelopment. Parasympathetic neurons originate from nerve-associated peripheral glial progenitors. Science *345*, 82-87.

Dyck PJ, T.P. (1993). Peripheral Neuropathy. WB Saunders.

Easton, D.F., Ponder, M.A., Huson, S.M., and Ponder, B.A. (1993). An analysis of variation in expression of neurofibromatosis (NF) type 1 (NF1): evidence for modifying genes. American journal of human genetics *53*, 305-313.

Echave, P., Machado-da-Silva, G., Arkell, R.S., Duchen, M.R., Jacobson, J., Mitter, R., and Lloyd, A.C. (2009). Extracellular growth factors and mitogens cooperate to drive mitochondrial biogenesis. J Cell Sci *122*, 4516-4525.

Egeblad, M., Rasch, M.G., and Weaver, V.M. (2010). Dynamic interplay between the collagen scaffold and tumor evolution. Curr Opin Cell Biol *22*, 697-706.

Ehlers, M.D. (2004). Deconstructing the axon: Wallerian degeneration and the ubiquitin-proteasome system. Trends Neurosci *27*, 3-6.

Eldridge, C.F., Bunge, M.B., Bunge, R.P., and Wood, P.M. (1987). Differentiation of axon-related Schwann cells in vitro. I. Ascorbic acid regulates basal lamina assembly and myelin formation. The Journal of cell biology *105*, 1023-1034.

Elenbaas, B., and Weinberg, R.A. (2001). Heterotypic signaling between epithelial tumor cells and fibroblasts in carcinoma formation. Experimental cell research *264*, 169-184.

Elinav, E., Nowarski, R., Thaiss, C.A., Hu, B., Jin, C., and Flavell, R.A. (2013). Inflammation-induced cancer: crosstalk between tumours, immune cells and microorganisms. Nat Rev Cancer *13*, 759-771.

Ellenbroek, S.I., and van Rheenen, J. (2014). Imaging hallmarks of cancer in living mice. Nat Rev Cancer *14*, 406-418.

Eming, S.A., Wynn, T.A., and Martin, P. (2017). Inflammation and metabolism in tissue repair and regeneration. Science *356*, 1026-1030.

Endrullat, C., Glokler, J., Franke, P., and Frohme, M. (2016). Standardization and quality management in next-generation sequencing. Appl Transl Genom *10*, 2-9.

Erlandson, R.A. (1985). Peripheral nerve sheath tumors. Ultrastructural pathology *9*, 113-122.

Erlandson, R.A. (1991). The enigmatic perineurial cell and its participation in tumors and in tumorlike entities. Ultrastructural pathology *15*, 335-351.

Erler, J.T., Bennewith, K.L., Cox, T.R., Lang, G., Bird, D., Koong, A., Le, Q.T., and Giaccia, A.J. (2009). Hypoxia-induced lysyl oxidase is a critical mediator of bone marrow cell recruitment to form the premetastatic niche. Cancer Cell *15*, 35-44.

Erler, J.T., Bennewith, K.L., Nicolau, M., Dornhofer, N., Kong, C., Le, Q.T., Chi, J.T., Jeffrey, S.S., and Giaccia, A.J. (2006). Lysyl oxidase is essential for hypoxia-induced metastasis. Nature *440*, 1222-1226.

Eshed, Y., Feinberg, K., Poliak, S., Sabanay, H., Sarig-Nadir, O., Spiegel, I., Bermingham, J.R., Jr., and Peles, E. (2005). Gliomedin mediates Schwann cell-axon interaction and the molecular assembly of the nodes of Ranvier. Neuron *47*, 215-229.

Esper, R.M., Pankonin, M.S., and Loeb, J.A. (2006). Neuregulins: versatile growth and differentiation factors in nervous system development and human disease. Brain research reviews *51*, 161-175.

Espinosa-Medina, I., Outin, E., Picard, C.A., Chettouh, Z., Dymecki, S., Consalez, G.G., Coppola, E., and Brunet, J.F. (2014). Neurodevelopment. Parasympathetic ganglia derive from Schwann cell precursors. Science *345*, 87-90.

Evans, D.G., Baser, M.E., McGaughran, J., Sharif, S., Howard, E., and Moran, A. (2002). Malignant peripheral nerve sheath tumours in neurofibromatosis 1. Journal of medical genetics *39*, 311-314.

Farid, M., Demicco, E.G., Garcia, R., Ahn, L., Merola, P.R., Cioffi, A., and Maki, R.G. (2014). Malignant peripheral nerve sheath tumors. The oncologist *19*, 193-201.

Fazal, S.V., Gomez-Sanchez, J.A., Wagstaff, L.J., Musner, N., Otto, G., Janz, M., Mirsky, R., and Jessen, K.R. (2017). Graded Elevation of c-Jun in Schwann Cells In Vivo: Gene Dosage Determines Effects on Development, Remyelination, Tumorigenesis, and Hypomyelination. The Journal of neuroscience : the official journal of the Society for Neuroscience *37*, 12297-12313.

Fearon, E.R. (2011). Molecular genetics of colorectal cancer. Annu Rev Pathol *6*, 479-507.

Fearon, E.R., and Vogelstein, B. (1990). A genetic model for colorectal tumorigenesis. Cell *61*, 759-767.

Feil, S., Valtcheva, N., and Feil, R. (2009). Inducible Cre mice. Methods Mol Biol *530*, 343-363.

Feltri, M.L., D'Antonio, M., Quattrini, A., Numerato, R., Arona, M., Previtali, S., Chiu, S.Y., Messing, A., and Wrabetz, L. (1999). A novel P0 glycoprotein transgene activates expression of lacZ in myelin-forming Schwann cells. The European journal of neuroscience *11*, 1577-1586.

Feltri, M.L., Poitelon, Y., and Previtali, S.C. (2016). How Schwann Cells Sort Axons: New Concepts. Neuroscientist *22*, 252-265.

Feng, Y.Q., Lorincz, M.C., Fiering, S., Greally, J.M., and Bouhassira, E.E. (2001). Position effects are influenced by the orientation of a transgene with respect to flanking chromatin. Mol Cell Biol *21*, 298-309.

Feng, Z., and Ko, C.P. (2008). Schwann cells promote synaptogenesis at the neuromuscular junction via transforming growth factor-beta1. J Neurosci *28*, 9599-9609.

Fernandes, K.J., Kobayashi, N.R., Gallagher, C.J., Barnabe-Heider, F., Aumont, A., Kaplan, D.R., and Miller, F.D. (2006). Analysis of the neurogenic potential of multipotent skin-derived precursors. Experimental neurology *201*, 32-48.

Fernandes, K.J., Toma, J.G., and Miller, F.D. (2008). Multipotent skin-derived precursors: adult neural crest-related precursors with therapeutic potential. Philosophical transactions of the Royal Society of London Series B, Biological sciences *363*, 185-198.

Ferner, R.E., and Gutmann, D.H. (2002). International consensus statement on malignant peripheral nerve sheath tumors in neurofibromatosis. Cancer research *62*, 1573-1577.

Ferro, E., and Trabalzini, L. (2010). RalGDS family members couple Ras to Ral signalling and that's not all. Cellular signalling *22*, 1804-1810.

Fetsch, J.F., Michal, M., and Miettinen, M. (2000). Pigmented (melanotic) neurofibroma: a clinicopathologic and immunohistochemical analysis of 19 lesions from 17 patients. The American journal of surgical pathology *24*, 331-343.

Fields, R.D., Woo, D.H., and Basser, P.J. (2015). Glial Regulation of the Neuronal Connectome through Local and Long-Distant Communication. Neuron *86*, 374-386.

Filbin, M.T., Walsh, F.S., Trapp, B.D., Pizzey, J.A., and Tennekoon, G.I. (1990). Role of myelin P0 protein as a homophilic adhesion molecule. Nature *344*, 871-872.

Finzsch, M., Schreiner, S., Kichko, T., Reeh, P., Tamm, E.R., Bosl, M.R., Meijer, D., and Wegner, M. (2010). Sox10 is required for Schwann cell identity and progression beyond the immature Schwann cell stage. J Cell Biol *189*, 701-712.

Folkman, J., and Kalluri, R. (2004). Cancer without disease. Nature *427*, 787.

Fontana, X., Hristova, M., Da Costa, C., Patodia, S., Thei, L., Makwana, M., Spencer-Dene, B., Latouche, M., Mirsky, R., Jessen, K.R.*, et al.* (2012). c-Jun in Schwann cells promotes axonal regeneration and motoneuron survival via paracrine signaling. J Cell Biol *198*, 127-141.

Franco, O.E., Shaw, A.K., Strand, D.W., and Hayward, S.W. (2010). Cancer associated fibroblasts in cancer pathogenesis. Seminars in cell & developmental biology *21*, 33-39.

Frank, S.A. (2007). In Dynamics of Cancer: Incidence, Inheritance, and Evolution (Princeton (NJ)).

Frantz, C., Stewart, K.M., and Weaver, V.M. (2010). The extracellular matrix at a glance. J Cell Sci *123*, 4195-4200.

Fregnan, F., Muratori, L., Simoes, A.R., Giacobini-Robecchi, M.G., and Raimondo, S. (2012). Role of inflammatory cytokines in peripheral nerve injury. Neural Regen Res *7*, 2259-2266.

Fricker, F.R., Antunes-Martins, A., Galino, J., Paramsothy, R., La Russa, F., Perkins, J., Goldberg, R., Brelstaff, J., Zhu, N., McMahon, S.B.*, et al.* (2013). Axonal neuregulin 1

is a rate limiting but not essential factor for nerve remyelination. Brain : a journal of neurology *136*, 2279-2297.

Fricker, F.R., Lago, N., Balarajah, S., Tsantoulas, C., Tanna, S., Zhu, N., Fageiry, S.K., Jenkins, M., Garratt, A.N., Birchmeier, C*., et al.* (2011). Axonally derived neuregulin-1 is required for remyelination and regeneration after nerve injury in adulthood. J Neurosci *31*, 3225-3233.

Friedl, P., and Alexander, S. (2011). Cancer invasion and the microenvironment: plasticity and reciprocity. Cell *147*, 992-1009.

Friedman, J.M. (1999). Neurofibromatosis: Phenotype, Natural History, and Pathogenesis. The Johns Hopkins University Press *3rd edition*, 400.

Friedman, J.M., and Birch, P.H. (1997). Type 1 neurofibromatosis: a descriptive analysis of the disorder in 1,728 patients. Am J Med Genet *70*, 138-143.

Funakoshi, H., Frisen, J., Barbany, G., Timmusk, T., Zachrisson, O., Verge, V.M., and Persson, H. (1993). Differential expression of mRNAs for neurotrophins and their receptors after axotomy of the sciatic nerve. J Cell Biol *123*, 455-465.

Galli, S.J., Tsai, M., and Wershil, B.K. (1993). The c-kit receptor, stem cell factor, and mast cells. What each is teaching us about the others. The American journal of pathology *142*, 965-974.

Garratt, A.N., Voiculescu, O., Topilko, P., Charnay, P., and Birchmeier, C. (2000). A dual role of erbB2 in myelination and in expansion of the schwann cell precursor pool. J Cell Biol *148*, 1035-1046.

Gay, L., Baker, A.M., and Graham, T.A. (2016). Tumour Cell Heterogeneity. F1000Res *5*.

Ge, Y., and Fuchs, E. (2018). Stretching the limits: from homeostasis to stem cell plasticity in wound healing and cancer. Nature reviews Genetics *19*, 311-325.

Ge, Y., Gomez, N.C., Adam, R.C., Nikolova, M., Yang, H., Verma, A., Lu, C.P., Polak, L., Yuan, S., Elemento, O*., et al.* (2017). Stem Cell Lineage Infidelity Drives Wound Repair and Cancer. Cell *169*, 636-650 e614.

Gentleman, R.C., Carey, V.J., Bates, D.M., Bolstad, B., Dettling, M., Dudoit, S., Ellis, B., Gautier, L., Ge, Y., Gentry, J*., et al.* (2004). Bioconductor: open software development for computational biology and bioinformatics. Genome Biol *5*, R80.

Gerdts, J., Sasaki, Y., Vohra, B., Marasa, J., and Milbrandt, J. (2011). Image-based screening identifies novel roles for IkappaB kinase and glycogen synthase kinase 3 in axonal degeneration. J Biol Chem *286*, 28011-28018.

Gerlinger, M., and Swanton, C. (2010). How Darwinian models inform therapeutic failure initiated by clonal heterogeneity in cancer medicine. Br J Cancer *103*, 1139-1143.

Geuna, S., Raimondo, S., Ronchi, G., Di Scipio, F., Tos, P., Czaja, K., and Fornaro, M. (2009). Chapter 3: Histology of the peripheral nerve and changes occurring during nerve regeneration. International review of neurobiology *87*, 27-46.

Ghazvini, M., Mandemakers, W., Jaegle, M., Piirsoo, M., Driegen, S., Koutsourakis, M., Smit, X., Grosveld, F., and Meijer, D. (2002). A cell type-specific allele of the POU gene Oct-6 reveals Schwann cell autonomous function in nerve development and regeneration. The EMBO journal *21*, 4612-4620.

Gherghiceanu, M., Manole, C.G., and Popescu, L.M. (2010). Telocytes in endocardium: electron microscope evidence. Journal of cellular and molecular medicine *14*, 2330-2334.

Giese, K.P., Martini, R., Lemke, G., Soriano, P., and Schachner, M. (1992). Mouse P0 gene disruption leads to hypomyelination, abnormal expression of recognition molecules, and degeneration of myelin and axons. Cell *71*, 565-576.

Giles, R.H., van Es, J.H., and Clevers, H. (2003). Caught up in a Wnt storm: Wnt signaling in cancer. Biochim Biophys Acta *1653*, 1-24.

Glass, J.D., Culver, D.G., Levey, A.I., and Nash, N.R. (2002). Very early activation of m-calpain in peripheral nerve during Wallerian degeneration. J Neurol Sci *196*, 9-20.

Glenn, T.D., and Talbot, W.S. (2013). Signals regulating myelination in peripheral nerves and the Schwann cell response to injury. Current opinion in neurobiology *23*, 1041-1048.

Goebbels, S., Oltrogge, J.H., Kemper, R., Heilmann, I., Bormuth, I., Wolfer, S., Wichert, S.P., Mobius, W., Liu, X., Lappe-Siefke, C*., et al.* (2010). Elevated phosphatidylinositol 3,4,5-trisphosphate in glia triggers cell-autonomous membrane wrapping and myelination. J Neurosci *30*, 8953-8964.

Goebbels, S., Oltrogge, J.H., Wolfer, S., Wieser, G.L., Nientiedt, T., Pieper, A., Ruhwedel, T., Groszer, M., Sereda, M.W., and Nave, K.A. (2012). Genetic disruption

of Pten in a novel mouse model of tomaculous neuropathy. EMBO Mol Med *4*, 486-499.

Gomez-Sanchez, J.A., Carty, L., Iruarrizaga-Lejarreta, M., Palomo-Irigoyen, M., Varela-Rey, M., Griffith, M., Hantke, J., Macias-Camara, N., Azkargorta, M., Aurrekoetxea, I.*, et al.* (2015). Schwann cell autophagy, myelinophagy, initiates myelin clearance from injured nerves. The Journal of cell biology *210*, 153-168.

Gomez-Sanchez, J.A., Pilch, K.S., van der Lans, M., Fazal, S.V., Benito, C., Wagstaff, L.J., Mirsky, R., and Jessen, K.R. (2017). After Nerve Injury, Lineage Tracing Shows That Myelin and Remak Schwann Cells Elongate Extensively and Branch to Form Repair Schwann Cells, Which Shorten Radically on Remyelination. J Neurosci *37*, 9086-9099.

Greaves, M., and Maley, C.C. (2012). Clonal evolution in cancer. Nature *481*, 306-313.

Green, J.E., and Hudson, T. (2005). The promise of genetically engineered mice for cancer prevention studies. Nat Rev Cancer *5*, 184-198.

Gregorian, C., Nakashima, J., Dry, S.M., Nghiemphu, P.L., Smith, K.B., Ao, Y., Dang, J., Lawson, G., Mellinghoff, I.K., Mischel, P.S.*, et al.* (2009). PTEN dosage is essential for neurofibroma development and malignant transformation. Proceedings of the National Academy of Sciences of the United States of America *106*, 19479-19484.

Gresset, A., Coulpier, F., Gerschenfeld, G., Jourdon, A., Matesic, G., Richard, L., Vallat, J.M., Charnay, P., and Topilko, P. (2015). Boundary Caps Give Rise to Neurogenic Stem Cells and Terminal Glia in the Skin. Stem Cell Reports *5*, 278-290.

Griffin, J.W., and Thompson, W.J. (2008). Biology and pathology of nonmyelinating Schwann cells. Glia *56*, 1518-1531.

Grivennikov, S.I., Greten, F.R., and Karin, M. (2010). Immunity, inflammation, and cancer. Cell *140*, 883-899.

Grivennikov, S.I., and Karin, M. (2011). Inflammatory cytokines in cancer: tumour necrosis factor and interleukin 6 take the stage. Ann Rheum Dis *70 Suppl 1*, i104-108.

Groden, J., Thliveris, A., Samowitz, W., Carlson, M., Gelbert, L., Albertsen, H., Joslyn, G., Stevens, J., Spirio, L., Robertson, M.*, et al.* (1991). Identification and characterization of the familial adenomatous polyposis coli gene. Cell *66*, 589-600.

Grubisic, V., and Gulbransen, B.D. (2017). Enteric glia: the most alimentary of all glia. J Physiol *595*, 557-570.

Guertin, A.D., Zhang, D.P., Mak, K.S., Alberta, J.A., and Kim, H.A. (2005). Microanatomy of axon/glial signaling during Wallerian degeneration. J Neurosci *25*, 3478-3487.

Guimaraes-Camboa, N., Cattaneo, P., Sun, Y., Moore-Morris, T., Gu, Y., Dalton, N.D., Rockenstein, E., Masliah, E., Peterson, K.L., Stallcup, W.B.*, et al.* (2017). Pericytes of Multiple Organs Do Not Behave as Mesenchymal Stem Cells In Vivo. Cell stem cell *20*, 345-359 e345.

Gutmann, D.H., Wood, D.L., and Collins, F.S. (1991). Identification of the neurofibromatosis type 1 gene product. Proc Natl Acad Sci U S A *88*, 9658-9662.

Habringer, S., Lapa, C., Herhaus, P., Schottelius, M., Istvanffy, R., Steiger, K., Slotta-Huspenina, J., Schirbel, A., Hanscheid, H., Kircher, S.*, et al.* (2018). Dual Targeting of Acute Leukemia and Supporting Niche by CXCR4-Directed Theranostics. Theranostics *8*, 369-383.

Hajra, A., Martin-Gallardo, A., Tarle, S.A., Freedman, M., Wilson-Gunn, S., Bernards, A., and Collins, F.S. (1994). DNA sequences in the promoter region of the NF1 gene are highly conserved between human and mouse. Genomics *21*, 649-652.

Hall, S. (2005). The response to injury in the peripheral nervous system. J Bone Joint Surg Br *87*, 1309-1319.

Hall, S.M., Li, H., and Kent, A.P. (1997). Schwann cells responding to primary demyelination in vivo express p75NTR and c-erbB receptors: a light and electron immunohistochemical study. J Neurocytol *26*, 679-690.

Hanahan, D., and Coussens, L.M. (2012). Accessories to the crime: functions of cells recruited to the tumor microenvironment. Cancer cell *21*, 309-322.

Hanahan, D., and Folkman, J. (1996). Patterns and emerging mechanisms of the angiogenic switch during tumorigenesis. Cell *86*, 353-364.

Hanahan, D., Wagner, E.F., and Palmiter, R.D. (2007). The origins of oncomice: a history of the first transgenic mice genetically engineered to develop cancer. Genes Dev *21*, 2258-2270.

Hanahan, D., and Weinberg, R.A. (2011). Hallmarks of cancer: the next generation. Cell *144*, 646-674.

Hanani, M. (2012). Intercellular communication in sensory ganglia by purinergic receptors and gap junctions: implications for chronic pain. Brain research *1487*, 183-191.

Harauz, G., Ladizhansky, V., and Boggs, J.M. (2009). Structural polymorphism and multifunctionality of myelin basic protein. Biochemistry *48*, 8094-8104.

Harno, E., Cottrell, E.C., and White, A. (2013). Metabolic pitfalls of CNS Cre-based technology. Cell Metab *18*, 21-28.

Harrisingh, M.C., Perez-Nadales, E., Parkinson, D.B., Malcolm, D.S., Mudge, A.W., and Lloyd, A.C. (2004). The Ras/Raf/ERK signalling pathway drives Schwann cell dedifferentiation. EMBO J *23*, 3061-3071.

Harty, B.L., and Monk, K.R. (2017). Unwrapping the unappreciated: recent progress in Remak Schwann cell biology. Current opinion in neurobiology *47*, 131-137.

Hayasaka, K., Himoro, M., Sato, W., Takada, G., Uyemura, K., Shimizu, N., Bird, T.D., Conneally, P.M., and Chance, P.F. (1993a). Charcot-Marie-Tooth neuropathy type 1B is associated with mutations of the myelin P0 gene. Nat Genet *5*, 31-34.

Hayasaka, K., Himoro, M., Sawaishi, Y., Nanao, K., Takahashi, T., Takada, G., Nicholson, G.A., Ouvrier, R.A., and Tachi, N. (1993b). De novo mutation of the myelin P0 gene in Dejerine-Sottas disease (hereditary motor and sensory neuropathy type III). Nat Genet *5*, 266-268.

He, X., Zhang, L., Queme, L.F., Liu, X., Lu, A., Waclaw, R.R., Dong, X., Zhou, W., Kidd, G., Yoon, S.O.*, et al.* (2018). A histone deacetylase 3-dependent pathway delimits peripheral myelin growth and functional regeneration. Nature medicine *24*, 338-351.

Heffner, C.S., Herbert Pratt, C., Babiuk, R.P., Sharma, Y., Rockwood, S.F., Donahue, L.R., Eppig, J.T., and Murray, S.A. (2012). Supporting conditional mouse mutagenesis with a comprehensive cre characterization resource. Nat Commun *3*, 1218.

Hidai, C., Zupancic, T., Penta, K., Mikhail, A., Kawana, M., Quertermous, E.E., Aoka, Y., Fukagawa, M., Matsui, Y., Platika, D.*, et al.* (1998). Cloning and characterization of developmental endothelial locus-1: an embryonic endothelial cell protein that binds the alphavbeta3 integrin receptor. Genes Dev *12*, 21-33.

Hikawa, N., and Takenaka, T. (1996). Myelin-stimulated macrophages release neurotrophic factors for adult dorsal root ganglion neurons in culture. Cellular and molecular neurobiology *16*, 517-528.

Hirata, K., and Kawabuchi, M. (2002). Myelin phagocytosis by macrophages and nonmacrophages during Wallerian degeneration. Microsc Res Tech *57*, 541-547.
Hirbe, A.C., and Gutmann, D.H. (2014). Neurofibromatosis type 1: a multidisciplinary approach to care. The Lancet Neurology *13*, 834-843.
Hjerling-Leffler, J., Marmigere, F., Heglind, M., Cederberg, A., Koltzenburg, M., Enerback, S., and Ernfors, P. (2005). The boundary cap: a source of neural crest stem cells that generate multiple sensory neuron subtypes. Development *132*, 2623-2632.
Hochberg, B.a. (1995). Controlling the False Discovery Rate: A Practical and Powerful Approach to Multiple Testing. Journal of the Royal Statistical Society.
Holt, K.H., Kasson, B.G., and Pessin, J.E. (1996). Insulin stimulation of a MEK-dependent but ERK-independent SOS protein kinase. Molecular and cellular biology *16*, 577-583.
Hoopfer, E.D., McLaughlin, T., Watts, R.J., Schuldiner, O., O'Leary, D.D., and Luo, L. (2006). Wlds protection distinguishes axon degeneration following injury from naturally occurring developmental pruning. Neuron *50*, 883-895.
Hsieh, S.T., Kidd, G.J., Crawford, T.O., Xu, Z., Lin, W.M., Trapp, B.D., Cleveland, D.W., and Griffin, J.W. (1994). Regional modulation of neurofilament organization by myelination in normal axons. J Neurosci *14*, 6392-6401.
Huang, E., Nocka, K., Beier, D.R., Chu, T.Y., Buck, J., Lahm, H.W., Wellner, D., Leder, P., and Besmer, P. (1990). The hematopoietic growth factor KL is encoded by the Sl locus and is the ligand of the c-kit receptor, the gene product of the W locus. Cell *63*, 225-233.
Huijbregts, R.P., Roth, K.A., Schmidt, R.E., and Carroll, S.L. (2003). Hypertrophic neuropathies and malignant peripheral nerve sheath tumors in transgenic mice overexpressing glial growth factor beta3 in myelinating Schwann cells. J Neurosci *23*, 7269-7280.
Ijichi, H., Chytil, A., Gorska, A.E., Aakre, M.E., Bierie, B., Tada, M., Mohri, D., Miyabayashi, K., Asaoka, Y., Maeda, S.*, et al.* (2011). Inhibiting Cxcr2 disrupts tumor-stromal interactions and improves survival in a mouse model of pancreatic ductal adenocarcinoma. The Journal of clinical investigation *121*, 4106-4117.
Imbeaud, S., Graudens, E., Boulanger, V., Barlet, X., Zaborski, P., Eveno, E., Mueller, O., Schroeder, A., and Auffray, C. (2005). Towards standardization of RNA quality

assessment using user-independent classifiers of microcapillary electrophoresis traces. Nucleic Acids Res *33*, e56.

Ingram, D.A., Hiatt, K., King, A.J., Fisher, L., Shivakumar, R., Derstine, C., Wenning, M.J., Diaz, B., Travers, J.B., Hood, A.*, et al.* (2001). Hyperactivation of p21(ras) and the hematopoietic-specific Rho GTPase, Rac2, cooperate to alter the proliferation of neurofibromin-deficient mast cells in vivo and in vitro. The Journal of experimental medicine *194*, 57-69.

Ingram, D.A., Yang, F.C., Travers, J.B., Wenning, M.J., Hiatt, K., New, S., Hood, A., Shannon, K., Williams, D.A., and Clapp, D.W. (2000). Genetic and biochemical evidence that haploinsufficiency of the Nf1 tumor suppressor gene modulates melanocyte and mast cell fates in vivo. The Journal of experimental medicine *191*, 181-188.

Ishii, A., Furusho, M., and Bansal, R. (2013). Sustained activation of ERK1/2 MAPK in oligodendrocytes and schwann cells enhances myelin growth and stimulates oligodendrocyte progenitor expansion. J Neurosci *33*, 175-186.

Ishii, A., Furusho, M., Dupree, J.L., and Bansal, R. (2016). Strength of ERK1/2 MAPK Activation Determines Its Effect on Myelin and Axonal Integrity in the Adult CNS. The Journal of neuroscience : the official journal of the Society for Neuroscience *36*, 6471-6487.

Ito, M., Liu, Y., Yang, Z., Nguyen, J., Liang, F., Morris, R.J., and Cotsarelis, G. (2005). Stem cells in the hair follicle bulge contribute to wound repair but not to homeostasis of the epidermis. Nature medicine *11*, 1351-1354.

Ito, M., Yang, Z., Andl, T., Cui, C., Kim, N., Millar, S.E., and Cotsarelis, G. (2007). Wnt-dependent de novo hair follicle regeneration in adult mouse skin after wounding. Nature *447*, 316-320.

Ito, T., Ikeda, K., Tomita, K., and Yokoyama, S. (2010). Interleukin-6 upregulates the expression of PMP22 in cultured rat Schwann cells via a JAK2-dependent pathway. Neurosci Lett *472*, 104-108.

Jacks, T., Shih, T.S., Schmitt, E.M., Bronson, R.T., Bernards, A., and Weinberg, R.A. (1994). Tumour predisposition in mice heterozygous for a targeted mutation in Nf1. Nat Genet *7*, 353-361.

Jackson, E.L., Willis, N., Mercer, K., Bronson, R.T., Crowley, D., Montoya, R., Jacks, T., and Tuveson, D.A. (2001). Analysis of lung tumor initiation and progression using conditional expression of oncogenic K-ras. Genes Dev *15*, 3243-3248.

Jacob, C., Christen, C.N., Pereira, J.A., Somandin, C., Baggiolini, A., Lotscher, P., Ozcelik, M., Tricaud, N., Meijer, D., Yamaguchi, T.*, et al.* (2011a). HDAC1 and HDAC2 control the transcriptional program of myelination and the survival of Schwann cells. Nat Neurosci *14*, 429-436.

Jacob, C., Lebrun-Julien, F., and Suter, U. (2011b). How histone deacetylases control myelination. Mol Neurobiol *44*, 303-312.

Jacob, C., Lotscher, P., Engler, S., Baggiolini, A., Varum Tavares, S., Brugger, V., John, N., Buchmann-Moller, S., Snider, P.L., Conway, S.J.*, et al.* (2014). HDAC1 and HDAC2 control the specification of neural crest cells into peripheral glia. J Neurosci *34*, 6112-6122.

Jaegle, M., Ghazvini, M., Mandemakers, W., Piirsoo, M., Driegen, S., Levavasseur, F., Raghoenath, S., Grosveld, F., and Meijer, D. (2003). The POU proteins Brn-2 and Oct-6 share important functions in Schwann cell development. Genes Dev *17*, 1380-1391.

Jagalur, N.B., Ghazvini, M., Mandemakers, W., Driegen, S., Maas, A., Jones, E.A., Jaegle, M., Grosveld, F., Svaren, J., and Meijer, D. (2011). Functional dissection of the Oct6 Schwann cell enhancer reveals an essential role for dimeric Sox10 binding. J Neurosci *31*, 8585-8594.

Jessen, K.R., Brennan, A., Morgan, L., Mirsky, R., Kent, A., Hashimoto, Y., and Gavrilovic, J. (1994). The Schwann cell precursor and its fate: a study of cell death and differentiation during gliogenesis in rat embryonic nerves. Neuron *12*, 509-527.

Jessen, K.R., and Mirsky, R. (1991). Schwann cell precursors and their development. Glia *4*, 185-194.

Jessen, K.R., and Mirsky, R. (2002). Signals that determine Schwann cell identity. J Anat *200*, 367-376.

Jessen, K.R., and Mirsky, R. (2005). The origin and development of glial cells in peripheral nerves. Nat Rev Neurosci *6*, 671-682.

Jessen, K.R., and Mirsky, R. (2008). Negative regulation of myelination: relevance for development, injury, and demyelinating disease. Glia *56*, 1552-1565.

Jessen, K.R., Mirsky, R., and Lloyd, A.C. (2015). Schwann Cells: Development and Role in Nerve Repair. Cold Spring Harb Perspect Biol *7*, a020487.

Jessen, K.R., Morgan, L., Stewart, H.J., and Mirsky, R. (1990). Three markers of adult non-myelin-forming Schwann cells, 217c(Ran-1), A5E3 and GFAP: development and regulation by neuron-Schwann cell interactions. Development *109*, 91-103.

Jessen, W.J., Miller, S.J., Jousma, E., Wu, J., Rizvi, T.A., Brundage, M.E., Eaves, D., Widemann, B., Kim, M.O., Dombi, E.*, et al.* (2013). MEK inhibition exhibits efficacy in human and mouse neurofibromatosis tumors. J Clin Invest *123*, 340-347.

Ji, R.R., Berta, T., and Nedergaard, M. (2013). Glia and pain: is chronic pain a gliopathy? Pain *154 Suppl 1*, S10-28.

Jia, H., Yan, T., Feng, Y., Zeng, C., Shi, X., and Zhai, Q. (2007). Identification of a critical site in Wld(s): essential for Nmnat enzyme activity and axon-protective function. Neurosci Lett *413*, 46-51.

Jiang, S.H., Wang, Y., Yang, J.Y., Li, J., Feng, M.X., Wang, Y.H., Yang, X.M., He, P., Tian, G.A., Zhang, X.X.*, et al.* (2016). Overexpressed EDIL3 predicts poor prognosis and promotes anchorage-independent tumor growth in human pancreatic cancer. Oncotarget *7*, 4226-4240.

Jin, J.J., Nikitin, A., and Rajewsky, M.F. (1993). Schwann cell lineage-specific neu (erbB-2) gene expression in the developing rat nervous system. Cell Growth Differ *4*, 227-237.

Johannessen, C.M., Johnson, B.W., Williams, S.M., Chan, A.W., Reczek, E.E., Lynch, R.C., Rioth, M.J., McClatchey, A., Ryeom, S., and Cichowski, K. (2008). TORC1 is essential for NF1-associated malignancies. Curr Biol *18*, 56-62.

Johannessen, C.M., Reczek, E.E., James, M.F., Brems, H., Legius, E., and Cichowski, K. (2005). The NF1 tumor suppressor critically regulates TSC2 and mTOR. Proc Natl Acad Sci U S A *102*, 8573-8578.

Jopling, C., Boue, S., and Izpisua Belmonte, J.C. (2011). Dedifferentiation, transdifferentiation and reprogramming: three routes to regeneration. Nature reviews Molecular cell biology *12*, 79-89.

Joseph, N.M., Mosher, J.T., Buchstaller, J., Snider, P., McKeever, P.E., Lim, M., Conway, S.J., Parada, L.F., Zhu, Y., and Morrison, S.J. (2008). The loss of Nf1

transiently promotes self-renewal but not tumorigenesis by neural crest stem cells. Cancer Cell *13*, 129-140.

Joseph, N.M., Mukouyama, Y.S., Mosher, J.T., Jaegle, M., Crone, S.A., Dormand, E.L., Lee, K.F., Meijer, D., Anderson, D.J., and Morrison, S.J. (2004). Neural crest stem cells undergo multilineage differentiation in developing peripheral nerves to generate endoneurial fibroblasts in addition to Schwann cells. Development *131*, 5599-5612.

Jouhilahti, E.M., Peltonen, S., Heape, A.M., and Peltonen, J. (2011). The pathoetiology of neurofibromatosis 1. Am J Pathol *178*, 1932-1939.

Joyce, J.A. (2005). Therapeutic targeting of the tumor microenvironment. Cancer cell *7*, 513-520.

Joyce, J.A., and Pollard, J.W. (2009). Microenvironmental regulation of metastasis. Nature reviews Cancer *9*, 239-252.

Kaller, M.S., Lazari, A., Blanco-Duque, C., Sampaio-Baptista, C., and Johansen-Berg, H. (2017). Myelin plasticity and behaviour-connecting the dots. Curr Opin Neurobiol *47*, 86-92.

Kalluri, R. (2016). The biology and function of fibroblasts in cancer. Nat Rev Cancer *16*, 582-598.

Kalluri, R., and Zeisberg, M. (2006). Fibroblasts in cancer. Nature reviews Cancer *6*, 392-401.

Kang, H., and Lichtman, J.W. (2013). Motor axon regeneration and muscle reinnervation in young adult and aged animals. J Neurosci *33*, 19480-19491.

Kang, H., Tian, L., Mikesh, M., Lichtman, J.W., and Thompson, W.J. (2014). Terminal Schwann cells participate in neuromuscular synapse remodeling during reinnervation following nerve injury. The Journal of neuroscience : the official journal of the Society for Neuroscience *34*, 6323-6333.

Kang, S.H., Fukaya, M., Yang, J.K., Rothstein, J.D., and Bergles, D.E. (2010). NG2+ CNS glial progenitors remain committed to the oligodendrocyte lineage in postnatal life and following neurodegeneration. Neuron *68*, 668-681.

Kao, S.C., Wu, H., Xie, J., Chang, C.P., Ranish, J.A., Graef, I.A., and Crabtree, G.R. (2009). Calcineurin/NFAT signaling is required for neuregulin-regulated Schwann cell differentiation. Science *323*, 651-654.

Kegel, L., Aunin, E., Meijer, D., and Bermingham, J.R. (2013). LGI proteins in the nervous system. ASN Neuro *5*, 167-181.

Kennedy, A.D., and DeLeo, F.R. (2009). Neutrophil apoptosis and the resolution of infection. Immunol Res *43*, 25-61.

Khwaja, A., Rodriguez-Viciana, P., Wennstrom, S., Warne, P.H., and Downward, J. (1997). Matrix adhesion and Ras transformation both activate a phosphoinositide 3-OH kinase and protein kinase B/Akt cellular survival pathway. EMBO J *16*, 2783-2793.

Kidd, G.J., Ohno, N., and Trapp, B.D. (2013). Biology of Schwann cells. Handbook of clinical neurology *115*, 55-79.

Kijima, T., Maulik, G., Ma, P.C., Tibaldi, E.V., Turner, R.E., Rollins, B., Sattler, M., Johnson, B.E., and Salgia, R. (2002). Regulation of cellular proliferation, cytoskeletal function, and signal transduction through CXCR4 and c-Kit in small cell lung cancer cells. Cancer research *62*, 6304-6311.

Kim, H.A., Ling, B., and Ratner, N. (1997). Nf1-deficient mouse Schwann cells are angiogenic and invasive and can be induced to hyperproliferate: reversion of some phenotypes by an inhibitor of farnesyl protein transferase. Mol Cell Biol *17*, 862-872.

Kim, H.A., Pomeroy, S.L., Whoriskey, W., Pawlitzky, I., Benowitz, L.I., Sicinski, P., Stiles, C.D., and Roberts, T.M. (2000). A developmentally regulated switch directs regenerative growth of Schwann cells through cyclin D1. Neuron *26*, 405-416.

Kim, H.A., Ratner, N., Roberts, T.M., and Stiles, C.D. (2001). Schwann cell proliferative responses to cAMP and Nf1 are mediated by cyclin D1. J Neurosci *21*, 1110-1116.

Kim, H.A., Rosenbaum, T., Marchionni, M.A., Ratner, N., and DeClue, J.E. (1995). Schwann cells from neurofibromin deficient mice exhibit activation of p21ras, inhibition of cell proliferation and morphological changes. Oncogene *11*, 325-335.

Kim, J.D., Choi, B.K., Bae, J.S., Lee, U.H., Han, I.S., Lee, H.W., Youn, B.S., Vinay, D.S., and Kwon, B.S. (2003). Cloning and characterization of GITR ligand. Genes Immun *4*, 564-569.

Kim, T.M., Jung, S.H., An, C.H., Lee, S.H., Baek, I.P., Kim, M.S., Park, S.W., Rhee, J.K., Lee, S.H., and Chung, Y.J. (2015). Subclonal Genomic Architectures of Primary and Metastatic Colorectal Cancer Based on Intratumoral Genetic Heterogeneity. Clin Cancer Res *21*, 4461-4472.

King, D., Yang, G., Thompson, M.A., and Hiebert, S.W. (2002). Loss of neurofibromatosis-1 and p19(ARF) cooperate to induce a multiple tumor phenotype. Oncogene *21*, 4978-4982.

Kirschner, D.A., and Ganser, A.L. (1980). Compact myelin exists in the absence of basic protein in the shiverer mutant mouse. Nature *283*, 207-210.

Klar, A., Baldassare, M., and Jessell, T.M. (1992). F-spondin: a gene expressed at high levels in the floor plate encodes a secreted protein that promotes neural cell adhesion and neurite extension. Cell *69*, 95-110.

Klein, D., and Martini, R. (2016). Myelin and macrophages in the PNS: An intimate relationship in trauma and disease. Brain Res *1641*, 130-138.

Klemm, F., and Joyce, J.A. (2015). Microenvironmental regulation of therapeutic response in cancer. Trends in cell biology *25*, 198-213.

Ko, C.P., and Robitaille, R. (2015). Perisynaptic Schwann Cells at the Neuromuscular Synapse: Adaptable, Multitasking Glial Cells. Cold Spring Harbor perspectives in biology *7*, a020503.

Kolodkin, A.L., Levengood, D.V., Rowe, E.G., Tai, Y.T., Giger, R.J., and Ginty, D.D. (1997). Neuropilin is a semaphorin III receptor. Cell *90*, 753-762.

Kondo, M., Wagers, A.J., Manz, M.G., Prohaska, S.S., Scherer, D.C., Beilhack, G.F., Shizuru, J.A., and Weissman, I.L. (2003). Biology of hematopoietic stem cells and progenitors: implications for clinical application. Annual review of immunology *21*, 759-806.

Kong, B., Michalski, C.W., Erkan, M., Friess, H., and Kleeff, J. (2011). From tissue turnover to the cell of origin for pancreatic cancer. Nature reviews Gastroenterology & hepatology *8*, 467-472.

Korinek, V., Barker, N., Morin, P.J., van Wichen, D., de Weger, R., Kinzler, K.W., Vogelstein, B., and Clevers, H. (1997). Constitutive transcriptional activation by a beta-catenin-Tcf complex in APC-/- colon carcinoma. Science *275*, 1784-1787.

Koshiba, T., Hosotani, R., Miyamoto, Y., Ida, J., Tsuji, S., Nakajima, S., Kawaguchi, M., Kobayashi, H., Doi, R., Hori, T.*, et al.* (2000). Expression of stromal cell-derived factor 1 and CXCR4 ligand receptor system in pancreatic cancer: a possible role for tumor progression. Clinical cancer research : an official journal of the American Association for Cancer Research *6*, 3530-3535.

Kreso, A., and Dick, J.E. (2014). Evolution of the cancer stem cell model. Cell stem cell *14*, 275-291.

Kreso, A., O'Brien, C.A., van Galen, P., Gan, O.I., Notta, F., Brown, A.M., Ng, K., Ma, J., Wienholds, E., Dunant, C.*, et al.* (2013). Variable clonal repopulation dynamics influence chemotherapy response in colorectal cancer. Science *339*, 543-548.

Kretzschmar, K., and Watt, F.M. (2012). Lineage tracing. Cell *148*, 33-45.

Kruger, G.M., Mosher, J.T., Bixby, S., Joseph, N., Iwashita, T., and Morrison, S.J. (2002). Neural crest stem cells persist in the adult gut but undergo changes in self-renewal, neuronal subtype potential, and factor responsiveness. Neuron *35*, 657-669.

Kuhlbrodt, K., Herbarth, B., Sock, E., Hermans-Borgmeyer, I., and Wegner, M. (1998). Sox10, a novel transcriptional modulator in glial cells. J Neurosci *18*, 237-250.

Kuhlmann, T., Bitsch, A., Stadelmann, C., Siebert, H., and Bruck, W. (2001). Macrophages are eliminated from the injured peripheral nerve via local apoptosis and circulation to regional lymph nodes and the spleen. J Neurosci *21*, 3401-3408.

Kuilman, T., Michaloglou, C., Vredeveld, L.C., Douma, S., van Doorn, R., Desmet, C.J., Aarden, L.A., Mooi, W.J., and Peeper, D.S. (2008). Oncogene-induced senescence relayed by an interleukin-dependent inflammatory network. Cell *133*, 1019-1031.

Kweh, F., Zheng, M., Kurenova, E., Wallace, M., Golubovskaya, V., and Cance, W.G. (2009). Neurofibromin physically interacts with the N-terminal domain of focal adhesion kinase. Mol Carcinog *48*, 1005-1017.

La Fleur, M., Underwood, J.L., Rappolee, D.A., and Werb, Z. (1996). Basement membrane and repair of injury to peripheral nerve: defining a potential role for macrophages, matrix metalloproteinases, and tissue inhibitor of metalloproteinases-1. J Exp Med *184*, 2311-2326.

Lakkis, M.M., and Epstein, J.A. (1998). Neurofibromin modulation of ras activity is required for normal endocardial-mesenchymal transformation in the developing heart. Development *125*, 4359-4367.

Lamouille, S., Xu, J., and Derynck, R. (2014). Molecular mechanisms of epithelial-mesenchymal transition. Nat Rev Mol Cell Biol *15*, 178-196.

Langley, R.R., and Fidler, I.J. (2011). The seed and soil hypothesis revisited--the role of tumor-stroma interactions in metastasis to different organs. International journal of cancer *128*, 2527-2535.

Lara-Ramirez, R., Segura-Anaya, E., Martinez-Gomez, A., and Dent, M.A. (2008). Expression of interleukin-6 receptor alpha in normal and injured rat sciatic nerve. Neuroscience *152*, 601-608.

Laverdiere, C., Hoang, B.H., Yang, R., Sowers, R., Qin, J., Meyers, P.A., Huvos, A.G., Healey, J.H., and Gorlick, R. (2005). Messenger RNA expression levels of CXCR4 correlate with metastatic behavior and outcome in patients with osteosarcoma. Clinical cancer research : an official journal of the American Association for Cancer Research *11*, 2561-2567.

Le Douarin, N.M., and Teillet, M.A. (1974). Experimental analysis of the migration and differentiation of neuroblasts of the autonomic nervous system and of neurectodermal mesenchymal derivatives, using a biological cell marking technique. Dev Biol *41*, 162-184.

Le, L.Q., Liu, C., Shipman, T., Chen, Z., Suter, U., and Parada, L.F. (2011). Susceptible stages in Schwann cells for NF1-associated plexiform neurofibroma development. Cancer Res *71*, 4686-4695.

Le, L.Q., Shipman, T., Burns, D.K., and Parada, L.F. (2009). Cell of origin and microenvironment contribution for NF1-associated dermal neurofibromas. Cell stem cell *4*, 453-463.

Le Magnen, C., Dutta, A., and Abate-Shen, C. (2016). Optimizing mouse models for precision cancer prevention. Nat Rev Cancer *16*, 187-196.

Le, N., Nagarajan, R., Wang, J.Y., Araki, T., Schmidt, R.E., and Milbrandt, J. (2005). Analysis of congenital hypomyelinating Egr2Lo/Lo nerves identifies Sox2 as an inhibitor of Schwann cell differentiation and myelination. Proc Natl Acad Sci U S A *102*, 2596-2601.

Lee, D.Y., Yeh, T.H., Emnett, R.J., White, C.R., and Gutmann, D.H. (2010). Neurofibromatosis-1 regulates neuroglial progenitor proliferation and glial differentiation in a brain region-specific manner. Genes & development *24*, 2317-2329.

Lee, J.E., Moon, P.G., Cho, Y.E., Kim, Y.B., Kim, I.S., Park, H., and Baek, M.C. (2016). Identification of EDIL3 on extracellular vesicles involved in breast cancer cell invasion. Journal of proteomics *131*, 17-28.

Lee, W., Teckie, S., Wiesner, T., Ran, L., Prieto Granada, C.N., Lin, M., Zhu, S., Cao, Z., Liang, Y., Sboner, A*., et al.* (2014). PRC2 is recurrently inactivated through EED or SUZ12 loss in malignant peripheral nerve sheath tumors. Nature genetics *46*, 1227-1232.

Lee, Y.I., Thompson, W.J., and Harlow, M.L. (2017). Schwann cells participate in synapse elimination at the developing neuromuscular junction. Current opinion in neurobiology *47*, 176-181.

Leevers, S.J., Paterson, H.F., and Marshall, C.J. (1994). Requirement for Ras in Raf activation is overcome by targeting Raf to the plasma membrane. Nature *369*, 411-414.

Lefcort, F., Venstrom, K., McDonald, J.A., and Reichardt, L.F. (1992). Regulation of expression of fibronectin and its receptor, alpha 5 beta 1, during development and regeneration of peripheral nerve. Development *116*, 767-782.

Lefort, S., Thuleau, A., Kieffer, Y., Sirven, P., Bieche, I., Marangoni, E., Vincent-Salomon, A., and Mechta-Grigoriou, F. (2017). CXCR4 inhibitors could benefit to HER2 but not to triple-negative breast cancer patients. Oncogene *36*, 1211-1222.

Lemke, G. (1988). Unwrapping the genes of myelin. Neuron *1*, 535-543.

Lemke, G., and Chao, M. (1988). Axons regulate Schwann cell expression of the major myelin and NGF receptor genes. Development *102*, 499-504.

Leone, D.P., Genoud, S., Atanasoski, S., Grausenburger, R., Berger, P., Metzger, D., Macklin, W.B., Chambon, P., and Suter, U. (2003). Tamoxifen-inducible glia-specific Cre mice for somatic mutagenesis in oligodendrocytes and Schwann cells. Mol Cell Neurosci *22*, 430-440.

Levental, K.R., Yu, H., Kass, L., Lakins, J.N., Egeblad, M., Erler, J.T., Fong, S.F., Csiszar, K., Giaccia, A., Weninger, W*., et al.* (2009). Matrix crosslinking forces tumor progression by enhancing integrin signaling. Cell *139*, 891-906.

Levy, P., Vidaud, D., Leroy, K., Laurendeau, I., Wechsler, J., Bolasco, G., Parfait, B., Wolkenstein, P., Vidaud, M., and Bieche, I. (2004). Molecular profiling of malignant

peripheral nerve sheath tumors associated with neurofibromatosis type 1, based on large-scale real-time RT-PCR. Molecular cancer *3*, 20.

Lewallen, K.A., Shen, Y.A., De la Torre, A.R., Ng, B.K., Meijer, D., and Chan, J.R. (2011). Assessing the role of the cadherin/catenin complex at the Schwann cell-axon interface and in the initiation of myelination. J Neurosci *31*, 3032-3043.

Li, H., Velasco-Miguel, S., Vass, W.C., Parada, L.F., and DeClue, J.E. (2002). Epidermal growth factor receptor signaling pathways are associated with tumorigenesis in the Nf1:p53 mouse tumor model. Cancer research *62*, 4507-4513.

Li, H., Yang, H., Liu, Y., Huan, W., Zhang, S., Wu, G., Lu, Q., Wang, Q., and Wang, Y. (2011). The cyclin-dependent kinase inhibitor p27(Kip1) is a positive regulator of Schwann cell differentiation in vitro. J Mol Neurosci *45*, 277-283.

Li, L., and Clevers, H. (2010). Coexistence of quiescent and active adult stem cells in mammals. Science *327*, 542-545.

Li, Y.M., Pan, Y., Wei, Y., Cheng, X., Zhou, B.P., Tan, M., Zhou, X., Xia, W., Hortobagyi, G.N., Yu, D.*, et al.* (2004). Upregulation of CXCR4 is essential for HER2-mediated tumor metastasis. Cancer cell *6*, 459-469.

Liebscher, I., Schon, J., Petersen, S.C., Fischer, L., Auerbach, N., Demberg, L.M., Mogha, A., Coster, M., Simon, K.U., Rothemund, S.*, et al.* (2014). A tethered agonist within the ectodomain activates the adhesion G protein-coupled receptors GPR126 and GPR133. Cell reports *9*, 2018-2026.

Lin, H.J., Zuo, T., Lin, C.H., Kuo, C.T., Liyanarachchi, S., Sun, S., Shen, R., Deatherage, D.E., Potter, D., Asamoto, L.*, et al.* (2008). Breast cancer-associated fibroblasts confer AKT1-mediated epigenetic silencing of Cystatin M in epithelial cells. Cancer research *68*, 10257-10266.

Lin, W.W., and Karin, M. (2007). A cytokine-mediated link between innate immunity, inflammation, and cancer. The Journal of clinical investigation *117*, 1175-1183.

Lindborg, J.A., Mack, M., and Zigmond, R.E. (2017). Neutrophils Are Critical for Myelin Removal in a Peripheral Nerve Injury Model of Wallerian Degeneration. The Journal of neuroscience : the official journal of the Society for Neuroscience *37*, 10258-10277.

Liu, K.M., and Shen, C.L. (1985). Ultrastructural sequence of myelin breakdown during Wallerian degeneration in the rat optic nerve. Cell Tissue Res *242*, 245-256.

Livet, J., Weissman, T.A., Kang, H., Draft, R.W., Lu, J., Bennis, R.A., Sanes, J.R., and Lichtman, J.W. (2007). Transgenic strategies for combinatorial expression of fluorescent proteins in the nervous system. Nature *450*, 56-62.

Lloyd, A.C., Obermuller, F., Staddon, S., Barth, C.F., McMahon, M., and Land, H. (1997). Cooperating oncogenes converge to regulate cyclin/cdk complexes. Genes Dev *11*, 663-677.

Lopez-Anido, C., Sun, G., Koenning, M., Srinivasan, R., Hung, H.A., Emery, B., Keles, S., and Svaren, J. (2015). Differential Sox10 genomic occupancy in myelinating glia. Glia *63*, 1897-1914.

Lopez-Verrilli, M.A., and Court, F.A. (2012). Transfer of vesicles from schwann cells to axons: a novel mechanism of communication in the peripheral nervous system. Frontiers in physiology *3*, 205.

Love, M.I., Huber, W., and Anders, S. (2014). Moderated estimation of fold change and dispersion for RNA-seq data with DESeq2. Genome Biol *15*, 550.

Lu, P., Takai, K., Weaver, V.M., and Werb, Z. (2011). Extracellular matrix degradation and remodeling in development and disease. Cold Spring Harb Perspect Biol *3*.

Lu, P., Weaver, V.M., and Werb, Z. (2012). The extracellular matrix: a dynamic niche in cancer progression. The Journal of cell biology *196*, 395-406.

Lundborg, G., Dahlin, L.B., Danielsen, N.P., Hansson, H.A., and Larsson, K. (1981). Reorganization and orientation of regenerating nerve fibres, perineurium, and epineurium in preformed mesothelial tubes - an experimental study on the sciatic nerve of rats. Journal of neuroscience research *6*, 265-281.

Ma, L., Chen, Z., Erdjument-Bromage, H., Tempst, P., and Pandolfi, P.P. (2005). Phosphorylation and functional inactivation of TSC2 by Erk implications for tuberous sclerosis and cancer pathogenesis. Cell *121*, 179-193.

MacInnis, B.L., and Campenot, R.B. (2005). Regulation of Wallerian degeneration and nerve growth factor withdrawal-induced pruning of axons of sympathetic neurons by the proteasome and the MEK/Erk pathway. Mol Cell Neurosci *28*, 430-439.

Mack, T.G., Reiner, M., Beirowski, B., Mi, W., Emanuelli, M., Wagner, D., Thomson, D., Gillingwater, T., Court, F., Conforti, L.*, et al.* (2001). Wallerian degeneration of injured axons and synapses is delayed by a Ube4b/Nmnat chimeric gene. Nat Neurosci *4*, 1199-1206.

Madisen, L., Zwingman, T.A., Sunkin, S.M., Oh, S.W., Zariwala, H.A., Gu, H., Ng, L.L., Palmiter, R.D., Hawrylycz, M.J., Jones, A.R.*, et al.* (2010). A robust and high-throughput Cre reporting and characterization system for the whole mouse brain. Nature neuroscience *13*, 133-140.

Madrid, R.E., Jaros, E., Cullen, M.J., and Bradley, W.G. (1975). Genetically determined defect of Schwann cell basement membrane in dystrophic mouse. Nature *257*, 319-321.

Mahar, M., and Cavalli, V. (2018). Intrinsic mechanisms of neuronal axon regeneration. Nature reviews Neuroscience *19*, 323-337.

Mallon, B.S., Shick, H.E., Kidd, G.J., and Macklin, W.B. (2002). Proteolipid promoter activity distinguishes two populations of NG2-positive cells throughout neonatal cortical development. The Journal of neuroscience : the official journal of the Society for Neuroscience *22*, 876-885.

Manabe, Y., Toda, S., Miyazaki, K., and Sugihara, H. (2003). Mature adipocytes, but not preadipocytes, promote the growth of breast carcinoma cells in collagen gel matrix culture through cancer-stromal cell interactions. The Journal of pathology *201*, 221-228.

Mangoura, D., Sun, Y., Li, C., Singh, D., Gutmann, D.H., Flores, A., Ahmed, M., and Vallianatos, G. (2006). Phosphorylation of neurofibromin by PKC is a possible molecular switch in EGF receptor signaling in neural cells. Oncogene *25*, 735-745.

Mantovani, A., Allavena, P., Sica, A., and Balkwill, F. (2008). Cancer-related inflammation. Nature *454*, 436-444.

Mantripragada, K.K., Spurlock, G., Kluwe, L., Chuzhanova, N., Ferner, R.E., Frayling, I.M., Dumanski, J.P., Guha, A., Mautner, V., and Upadhyaya, M. (2008). High-resolution DNA copy number profiling of malignant peripheral nerve sheath tumors using targeted microarray-based comparative genomic hybridization. Clinical cancer research : an official journal of the American Association for Cancer Research *14*, 1015-1024.

Mao, T.L., Fan, K.F., and Liu, C.L. (2017). Targeting the CXCR4/CXCL12 axis in treating epithelial ovarian cancer. Gene therapy *24*, 621-629.

Marais, R., Light, Y., Paterson, H.F., and Marshall, C.J. (1995). Ras recruits Raf-1 to the plasma membrane for activation by tyrosine phosphorylation. EMBO J *14*, 3136-3145.

Marchuk, D.A., Saulino, A.M., Tavakkol, R., Swaroop, M., Wallace, M.R., Andersen, L.B., Mitchell, A.L., Gutmann, D.H., Boguski, M., and Collins, F.S. (1991). cDNA cloning of the type 1 neurofibromatosis gene: complete sequence of the NF1 gene product. Genomics *11*, 931-940.

Maro, G.S., Vermeren, M., Voiculescu, O., Melton, L., Cohen, J., Charnay, P., and Topilko, P. (2004). Neural crest boundary cap cells constitute a source of neuronal and glial cells of the PNS. Nat Neurosci *7*, 930-938.

Marshall, C.J. (1995). Specificity of receptor tyrosine kinase signaling: transient versus sustained extracellular signal-regulated kinase activation. Cell *80*, 179-185.

Martin, G.A., Viskochil, D., Bollag, G., McCabe, P.C., Crosier, W.J., Haubruck, H., Conroy, L., Clark, R., O'Connell, P., Cawthon, R.M.*, et al.* (1990). The GAP-related domain of the neurofibromatosis type 1 gene product interacts with ras p21. Cell *63*, 843-849.

Martin, M. (2011). Cutadapt Removes Adapter Sequences From High-Throughput Sequencing Reads. EMBnetjournal *17*, 10-12.

Martin, S., Levine, A.K., Chen, Z.J., Ughrin, Y., and Levine, J.M. (2001). Deposition of the NG2 proteoglycan at nodes of Ranvier in the peripheral nervous system. The Journal of neuroscience : the official journal of the Society for Neuroscience *21*, 8119-8128.

Martini, R., Fischer, S., Lopez-Vales, R., and David, S. (2008). Interactions between Schwann cells and macrophages in injury and inherited demyelinating disease. Glia *56*, 1566-1577.

Martini, R., Mohajeri, M.H., Kasper, S., Giese, K.P., and Schachner, M. (1995a). Mice doubly deficient in the genes for P0 and myelin basic protein show that both proteins contribute to the formation of the major dense line in peripheral nerve myelin. The Journal of neuroscience : the official journal of the Society for Neuroscience *15*, 4488-4495.

Martini, R., Zielasek, J., Toyka, K.V., Giese, K.P., and Schachner, M. (1995b). Protein zero (P0)-deficient mice show myelin degeneration in peripheral nerves characteristic of inherited human neuropathies. Nat Genet *11*, 281-286.
Martins-Green, M., Boudreau, N., and Bissell, M.J. (1994). Inflammation is responsible for the development of wound-induced tumors in chickens infected with Rous sarcoma virus. Cancer Res *54*, 4334-4341.
Marusyk, A., Almendro, V., and Polyak, K. (2012). Intra-tumour heterogeneity: a looking glass for cancer? Nature reviews Cancer *12*, 323-334.
Mascre, G., Dekoninck, S., Drogat, B., Youssef, K.K., Brohee, S., Sotiropoulou, P.A., Simons, B.D., and Blanpain, C. (2012). Distinct contribution of stem and progenitor cells to epidermal maintenance. Nature *489*, 257-262.
Mathon, N.F., and Lloyd, A.C. (2001). Cell senescence and cancer. Nature reviews Cancer *1*, 203-213.
Maurel, P., Einheber, S., Galinska, J., Thaker, P., Lam, I., Rubin, M.B., Scherer, S.S., Murakami, Y., Gutmann, D.H., and Salzer, J.L. (2007). Nectin-like proteins mediate axon Schwann cell interactions along the internode and are essential for myelination. J Cell Biol *178*, 861-874.
McCarthy, D.J., Chen, Y., and Smyth, G.K. (2012). Differential expression analysis of multifactor RNA-Seq experiments with respect to biological variation. Nucleic Acids Res *40*, 4288-4297.
McClatchey, A.I. (2007). Neurofibromatosis. Annual review of pathology *2*, 191-216.
McDonald, D., Cheng, C., Chen, Y., and Zochodne, D. (2006). Early events of peripheral nerve regeneration. Neuron glia biology *2*, 139-147.
McGillicuddy, L.T., Fromm, J.A., Hollstein, P.E., Kubek, S., Beroukhim, R., De Raedt, T., Johnson, B.W., Williams, S.M., Nghiemphu, P., Liau, L.M.*, et al.* (2009). Proteasomal and genetic inactivation of the NF1 tumor suppressor in gliomagenesis. Cancer cell *16*, 44-54.
McGranahan, N., and Swanton, C. (2017). Clonal Heterogeneity and Tumor Evolution: Past, Present, and the Future. Cell *168*, 613-628.
McKee, K.K., Yang, D.H., Patel, R., Chen, Z.L., Strickland, S., Takagi, J., Sekiguchi, K., and Yurchenco, P.D. (2012). Schwann cell myelination requires integration of laminin activities. J Cell Sci *125*, 4609-4619.

McKenzie, I.A., Biernaskie, J., Toma, J.G., Midha, R., and Miller, F.D. (2006). Skin-derived precursors generate myelinating Schwann cells for the injured and dysmyelinated nervous system. The Journal of neuroscience : the official journal of the Society for Neuroscience *26*, 6651-6660.

McKenzie, I.A., Ohayon, D., Li, H., de Faria, J.P., Emery, B., Tohyama, K., and Richardson, W.D. (2014). Motor skill learning requires active central myelination. Science *346*, 318-322.

Mei, L., and Nave, K.A. (2014). Neuregulin-ERBB signaling in the nervous system and neuropsychiatric diseases. Neuron *83*, 27-49.

Meier, C., Parmantier, E., Brennan, A., Mirsky, R., and Jessen, K.R. (1999). Developing Schwann cells acquire the ability to survive without axons by establishing an autocrine circuit involving insulin-like growth factor, neurotrophin-3, and platelet-derived growth factor-BB. J Neurosci *19*, 3847-3859.

Menon, A.G., Anderson, K.M., Riccardi, V.M., Chung, R.Y., Whaley, J.M., Yandell, D.W., Farmer, G.E., Freiman, R.N., Lee, J.K., Li, F.P.*, et al.* (1990). Chromosome 17p deletions and p53 gene mutations associated with the formation of malignant neurofibrosarcomas in von Recklinghausen neurofibromatosis. Proc Natl Acad Sci U S A *87*, 5435-5439.

Merrell, A.J., and Stanger, B.Z. (2016). Adult cell plasticity in vivo: de-differentiation and transdifferentiation are back in style. Nature reviews Molecular cell biology *17*, 413-425.

Messing, A., Behringer, R.R., Hammang, J.P., Palmiter, R.D., Brinster, R.L., and Lemke, G. (1992). P0 promoter directs expression of reporter and toxin genes to Schwann cells of transgenic mice. Neuron *8*, 507-520.

Messing, A., Behringer, R.R., Wrabetz, L., Hammang, J.P., Lemke, G., Palmiter, R.D., and Brinster, R.L. (1994). Hypomyelinating peripheral neuropathies and schwannomas in transgenic mice expressing SV40 T-antigen. J Neurosci *14*, 3533-3539.

Meyer, D., and Birchmeier, C. (1995). Multiple essential functions of neuregulin in development. Nature *378*, 386-390.

Meyer, D., Yamaai, T., Garratt, A., Riethmacher-Sonnenberg, E., Kane, D., Theill, L.E., and Birchmeier, C. (1997). Isoform-specific expression and function of neuregulin. Development *124*, 3575-3586.

Mi, H., Muruganujan, A., Casagrande, J.T., and Thomas, P.D. (2013). Large-scale gene function analysis with the PANTHER classification system. Nature protocols *8*, 1551-1566.

Michailov, G.V., Sereda, M.W., Brinkmann, B.G., Fischer, T.M., Haug, B., Birchmeier, C., Role, L., Lai, C., Schwab, M.H., and Nave, K.A. (2004). Axonal neuregulin-1 regulates myelin sheath thickness. Science *304*, 700-703.

Michalopoulos, G.K., Barua, L., and Bowen, W.C. (2005). Transdifferentiation of rat hepatocytes into biliary cells after bile duct ligation and toxic biliary injury. Hepatology *41*, 535-544.

Miller, S.J., Jessen, W.J., Mehta, T., Hardiman, A., Sites, E., Kaiser, S., Jegga, A.G., Li, H., Upadhyaya, M., Giovannini, M.*, et al.* (2009). Integrative genomic analyses of neurofibromatosis tumours identify SOX9 as a biomarker and survival gene. EMBO molecular medicine *1*, 236-248.

Miller, S.J., Rangwala, F., Williams, J., Ackerman, P., Kong, S., Jegga, A.G., Kaiser, S., Aronow, B.J., Frahm, S., Kluwe, L.*, et al.* (2006). Large-scale molecular comparison of human schwann cells to malignant peripheral nerve sheath tumor cell lines and tissues. Cancer research *66*, 2584-2591.

Min, Y., Kristiansen, K., Boggs, J.M., Husted, C., Zasadzinski, J.A., and Israelachvili, J. (2009). Interaction forces and adhesion of supported myelin lipid bilayers modulated by myelin basic protein. Proceedings of the National Academy of Sciences of the United States of America *106*, 3154-3159.

Mirancea, N. (2016). Telocyte - a particular cell phenotype. Infrastructure, relationships and putative functions. Romanian journal of morphology and embryology = Revue roumaine de morphologie et embryologie *57*, 7-21.

Mirsky, R., Woodhoo, A., Parkinson, D.B., Arthur-Farraj, P., Bhaskaran, A., and Jessen, K.R. (2008). Novel signals controlling embryonic Schwann cell development, myelination and dedifferentiation. J Peripher Nerv Syst *13*, 122-135.

Misale, S., Yaeger, R., Hobor, S., Scala, E., Janakiraman, M., Liska, D., Valtorta, E., Schiavo, R., Buscarino, M., Siravegna, G.*, et al.* (2012). Emergence of KRAS mutations

and acquired resistance to anti-EGFR therapy in colorectal cancer. Nature *486*, 532-536.

Mo, W., Chen, J., Patel, A., Zhang, L., Chau, V., Li, Y., Cho, W., Lim, K., Xu, J., Lazar, A.J.*, et al.* (2013). CXCR4/CXCL12 mediate autocrine cell- cycle progression in NF1-associated malignant peripheral nerve sheath tumors. Cell *152*, 1077-1090.

Moalem, G., Xu, K., and Yu, L. (2004). T lymphocytes play a role in neuropathic pain following peripheral nerve injury in rats. Neuroscience *129*, 767-777.

Mogha, A., Benesh, A.E., Patra, C., Engel, F.B., Schoneberg, T., Liebscher, I., and Monk, K.R. (2013). Gpr126 functions in Schwann cells to control differentiation and myelination via G-protein activation. The Journal of neuroscience : the official journal of the Society for Neuroscience *33*, 17976-17985.

Mogha, A., Harty, B.L., Carlin, D., Joseph, J., Sanchez, N.E., Suter, U., Piao, X., Cavalli, V., and Monk, K.R. (2016). Gpr126/Adgrg6 Has Schwann Cell Autonomous and Nonautonomous Functions in Peripheral Nerve Injury and Repair. The Journal of neuroscience : the official journal of the Society for Neuroscience *36*, 12351-12367.

Monk, K.R., Feltri, M.L., and Taveggia, C. (2015). New insights on Schwann cell development. Glia *63*, 1376-1393.

Monk, K.R., Naylor, S.G., Glenn, T.D., Mercurio, S., Perlin, J.R., Dominguez, C., Moens, C.B., and Talbot, W.S. (2009). A G protein-coupled receptor is essential for Schwann cells to initiate myelination. Science *325*, 1402-1405.

Monk, K.R., Oshima, K., Jors, S., Heller, S., and Talbot, W.S. (2011). Gpr126 is essential for peripheral nerve development and myelination in mammals. Development *138*, 2673-2680.

Monuki, E.S., Kuhn, R., Weinmaster, G., Trapp, B.D., and Lemke, G. (1990). Expression and activity of the POU transcription factor SCIP. Science *249*, 1300-1303.

Monvoisin, A., Alva, J.A., Hofmann, J.J., Zovein, A.C., Lane, T.F., and Iruela-Arispe, M.L. (2006). VE-cadherin-CreERT2 transgenic mouse: a model for inducible recombination in the endothelium. Dev Dyn *235*, 3413-3422.

Moon, L.D., Asher, R.A., Rhodes, K.E., and Fawcett, J.W. (2001). Regeneration of CNS axons back to their target following treatment of adult rat brain with chondroitinase ABC. Nature neuroscience *4*, 465-466.

Morgan, L., Jessen, K.R., and Mirsky, R. (1991). The effects of cAMP on differentiation of cultured Schwann cells: progression from an early phenotype (04+) to a myelin phenotype (P0+, GFAP-, N-CAM-, NGF-receptor-) depends on growth inhibition. The Journal of cell biology *112*, 457-467.

Morgenstern, D.A., Asher, R.A., Naidu, M., Carlstedt, T., Levine, J.M., and Fawcett, J.W. (2003). Expression and glycanation of the NG2 proteoglycan in developing, adult, and damaged peripheral nerve. Molecular and cellular neurosciences *24*, 787-802.

Mori, M., Nakajima, M., Mikami, Y., Seki, S., Takigawa, M., Kubo, T., and Ikegawa, S. (2006). Transcriptional regulation of the cartilage intermediate layer protein (CILP) gene. Biochem Biophys Res Commun *341*, 121-127.

Morris, J.H., Hudson, A.R., and Weddell, G. (1972). A study of degeneration and regeneration in the divided rat sciatic nerve based on electron microscopy. IV. Changes in fascicular microtopography, perineurium and endoneurial fibroblasts. Zeitschrift fur Zellforschung und mikroskopische Anatomie *124*, 165-203.

Morrison, K., Challita-Eid, P.M., Raitano, A., An, Z., Yang, P., Abad, J.D., Liu, W., Lortie, D.R., Snyder, J.T., Capo, L.*, et al.* (2016). Development of ASG-15ME, a Novel Antibody-Drug Conjugate Targeting SLITRK6, a New Urothelial Cancer Biomarker. Mol Cancer Ther *15*, 1301-1310.

Morrison, S.J., Perez, S.E., Qiao, Z., Verdi, J.M., Hicks, C., Weinmaster, G., and Anderson, D.J. (2000). Transient Notch activation initiates an irreversible switch from neurogenesis to gliogenesis by neural crest stem cells. Cell *101*, 499-510.

Morrison, S.J., White, P.M., Zock, C., and Anderson, D.J. (1999). Prospective identification, isolation by flow cytometry, and in vivo self-renewal of multipotent mammalian neural crest stem cells. Cell *96*, 737-749.

Mortazavi, A., Williams, B.A., McCue, K., Schaeffer, L., and Wold, B. (2008). Mapping and quantifying mammalian transcriptomes by RNA-Seq. Nat Methods *5*, 621-628.

Morton, P.D., Dellarole, A., Theus, M.H., Walters, W.M., Berge, S.S., and Bethea, J.R. (2013). Activation of NF-kappaB in Schwann cells is dispensable for myelination in vivo. J Neurosci *33*, 9932-9936.

Mroz, E.A., Tward, A.D., Pickering, C.R., Myers, J.N., Ferris, R.L., and Rocco, J.W. (2013). High intratumor genetic heterogeneity is related to worse outcome in patients with head and neck squamous cell carcinoma. Cancer *119*, 3034-3042.
Mueller, M., Leonhard, C., Wacker, K., Ringelstein, E.B., Okabe, M., Hickey, W.F., and Kiefer, R. (2003). Macrophage response to peripheral nerve injury: the quantitative contribution of resident and hematogenous macrophages. Laboratory investigation; a journal of technical methods and pathology *83*, 175-185.
Mueller, M., Wacker, K., Ringelstein, E.B., Hickey, W.F., Imai, Y., and Kiefer, R. (2001). Rapid response of identified resident endoneurial macrophages to nerve injury. The American journal of pathology *159*, 2187-2197.
Mueller, M.M., and Fusenig, N.E. (2004). Friends or foes - bipolar effects of the tumour stroma in cancer. Nat Rev Cancer *4*, 839-849.
Mueller O., L.S., Schroeder A. (2004). RNA Integrity Number (RIN) – Standardization of RNA Quality Control. In: https://wwwchemagilentcom/Library/applications/5989-1165ENpdf.
Muir, D. (1995). Differences in proliferation and invasion by normal, transformed and NF1 Schwann cell cultures are influenced by matrix metalloproteinase expression. Clinical & experimental metastasis *13*, 303-314.
Mukhopadhyay, G., Doherty, P., Walsh, F.S., Crocker, P.R., and Filbin, M.T. (1994). A novel role for myelin-associated glycoprotein as an inhibitor of axonal regeneration. Neuron *13*, 757-767.
Mukouyama, Y.S., Gerber, H.P., Ferrara, N., Gu, C., and Anderson, D.J. (2005). Peripheral nerve-derived VEGF promotes arterial differentiation via neuropilin 1-mediated positive feedback. Development *132*, 941-952.
Muller, A., Homey, B., Soto, H., Ge, N., Catron, D., Buchanan, M.E., McClanahan, T., Murphy, E., Yuan, W., Wagner, S.N.*, et al.* (2001). Involvement of chemokine receptors in breast cancer metastasis. Nature *410*, 50-56.
Murdoch, C., Muthana, M., Coffelt, S.B., and Lewis, C.E. (2008). The role of myeloid cells in the promotion of tumour angiogenesis. Nature reviews Cancer *8*, 618-631.
Murinson, B.B., Archer, D.R., Li, Y., and Griffin, J.W. (2005). Degeneration of myelinated efferent fibers prompts mitosis in Remak Schwann cells of uninjured C-fiber afferents. J Neurosci *25*, 1179-1187.

Nagy, A. (2000). Cre recombinase: the universal reagent for genome tailoring. Genesis *26*, 99-109.

Napoli, I., Noon, L.A., Ribeiro, S., Kerai, A.P., Parrinello, S., Rosenberg, L.H., Collins, M.J., Harrisingh, M.C., White, I.J., Woodhoo, A.*, et al.* (2012). A central role for the ERK-signaling pathway in controlling Schwann cell plasticity and peripheral nerve regeneration in vivo. Neuron *73*, 729-742.

Nathan, C. (2006). Neutrophils and immunity: challenges and opportunities. Nat Rev Immunol *6*, 173-182.

Nave, K.A., and Salzer, J.L. (2006). Axonal regulation of myelination by neuregulin 1. Curr Opin Neurobiol *16*, 492-500.

Nave, K.A., and Werner, H.B. (2014). Myelination of the nervous system: mechanisms and functions. Annu Rev Cell Dev Biol *30*, 503-533.

Nazareth, L., Lineburg, K.E., Chuah, M.I., Tello Velasquez, J., Chehrehasa, F., St John, J.A., and Ekberg, J.A. (2015). Olfactory ensheathing cells are the main phagocytic cells that remove axon debris during early development of the olfactory system. The Journal of comparative neurology *523*, 479-494.

Nazarian, R., Shi, H., Wang, Q., Kong, X., Koya, R.C., Lee, H., Chen, Z., Lee, M.K., Attar, N., Sazegar, H.*, et al.* (2010). Melanomas acquire resistance to B-RAF(V600E) inhibition by RTK or N-RAS upregulation. Nature *468*, 973-977.

Nervi, B., Ramirez, P., Rettig, M.P., Uy, G.L., Holt, M.S., Ritchey, J.K., Prior, J.L., Piwnica-Worms, D., Bridger, G., Ley, T.J.*, et al.* (2009). Chemosensitization of acute myeloid leukemia (AML) following mobilization by the CXCR4 antagonist AMD3100. Blood *113*, 6206-6214.

Newbern, J., and Birchmeier, C. (2010). Nrg1/ErbB signaling networks in Schwann cell development and myelination. Semin Cell Dev Biol *21*, 922-928.

Newbern, J.M., Li, X., Shoemaker, S.E., Zhou, J., Zhong, J., Wu, Y., Bonder, D., Hollenback, S., Coppola, G., Geschwind, D.H.*, et al.* (2011). Specific functions for ERK/MAPK signaling during PNS development. Neuron *69*, 91-105.

Nguyen, L.V., Vanner, R., Dirks, P., and Eaves, C.J. (2012). Cancer stem cells: an evolving concept. Nature reviews Cancer *12*, 133-143.

Nguyen, Q.T., Sanes, J.R., and Lichtman, J.W. (2002). Pre-existing pathways promote precise projection patterns. Nature neuroscience *5*, 861-867.

Nickols, J.C., Valentine, W., Kanwal, S., and Carter, B.D. (2003). Activation of the transcription factor NF-kappaB in Schwann cells is required for peripheral myelin formation. Nat Neurosci *6*, 161-167.

Nitzan, E., Pfaltzgraff, E.R., Labosky, P.A., and Kalcheim, C. (2013). Neural crest and Schwann cell progenitor-derived melanocytes are two spatially segregated populations similarly regulated by Foxd3. Proc Natl Acad Sci U S A *110*, 12709-12714.

Nocentini, G., and Riccardi, C. (2009). GITR: a modulator of immune response and inflammation. Adv Exp Med Biol *647*, 156-173.

Nodari, A., Previtali, S.C., Dati, G., Occhi, S., Court, F.A., Colombelli, C., Zambroni, D., Dina, G., Del Carro, U., Campbell, K.P.*, et al.* (2008). Alpha6beta4 integrin and dystroglycan cooperate to stabilize the myelin sheath. J Neurosci *28*, 6714-6719.

Nowell, P.C. (1976). The clonal evolution of tumor cell populations. Science *194*, 23-28.

Nwabo Kamdje, A.H., Takam Kamga, P., Tagne Simo, R., Vecchio, L., Seke Etet, P.F., Muller, J.M., Bassi, G., Lukong, E., Kumar Goel, R., Mbo Amvene, J.*, et al.* (2017). Developmental pathways associated with cancer metastasis: Notch, Wnt, and Hedgehog. Cancer Biol Med *14*, 109-120.

Ochoa, J., and Mair, W.G. (1969). The normal sural nerve in man. I. Ultrastructure and numbers of fibres and cells. Acta Neuropathol *13*, 197-216.

Ogata, T., Iijima, S., Hoshikawa, S., Miura, T., Yamamoto, S., Oda, H., Nakamura, K., and Tanaka, S. (2004). Opposing extracellular signal-regulated kinase and Akt pathways control Schwann cell myelination. J Neurosci *24*, 6724-6732.

Oh, J.W., Drabik, K., Kutsch, O., Choi, C., Tousson, A., and Benveniste, E.N. (2001). CXC chemokine receptor 4 expression and function in human astroglioma cells. Journal of immunology *166*, 2695-2704.

Ohara, P.T., Vit, J.P., Bhargava, A., Romero, M., Sundberg, C., Charles, A.C., and Jasmin, L. (2009). Gliopathic pain: when satellite glial cells go bad. Neuroscientist *15*, 450-463.

Osawa, M., Hanada, K., Hamada, H., and Nakauchi, H. (1996). Long-term lymphohematopoietic reconstitution by a single CD34-low/negative hematopoietic stem cell. Science *273*, 242-245.

Ostman, A. (2012). The tumor microenvironment controls drug sensitivity. Nat Med *18*, 1332-1334.

Paavola, K.J., Sidik, H., Zuchero, J.B., Eckart, M., and Talbot, W.S. (2014). Type IV collagen is an activating ligand for the adhesion G protein-coupled receptor GPR126. Science signaling *7*, ra76.

Paget, S. (1989). The distribution of secondary growths in cancer of the breast. 1889. Cancer metastasis reviews *8*, 98-101.

Panni, P., Ferguson, I.A., Beacham, I., Mackay-Sim, A., Ekberg, J.A., and St John, J.A. (2013). Phagocytosis of bacteria by olfactory ensheathing cells and Schwann cells. Neuroscience letters *539*, 65-70.

Paratore, C., Goerich, D.E., Suter, U., Wegner, M., and Sommer, L. (2001). Survival and glial fate acquisition of neural crest cells are regulated by an interplay between the transcription factor Sox10 and extrinsic combinatorial signaling. Development *128*, 3949-3961.

Pardal, R., Clarke, M.F., and Morrison, S.J. (2003). Applying the principles of stem-cell biology to cancer. Nat Rev Cancer *3*, 895-902.

Park, E.J., Sun, X., Nichol, P., Saijoh, Y., Martin, J.F., and Moon, A.M. (2008). System for tamoxifen-inducible expression of cre-recombinase from the Foxa2 locus in mice. Dev Dyn *237*, 447-453.

Park, S.J., Sawitzki, B., Kluwe, L., Mautner, V.F., Holtkamp, N., and Kurtz, A. (2013). Serum biomarkers for neurofibromatosis type 1 and early detection of malignant peripheral nerve-sheath tumors. BMC Med *11*, 109.

Parkhomchuk, D., Borodina, T., Amstislavskiy, V., Banaru, M., Hallen, L., Krobitsch, S., Lehrach, H., and Soldatov, A. (2009). Transcriptome analysis by strand-specific sequencing of complementary DNA. Nucleic Acids Res *37*, e123.

Parkinson, D.B., Bhaskaran, A., Arthur-Farraj, P., Noon, L.A., Woodhoo, A., Lloyd, A.C., Feltri, M.L., Wrabetz, L., Behrens, A., Mirsky, R.*, et al.* (2008). c-Jun is a negative regulator of myelination. J Cell Biol *181*, 625-637.

Parkinson, D.B., Bhaskaran, A., Droggiti, A., Dickinson, S., D'Antonio, M., Mirsky, R., and Jessen, K.R. (2004). Krox-20 inhibits Jun-NH2-terminal kinase/c-Jun to control Schwann cell proliferation and death. J Cell Biol *164*, 385-394.

Parmantier, E., Lynn, B., Lawson, D., Turmaine, M., Namini, S.S., Chakrabarti, L., McMahon, A.P., Jessen, K.R., and Mirsky, R. (1999). Schwann cell-derived Desert hedgehog controls the development of peripheral nerve sheaths. Neuron *23*, 713-724.

Parrinello, S., and Lloyd, A.C. (2009). Neurofibroma development in NF1--insights into tumour initiation. Trends in cell biology *19*, 395-403.

Parrinello, S., Napoli, I., Ribeiro, S., Wingfield Digby, P., Fedorova, M., Parkinson, D.B., Doddrell, R.D., Nakayama, M., Adams, R.H., and Lloyd, A.C. (2010). EphB signaling directs peripheral nerve regeneration through Sox2-dependent Schwann cell sorting. Cell *143*, 145-155.

Parrinello, S., Noon, L.A., Harrisingh, M.C., Wingfield Digby, P., Rosenberg, L.H., Cremona, C.A., Echave, P., Flanagan, A.M., Parada, L.F., and Lloyd, A.C. (2008). NF1 loss disrupts Schwann cell-axonal interactions: a novel role for semaphorin 4F. Genes Dev *22*, 3335-3348.

Pedersen, T.X., Leethanakul, C., Patel, V., Mitola, D., Lund, L.R., Dano, K., Johnsen, M., Gutkind, J.S., and Bugge, T.H. (2003). Laser capture microdissection-based in vivo genomic profiling of wound keratinocytes identifies similarities and differences to squamous cell carcinoma. Oncogene *22*, 3964-3976.

Pellegrino, R.G., and Spencer, P.S. (1985). Schwann cell mitosis in response to regenerating peripheral axons in vivo. Brain Res *341*, 16-25.

Pereira, J.A., Lebrun-Julien, F., and Suter, U. (2012). Molecular mechanisms regulating myelination in the peripheral nervous system. Trends Neurosci *35*, 123-134.

Perkins, N.M., and Tracey, D.J. (2000). Hyperalgesia due to nerve injury: role of neutrophils. Neuroscience *101*, 745-757.

Perlson, E., Hanz, S., Ben-Yaakov, K., Segal-Ruder, Y., Seger, R., and Fainzilber, M. (2005). Vimentin-dependent spatial translocation of an activated MAP kinase in injured nerve. Neuron *45*, 715-726.

Perry, A., Kunz, S.N., Fuller, C.E., Banerjee, R., Marley, E.F., Liapis, H., Watson, M.A., and Gutmann, D.H. (2002). Differential NF1, p16, and EGFR patterns by interphase cytogenetics (FISH) in malignant peripheral nerve sheath tumor (MPNST) and

morphologically similar spindle cell neoplasms. Journal of neuropathology and experimental neurology *61*, 702-709.

Peters, A., Palay, Sanford L., Webster, HenrydeF (1991). The Fine Structure of the Nervous System: Neurons and Their Supporting Cells. OUP USA *3 edition*, 514.

Petersen, J., and Adameyko, I. (2017). Nerve-associated neural crest: peripheral glial cells generate multiple fates in the body. Current opinion in genetics & development *45*, 10-14.

Petersen, S.C., Luo, R., Liebscher, I., Giera, S., Jeong, S.J., Mogha, A., Ghidinelli, M., Feltri, M.L., Schoneberg, T., Piao, X.*, et al.* (2015). The adhesion GPCR GPR126 has distinct, domain-dependent functions in Schwann cell development mediated by interaction with laminin-211. Neuron *85*, 755-769.

Petersson, M., Reuter, K., Brylka, H., Kraus, A., Schettina, P., and Niemann, C. (2015). Interfering with stem cell-specific gatekeeper functions controls tumour initiation and malignant progression of skin tumours. Nature communications *6*, 5874.

Pickup, M.W., Mouw, J.K., and Weaver, V.M. (2014). The extracellular matrix modulates the hallmarks of cancer. EMBO Rep *15*, 1243-1253.

Pinkert, C.A. (2014). Transgenic Animal Technology: A Laboratory Handbook. Elsevier *Third edition*.

Pittet, M.J., and Weissleder, R. (2011). Intravital imaging. Cell *147*, 983-991.

Pogoda, H.M., Sternheim, N., Lyons, D.A., Diamond, B., Hawkins, T.A., Woods, I.G., Bhatt, D.H., Franzini-Armstrong, C., Dominguez, C., Arana, N.*, et al.* (2006). A genetic screen identifies genes essential for development of myelinated axons in zebrafish. Developmental biology *298*, 118-131.

Polakis, P. (2007). The many ways of Wnt in cancer. Curr Opin Genet Dev *17*, 45-51.

Poliak, S., and Peles, E. (2003). The local differentiation of myelinated axons at nodes of Ranvier. Nat Rev Neurosci *4*, 968-980.

Pollak, M. (2008). Insulin and insulin-like growth factor signalling in neoplasia. Nature reviews Cancer *8*, 915-928.

Pollak, M. (2012). The insulin and insulin-like growth factor receptor family in neoplasia: an update. Nature reviews Cancer *12*, 159-169.

Popescu, L.M., and Faussone-Pellegrini, M.S. (2010). TELOCYTES - a case of serendipity: the winding way from Interstitial Cells of Cajal (ICC), via Interstitial Cajal-

Like Cells (ICLC) to TELOCYTES. Journal of cellular and molecular medicine *14*, 729-740.

Porrello, E., Rivellini, C., Dina, G., Triolo, D., Del Carro, U., Ungaro, D., Panattoni, M., Feltri, M.L., Wrabetz, L., Pardi, R.*, et al.* (2014). Jab1 regulates Schwann cell proliferation and axonal sorting through p27. J Exp Med *211*, 29-43.

Prada, C.E., Jousma, E., Rizvi, T.A., Wu, J., Dunn, R.S., Mayes, D.A., Cancelas, J.A., Dombi, E., Kim, M.O., West, B.L.*, et al.* (2013). Neurofibroma-associated macrophages play roles in tumor growth and response to pharmacological inhibition. Acta Neuropathol *125*, 159-168.

Prahallad, A., Sun, C., Huang, S., Di Nicolantonio, F., Salazar, R., Zecchin, D., Beijersbergen, R.L., Bardelli, A., and Bernards, R. (2012). Unresponsiveness of colon cancer to BRAF(V600E) inhibition through feedback activation of EGFR. Nature *483*, 100-103.

Provenzano, P.P., Inman, D.R., Eliceiri, K.W., and Keely, P.J. (2009). Matrix density-induced mechanoregulation of breast cell phenotype, signaling and gene expression through a FAK-ERK linkage. Oncogene *28*, 4326-4343.

Pruitt, K., and Der, C.J. (2001). Ras and Rho regulation of the cell cycle and oncogenesis. Cancer Lett *171*, 1-10.

Psachoulia, K., Jamen, F., Young, K.M., and Richardson, W.D. (2009). Cell cycle dynamics of NG2 cells in the postnatal and ageing brain. Neuron glia biology *5*, 57-67.

Pylayeva-Gupta, Y., Grabocka, E., and Bar-Sagi, D. (2011). RAS oncogenes: weaving a tumorigenic web. Nature reviews Cancer *11*, 761-774.

Qian, B.Z., and Pollard, J.W. (2010). Macrophage diversity enhances tumor progression and metastasis. Cell *141*, 39-51.

Quail, D.F., and Joyce, J.A. (2013). Microenvironmental regulation of tumor progression and metastasis. Nature medicine *19*, 1423-1437.

Radtke, F., and Raj, K. (2003). The role of Notch in tumorigenesis: oncogene or tumour suppressor? Nat Rev Cancer *3*, 756-767.

Ramon-Cueto, A., and Avila, J. (1998). Olfactory ensheathing glia: properties and function. Brain research bulletin *46*, 175-187.

Rangarajan, A., and Weinberg, R.A. (2003). Opinion: Comparative biology of mouse versus human cells: modelling human cancer in mice. Nat Rev Cancer *3*, 952-959.
Rapp, U.R., Goldsborough, M.D., Mark, G.E., Bonner, T.I., Groffen, J., Reynolds, F.H., Jr., and Stephenson, J.R. (1983). Structure and biological activity of v-raf, a unique oncogene transduced by a retrovirus. Proceedings of the National Academy of Sciences of the United States of America *80*, 4218-4222.
Rasband, M.N. (2010). The axon initial segment and the maintenance of neuronal polarity. Nature reviews Neuroscience *11*, 552-562.
Rasband, M.N., and Peles, E. (2015). The Nodes of Ranvier: Molecular Assembly and Maintenance. Cold Spring Harbor perspectives in biology *8*, a020495.
Rassoulzadegan, M., Magliano, M., and Cuzin, F. (2002). Transvection effects involving DNA methylation during meiosis in the mouse. EMBO J *21*, 440-450.
Ratner, N., and Miller, S.J. (2015). A RASopathy gene commonly mutated in cancer: the neurofibromatosis type 1 tumour suppressor. Nature reviews Cancer *15*, 290-301.
Real, C., Glavieux-Pardanaud, C., Vaigot, P., Le-Douarin, N., and Dupin, E. (2005). The instability of the neural crest phenotypes: Schwann cells can differentiate into myofibroblasts. The International journal of developmental biology *49*, 151-159.
Rebustini, I.T., Myers, C., Lassiter, K.S., Surmak, A., Szabova, L., Holmbeck, K., Pedchenko, V., Hudson, B.G., and Hoffman, M.P. (2009). MT2-MMP-dependent release of collagen IV NC1 domains regulates submandibular gland branching morphogenesis. Dev Cell *17*, 482-493.
Reeves, M.Q., Kandyba, E., Harris, S., Del Rosario, R., and Balmain, A. (2018). Multicolour lineage tracing reveals clonal dynamics of squamous carcinoma evolution from initiation to metastasis. Nature cell biology *20*, 699-709.
Reichert, F., Levitzky, R., and Rotshenker, S. (1996). Interleukin 6 in intact and injured mouse peripheral nerves. Eur J Neurosci *8*, 530-535.
Reichert, F., Saada, A., and Rotshenker, S. (1994). Peripheral nerve injury induces Schwann cells to express two macrophage phenotypes: phagocytosis and the galactose-specific lectin MAC-2. J Neurosci *14*, 3231-3245.

Reinert, R.B., Kantz, J., Misfeldt, A.A., Poffenberger, G., Gannon, M., Brissova, M., and Powers, A.C. (2012). Tamoxifen-Induced Cre-loxP Recombination Is Prolonged in Pancreatic Islets of Adult Mice. PLoS One *7*, e33529.

Rempe, D., Vangeison, G., Hamilton, J., Li, Y., Jepson, M., and Federoff, H.J. (2006). Synapsin I Cre transgene expression in male mice produces germline recombination in progeny. Genesis *44*, 44-49.

Repasky, G.A., Chenette, E.J., and Der, C.J. (2004). Renewing the conspiracy theory debate: does Raf function alone to mediate Ras oncogenesis? Trends Cell Biol *14*, 639-647.

Reya, T., Morrison, S.J., Clarke, M.F., and Weissman, I.L. (2001). Stem cells, cancer, and cancer stem cells. Nature *414*, 105-111.

Reynolds, A.J., Hendry, I.A., and Bartlett, S.E. (2001). Anterograde and retrograde transport of active extracellular signal-related kinase 1 (ERK1) in the ligated rat sciatic nerve. Neuroscience *105*, 761-771.

Rezaee, M., Penta, K., and Quertermous, T. (2002). Del1 mediates VSMC adhesion, migration, and proliferation through interaction with integrin alpha(v)beta(3). American journal of physiology Heart and circulatory physiology *282*, H1924-1932.

Ribeiro, S., Napoli, I., White, I.J., Parrinello, S., Flanagan, A.M., Suter, U., Parada, L.F., and Lloyd, A.C. (2013). Injury signals cooperate with Nf1 loss to relieve the tumor-suppressive environment of adult peripheral nerve. Cell Rep *5*, 126-136.

Riccardi, V.M. (1981). Von Recklinghausen neurofibromatosis. N Engl J Med *305*, 1617-1627.

Riccardi, V.M. (1992a). Neurofibromatosis: Phenotype, natural history and pathogenesis.

Riccardi, V.M. (1992b). Neurofibromatosis: Phenotype, natural history and pathogenesis. Johns Hopkins Press.

Richard, L., Vedrenne, N., Vallat, J.M., and Funalot, B. (2014). Characterization of Endoneurial Fibroblast-like Cells from Human and Rat Peripheral Nerves. The journal of histochemistry and cytochemistry : official journal of the Histochemistry Society *62*, 424-435.

Richardson, W.D., Young, K.M., Tripathi, R.B., and McKenzie, I. (2011). NG2-glia as multipotent neural stem cells: fact or fantasy? Neuron *70*, 661-673.

Ridley, A.J., Paterson, H.F., Noble, M., and Land, H. (1988). Ras-mediated cell cycle arrest is altered by nuclear oncogenes to induce Schwann cell transformation. The EMBO journal *7*, 1635-1645.

Rieley, M.B., Stevenson, D.A., Viskochil, D.H., Tinkle, B.T., Martin, L.J., and Schorry, E.K. (2011). Variable expression of neurofibromatosis 1 in monozygotic twins. American journal of medical genetics Part A *155A*, 478-485.

Riethmacher, D., Sonnenberg-Riethmacher, E., Brinkmann, V., Yamaai, T., Lewin, G.R., and Birchmeier, C. (1997). Severe neuropathies in mice with targeted mutations in the ErbB3 receptor. Nature *389*, 725-730.

Righi, E., Kashiwagi, S., Yuan, J., Santosuosso, M., Leblanc, P., Ingraham, R., Forbes, B., Edelblute, B., Collette, B., Xing, D*., et al.* (2011). CXCL12/CXCR4 blockade induces multimodal antitumor effects that prolong survival in an immunocompetent mouse model of ovarian cancer. Cancer research *71*, 5522-5534.

Rios, A.C., Fu, N.Y., Cursons, J., Lindeman, G.J., and Visvader, J.E. (2016). The complexities and caveats of lineage tracing in the mammary gland. Breast Cancer Res *18*, 116.

Rios, J.C., Melendez-Vasquez, C.V., Einheber, S., Lustig, M., Grumet, M., Hemperly, J., Peles, E., and Salzer, J.L. (2000). Contactin-associated protein (Caspr) and contactin form a complex that is targeted to the paranodal junctions during myelination. J Neurosci *20*, 8354-8364.

Rios, J.C., Rubin, M., St Martin, M., Downey, R.T., Einheber, S., Rosenbluth, J., Levinson, S.R., Bhat, M., and Salzer, J.L. (2003). Paranodal interactions regulate expression of sodium channel subtypes and provide a diffusion barrier for the node of Ranvier. J Neurosci *23*, 7001-7011.

Rizvi, T.A., Huang, Y., Sidani, A., Atit, R., Largaespada, D.A., Boissy, R.E., and Ratner, N. (2002). A novel cytokine pathway suppresses glial cell melanogenesis after injury to adult nerve. The Journal of neuroscience : the official journal of the Society for Neuroscience *22*, 9831-9840.

Roberts, S.L., Dun, X.P., Doddrell, R.D.S., Mindos, T., Drake, L.K., Onaitis, M.W., Florio, F., Quattrini, A., Lloyd, A.C., D'Antonio, M*., et al.* (2017). Sox2 expression in Schwann cells inhibits myelination in vivo and induces influx of macrophages to the nerve. Development *144*, 3114-3125.

Robertson, G., Garrick, D., Wilson, M., Martin, D.I., and Whitelaw, E. (1996). Age-dependent silencing of globin transgenes in the mouse. Nucleic Acids Res *24*, 1465-1471.

Robertson, K.A., Nalepa, G., Yang, F.C., Bowers, D.C., Ho, C.Y., Hutchins, G.D., Croop, J.M., Vik, T.A., Denne, S.C., Parada, L.F*., et al.* (2012). Imatinib mesylate for plexiform neurofibromas in patients with neurofibromatosis type 1: a phase 2 trial. The Lancet Oncology *13*, 1218-1224.

Rodriguez-Viciana, P., Warne, P.H., Dhand, R., Vanhaesebroeck, B., Gout, I., Fry, M.J., Waterfield, M.D., and Downward, J. (1994). Phosphatidylinositol-3-OH kinase as a direct target of Ras. Nature *370*, 527-532.

Rotshenker, S. (2011). Wallerian degeneration: the innate-immune response to traumatic nerve injury. J Neuroinflammation *8*, 109.

Rubin, J.B., and Gutmann, D.H. (2005). Neurofibromatosis type 1 - a model for nervous system tumour formation? Nat Rev Cancer *5*, 557-564.

Ruhl, A. (2005). Glial cells in the gut. Neurogastroenterology and motility : the official journal of the European Gastrointestinal Motility Society *17*, 777-790.

Rusu, M.C., Pop, F., Hostiuc, S., Curca, G.C., Jianu, A.M., and Paduraru, D. (2012). Telocytes form networks in normal cardiac tissues. Histology and histopathology *27*, 807-816.

Sabbagh, A., Pasmant, E., Laurendeau, I., Parfait, B., Barbarot, S., Guillot, B., Combemale, P., Ferkal, S., Vidaud, M., Aubourg, P*., et al.* (2009). Unravelling the genetic basis of variable clinical expression in neurofibromatosis 1. Human molecular genetics *18*, 2768-2778.

Saher, G., and Simons, M. (2010). Cholesterol and myelin biogenesis. Sub-cellular biochemistry *51*, 489-508.

Salonen, V., Aho, H., Roytta, M., and Peltonen, J. (1988). Quantitation of Schwann cells and endoneurial fibroblast-like cells after experimental nerve trauma. Acta neuropathologica *75*, 331-336.

Salzer, J.L. (2003). Polarized domains of myelinated axons. Neuron *40*, 297-318.

Salzer, J.L. (2012). Axonal regulation of Schwann cell ensheathment and myelination. Journal of the peripheral nervous system : JPNS *17 Suppl 3*, 14-19.

Salzer, J.L. (2015). Schwann cell myelination. Cold Spring Harb Perspect Biol *7*, a020529.

Salzer, J.L., Brophy, P.J., and Peles, E. (2008). Molecular domains of myelinated axons in the peripheral nervous system. Glia *56*, 1532-1540.

Sanders, F.K., and Young, J.Z. (1946). The influence of peripheral connexion on the diameter of regenerating nerve fibres. The Journal of experimental biology *22*, 203-212.

Sato, T., van Es, J.H., Snippert, H.J., Stange, D.E., Vries, R.G., van den Born, M., Barker, N., Shroyer, N.F., van de Wetering, M., and Clevers, H. (2011). Paneth cells constitute the niche for Lgr5 stem cells in intestinal crypts. Nature *469*, 415-418.

Sauer, B., and Henderson, N. (1988). Site-specific DNA recombination in mammalian cells by the Cre recombinase of bacteriophage P1. Proceedings of the National Academy of Sciences of the United States of America *85*, 5166-5170.

Savidge, T.C., Newman, P., Pothoulakis, C., Ruhl, A., Neunlist, M., Bourreille, A., Hurst, R., and Sofroniew, M.V. (2007). Enteric glia regulate intestinal barrier function and inflammation via release of S-nitrosoglutathione. Gastroenterology *132*, 1344-1358.

Savva, E., Vargas, M.I., Beaulieu, J.Y., Truffert, A., Burkhardt, K., Lobrinus, J.A., and Burkhard, P.R. (2010). Giant plexiform neurofibroma in neurofibromatosis type 1. Archives of neurology *67*, 356-357.

Schafer, M., Fruttiger, M., Montag, D., Schachner, M., and Martini, R. (1996). Disruption of the gene for the myelin-associated glycoprotein improves axonal regrowth along myelin in C57BL/Wlds mice. Neuron *16*, 1107-1113.

Scherer, S.S. (1999). Nodes, Paranodes, and Incisures: From Form to Function. Ann N Y Acad Sci *883*, 131-142.

Scherer, S.S., Wang, D.Y., Kuhn, R., Lemke, G., Wrabetz, L., and Kamholz, J. (1994). Axons regulate Schwann cell expression of the POU transcription factor SCIP. J Neurosci *14*, 1930-1942.

Schindelin, J., Arganda-Carreras, I., Frise, E., Kaynig, V., Longair, M., Pietzsch, T., Preibisch, S., Rueden, C., Saalfeld, S., Schmid, B.*, et al.* (2012). Fiji: an open-source platform for biological-image analysis. Nature methods *9*, 676-682.

Schreiner, S., Cossais, F., Fischer, K., Scholz, S., Bosl, M.R., Holtmann, B., Sendtner, M., and Wegner, M. (2007). Hypomorphic Sox10 alleles reveal novel protein functions and unravel developmental differences in glial lineages. Development *134*, 3271-3281.

Schroder, J.M. (1972). Altered ratio between axon diameter and myelin sheath thickness in regenerated nerve fibers. Brain research *45*, 49-65.

Schroeder, A., Mueller, O., Stocker, S., Salowsky, R., Leiber, M., Gassmann, M., Lightfoot, S., Menzel, W., Granzow, M., and Ragg, T. (2006). The RIN: an RNA integrity number for assigning integrity values to RNA measurements. BMC Mol Biol *7*, 3.

Schubbert, S., Shannon, K., and Bollag, G. (2007). Hyperactive Ras in developmental disorders and cancer. Nat Rev Cancer *7*, 295-308.

Schulz, T.J., Glaubitz, M., Kuhlow, D., Thierbach, R., Birringer, M., Steinberg, P., Pfeiffer, A.F., and Ristow, M. (2007). Variable expression of Cre recombinase transgenes precludes reliable prediction of tissue-specific gene disruption by tail-biopsy genotyping. PLoS One *2*, e1013.

Sehgal, A., Keener, C., Boynton, A.L., Warrick, J., and Murphy, G.P. (1998). CXCR-4, a chemokine receptor, is overexpressed in and required for proliferation of glioblastoma tumor cells. Journal of surgical oncology *69*, 99-104.

Seki, S., Kawaguchi, Y., Chiba, K., Mikami, Y., Kizawa, H., Oya, T., Mio, F., Mori, M., Miyamoto, Y., Masuda, I.*, et al.* (2005). A functional SNP in CILP, encoding cartilage intermediate layer protein, is associated with susceptibility to lumbar disc disease. Nat Genet *37*, 607-612.

Sengupta, R., Dubuc, A., Ward, S., Yang, L., Northcott, P., Woerner, B.M., Kroll, K., Luo, J., Taylor, M.D., Wechsler-Reya, R.J.*, et al.* (2012). CXCR4 activation defines a new subgroup of Sonic hedgehog-driven medulloblastoma. Cancer research *72*, 122-132.

Serra, E., Puig, S., Otero, D., Gaona, A., Kruyer, H., Ars, E., Estivill, X., and Lazaro, C. (1997). Confirmation of a double-hit model for the NF1 gene in benign neurofibromas. Am J Hum Genet *61*, 512-519.

Serra, E., Rosenbaum, T., Winner, U., Aledo, R., Ars, E., Estivill, X., Lenard, H.G., and Lazaro, C. (2000). Schwann cells harbor the somatic NF1 mutation in neurofibromas:

evidence of two different Schwann cell subpopulations. Hum Mol Genet *9*, 3055-3064.

Serrano, M., Lin, A.W., McCurrach, M.E., Beach, D., and Lowe, S.W. (1997). Oncogenic ras provokes premature cell senescence associated with accumulation of p53 and p16INK4a. Cell *88*, 593-602.

Shah, N.M., Marchionni, M.A., Isaacs, I., Stroobant, P., and Anderson, D.J. (1994). Glial growth factor restricts mammalian neural crest stem cells to a glial fate. Cell *77*, 349-360.

Shamash, S., Reichert, F., and Rotshenker, S. (2002). The cytokine network of Wallerian degeneration: tumor necrosis factor-alpha, interleukin-1alpha, and interleukin-1beta. J Neurosci *22*, 3052-3060.

Shapiro, L., Doyle, J.P., Hensley, P., Colman, D.R., and Hendrickson, W.A. (1996). Crystal structure of the extracellular domain from P0, the major structural protein of peripheral nerve myelin. Neuron *17*, 435-449.

Sheean, M.E., McShane, E., Cheret, C., Walcher, J., Muller, T., Wulf-Goldenberg, A., Hoelper, S., Garratt, A.N., Kruger, M., Rajewsky, K.*, et al.* (2014). Activation of MAPK overrides the termination of myelin growth and replaces Nrg1/ErbB3 signals during Schwann cell development and myelination. Genes & development *28*, 290-303.

Sheela, S., Riccardi, V.M., and Ratner, N. (1990). Angiogenic and invasive properties of neurofibroma Schwann cells. The Journal of cell biology *111*, 645-653.

Shellenberger, T.D., Wang, M., Gujrati, M., Jayakumar, A., Strieter, R.M., Burdick, M.D., Ioannides, C.G., Efferson, C.L., El-Naggar, A.K., Roberts, D.*, et al.* (2004). BRAK/CXCL14 is a potent inhibitor of angiogenesis and a chemotactic factor for immature dendritic cells. Cancer Res *64*, 8262-8270.

Shen, X.H., Lin, W.R., Xu, M.D., Qi, P., Dong, L., Zhang, Q.Y., Ni, S.J., Weng, W.W., Tan, C., Huang, D.*, et al.* (2015). Prognostic significance of Versican expression in gastric adenocarcinoma. Oncogenesis *4*, e178.

Shen, Y.J., DeBellard, M.E., Salzer, J.L., Roder, J., and Filbin, M.T. (1998). Myelin-associated glycoprotein in myelin and expressed by Schwann cells inhibits axonal regeneration and branching. Molecular and cellular neurosciences *12*, 79-91.

Sherman, D.L., and Brophy, P.J. (2005). Mechanisms of axon ensheathment and myelin growth. Nature reviews Neuroscience *6*, 683-690.

Sherman, D.L., Wu, L.M., Grove, M., Gillespie, C.S., and Brophy, P.J. (2012). Drp2 and periaxin form Cajal bands with dystroglycan but have distinct roles in Schwann cell growth. The Journal of neuroscience : the official journal of the Society for Neuroscience *32*, 9419-9428.

Sherman, L.S., Atit, R., Rosenbaum, T., Cox, A.D., and Ratner, N. (2000). Single cell Ras-GTP analysis reveals altered Ras activity in a subpopulation of neurofibroma Schwann cells but not fibroblasts. J Biol Chem *275*, 30740-30745.

Sherman, M.H., Yu, R.T., Engle, D.D., Ding, N., Atkins, A.R., Tiriac, H., Collisson, E.A., Connor, F., Van Dyke, T., Kozlov, S*., et al.* (2014). Vitamin D receptor-mediated stromal reprogramming suppresses pancreatitis and enhances pancreatic cancer therapy. Cell *159*, 80-93.

Sheu, J.Y., Kulhanek, D.J., and Eckenstein, F.P. (2000). Differential patterns of ERK and STAT3 phosphorylation after sciatic nerve transection in the rat. Exp Neurol *166*, 392-402.

Shimshek, D.R., Kim, J., Hubner, M.R., Spergel, D.J., Buchholz, F., Casanova, E., Stewart, A.F., Seeburg, P.H., and Sprengel, R. (2002). Codon-improved Cre recombinase (iCre) expression in the mouse. Genesis *32*, 19-26.

Shoshkes-Carmel, M., Wang, Y.J., Wangensteen, K.J., Toth, B., Kondo, A., Massasa, E.E., Itzkovitz, S., and Kaestner, K.H. (2018). Subepithelial telocytes are an important source of Wnts that supports intestinal crypts. Nature *557*, 242-246.

Shuman, S., Hardy, M., Sobue, G., and Pleasure, D. (1988). A cyclic AMP analogue induces synthesis of a myelin-specific glycoprotein by cultured Schwann cells. Journal of neurochemistry *50*, 190-194.

Shurin, G.V., Ferris, R.L., Tourkova, I.L., Perez, L., Lokshin, A., Balkir, L., Collins, B., Chatta, G.S., and Shurin, M.R. (2005). Loss of new chemokine CXCL14 in tumor tissue is associated with low infiltration by dendritic cells (DC), while restoration of human CXCL14 expression in tumor cells causes attraction of DC both in vitro and in vivo. J Immunol *174*, 5490-5498.

Shy, M.E., Arroyo, E., Sladky, J., Menichella, D., Jiang, H., Xu, W., Kamholz, J., and Scherer, S.S. (1997). Heterozygous P0 knockout mice develop a peripheral neuropathy that resembles chronic inflammatory demyelinating polyneuropathy (CIDP). J Neuropathol Exp Neurol *56*, 811-821.

Silva, A.J., Frankland, P.W., Marowitz, Z., Friedman, E., Laszlo, G.S., Cioffi, D., Jacks, T., and Bourtchuladze, R. (1997). A mouse model for the learning and memory deficits associated with neurofibromatosis type I. Nature genetics *15*, 281-284.

Simanshu, D.K., Nissley, D.V., and McCormick, F. (2017). RAS Proteins and Their Regulators in Human Disease. Cell *170*, 17-33.

Simmons, G.W., Pong, W.W., Emnett, R.J., White, C.R., Gianino, S.M., Rodriguez, F.J., and Gutmann, D.H. (2011). Neurofibromatosis-1 heterozygosity increases microglia in a spatially and temporally restricted pattern relevant to mouse optic glioma formation and growth. Journal of neuropathology and experimental neurology *70*, 51-62.

Simon, A., and Frisen, J. (2007). From stem cell to progenitor and back again. Cell *128*, 825-826.

Simons, B.D., and Clevers, H. (2011). Strategies for homeostatic stem cell self-renewal in adult tissues. Cell *145*, 851-862.

Singh, S.K., Hawkins, C., Clarke, I.D., Squire, J.A., Bayani, J., Hide, T., Henkelman, R.M., Cusimano, M.D., and Dirks, P.B. (2004). Identification of human brain tumour initiating cells. Nature *432*, 396-401.

Smith, H.W., and Muller, W.J. (2013). Transgenic mouse models--a seminal breakthrough in oncogene research. Cold Spring Harb Protoc *2013*, 1099-1108.

Smith, I.W., Mikesh, M., Lee, Y., and Thompson, W.J. (2013). Terminal Schwann cells participate in the competition underlying neuromuscular synapse elimination. The Journal of neuroscience : the official journal of the Society for Neuroscience *33*, 17724-17736.

Smith M.M., H.B.K. (1993). A Developmental Model for Evolution of the Vertebrate Exoskeleton and Teeth. Evolutionary Biology, Evolutionary Biology, Springer, Boston, MA *27*.

Snaidero, N., and Simons, M. (2014). Myelination at a glance. J Cell Sci *127*, 2999-3004.

Snippert, H.J., and Clevers, H. (2011). Tracking adult stem cells. EMBO reports *12*, 113-122.

Snippert, H.J., van der Flier, L.G., Sato, T., van Es, J.H., van den Born, M., Kroon-Veenboer, C., Barker, N., Klein, A.M., van Rheenen, J., Simons, B.D.*, et al.* (2010).

Intestinal crypt homeostasis results from neutral competition between symmetrically dividing Lgr5 stem cells. Cell *143*, 134-144.
Sobue, G., and Pleasure, D. (1984). Schwann cell galactocerebroside induced by derivatives of adenosine 3',5'-monophosphate. Science *224*, 72-74.
Sobue, G., Shuman, S., and Pleasure, D. (1986). Schwann cell responses to cyclic AMP: proliferation, change in shape, and appearance of surface galactocerebroside. Brain research *362*, 23-32.
Sondell, M., Lundborg, G., and Kanje, M. (1999). Vascular endothelial growth factor has neurotrophic activity and stimulates axonal outgrowth, enhancing cell survival and Schwann cell proliferation in the peripheral nervous system. The Journal of neuroscience : the official journal of the Society for Neuroscience *19*, 5731-5740.
Song, X.Y., Zhou, F.H., Zhong, J.H., Wu, L.L., and Zhou, X.F. (2006). Knockout of p75(NTR) impairs re-myelination of injured sciatic nerve in mice. J Neurochem *96*, 833-842.
Soriano, P.M.W.a.P. (2010). Guide to Techniques in Mouse Development, Part B. Academic Press.
Soteriou, D., and Fuchs, Y. (2018). A matter of life and death: stem cell survival in tissue regeneration and tumour formation. Nature reviews Cancer *18*, 187-201.
Sottoriva, A., Kang, H., Ma, Z., Graham, T.A., Salomon, M.P., Zhao, J., Marjoram, P., Siegmund, K., Press, M.F., Shibata, D.*, et al.* (2015). A Big Bang model of human colorectal tumor growth. Nature genetics *47*, 209-216.
Spiegel, I., Adamsky, K., Eshed, Y., Milo, R., Sabanay, H., Sarig-Nadir, O., Horresh, I., Scherer, S.S., Rasband, M.N., and Peles, E. (2007). A central role for Necl4 (SynCAM4) in Schwann cell-axon interaction and myelination. Nat Neurosci *10*, 861-869.
Srinivas, S., Watanabe, T., Lin, C.S., William, C.M., Tanabe, Y., Jessell, T.M., and Costantini, F. (2001). Cre reporter strains produced by targeted insertion of EYFP and ECFP into the ROSA26 locus. BMC developmental biology *1*, 4.
Srinivasan, R., Sun, G., Keles, S., Jones, E.A., Jang, S.W., Krueger, C., Moran, J.J., and Svaren, J. (2012). Genome-wide analysis of EGR2/SOX10 binding in myelinating peripheral nerve. Nucleic acids research *40*, 6449-6460.
Stange, D.E., Koo, B.K., Huch, M., Sibbel, G., Basak, O., Lyubimova, A., Kujala, P., Bartfeld, S., Koster, J., Geahlen, J.H.*, et al.* (2013). Differentiated Troy+ chief cells act

as reserve stem cells to generate all lineages of the stomach epithelium. Cell *155*, 357-368.

Starnes, T., Rasila, K.K., Robertson, M.J., Brahmi, Z., Dahl, R., Christopherson, K., and Hromas, R. (2006). The chemokine CXCL14 (BRAK) stimulates activated NK cell migration: implications for the downregulation of CXCL14 in malignancy. Exp Hematol *34*, 1101-1105.

Staser, K., Yang, F.C., and Clapp, D.W. (2010). Mast cells and the neurofibroma microenvironment. Blood *116*, 157-164.

Stassart, R.M., Fledrich, R., Velanac, V., Brinkmann, B.G., Schwab, M.H., Meijer, D., Sereda, M.W., and Nave, K.A. (2013). A role for Schwann cell-derived neuregulin-1 in remyelination. Nat Neurosci *16*, 48-54.

Stetler-Stevenson, W.G., and Yu, A.E. (2001). Proteases in invasion: matrix metalloproteinases. Seminars in cancer biology *11*, 143-152.

Stevens, B., and Fields, R.D. (2002). Regulation of the cell cycle in normal and pathological glia. Neuroscientist *8*, 93-97.

Stewart, H., Bowker, C., Edees, S., Smalley, S., Crocker, M., Mechan, D., Forrester, N., Spurlock, G., and Upadhyaya, M. (2008). Congenital disseminated neurofibromatosis type 1: a clinical and molecular case report. American journal of medical genetics Part A *146A*, 1444-1452.

Stickens, D., Behonick, D.J., Ortega, N., Heyer, B., Hartenstein, B., Yu, Y., Fosang, A.J., Schorpp-Kistner, M., Angel, P., and Werb, Z. (2004). Altered endochondral bone development in matrix metalloproteinase 13-deficient mice. Development *131*, 5883-5895.

Straussman, R., Morikawa, T., Shee, K., Barzily-Rokni, M., Qian, Z.R., Du, J., Davis, A., Mongare, M.M., Gould, J., Frederick, D.T.*, et al.* (2012). Tumour micro-environment elicits innate resistance to RAF inhibitors through HGF secretion. Nature *487*, 500-504.

Suadicani, S.O., Cherkas, P.S., Zuckerman, J., Smith, D.N., Spray, D.C., and Hanani, M. (2010). Bidirectional calcium signaling between satellite glial cells and neurons in cultured mouse trigeminal ganglia. Neuron glia biology *6*, 43-51.

Sun, Y., Campisi, J., Higano, C., Beer, T.M., Porter, P., Coleman, I., True, L., and Nelson, P.S. (2012). Treatment-induced damage to the tumor microenvironment

promotes prostate cancer therapy resistance through WNT16B. Nat Med *18*, 1359-1368.

Svaren, J., and Meijer, D. (2008). The molecular machinery of myelin gene transcription in Schwann cells. Glia *56*, 1541-1551.

Syed, N., Reddy, K., Yang, D.P., Taveggia, C., Salzer, J.L., Maurel, P., and Kim, H.A. (2010). Soluble neuregulin-1 has bifunctional, concentration-dependent effects on Schwann cell myelination. J Neurosci *30*, 6122-6131.

Tacke, R., and Martini, R. (1990). Changes in expression of mRNA specific for cell adhesion molecules (L1 and NCAM) in the transected peripheral nerve of the adult rat. Neurosci Lett *120*, 227-230.

Takahashi, K., and Yamanaka, S. (2006). Induction of pluripotent stem cells from mouse embryonic and adult fibroblast cultures by defined factors. Cell *126*, 663-676.

Takahashi, T., Fournier, A., Nakamura, F., Wang, L.H., Murakami, Y., Kalb, R.G., Fujisawa, H., and Strittmatter, S.M. (1999). Plexin-neuropilin-1 complexes form functional semaphorin-3A receptors. Cell *99*, 59-69.

Takeda, M., Takahashi, M., and Matsumoto, S. (2009). Contribution of the activation of satellite glia in sensory ganglia to pathological pain. Neuroscience and biobehavioral reviews *33*, 784-792.

Taniuchi, M., Clark, H.B., and Johnson, E.M., Jr. (1986). Induction of nerve growth factor receptor in Schwann cells after axotomy. Proc Natl Acad Sci U S A *83*, 4094-4098.

Tarazona, S., Garcia-Alcalde, F., Dopazo, J., Ferrer, A., and Conesa, A. (2011). Differential expression in RNA-seq: a matter of depth. Genome Res *21*, 2213-2223.

Tarlow, B.D., Pelz, C., Naugler, W.E., Wakefield, L., Wilson, E.M., Finegold, M.J., and Grompe, M. (2014). Bipotential adult liver progenitors are derived from chronically injured mature hepatocytes. Cell stem cell *15*, 605-618.

Tata, P.R., Mou, H., Pardo-Saganta, A., Zhao, R., Prabhu, M., Law, B.M., Vinarsky, V., Cho, J.L., Breton, S., Sahay, A.*, et al.* (2013). Dedifferentiation of committed epithelial cells into stem cells in vivo. Nature *503*, 218-223.

Tata, P.R., and Rajagopal, J. (2016). Cellular plasticity: 1712 to the present day. Current opinion in cell biology *43*, 46-54.

Taupin, P. (2007). BrdU immunohistochemistry for studying adult neurogenesis: paradigms, pitfalls, limitations, and validation. Brain Res Rev *53*, 198-214.

Taveggia, C., Zanazzi, G., Petrylak, A., Yano, H., Rosenbluth, J., Einheber, S., Xu, X., Esper, R.M., Loeb, J.A., Shrager, P.*, et al.* (2005). Neuregulin-1 type III determines the ensheathment fate of axons. Neuron *47*, 681-694.

Team, R.C. (2014). R: A Language and Environment for Statistical Computing. R Foundation for Statistical Computing.

Tekin, M., Chioza, B.A., Matsumoto, Y., Diaz-Horta, O., Cross, H.E., Duman, D., Kokotas, H., Moore-Barton, H.L., Sakoori, K., Ota, M.*, et al.* (2013). SLITRK6 mutations cause myopia and deafness in humans and mice. J Clin Invest *123*, 2094-2102.

Tetteh, P.W., Basak, O., Farin, H.F., Wiebrands, K., Kretzschmar, K., Begthel, H., van den Born, M., Korving, J., de Sauvage, F., van Es, J.H.*, et al.* (2016). Replacement of Lost Lgr5-Positive Stem Cells through Plasticity of Their Enterocyte-Lineage Daughters. Cell stem cell *18*, 203-213.

Thomas, L., Kluwe, L., Chuzhanova, N., Mautner, V., and Upadhyaya, M. (2010). Analysis of NF1 somatic mutations in cutaneous neurofibromas from patients with high tumor burden. Neurogenetics *11*, 391-400.

Thornton, M.R., Mantovani, C., Birchall, M.A., and Terenghi, G. (2005). Quantification of N-CAM and N-cadherin expression in axotomized and crushed rat sciatic nerve. J Anat *206*, 69-78.

Tian, H., Biehs, B., Warming, S., Leong, K.G., Rangell, L., Klein, O.D., and de Sauvage, F.J. (2011). A reserve stem cell population in small intestine renders Lgr5-positive cells dispensable. Nature *478*, 255-259.

Tlsty, T.D., and Coussens, L.M. (2006). Tumor stroma and regulation of cancer development. Annu Rev Pathol *1*, 119-150.

Toma, J.G., Akhavan, M., Fernandes, K.J., Barnabe-Heider, F., Sadikot, A., Kaplan, D.R., and Miller, F.D. (2001). Isolation of multipotent adult stem cells from the dermis of mammalian skin. Nature cell biology *3*, 778-784.

Toma, J.G., McKenzie, I.A., Bagli, D., and Miller, F.D. (2005). Isolation and characterization of multipotent skin-derived precursors from human skin. Stem cells *23*, 727-737.

Tomer, R., Ye, L., Hsueh, B., and Deisseroth, K. (2014). Advanced CLARITY for rapid and high-resolution imaging of intact tissues. Nature protocols *9*, 1682-1697.

Topilko, P., Schneider-Maunoury, S., Levi, G., Baron-Van Evercooren, A., Chennoufi, A.B., Seitanidou, T., Babinet, C., and Charnay, P. (1994). Krox-20 controls myelination in the peripheral nervous system. Nature *371*, 796-799.

Torres, K.C., Lima, G., Simoes, E.S.A.C., Lubambo, I., Rodrigues, L.O., Rodrigues, L., Silveira, K.D., Vieira, E.L., Romano-Silva, M.A., and Miranda, D.M. (2016). Immune markers in the RASopathy neurofibromatosis type 1. J Neuroimmunol *295-296*, 122-129.

Toyota, B., Carbonetto, S., and David, S. (1990). A dual laminin/collagen receptor acts in peripheral nerve regeneration. Proc Natl Acad Sci U S A *87*, 1319-1322.

Trapp, B.D., Hauer, P., and Lemke, G. (1988). Axonal regulation of myelin protein mRNA levels in actively myelinating Schwann cells. J Neurosci *8*, 3515-3521.

True, L.D., Zhang, H., Ye, M., Huang, C.Y., Nelson, P.S., von Haller, P.D., Tjoelker, L.W., Kim, J.S., Qian, W.J., Smith, R.D.*, et al.* (2010). CD90/THY1 is overexpressed in prostate cancer-associated fibroblasts and could serve as a cancer biomarker. Modern pathology : an official journal of the United States and Canadian Academy of Pathology, Inc *23*, 1346-1356.

Tucker, T., Wolkenstein, P., Revuz, J., Zeller, J., and Friedman, J.M. (2005). Association between benign and malignant peripheral nerve sheath tumors in NF1. Neurology *65*, 205-211.

Tuveson, D.A., Shaw, A.T., Willis, N.A., Silver, D.P., Jackson, E.L., Chang, S., Mercer, K.L., Grochow, R., Hock, H., Crowley, D.*, et al.* (2004). Endogenous oncogenic K-ras(G12D) stimulates proliferation and widespread neoplastic and developmental defects. Cancer Cell *5*, 375-387.

Uesaka, T., Nagashimada, M., and Enomoto, H. (2015). Neuronal Differentiation in Schwann Cell Lineage Underlies Postnatal Neurogenesis in the Enteric Nervous System. The Journal of neuroscience : the official journal of the Society for Neuroscience *35*, 9879-9888.

Upadhyaya, M., Cooper, David (Eds.) (2012). Neurofibromatosis Type 1: Molecular and Cellular Biology. Springer.

Upadhyaya, M., Shaw, D.J., and Harper, P.S. (1994). Molecular basis of neurofibromatosis type 1 (NF1): mutation analysis and polymorphisms in the NF1 gene. Hum Mutat *4*, 83-101.

Upadhyaya, M., Spurlock, G., Monem, B., Thomas, N., Friedrich, R.E., Kluwe, L., and Mautner, V. (2008). Germline and somatic NF1 gene mutations in plexiform neurofibromas. Human mutation *29*, E103-111.

Vabnick, I., and Shrager, P. (1998). Ion channel redistribution and function during development of the myelinated axon. Journal of neurobiology *37*, 80-96.

Valkenburg, K.C., de Groot, A.E., and Pienta, K.J. (2018). Targeting the tumour stroma to improve cancer therapy. Nature reviews Clinical oncology *15*, 366-381.

van der Flier, L.G., and Clevers, H. (2009). Stem cells, self-renewal, and differentiation in the intestinal epithelium. Annual review of physiology *71*, 241-260.

Van Dyke, T., and Jacks, T. (2002). Cancer modeling in the modern era: progress and challenges. Cell *108*, 135-144.

van Es, J.H., Sato, T., van de Wetering, M., Lyubimova, A., Yee Nee, A.N., Gregorieff, A., Sasaki, N., Zeinstra, L., van den Born, M., Korving, J.*, et al.* (2012). Dll1+ secretory progenitor cells revert to stem cells upon crypt damage. Nature cell biology *14*, 1099-1104.

Van Keymeulen, A., and Blanpain, C. (2012). Tracing epithelial stem cells during development, homeostasis, and repair. J Cell Biol *197*, 575-584.

Vandenbroucke, I., Van Oostveldt, P., Coene, E., De Paepe, A., and Messiaen, L. (2004). Neurofibromin is actively transported to the nucleus. FEBS Lett *560*, 98-102.

Varga, J., and Greten, F.R. (2017). Cell plasticity in epithelial homeostasis and tumorigenesis. Nature cell biology *19*, 1133-1141.

Vargas, M.E., Watanabe, J., Singh, S.J., Robinson, W.H., and Barres, B.A. (2010). Endogenous antibodies promote rapid myelin clearance and effective axon regeneration after nerve injury. Proceedings of the National Academy of Sciences of the United States of America *107*, 11993-11998.

Verma, P., Chierzi, S., Codd, A.M., Campbell, D.S., Meyer, R.L., Holt, C.E., and Fawcett, J.W. (2005). Axonal protein synthesis and degradation are necessary for efficient growth cone regeneration. The Journal of neuroscience : the official journal of the Society for Neuroscience *25*, 331-342.

Vermeulen, L., De Sousa, E.M.F., van der Heijden, M., Cameron, K., de Jong, J.H., Borovski, T., Tuynman, J.B., Todaro, M., Merz, C., Rodermond, H.*, et al.* (2010). Wnt activity defines colon cancer stem cells and is regulated by the microenvironment. Nature cell biology *12*, 468-476.

Viader, A., Golden, J.P., Baloh, R.H., Schmidt, R.E., Hunter, D.A., and Milbrandt, J. (2011). Schwann cell mitochondrial metabolism supports long-term axonal survival and peripheral nerve function. J Neurosci *31*, 10128-10140.

Viader, A., Sasaki, Y., Kim, S., Strickland, A., Workman, C.S., Yang, K., Gross, R.W., and Milbrandt, J. (2013). Aberrant Schwann cell lipid metabolism linked to mitochondrial deficits leads to axon degeneration and neuropathy. Neuron *77*, 886-898.

Vigil, D., Cherfils, J., Rossman, K.L., and Der, C.J. (2010). Ras superfamily GEFs and GAPs: validated and tractable targets for cancer therapy? Nature reviews Cancer *10*, 842-857.

Vivanco, I., and Sawyers, C.L. (2002). The phosphatidylinositol 3-Kinase AKT pathway in human cancer. Nat Rev Cancer *2*, 489-501.

Vogel, K.S., Klesse, L.J., Velasco-Miguel, S., Meyers, K., Rushing, E.J., and Parada, L.F. (1999). Mouse tumor model for neurofibromatosis type 1. Science *286*, 2176-2179.

Vogelezang, M.G., Liu, Z., Relvas, J.B., Raivich, G., Scherer, S.S., and ffrench-Constant, C. (2001). Alpha4 integrin is expressed during peripheral nerve regeneration and enhances neurite outgrowth. J Neurosci *21*, 6732-6744.

Wakamatsu, Y., Maynard, T.M., and Weston, J.A. (2000). Fate determination of neural crest cells by NOTCH-mediated lateral inhibition and asymmetrical cell division during gangliogenesis. Development *127*, 2811-2821.

Waldner, M.J., Foersch, S., and Neurath, M.F. (2012). Interleukin-6--a key regulator of colorectal cancer development. Int J Biol Sci *8*, 1248-1253.

Walikonis, R.S., and Poduslo, J.F. (1998). Activity of cyclic AMP phosphodiesterases and adenylyl cyclase in peripheral nerve after crush and permanent transection injuries. J Biol Chem *273*, 9070-9077.

Wallace, M.R., Marchuk, D.A., Andersen, L.B., Letcher, R., Odeh, H.M., Saulino, A.M., Fountain, J.W., Brereton, A., Nicholson, J., Mitchell, A.L.*, et al.* (1990). Type 1 neurofibromatosis gene: identification of a large transcript disrupted in three NF1 patients. Science *249*, 181-186.

Wang, G.Y., Wang, J., Mancianti, M.L., and Epstein, E.H., Jr. (2011). Basal cell carcinomas arise from hair follicle stem cells in Ptch1(+/-) mice. Cancer cell *19*, 114-124.

Wang, H., Kunkel, D.D., Martin, T.M., Schwartzkroin, P.A., and Tempel, B.L. (1993). Heteromultimeric K+ channels in terminal and juxtaparanodal regions of neurons. Nature *365*, 75-79.

Wang, J., Zhai, Q., Chen, Y., Lin, E., Gu, W., McBurney, M.W., and He, Z. (2005). A local mechanism mediates NAD-dependent protection of axon degeneration. J Cell Biol *170*, 349-355.

Wang, Z., Ma, Q., Liu, Q., Yu, H., Zhao, L., Shen, S., and Yao, J. (2008). Blockade of SDF-1/CXCR4 signalling inhibits pancreatic cancer progression in vitro via inactivation of canonical Wnt pathway. British journal of cancer *99*, 1695-1703.

Wanner, I.B., and Wood, P.M. (2002). N-cadherin mediates axon-aligned process growth and cell-cell interaction in rat Schwann cells. J Neurosci *22*, 4066-4079.

Warbey, V.S., Ferner, R.E., Dunn, J.T., Calonje, E., and O'Doherty, M.J. (2009). [18F]FDG PET/CT in the diagnosis of malignant peripheral nerve sheath tumours in neurofibromatosis type-1. European journal of nuclear medicine and molecular imaging *36*, 751-757.

Warner, L.E., Hilz, M.J., Appel, S.H., Killian, J.M., Kolodry, E.H., Karpati, G., Carpenter, S., Watters, G.V., Wheeler, C., Witt, D*., et al.* (1996). Clinical phenotypes of different MPZ (P0) mutations may include Charcot-Marie-Tooth type 1B, Dejerine-Sottas, and congenital hypomyelination. Neuron *17*, 451-460.

Watson, A.L., Anderson, L.K., Greeley, A.D., Keng, V.W., Rahrmann, E.P., Halfond, A.L., Powell, N.M., Collins, M.H., Rizvi, T., Moertel, C.L*., et al.* (2014). Co-targeting the MAPK and PI3K/AKT/mTOR pathways in two genetically engineered mouse models of schwann cell tumors reduces tumor grade and multiplicity. Oncotarget *5*, 1502-1514.

Watt, F.M., and Driskell, R.R. (2010). The therapeutic potential of stem cells. Philosophical transactions of the Royal Society of London Series B, Biological sciences *365*, 155-163.

Watters, J.J., Schartner, J.M., and Badie, B. (2005). Microglia function in brain tumors. Journal of neuroscience research *81*, 447-455.

Webster, H.D., Martin, R., and O'Connell, M.F. (1973). The relationships between interphase Schwann cells and axons before myelination: a quantitative electron microscopic study. Dev Biol *32*, 401-416.

Weider, M., Reiprich, S., and Wegner, M. (2013). Sox appeal - Sox10 attracts epigenetic and transcriptional regulators in myelinating glia. Biol Chem *394*, 1583-1593.

Weis, S.M., and Cheresh, D.A. (2011). Tumor angiogenesis: molecular pathways and therapeutic targets. Nat Med *17*, 1359-1370.

Weiss, B., Bollag, G., and Shannon, K. (1999). Hyperactive Ras as a therapeutic target in neurofibromatosis type 1. Am J Med Genet *89*, 14-22.

Weissman, I.L. (2000). Stem cells: units of development, units of regeneration, and units in evolution. Cell *100*, 157-168.

Wells, J.M., and Watt, F.M. (2018). Diverse mechanisms for endogenous regeneration and repair in mammalian organs. Nature *557*, 322-328.

Wente, M.N., Mayer, C., Gaida, M.M., Michalski, C.W., Giese, T., Bergmann, F., Giese, N.A., Buchler, M.W., and Friess, H. (2008). CXCL14 expression and potential function in pancreatic cancer. Cancer Lett *259*, 209-217.

Weston, J.A. (1963). A radioautographic analysis of the migration and localization of trunk neural crest cells in the chick. Dev Biol *6*, 279-310.

Widemann, B.C. (2009). Current status of sporadic and neurofibromatosis type 1-associated malignant peripheral nerve sheath tumors. Current oncology reports *11*, 322-328.

Widera, D., Heimann, P., Zander, C., Imielski, Y., Heidbreder, M., Heilemann, M., Kaltschmidt, C., and Kaltschmidt, B. (2011). Schwann cells can be reprogrammed to multipotency by culture. Stem cells and development *20*, 2053-2064.

Wight, T.N. (2002). Versican: a versatile extracellular matrix proteoglycan in cell biology. Curr Opin Cell Biol *14*, 617-623.

Williams, A., Piaton, G., Aigrot, M.S., Belhadi, A., Theaudin, M., Petermann, F., Thomas, J.L., Zalc, B., and Lubetzki, C. (2007). Semaphorin 3A and 3F: key players in myelin repair in multiple sclerosis? Brain : a journal of neurology *130*, 2554-2565.

Wimmer, K., Roca, X., Beiglbock, H., Callens, T., Etzler, J., Rao, A.R., Krainer, A.R., Fonatsch, C., and Messiaen, L. (2007). Extensive in silico analysis of NF1 splicing

defects uncovers determinants for splicing outcome upon 5' splice-site disruption. Human mutation *28*, 599-612.

Wimmer, K., Yao, S., Claes, K., Kehrer-Sawatzki, H., Tinschert, S., De Raedt, T., Legius, E., Callens, T., Beiglbock, H., Maertens, O.*, et al.* (2006). Spectrum of single- and multiexon NF1 copy number changes in a cohort of 1,100 unselected NF1 patients. Genes, chromosomes & cancer *45*, 265-276.

Witsch, E., Sela, M., and Yarden, Y. (2010). Roles for growth factors in cancer progression. Physiology *25*, 85-101.

Woldeyesus, M.T., Britsch, S., Riethmacher, D., Xu, L., Sonnenberg-Riethmacher, E., Abou-Rebyeh, F., Harvey, R., Caroni, P., and Birchmeier, C. (1999). Peripheral nervous system defects in erbB2 mutants following genetic rescue of heart development. Genes Dev *13*, 2538-2548.

Wong, S.Y., and Reiter, J.F. (2011). Wounding mobilizes hair follicle stem cells to form tumors. Proceedings of the National Academy of Sciences of the United States of America *108*, 4093-4098.

Woodhoo, A., Alonso, M.B., Droggiti, A., Turmaine, M., D'Antonio, M., Parkinson, D.B., Wilton, D.K., Al-Shawi, R., Simons, P., Shen, J.*, et al.* (2009). Notch controls embryonic Schwann cell differentiation, postnatal myelination and adult plasticity. Nat Neurosci *12*, 839-847.

Woodruff, J.M. (1999). Pathology of tumors of the peripheral nerve sheath in type 1 neurofibromatosis. Am J Med Genet *89*, 23-30.

Wu, J., Keng, V.W., Patmore, D.M., Kendall, J.J., Patel, A.V., Jousma, E., Jessen, W.J., Choi, K., Tschida, B.R., Silverstein, K.A.*, et al.* (2016). Insertional Mutagenesis Identifies a STAT3/Arid1b/beta-catenin Pathway Driving Neurofibroma Initiation. Cell Rep *14*, 1979-1990.

Wu, J., Patmore, D.M., Jousma, E., Eaves, D.W., Breving, K., Patel, A.V., Schwartz, E.B., Fuchs, J.R., Cripe, T.P., Stemmer-Rachamimov, A.O.*, et al.* (2014). EGFR-STAT3 signaling promotes formation of malignant peripheral nerve sheath tumors. Oncogene *33*, 173-180.

Wu, J., Williams, J.P., Rizvi, T.A., Kordich, J.J., Witte, D., Meijer, D., Stemmer-Rachamimov, A.O., Cancelas, J.A., and Ratner, N. (2008). Plexiform and dermal

neurofibromas and pigmentation are caused by Nf1 loss in desert hedgehog-expressing cells. Cancer Cell *13*, 105-116.

Wyckoff, J.B., Wang, Y., Lin, E.Y., Li, J.F., Goswami, S., Stanley, E.R., Segall, J.E., Pollard, J.W., and Condeelis, J. (2007). Direct visualization of macrophage-assisted tumor cell intravasation in mammary tumors. Cancer research *67*, 2649-2656.

Xia, H., Chen, J., Shi, M., Gao, H., Sekar, K., Seshachalam, V.P., Ooi, L.L., and Hui, K.M. (2015). EDIL3 is a novel regulator of epithelial-mesenchymal transition controlling early recurrence of hepatocellular carcinoma. J Hepatol *63*, 863-873.

Xu, G.F., Lin, B., Tanaka, K., Dunn, D., Wood, D., Gesteland, R., White, R., Weiss, R., and Tamanoi, F. (1990). The catalytic domain of the neurofibromatosis type 1 gene product stimulates ras GTPase and complements ira mutants of S. cerevisiae. Cell *63*, 835-841.

Yan, T., Feng, Y., Zheng, J., Ge, X., Zhang, Y., Wu, D., Zhao, J., and Zhai, Q. (2010). Nmnat2 delays axon degeneration in superior cervical ganglia dependent on its NAD synthesis activity. Neurochem Int *56*, 101-106.

Yang, B., Treweek, J.B., Kulkarni, R.P., Deverman, B.E., Chen, C.K., Lubeck, E., Shah, S., Cai, L., and Gradinaru, V. (2014). Single-cell phenotyping within transparent intact tissue through whole-body clearing. Cell *158*, 945-958.

Yang, F.C., Chen, S., Clegg, T., Li, X., Morgan, T., Estwick, S.A., Yuan, J., Khalaf, W., Burgin, S., Travers, J.*, et al.* (2006). Nf1+/- mast cells induce neurofibroma like phenotypes through secreted TGF-beta signaling. Hum Mol Genet *15*, 2421-2437.

Yang, F.C., Ingram, D.A., Chen, S., Hingtgen, C.M., Ratner, N., Monk, K.R., Clegg, T., White, H., Mead, L., Wenning, M.J.*, et al.* (2003). Neurofibromin-deficient Schwann cells secrete a potent migratory stimulus for Nf1+/- mast cells. J Clin Invest *112*, 1851-1861.

Yang, F.C., Ingram, D.A., Chen, S., Zhu, Y., Yuan, J., Li, X., Yang, X., Knowles, S., Horn, W., Li, Y.*, et al.* (2008a). Nf1-dependent tumors require a microenvironment containing Nf1+/-- and c-kit-dependent bone marrow. Cell *135*, 437-448.

Yang, L., Huang, J., Ren, X., Gorska, A.E., Chytil, A., Aakre, M., Carbone, D.P., Matrisian, L.M., Richmond, A., Lin, P.C.*, et al.* (2008b). Abrogation of TGF beta signaling in mammary carcinomas recruits Gr-1+CD11b+ myeloid cells that promote metastasis. Cancer cell *13*, 23-35.

Yanger, K., Zong, Y., Maggs, L.R., Shapira, S.N., Maddipati, R., Aiello, N.M., Thung, S.N., Wells, R.G., Greenbaum, L.E., and Stanger, B.Z. (2013). Robust cellular reprogramming occurs spontaneously during liver regeneration. Genes & development *27*, 719-724.

Yao, X., Huang, J., Zhong, H., Shen, N., Faggioni, R., Fung, M., and Yao, Y. (2014). Targeting interleukin-6 in inflammatory autoimmune diseases and cancers. Pharmacol Ther *141*, 125-139.

Young, K.M., Psachoulia, K., Tripathi, R.B., Dunn, S.J., Cossell, L., Attwell, D., Tohyama, K., and Richardson, W.D. (2013). Oligodendrocyte dynamics in the healthy adult CNS: evidence for myelin remodeling. Neuron *77*, 873-885.

Yu, W.M., Feltri, M.L., Wrabetz, L., Strickland, S., and Chen, Z.L. (2005). Schwann cell-specific ablation of laminin gamma1 causes apoptosis and prevents proliferation. The Journal of neuroscience : the official journal of the Society for Neuroscience *25*, 4463-4472.

Yu, W.M., Yu, H., Chen, Z.L., and Strickland, S. (2009). Disruption of laminin in the peripheral nervous system impedes nonmyelinating Schwann cell development and impairs nociceptive sensory function. Glia *57*, 850-859.

Zanazzi, G., Einheber, S., Westreich, R., Hannocks, M.J., Bedell-Hogan, D., Marchionni, M.A., and Salzer, J.L. (2001). Glial growth factor/neuregulin inhibits Schwann cell myelination and induces demyelination. J Cell Biol *152*, 1289-1299.

Zeng, J., Yang, X., Cheng, L., Liu, R., Lei, Y., Dong, D., Li, F., Lau, Q.C., Deng, L., Nice, E.C.*, et al.* (2013). Chemokine CXCL14 is associated with prognosis in patients with colorectal carcinoma after curative resection. J Transl Med *11*, 6.

Zeng, Z., Shi, Y.X., Samudio, I.J., Wang, R.Y., Ling, X., Frolova, O., Levis, M., Rubin, J.B., Negrin, R.R., Estey, E.H.*, et al.* (2009). Targeting the leukemia microenvironment by CXCR4 inhibition overcomes resistance to kinase inhibitors and chemotherapy in AML. Blood *113*, 6215-6224.

Zhang, J., Fujimoto, J., Zhang, J., Wedge, D.C., Song, X., Zhang, J., Seth, S., Chow, C.W., Cao, Y., Gumbs, C.*, et al.* (2014a). Intratumor heterogeneity in localized lung adenocarcinomas delineated by multiregion sequencing. Science *346*, 256-259.

Zhang, J.Y., Luo, X.G., Xian, C.J., Liu, Z.H., and Zhou, X.F. (2000). Endogenous BDNF is required for myelination and regeneration of injured sciatic nerve in rodents. Eur J Neurosci *12*, 4171-4180.

Zhang, M., Wang, Y., Jones, S., Sausen, M., McMahon, K., Sharma, R., Wang, Q., Belzberg, A.J., Chaichana, K., Gallia, G.L.*, et al.* (2014b). Somatic mutations of SUZ12 in malignant peripheral nerve sheath tumors. Nature genetics *46*, 1170-1172.

Zhang, Y., Patel, S., Abdelouahab, H., Wittner, M., Willekens, C., Shen, S., Betems, A., Joulin, V., Opolon, P., Bawa, O.*, et al.* (2012). CXCR4 inhibitors selectively eliminate CXCR4-expressing human acute myeloid leukemia cells in NOG mouse model. Cell death & disease *3*, e396.

Zhang, Y., Saavedra, E., Tang, R., Gu, Y., Lappin, P., Trajkovic, D., Liu, S.H., Smeal, T., Fantin, V., De Botton, S.*, et al.* (2017). Targeting primary acute myeloid leukemia with a new CXCR4 antagonist IgG1 antibody (PF-06747143). Scientific reports *7*, 7305.

Zhao, H., and Peehl, D.M. (2009). Tumor-promoting phenotype of CD90hi prostate cancer-associated fibroblasts. The Prostate *69*, 991-1000.

Zheng, H., Chang, L., Patel, N., Yang, J., Lowe, L., Burns, D.K., and Zhu, Y. (2008). Induction of abnormal proliferation by nonmyelinating schwann cells triggers neurofibroma formation. Cancer Cell *13*, 117-128.

Zhou, Y., Larsen, P.H., Hao, C., and Yong, V.W. (2002). CXCR4 is a major chemokine receptor on glioma cells and mediates their survival. The Journal of biological chemistry *277*, 49481-49487.

Zhu, J., Thakolwiboon, S., Liu, X., Zhang, M., and Lubman, D.M. (2014). Overexpression of CD90 (Thy-1) in pancreatic adenocarcinoma present in the tumor microenvironment. PloS one *9*, e115507.

Zhu, X., Bergles, D.E., and Nishiyama, A. (2008). NG2 cells generate both oligodendrocytes and gray matter astrocytes. Development *135*, 145-157.

Zhu, Y., Ghosh, P., Charnay, P., Burns, D.K., and Parada, L.F. (2002). Neurofibromas in NF1: Schwann cell origin and role of tumor environment. Science *296*, 920-922.

Zhu, Y., Guignard, F., Zhao, D., Liu, L., Burns, D.K., Mason, R.P., Messing, A., and Parada, L.F. (2005). Early inactivation of p53 tumor suppressor gene cooperating with NF1 loss induces malignant astrocytoma. Cancer cell *8*, 119-130.

Zhu, Y., Li, H., Li, K., Zhao, X., An, T., Hu, X., Park, J., Huang, H., Bin, Y., Qiang, B.*, et al.* (2013). Necl-4/SynCAM-4 is expressed in myelinating oligodendrocytes but not required for axonal myelination. PLoS One *8*, e64264.

Zochodne, D.W. (2008). Neurobiology of Peripheral Nerve Regeneration. Cambridge University Press

Zorick, T.S., Syroid, D.E., Arroyo, E., Scherer, S.S., and Lemke, G. (1996). The Transcription Factors SCIP and Krox-20 Mark Distinct Stages and Cell Fates in Schwann Cell Differentiation. Mol Cell Neurosci *8*, 129-145.

Zou, X., Qiao, H., Jiang, X., Dong, X., Jiang, H., and Sun, X. (2009). Downregulation of developmentally regulated endothelial cell locus-1 inhibits the growth of colon cancer. J Biomed Sci *16*, 33.

Zuchero, J.B., and Barres, B.A. (2015). Glia in mammalian development and disease. Development *142*, 3805-3809.

Zujovic, V., Thibaud, J., Bachelin, C., Vidal, M., Deboux, C., Coulpier, F., Stadler, N., Charnay, P., Topilko, P., and Baron-Van Evercooren, A. (2011). Boundary cap cells are peripheral nervous system stem cells that can be redirected into central nervous system lineages. Proc Natl Acad Sci U S A *108*, 10714-10719.

Zuo, J., Hernandez, Y.J., and Muir, D. (1998a). Chondroitin sulfate proteoglycan with neurite-inhibiting activity is up-regulated following peripheral nerve injury. J Neurobiol *34*, 41-54.

Zuo, J., Neubauer, D., Dyess, K., Ferguson, T.A., and Muir, D. (1998b). Degradation of chondroitin sulfate proteoglycan enhances the neurite-promoting potential of spinal cord tissue. Exp Neurol *154*, 654-662.

Zuo, J., Neubauer, D., Graham, J., Krekoski, C.A., Ferguson, T.A., and Muir, D. (2002). Regeneration of axons after nerve transection repair is enhanced by degradation of chondroitin sulfate proteoglycan. Exp Neurol *176*, 221-228.

Zurkirchen, L., and Sommer, L. (2017). Quo vadis: tracing the fate of neural crest cells. Current opinion in neurobiology *47*, 16-23.

Appendix

Complete RNA seq analysis (Located on the CD at the back of this thesis):

1. Analysis by the Genomic Facility in Liverpool: This analysis contains the trimmed reads (fastq format) and the differential expression (DE) analysis tables. The data can also be accessed via http://cgr.liv.ac.uk/illum/LIMS11184_9e0728efb51e3121/ (for trimmed reads) and http://www.cgr.liv.ac.uk/illum/LIMS11184Results_ba3c2a163baf7ea1/ (for alignments and DE tables)
2. Analysis by the Dr. Christina Venturini: This analysis can be accessed via file:///Users/salomestierli/Desktop/RNA%20seq/salome_data/Salome's%20project_report.html and all Figures and DE analysis tables have been included here.